



HAL
open science

Rôle des conditions océaniques et des ice-shelves en périphérie des calottes européennes lors des événements climatiques abrupts de la dernière période glaciaire

Mélanie Wary

► **To cite this version:**

Mélanie Wary. Rôle des conditions océaniques et des ice-shelves en périphérie des calottes européennes lors des événements climatiques abrupts de la dernière période glaciaire. Sciences de la Terre. Université de Bordeaux, 2015. Français. NNT : 2015BORD0316 . tel-01276330

HAL Id: tel-01276330

<https://theses.hal.science/tel-01276330>

Submitted on 19 Feb 2016

HAL is a multi-disciplinary open access archive for the deposit and dissemination of scientific research documents, whether they are published or not. The documents may come from teaching and research institutions in France or abroad, or from public or private research centers.

L'archive ouverte pluridisciplinaire **HAL**, est destinée au dépôt et à la diffusion de documents scientifiques de niveau recherche, publiés ou non, émanant des établissements d'enseignement et de recherche français ou étrangers, des laboratoires publics ou privés.

THÈSE

PRESENTEE A

L'UNIVERSITE DE BORDEAUX

ÉCOLE DOCTORALE : SCIENCES ET ENVIRONNEMENTS

Par **Mélanie WARY**

POUR OBTENIR LE GRADE DE

DOCTEUR

SPECIALITE : Sédimentologie Marine et Paléoclimats

**ROLE DES CONDITIONS OCEANIQUES ET DES *ICE-SHELVES* EN
PERIPHERIE DES CALOTTES EUROPEENNES LORS DES
EVENEMENTS CLIMATIQUES ABRUPTS DE LA DERNIERE PERIODE
GLACIAIRE**

DIRIGEE PAR : **Frédérique EYNAUD**

Soutenue le 10 décembre 2015

DEVANT LA COMMISSION D'EXAMEN COMPOSEE DE :

Mme Mary ELLIOT, Professeur, Université de Nantes	Rapporteur
Mme Masa KAGEYAMA, Directeur de Recherche CNRS, LSCE	Rapporteur
Mme Fabienne MARRET-DAVIES, Senior Reader, Université de Liverpool	Rapporteur
Mme Aurélie PENAUD, Maître de Conférences, IUEM-UBO	Examineur
Mme Maria Fernanda SANCHEZ GOÑI, Professeur/Directeur d'Étude EPHE, Université de Bordeaux	Examineur et Présidente du Jury
Mme Frédérique EYNAUD, Maître de Conférences, Université de Bordeaux	Directrice de thèse

Remerciements

Voilà enfin venu le moment des remerciements à toutes les personnes qui m'ont accompagnée au cours de ces dernières années... ou disons plutôt au cours de mes premières années de recherche !!! Les dernières pages à écrire – et que j'ai failli oublier d'écrire ! – mais finalement pas les plus faciles : il ne faut oublier personne !!! J'avais justement commencé une liste, mais impossible de la retrouver, alors si jamais j'oubliais certaines personnes, qu'elles veuillent bien m'en excuser, car il est clair que ce travail de thèse aurait été tout autre sans leur aide/soutien/contribution/... !

Je tiens tout d'abord à remercier les membres de l'équipe paléo en tant que « mes profs de paléo de licence et de master », car c'est avant tout vous qui m'avez fait découvrir, et petit à petit me passionner pour, cette discipline. Et c'est donc grâce à vous que je me suis petit à petit éloignée de mon projet professionnel initial (qui se résumait, en L1, à un « métier bien payé en lien avec la géologie et qu'on trouve rapidement à la fin des études »... alors oui, c'est vrai qu'on est un peu à côté de la plaque là, mais je maintiens le « grâce à vous » et vous allez comprendre pourquoi!). Parmi « mes profs de paléo », je me dois de remercier tout particulièrement Bruno, qui a été le premier, à travers un cours de licence, à me faire me passionner pour les événements d'Heinrich (et oui Fred, ça remonte à aussi loin ! du coup, un premier grand merci à toi pour m'avoir offert le sujet de thèse dont je rêvais depuis longtemps !)... et de fil en aiguille, me voilà, début M1, aller voir Bruno avec ma demande de stage (un peu naïve) : « Monsieur, je voudrais faire un stage avec vous sur les événements d'Heinrich avec les isotopes parce que je ne me vois pas compter des petites bêtes » (!) ... Et toujours de fil en aiguille (avec, au passage, un énorme merci à Bruno + Fred, et Séb + Fred + Catherine Kissel, pour les supers stages de M1 et M2 que j'ai passés avec vous), me voilà finalement quelques années plus tard, complètement dingue des dinos (deuxième merci à Fred pour m'avoir fait découvrir et m'avoir formée à ce super outil !) et à vouloir faire un métier, soyons honnêtes, pas très bien payé et avec peu de postes disponibles... Mais... un métier de passion ! Et de grande passion en l'occurrence! Alors merci mille fois à vous tous pour ça !

Je tiens également à vous remercier en tant que collègues, car, même si on aurait pu faire un peu plus de « réunions-goûters » (non, réflexion faite, juste « goûters »), c'était drôlement chouette de partager ces années avec vous ! Et merci aussi pour votre disponibilité quand je débarquais à l'imprévu dans vos bureaux ! Je tiens à remercier plus particulièrement Anne-Laure, pour son soutien inestimable tout au long de ma thèse ; Didier, pour m'avoir fait

comprendre que la modélisation ça ne servait pas à rien (Rrrro, j'ai honte) et m'avoir même finalement convaincue que modélisation et paléoreconstructions étaient plus que complémentaires ! (ça compense mon avis initial sur la modélisation, non ?!) ; Jérôme, pour ton soutien et nos séances de rigolades, et aussi pour les apéros, bbq et autres ! ; Bruno, pour ton aide sur le $\delta^{18}\text{O}$ et les calculs de SSS, et pour tes corrections d'article en mode « reviewer » ! ; Linda et Marie-Hélène, pour les lavages / préparations palyno / comptages / piquages (parfois en urgence !), et j'en passe, mais aussi pour les moments papotages / rigolades / chocolats chauds-madeleines passés dans votre bureau ; Laurent, pour ton aide avec les dinos (verre de montre compris... Grrr...) et pour m'avoir fait manger une vraie poutine (au moins 2 en fait !) à Montréal ! ; Mumu, Olivier et Ludo, pour votre aide et surtout pour les moments de rigolades dans votre bureau ! Et, Mumu, pour nos petites discussions aussi ! ; et bien sûr tous les autres : Philippe, Maria, Stéphan (notamment pour tes réponses à mes « questions débiles »... je sais pas pourquoi ça tombait souvent sur toi !), Jacques, Thierry (pour ton aide sur le Mg/Ca), Xavier, Loïc, Karine, Thibaut, Isa.

En tant que « pseudo-membre » de l'équipe, je tiens également à remercier le « spectro », qui au bout de 4 ans m'a enfin autorisé à l'utiliser pour passer mes échantillons ! Petit spectro, sache que je ne t'en veux plus pour ces 4 premières années ! Et merci à toi Karine, pour avoir tant de fois réparé ses caprices intempestifs ! Et pour m'avoir formée à son utilisation, même si ça m'a fait râler au début... !

Enfin, dernier membre de paléo, mais pas des moindres... Fred !!! Mille énormes mercis à toi, pour avoir été la meilleure directrice de thèse, qui m'a offert le meilleur sujet de thèse (oui, je sais, je dévie un peu dans le cul-cul la praline, mais là je peux pas faire autrement !... et si, si, je suis totalement objective !!) !!! Merci pour m'avoir si bien encadrée, soutenue, et aidée, pendant la thèse et encore maintenant ! Merci de m'avoir fait confiance (même si mes comptages n'avançaient pas très vite en première année !) et de m'avoir poussée à être autonome (hormis ces tout derniers mois, je débarque moins dans ton bureau, hein !?!). Merci aussi pour nos nombreuses discussions (scientifiques ou pas !) et pour ton enthousiasme constant et communicatif !! Et j'en passe, parce qu'il y en aurait trop à dire, et que je ne pourrais jamais assez te remercier pour tout ce que tu m'as apporté et tout ce que tu as fait pour moi ! Bref, ça a vraiment été génial de faire cette thèse avec toi, je me suis éclatée !! Et il me tarde déjà la suite de notre collaboration !!!

Un énorme merci à Seb également, pour toute ton aide au cours de ces années, pour m'avoir formée à la sédimento et m'avoir permis de conserver cet aspect sédimento si nécessaire en paléo (merci pour mes mesures granulo notamment!!), pour m'avoir formée à

ArcGIS (trop cool !), pour m'avoir donné comme « réponse rapide » à ma « question rapide » : « je sais pas » (!!!), pour m'avoir permis de partir en mer (un grand merci au passage aux membres de la mission MOCOSED 2014 pour cette incroyable expérience !), ... et j'en oublie sans doute, alors merci pour tout Seb ! P.S. : si jamais t'as une place dispo pour une nouvelle mission (genre la prochaine mission MOCOSED au Groenland, comme ça, par exemple...), pense à moi !! ;-)

Sauf si tu décides de te casser un genou avant bien sûr, parce que sans ravitaillement en schtroumpfs et chocolat ça sera moins bien quand même... ! :-)

Merci à Pierre-Yves et Loïc, ainsi qu'à Hélène Rebaubier et Nicolas Caillon du LSCE, pour leur aide plus qu'incalculable sur le Mg/Ca ! Heureusement que vous avez été là !! Merci aussi aux stagiaires que j'ai co-encadrés pendant ma thèse et qui ont grandement contribué à ce travail : Marjolaine, Joanna, Pierre et Camille.

Je tiens également à remercier les autres membres du labo EPOC que j'ai côtoyés au cours de ces années, pour leur bonne humeur, leur aide et leur soutien, tant du point de vue perso que du boulot... Et ils sont nombreux !! Je ne vais pas prendre le risque de citer tout le monde ici (j'en oublierais forcément !), mais au moins quelques noms (sans ordre de préférence, mais plutôt de couloirs !) : Domi, Bruno D., Jean-Michel et Hubert, Vincent M., Manue, Michel, Béa, Vincent H., Lionel et Cécile, Hervé D., Pascal... et pardon pour ceux que je ne cite pas !

Un grand merci également à TOUTES (☺) les membres de mon jury, qui ont accepté de lire ce travail de thèse, et m'ont donné de nombreux conseils !

Merci également à mes collègues thésards et collègues de Master, ainsi qu'à mes amis (là encore, dans le désordre, et tout confondu, car certains vont bien évidemment dans plusieurs catégories !!): Elsa, Damien et Loris (génial d'avoir partagé le même bureau !!), Cécile, Fred, Mylène et Sarah (merci pour votre soutien incalculable! Et pour le reste aussi bien sûr – shopping, soirées, aprem glandouille, dimanches jardiland, ... et j'en passe !), Léo et Léa (quelle belle rencontre !), Mélanie et Sophie (les M&M's !!), Ludo, Alex, Max, Philippine, Salomé, Ludivine, PA, Mélina, Mathylde, Arnaud, Mélanie, Hélène, Arthur, Aurélie et Marylise (merci pour votre accueil), Jérémie, Sonia, Junior, Christian, Emanuela... et tous ceux que j'oublie ! Merci à tous pour tous les moments passés ensemble !

Et enfin, dix-mille énormes mercis à ma famille (ma mère, mon père, mon frère, mes grands-mères, oncles, tantes, cousins et cousines), sans qui je n'en serai pas là aujourd'hui. Merci d'avoir supporté mes bonnes et mauvaises humeurs de ces derniers mois et de m'avoir continuellement soutenue !!! Et merci pour tout le reste !

Sommaire général

** Ce sommaire n'est que partiel, chaque chapitre incluant son propre sommaire détaillé*

<u>INTRODUCTION GENERALE</u>	1
<u>CHAPITRE 1 : CONTEXTE ENVIRONNEMENTAL ET PALEOCLIMATIQUE</u>	5
<u>Partie 1</u> : Cadre temporel de l'étude et problématiques.....	7
<u>Partie 2</u> : Cadre environnemental actuel et passé	13
<u>Partie 3</u> : Etat de l'art sur la paléoclimatologie de notre période et zone d'étude	25
<u>CHAPITRE 2 : MATERIEL ET METHODES</u>	31
<u>Partie 1</u> : Stratégie analytique	33
<u>Partie 2</u> : Principaux outils mis en œuvre	36
<u>Partie 3</u> : Outils complémentaires	74
<u>CHAPITRE 3 : CHANGEMENTS HYDROGRAPHIQUES DE PART ET D'AUTRE DE LA RIDE ISLANDE-ECOSSE AU COURS DES DERNIERS 45 KA</u>	77
<u>Partie 1</u> : Paléocéanographie du pourtour des Iles féroé au cours des derniers 45 ka	83
<u>Partie 2</u> : Processus hydrographiques et mécanismes de déclenchement en jeu lors des évènements climatiques abrupts avant, pendant et après un HE : zoom sur la période 35-41 ka autour d'HE4.....	163
<u>Partie 3</u> : Vue synthétique et synoptique de la paléocéanographie de l'Atlantique subboreale et de ses mers bordières au cours des évènements millénaires de la dernière période glaciaire.....	227
<u>CONCLUSIONS GENERALES ET PERSPECTIVES</u>	283
<u>REFERENCES BIBLIOGRAPHIQUES (HORS ARTICLES)</u>	291
<u>ANNEXES</u>	303
<u>Annexe 1</u> : Zumaque et al., 2012	305
<u>Annexe 2</u> : Caulle et al., 2013.....	307

Liste des Figures et Tables

CHAPITRE 1

Partie 1

- Figure 1 : Variations glaciaires/interglaciaires au cours du Quaternaire (haut) et des derniers 150 ka (bas) mises en évidence au travers de la courbe isotopique composite LR04 de Lisiecki et Raymo (2005). 8
- Figure 2 Enregistrement isotopique NGRIP (a) au cours des derniers 120 ka et (b) au cours des derniers 60 ka. Sur la Figure 2b, les portions de courbe en rouge représentent les interstadias (numérotés d'après Dansgaard et al., 1993), les portions en bleu les stadias. Les rectangles bleus illustrent les intervalles de temps correspondant aux « Heinrich stadials » (numérotés de H0 à H6). YD : Younger Dryas, BA : Bølling-Allerød. 9
- Figure 3 : (a) Localisation de la bande de Ruddiman (modifié d'après Ruddiman, 2001), zone de dépôt préférentielle des IRD, et (b) mécanismes de formation, transport et libération des IRD depuis le continent jusqu'aux sédiments marins (source : <http://access.ens-lyon.fr>). 11
- Figure 4 : Schéma conceptuel de l'interface calotte de glace – océan - atmosphère 12

Partie 2

- Figure 5 : Représentation schématique de la circulation océanique globale (issue de Rahmstorf, 2002), où les courants de surface sont représentés en rouge, les courants profonds en bleu, les courants de grand fond en violet, et les centres de convection par des cercles jaunes. 13
- Figure 6 : Circulation océanique en Atlantique Nord. (a) Circulation de surface (GS : Gulf Stream, NAD : North Atlantic Drift, NAC : North Atlantic Current, IC : Irminger Current, LC : Labrador Current, EIC : East Icelandic Current, EGC : East Greenland Current, WGC : West Greenland Current). (b) Circulation intermédiaire et profonde

(LSW : Labrador Sea Water, ISOW : Iceland-Scotland Overflow Water, DSOW : Denmark Strait Overflow Water, DWBC : Deep Western Boundary Current, NADW : North Atlantic Deep Water, AABW : Antarctic Bottom Water). Circulation d'après Stanford et al., 2011. Bathymétrie GEBCO (www.gebco.net). WGS 1984 Mercator 55°N..... 15

Figure 7 : Cadre environnemental de la zone d'étude. (a) Localisation des deux sites d'étude et circulation océanique de surface (NAC : North Atlantic Current, CSC : Continental Slope Current, EIC : East Icelandic Current, IC : Irminger Current). (b) Circulation profonde (ISOW : Iceland Scotland Overflow Water), bassins océaniques, et structures topographiques majeures (RT : Rockall Trough, RP : Rockall Plateau, LB : Louisy Bank, BBB : Bill Bailey Bank, FB : Faeroe Bank, WTR : Wyville-Thompson Ridge, FIR : Faeroe-Iceland Ridge, FBC : Faeroe Bank Channel, FSC : Faeroe Shetland Channel). Isobathes grises : 200 mètres de profondeur. Intervalle des isobathes noires : 500 mètres. (c et d) Profils Est-Ouest et Nord-Sud de températures océaniques (NAW : North Atlantic Water), réalisé avec Ocean Data View (Schlitzer, 2011). Leur localisation est indiquée sur les cartes a et b. Bathymétrie EMODNET (www.emodnet.eu). WGS 1984, Mercator 55°N..... 17

Figure 8 : Calottes de glace et couloirs d'écoulement de la glace au niveau de la zone d'étude lors de la dernière période glaciaire. (a) Etendue des calottes de glace au cours du Dernier Maximum Glaciaire (FIS : Fennoscandian Ice Sheet, BIIS : British Irish Ice Sheet), d'après Ehlers & Gibbard (2007) et paleo-ice streams d'après Stokes & Clark (2001). (b) Etendue des calottes de glace européennes vers 50-60 ka (marron) et au Dernier Maximum Glaciaire (beige), d'après Svendsen et al. (2004), et paleo-ice streams drainant les calottes européennes (MNIS : Minch Ice Stream, NCIS : Norwegian Channel Ice Stream), d'après Sejrup et al. (2003) et Bradwell et al. (2008). Bathymétrie EMODNET (www.emodnet.eu). WGS 1984, Mercator 55°N. 18

Figure 9 : Iceberg ploughmarks proches de la zone d'étude (localisation indiquée sur la Figure 8b). Données EMODNET (www.emodnet.eu)..... 19

Figure 10 : Répartition schématique des zones de dépôt contouritique (rouge), de trough mouth fan (vert) et de glissement (jaune), d'après Laberg et al. (2005). Les sites d'études sont localisés par des points blancs. Bathymétrie EMODNET

(www.emodnet.eu), isobathes pleins tous les 1000 m, isobathes 200 m en pointillés. WGS 1984, Mercator 55°N. 20

Figure 11 : Représentation simplifiée des vitesses de courant de fond nécessaires pour éroder, transporter et déposer des particules sédimentaires de différentes tailles et différentes natures (issue de Zenk, 2008). 21

Figure 12 : Contexte sédimentaire des sites d'étude et localisation des carottes proches référencées dans le texte. (a) Carte générale de localisation des sites. (b et c) Zoom au niveau des sites MD99-2285 (b) et MD99-2281 (c) illustrant les zones de dépôt contouritique, de glissement, et d'activité maximale du courant de fond, d'après Kuijpers (1998b, 2001), van Weering et al. (1998), Nielsen et al. (2007). (d) Profil sismique obtenu au niveau du site MD99-2281, issu de Boldreel et al. (1998). Bathymétrie EMODNET (www.emodnet.eu), isobathes pleins tous les 500 m, isobathes 200 m en pointillés. WGS 1984, Mercator 55°N..... 23

Tableau 1 : Localisation et caractéristiques générales des carottes sédimentaires étudiées 21

CHAPITRE 2

Partie 1

Tableau 2 : Stratégie analytique (outils et résolution temporelle). Les coches rouges indiquent les analyses que j'ai moi-même réalisées. Les noms en bleu correspondent à des stagiaires que j'ai co-encadrés (le nom du co-encadrant étant précisé entre parenthèses). Les informations en gris indiquent des données disponibles avant le début de ma thèse (Zumaque et al., 2012 et Caille et al., 2013 disponibles en Annexes 1 et 2)..... 34/35

Partie 2

Figure 13 : Cartes de distribution (en pourcentages) d'*Islandinium minutum* var *minutum* (a) dans la base de données modernes n = 1207, carte construite sous ARCGIS et (b) issue de l'atlas mondial de Zonneveld et al. (2013). 38

Figure 14 : Cartes de distribution (en pourcentages) de *Bitectatodinium tepikiense* (a) dans la base de données modernes n = 1207, carte construite sous ARCGIS et (b) issue de l'atlas mondial de Zonneveld et al. (2013). 39

Figure 15 : Cartes de distribution (en pourcentages) d'*Operculodinium centrocarpum* (a) dans la base de données modernes n = 1207, carte construite sous ARCGIS et (b) issue de l'atlas mondial de Zonneveld et al. (2013). 40

Figure 16 : Cartes de distribution (en pourcentages) de *Pentapharsodinium dalei* (a) dans la base de données modernes n = 1207, carte construite sous ARCGIS et (b) issue de l'atlas mondial de Zonneveld et al. (2013). 41

Figure 17 : Cartes de distribution (en pourcentages) de *Nematosphaeropsis labyrinthus* (a) dans la base de données modernes n = 1207, carte construite sous ARCGIS et (b) issue de l'atlas mondial de Zonneveld et al. (2013). 42

Figure 18 : Cartes de distribution (en pourcentages) de *Brigantedinium* spp. (a) dans la base de données modernes n = 1207, carte construite sous ARCGIS et (b) issue de l'atlas mondial de Zonneveld et al. (2013). 43

Figure 19 : Cartes de distribution (en pourcentages) de *Lingulodinium machaerophorum* (a) dans la base de données modernes n = 1207, carte construite sous ARCGIS et (b) issue de l'atlas mondial de Zonneveld et al. (2013). 44

Figure 20 : Cartes de distribution (en pourcentages) de *Spiniferites ramosus* (a) dans la base de données modernes n = 1207, carte construite sous ARCGIS et (b) issue de l'atlas mondial de Zonneveld et al. (2013). 45

Figure 21 : Cartes de distribution (en pourcentages) de *Spiniferites elongatus*/S. *frigidus* (a) dans la base de données modernes n = 1207, carte construite sous ARCGIS et (b) issue de l'atlas mondial de Zonneveld et al. (2013). 46

Figure 22 : Cartes de distribution (en pourcentages) d'Impagidinium pallidum (a) dans la base de données modernes n = 1207, carte construite sous ARCGIS et (b) issue de l'atlas mondial de Zonneveld et al. (2013).	47
Figure 23 : Cartes de distribution (en pourcentages) de Selenopemphix quanta (a) dans la base de données modernes n = 1207, carte construite sous ARCGIS et (b) issue de l'atlas mondial de Zonneveld et al. (2013).	48
Figure 24 : Cartes de distribution (en pourcentages) d'Echinidinium granulatum (a) dans la base de données modernes n = 1207, carte construite sous ARCGIS et (b) issue de l'atlas mondial de Zonneveld et al. (2013).	49
Figure 25 : Cartes de distribution (en pourcentages) de Polykrikos schwartzii sensu Bütschli, 1873 (a) dans la base de données modernes n = 1207, carte construite sous ARCGIS et (b) issue de l'atlas mondial de Zonneveld et al. (2013).	50
Figure 26 : Résultat des mesures de calcimétrie et droite de calibration Ca (XRF NIOZ) – taux de CaCO ₃	58
Figure 27 : Evolution du taux de CaCO ₃ d'après calibration XRF dans la carotte MD99-2281	58
Figure 28 : Evolution du taux de CaCO ₃ d'après calibration XRF dans la carotte MD99-2285	58
Figure 29 : Schéma de fonctionnement d'un ICP-OES	61
Figure 30 : Notions de justesse et de répétabilité	62
Figure 31 : Capture d'écran du logiciel de l'ICP illustrant la détermination des droites de calibration (en vert) à partir des intensités relatives mesurées pour chaque standard (en rouge) de la gamme étalon.	66
Figure 32 : Illustration de la méthode de calibration dite des ratios d'intensité.	67
Figure 33 : Comparaison des signaux de température issus de la méthode Mg/Ca sur PF (courbes noires) et de la méthode fonction de transfert sur assemblages de PF (courbes rouges) sur les portions (a) 1 – 1.3 Ma BP et (b) 1.8 – 2 Ma BP de la carotte MD96-2048 (figure modifiée d'après Extier, 2015).	71
Figure 34 : Résultat des analyses Mg/Ca sur la carotte MD99-2285. (a) NGRIP $\delta^{18}\text{O}$. (b) Susceptibilité magnétique. (c) Abondance relative de <i>N. pachyderma</i> senestre. (d)	

Reconstructions quantifiées des températures océaniques estivale et hivernale issues des assemblages de PF via l’application d’une fonction de transfert. (e) Ratio Mg/Ca mesuré sur *N. pachyderma* senestre et température équivalente d’après la calibration de Nürnberg et al. (1995)..... 72

Planche 1 : Micro-photographies de certains taxons de dinokystes rencontrés dans cette thèse. 51

Planche 2 : Micro-photographies de certains taxons de dinokystes rencontrés dans cette thèse. 52

Tableau 1 : Comparaison des deux méthodes de calibration à partir des mesures réalisées sur du BAM-RS3. 68

CHAPITRE 3

Partie 1

Section 1

Figure 1: (a) General map of the studied area, showing the location of the studied core MD99-2281 (red cross) and of nearby cores referred to in the present study (black dots; ENAM93-21 and ENAM33, Rasmussen et al., 1996a,b, Rasmussen and Thomsen, 2004; MD99-2284, Dokken et al., 2013; LO09-18GC and SO82-05GGC, Snowball and Moros, 2003; Na87-22 and SU90-24, Elliot et al., 2002). The hatched areas represent the maximal last glacial extension of the proximal ice-sheets (after Ehlers and Gibbard, 2007; FIS: Fennoscandian Ice-Sheet; BIIS: British-Irish Ice-Sheet). The yellow arrows indicate the major pathways of the warm and saline surface water conveyed by the North Atlantic Drift (NAD, after Orvik and Niiler, 2002 and Stanford et al., 2011). Purple square indicates the area shown in Fig. 1b. Blue line indicates the location of the profile shown in Fig. 1c. (b) Detailed physiography of the studied area. Bathymetry is from GEBCO (www.gebco.net, isobaths every 200 m). Remarkable sub-marine

structures are indicated (bathymetric heights: FB, Faeroe Bank; BBB, Bill Bailey Bank; LB, Lousy Bank; WTR, Wyville-Thompson Ridge – trough: RT, Rockall Trough – and channels: FSC, Faeroe-Shetland Channel; FBC, Faeroe Bank Channel). Purple arrows show the major (full lines) and intermittent (dotted lines) deep Iceland Scotland Overflow Water (ISOW) pathways, after Boldreel et al., (1998), Kuijpers et al. (1998b, 2002), and Howe et al. (2006). Blue line indicates the location of the profile shown in Fig. 1c. (c) East-west profile of oceanic temperatures. Temperature data are derived from WOA09 (Locarnini et al., 2010) and plot using Ocean Data View (Schlitzer, 2012); bathymetric data are from GEBCO (www.gebco.net). Locations of the studied core and of the main sub-marine structures are indicated. Geographic coordinate system: WGS 1984 – Projection: Mercator 55°N. 111

Figure 2: Evolution of index micro-planktonic assemblages compared to (a) NGRIP-GICC05 $\delta 18\text{O}$ record: (b) Relative abundances of the dominant planktonic foraminifera species – (c) Absolute abundances (nb. of specimen in the sediment) of dinocysts and planktonic foraminifera – (d) Relative abundances of dominant dinocyst species – (e) Planktonic foraminifera diversity and dominance (see calculations in Sect. 3.2.) – (f) Dinocyst diversity and dominance. Red stars indicate AMS 14C dates used, and blue stars show the tie-points obtained by comparing the MD99-2281 magnetic susceptibility record to the NGRIP $\delta 18\text{O}$ signal (see Zumaque et al., 2012). GS and HS are highlighted by light and dark grey bands respectively (age limits after Wolff et al., 2010). DO are numbered according to corresponding GI numbers in Dansgaard et al. (1993), except for GI 5 which was divided in GI 5.2 and GI 5.1 according to Rasmussen et al. (2014). LGM is for Last Glacial Maximum, BA for Bølling-Allerød, and YD for Younger Dryas. 112

Figure 3: Reconstructed hydrological parameters derived from dinocyst and planktonic foraminifera assemblages compared to (a) NGRIP-GICC05 $\delta 18\text{O}$ record: – (b) Temperatures – (c) Seasonality (mean summer minus mean winter temperatures) – (d) SSS derived from dinocysts – (e) Abundances of coenobia of the freshwater algae *Pediastrum* spp. – (f) $\delta 18\text{O}$ measured on *N. pachyderma* – (g) Local $\delta 18\text{OSW}$ derived from $\delta 18\text{O}$ on *N. pachyderma* – (h) Large Lithic Grains (LLG) concentration, plotted on a reverse scale. Stars, bands, DO number and acronyms: same legend as Fig. 2. 113

Figure 4: Evolution of oceanic bottom conditions. (a) NGRIP-GICC05 $\delta 18\text{O}$ record – (b) Sedimentation rate (calculated between two consecutive tie-points) – (c) Grain-size

distribution on the background, and D10, D50, and D90 represented as black curves in the foreground – (d) Mean size of the silt (10-63 μm) fraction for bulk samples and pretreated samples (carbonates and organic matter removed) – (e) Silt ratio between 26-63 μm and 10-26 μm fractions for bulk and pretreated samples – (f) Mean diameter of the dominant grain-size mode for bulk and pretreated samples – (g) Magnetic susceptibility record – (h) Absolute abundances of benthic foraminifera. Stars, bands, DO number and acronyms: same legend as Fig. 2. 114

Figure 5: Comparative figure showing the evolution through time of proxies indicative of the ISOW bottom dynamics (left framed panel), the subsurface NAD intensity (middle framed panel), and the surface sensu stricto conditions (right framed panel). Absolute abundances of benthic foraminifera, planktonic foraminifera, and dinocysts are shown in the middle unframed panel. NGRIP $\delta^{18}\text{O}$ record is shown at the far left to illustrate the chronological framework. Stars, bands, DO number and acronyms: same legend as Fig. 2. Red arrows highlight the progressive trends. 115

Figure 6: Synthetic figure illustrating the hydrological processes occurring during Dansgaard-Oeschger cycles at the study site. (a) Zoom in on DO 8, 7, 6 and 5 showing the evolution of some selected proxies shown in Fig. 5, as well as the schematic evolution through DO of the ISOW activity, the NAD vigor, the intensity of mixing between surface and subsurface waters, and the degree of surface stratification. (b) Conceptual representation of the hydrological processes occurring during the different phases of DO as depicted in Fig. 6a. 116

Table 1: Synthesis of the main hydrologic features depicted at the study site during Heinrich stadials (HS) 1 to 4. 117

Supplementary Table 1: raw planktonic foraminifera counts. 122-126

Section 2

Figure 1: Map of the study area showing the locations of the studied core and of nearby cores referenced to in the present study, as well as past and modern environmental settings. (a) Surface hydrology (after Kenyon, 1986; Valdimarsson and Malmberg, 1999, Orvik and Niiler, 2002), last glacial ice-sheet extensions (after Svendsen et al., 2004) and major paleo-ice streams (after Sejrup et al., 2003 and Bradwell et al., 2008). (b) Detailed bottom physiography and deep Iceland Scotland Overflow Water (ISOW) major pathways across the Greenland Scotland Ridge via the bottom current (after Kuijpers et al., 1998). The first isobath (dotted) is at 200 m, then isobath interval is 500 m. Major bathymetric structures are indicated (FIR: Faeroe Iceland Ridge, FSC: Faeroe Shetland Channel, FBC: Faeroe Bank Channel; WTR: Wyville-Thomson Ridge, FB: Faeroe Bank). Location of the north-south temperature profile shown in Fig. 1d is indicated by the yellow line. (c) Modern sedimentary regimes, with indication of the area of contourite deposit (van Weering et al., 1998), the sector affected by down-slope mass transport (Kuijpers et al., 2001; Nielsen et al., 2007), and the location of the erosive channel formed through the bottom current action (van Weering et al., 1998). Isobath intervals is 200 m. (d) North-south temperature profile illustrating the structure of the water column over the study area. Temperature data are derived from WOA09 data (Locarnini et al., 2010) and plot using Ocean Data View (Schlitzer, 2012). Bathymetry is from EMODnet (www.emodnet.eu). Geographic coordinate system: WGS 1984 – Projection: Mercator 55°N..... 156

Figure 2: Age model, sedimentation rate and resolution of analyses on core MD99-2285 for the last 50 ka. (a) Linear interpolation (black curve) between tie-points, i.e. selected AMS14C dates (red dots) and age-control points (blue dots) obtained by correlation of the magnetic susceptibility signal of the core to the NGRIP $\delta^{18}O$ record (Wolff et al., 2010). Incoherent dates (unconsidered for the establishment of the age model) are also shown (grey squares with corresponding ages in brackets). (b) Graph showing the correspondence between the magnetic susceptibility signal of the core (plotted according to the resulting calendar BP age scale) and the NGRIP $\delta^{18}O$ record. (c) Comparison of MD99-2281 MS record with nearby core MD95-2009 (cf. Fig. 1c) MS signal from Kissel et al. (1999). (d) Evolution through time of sedimentation rates of the

studied core. (e) Resolution of the three principal analyses conducted on core MD99-2285 for the present work. 157

Figure 3: Results from dinocyst and planktonic foraminifera assemblages over the section 0-600 cm of core MD99-2285. (a) Magnetic susceptibility signal, tie-points used to establish the age model (with blue stars = age control points obtained by correlating the core magnetic susceptibility signal to NGRIP $\delta 18O$ record, and red stars = AMS 14C dates; cf. Figure 2 and Table 1) and chronostratigraphic framework. (b) Relative abundances of dominant and major subordinate modern dinocyst species. (c) Concentration of modern dinocysts. (d) Dinocyst diversity and dominance indices. (e) Relative abundances of dominant and major subordinate planktonic foraminifera species. (f) Concentration of planktonic foraminifera. (g) Planktonic foraminifera diversity and dominance indices. Key cold periods highlighted by grey bands (delimited according to our age model with age limits defined by Wolff et al., 2010, Sanchez-Goñi and Harrison, 2010, and Rasmussen et al., 2014; YD = Younger Dryas, HS# = Heinrich stadial number #, GS# = Greenland stadial number #)..... 158

Figure 4: Age compilation of hydrological signals recorded on core MD99-2285. (a) NGRIP $\delta 18O$ regional stratotype. (b to e) Indicators of deep current activity, with (b) magnetic susceptibility, (c) Xrf K/Ti ratio, plotted on a reverse scale, (d) mapping of grain-size distribution, D10, D50, and D90, (e and f) mean sizes of the clay to silty clay size fractions. (g) Large Lithic Grains concentration, indicative of iceberg calving. (h to l) indicators of surface and subsurface hydrological conditions, with (h) seasonal SSSdino, (i) seasonal SSTdino and PF-Temp, (j) temperature seasonal contrast calculated from seasonal SSTdino and PF-Temp, (k) SICdino, and (l) salinity seasonal contrast calculated from seasonal SSSdino. (m) Obliquity signal, which displays relatively similar trends to some of our dinocyst-derived records and especially those related to sea ice. Stars and grey bands: same legend as Fig. 3. Mean modern hydrological values (after WOA09 data; Antonov et al., 2010; Locarnini et al., 2010) and undated core-top values are also indicated. 159

Table 1: Radiocarbon dates on MD99-2285 and age control points obtained by correlation of the magnetic susceptibility signal of core MD99-2285 to NGRIP $\delta 18O$ record

(Svensson et al., 2008; Wolff et al., 2010). Selected and eliminated tie points are shown.

..... 160

Table 2: Modern hydrological conditions (WOA09 data, Locarnini et al., 2010; Antonov et al., 2010) and core-top (0-1 cm) reconstructed hydrological parameters at 10 m water depth..... 161

Partie 2

Section 1

Figure 1: Map of the study area showing the locations of the studied core and of nearby cores referenced to in the present study, as well as past and modern environmental settings. (a) Surface hydrology (after Kenyon, 1986; Valdimarsson and Malmberg, 1999, Orvik and Niiler, 2002), last glacial ice-sheet extensions (after Svendsen et al., 2004) and major paleo-ice streams (after Sejrup et al., 2003 and Bradwell et al., 2008). (b) Detailed bottom physiography and deep Iceland Scotland Overflow Water (ISOW) major pathways across the Greenland Scotland Ridge via the bottom current (after Kuijpers et al., 1998). The first isobath (dotted) is at 200 m, then isobath interval is 500 m. Major bathymetric structures are indicated (FIR: Faeroe Iceland Ridge, FSC: Faeroe Shetland Channel, FBC: Faeroe Bank Channel; WTR: Wyville-Thomson Ridge, FB: Faeroe Bank). Location of the north-south temperature profile shown in Fig. 1d is indicated by the yellow line. (c) Modern sedimentary regimes, with indication of the area of contourite deposit (van Weering et al., 1998), the sector affected by down-slope mass transport (Kuijpers et al., 2001; Nielsen et al., 2007), and the location of the erosive channel formed through the bottom current action (van Weering et al., 1998). Isobath intervals is 200 m. (d) North-south temperature profile illustrating the structure of the water column over the study area. Temperature data are derived from WOA09 data (Locarnini et al., 2010) and plot using Ocean Data View (Schlitzer, 2012). Bathymetry is from EMODnet (www.emodnet.eu). Geographic coordinate system: WGS 1984 – Projection: Mercator 55°N..... 191

Figure 2: Age model and sedimentation rates of core MD99-2285 for the last 50 ka. (a) Linear interpolation (black curve) between tie-points, i.e. selected AMS14C dates (red dots)

and age-control points (blue dots) obtained by correlation of the magnetic susceptibility signal of the core to the NGRIP $\delta^{18}\text{O}$ record (Wolff et al., 2010). Incoherent dates (unconsidered for the establishment of the age model) are also shown (grey squares with corresponding ages in brackets). (b) Graph showing the correspondence between the magnetic susceptibility signal of the core (plotted according to the resulting calendar BP age scale) and the NGRIP $\delta^{18}\text{O}$ record. (c) Evolution through time of sedimentation rates of the studied core. 192

Figure 3: Evolution through depth on the studied interval (444-600 cm) of core MD99-2285 of selected parameters that enable the identification of allochthonous versus autochthonous signals. (a) Diversity and dominance indices calculated on dinocyst assemblages. (b) Concentrations of advected palynomorphs: *Halodinium* spp. and coenobia of *Pediastrum* spp. (c) SST stemming from dinocyst analyses (SSTdino) and from alkenones quantifications (SSTalk), compared to the concentration of advected pre-Quaternary dinocysts. (d) Relative abundance of *O. centrocarpum*, a dinocyst species related to the warm Atlantic inflow pathways. (e) Sea-ice cover duration derived from dinocyst analyses (SICdino) compared to IP25 abundances. The yellow bands highlight the intervals where coeval high SSTalk and high concentrations of advected palynomorphs are recorded. 193

Figure 4: Compilation of autochthonous signals indicative of regional surface and subsurface hydrological conditions through time on the 35-41 ka cal BP section of core MD99-2285. (a) NGRIP $\delta^{18}\text{O}$ regional stratotype compared to the magnetic susceptibility signal of the studied core. (b) Sea-ice cover indicators: SICdino, IP25 abundances, and relative abundance of the dinocyst polar taxa *I. minutum*. (c) Seasonal SSTdino and relative abundance of *O. centrocarpum*, a dinocyst taxa associated to the warm Atlantic inflow pathways. Triangles indicate mean modern SST values in summer (light red) and winter (dark red), after WOA09 data (Locarnini et al., 2010). (d) Seasonal sea-surface salinities derived from dinocyst analyses (SSSdino). The green triangle indicate mean modern SSS value (equal for both seasons) after WOA09 data (Antonov et al., 2010). (e) Ice-rafted debris (IRD) concentration. (f) $\delta^{18}\text{O}$ signal measured on *N. pachyderma* s. ($\delta^{18}\text{ONPS}$) and its associated potential ways of interpretation. (g) Concentration of the planktonic foraminifera polar taxa *N. pachyderma* s. (NPS), and relative abundance of dinocyst taxa *B. tepikiense*, both indicative of upper stratification favorable to NPS

development in subsurface. Hatched bands highlight stadial intervals (age limits after Wolff et al., 2010)..... 194/195

Figure 5: Selected hydrological parameters highlighting the sequencing of processes and ocean-cryosphere interactions occurring during Dansgaard-Oeschger and Heinrich events and associated ice-sheet collapses in core MD99-2285. (a) NGRIP $\delta^{18}O$ regional stratotype. (b) Indicator of (at least seasonally) open-ocean conditions (presence of sterols) versus more chaotic surface conditions (absence of sterols). (c) Sea-ice cover indicators. (d) Iceberg calving indicator. (e) Sea surface temperature record. (f) Sea surface salinity record. (g) Indirect indicators of warm Atlantic waters advection. (h) Indirect and relative indicator of subsurface warming versus propagation of sea-ice melting in subsurface, i.e. the two main factors impacting on local variations of $\delta^{18}ONPS$. (i) Indirect indicator of upper stratification. Hatched bands highlight stadial intervals (age limits after Wolff et al., 2010). Colored bands highlight the different sequences of hydrological processes (numbered at the top of the graph, including the subphases of phase 2). 195/196

Figure 6: Conceptual scheme of the sequencing of hydrological processes occurring during Dansgaard-Oeschger and Heinrich events in the southern Norwegian Sea..... 197

Table 1: Location and water depth of the studied core MD99-2285 and cores cited in the present study. 198

Table 2: Paleoceanographic studies conducted on Norwegian cores and using identical or equivalent analyses to some of those used in the present study. 199

Section 2

Figure 1: Map of the study area showing the location of the studied core (MD99-2281) and of the compared core (MD99-2285), the modern surface currents (after Kenyon, 1986; Orvik and Niiler, 2002) and deep currents (after Boldreel, 1998; Kuijpers et al., 1998a,b), the last glacial ice-sheet extensions (after Svendsen et al., 2004) and locations of major paleo-ice streams (after Sejrup et al., 2003 and Bradwell et al., 2008). 219

Figure 2: Age compilation of proxies indicative of surface advection and chronological framework for cores MD99-2281 (red) and MD99-2285 (black). (a) NGRIP $\delta^{18}\text{O}$ record. (b) Magnetic susceptibility (MS) and low field magnetic susceptibility (κ). (c) Ca/Sr Xrf ratio. (d) Ice-rafted debris concentration. (e) Reworked dinocyst concentration. (f) Concentration of *Coenobia* or *Pediastrum* spp. (g) Concentration of *Halodinium* spp. 220

Figure 3: Age compilation of proxies indicative of in situ hydrological conditions and chronological framework for cores MD99-2281 (red) and MD99-2285 (black). (a) NGRIP $\delta^{18}\text{O}$ record. (b) Magnetic susceptibility (MS) and low field magnetic susceptibility (κ). (c) SST stemming from dinocyst analyses. (d) SSS stemming from dinocyst analyses. (e) Ice-rafted debris concentration. (f) Concentration of *N. pachyderma* sinistral coiling. (g) Relative abundance of *N. pachyderma* sinistral coiling. 221

Table 1: Temporal resolution of the different analyses conducted on section 1792-1941 cm (i.e. ~ 37-40 ka cal BP) of core MD99-2281. 222

Section 3

Figure 35 : Evolution temporelle sur la section 3-41 ka cal BP de la carotte MD99-2285 de certains paramètres hydrologiques de surface et subsurface utilisés pour mettre en évidence le séquençage des processus hydrologiques au cours des événements de Dansgaard-Oeschger 10 à 8 incluant l'évènement d'Heinrich 4. (a) Enregistrement du $\delta^{18}\text{O}$ de NGRIP, et cadre chrono-stratigraphique. (b) SIC_{dino} . (c) Concentration en IRD > 150 μm . (d) SST_{dino} pour la période estivale. (e) Concentration en dinokystes remaniés. (f) Concentration des colonies de *Pediastrum* spp. (g) Concentration en *Halodinium* spp. (h) $\delta^{18}\text{O}$ mesuré sur *N. pachyderma* senestre. (i) Concentration absolue en *N. pachyderma* senestre. 224

Partie 3

Section 1

Figure 1: Five-member ensemble mean of temperature differences. a, Map showing the cores location (from north to south: MD95-2010, 66.68°N, 4.57°E, 1,226 m depth; MD95-2009, 62.74°N, -4.00°E, 1,027 m depth; MD99-2285, 62.69°N, -3.57°E, 885 m depth; MD99-2281, 60.34°N, -9.46°E, 1,197m depth) as well as SST differences (°C) between hosing and control experiments averaged over the 4th decade. The study area constitutes a nodal point regarding the modern surface oceanic circulation. It is indeed located at the convergence of (i) the northward warm North Atlantic water inflow and (ii) the southward polar water outflow through the East Greenland current terminal limb, i.e. the East Icelandic Current. Previous paleoclimatic studies^{34,35} evidenced that this area was also a key sector during the Last Glacial Maximum when, similarly to the SST pattern shown on the present map, warmer SST were recorded within the Nordic Seas and colder ones within the North Atlantic. This suggests that such a situation might represent a regular feature, at least for glacial periods. b, Latitude-depth section of the temperature differences (in °C, averaged over the whole Atlantic basin) between hosing and control experiments averaged over the 4th decade. 234

Figure 2: SST and SIC records from the four studied cores, with from the south to the north of the considered area: (a) core MD99-2281, (b) core MD99-2285, (c) core MD95-2009 and (d) core MD95-2010. To highlight the phase/antiphase of signals, SST and SIC signals have been shaded relatively to a threshold that corresponds to the mean value of the parameter over the studied period (red / dark blue for SST, and green / light blue for SIC). The value of this threshold is indicated in grey next to each signal. Worth is noting the latitudinal gradient expressed in the SIC mean values and especially the discrepancy between Norwegian Sea versus Atlantic sites. Magnetic susceptibility (MS) signals (black dotted curves) have been added for each core as they can be directly related to (f) the NGRIP $\delta^{18}O$ record⁵ (GICC05 age scale). Results are also compared to (e) the temperature anomaly (compared to modern value of ~ 20 °C) of the evaporative moisture source region for Greenland precipitation (shaded relatively to its mean value over 30-48 ka cal BP) deduced from GRIP deuterium excess signal, and superposed to the NGRIP deuterium excess record (black curve). Grey bands highlight

low NGRIP $\delta^{18}O$ and low MS values, i.e. stadial periods. Their position is highly coherent in core sections constrained by the MS/ $\delta^{18}O$ tuning but appears shifted when it is not the case (see methods). For core MD95-2010, the %I.MIN, indicative of colder SST and longer SIC duration, is also shown. 235/236

Figure 3: Polar water protrusions vs sea-surface seasonality contrasts. Indices of subsurface migration of polar waters (a), as deduced from the NPS abundances in the respective cores (with a shading in core MD99-2281 thanks to an arbitrary threshold of 75 % used to better evidence changes), are here plotted against the seasonality ranges calculated in the different cores (from b to e) as Summer SST minus Winter SST and compared to the reference (f) NGRIP $\delta^{18}O$ (GICC05 age scale) stratotype. Sea-surface seasonality values are shaded relatively to the mean value obtained over the studied period within each core (threshold value indicated in grey next to each record). Triangles indicate modern values of summer SST (red), winter SST (blue), and seasonality (black) for each study site (WOA09 data³⁶). As in Fig. 2, grey bands highlight low NGRIP $\delta^{18}O$ and low MS values, i.e. stadial periods..... 236/237

Figure 4: Conceptual hydrological scheme. The diagrams depict the mean conditions in the suboreal Atlantic area during stadials/interstadials, and summer/winter. Section location is indicated on the top maps. Bathymetry is from GEBCO (www.gebco.net), and has been simplified for sections. Ice-sheet extent on maps corresponds to the last glacial maximal extension, after³⁷. Colors indicate temperature range, as indicated by the bottom scale. 238

Extended data Figure 1: Information regarding the age model construction of the studied cores. a, age versus depth plots of the respective chronological constrains used to built the chronology (see Supplementary Information Table 1). b, Correlation of the NGRIP GICC05 $\delta^{18}O$ record³⁸ (a thick grey line has been chosen to circumscribe issues due to the b2k versus BP age scaling) to the magnetic susceptibility records of the respective studied cores. 243

Extended Data Figure 2: *Islandinium minutum* distribution within the modern dinocyst database made of 1207 points. This map clearly shows that this dinocyst taxon is strongly linked to cold and seasonally sea-ice covered surface environments..... 244

Extended Data Figure 3: Records of the relative percentage of *Islandinium minutum* within the four studied cores. For each core (from a to d) the %I.MIN records, indicative of colder SST and longer SIC, are compared to the magnetic susceptibility signals which can be directly correlated to Greenland climate variability as detected within the NGRIP $\delta^{18}O$ record (e). Grey bands highlight low NGRIP $\delta^{18}O$ and low MS values, i.e. stadial periods. It is worth noting the opposite scheme described by %I.MIN variations within the Nordic Seas versus in the Atlantic sector, which again illustrates the different patterns observed within the Nordic Seas and within the North Atlantic Ocean. 245

Extended Data Figure 4: Five-member ensemble mean of SSS differences. Anomalies between hosing and control experiments averaged over the 4th decade. 246

Extended Data Table 1: Characteristics of the five models considered. 247

Extended Data Table 2: SST anomalies. 247

Extended Data Table 3: SSS anomalies. 247

Supplementary Information Table 1: Age constrains for each of the studied cores. Lab. ID.: KIA – Tandetron AMS facility at Kiel Leibniz Laboratory (Germany); GifA – Tandetron AMS facility at Gif-Sur-Yvette (France); SacA– ARTEMIS Tandetron AMS facility at Saclay (France). 250-254

Section 2

Figure 1: Map of the study area showing the locations of the studied cores (MD99-2281 and MD99-2285) and of nearby core (MD99-2284), as well as past and modern environmental settings. Last glacial ice-sheet extensions are from Svendsen et al. (2004). Major paleo-ice streams are from Sejrup et al. (2003) and Bradwell et al. (2008). Surface current pathways are from Kenyon (1986), Valdimarsson and Malmberg (1999) and Orvik and Niiler (2002). Deep bottom flow pathways of ISOW are from Kuijpers et al. (1998) and Boldreel et al. (1998). Bathymetry is from EMODnet (www.emodnet.eu). Geographic coordinate system: WGS 1984 – Projection: Mercator 55°N. 276

Figure 2: Age compilation of records from cores MD99-2281 (in red and dark red) and MD99-2285 (in black and gray) indicative of AMOC strength and potential triggering mechanisms of its slowdowns at GI to GS/HS transitions. (a) NGRIP $\delta^{18}\text{O}$ regional stratotype, compared to (b) the magnetic susceptibility (MS) and/or low field magnetic susceptibility (κ) of both cores. (c) ISOW strength indicators. (d and e) NAD strength indicators (after Wary et al., CP, in press), with PF-derived temperature reconstructions (d) and relative percentages of temperate and polar PF species (e). Note the reverse scale of the relative percentage of *N. pachyderma* sinistral form (NPS). (f) Summed up concentrations of *Halodinium* spp. (light gray and red), *Pediastrum* spp. (medium gray and red), and reworked dinocysts (black and dark red), indicative of glacio-fluvial inputs after Wary et al. (QSR, to be submitted, and EPSL, to be submitted). (g) Indicators of sea-ice cover in the Norwegian Sea, i.e. IP25 abundances indicative of sea ice formation, and sea-ice cover duration derived from dinocyst assemblages, from Wary et al. (QSR, to be submitted). Hatched bands indicate GS intervals (age limits after Wolff et al., 2010). Green bands highlight periods when NAD strength decreases while ISOW flow is strong (phase 1). Light blue bands highlight periods when both NAD and ISOW strength decrease (phase 2 and sub-phase 2.1). Dark blue band highlight the period when ISOW strength decreases while NAD strength is reduced (sub-phase 2.2). Green horizontal double arrows indicate time intervals when glacio-fluvial inputs occur. Green simple arrows indicate NAD strength decreases. Blue arrows indicate ISOW strength and Norwegian Sea ice cover dynamics at GI to GS/HS transitions..... 277/278

Figure 3: Age compilation of records from cores MD99-2281 (in red and dark red) and MD99-2285 (in black) indicative of ice-sheet decays and potential triggering mechanisms of ice-sheet collapses at GI to GS/HS transitions. (a) NGRIP $\delta^{18}\text{O}$ regional stratotype, compared to (b) the magnetic susceptibility (MS) and/or low field magnetic susceptibility (κ) of both cores. (c) IRD concentrations indicative of iceberg calving, i.e. ice-sheet destabilization, after Wary et al. (QSR, to be submitted, and EPSL, to be submitted). (d) SST reconstructions derived from alkenone analyses, indicative of surface advection of warm Atlantic waters after Wary et al. (QSR, to be submitted). (e) summer SST reconstructions stemming from dinocyst analyses, indicative of in situ Norwegian Sea summer SST after Wary et al. (QSR, to be submitted). (f) $\delta^{18}\text{O}$ measured on *N. pachyderma* sinistral form, indicative of subsurface temperatures during

GS and HS, according to the present study and to Wary et al. (QSR, to be submitted). (g) PF-derived temperature reconstructions. Hatched bands indicate GS intervals (age limits after Wolff et al., 2010). Green bands and arrows highlight the beginning of ice-sheet destabilization, of surface advection of warm Atlantic waters in the Nordic Seas, and of increase of Norwegian Sea summer SST. Blue bands and arrows highlight periods of massive ice-sheet collapse, maximal Norwegian Sea summer SST, strong surface advection of warm Atlantic waters in the Nordic Seas, and moderate subsurface warming. 278/279

Figure 4: Comparison between (a) NGRIP $\delta^{18}O$ signal, indicative of atmospheric temperatures above Greenland ice-sheet, (b) PF-Temp record from core MD99-2281, indicative of NAD strength, and (c) SSTalk signal from core MD99-2285 indicative of enhanced advection of warm Atlantic waters seemingly through the Continental Slope Current. This figure highlights the more than striking resemblance between NGRIP $\delta^{18}O$ and PF-Temp signals, which suggests that a rapid re-intensification of the NAD might be the triggering mechanism of the abrupt atmospheric warming recorded in NGRIP at the onset of GI. It also highlights the remarkable anti-phase between PF-Temp and SSTalk records, which suggests that this rapid NAD re-intensification might be due to an abrupt re-organization of the North Atlantic gyres and circulation. Hatched bands indicate GS intervals (age limits after Wolff et al., 2010)..... 280

Table 1: List of previously published records used in the present study, their provenance, and their main interpretation in the related study(ies)/core(s)..... 281

Introduction générale

Les ruptures successives de plates-formes de glace flottantes (connues sous le terme anglais d'*ice-shelves*) survenues en Antarctique au cours des dernières décennies (e.g. [Cook & Vaughan, 2010](#)), ainsi que l'accélération du recul de la glace de mer en Arctique enregistrée au cours des dernières années (e.g. [Comiso et al., 2008](#)), ont suscité une prise de conscience majeure quant à la sensibilité de la cryosphère face au changement climatique actuel. Si l'atmosphère a largement été envisagée comme principal facteur de déstabilisation de ces marges glaciaires, l'océan qui jouxte les grands glaciers boréaux et la calotte australe a également été mis en cause (e.g. [Shepherd et al., 2003](#) ; [Woodgate et al., 2010](#)). Il en ressort aujourd'hui la nécessité d'approfondir nos connaissances sur les interactions et les rétroactions entre océan, glace et atmosphère, ces processus restant pour l'heure encore assez mal appréhendés du fait notamment d'un recul temporel trop court (période instrumentale limitée au derniers 70 ans) pour apprécier correctement l'ensemble des mécanismes en jeu.

L'analyse des archives sédimentaires du Quaternaire offre cependant l'accès à des événements climatiques où vitesse et amplitude des changements enregistrés sont très proches de celles aujourd'hui détectées. Ces archives présentent également l'avantage de couvrir des périodes dépourvues de tout impact anthropique et permettent donc d'étudier la variabilité naturelle du climat. La dernière période glaciaire a notamment été ponctuée d'oscillations climatiques abruptes (appelées événements de Dansgaard-Oeschger) qui débutent par une phase chaude (appelée interstadaire) où les températures atmosphériques de l'hémisphère Nord augmentent très rapidement (d'une dizaine de degrés en plusieurs décennies) puis diminuent progressivement pendant quelques centaines d'années, et se terminent par une phase très froide (appelée stadaire) de plusieurs centaines d'années (e.g. [Dansgaard et al., 1993](#)). La dynamique de la glace de mer boréale semble avoir été largement impactée par cette variabilité climatique (e.g. [Li et al., 2010](#)). Par ailleurs, les phases froides de ces oscillations climatiques semblent être associées à des décharges d'icebergs, issues des calottes de glace boréales, dans l'Océan Atlantique Nord (e.g. [Bond & Lotti, 1995](#)), ces décharges ayant été particulièrement massives lors des épisodes les plus froids (connus sous le nom d'événements d'Heinrich ; [Heinrich, 1988](#)). L'origine mécanistique de ces effondrements glaciaires est encore méconnue, mais le rôle potentiel de l'océan et des *ice-shelves* a récemment été suggéré (e.g. [Alvarez-Solas et al., 2010](#)). Ainsi, la dernière période glaciaire offre un cadre idéal à l'étude des interactions océan-glace-atmosphère.

Cette thèse se propose ainsi d'étendre nos connaissances sur la variabilité climatique rapide des derniers 45 000 ans, et notamment sur les interactions, processus et mécanismes

associés à la dynamique océanique. Pour cela, ce travail se focalise sur l'étude des changements hydrographiques tels qu'enregistrés dans deux archives sédimentaires prélevées sur le pourtour des îles Féroé, i.e. un secteur clé situé à la jonction du bassin nord-atlantique et des bassins nordiques et sous influence des glaciers européens lors de la dernière période glaciaire. La rapidité et la complexité des processus en jeu nécessitent une approche analytique à haute résolution temporelle et couplant un maximum de traceurs. A ce titre, nous documentons ces variations hydrographiques à travers des outils complémentaires : approches micropaléontologiques (assemblages de dinokystes et de foraminifères planctoniques et reconstructions quantifiées dérivées de ces assemblages par le biais de fonction de transfert, concentrations en foraminifères benthiques et autres palynomorphes), géochimiques ($\delta^{18}\text{O}$ dans les tests de foraminifères planctoniques, biomarqueurs – alcénones et IP25 –, analyses Xrf du sédiment), et sédimentologiques (granularité du sédiment et concentration en IRD). Ces analyses sont conduites à haute voire très haute résolution temporelle (résolution moyenne minimale d'environ 350 ans, et maximale d'environ 30 ans). Ceci nous permet ainsi de retracer la dynamique des masses d'eau de surface, de subsurface, et de fond, ainsi que des calottes de glace et de la glace de mer.

Notre analyse s'est alors axée selon trois défis principaux :

- (i) Une meilleure caractérisation des conditions hydrographiques associées aux périodes chaudes (interstadias), aux périodes froides (stadias et événements d'Heinrich), et à leur enchaînement, ainsi qu'à leurs implications en termes de circulation océanique.
- (ii) La détermination des processus hydrographiques en jeu, et de leurs dimensions spatiale et temporelle.
- (iii) L'identification des interactions océan-atmosphère-cryosphère, et de la chronologie des mécanismes impliqués dans le déclenchement de cette variabilité rapide.

Ce manuscrit s'organise en trois chapitres. Le Chapitre 1 présente le cadre temporel et environnemental de notre étude, et dresse un état de l'art sur la paléoclimatologie de notre période et zone d'étude. Le Chapitre 2 expose notre stratégie analytique, et présente une description des outils utilisés. Enfin, le Chapitre 3 présente l'ensemble des résultats et interprétations obtenus dans le cadre de cette thèse.

Chapitre 1 : Contexte environnemental et paléoclimatique

Le **chapitre 1** dresse un **état de l'art synthétique** sur :

- les **variations climatiques du Quaternaire** et notamment les variations climatiques rapides de la dernière période glaciaire (**Partie 1**),
- le **cadre environnemental** passé et actuel de l'Atlantique Nord et des mers adjacentes, avec un focus sur notre zone d'étude (pourtour des îles Féroé), en termes d'hydrographie, de dynamique cryosphérique, et de processus sédimentaires (**Partie 2**),
- l'état actuel des connaissances et des observations documentant la **variabilité climatique rapide glaciaire en Atlantique Nord et dans les Mers Nordiques** (**Partie 3**).

Sommaire

<u>PARTIE 1 : CADRE TEMPOREL DE L'ETUDE ET PROBLEMATIQUES</u>	7
<u>PARTIE 2 : CADRE ENVIRONNEMENTAL ACTUEL ET PASSE</u>	13
<i>Section 1. Circulation océanique moderne</i>	13
1. Circulation en Atlantique Nord	14
2. Circulation à la frontière Atlantique Nord – Mers Nordiques.....	16
<i>Section 2. Dynamique passée des calottes de glaces proximales</i>	18
<i>Section 3. Contexte sédimentaire et sites d'étude</i>	20
<u>PARTIE 3 : ETAT DE L'ART SUR LA PALEOCLIMATOLOGIE DE NOTRE PERIODE ET ZONE D'ETUDE</u>	25

Partie 1 : Cadre temporel de l'étude et problématiques

A l'échelle des temps géologiques, la Terre a connu de grandes variations climatiques, oscillant entre des périodes chaudes (« greenhouse ») et des périodes froides (« icehouse »). Le Quaternaire, débuté il y a 2.6 millions d'années (étage du Gélasién inclus, [Pillans & Naish, 2004](#)), constitue une période « icehouse » marquée par l'alternance entre périodes relativement froides dites « glaciaires », et périodes relativement chaudes dites « interglaciaires » ([Figure 1a](#)). Les périodes glaciaires se caractérisent par un volume de glaces continentales conséquent et un niveau marin relativement faible. A l'inverse, les périodes interglaciaires se caractérisent par un volume des glaces continentales fortement réduit et un niveau marin relativement élevé. Cette alternance glaciaire/interglaciaire apparaît étroitement liée aux variations orbitales de la Terre (i.e. les variations de sa position par rapport au Soleil, contrôlées par trois paramètres orbitaux : l'excentricité, l'obliquité, et la précession) qui conditionnent la quantité et la distribution de chaleur reçue par notre planète (e.g. [Milankovitch, 1941](#) ; [Berger & Loutre, 1991](#)). Cette variabilité climatique est particulièrement bien identifiée au sein des sédiments marins, et notamment au travers des enregistrements du signal isotopique de l'oxygène des foraminifères (zooplancton/benthos marin) sensible aux variations du volume des glaces et des conditions océaniques. Plusieurs enregistrements benthiques ont ainsi été combinés pour établir une stratigraphie isotopique de référence (i.e. courbe composite appelée LR04, [Lisiecki & Raymo, 2005](#)) où, classiquement, les stades isotopiques marins (ou MIS pour *Marine Isotopic Stage*) impairs correspondent aux périodes interglaciaires, et les stades pairs aux périodes glaciaires ([Figure 1b](#)).

Actuellement, la Terre connaît une période interglaciaire, le MIS1 ou Holocène, débutée il y a 11.65 ka cal BP (milliers d'années calendaires avant 1950 ; [Walker et al., 2009](#) ; [Figure 1](#)). Cette période interglaciaire se caractérise par un climat qui peut être qualifié de relativement stable au niveau global, principalement marqué par des fluctuations climatiques de faible amplitude (e.g. la Période Chaude Médiévale, enregistrée du X^{ème} au XIV^{ème} siècle, suivi de l'épisode froid du Petit Age Glaciaire, qui s'étend du XVI^{ème} siècle à la moitié du XIX^{ème} siècle, e.g. [Mann, 2002a,b](#)). Cette variabilité climatique intra-Holocène semble être principalement liée aux variations d'activité solaire et/ou d'activité volcanique, combinées et/ou superposées aux variations orbitales lentes (e.g. [Mayewski et al., 2004](#) ; [Sicre et al., 2013](#) ; [Swingedouw et al., 2015](#)). Par ailleurs, certains événements abrupts et de plus forte amplitude se sont également produits au cours de l'Holocène, tels que l'évènement 8.2 à

~ 8200 ans BP dont l'origine, vraisemblablement interne au système terrestre, est encore débattue (e.g. Alley et al., 1997 ; Hillaire-Marcel et al., 2007 ; Wagner et al., 2013), ou encore le réchauffement climatique actuel (5^{ème} rapport du GIEC, volume 1, <http://www.ipcc.ch/>) dont l'origine anthropique est encore parfois déniée.

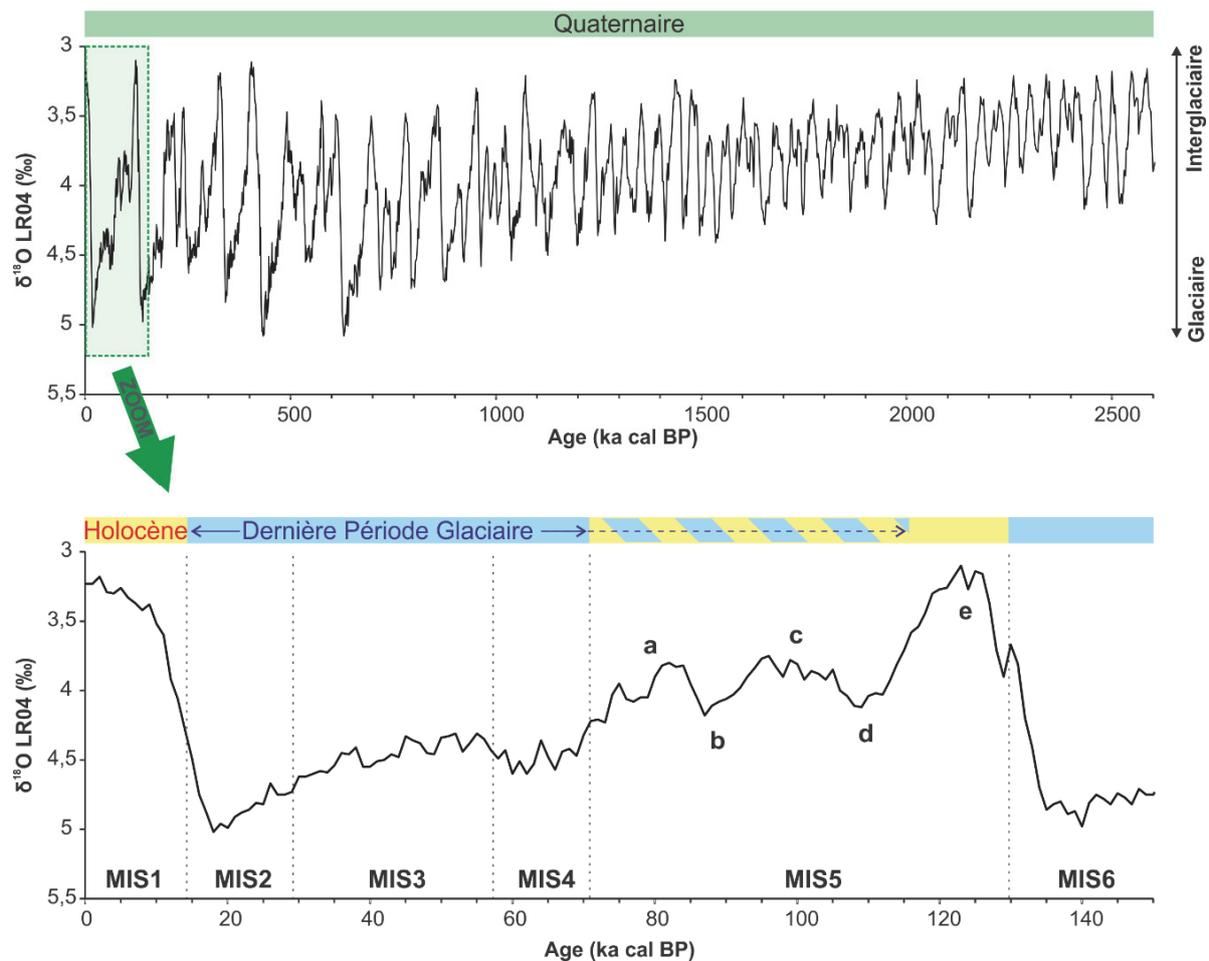


Figure 1 : Variations glaciaires/interglaciaires au cours du Quaternaire (haut) et des derniers 150 ka (bas) mises en évidence au travers de la courbe isotopique composite LR04 de Lisiecki et Raymo (2005).

A l'inverse, la dernière période glaciaire (qui peut être considérée comme englobant les MIS2, 3, et 4, commençant alors vers 70 ka, voire même les MIS5a à 5d, et commençant alors vers 120 ka ; Figure 1b) a été ponctuée de nombreux événements climatiques abrupts (Figure 2a). Ces événements ont tout d'abord été mis en évidence dans les enregistrements isotopiques des glaces du Groenland (e.g. Dansgaard et al., 1993). Ils correspondent à des

oscillations des températures atmosphériques se produisant tous les 1000 à 4000 ans, et sont connus sous le nom d'évènements de Dansgaard-Oeschger (DO). Chaque DO se caractérise par une phase chaude, appelée « interstadienne » (ou GI pour *Greenland Interstadial*) et marquée par une augmentation rapide des températures atmosphériques en quelques décennies (e.g. Johnsen et al., 1992 ; Lang et al., 1999) puis d'une diminution progressive des températures pendant quelques siècles, suivie d'une phase froide, appelée « stadienne » (ou GS pour *Greenland Stadial*) et durant généralement de un à quelques milliers d'années (Figure 2b). Le Bølling-Allerød, phase chaude s'étant produite au cours de la transition MIS2-MIS1 (également appelée dernière déglaciation ou terminaison glaciaire I), est souvent considéré comme étant le GI1. Très vite, les DO ont été identifiés dans les autres archives climatiques, et notamment dans les sédiments marins de l'Océan Atlantique Nord subpolaire et ses mers adjacentes (e.g. Bond et al., 1993 ; Voelker et al., 2002) comme des changements hydrographiques majeurs (qui seront détaillés dans la Partie 3 de ce chapitre).

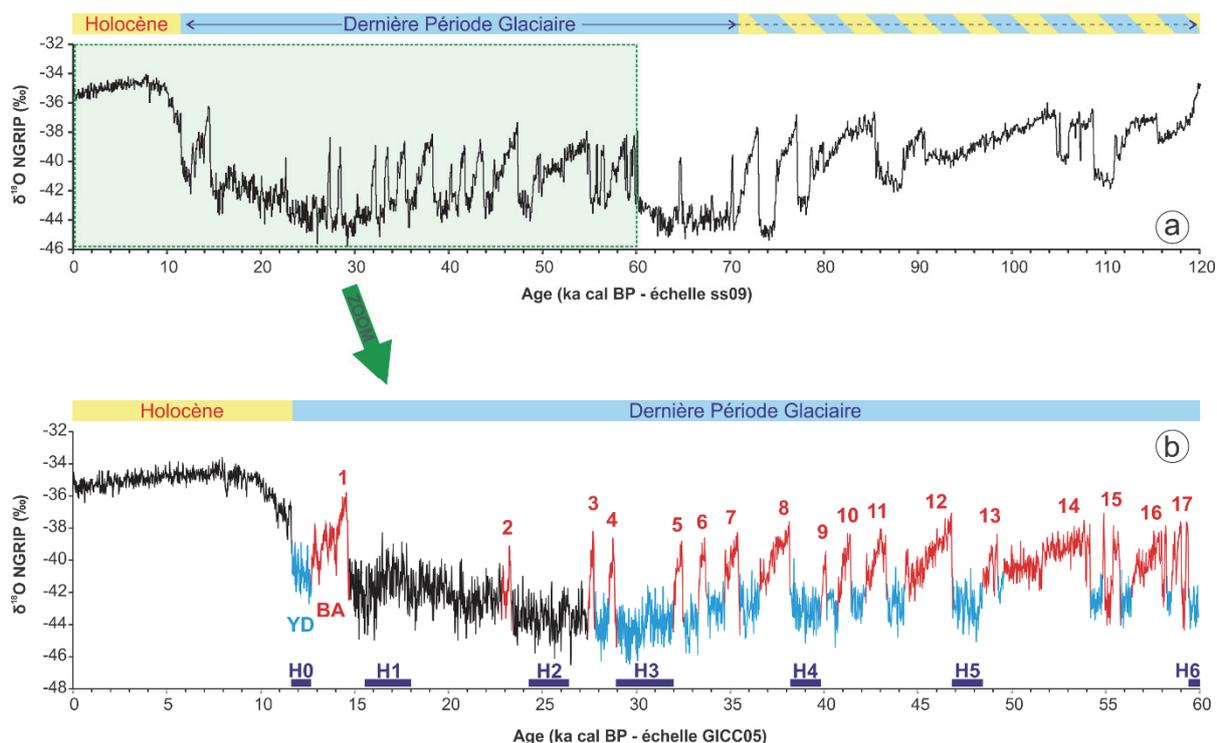


Figure 2 Enregistrement isotopique NGRIP (a) au cours des derniers 120 ka et (b) au cours des derniers 60 ka. Sur la Figure 2b, les portions de courbe en rouge représentent les interstadiennes (numérotés d'après Dansgaard et al., 1993), les portions en bleu les stadiennes. Les rectangles bleus illustrent les intervalles de temps correspondant aux « Heinrich stadials » (numérotés de H0 à H6). YD : Younger Dryas, BA : Bølling-Allerød.

De surcroît, au sein de ces systèmes océaniques boréaux, certains GS sont associés à des niveaux sédimentaires riches en particules détritiques grossières (micrométriques à décimétriques). Ces niveaux sont appelés niveaux d'Heinrich (Heinrich, 1988 ; Bond et al., 1992 ; Broecker et al., 1992 ; Figure 2b), et les GS auxquels ils correspondent sont appelés *Heinrich Stadials* (ou HS ; e.g. Sanchez Goñi & Harrison, 2010). Ces niveaux d'Heinrich sont particulièrement bien enregistrés dans une bande latitudinale localisée en Atlantique Nord entre environ 40 et 55 °N, appelée « bande de Ruddiman » (Ruddiman, 1977 ; Figure 3a). L'origine des particules détritiques grossières constituant ces niveaux a été attribuée à la fonte d'icebergs résultant d'une décharge en masse lors d'effondrements répétitifs des calottes de glaces boréales (Broecker et al., 1992 et les références qui ont suivis). Ces particules sont de ce fait appelées *Ice-Rafted Debris* (ou IRD). En effet, les calottes de glace, via le fluage de la glace, incorporent à leur base des particules terrigènes arrachées au continent sur lequel elles reposent. Ces particules se retrouvent alors incluses dans les icebergs délivrés à l'océan lors des effondrements brutaux. En se déplaçant vers de plus basses latitudes, les icebergs fondent et libèrent alors les IRD qu'ils contenaient dans l'océan. Ces IRD vont alors se déposer au fond de l'océan, formant alors les niveaux d'Heinrich (Figure 3b). Le Younger-Dryas, phase froide s'étant produite au cours de la transition MIS2-MIS1, est dans certaines zones également associé à des dépôts riches en IRD dont la nature est similaire à ceux retrouvés dans les niveaux d'Heinrich de la bande de Ruddiman (Andrews et al., 1995). De ce fait, il est parfois considéré comme un « *Heinrich-like event* », et alors appelé H0.

Dans l'Atlantique Nord subpolaire, GS et HS sont tous deux associés à des dépôts d'IRD (e.g. Bond & Lotti, 1995 ; Elliot et al., 2001), i.e. à des décharges importantes d'icebergs issues de la déstabilisation des calottes de glaces proximales. Cette similitude a conduit à la théorie que les GS et HS résultaient de mécanismes de déclenchement communs, dont l'origine demeure toutefois encore débattue. On a pendant longtemps opposé deux mécanismes, qui sembleraient en fait jouer de pair dans ce déclenchement. On distingue ainsi :

(1) La dynamique interne des glaciers, qui pourrait être, à elle-seule, l'élément déclencheur, avec un cycle de construction / ablation auto-entretenu par la charge de glace accumulée. Cette hypothèse, initialement proposée par MacAyeal (1993), correspond au mécanisme de « *binge-purge* ».

(2) L'océan, qui par le biais d'apports de chaleur sous-marins, aurait un rôle prépondérant dans ces effondrements, notamment à l'interface des extensions marines des glaciers (i.e. les plates-formes de glace flottantes terminant les couloirs d'écoulement des

glaciers, connues sous le terme anglais d'*ice-shelves* ; Figure 4) où il accélérerait l'ablation de ces plates-formes. Ces dernières jouant un important rôle de soutien pour les calottes (en ralentissant l'écoulement de la glace en amont), leur réduction *in fine* conduirait à l'effondrement du glacier dans l'océan. Plusieurs ruptures successives d'*ice-shelves* suivies de décharges d'icebergs dans l'océan ont d'ailleurs été récemment observées en Antarctique (LarsenA en 1998, LarsenB en 2002 et Wilkins en 2008 ; Cook & Vaughan, 2010). Ce type d'interaction glace-océan a par ailleurs été mis en évidence pour les glaciers groenlandais lors de la dernière déglaciation (Knutz et al., 2011). Plusieurs expériences de modélisation ont en outre démontré le potentiel d'un tel mécanisme dans le déclenchement des débâcles d'icebergs de la dernière période glaciaire (e.g. Alvarez-Solas et al., 2010, 2012).

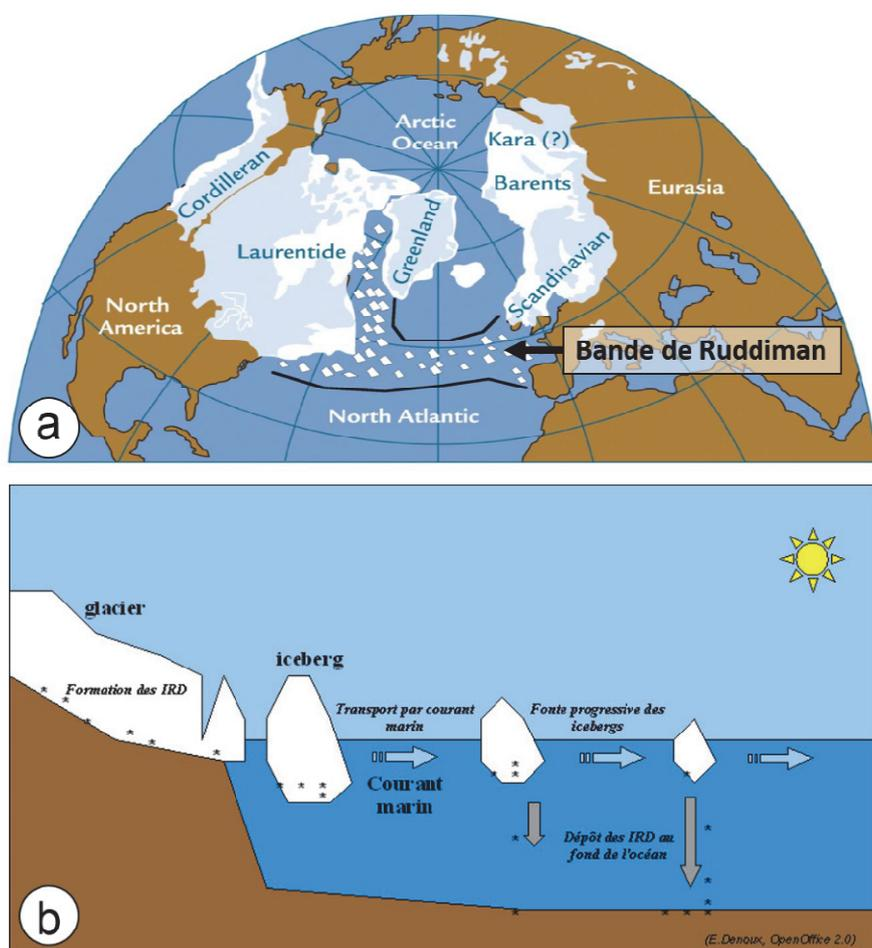


Figure 3 : (a) Localisation de la bande de Ruddiman (modifié d'après Ruddiman, 2001), zone de dépôt préférentielle des IRD, et (b) mécanismes de formation, transport et libération des IRD depuis le continent jusqu'aux sédiments marins (source : <http://access.ens-lyon.fr>).

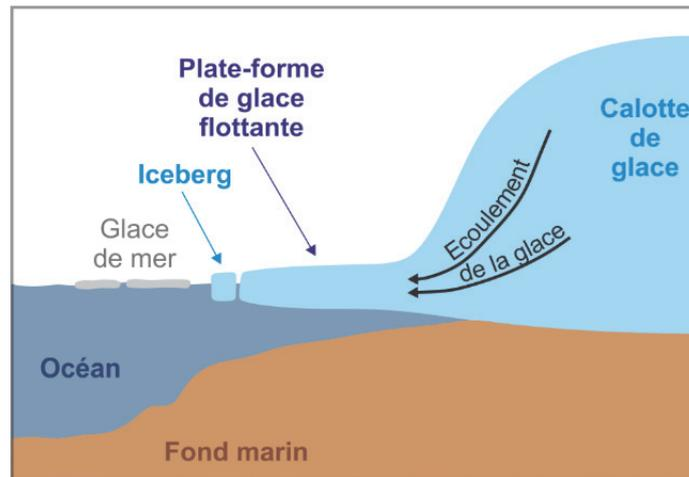


Figure 4 : Schéma conceptuel de l'interface calotte de glace – océan - atmosphère

*Les mécanismes mis en jeu lors de la dernière période glaciaire constituent ainsi des cas de figure types d'interactions rapides océan-glace-atmosphère. Il apparaît donc nécessaire de chercher à reconstruire de manière détaillée l'histoire paléocéanographique qui entoure ces évènements abrupts afin de (1) **déterminer qui, de l'océan, de l'atmosphère ou de la cryosphère, ou de quelle combinaison plurifactorielle naissent ces évènements**, (2) **mieux comprendre les mécanismes, inter- et rétro- actions impliqués** et (3) **estimer les impacts (et leur durée) de telles bascules climatiques (changements de circulation océanique, fonte des glaces et élévation du niveau marin, climat global, biodiversité...)**.*

Partie 2 : Cadre environnemental actuel et passé

Section 1. Circulation océanique moderne

La circulation océanique globale, ou *Meridional Overturning Circulation*, est le principal facteur de redistribution de chaleur à la surface de la Terre depuis l'équateur vers les pôles. Elle est régie par les vents, qui entraînent les courants de surface, et par des gradients de densité liés aux contrastes et échanges de température et salinité des masses d'eau, qui conditionnent les courants marins depuis la surface jusqu'aux fonds océaniques. Elle peut être représentée, de façon très schématique, comme une sorte de « tapis roulant » ou « *conveyor belt* » (e.g. Broecker, 1991) où les eaux de surface sont entraînées vers quatre centres de formation d'eaux intermédiaires et profondes localisés aux hautes latitudes (les Mers Nordiques, la Mer du Labrador, la Mer de Weddel, et la Mer de Ross), puis re-circulent en profondeur (Figure 5, e.g. Hansen & Østerhus, 2000 ; Wunsch, 2002 ; Rahmstorf, 2002, 2003).

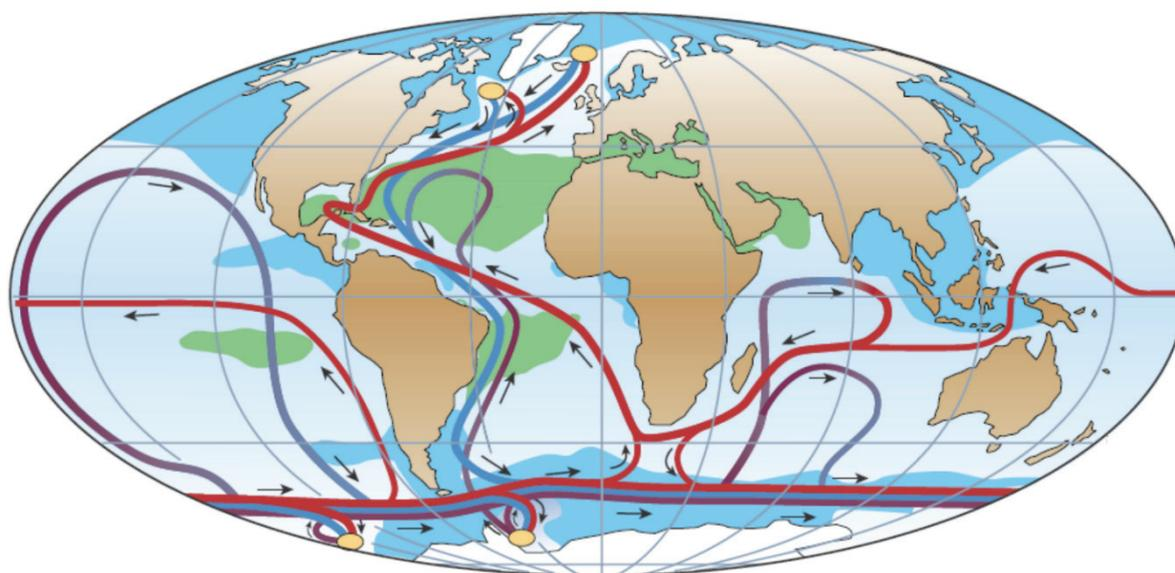


Figure 5 : Représentation schématique de la circulation océanique globale (issue de Rahmstorf, 2002), où les courants de surface sont représentés en rouge, les courants profonds en bleu, les courants de grand fond en violet, et les centres de convection par des cercles jaunes.

1. Circulation en Atlantique Nord

L'Atlantique Nord abritant deux zones de convection majeures, il constitue une zone clé dans la circulation océanique globale. De façon schématique, la circulation s'y traduit par un flux trans-latitudinal où les eaux de surface remontent du Sud vers les hautes latitudes Nord, plongent au niveau des centres de convection, et re-circulent en profondeur vers les basses latitudes, d'où le terme d'*Atlantique Meridional Overturning Circulation* (AMOC).

De façon plus détaillée, la circulation de surface s'y organise sous forme de gyres océaniques : la gyre anticyclonique subtropicale, et la gyre cyclonique subpolaire (e.g. Schmitz & McCartney, 1993 ; Stanford et al., 2011 et références incluses ; Figure 6). Parmi les courants d'intérêt notoire dans le cadre de notre étude se trouve en premier lieu le *Gulf Stream*, courant chaud et salé prenant naissance au niveau du Golfe du Mexique et constituant le segment Nord de la gyre subtropicale. Au cours de son trajet vers les côtes Nord européennes, le *Gulf Stream* se divise en deux branches : une branche qui se propage vers le Sud et *in fine* vient « boucler » la gyre subtropicale, et une branche, appelée Dérive Nord Atlantique (ou *North Atlantic Drift*, NAD), qui rejoint le segment sud de la gyre subpolaire et se propage vers les Mers Nordiques. A son tour, la NAD se divise en plusieurs branches lors de son trajet vers les hautes latitudes : une branche qui se propage vers l'Ouest, le Courant d'Irminger (*Irminger Current*), puis rejoint le Courant du Labrador (*Labrador Current*) froid et dessalé, fermant ainsi la gyre subpolaire, et une branche qui se répand dans les Mers Nordiques, en prolongement direct de la NAD, appelée Courant Nord Atlantique (*North Atlantic Current*). En parallèle, des courants de surface froids vecteurs d'eau douce et de glace se propagent depuis le domaine Arctique le long des côtes groenlandaises (*East Greenland Current*, et *West Greenland Current*) et dans les Mers Nordiques (*East Icelandic Current*).

En se propageant vers les hautes latitudes, ces masses d'eau de surface, initialement chaudes et salées, vont progressivement se refroidir en libérant de la chaleur latente vers l'atmosphère. Arrivées dans les Mers Nordiques et en Mer du Labrador, ces eaux vont être suffisamment denses (froides et salées) pour plonger, et se transformer en masses d'eaux intermédiaires et profondes. Eventuellement, la formation saisonnière de glace de mer, qui s'accompagne d'une libération de sel, peut contribuer à favoriser la formation d'eau profonde en augmentant la salinité et donc la densité des eaux sous-jacentes à la glace néoformée.

Les masses d'eau intermédiaires et profondes ainsi formées (dont la *Labrador Sea Water* formée en Mer du Labrador, l'*Iceland-Scotland Overflow Water* formée en Mer de Norvège, la *Denmark Strait Overflow Water* formée en Mer du Groenland) vont alors se répandre en profondeur sous l'action de courants intermédiaires et profonds, se rejoindre, et *in fine* former la *North Atlantic Deep Water* (NADW), principale masse d'eau profonde de l'Atlantique Nord et composante importante de l'AMOC, qui s'écoule vers le Sud. En parallèle, la masse d'eau profonde formée dans les centres de convections antarctiques (l'*Antarctic Bottom Water*) remonte vers le Nord.

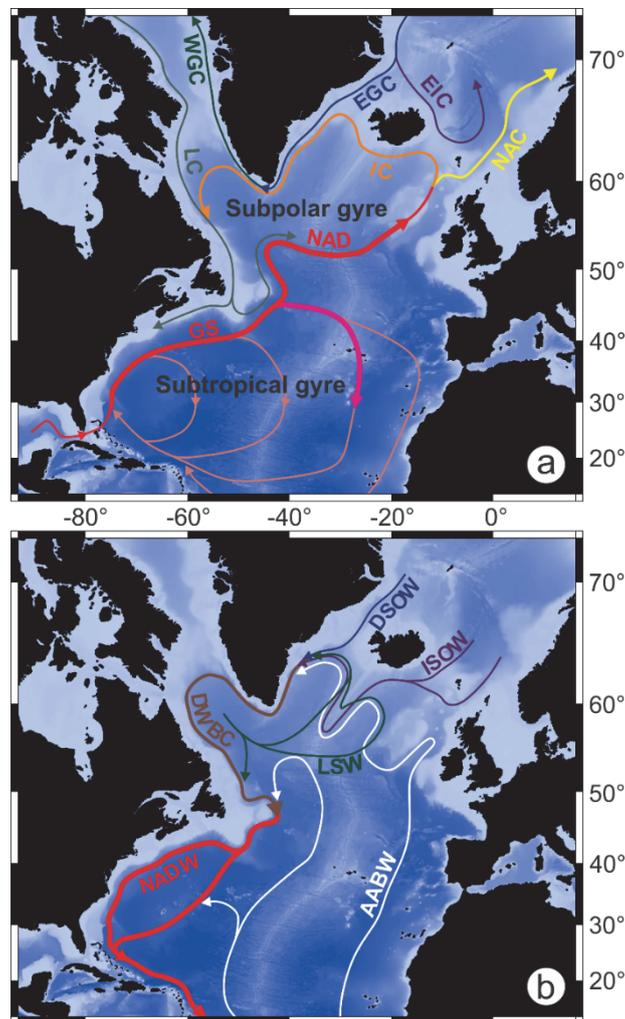


Figure 6 : Circulation océanique en Atlantique Nord. (a) Circulation de surface (GS : Gulf Stream, NAD : North Atlantic Drift, NAC : North Atlantic Current, IC : Irminger Current, LC : Labrador Current, EIC : East Icelandic Current, EGC : East Greenland Current, WGC : West Greenland Current). (b) Circulation intermédiaire et profonde (LSW : Labrador Sea Water, ISOW : Iceland-Scotland Overflow Water, DSOW : Denmark Strait Overflow Water, DWBC : Deep Western Boundary Current, NADW : North Atlantic Deep Water, AABW : Antarctic Bottom Water). Circulation d'après Stanford et al., 2011. Bathymétrie GEBCO (www.gebco.net). WGS 1984 Mercator 55°N.

2. Circulation à la frontière Atlantique Nord – Mers Nordiques

La zone d'étude de cette thèse se situe au niveau des îles Féroé (cf. Section 3 où sont présentés les sites d'étude), à la frontière entre l'Atlantique Nord et les Mers Nordiques, un point nodal du point de vue la circulation océanique (Figure 7).

En effet, cette zone se trouve sous l'influence directe de la masse d'eau chaude ($T > 8^{\circ}\text{C}$) et salée de surface composant la *North Atlantic Water* (e.g. Mauritzen et al., 2005). Ces eaux sont entraînées vers le Nord par le Courant Nord Atlantique décrit précédemment, ainsi que par le *Continental Slope Current* qui s'écoule le long de la pente Nord-Ouest de l'Europe et dont le cœur salin se situe vers 200 mètres de profondeur (Booth & Ellet, 1983 ; Kenyon, 1986 ; Hill & Mitchelson-Jacob, 1993 ; Orvik & Niiler, 2002 ; Mauritzen et al., 2005). La contribution respective de chaque courant est très mal définie, les deux courants se rejoignant et se mélangeant partiellement dès le bassin de Rockall (Hansen & Østerhus, 2000). L'origine du *Continental Slope Current* reste débattue, certaines études suggérant un lien direct avec la masse d'eau profonde issue de la Mer Méditerranée (*Mediterranean Outflow Water* ou MOW ; e.g. Reid, 1979), et d'autres, plus récentes, prônant un lien direct avec le continuum *Gulf Stream* – Dérive Nord Atlantique – Courant Nord Atlantique mais confirmant une signature de la MOW via sa contribution à la gyre subtropicale (e.g. McCartney & Mauritzen, 2001). De plus, le secteur situé au Nord des îles Féroé est également influencé par une seconde masse d'eau, plus froide et moins salée, issue du mélange entre la *North Atlantic Water* et les eaux froides et dessalées polaires ($T < 0^{\circ}\text{C}$ à 2°C) transportées depuis l'Arctique par le Courant Est Groenlandais et son extension *l'East Icelandic Current* (Valdimarsson & Malmberg, 1999). Dans la zone peu profonde du plateau continental des îles Féroé a lieu un fort mélange des masses d'eau responsable de la présence d'une masse d'eau très homogène, la *Faeroe Shelf Water*, séparée des masses d'eau offshore par un front hydrographique appelé le *Faeroe Shelf Front* (Larsen et al., 2008, 2009).

La zone d'étude se trouve également sous l'influence de la masse d'eau profonde formée en Mer de Norvège : *l'Iceland Scotland Overflow Water* (ISOW). Cette masse d'eau se compose de plusieurs masses d'eau intermédiaires et profondes formées dans les Mers Nordiques. La masse d'eau intermédiaire supérieure (*Arctic Intermediate/North Iceland Water* ou *Modified East Atlantic Water*) présente des températures inférieures à 5.5°C , et les masses d'eau les plus profondes (*Norwegian Sea Arctic Intermediate Water*, et *Norwegian Sea Deep Water*) des températures inférieures à 0.5°C (Hansen & Østerhus, 2000 ; Borenäs &

Lundberg, 2004 ; Mauritzen et al., 2005). Ces eaux transitent en profondeur depuis les Mers Nordiques vers l'Océan Atlantique, au gré d'un courant profond s'écoulant le long de la marge Nord-Est des îles Féroé, bifurquant ensuite vers le Sud-Ouest à travers le *Faeroe-Shetland Channel* puis vers le Nord-Ouest à travers le *Faeroe Bank Channel* (e.g. Kuijpers et al., 1998a). De manière intermittente, une portion mineure de ce flux d'eau profonde franchit la Ride de Wyville-Thompson (i.e. barrière topographique reliant le plateau des Shetland au *Faeroe Bank* et culminant à environ 600 mètres de profondeur) et s'écoule alors vers le Sud dans la fosse de Rockall et vers le Nord-Ouest dans la vallée sous-marine séparant le *Bill Bailey Bank* du *Louisy Bank* (e.g. Boldreel et al., 1998 ; Kuijpers et al., 1998a,b, 2002 ; Hansen & Østerhus, 2000 ; Laberg et al., 2005). Le *Faeroe-Shetland Channel* étant le passage le plus profond à travers la Ride Groenland-Ecosse, cette branche de l'ISOW constitue une importante source pour la NADW (Borenäs & Lundberg, 2004).

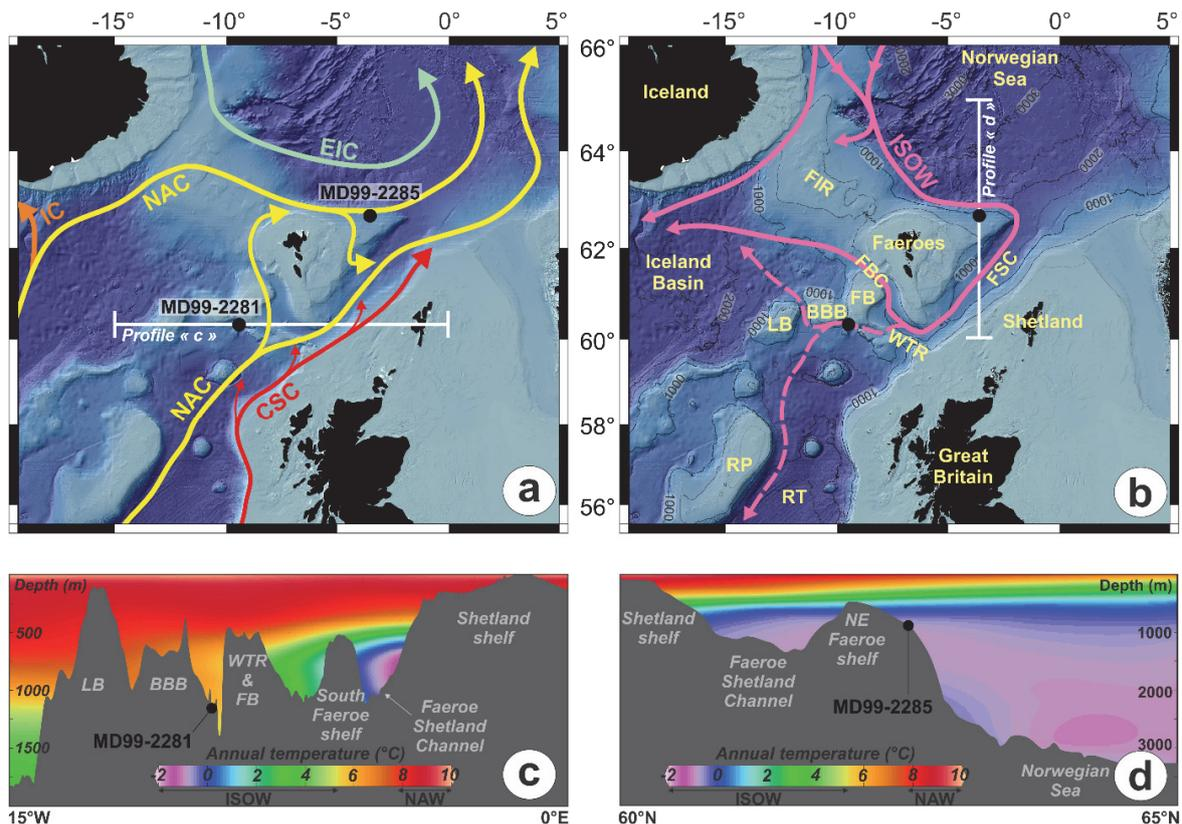


Figure 7 : Cadre environnemental de la zone d'étude. (a) Localisation des deux sites d'étude et circulation océanique de surface (NAC : North Atlantic Current, CSC : Continental Slope Current, EIC : East Icelandic Current, IC : Irminger Current). (b) Circulation profonde (ISOW : Iceland Scotland Overflow Water), bassins océaniques, et structures topographiques majeures (RT : Rockall Trough, RP : Rockall Plateau, LB : Louisy Bank, BBB : Bill Bailey Bank, FB : Faeroe Bank, WTR : Wyville-Thompson Ridge, FIR : Faeroe-Iceland Ridge, FBC : Faeroe Bank Channel, FSC : Faeroe Shetland Channel). Isobathes grises : 200 mètres de profondeur. Intervalle des isobathes noires : 500 mètres. (c et d) Profils Est-Ouest et Nord-Sud de températures océaniques (NAW : North Atlantic Water), réalisé avec Ocean Data View (Schlitzer, 2011). Leur localisation est indiquée sur les cartes a et b. Bathymétrie EMODNET (www.emodnet.eu). WGS 1984, Mercator 55°N.

Section 2. Dynamique passée des calottes de glaces proximales

Lors de la dernière période glaciaire, la zone d'étude se trouvait encerclée de glaciers proximaux : la calotte fennoscandienne (*Fennoscandian Ice Sheet*, FIS), la calotte britannique (*British Irish Ice Sheet*, BIIS), et le glacier des Féroé (Figure 8a). Au cours de cette période, les FIS et BIIS se sont largement étendues (Svendsen et al., 2004), devenant alors vraisemblablement reliées par un pont de glace dès 29 ka et jusqu'à environ 17-18 ka BP, (Sejrup et al., 2009 ; Toucanne et al., 2010 ; Clark et al., 2012 ; Figure 8b). Le glacier des Féroé n'a lui connu que de faibles avancées, s'étendant alors au maximum jusqu'à une limite située à présent vers 200 mètres de profondeur (Nielsen et al., 2007).

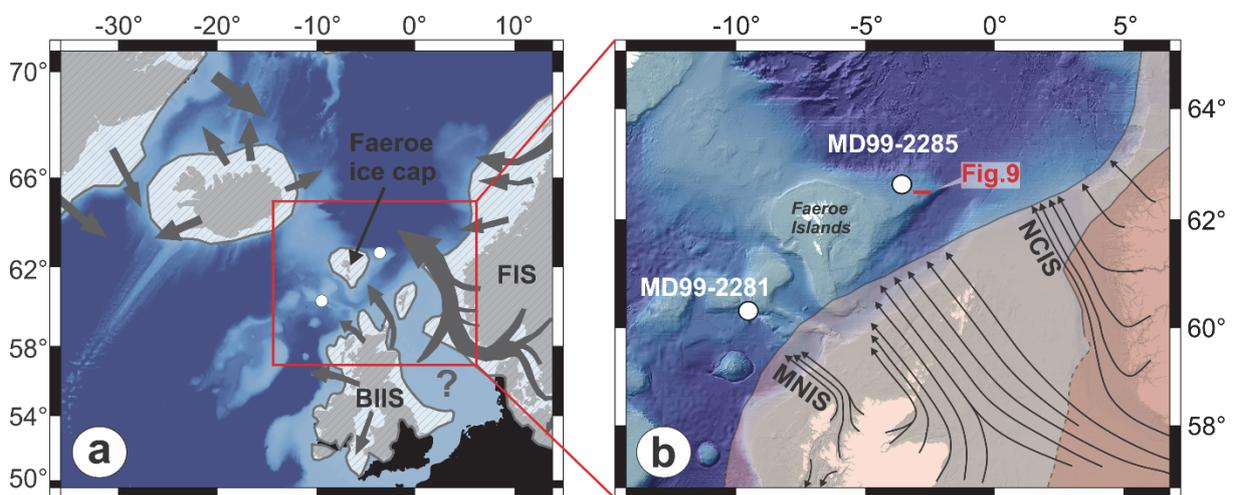


Figure 8 : Calottes de glace et couloirs d'écoulement de la glace au niveau de la zone d'étude lors de la dernière période glaciaire. (a) Etendue des calottes de glace au cours du Dernier Maximum Glaciaire (FIS : Fennoscandian Ice Sheet, BIIS : British Irish Ice Sheet), d'après Ehlers & Gibbard (2007) et paleo-ice streams d'après Stokes & Clark (2001). (b) Etendue des calottes de glace européennes vers 50-60 ka (marron) et au Dernier Maximum Glaciaire (beige), d'après Svendsen et al. (2004), et paleo-ice streams drainant les calottes européennes (MNIS : Minch Ice Stream, NCIS : Norwegian Channel Ice Stream), d'après Sejrup et al. (2003) et Bradwell et al. (2008). Bathymétrie EMODNET (www.emodnet.eu). WGS 1984, Mercator 55°N.

Plusieurs études ont permis de mettre en évidence les différents paléo-couloirs d'écoulement de la glace (*paleo-ice streams*), notamment ceux ayant drainé les FIS et BIIS, le glacier des Féroé ayant quant à lui été beaucoup moins étudié (Figure 8a). Parmi les principaux *paleo-ice streams* identifiés, certains se déversent au niveau de la zone d'étude : le *Norwegian Channel*

Ice Stream (NCIS), qui drainait la partie Sud de la FIS, le *Minch Ice Stream* (MNIS), qui drainait le secteur Nord de la BIIS, et le *paleo-ice stream* drainant le Nord-Est de la BIIS ainsi que la Mer du Nord au moment où elle était englacée (e.g. Sejrup et al., 2003 ; Bradwell et al., 2008 ; Hughes et al., 2014 ; Dove et al., 2015 ; Figure 8b). La localisation de la zone d'étude au débouché de ces *paleo-ice streams* majeurs suggèrent fortement que : (i) cette zone était probablement bordée d'*ice-shelves*, et (ii) elle a probablement subi l'influence directe des décharges de glace de ces deux calottes. Bien qu'il n'existe à ce jour aucune archive (sédimentaire/géomorphologique/glaciologique/sismique/...) permettant d'attester la présence d'*ice-shelves* en général, plusieurs jeux de données sismiques et de sonar latéral obtenus sur le pourtour des îles Féroé révèlent l'existence d'empreintes sédimentaires formées par le frottement d'icebergs sur le fond marin (i.e. des « *iceberg ploughmarks* » ou « *iceberg scours* », e.g. Nielsen & van Weering, 1998 ; van Weering et al., 1998 ; Nielsen & Kuijpers, 2000 ; Nielsen et al., 2007). Ces « cicatrices » se rencontrent jusqu'à une profondeur maximale de 800 mètres. Au vu de l'orientation et de la forte concentration de certaines de ces marques, Nielsen et al. (2007) ont attribué leur origine à d'intenses décharges d'icebergs provenant principalement de calottes relativement distantes, et non du glacier des Féroé. De plus, du fait de leur présence en surface du sédiment, les auteurs ont suggéré que les décharges massives d'icebergs à l'origine de ces empreintes sédimentaires se soient produites durant la dernière période glaciaire, et plus probablement durant la dernière déglaciation. Ainsi, malgré des changements morphobathymétriques depuis la dernière glaciaire (dus aux réajustements isostatiques liés au retrait des calottes de glace, e.g. Peltier, 2004), ces empreintes attestent de l'influence directe d'icebergs dérivés des calottes européennes sur la zone d'étude, potentiellement durant la dernière période glaciaire, et vraisemblablement durant la dernière déglaciation.



Figure 9 : *Iceberg ploughmarks* proches de la zone d'étude (localisation indiquée sur la Figure 8b).
Données EMODNET (www.emodnet.eu).

Section 3. Contexte sédimentaire et sites d'étude

La sédimentation quaternaire de la zone d'étude se caractérise principalement par (i) des dépôts contouritiques formés sous l'action des courants profonds, (ii) des apports glacio-fluviaux issus des calottes de glace proximales, organisés sous forme de sortes de cônes de dépôts situés au débouché des paleo-ice streams et appelés *trough mouth fans*, et (iii) des glissements en masse résultant de la déstabilisation des deux types de dépôts précédents (van Weering et al., 1998 ; Andersen et al., 2000 ; Kuijpers et al., 2001 ; Laberg et al., 2005 ; Nielsen et al., 2007 ; Figure 10).

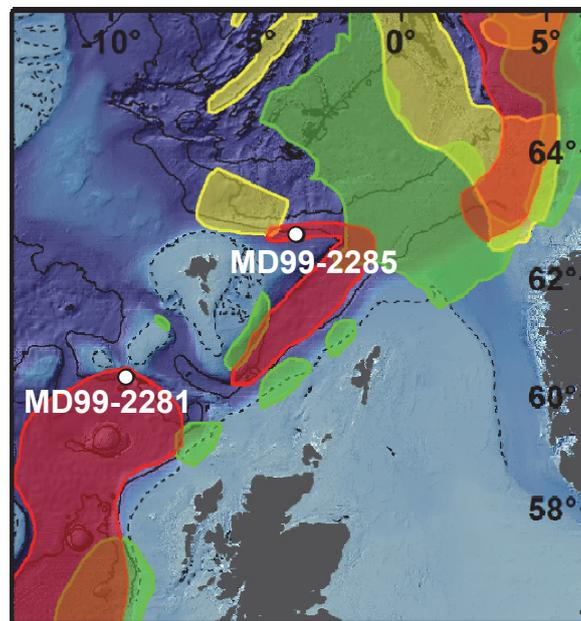


Figure 10 : Répartition schématique des zones de dépôt contouritique (rouge), de *trough mouth fan* (vert) et de glissement (jaune), d'après Laberg et al. (2005). Les sites d'études sont localisés par des points blancs. Bathymétrie EMODNET (www.emodnet.eu), isobathes pleins tous les 1000 m, isobathes 200 m en pointillés. WGS 1984, Mercator 55°N.

Les deux carottes sédimentaires étudiées dans le cadre de cette thèse ont été prélevées dans des secteurs principalement affectés par des processus contouritiques liés au courant profond transportant l'ISOW, i.e. au pied de la pente Sud de *Faeroe Bank* (site MD99-2281) et au niveau de la pente Nord-Est du plateau des îles Féroé (MD99-2285 ; Tableau 1 ; Figure 10). Elles ont été prélevées lors de la mission IMAGES (International Marine Global Change

Study) V – MD99-114 (GINNA) à bord du N/O *Marion Dufresne*, et sont principalement composées d'argiles silteuses hémipélagiques (Labeyrie et al., 1999).

Carotte	Latitude (°N)	Longitude (°E)	Profondeur (m)	Longueur (m)
MD99-2281	60,3418	-9,4557	1197	29,02
MD99-2285	62,6938	-3,5723	885	46,92

Tableau 1 : Localisation et caractéristiques générales des carottes sédimentaires étudiées

En fonction de l'intensité des courants profonds, de la nature sédimentaire des fonds qu'ils parcourent, et des particules sédimentaires qu'ils transportent, ces courants peuvent être pourvoyeurs de sédiments ou au contraire érosifs (Figure 11). Au niveau des zones de pente des Féroé, les séquences sédimentaires datant de la dernière période glaciaire sont principalement composées de particules fines et caractérisées par de forts taux de sédimentation. Ceci révèle l'influence de courants profonds relativement peu intenses et responsables de forts apports sédimentaires. A l'inverse, les séquences interglaciaires sont généralement fortement réduites voire absentes du fait d'un intense vannage des sédiments fins (ou même de la non-déposition) par des courants de fond plus intenses (Kuijpers et al., 1998b ; Nielsen et al., 2007).

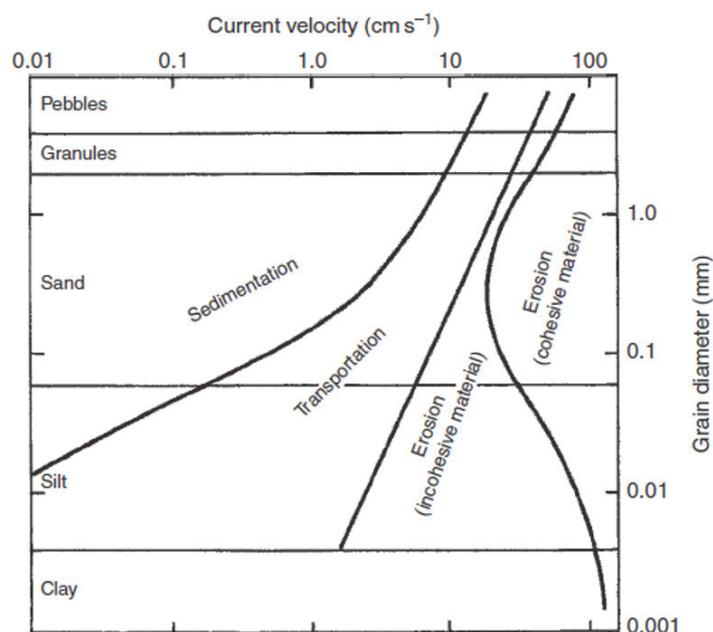


Figure 11 : Représentation simplifiée des vitesses de courant de fond nécessaires pour éroder, transporter et déposer des particules sédimentaires de différentes tailles et différentes natures (issue de Zenk, 2008).

Ce schéma de sédimentation se rencontre notamment dans le secteur où a été prélevée la carotte MD99-2281, où, sur la base de données sismiques et d'analyses lithologiques et granulométriques de carottes (notamment la carotte proche ENAM94-09, 60°3357 °N, -9.4333 °E, 1286 mètres de profondeur, 6.03 mètres de long ; [Figure 12d](#)), [Kuijpers et al. \(1998b\)](#) ont mis évidence l'existence d'une surface holocène peu épaisse (quelques centimètres) composée de silts et sables fins à très fins, recouvrant une séquence glaciaire plus épaisse composée d'argiles silteuses et caractérisée par de forts taux de sédimentation (supérieurs à 15 cm.ka⁻¹). Les profils sismiques acquis dans cette zone révèlent que l'unité sédimentaire supérieure, d'âge Néogène, est constituée de réflecteurs continus parallèles d'amplitude moyenne venant draper l'unité inférieure ([Figure 12d](#)). [Boldreel et al. \(1998\)](#) ont interprété ce faciès comme résultant d'une sédimentation pélagique en environnement profond de faible énergie, non affectée par la forte activité du courant profond transportant l'ISOW. En effet, la zone d'activité maximale de ce courant intermittent semble être restreinte le long de l'isobathe 1000 mètres, i.e. quelques 200 mètres au-dessus du site MD99-2281 ([Figure 12c](#)).

Le site MD99-2285 est quant à lui situé dans une zone où l'activité du courant profond semble avoir été plus faible. En effet, les séquences holocènes sont plus développées dans ce secteur, mesurant 40 centimètres dans la carotte proche ENAM93-21 (62.7383 °N ; -3.9987 °E ; 1020 mètres de profondeur, 11 mètres de long ; [Rasmussen et al., 1996b](#)), et environ 180 centimètres dans la carotte NA81-10 (62.9667 °N, -2.3667 °E, 1750 mètres de profondeur, > 800 centimètres de long ; [Rasmussen et al., 1996c](#) ; [Figure 12a et b](#)). Par ailleurs, sur la base de données sismiques et de sonar latéral, [van Weering et al. \(1998\)](#) ont montré que ce site se trouve (i) dans une zone où les apports sédimentaires via le courant profond transportant l'ISOW ont été relativement faibles, i.e. où l'activité de ce courant profond est relativement faible, et (ii) au-dessus du chenal érosif où se concentre l'activité maximale de ce courant ([Figure 12b](#)). Cependant, les taux de sédimentation enregistrés dans ce secteur sont généralement plus importants en période glaciaire qu'interglaciaire, notamment lors des MIS 3 et 2 où ils sont compris entre 8 et 28 cm.ka⁻¹ ([Nielsen et al., 2007](#)). Or, ces apports sédimentaires conséquents lors de la dernière période glaciaire ont conduit à des épisodes simultanés de déstabilisation de pente ([van Weering et al., 1998](#) ; [Kuijpers et al., 2001](#) ; [Nielsen et al., 2007](#)). Toutefois, des données sismiques et de sonar latéral ([van Weering et al., 1998](#) ; [Kuijpers et al., 2001](#)) révèlent que le site MD99-2285 se situe largement au-dessus de la zone affectée par ces processus de glissements en masse (appelée *North Faeroe Slide*

Complex ; Figure 12b), et donc que notre carotte n'a pas souffert de tels processus de remaniement.

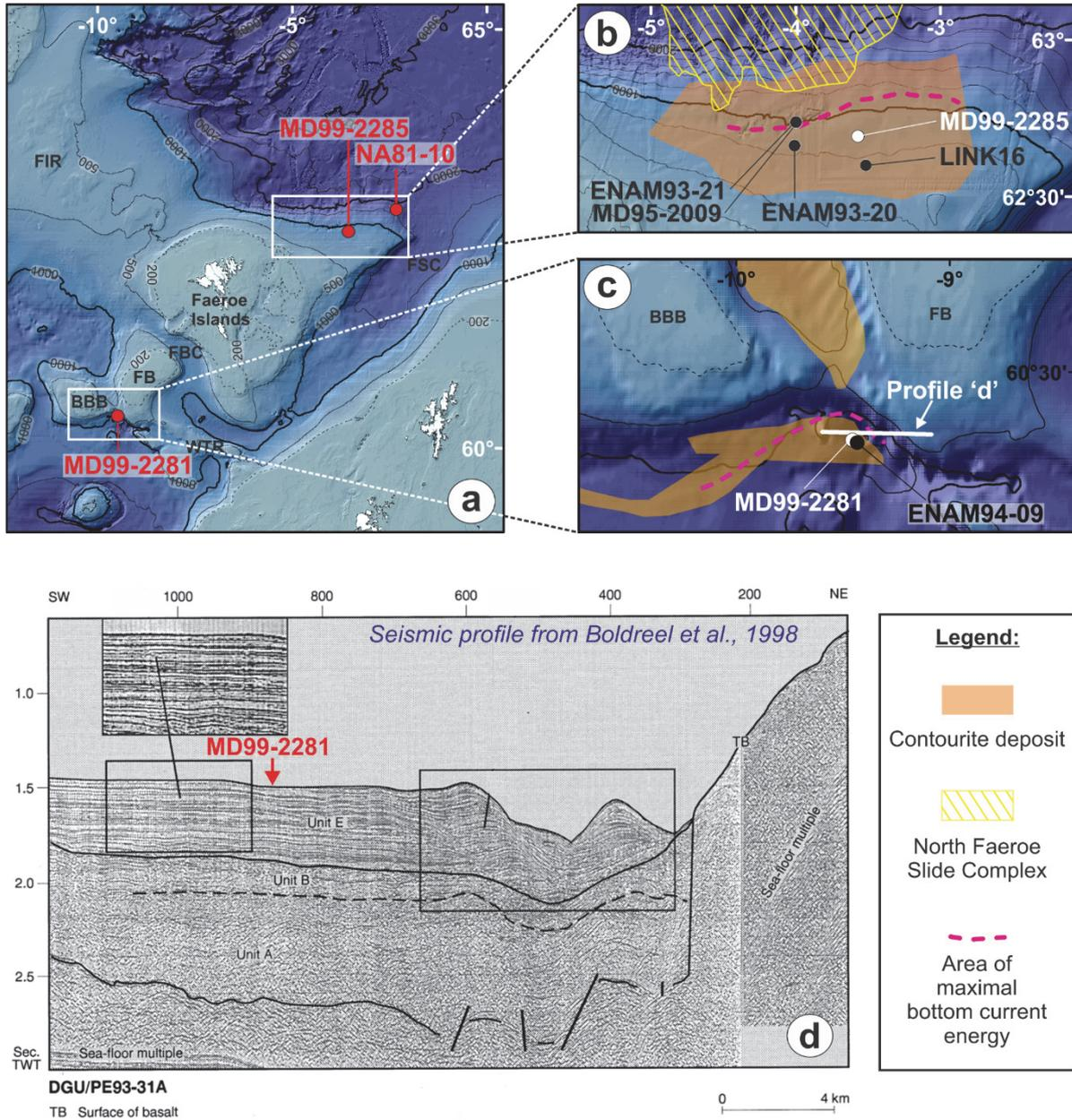


Figure 12 : Contexte sédimentaire des sites d'étude et localisation des carottes proches référencées dans le texte. (a) Carte générale de localisation des sites. (b et c) Zoom au niveau des sites MD99-2285 (b) et MD99-2281 (c) illustrant les zones de dépôt contouritique, de glissement, et d'activité maximale du courant de fond, d'après Kuijpers (1998b, 2001), van Weering et al. (1998), Nielsen et al. (2007). (d) Profil sismique obtenu au niveau du site MD99-2281, issu de Boldreel et al. (1998). Bathymétrie EMODNET (www.emodnet.eu), isobathes pleins tous les 500 m, isobathes 200 m en pointillés. WGS 1984, Mercator 55°N.

Par ailleurs, il est important de rappeler que les « cicatrices d'icebergs » observées sur le fond marin dans la zone d'étude se situent toutes au-dessus des sites étudiés. De telles marques ont été rencontrées jusqu'à 960 mètres de profondeur, mais dans un secteur plus éloigné, au niveau de la Ride Islande-Féroé (e.g. Kuijpers, 1997), qui a pu constituer une voie majeure de transit des icebergs lors des épisodes d'effondrements glaciaires de la dernière période glaciaire. A l'inverse, dans notre secteur d'étude et à cette époque, le *Faeroe Bank* et la pointe Sud-Est du plateau des Féroé étaient vraisemblablement en partie émergés, et la tranche d'eau au niveau de la Ride de Wyville-Thompson potentiellement inférieure à 500 mètres par endroits. Ainsi, comme cela a déjà été suggéré par Kuijpers et al. (1998b), ces structures topographiques formaient alors probablement une barrière entre l'Atlantique Nord-Est et le Sud-Est de la Mer de Norvège, entravant le passage des icebergs d'un domaine à l'autre. Par conséquent, il est vraisemblable que les icebergs n'aient pas non plus remanié les séquences sédimentaires prélevées sur nos deux sites d'études.

Au terme de ce chapitre 2, il apparaît clairement que la zone d'étude et les sites d'étude sont idéalement localisés pour tracer les changements hydrographiques majeurs en lien avec la dynamique passée des calottes de glace de la dernière période glaciaire. Le contexte sédimentaire des secteurs d'étude, et notamment les forts taux de sédimentation enregistrés pour la dernière période glaciaire, laissent supposer que ces archives sédimentaires sont idéales pour reconstruire ces variations à une échelle infra-millénaire.

Partie 3 : Etat de l'art sur la paléoclimatologie de notre période et zone d'étude

La variabilité climatique rapide de la dernière période glaciaire a fait l'objet d'un grand nombre d'études paléoclimatiques et expériences de modélisation. Néanmoins, de nombreuses incertitudes et plusieurs incohérences ou désaccords persistent. La plupart des études conduites en Atlantique Nord et dans les mers adjacentes s'accordent toutefois sur un schéma hydrographique général où les phases atmosphériques froides (GS et HS) sont associées à :

- des dépôts d'IRD dans la zone subpolaire (e.g. [Bond & Lotti, 1995](#) ; [Elliot et al., 1998](#)), et même dans l'ensemble de l'Atlantique Nord lors des HS (e.g. [Bond et al., 1992](#)), ces dépôts résultant des effondrements des calottes de glace boréales et des décharges d'icebergs consécutives,
- un ralentissement de l'AMOC, caractérisé par une réduction de l'afflux d'eau chaude Atlantique vers les hautes latitudes (e.g. [Van Kreveld et al., 2000](#) ; [Dickson et al., 2008](#)), une diminution de la formation d'eau profonde dans les centres de convection actuels, et par conséquent un ralentissement (et une remontée vers des profondeurs d'eau intermédiaires) des veines d'eau profondes et courants associés tels que la NADW (e.g. [McCave et al., 1995a](#) ; [Moros et al., 1997](#) ; [Kissel et al., 1999](#) ; [Rahmstorf, 2002](#) ; [Böhm et al., 2015](#)). Ceci aurait alors permis la propagation vers des latitudes plus septentrionales des eaux profondes formées dans l'hémisphère Sud (e.g. [Elliot et al., 2002](#)). Par ailleurs, des expériences de modélisation (e.g. [Manabe & Stouffer, 1995](#) ; [Ganopolski & Rahmstorf, 2001](#) ; [Bigg et al., 2011](#)) ont montré que ce ralentissement de l'AMOC pourrait être dû aux importants flux d'eau douce issus de la fonte des icebergs, qui, en diminuant la densité des eaux de surface dans les zones de convection, entraveraient la formation d'eau profonde. Les centres de convection migreraient alors vers de plus basses latitudes, moins affectées par les décharges d'icebergs et flux d'eau douce (e.g. [Vidal et al., 1997](#)).
- de faibles températures de surface (ci-après SST pour *Sea Surface Temperatures*) en Atlantique Nord et dans les mers adjacentes (e.g. [Bond et al., 1993](#) ; [Cortijo et al., 1997](#) ; [Sachs & Lehman, 1999](#) ; [Rasmussen & Thomsen, 2004](#)), étroitement liées aux décharges d'icebergs et au ralentissement de la branche supérieure de l'AMOC (NAD et extensions).

Inversement, les phases atmosphériques chaudes (GI), seraient caractérisées par un schéma hydrographique comparable à la situation actuelle, avec des décharges d'icebergs fortement réduites, une AMOC relativement active et des centres de convection profonde localisés aux hautes latitudes.

La synchronicité relative des décharges d'icebergs et des ralentissements de l'AMOC, et l'occurrence de ces changements majeurs à la fois lors des GS et des HS, ont conduit à l'hypothèse que GS et HS résulteraient de mécanismes de déclenchement communs et étroitement liés à la circulation océanique en Atlantique. Les changements de circulation impliqués pourraient alors être soit la cause (e.g. Alvarez-Solas et al., 2010 ; Alvarez-Solas & Ramstein, 2011), soit la conséquence (e.g. Manabe & Stouffer, 1995 ; Ganopolski & Rahmstorf, 2001 ; Levine & Bigg, 2008) de ces instabilités glaciaires périodiques. Ils seraient également étroitement liés aux fluctuations plurimillénaires de températures atmosphériques enregistrées dans les glaces du continent Antarctique (les « *Antarctic warm events* », enregistrés lors des événements d'Heinrich ; e.g. Blunier et al., 1998) par le biais d'oscillations inter-hémisphériques caractérisées par un comportement de type « *bipolar seesaw* » (e.g. Stocker, 1998 ; Banderas et al., 2015). Les simulations numériques issues des expériences de modélisation testant ces deux principales hypothèses (cause *versus* conséquence) révèlent dans les deux cas des changements de température atmosphérique cohérents avec l'évolution des températures atmosphériques au Groenland. Dans les deux cas également, la glace de mer et les *ice-shelves*, toutes deux localisées à l'interface entre les calottes et l'océan, semblent jouer un rôle clé dans les processus impliqués (voir également e.g. Li et al., 2010). Ces constats et hypothèses ont mené la communauté scientifique à étudier la dynamique océanique et cryosphérique, et les interactions entre ces deux composantes, lors des changements rapides de la dernière période glaciaire, et dans des secteurs géographiques clés tels que la frontière entre l'Atlantique Nord-Est et les Mers Nordiques. Les études ainsi conduites ont démontré le fort potentiel de cette zone pour étudier de telles problématiques à une échelle infra-millénaire. Une grande partie de ces études se sont notamment concentrées dans des secteurs proches des calottes européennes, susceptibles d'avoir joué un rôle précurseur lors de certains HS (e.g. Bond & Lotti, 1995 ; Snoeckx et al., 1999 ; Grousset et al., 2000 ; Hemming, 2004).

La plupart de ces travaux délivrent des conclusions en accord avec le schéma hydrographique général décrit précédemment. En effet, le long des côtes Nord-Ouest européennes, les GI apparaissent caractérisés par un important afflux d'eau Atlantique dans

les Mers Nordiques via le Courant Nord Atlantique (NAC pour *North Atlantic Current*) et une circulation de fond active liée au fort taux de production d'ISOW dans les Mers Nordiques (e.g. Rasmussen et al., 1996a,b, 1997, 1999 ; Dokken & Jansen, 1999 ; Kissel et al., 1999 ; van Kreveld et al., 2000 ; Rasmussen & Thomsen, 2004, 2009 ; Ballini et al., 2006 ; Dickson et al., 2008 ; Ezat et al., 2014). A l'inverse, les GS et HS sont marqués par des flux accrus d'icebergs et d'eau douce (Rasmussen et al., 1996a,b, 1997 ; Dokken & Jansen, 1999 ; Elliot et al., 2001 ; Eynaud et al., 2002 ; Rasmussen & Thomsen, 2009) et un ralentissement de la boucle NAC – convection dans les Mers Nordiques - ISOW (Rasmussen et al., 1996a,b, 1997, 1999 ; Dokken & Jansen, 1999 ; Kissel et al., 1999 ; Elliot et al., 2002 ; Ballini et al., 2006 ; Rasmussen & Thomsen, 2004, 2009 ; Ezat et al., 2014). Par ailleurs, certains ont suggéré l'existence lors des GS et HS d'une forte stratification de la colonne d'eau dans les Mers Nordiques liée à la mise en place d'une halocline lors des débâcles d'icebergs (Rasmussen et al., 1996a,b ; Rasmussen & Thomsen, 2004 ; Dokken et al., 2013). Une telle stratification a de plus été également mise en évidence dans le bassin d'Irminger (van Kreveld et al., 2000). Par la suite, Rasmussen & Thomsen (2009) ont suggéré que cette halocline ait pu jouer un rôle majeur dans le ralentissement de l'AMOC en inhibant la formation d'eau profonde dans les Mers Nordiques, supportant ainsi l'hypothèse que ce ralentissement soit lié aux décharges d'icebergs et flux d'eau douce associés.

En parallèle, plusieurs de ces études ont suggéré l'occurrence de faibles SST dans les Mers Nordiques lors des GS et HS, et inversement lors des GI (e.g. Rasmussen et al., 1996a,b, 1997 ; Rasmussen & Thomsen, 2004 ; Van Kreveld et al., 2000 ; Dokken et al., 2013). Un tel schéma de SST, similaire à celui décrit pour l'Atlantique Nord, est également reproduit dans certaines expériences de modélisation testant l'impact d'un flux d'eau douce aux hautes latitudes (e.g. Stouffer et al., 2006). De plus, ce schéma apparaît cohérent avec les variations de températures atmosphériques enregistrées dans les glaces du Groenland, ainsi qu'avec les décharges massives d'icebergs enregistrées au cours des GS et HS. Il est toutefois important de préciser que, dans les Mers Nordiques, ce schéma de SST a été déduit sur la base de proxies pouvant être qualifiés d'indirects. En effet, il émane de résultats principalement issus de foraminifères planctoniques (assemblages et contenu isotopique en oxygène). Or, il est désormais admis que ces organismes zooplanctoniques migrent au cours de leur cycle de vie au sein d'une section relativement importante de la colonne d'eau (e.g. Schiebel et al., 2001), et peuvent également adapter leur profondeur de vie en fonction des conditions hydrologiques de surface (e.g. Carstens et al., 1997 ; Simstich et al., 2003). De façon assez similaire, les

faibles SST assignées aux GS et HS ont régulièrement été associées à un large couvert de glace de mer dans les Mers Nordiques (e.g. Rasmussen et al., 1999 ; Gildor & Tziperman, 2003 ; Rasmussen & Thomsen, 2004 ; Dokken et al., 2013). Ceci est conforté par des mesures isotopiques ($\delta^{18}\text{O}$) effectuées au sein de tests de foraminifères planctoniques et benthiques (Dokken & Jansen, 1999 ; Dokken et al., 2013), ainsi que par diverses expériences de modélisation (e.g. Li et al., 2010 ; Petersen et al., 2013 ; Singh et al., 2014) où la dynamique de la glace de mer dans les Mers Nordiques semble jouer un rôle primordial sur les températures atmosphériques de l'hémisphère Nord.

Cependant, en mer de Norvège, Eynaud et al. (2002) ont mis en évidence un schéma tout autre, où les GS et HS sont associés à des SST élevées et un couvert de glace de mer réduit, et inversement les GI sont associés à des SST faibles et un couvert de glace plus étendu. Ce schéma, bien que paradoxal, s'appuie toutefois sur des proxies plus directement liés aux conditions océaniques de surface : les assemblages de kystes de dinoflagellés (ou dinokystes), et les reconstructions hydrologiques quantifiées obtenues en appliquant une fonction de transfert à ces assemblages. Les dinoflagellés constituent en effet des organismes phytoplanctoniques qui, contrairement aux foraminifères planctoniques, sont principalement restreints à la zone euphotique (e.g. Sarjeant, 1974). Bien que les enregistrements d'Eynaud et al. (2002) constituent les seules reconstructions directes couplant SST et couvert de glace de mer au sein des Mers Nordiques, les interprétations atypiques qui en ont été déduites n'ont été que peu prises en considération. Pourtant, de récentes études de modélisation (Kleinen et al., 2009 ; Swingedouw et al., 2013) viennent conforter ces résultats. En effet, elles suggèrent qu'une libération massive d'eau douce aux hautes latitudes de l'Atlantique Nord, en plus d'induire une diminution de la vigueur de l'AMOC et un refroidissement de surface en Atlantique Nord, puisse également s'accompagner d'une advection accrue d'eau chaude et salée atlantique se propageant en subsurface dans l'Atlantique Nord et ré-émergeant en surface des Mers Nordiques, générant ainsi un réchauffement de surface dans ce bassin. Là encore, la réaction de la composante atmosphérique dans ces simulations est cohérente avec les observations. Malgré des différences notoires, ce scénario rappelle ceux suggérés par Rasmussen & Thomsen (2004) et Dokken et al. (2013) où, lors des GS et HS, l'afflux d'eau atlantique dans les Mers Nordiques n'est pas inhibé mais se propage en subsurface, sous la halocline et la couverture de glace de mer (mais sans pour autant remonter en surface donc). En effet, les reconstructions de températures de Dokken et al. (2013) au niveau du *Faeroe-Shetland Channel*, obtenues en appliquant une fonction de transfert aux assemblages de

foraminifères planctoniques et interprétées comme des signaux de subsurface par les auteurs, indiquent un réchauffement de cette masse d'eau lors des GS et HS. Il est toutefois important de noter que, parmi toutes les études menées dans les Mers Nordiques sur la base des assemblages de foraminifères planctoniques, celle de [Dokken et al. \(2013\)](#) est la seule à mettre en évidence des faunes plus chaudes lors des GS et HS que lors des GI. Par contre, en dehors des Mers Nordiques, malgré la présence d'assemblages également polaires lors des GS et HS, certaines études ont mis en évidence un réchauffement modéré des eaux de surface/subsurface sur la base de mesures Mg/Ca réalisées sur des tests de foraminifères planctoniques (e.g. [Peck et al. \(2008\)](#) au niveau de la baie de Porcupine, et [Jonkers et al. \(2010a\)](#) au niveau de la Ride de Reykjanes). Contrairement à [Dokken et al. \(2013\)](#), [Rasmussen & Thomsen \(2004\)](#) suggèrent que cet afflux d'eau atlantique s'étende jusqu'à des profondeurs qualifiées d' « intermédiaires » par les auteurs (i.e. à partir d'au moins 850 mètres, et au moins jusqu'à 1760 mètres de profondeurs lors de certains HS). Cette suggestion est basée sur la présence lors des GS et HS d'espèces de foraminifères benthiques actuellement présentes dans le domaine Atlantique, ainsi que sur les faibles valeurs de $\delta^{18}\text{O}$ benthique enregistrées lors de ces périodes. [Dokken et al. \(2013\)](#), ainsi que [Dokken & Jansen \(1999\)](#), relient quant à eux ces faibles valeurs isotopiques principalement au rejet de saumures, ou *brines*, lors de la formation saisonnière de glace de mer. L'hypothèse de [Rasmussen & Thomsen \(2004\)](#) est toutefois confortée par des mesures Mg/Ca réalisées sur des foraminifères benthiques ([Marcott et al., 2011](#) ; [Ezat et al., 2014](#)), ainsi que par des expériences de modélisation ([Shaffer et al., 2004](#)) qui mettent en évidence la possibilité d'un réchauffement des eaux intermédiaires (jusqu'à environ 2500 mètres de profondeur) dans l'Atlantique Nord et les mers adjacentes lors des GS et HS. Néanmoins, l'origine de cette masse d'eau atlantique intermédiaire, et sa présence en elle-même au sein des Mers Nordiques durant les stadiers, restent toujours controversées (e.g. [Rasmussen et al., 1996a, 2002](#) ; [Dokken & Jansen, 1999](#) ; [Lassen et al., 2002](#) ; [Rasmussen & Thomsen, 2004](#) ; [Dokken et al., 2013](#)). Par ailleurs, [Dokken et al. \(2013\)](#) ont émis l'hypothèse que cet afflux d'eau atlantique et le réchauffement de subsurface associé aient pu déclencher les débâcles d'icebergs en induisant une fonte basale des *ice-shelves* et *in fine* leur dislocation, tel que suggéré par e.g. [Alvarez-Solas et al. \(2010\)](#). Il n'existe toutefois à ce jour aucune preuve directe d'un tel mécanisme. De plus, [Rasmussen & Thomsen \(2004\)](#) et [Dokken et al. \(2013\)](#) ont également suggéré que cet afflux d'eau atlantique ait conduit à une importante accumulation de chaleur sous la halocline, rendant progressivement la colonne d'eau instable, aboutissant *in fine* à la rupture de la halocline et à la libération massive de chaleur dans l'atmosphère, et générant

alors le réchauffement atmosphérique abrupt enregistré dans les glaces du Groenland au début des GI. Là encore, il n'existe aucune preuve directe de rupture abrupte de cette halocline à la transition GS/HS – GI.

Ainsi, bien que les nombreux travaux focalisés sur la variabilité climatique rapide de la dernière période glaciaire dans la zone d'étude nous aient permis de mieux comprendre les processus impliqués, de nombreuses incertitudes demeurent.

*Cette thèse a donc pour objectifs de reconstruire les variations hydrologiques enregistrées dans nos deux archives sédimentaires en combinant de nombreux proxys principalement indicateurs de la **dynamique des masses d'eau de surface, de subsurface, et de fond**, ainsi que de la **dynamique des calottes de glace et de la glace de mer**, afin d'améliorer nos connaissances concernant :*

- les **conditions caractérisant les GS/HS et les GI de part et d'autre de la Ride Féroé-Ecosse**,*
- les **processus hydrographiques en jeu**,*
- les **interactions océan-atmosphère-cryosphère**,*
- et les **mécanismes de déclenchement impliqués**.*

Chapitre 2 : Matériel et méthodes

Le **chapitre 2** regroupe une première partie (**Partie 1**) présentant la **stratégie analytique** des deux archives sédimentaires (en terme d'outils et de résolution), puis une description des **principaux outils** que j'ai moi-même mis en œuvre (**Partie 2**), et enfin une description des **données complémentaires (Partie 3)** produites par les collaborateurs à cette thèse et utilisées dans le cadre de ce manuscrit et des articles qu'il intègre.

Sommaire

<u>PARTIE 1 : STRATEGIE ANALYTIQUE</u>	33
<u>PARTIE 2 : PRINCIPAUX OUTILS MIS EN ŒUVRE</u>	36
<i>Section 1. Assemblages de dinokystes quaternaires et reconstructions associées</i>	36
1. Généralités sur les kystes de dinoflagellés	36
2. Distribution géographique actuelle des dinokystes	37
3. Reconstructions des conditions de surface passées : fonction de transfert	53
<i>Section 2. Autres palynomorphes</i>	54
<i>Section 3. $\delta^{18}O$ dans les tests de foraminifères planctoniques</i>	55
<i>Section 4. Granularité du sédiment et mesure de calcimétrie</i>	56
<i>Section 5. Mg/Ca dans les tests de foraminifères planctoniques</i>	60
1. Principe général de la méthode de dosage du Mg/Ca sur les tests de PF via ICP-OES	60
2. Résumé synthétique du développement de méthode.....	62
2.1. Optimisation du dosage.....	62
2.2. Gammes étalons et certifiés	64
2.3. Méthodes de calibration	65
2.4. Protocole de chimie.....	68
3. Mesures tests sur des échantillons de <i>N. pachyderma</i> senestre (carotte KI02 - MOCOSED2014)	69
4. Résultats des mesures sur la carotte MD96-2048 (stage T. Extier)	70
5. Résultats des mesures sur la carotte MD99-2285	71
6. Conclusion.....	73
<u>PARTIE 3 : OUTILS COMPLEMENTAIRES</u>	74
<i>Section 1. Assemblages de foraminifères planctoniques et reconstructions associées</i> ..	74
<i>Section 2. IRD</i>	75
<i>Section 3. Biomarqueurs : alcénones et IP25</i>	75
<i>Section 4. Xrf</i>	76

Partie 1 : Stratégie analytique

Les problématiques de cette thèse impliquent une stratégie analytique couplant approche multi-outils et haute résolution temporelle, synthétisée dans le [Tableau 2](#). Les nombreux outils mis en œuvre sur les deux carottes étudiées, décrits de façon plus détaillée dans les deux parties suivantes, permettent de reconstruire les variations hydrographiques de surface (température, salinité, couvert de glace, décharges d'icebergs), de subsurface (température, salinité), et de fond (intensité de courant profond transportant l'ISOW). Les analyses ont été conduites à « basse résolution » sur les sections 12 – 42 ka cal BP (300 – 2170 cm) de la carotte MD99-2281, et 3 – 41 ka cal BP (0 – 600 cm) de la carotte MD99-2285, dans le but premier d'identifier les variations hydrographiques générales caractérisant ces périodes de temps. Elles ont également été conduites à haute voire très haute résolution (résolution moyenne < 155 ans) sur les sections 37-40 ka cal BP de la carotte MD99-2281 et 35-41 cal BP ka de la carotte MD99-2285, i.e. de part et d'autres d'HS4, afin de mettre en évidence le séquençage précis des processus hydrographiques en jeu lors des transitions GI à GS/HS, et GS/HS à GI.

La stratigraphie de chaque carotte est présentée de manière détaillée dans [Zumaque et al. \(2012\)](#), disponible en [Annexe 1](#) pour la carotte MD99-2281, et dans le Chapitre 3 de ce manuscrit (Partie 1, Section 2) pour la carotte MD99-2285. Néanmoins, et très brièvement, les modèles d'âge des carottes étudiées dans cette thèse ont été établis conformément à la méthodologie couramment employée pour établir la stratigraphie des archives sédimentaires marines prélevées dans la zone d'étude (e.g. [Rasmussen et al., 1996a,b](#) ; [Kissel et al., 1999](#) ; [Laj et al., 2000](#) ; [Elliot et al., 2002](#) ; [Ballini et al., 2006](#) ; [Rasmussen & Thomsen, 2009](#)), i.e. en combinant deux types de points de contrôle :

- des datations ^{14}C , obtenues dans le cadre du programme ARTEMIS, sur des échantillons de PF, souvent monospécifiques (*G. bulloides* ou *N. pachyderma* senestre). 13 dates (dont 3 non retenues pour l'établissement du modèle d'âge) ont été obtenues pour la carotte MD99-2281, et 17 (dont 9 non retenues) pour la carotte MD99-2285.
- des points de contrôle obtenus en comparant le signal de susceptibilité magnétique (MS) de nos carottes à l'enregistrement de $\delta^{18}\text{O}$ de NGRIP (stratotype régional Nord Atlantique recommandé par [Austin & Hibbert, 2012](#) ; échelle d'âge GICC05, [Svensson et al., 2008](#)), et plus précisément en corrélant les augmentations de MS au début des GI,

et les baisses de MS à la terminaison des GI (en utilisant les limites d'âge de GI fournies par Wolff et al., 2010). En effet, les travaux de Kissel et al. (1999) ont montré que dans l'Atlantique Nord subpolaire, le long du trajet des veines d'eau profondes nourrissant la NADW, (i) les variations de susceptibilité magnétique sont directement liées aux variations d'intensité de ces veines d'eau profondes, et (ii) les faibles valeurs de susceptibilité magnétique coïncident avec les GS et HS, et inversement les valeurs élevées avec les GI. Les signaux de susceptibilité magnétique utilisés sont ceux produits à bord du Marion Dufresne lors de la mission GINNA, mesurés tous les 2 cm avec le banc GEOTEK (ou *GEOTEK Multi-Sensor Core Logger*; Labeyrie & Cortijo, 2005a,b).

Il est important de préciser que d'autres mesures des propriétés magnétiques du sédiment ont été effectuées de manière plus détaillée mais discontinue sur la carotte MD99-2281 par C. Kissel au LSCE. Parmi les signaux mesurés, celui de susceptibilité magnétique κ (*low field magnetic susceptibility*) montre des tendances très similaires au signal de MS mesuré à bord. Par ailleurs, le signal de paléo-intensité relative du champ magnétique terrestre met en évidence des points de contrôle stratigraphiques supplémentaires, indépendants des variations climatiques. Il s'agit des excursions magnétiques (de faibles valeurs) du Mono Lake (~ 34 ka cal BP) et du Laschamp (~ 41 ka cal BP; Laj et al., 2000), également identifiées dans plusieurs autres carottes de notre secteur d'étude (e.g. Kissel et al., 1999; Laj et al., 2000; Ballini et al., 2006). La position stratigraphique donnée à ces deux excursions par le modèle d'âge établi pour cette carotte, en accord avec les âges données dans la bibliographie, conforte ce modèle d'âge (cf. Fig. 3 et Fig. 4 de Zumaque et al., 2012 – Annexe 1).

Sur la base de ces modèles d'âge, les taux de sédimentation moyens estimés sont de 61 cm.ka⁻¹ pour la section 12 – 42 ka cal BP de la carotte MD99-2281, et de 16 cm.ka⁻¹ pour la section étudiée 3 – 41 ka cal BP de la carotte MD99-2285.

Tableau 2 : Stratégie analytique (outils et résolution temporelle). Les coches rouges indiquent les analyses que j'ai moi-même réalisées. Les noms en bleu correspondent à des stagiaires que j'ai co-encadrés (le nom du co-encadrant étant précisé entre parenthèses). Les informations en gris indiquent des données disponibles avant le début de ma thèse (Zumaque et al., 2012 et Caille et al., 2013 disponibles en Annexes 1 et 2).

<u>Outils</u>	MD99-2281		MD99-2285	
	12 - 42ka	37-40 ka	3-41 ka	35-41 ka
Assemblages de dinokystes	Zumaque et al., 2012 Caulle et al., 2013	✓	✓	✓
Fonction de transfert dinokystes	Zumaque et al., 2012 Caulle et al., 2013	✓	F. Eynaud	F. Eynaud
Autres palynomorphes (concentration uniquement)	Zumaque et al., 2012 Caulle et al., 2013	✓	✓	✓
Assemblages foraminifères planctoniques (PF)	L. Rossignol	L. Rossignol	L. Rossignol	L. Rossignol
Fonction de transfert PF	F. Eynaud	F. Eynaud	F. Eynaud	F. Eynaud
Concentration Foraminifères benthiques	L. Rossignol	L. Rossignol	L. Rossignol	L. Rossignol
Assemblages foraminifères benthiques	/	/	/	C. Grimaldi (J. Bonnin), ✓
δ ¹⁸ O sur foraminifères planctoniques (PF)	Zumaque et al., 2012 Caulle et al., 2013	✓	✓	✓
Quantification SSS à partir δ ¹⁸ O et températures PF	B. Malaizé, ✓	/	/	/
Granularité du sédiment	M. Sabine (S. Zaragosi), ✓	M. Sabine (S. Zaragosi)	M. Sabine (S. Zaragosi), ✓	M. Sabine (S. Zaragosi), ✓
Calcimétrie	✓		✓	
IRD (concentration uniquement)	Zumaque et al., 2012 Caulle et al., 2013	L. Rossignol	L. Rossignol	J. Lapuyade (L. Londeix)
Mg/Ca sur PF	/	/	✓	✓
Biomarqueurs (IP25 et alcénones)	/	/	/	M.-A. Sicre (LOCEAN)
XRF	T. Richter (NIOZ, Pays-Bas) S. Zaragosi, Plate-forme PAACS			
Susceptibilité magnétique	C. Kissel (LSCE) + Mesures effectuées à bord			
Datations ¹⁴ C (piquages PF)	Zumaque et al., 2012 Caulle et al., 2013	M.-H. Castéra, L. Rossignol, ✓		
Construction des modèles d'âge	Zumaque et al., 2012 Caulle et al., 2013	F. Eynaud, ✓		
<u>Autres</u>				
Echantillonnage des carottes (sur plaquettes)	Echantillons déjà disponibles	✓	✓	✓
Préparation palynologique		M.-H. Castéra	M.-H. Castéra	M.-H. Castéra
Piquages PF pour analyses δ ¹⁸ O et Mg/Ca	/	M.-C. Gasparotto, L. Rossignol, ✓		
Imagerie rX	S. Zaragosi, Plate-forme PAACS			
<u>Résolution temporelle moyenne (et minimale à maximale) des principales analyses, en années</u>	165 (25 à 525)	19 à 38 selon les outils (10 à 66)	Variable selon les outils, ≈350 (17 à 1235)	55 à 155 selon les outils (15 à 492)

Partie 2 : Principaux outils mis en œuvre

Section 1. Assemblages de dinokystes quaternaires et reconstructions associées

Les kystes de dinoflagellés, ou dinokystes, constituent de précieux outils pour retracer les conditions hydrographiques de surface passées (e.g. Rochon et al., 2008), notamment aux hautes latitudes où les assemblages sont nettement plus diversifiés que ceux d'autres organismes tels que les foraminifères planctoniques.

1. Généralités sur les kystes de dinoflagellés

Les dinoflagellés sont des organismes phytoplanctoniques unicellulaires microscopiques essentiellement marins. Ils se rencontrent à toutes les latitudes et affectionnent particulièrement les zones côtières et néritiques. Ils vivent principalement dans la zone euphotique (e.g. Sarjeant, 1974), la grande majorité des espèces (~ 50%) étant autotrophe, l'autre partie étant hétérotrophe, mixotrophe, parasitaire ou symbiotique (e.g. de Vernal & Marret, 2007). Avec les diatomées et les coccolithophoridées, ils sont responsables d'une part importante de la productivité primaire globale. Leur distribution spatiale dépend principalement de la pénétration de la lumière, de la température, de la salinité, et de la teneur en éléments nutritifs.

Les dinoflagellés en eux-mêmes ne sont pas fossilisables, leur forme vivante étant entourée d'une thèque cellulosique se dégradant rapidement à la mort de l'organisme. Néanmoins, au cours de leur complexe cycle de vie, et plus précisément lors de la phase sexuée de leur reproduction, certains dinoflagellés (de 13 à 16 % des populations actuelles) produisent un kyste qui va sédimenter et se fossiliser. Ce kyste, généralement de nature organique (dinosporine) très résistante à la dissolution, va constituer une protection pour la cellule diploïde néo-formée lors de sa phase de dormance (e.g. Wall & Dale, 1968). Cette phase d'enkystement se produit généralement en automne. La phase d'exkystement (via l'archéopyle) se produit quant à elle lors de l'amélioration des conditions thermiques du milieu, généralement au printemps (e.g. Penaud, 2009 ; Ellegaard et al., 2013). Actuellement, plus de 75 espèces de dinokystes sont recensées (e.g. Zonneveld et al., 2013). Cependant, les connaissances concernant les relations forme thécale – kyste restent assez limitées.

2. Distribution géographique actuelle des dinokystes

Bien que les assemblages de dinokystes ne constituent qu'une image fragmentaire des populations phytoplanctoniques, et que les relations thèque-kyste soient assez mal définies pour de nombreuses espèces, la distribution géographique des dinokystes quaternaires à la surface des sédiments marins semble être étroitement liée aux paramètres environnementaux caractérisant la surface océanique. Ce constat émane de plusieurs travaux ayant permis de mieux caractériser la distribution spécifique des dinokystes dans les sédiments de surface (e.g. Williams, 1971 ; Wall et al., 1977 ; Harland, 1983 ; Turon, 1984). Les résultats de ces travaux ont par la suite été synthétisés au sein de divers ouvrages qui font actuellement référence en la matière et constituent la base des reconstructions paléoenvironnementales (e.g. Rochon et al., 1999 ; Marret & Zonneveld, 2003 ; Zonneveld et al., 2013).

Dans le cadre de cette approche paléoenvironnementale (dans laquelle s'inclut cette thèse), il est important de préciser que plusieurs processus sont susceptibles d'altérer les assemblages de kystes entre leur production dans la zone euphotique et leur dépôt sur les fonds marins, notamment la dissolution et le transport par les courants. Ceci appuie et justifie la démarche de référencement des assemblages modernes sur la base du sédiment superficiel qui intègre déjà ces processus taphonomiques. Concernant la dissolution, il a été démontré que celle-ci affecte préférentiellement certaines espèces sensibles à l'oxydation (e.g. Zonneveld et al., 1997), dont quelques-unes se retrouvent dans nos assemblages, et parfois en tant qu'espèces dominantes (e.g. *Operculodinium centrocarpum*). Aussi, il apparaît peu probable que ce paramètre ait biaisé nos assemblages lors de leur transfert vers le fond. Par contre, étant donné la localisation de nos sites d'étude à un point nodal de la circulation océanique de surface et de fond, ce paramètre dynamique pourrait constituer un biais significatif (Dale, 1976). Il n'est d'ailleurs pas uniquement restreint aux dinokystes, mais également à tous les organismes utilisés en micropaléontologie tels que les foraminifères planctoniques et benthiques, les coccolithophoridées, ou encore les diatomées. Toutefois, il est important de garder à l'esprit que les signaux paléoenvironnementaux reconstruits représentent toujours des signaux moyennés à la fois dans le temps et l'espace. Par ailleurs, plusieurs éléments issus des analyses menées dans le cadre de cette thèse, et exposés en détails dans le Chapitre 3 (page 77 et suivantes de ce manuscrit), permettent (i) de discriminer les signaux principalement représentatifs de conditions de surface/subsurface régionales (que l'on peut qualifier d'« autochtones ») de ceux résultant principalement d'advection par les

courants de surface/subsurface (« allochtones »), et (ii) d'établir que nos assemblages n'ont pas significativement souffert d'un éventuel remaniement par les courants profonds.

Dans le cadre de cette thèse, 42 espèces de dinokystes ont été identifiées. La distribution écologique des espèces dominantes et subordonnées, ainsi que de certains taxons annexes d'intérêt, est présentée ci-dessous de manière très succincte (cf. Rochon et al., 1999 ; Marret & Zonneveld, 2003 ; Zonneveld et al., 2013 ; et références ci-dessous).

- *Islandinium minutum* var *minutum* (Figure 13 ; Planche 1) : taxon polaire associé à des eaux de surface froides et saisonnièrement couvertes par de la glace de mer, dont les abondances maximales sont observées sous couvert de glace de 8 à 12 mois par an.

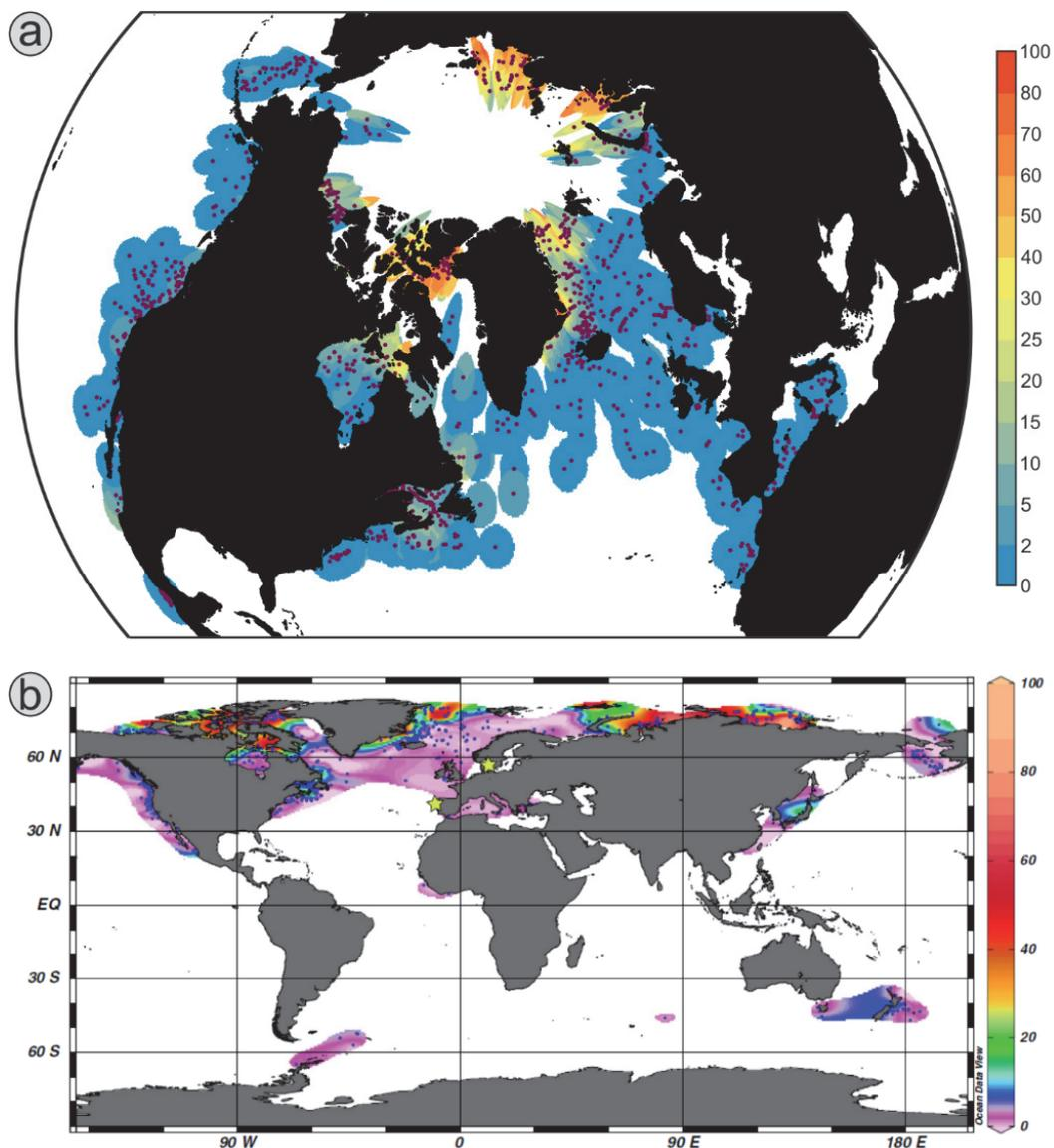


Figure 13 : Cartes de distribution (en pourcentages) d'*Islandinium minutum* var *minutum* (a) dans la base de données modernes n = 1207, carte construite sous ARCGIS et (b) issue de l'atlas mondial de Zonneveld et al. (2013).

- *Bitectatodinium tepikiense* (Figure 14 ; Planche 1) : taxon tempéré à subpolaire présentant une forte affinité pour les eaux de surface stratifiées caractérisées par de forts contrastes de saisonnalité.

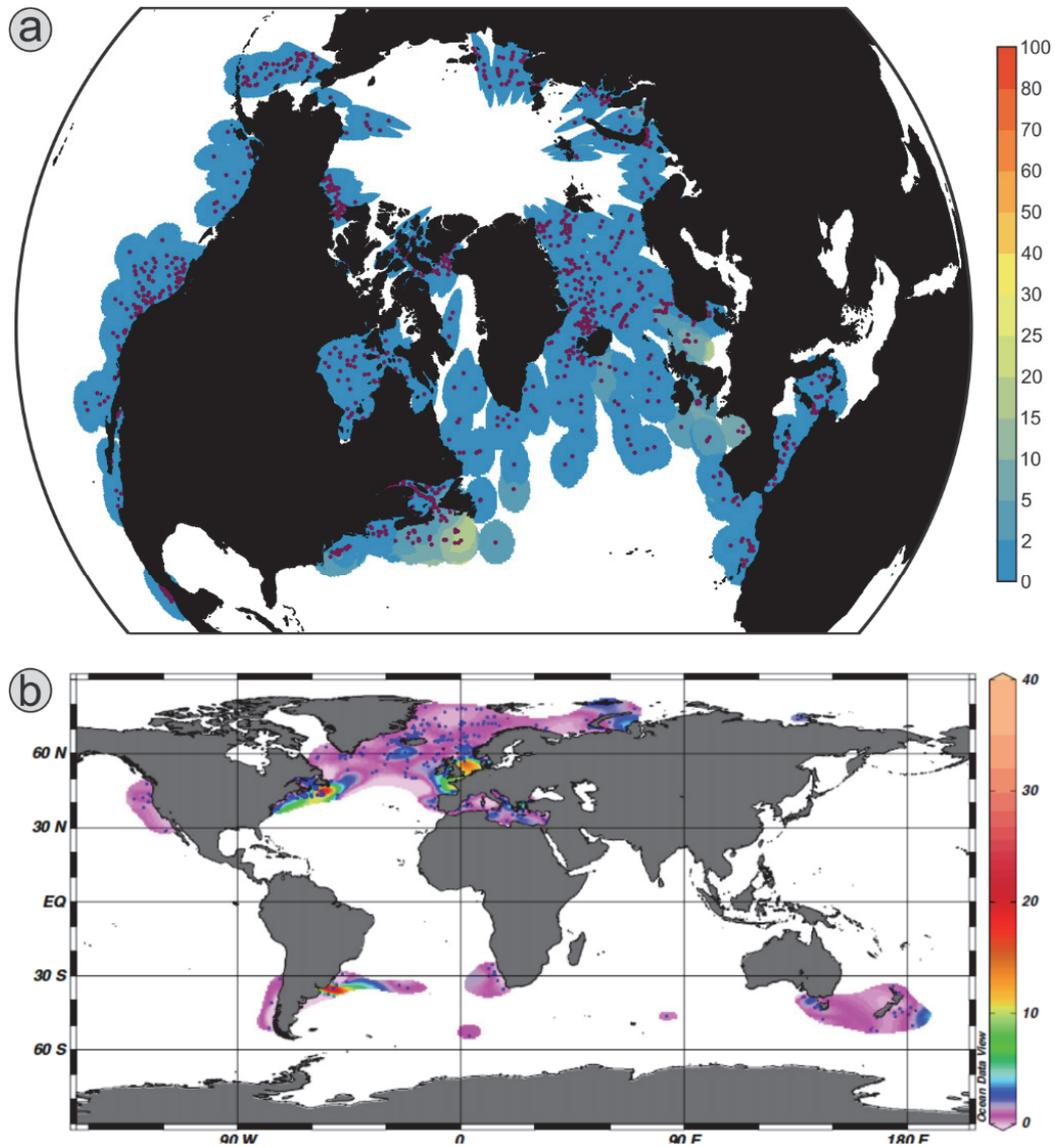


Figure 14 : Cartes de distribution (en pourcentages) de *Bitectatodinium tepikiense* (a) dans la base de données modernes $n = 1207$, carte construite sous ARCGIS et (b) issue de l'atlas mondial de Zonneveld et al. (2013).

- *Operculodinium centrocarpum* (Figure 15 ; Planche 1) : espèce cosmopolite par excellence, son schéma de distribution en Atlantique Nord et dans les Mers Nordiques est toutefois étroitement lié au tracé de la Dérive Nord Atlantique et ses extensions. La longueur des processus pourrait être un indicateur de salinité (e.g. Mertens et al., 2012).

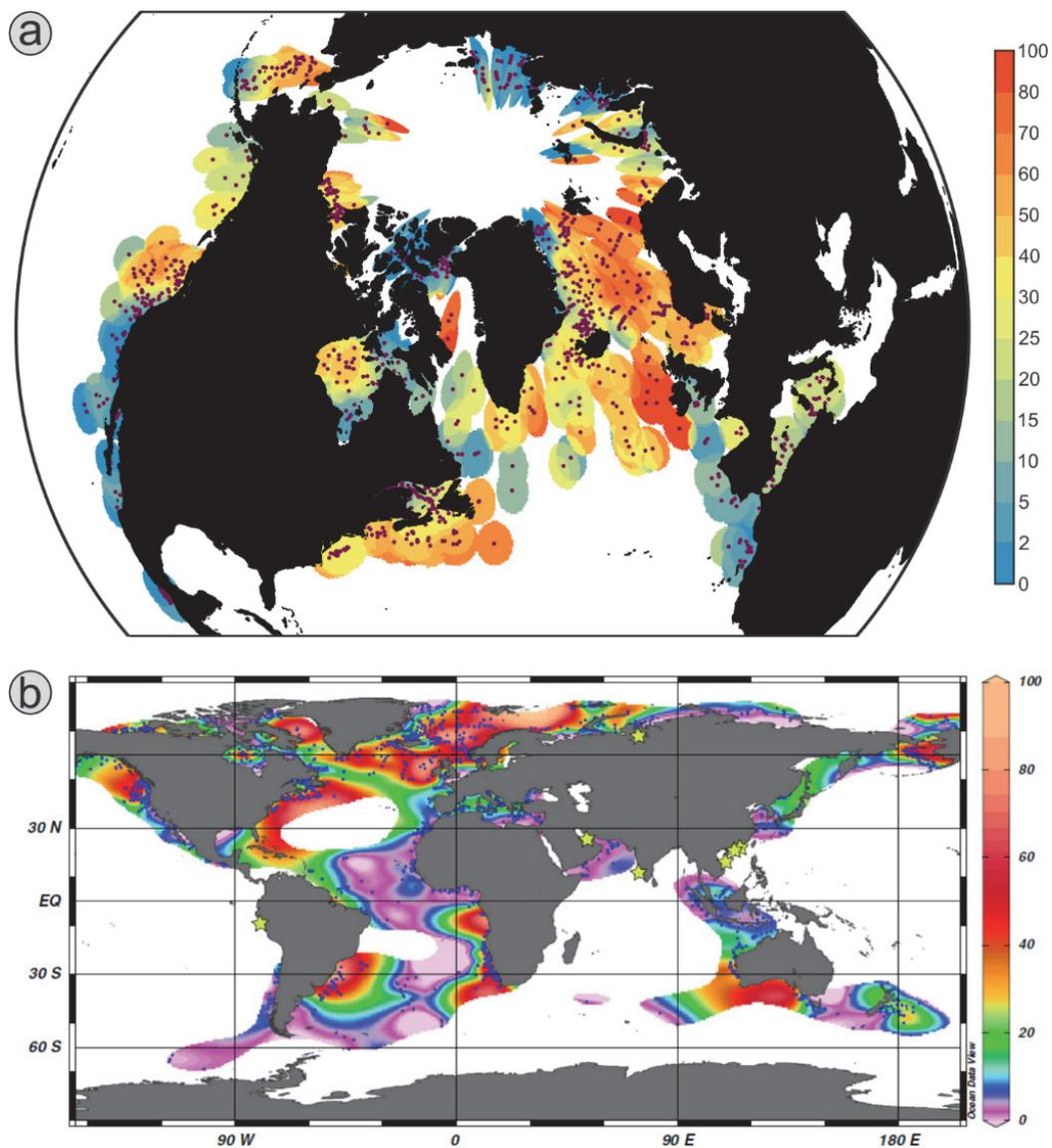


Figure 15 : Cartes de distribution (en pourcentages) d'*Operculodinium centrocarpum* (a) dans la base de données modernes $n = 1207$, carte construite sous ARCGIS et (b) issue de l'atlas mondial de Zonneveld et al. (2013).

- *Pentapharsodinium dalei* (Figure 16 ; Planche 1) : espèce présente des domaines polaires à équatorial, dont les abondances maximales se rencontrent principalement en domaine subpolaire, et affectionnant particulièrement les zones marquées par une forte saisonnalité.

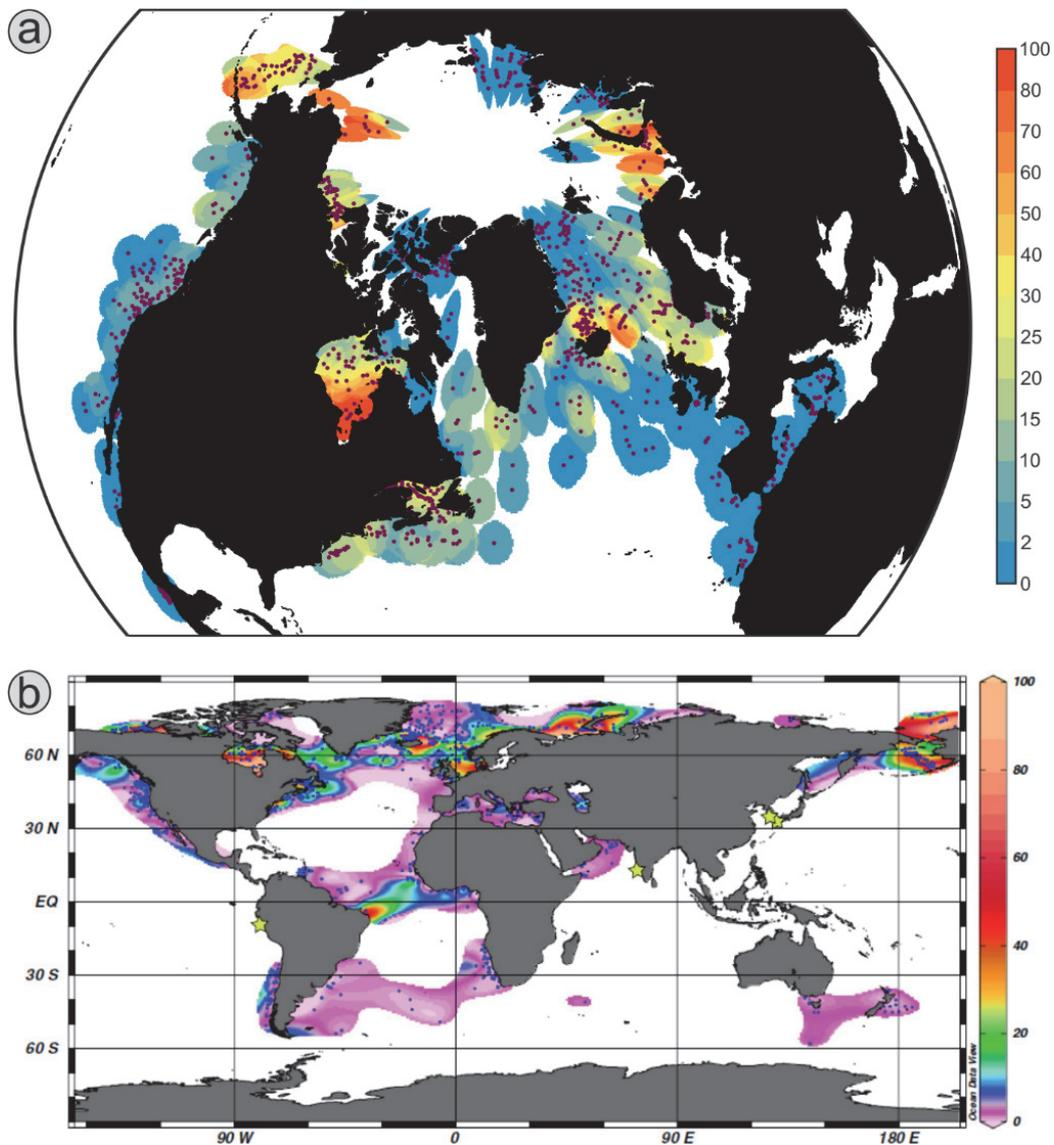


Figure 16 : Cartes de distribution (en pourcentages) de *Pentapharsodinium dalei* (a) dans la base de données modernes $n = 1207$, carte construite sous ARCGIS et (b) issue de l'atlas mondial de Zonneveld et al. (2013).

- *Nematosphaeropsis labyrinthus* (Figure 17 ; Planche 1) : taxon tempéré à subpolaire dont les abondances relatives maximales enregistrées en Atlantique Nord et dans les mers adjacentes se rencontrent dans les zones où les eaux froides arctiques se mélangent aux eaux chaudes nord-atlantiques.

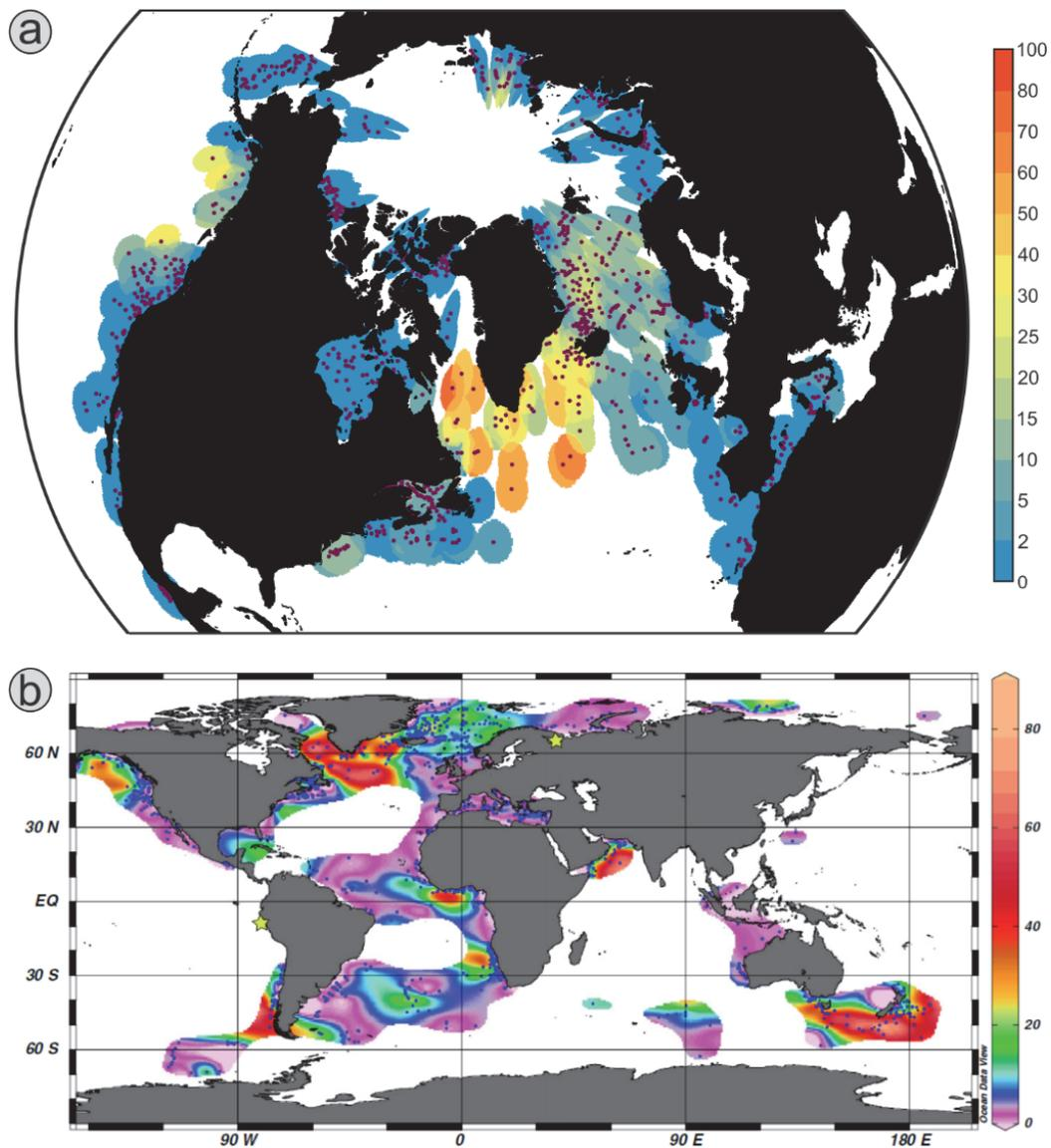


Figure 17 : Cartes de distribution (en pourcentages) de *Nematosphaeropsis labyrinthus* (a) dans la base de données modernes $n = 1207$, carte construite sous ARCGIS et (b) issue de l'atlas mondial de Zonneveld et al. (2013).

- *Brigantedinium* spp. (Figure 18 ; Planche 1) : *B. simplex* et *B. cariacoense* constituent des espèces ubiquistes hétérotrophes, dont les abondances relatives maximales se retrouvent principalement dans les environnements néritiques subarctiques à arctiques, et dont la présence semble être étroitement liée à la disponibilité en nourriture.

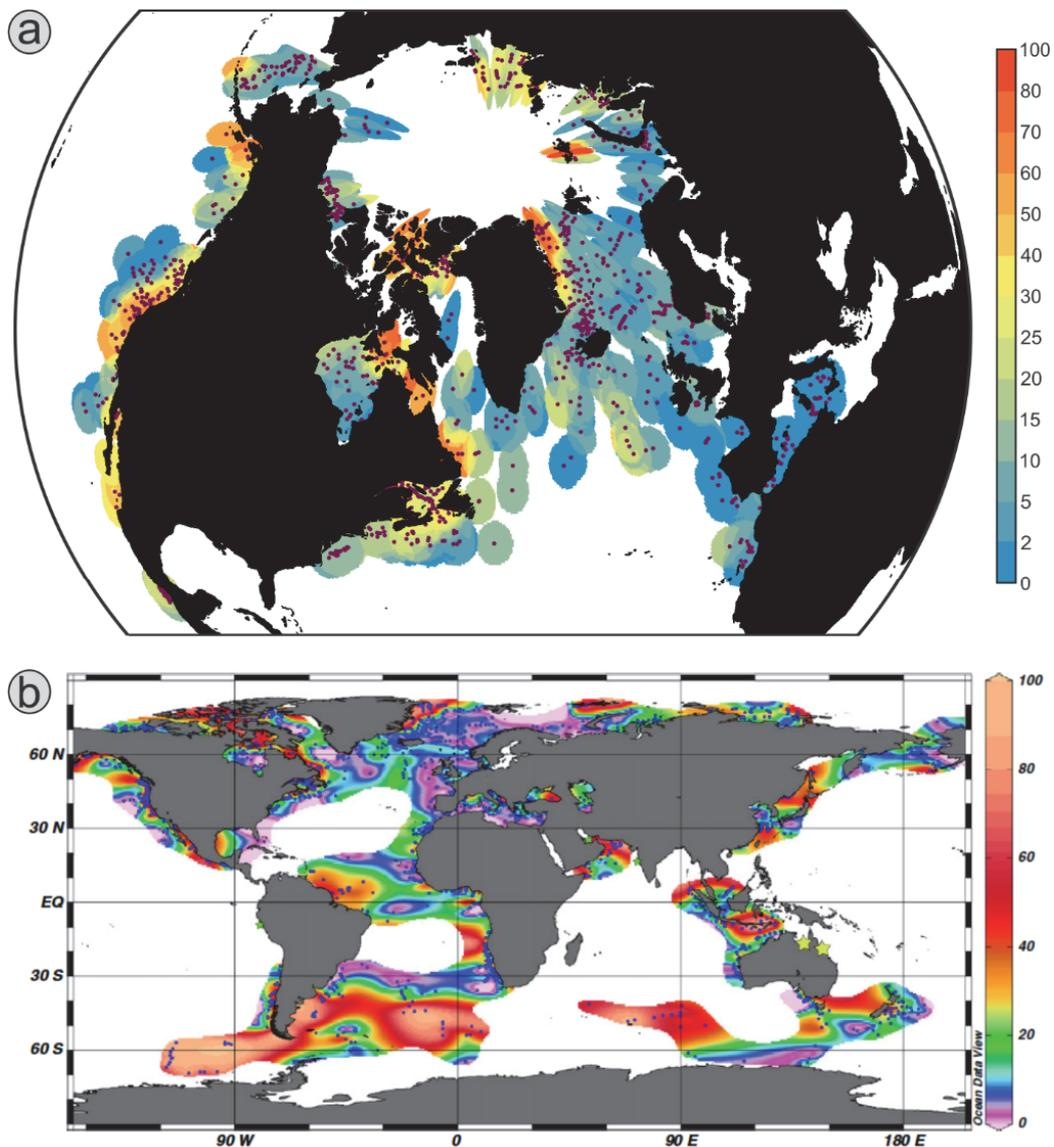


Figure 18 : Cartes de distribution (en pourcentages) de *Brigantedinium* spp. (a) dans la base de données modernes $n = 1207$, carte construite sous ARCGIS et (b) issue de l'atlas mondial de Zonneveld et al. (2013).

- *Lingulodinium machaerophorum* (Figure 19 ; Planche 2) : taxon tempéré à tropical, présent aussi bien dans les milieux estuariens saumâtres que dans les domaines néritiques à salinité normale, mais semblant affectionner les eaux de surface (saisonnement) stratifiées telles qu'au débouché des fleuves, dans les fjords, ...

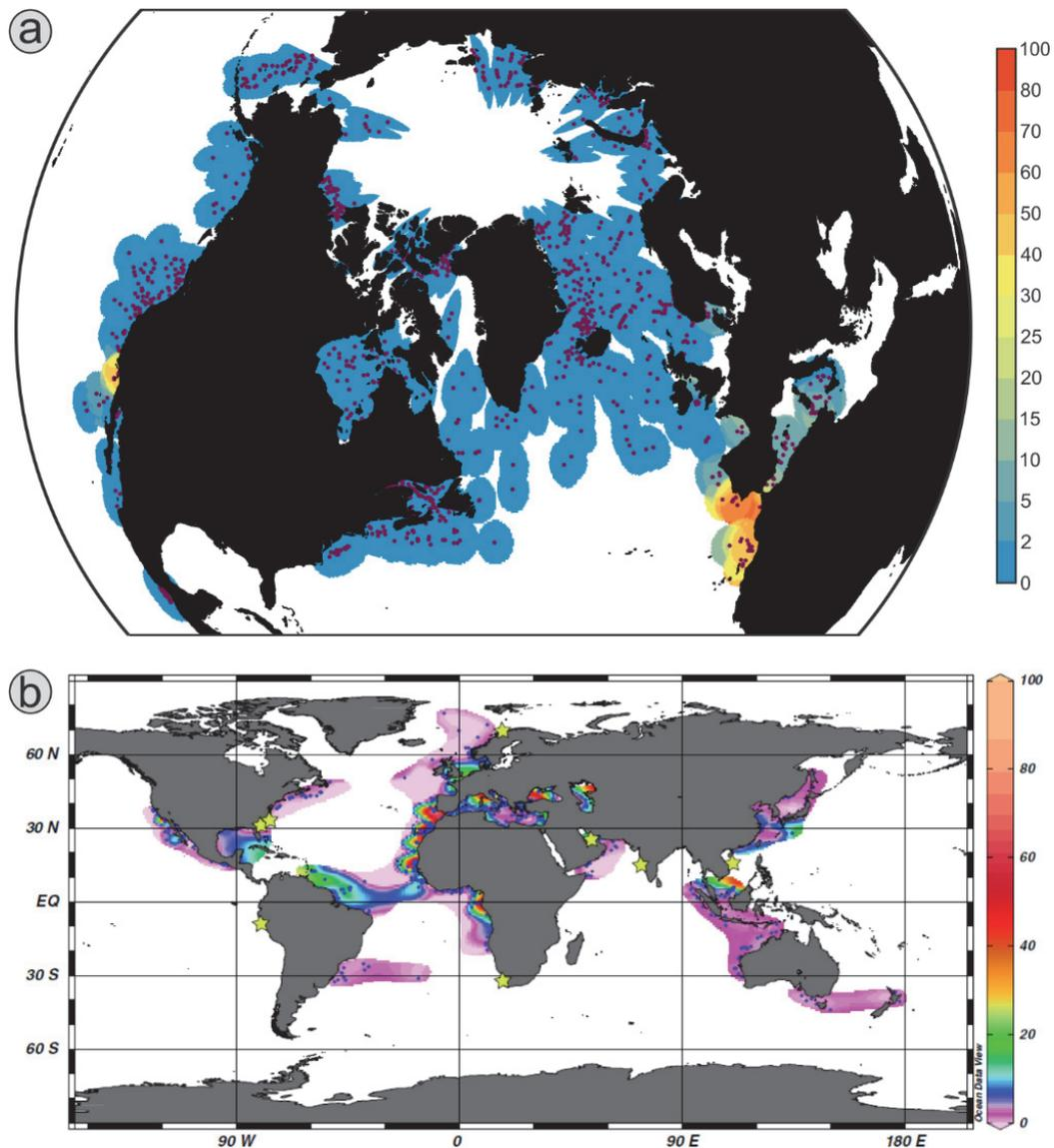


Figure 19 : Cartes de distribution (en pourcentages) de *Lingulodinium machaerophorum* (a) dans la base de données modernes $n = 1207$, carte construite sous ARCGIS et (b) issue de l'atlas mondial de Zonneveld et al. (2013).

- *Spiniferites ramosus* (Figure 20 ; Planche 2) : espèce cosmopolite présente aussi bien en domaine néritique qu'océanique, supportant une large gamme de température/salinité/durée de couvert de glace, mais limitée au Sud de 70°N.

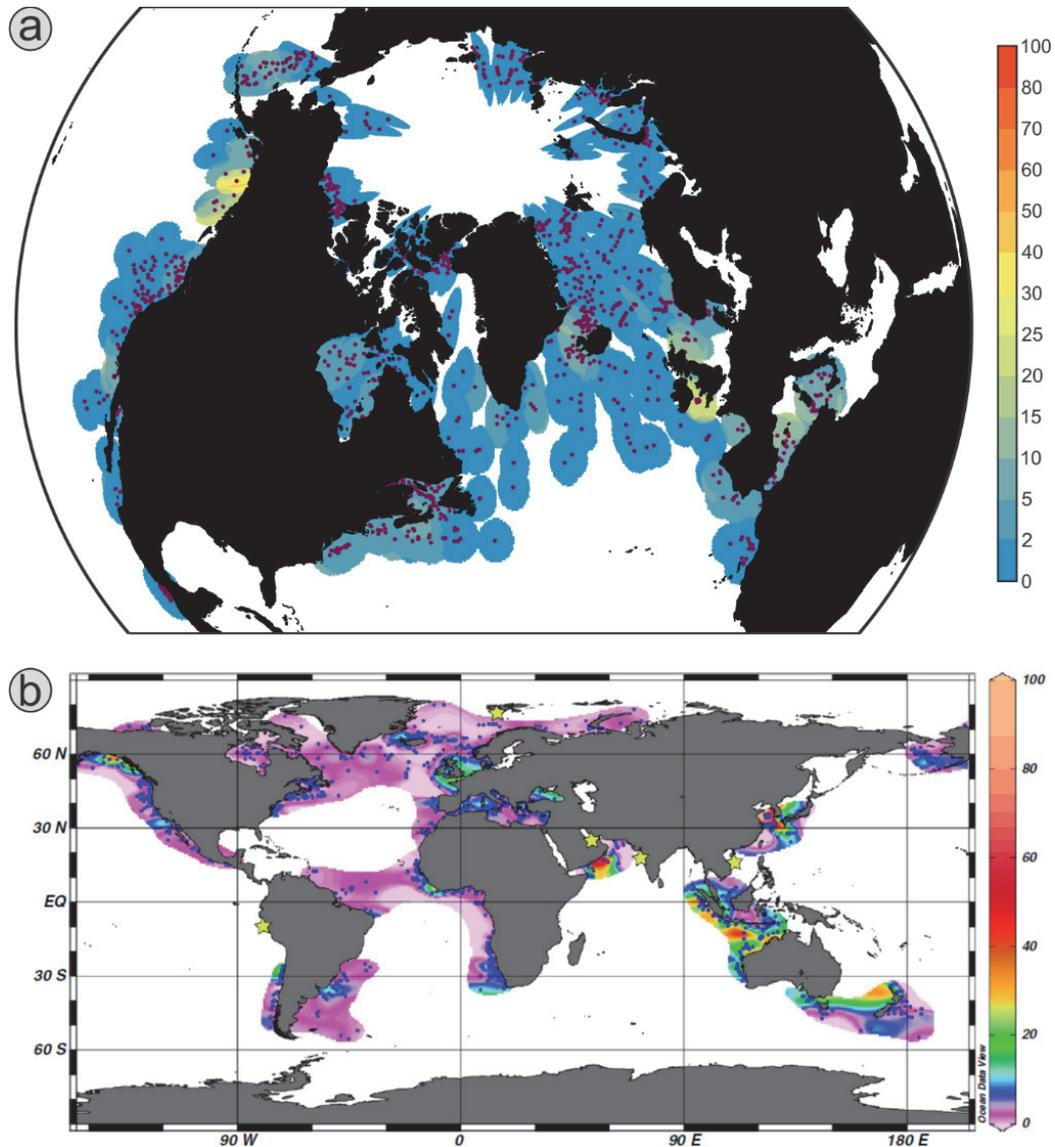


Figure 20 : Cartes de distribution (en pourcentages) de *Spiniferites ramosus* (a) dans la base de données modernes $n = 1207$, carte construite sous ARCGIS et (b) issue de l'atlas mondial de Zonneveld et al. (2013).

- *Spiniferites elongatus/S. frigidus* (Figure 21 ; Planche 2) : *S. frigidus* apparaît comme une espèce polaire peuplant des eaux de surface < 4°C, alors que *S. elongatus* peut être considéré comme une espèce tempérée fraîche supportant une plus large gamme de températures.

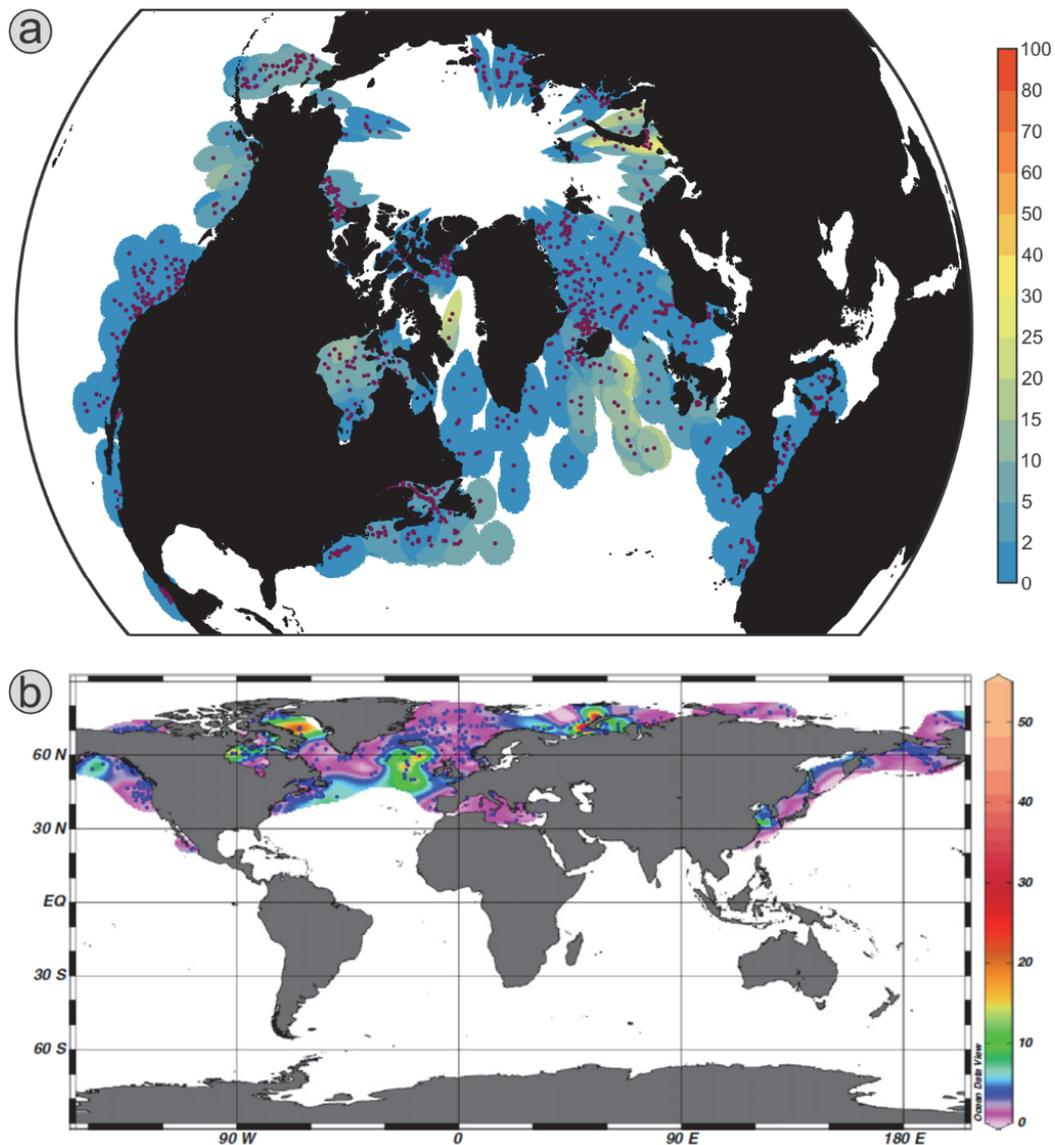


Figure 21 : Cartes de distribution (en pourcentages) de *Spiniferites elongatus/S. frigidus* (a) dans la base de données modernes $n = 1207$, carte construite sous ARCGIS et (b) issue de l'atlas mondial de Zonneveld et al. (2013).

- *Impagidinium pallidum* (Figure 22 ; Planche 1) : taxon franchement océanique colonisant les domaines polaires à subpolaires, il peut être considéré comme un indicateur de conditions de surface froides de type océan ouvert.

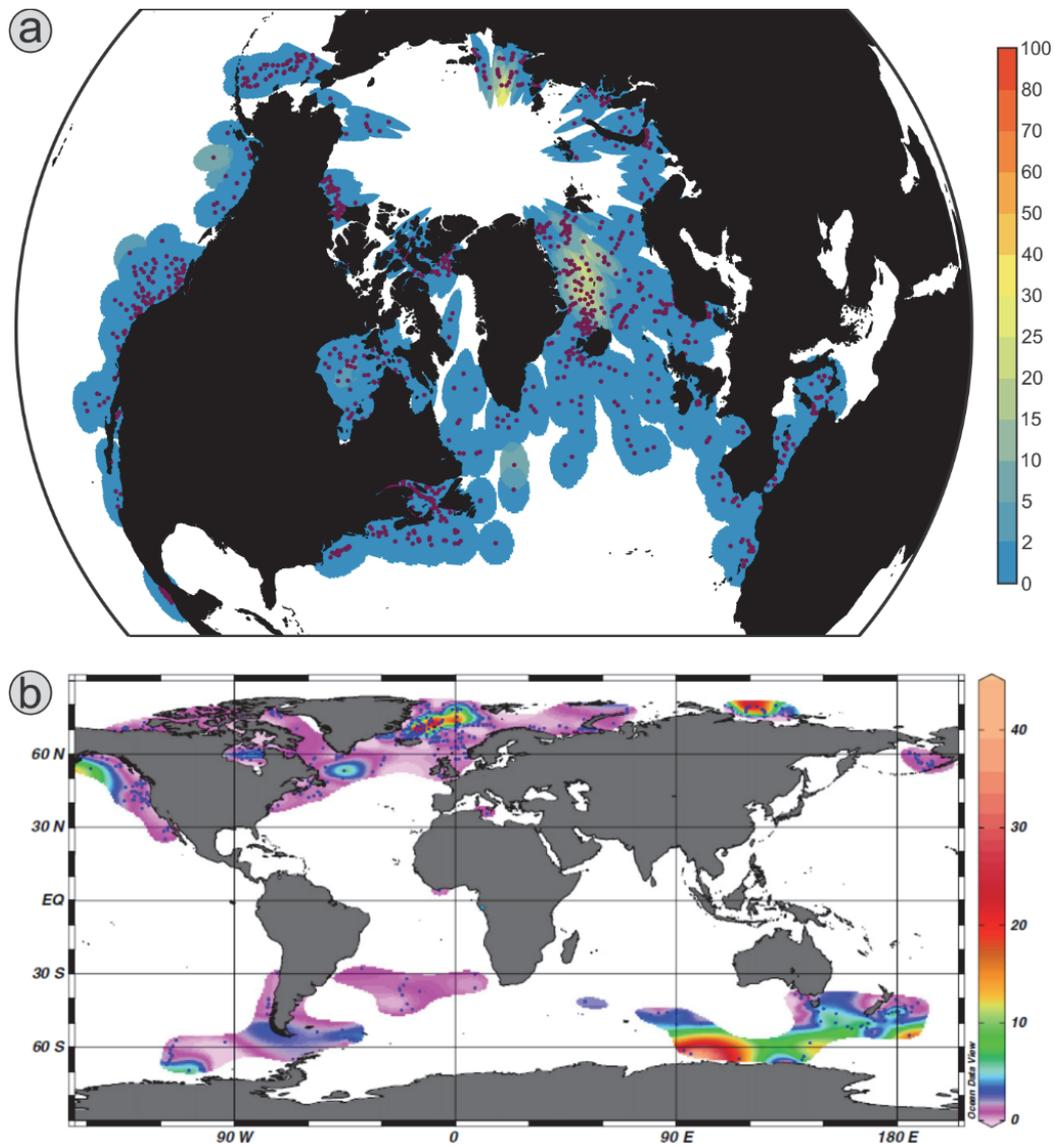


Figure 22 : Cartes de distribution (en pourcentages) d'*Impagidinium pallidum* (a) dans la base de données modernes $n = 1207$, carte construite sous ARCGIS et (b) issue de l'atlas mondial de Zonneveld et al. (2013).

- *Selenopemphix quanta* (Figure 23 ; Planche 2) : taxon hétérotrophe cosmopolite, essentiellement concentré autour de 60°N dans l'Atlantique Nord.

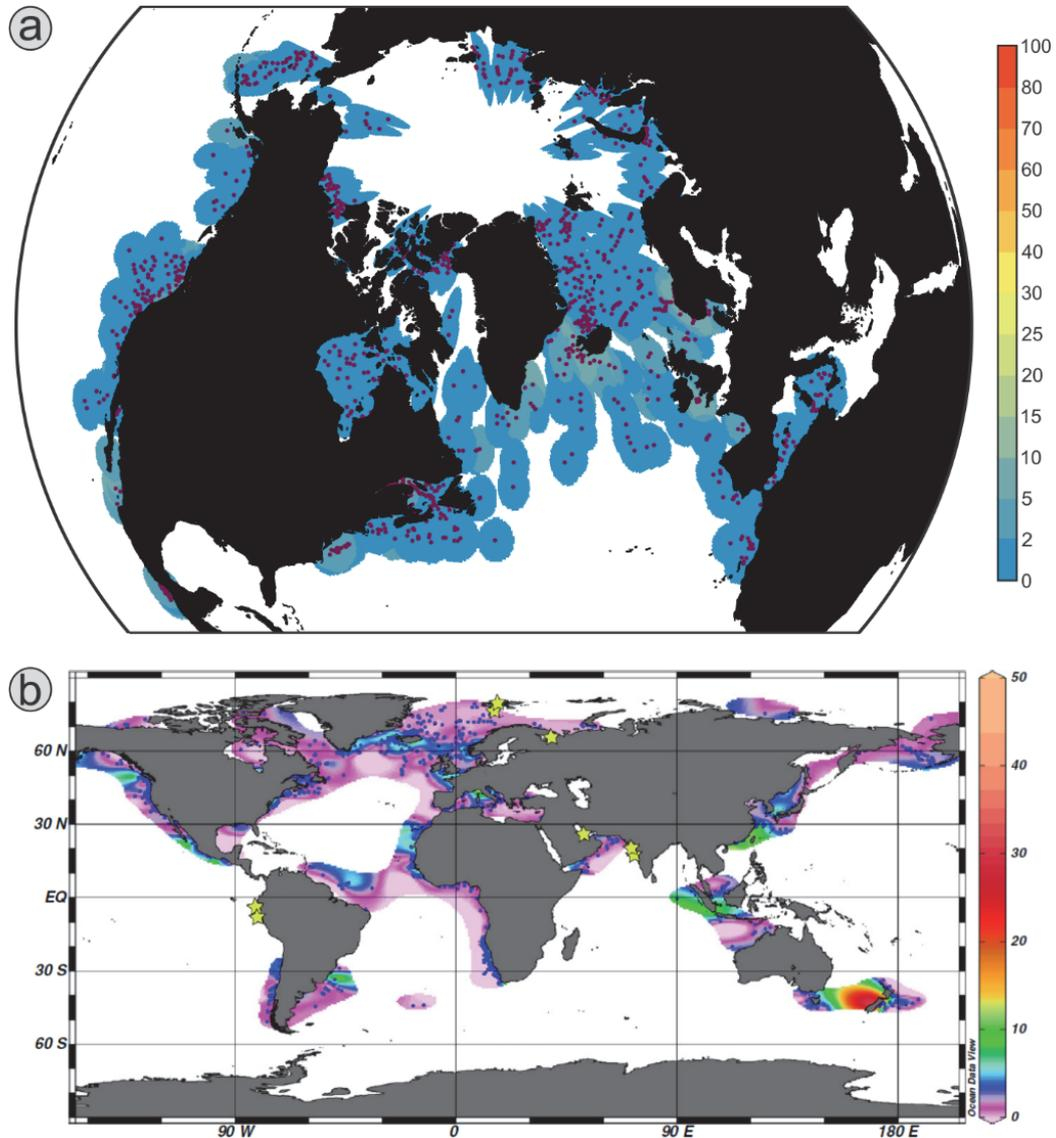


Figure 23 : Cartes de distribution (en pourcentages) de *Selenopemphix quanta* (a) dans la base de données modernes $n = 1207$, carte construite sous ARCGIS et (b) issue de l'atlas mondial de Zonneveld et al. (2013).

- *Echinidinium granulatum* (Figure 24 ; Planche 2) : rare taxon hétérotrophe présent en domaines équatorial à subpolaire, marin à estuarien, et caractérisés par une productivité primaire relativement élevée (Radi et al., 2013).

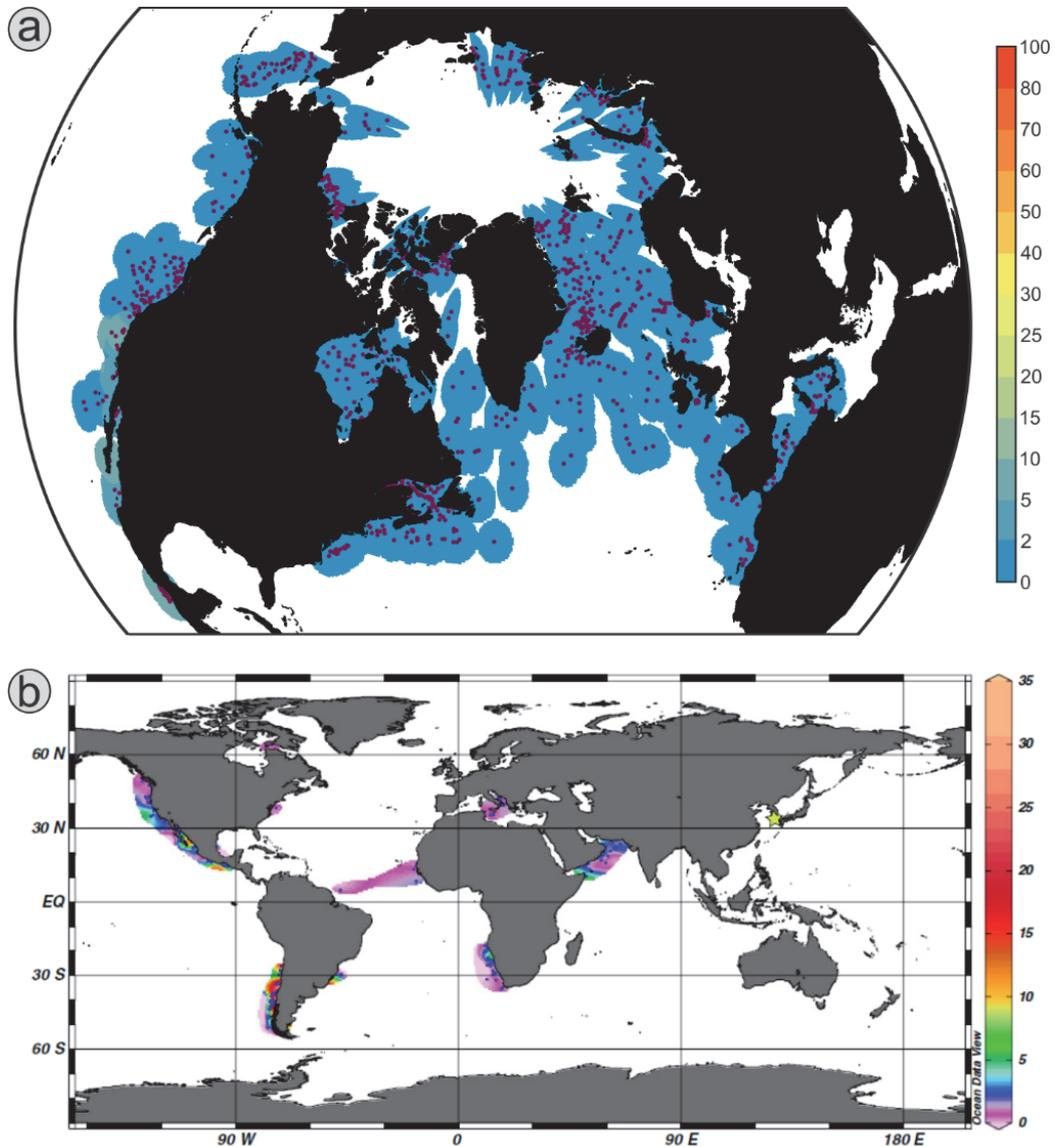


Figure 24 : Cartes de distribution (en pourcentages) d'*Echinidinium granulatum* (a) dans la base de données modernes $n = 1207$, carte construite sous ARCGIS et (b) issue de l'atlas mondial de Zonneveld et al. (2013).

- *Polykrikos schwartzii* sensu Bütschli, 1873 (i.e. *Polykrikos kofoidii* (Chatton 1914) sensu Matsuoka et al., 2009 ; Figure 25 ; Planche 2) : espèce tempérée fraîche à subpolaire présente dans une large gamme d'environnements océaniques francs à côtiers.

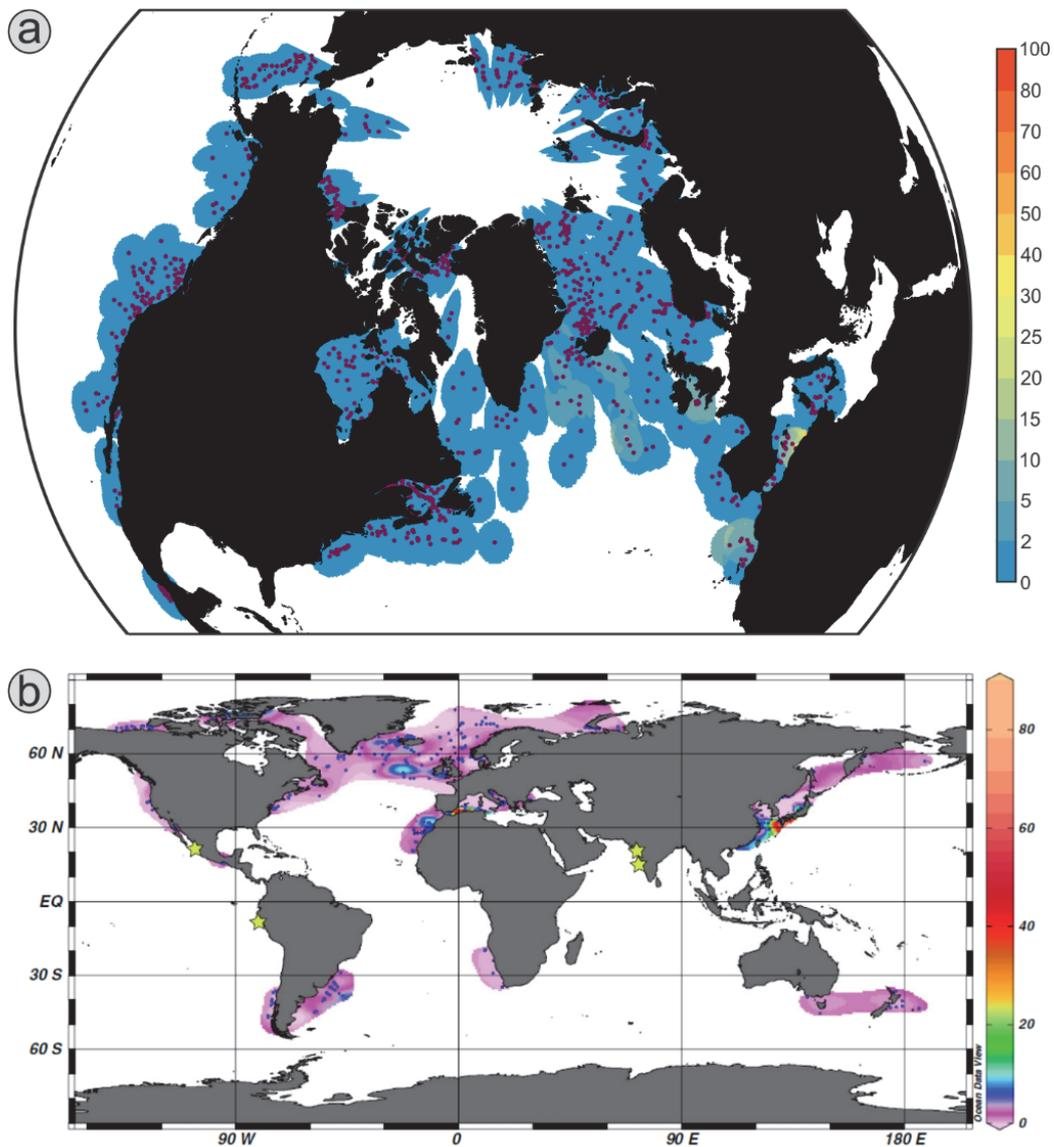


Figure 25 : Cartes de distribution (en pourcentages) de *Polykrikos schwartzii* sensu Bütschli, 1873 (a) dans la base de données modernes $n = 1207$, carte construite sous ARCGIS et (b) issue de l'atlas mondial de Zonneveld et al. (2013).

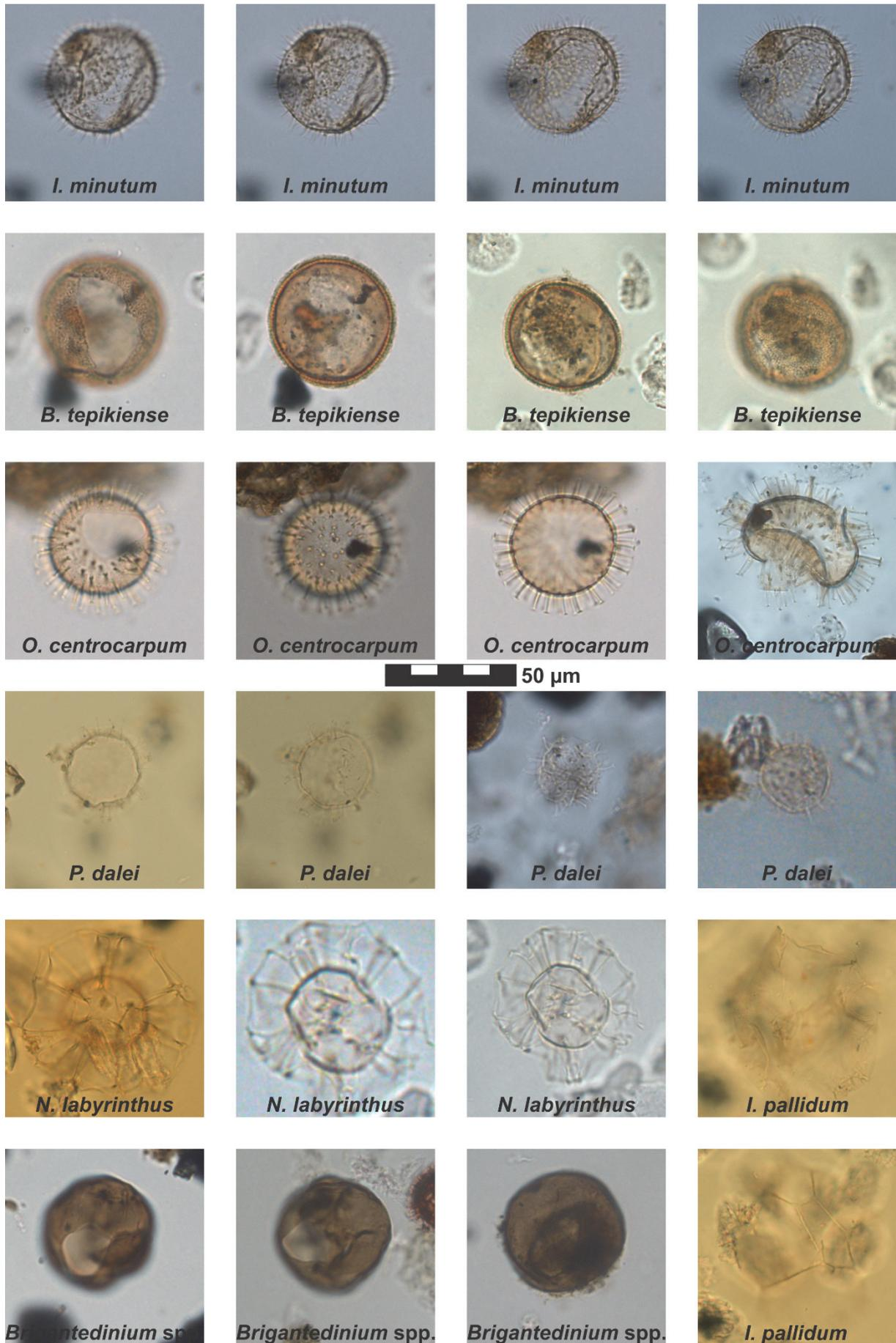


Planche 1 : Micro-photographies de certains taxons de dinokystes rencontrés dans cette thèse.

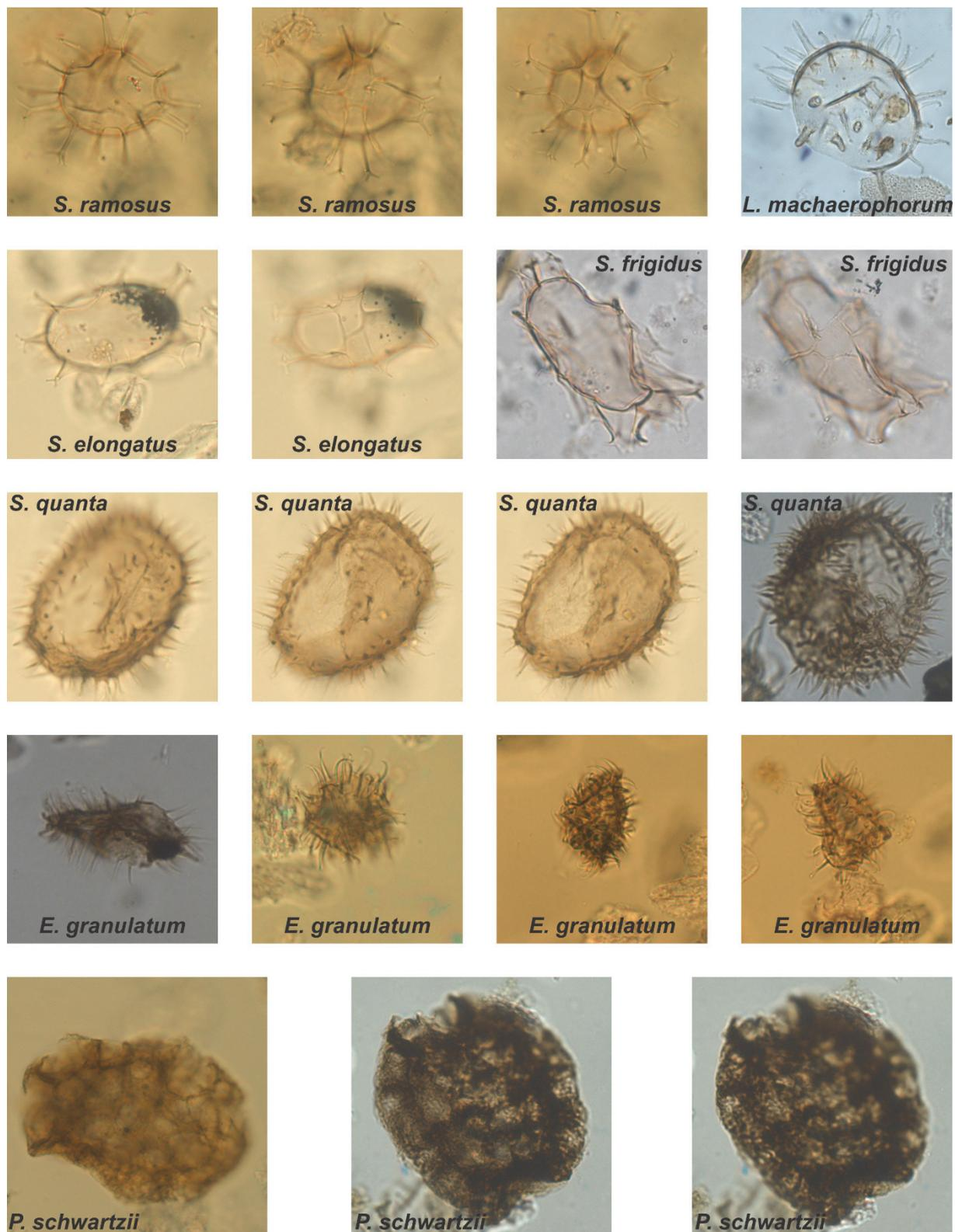


Planche 2 : Micro-photographies de certains taxons de dinokystes rencontrés dans cette thèse.

3. Reconstructions des conditions de surface passées : fonction de transfert

L'application de fonctions de transfert aux assemblages fossiles de dinokystes (mais également aux assemblages d'autres organismes tels que les foraminifères planctoniques) permet d'obtenir des reconstructions quantifiées des paramètres environnementaux caractérisant le milieu de vie de ces organismes. Cette approche repose sur le principe de l'actualisme, qui suppose que les relations liant paramètres biotiques et abiotiques n'ont pas changé au cours du temps. Concrètement, toute fonction de transfert compare les assemblages fossiles contenus dans les archives sédimentaires, à des assemblages modernes contenus dans des échantillons de sédiments de surface. Ces assemblages modernes sont répertoriés dans une base de données qui combine, pour chaque échantillon/site de surface, assemblages et paramètres environnementaux actuels correspondants (e.g. température, salinité, ... issus d'atlas océanographiques modernes). Plusieurs méthodes de comparaison peuvent être utilisées, dont la méthode des meilleurs analogues (ou *Modern Analogue technique*, MAT, voir [Guiot & de Vernal, 2007, 2011a,b](#) pour une revue complète de la méthode et de ses limites). Les fonctions de transfert basées sur la méthode MAT vont calculer la distance statistique, ou coefficient de dissimilarité, entre spectres fossiles et spectres modernes, et ainsi déterminer les N_x (souvent 5) meilleurs analogues modernes (i.e. ceux présentant les plus faibles distances statistiques). Ces fonctions de transfert permettent alors de calculer les paramètres environnementaux passés associés à l'assemblage fossile analysé par une moyenne pondérée des paramètres environnementaux modernes associés à chaque meilleur analogue ; cette pondération est calculée en multipliant chaque paramètre des N_x par l'inverse de la distance statistique correspondante, de manière à donner plus de poids au meilleur analogue.

Dans le cadre de cette thèse, pour les deux carottes étudiées, les assemblages de dinokystes ont été déterminés dans la fraction 10-150 μm après traitement palynologique des échantillons de sédiment (175 niveaux en tout) (protocole disponible à l'adresse suivante : http://www.epoc.u-bordeaux.fr/index.php?lang=fr&page=eq_paleo_pollens). Un minimum de 300 dinokystes, ou 1000 grains exotiques, ont été comptés dans chaque niveau lorsque cela était possible. L'identification des espèces est conforme à [Rochon et al. \(1999\)](#), [Head et al. \(2001\)](#), et [Radi et al. \(2013\)](#). Les abondances relatives de chaque espèce ont ensuite été calculées par rapport au nombre total de dinokystes quaternaires. Une fonction de transfert « spécial dinokystes » basée sur la méthode MAT a alors été appliquée aux assemblages de dinokystes en utilisant le logiciel R (version 2.7.0; <http://www.r-project.org/>), le script

« ReconstMAT » développé par J. Guiot (progiciel BIOINDIC, <https://www.eccorev.fr/spip.php?article389>). La base de données modernes utilisée ici inclut 1207 sites localisés dans les bassins Nord Atlantique, Arctique, sub-Arctique, méditerranéen, et Nord Pacifique (base de données présentée lors du workshop DINO9, <http://pcwww.liv.ac.uk/~dino9/workshops.html>, paramètres environnementaux utilisés issus de la version 2001 du *World Ocean Atlas* et de données fournies par le *National Snow and Ice Data Center*). Parmi les reconstructions quantifiées fournies par cette fonction de transfert, celles utilisées dans cette thèse sont :

- les SST moyennes estivales (Juillet-Août-Septembre) et hivernales (Janvier-Février-Mars), avec des incertitudes (ou erreurs moyennes de prédiction / *root mean square errors of prediction* – RMSEP) respectives de 1.5 °C et 1.05 °C.
- les salinités de surface (SSS, *sea-surface salinities*) moyennes estivales et hivernales (RMSEP respectives de 2.4 et 2.3 psu).
- la durée moyenne annuelle du couvert de glace de mer (RMSEP de 1.2 mois/an).

Section 2. Autres palynomorphes

Plusieurs autres palynomorphes ont été identifiés et comptés en parallèle des dinokystes modernes. Il s'agit des dinokystes remaniés (i.e. provenant de formation géologiques anté-quadernaires), des colonies de *Pediastrum* spp., et des *Halodinium* spp.

Ces palynomorphes (et notamment leurs concentrations absolues) constituent des indicateurs d'apports allochtones d'origine fluviale / continentale (e.g. [Matthiessen et al., 2000](#) ; [Zaragosi et al., 2001](#) ; [Eynaud et al., 2007](#) ; [Penaud et al., 2009](#)). En effet, les dinokystes remaniés peuvent être transportés du continent à l'océan via les icebergs ou par transport fluvial (incluant les panaches d'eau de fonte glaciaire, e.g. [Rahman, 1995](#) ; [Eynaud et al., 2007](#)). Les algues d'eau douce de type *Pediastrum* spp. et *Halodinium* spp. semblent quant à elles être exclusivement amenées jusqu'aux zones côtières par transport (glacio-) fluvial (e.g. [Mudie, 1992](#)). Elles peuvent être par la suite acheminées vers des secteurs plus profonds à travers divers processus de remaniement des sédiments côtiers. Par exemple, les saumures libérées lors de la formation de glace de mer côtière peuvent induire une remise en suspension des sédiments côtiers puis le transport de ces sédiments vers des domaines plus profonds ([Matthiessen et al., 2000](#)). Les sédiments ainsi remis en suspension peuvent

également être incorporés à la glace de mer néo-formée par « *basal-freezing* » puis être acheminés vers des sites plus profonds lors du vêlage et de la fonte de cette glace de mer (e.g. Mudie, 1992 ; Matthiessen et al., 2000). Les courants côtiers, ainsi que les processus gravitaires affectant le haut de pente, peuvent également être envisagés comme des vecteurs potentiels de remaniement et de transport de ces sédiments et palynomorphes non produits *in situ*.

Section 3. $\delta^{18}\text{O}$ dans les tests de foraminifères planctoniques

De nombreuses études focalisées sur la variabilité climatique rapide de la dernière période glaciaire et conduites dans l'Atlantique Nord subpolaire (incluant les mers adjacentes) utilisent le rapport isotopique de l'oxygène ($\delta^{18}\text{O}$) contenu dans les tests de foraminifères planctoniques (PF) comme indicateur hydrologique de la masse d'eau dans laquelle ils se sont développés. Dans ces études, les variations de $\delta^{18}\text{O}$ (généralement mesuré sur *N. pachyderma* senestre) ont souvent été reliées aux variations de salinité induites par les décharges d'eau douce liées à la fonte des icebergs (e.g. Bond et al., 1992, 1993 ; Cortijo et al., 1997). Cependant, il est important de rappeler que le $\delta^{18}\text{O}$ planctonique est également fonction des températures océaniques locales et du volume global de glace stocké sur les continents (e.g. Shackleton, 1974 ; Malaizé & Caley, 2009). Par ailleurs, de récentes études ont démontré que le $\delta^{18}\text{O}$ mesuré sur *N. pachyderma* senestre pouvait également être influencé par la production de saumures, appauvries en $\delta^{18}\text{O}$, lors de la formation de glace de mer, et inversement par les eaux de fonte de cette glace de mer, enrichies en $\delta^{18}\text{O}$ malgré leur faible salinité (e.g. Dokken & Jansen, 1999 ; Hillaire-Marcel & de Vernal, 2008).

Dans le cadre de cette thèse, des mesures de $\delta^{18}\text{O}$ ont été effectuées sur des échantillons monospécifiques de *N. pachyderma* senestre (200-250 μm), l'espèce de PF la plus abondante dans les carottes étudiées, et dont la profondeur de calcification dans la zone d'étude se situe entre quelques dizaines de mètres et environ 250 mètres de profondeur (e.g. Carstens et al., 1997 ; Simstich et al., 2003 ; Peck et al., 2008 ; Jonkers et al., 2010b). Ces mesures ont été réalisées au laboratoire EPOC avec un spectromètre de masse « Optima Micromass ». Etant donné les différents facteurs influençant le $\delta^{18}\text{O}$ planctonique, et le cadre temporel et géographique dans lequel s'inscrivent nos travaux de recherche, l'interprétation de ces signaux dans les deux carottes étudiées n'est pas triviale. Néanmoins, notre approche multi-

proxy fournit de précieux indices permettant souvent d'identifier la principale source responsable des variations de $\delta^{18}\text{O}$.

Par ailleurs, pour la carotte MD99-2281, nous avons tenté d'estimer les variations locales du $\delta^{18}\text{O}$ de l'eau de mer ($\delta^{18}\text{O}_{\text{SW}}$). Les variations locales de ce signal sont liées aux variations locales de salinité. Elles se surimposent aux variations globales de ce signal, liées aux variations du volume global de glace continentale. Le $\delta^{18}\text{O}$ des tests carbonatés permet d'accéder à ce signal, puisqu'il est lui-même fonction du $\delta^{18}\text{O}_{\text{SW}}$ (global + local) et de la température océanique locale. Pour estimer les variations locales du $\delta^{18}\text{O}_{\text{SW}}$, nous avons donc utilisé l'équation de paléo-température développée successivement par Epstein & Mayeda (1953) puis Shackleton (1974), et qui relie le $\delta^{18}\text{O}_{\text{SW}}$ (local + global), le $\delta^{18}\text{O}$ de tests carbonatés ($\delta^{18}\text{O}_{\text{C}}$) et la température de calcification (T) comme suit : $T = 16.9 - 4.38 (\delta^{18}\text{O}_{\text{C}} - \delta^{18}\text{O}_{\text{SW}}) + 0.13 (\delta^{18}\text{O}_{\text{C}} - \delta^{18}\text{O}_{\text{SW}})^2$. Appliquant tout d'abord la même méthodologie que Duplessy et al. (1991), nous avons utilisé le $\delta^{18}\text{O}$ mesuré sur *N. pachyderma* senestre en tant que $\delta^{18}\text{O}_{\text{C}}$, et les reconstructions de température d'été issues de l'application d'une fonction de transfert aux assemblages de PF (cf. Section 1, Partie 3 de ce chapitre), corrigées de 2.5 °C, en tant que T (cette correction empirique de 2.5 °C, issue des travaux de Duplessy et al., 1991, reflétant la différence entre températures d'été et température moyenne estimée de calcification du taxon *N. pachyderma* senestre). Nous avons alors suivie la méthodologie récemment décrite par Malaizé & Caley (2009) pour extraire le signal local de $\delta^{18}\text{O}_{\text{SW}}$. Pour cela, nous avons corrigé le signal de $\delta^{18}\text{O}_{\text{SW}}$ (local + global) précédemment obtenu des variations globales de $\delta^{18}\text{O}_{\text{SW}}$ fournies par les travaux de Waelbroeck et al. (2002). L'ensemble de ces manipulations permettent ainsi d'obtenir un signal de variations locales du $\delta^{18}\text{O}_{\text{SW}}$, qui peut être considéré comme un indicateur des changements locaux de salinité à la profondeur de calcification de *N. pachyderma* senestre. Cette méthodologie n'a pas été appliquée à la carotte MD99-2285, pour laquelle les reconstructions de température ne montrent pas de variations significatives sur la dernière période glaciaires car issues d'assemblages de PF quasiment monospécifiques.

Section 4. Granularité du sédiment et mesure de calcimétrie

L'analyse de la granularité du sédiment fournit de précieuses informations sur les processus sédimentaires affectant les dépôts (en termes de sources, de dépôt, d'érosion, ...).

Dans le cas de séquences sédimentaires affectées par un courant profond, ce type d'analyse permet de reconstruire les variations d'intensité de ce courant. Ceci repose sur le fait que les courants profonds vont avoir pour effet de trier les particules sédimentaires, de telle sorte que plus les courants sont forts, plus les particules sédimentaires vont être grossières (d'une part, parce que ces courants vont transporter et déposer des particules plus grossières, et d'autre part parce que, si ces courants sont suffisamment intenses, ils vont vanner les particules fines, e.g. [McCave et al., 1995a](#); [McCave, 2007](#)). Ainsi, dans le but de reconstituer les variations d'intensité du courant profond transportant l'ISOW, des mesures de granularité du sédiment ont été effectuées sur les deux carottes étudiées, toutes deux situées sur le trajet de ce courant profond. Ces mesures ont été réalisées au laboratoire EPOC avec un granulomètre laser de type Malvern (MASTER SIZER S). Une grande partie de ces analyses a été réalisée par M. Sabine lors d'un stage co-encadré par S. Zaragosi et moi-même.

Les analyses ont été effectuées sur des échantillons de sédiment bruts. Néanmoins, il est communément admis que les variations d'apports biogènes (i.e. les variations de productivité primaire) pourraient diluer les apports terrigènes (qui seraient quant à eux principalement issus du courant profond) et ainsi biaiser les reconstructions d'intensité du courant profond (e.g. [McCave et al., 1995b](#)). Aussi, afin de s'assurer que ces mesures de granularité sur sédiment brut reflètent bien la granularité de la fraction terrigène, des mesures de calcimétrie ont été effectuées dans les deux carottes, et des mesures de granularité ont été effectuées sur une vingtaine d'échantillons ayant subi au préalable un traitement chimique permettant d'éliminer les fractions organique (ajout d' H_2O_2 à 35%) et carbonatée (ajout d' HCl à 10%). Ce set d'échantillons a été prélevé sur la carotte MD99-2281 (celle contenant les plus forts taux de $CaCO_3$; [Figure 26](#)), sur la section de cette carotte présentant les plus grandes variations du taux de $CaCO_3$ ([Figure 27](#)), et sur des niveaux pour lesquels la granularité a également été mesurée sur des échantillons bruts.

Les mesures de calcimétrie ont permis de définir une droite de calibration commune aux deux carottes (et pouvant probablement être étendue à l'ensemble de la zone d'étude si nécessaire) permettant de convertir les concentrations relatives en Ca obtenues par mesures de fluorescence X (XRF) sur l'appareil XRF du NIOZ (données fournies par T. Richter, cf. Partie 3, Section 4) en taux de $CaCO_3$ ([Figure 26](#)). L'application de cette calibration à l'ensemble des signaux de Ca (XRF) obtenus sur les deux carottes étudiées révèle que le taux de $CaCO_3$ reste inférieur à 30 % sur la section étudiée de la carotte MD99-2281 ([Figure 27](#)), et inférieur à 12 % sur la section étudiée de la carotte MD99-2285 ([Figure 28](#)).

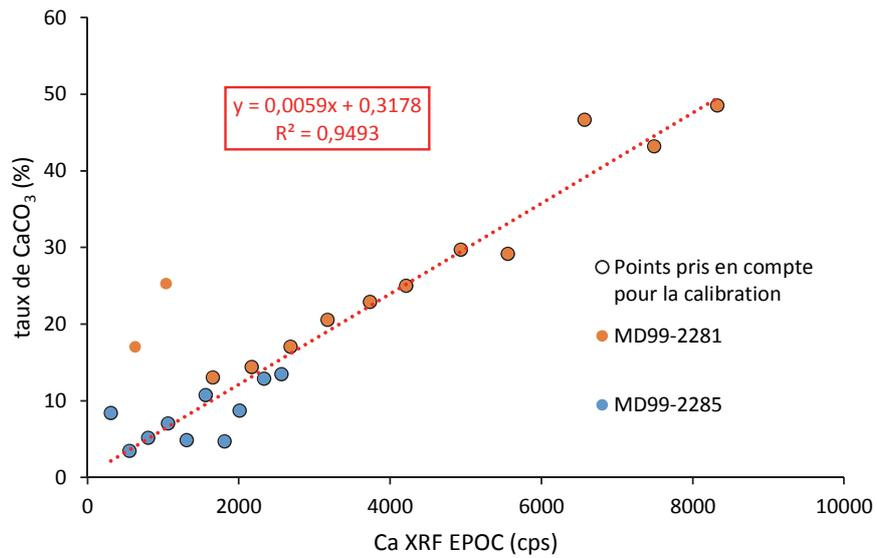


Figure 26 : Résultat des mesures de calcimétrie et droite de calibration Ca (XRF NIOZ) – taux de $CaCO_3$

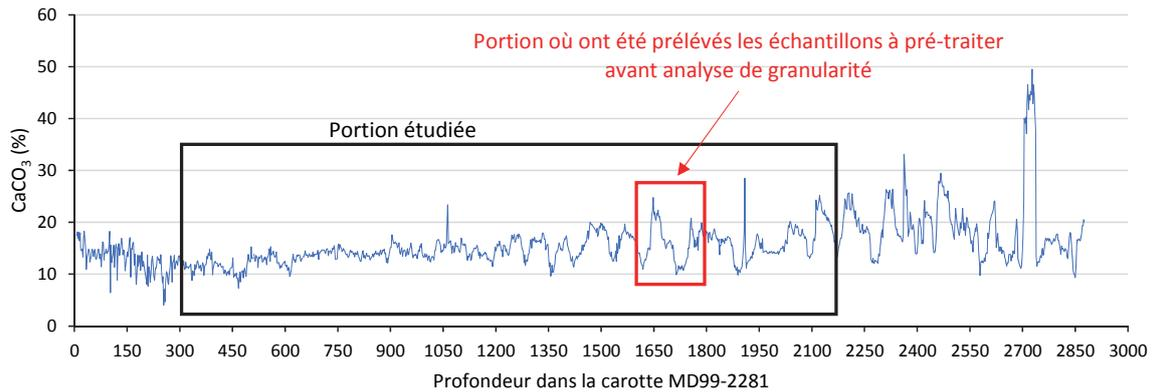


Figure 27 : Evolution du taux de $CaCO_3$ d'après calibration XRF dans la carotte MD99-2281

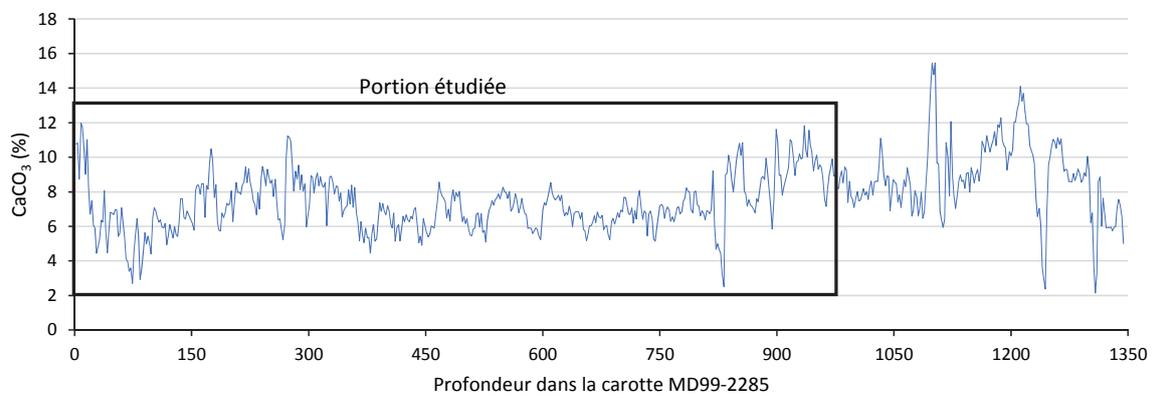


Figure 28 : Evolution du taux de $CaCO_3$ d'après calibration XRF dans la carotte MD99-2285

La comparaison des données granulométriques obtenues sur les échantillons bruts et sur les échantillons pré-traités révèle une étonnante correspondance entre ces deux jeux de données (cf. Chapitre 3, Partie 1, Section 1, Fig. 4). Ceci atteste que les données granulométriques obtenues sur les échantillons de sédiments bruts reflètent bien la distribution granulométrique de la fraction terrigène contenue dans ces échantillons, et constituent donc un indicateur valide de l'intensité du courant profond transportant l'ISOW. Cela signifie par ailleurs que les apports biogènes ne sont pas suffisamment conséquents comparés aux apports terrigènes issus du courant profond pour les diluer (malgré des taux de CaCO_3 pouvant atteindre 25% sur la section testée), ou bien que la fraction terrigène et la fraction biogène sont toutes deux affectées de la même façon par le courant profond. La deuxième option est assez problématique pour les reconstructions paléoenvironnementales basées sur les outils micropaléontologiques. Néanmoins, comme mentionné en Section 1 de ce chapitre, plusieurs éléments issus des analyses menées dans le cadre de cette thèse nous permettent d'établir que nos assemblages n'ont pas significativement souffert d'un éventuel remaniement par les courants profonds.

Bien que l'ensemble de la distribution granulométrique du sédiment soit indicatrice de l'influence du courant profond, elle témoigne également des autres processus affectant les dépôts, comme par exemple les apports d'IRD. Ces influences annexes peuvent rendre la lecture du signal total assez complexe, aussi certains paramètres granulométriques sont souvent calculés et utilisés pour accéder plus facilement aux variations d'intensité des courants profonds. Généralement, la fraction de taille principalement affectée par le courant profond est la fraction silteuse (10 – 63 μm), et les paramètres granulométriques principalement utilisés sont donc logiquement la taille moyenne de la fraction silteuse et le rapport entre fraction silteuse grossière (26 – 63 μm) et fraction silteuse fine (10 – 26 μm) (e.g. McCave et al., 1995a,b ; McCave, 2007 ; Bianchi & McCave, 1999 ; Hodell et al., 2009). Néanmoins, lorsque le courant profond est peu intense comme sur le site MD99-2285, la fraction argileuse à finement silteuse (0.5 – 10 μm , ou 0.5 – 20 μm) peut constituer un meilleur indicateur, notamment en environnement glaciaire influencé par des apports d'IRD (e.g. Prins et al., 2002 ; Snowball & Moros, 2003 ; Ballini et al., 2006). De ce fait, les principaux paramètres granulométriques utilisés dans le cadre de cette thèse pour estimer les variations d'intensité de l'ISOW diffèrent sur les deux carottes étudiées (paramètres de la fraction silteuse pour la carotte MD99-2281, et paramètres de la fraction < 20 μm pour la carotte MD99-2285).

Section 5. Mg/Ca dans les tests de foraminifères planctoniques

Dans le but d'étoffer notre approche multi-proxies par des outils supplémentaires de reconstructions de températures océaniques, et qui plus est pour palier au fait que ces reconstructions issues des assemblages de PF sur la carotte MD99-2285 ne révèlent aucune variation significative sur la dernière période glaciaire, des mesures Mg/Ca ont été effectuées sur des échantillons monospécifiques de *N. pachyderma* senestre provenant de cette carotte. Cette méthode est basée sur le principe suivant : l'incorporation préférentielle de l'élément Mg *versus* Ca dans les tests de PF dépend de la température de la masse d'eau dans laquelle ils calcifient. Les différents travaux menés sur cette méthode ont permis d'établir des relations empiriques reliant température et ratio Mg/Ca de manière exponentielle, où les coefficients des équations des courbes de calibration varient en fonction de l'espèce considérée (e.g. Nürnberg et al., 1996 ; Elderfield & Ganssen, 2000 ; Anand et al., 2003).

Le laboratoire EPOC disposant de l'appareil nécessaire à la réalisation de ces mesures (ICP-OES acquis par T. Corrège dans le cadre de l'ANR « EL PASO »), mais la méthode « Mg/Ca sur PF » n'y étant pas pratiquée, une grande partie de mon travail de thèse a consisté à mettre en place et développer cette méthode au sein du laboratoire EPOC, avec le soutien technique de P.-Y. Gourves et L. Thiao-Layel, et l'aide du LSCE (N. Caillon et H. Rebaubier).

1. Principe général de la méthode de dosage du Mg/Ca sur les tests de PF via ICP-OES

Les mesures du ratio Mg/Ca dans les tests de PF consistent à :

- Mettre en solution les éléments constituant les tests de foraminifères, en ayant au préalable éliminé les restes de sédiment et de matière organique emprisonnés dans les loges.
- Analyser les solutions ainsi produites pour chaque échantillon, ainsi que des solutions standards de concentrations connues, avec un ICP-OES (*Induction Coupled Plasma – Optical Emission Spectrometer*).
 - ↳ Principe de l'ICP-OES (Figure 29): La solution peut être prélevée par le passeur automatique, ou le tuyau de prélèvement inséré manuellement dans l'échantillon. La pompe péristaltique permet alors d'entraîner la solution dans le circuit jusqu'au couple nébuliseur-chambre de nébulisation où la

solution va être vaporisée. Cette solution vaporisée va alors être entraînée jusqu'à un plasma d'argon, où elle va être ionisée. Lors de cette ionisation, chaque atome va émettre un photon dont la longueur d'onde lui est caractéristique. Ces photons vont alors être détectés par l'analyseur (spectromètre d'émission optique), qui va quantifier le nombre de photons pour chaque longueur d'onde, i.e. pour chaque élément chimique.

- Déterminer les concentrations élémentaires (Mg, Ca, et autres éléments souhaités, notamment les éléments indicateurs de pollution / altération du Mg/Ca), et les ratios recherchés, en établissant les équations de calibration à partir des mesures des solutions standards.

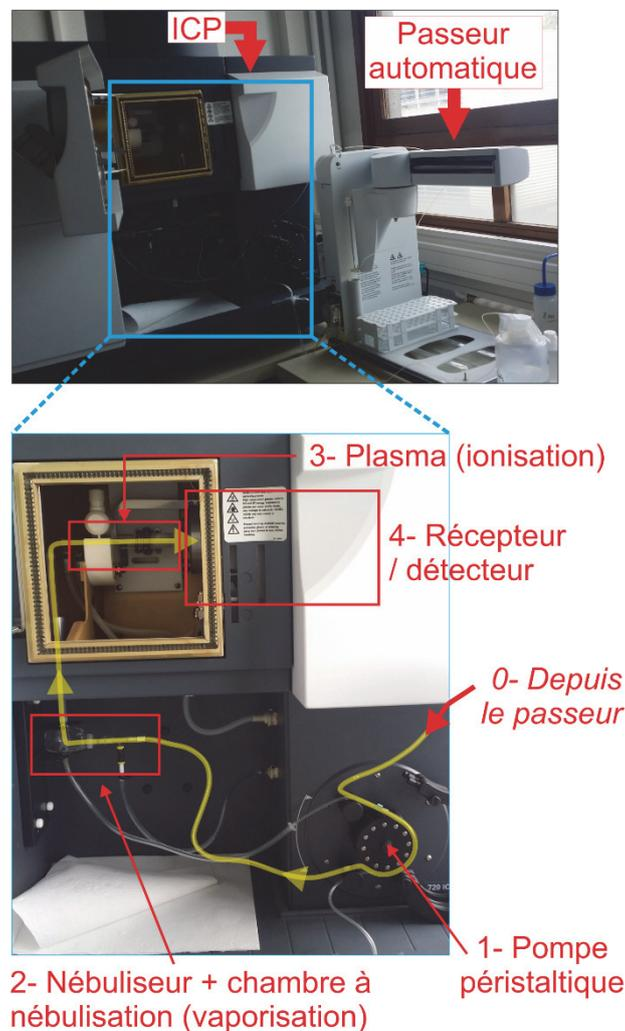


Figure 29 : Schéma de fonctionnement d'un ICP-OES

2. Résumé synthétique du développement de méthode

2.1. Optimisation du dosage

Le principal objectif technique était de pouvoir réaliser des mesures justes et répétables (Figure 30), la justesse et la répétabilité des mesures dépendant de divers facteurs techniques (concentration proche de la limite de quantification, stabilisation du plasma, temps d'analyse, qualité de la gamme étalon, ...). Une solution (appelée « *Ice-pacman* ») composée de PF, dissous dans de l'acide HNO₃ 0.075M, dans les mêmes proportions que celles utilisées dans le cadre de mesures classiques, a été fabriquée en grande quantité et utilisée tout au long du développement de cette méthode afin de pouvoir estimer et comparer la justesse et la répétabilité des mesures entre les différentes configurations testées.

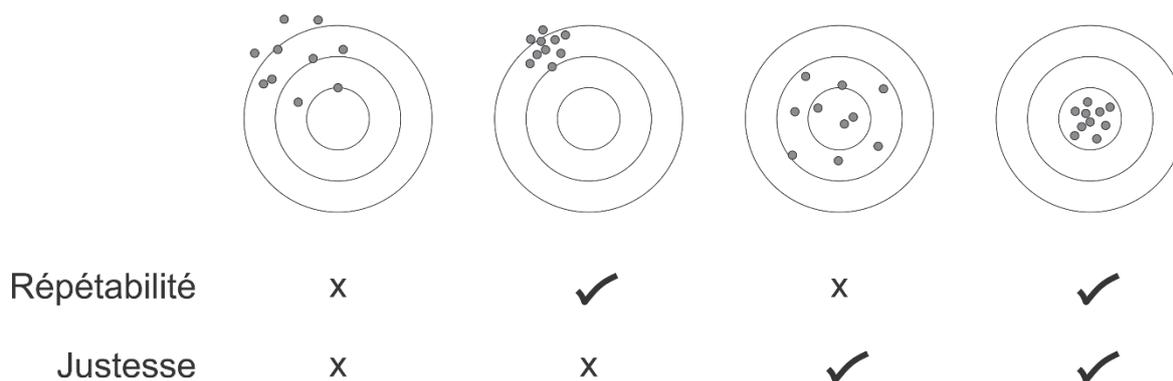


Figure 30 : Notions de justesse et de répétabilité

Les étapes de l'optimisation du dosage sont décrites très succinctement ci-dessous. Pour chaque étape/configuration testée, différents paramètres en plus de ceux décrits ci-dessous ont été testés et optimisés (débit du nébuliseur, délai de prélèvement, délai de stabilisation, nombre de répliques, durée de chaque réplique, temps de rinçage).

- 1^{ère} configuration testée : passeur + nébuliseur *sea-spray* + chambre *double-pass* + avec ou sans pompe péristaltique (sans la pompe, le passeur est directement connecté au nébuliseur, et l'échantillon est alors entraîné par effet venturi) = matériel disponible à EPOC et utilisé dans le cadre des mesures Mg/Ca et Ba/Ca dans les coraux.

- ↳ Résultats : le fait de ne pas utiliser la pompe péristaltique fournit de meilleurs résultats (meilleure répétabilité) et réduit le volume de solution nécessaire à l'analyse. Néanmoins, dans cette configuration, le volume minimal de solution nécessaire à l'analyse (1.1 mL) implique des solutions dont la concentration maximale en Ca ([Ca]) est de 25 ppm. Or, de Villiers et al. (2002) indique que la [Ca] optimale pour avoir des mesures justes doit être comprise entre 40 et 60 ppm. Ceci est lié au fait que dans les tests de PF, la [Ca] est plusieurs centaines à plusieurs milliers de fois supérieure à la concentration des autres éléments, ce qui induit un « effet de matrice ». Cet effet de matrice perturbe la mesure des concentrations des autres éléments et donc des ratios (dont le Mg/Ca). D'après de Villiers et al. (2002), cet effet de matrice serait minimum pour une [Ca] comprise entre 40 et 50 ppm.
- ↳ Conclusion : nécessité de mettre au point une nouvelle méthode / configuration permettant d'analyser des volumes plus faibles (< 0.5 mL) et/ou des concentrations plus élevées.

- 2^{ème} configuration testée : nébuliseur ultrasonique (disponible à EPOC) + chambre *double-pass* + avec/sans pompe péristaltique
 - ↳ Résultats : le nébuliseur ultrasonique permet d'abaisser la limite de quantification de l'appareil et d'analyser des échantillons plus dilués, le fait de ne pas utiliser la pompe péristaltique permet bien de diminuer le volume nécessaire à l'analyse. Néanmoins, les volumes nécessaires restent beaucoup trop importants.
 - ↳ Conclusion : le nébuliseur ultrasonique ne convient pas.

- 3^{ème} configuration testée : 1^{ère} configuration, avec un « volume mort » (c'est-à-dire le volume de solution non analysé mais nécessaire pour effectuer le circuit d'analyse) optimisé, i.e. des tuyaux raccourcis au maximum. Objectif de cette étape : évaluer l'influence de la pompe péristaltique et optimiser son utilisation, en faisant varier la vitesse de la pompe ou en la court-circuitant (effet venturi).
 - ↳ Résultats : le fait de diminuer la vitesse de la pompe permet de diminuer le volume de solution nécessaire, mais fournit des mesures moins répétables. Si l'on supprime la pompe, on diminue le volume nécessaire et on augmente la répétabilité. Toutefois, le temps analytique et le volume nécessaires restent trop élevés.

- ↳ Conclusion : Il est nécessaire de ne pas utiliser la pompe péristaltique, mais ce n'est pas suffisant.

- 4^{ème} configuration testée : nébuliseur *micromist* + chambre *simple-pass* + tuyaux raccourcis + avec/sans passeur. Le nébuliseur et la chambre de nébulisation ont été achetés spécialement pour les PF car ils permettent de réduire le débit dans le circuit d'analyse.
 - ↳ Résultats : Les débits sont effectivement plus faibles. Mais, avec le passeur, le volume nécessaire reste trop élevé. Le fait d'enlever le passeur permet de réduire au maximum le « volume mort », implique un volume minimal de solution de 0.4 mL par analyse, et fournit des mesures justes et répétables.
 - ↳ Conclusion : Cette 4^{ème} configuration, sans le passeur, permet d'effectuer des mesures Mg/Ca sur PF justes et répétables, mais les échantillons sont introduits manuellement.

- 5^{ème} configuration testée : nébuliseur *micromist* + chambre *simple-pass* + tuyaux raccourcis ET de diamètre plus fin + passeur et pompe péristaltique, dans le but d'automatiser les analyses.
 - ↳ Résultats : Le volume nécessaire par analyse est beaucoup trop élevé.
 - ↳ Conclusion : Les analyses vont devoir être effectuées en manuel (i.e. avec la 4^{ème} configuration testée). Le passage en automatique nécessiterait l'achat d'un micro-passeur (~ 10 k€).

2.2. Gammes étalons et certifiés

Une fois la méthode mise au point, il a été nécessaire d'élaborer des gammes étalons, indispensables à la calibration des mesures et leur conversion en concentration. Etant donné que les mesures sont effectuées de manière optimale lorsque la [Ca] est comprise entre 40 et 60 ppm, il est nécessaire de mesurer deux fois chaque série d'échantillons : une première fois (« run 1 ») pour quantifier leur [Ca] initiale, puis une deuxième fois (« run 2 ») où tous les échantillons sont dilués de telle sorte à ce que leur [Ca] soit égale à ~ 40 ppm et où leur ratio Mg/Ca est alors estimé. Par ailleurs, il est également nécessaire de quantifier la concentration d'autres éléments, dits éléments mineurs, indicateurs de pollution du ratio Mg/Ca (e.g. [Mn])

et [Fe], qui vont traduire la présence d'oxydations secondaires susceptibles d'altérer le ratio Mg/Ca).

Ainsi, plusieurs gammes étalon ont dû être établies : (i) une gamme à différentes [Ca] (utilisées pour les runs 1 et 2), (ii) une gamme avec [Ca] ~ 40 ppm et différents ratio Mg/Ca (et autres ratios recherchés ; run 2), et (iii) une gamme avec différentes concentrations en éléments mineurs (run 2). Chaque gamme comporte un « blanc », constitué uniquement de l'acide ayant servi à préparer chaque gamme étalon.

La conception de ces gammes s'est fortement inspirée de celles utilisées au LSCE, où Ca, Mg et Sr sont des éléments majeurs (les ratios recherchés étant Mg/Ca et Sr/Ca), et Al, Fe, Ba, Li, Mn, Ti, ZN, K, NA, et Si sont des éléments mineurs. A la différence du LSCE, nous avons choisi d'utiliser le Ba comme élément majeur dans le but de quantifier avec précision le ratio Ba/Ca, récemment identifié comme potentiel proxy d'apports d'eau douce (e.g. [Hall & Chan, 2004](#)).

Il a par ailleurs été nécessaire d'introduire un certifié lors de nos analyses, afin de garantir la justesse de nos résultats et de corriger toute éventuelle dérive de l'appareil. Le matériel que nous avons choisi d'utiliser en tant que certifié pour nos analyses est le BAM-RS3 (échantillon fourni par le LSCE) qui est issu de calcite (donc proche de la composition des PF) et qui dispose de [Ca], [Mg] et [Sr] certifiées. Le ratio Mg/Ca de ce composé n'est quant à lui pas certifié (sa valeur calculée à partir des concentrations certifiées est de 0.8 mmol/mol), mais il a fait l'objet d'une inter-calibration entre laboratoires qui a fourni une valeur moyenne entre 0.77 et 0.78 mmol/mol (les valeurs minimale et maximale mesurées étant respectivement de 0.671 et 0.847 mmol/mol ; [Greaves et al., 2008](#)).

2.3. Méthodes de calibration

Il existe deux méthodes de calibration. La première est la méthode dite des concentrations. Elle consiste à calculer les ratios élémentaires à partir des concentrations élémentaires calculées automatiquement par le logiciel de l'ICP. En effet, pour chaque élément, le logiciel de l'ICP détermine la droite de calibration reliant les intensités relatives mesurées (en coups par seconde) et les concentrations absolues connues (rentrées dans le logiciel en ppm) des différents standards et blanc de chaque gamme étalon ([Figure 31](#)). Il applique alors ces équations de calibration aux intensités relatives mesurées pour chaque

élément et dans chaque échantillon, et les convertit en concentrations absolues. Le calcul des ratios élémentaires se fait alors en appliquant la formule suivant : $X/Ca = (([X]/[Ca]) \cdot (M_X/M_{Ca})) \cdot 1000$ où X/Ca est le ratio de l'élément X sur l'élément Ca (en mmol/mol), $[X]$ et $[Ca]$ sont les concentrations élémentaires en X et en Ca (en ppm, i.e. mg/L, calculées automatiquement par le logiciel), et M_X et M_{Ca} sont les masses molaires de X et de Ca (en g/mol).

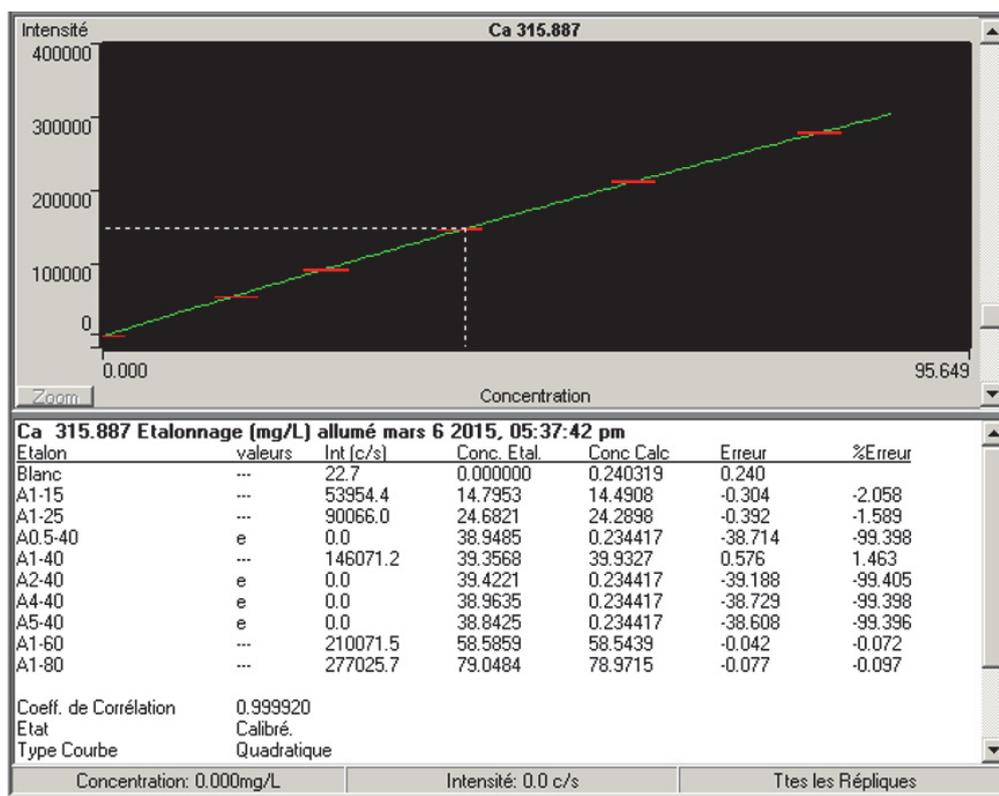


Figure 31 : Capture d'écran du logiciel de l'ICP illustrant la détermination des droites de calibration (en vert) à partir des intensités relatives mesurées pour chaque standard (en rouge) de la gamme étalon.

La deuxième méthode est la méthode dite des ratios d'intensité, décrite par de Villiers et al. (2002), et qui, d'après ces auteurs, fournirait de meilleurs résultats. Elle consiste à (i) déterminer les droites de calibrations reliant les ratios R d'intensité des standards aux valeurs supposées / « connues » des ratios élémentaires correspondants, puis (ii) d'appliquer ces droites de calibrations aux ratios R d'intensité des échantillons, et ainsi déterminer leurs ratios élémentaires en mmol/mol. Pour le ratio Mg/Ca par exemple, le ratio R d'intensité des standards est défini comme suit : $R[Mg/Ca]_{standard} = [(Int_Mg)_{standard} - (IntMg)_{blanc_std}] / [(IntCa)_{standard} - (IntCa315)_{blanc_std}]$ où $(Int_X)_{standard}$ est l'intensité mesurée pour l'élément X et

dans chaque standard, et $(Int_X)_{blanc_std}$ est l'intensité mesurée pour l'élément X dans le blanc de la gamme étalon. Le ratio R d'intensité des échantillons est alors défini comme suit : $R[Mg/Ca]_{échantillon} = [(Int_Mg285)_{échantillon} - (IntMg285)_{blanc_éch}] / [(IntCa315)_{échantillon} - (IntCa315)_{blanc_éch}]$ où $(Int_X)_{échantillon}$ est l'intensité mesurée pour l'élément X dans l'échantillon, et $(Int_X)_{blanc_éch}$ est l'intensité mesurée pour l'élément X dans le blanc de la série d'échantillon. Cette méthode est illustrée dans la Figure 32.

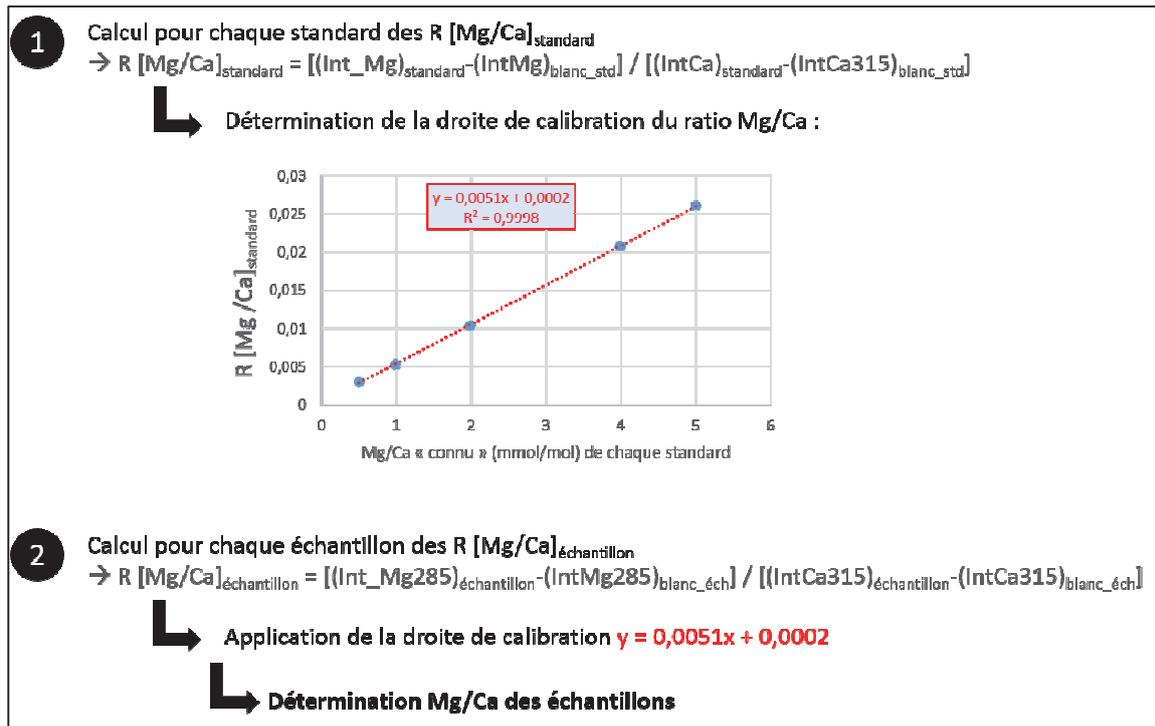


Figure 32 : Illustration de la méthode de calibration dite des ratios d'intensité.

La comparaison des deux méthodes à partir de l'analyse répétée de BAM-RS3 (matériel certifié) semble indiquer que les deux méthodes fournissent des résultats similaires et justes (Tableau 3). La longueur d'onde de Mg considérée (279, 280 ou 285) semble avoir peu d'importance, les différences entre les ratios Mg/Ca correspondants étant faibles. Néanmoins, le nombre relativement limité de mesures effectuées nous empêche de conclure de manière définitive à ce sujet. Il serait donc pertinent de mettre en œuvre de nouveaux tests.

Valeurs de références du BAM-RS3		Mg/Ca (mmol/mol)	
Calculé (Greaves et al., 2008) à partir des concentrations		0,8	
Mesuré dans différents laboratoires (inter-calibration ; Greaves et al., 2008)		Min.	0,671
		Max.	0,847
		Moyenne	entre 0,774 et 0,777

	Mesures du BAM-RS3 à EPOC	Mg(285)/Ca(315) (mmol/mol)		Mg(280)/Ca(315) (mmol/mol)		Mg(279)/Ca(315) (mmol/mol)		Toutes les valeurs issues de la méthode des concentrations	Toutes les valeurs issues de la méthode des ratios d'intensité
		Méth. Conc.	Méth. Ratio Intensité	Méth. Conc.	Méth. Ratio Intensité	Méth. Conc.	Méth. Ratio Intensité		
1	26/02/2015	0,78710855	0,77752336	0,76639837	0,7694701	0,76625114	0,7757663		
2	25/03/2015	0,78747922	0,80448021	0,75899354	0,78472804	0,77170525	0,79110918		
3	09/04/2015	0,77071968	0,80928811	0,75598036	0,80804771	0,75143308	0,79760696		
4	09/04/2015	0,77751754	0,81645219	0,75566676	0,80772033	0,74796899	0,79398708		
5	09/04/2015	0,77484481	0,81361755	0,7515057	0,80332733	0,74746894	0,79345803		
6	09/04/2015	0,77398839	0,8127359	0,75310484	0,80502143	0,74851557	0,79455677		
7	09/04/2015	0,77348685	0,81218857	0,75555522	0,80759415	0,74935663	0,79542994		
8	09/04/2015	0,76395203	0,80212196	0,75787133	0,81003054	0,75190569	0,79809733		
9	09/04/2015	0,77021124	0,80869395	0,75423751	0,80619817	0,75109821	0,79724968		
10	20/04/2015	0,78738925	0,77942737	0,76926822	0,77789019	0,76662763	0,7737022		
11	20/04/2015	0,78129868	0,77260204	0,77313937	0,78157195	0,76797212	0,77476872		
12	20/04/2015	0,78796893	0,77951288	0,77072019	0,7790564	0,76869302	0,77551041		
13	20/04/2015	0,78422224	0,77530713	0,77185396	0,78000738	0,77031901	0,77698508		
14	20/04/2015	0,7884176	0,77959943	0,77124516	0,7793376	0,77036771	0,77699983		
15	20/04/2015	0,77982016	0,77072837	0,77658657	0,78490949	0,77459368	0,78140812		
16	20/04/2015	0,78701923	0,77805987	0,76984154	0,77782378	0,77231409	0,7789584		
17	20/04/2015	0,77988441	0,77034661	0,76806137	0,77575627	0,77533461	0,78187427		
18	20/04/2015	0,7792089	0,76984602	0,77641987	0,78455413	0,77500192	0,78165808		
19	20/04/2015	0,78186525	0,77277016	0,77095472	0,77901067	0,7711557	0,77779086		
	Ecart-type	0,00714324	0,01818294	0,00856026	0,01402489	0,01082671	0,00921432	0,0117	0,0142
	Différence max.	0,02446557	0,04660617	0,02508087	0,04056044	0,02786568	0,02439513	0,0409	0,047
	Temp. équiv.	< 1°C	< 1°C	< 1°C	< 1°C	< 1°C	< 1°C	< 1°C	< 1°C

Tableau 3 : Comparaison des deux méthodes de calibration à partir des mesures réalisées sur du BAM-RS3.

2.4. Protocole de chimie

Le protocole de chimie utilisé pour préparer les échantillons avant les analyses est celui défini par Barker et al. (2003). Il se compose de plusieurs étapes, qui peuvent être décrites de manière synthétique comme suit :

- 1) « *Crushing* » → ouverture des loges en écrasant les PF entre deux lames de verre
 - ↳ Introduction de l'échantillon dans un micro-tube (type eppendorf) numéroté.
- 2) Extraction argiles → plusieurs rinçages à l'eau mQ (EmQ)
- 3) Extraction argiles récalcitrantes → 2 rinçages éthanol + 2 rinçages EmQ

- 4) Extraction matière organique → attaque H₂O₂ à chaud (bain-marie) + 2 rinçages EmQ
- 5) « Leaching » → attaque acide HNO₃ faible (0,001M) pour décontaminer l'échantillon + 2 rinçages EmQ
- 6) Dissolution → attaque acide HNO₃ « fort » (0,075M) → on obtient alors la solution mère (300 µL)
- 7) Prélèvement d'une partie de la solution mère et dilution facteur 4
 - ↳ 1^{er} RUN ICP
- 8) Dilution pour ramener tous les échantillons à [Ca] = 40 ppm
 - ↳ 2^{ème} RUN ICP

3. Mesures tests sur des échantillons de *N. pachyderma senestre* (carotte KI02 - MOCOSED2014)

Une fois la méthode d'analyse, le protocole de chimie et le protocole d'analyse mis en place, et les gammes étalons et certifié réalisés, des mesures « tests » ont été réalisées en conditions réelles sur des échantillons monospécifiques de *N. pachyderma senestre* issus de l'intervalle 1-2 cm de la carotte KI02 (74.5280 °N ; 12.0326 °E ; 2340 mètres de profondeur) prélevée à bord du Pourquoi Pas ? lors de la mission MOCOSED2014. Les spécimens ont été sélectionnés dans trois gammes de taille : 150 – 200 µm, 200-250 µm, et > 250 µm. Ils ont été traités selon le protocole de [Barker et al. \(2003\)](#) puis analysés selon la méthode mise au point à EPOC et décrite précédemment.

Les résultats issus de ces analyses révèlent que :

- **La méthode mise au point et les volumes de solution nécessaires associés sont adaptés** : il est possible d'analyser des échantillons à 40 ppm de [Ca] lors du run 2.
- **Les gammes étalons semblent adaptées**, exceptées pour le Ba. En effet, la [Ba] et le ratio Ba/Ca sont 10 fois plus élevés que les valeurs maximales fournies dans la littérature (et donc que les concentrations de notre gamme étalon, établie en fonction des valeurs fournis dans la littérature). Cela semble toutefois être lié au protocole de chimie utilisé, qui n'est pas adapté aux mesures Ba/Ca. En effet, les protocoles de chimie appliqués en amont des mesures Ba/Ca incluent une étape de dissolution de la baryte sédimentaire (e.g. [Hall & Chan, 2004](#)).
- Les valeurs obtenues sur le blanc de la série d'échantillons sont très faibles, ce qui suggère que **la préparation chimique est réalisée dans de bonnes conditions**

(solvants suffisamment purs, pas de contamination inter-échantillons lors des manipulations, *leaching* efficace, ...).

- Les mesures effectuées sur les spécimens 200-250 μm fournissent un Mg/Ca moyen de ~ 1.75 mmol/mol, soit ~ 11.7 °C d'après la calibration de Nürnberg et al., (1995) (calibration la plus adaptée car spécifique à *N. pachyderma* senestre et établie dans les Mers Nordiques). Cette valeur est supérieure à celle rencontrée actuellement en été au niveau du site KI02 (6.8°C d'après les données 2009 du WOA ; Locarnini et al., 2010), mais ne semble pas incohérente dans la mesure où les échantillons proviennent de l'intervalle 1-2 cm de la carotte.
- Il semblerait qu'il y ait un effet vital lié à la taille, mais le nombre trop limité de mesures effectuées nous empêche de l'affirmer.

4. Résultats des mesures sur la carotte MD96-2048 (stage T. Extier)

Dans le cadre de son stage de Master 1, T. Extier a réalisé quelques points de mesures Mg/Ca en utilisant la méthode développée dans le cadre de cette thèse. Les mesures ont été réalisées sur la carotte MD96-2048 (26.1747 °S ; 34.0191 °E ; 660 mètres de profondeur) prélevée au large de la côte Sud-Est africaine lors de la mission MOZAPHARE à bord du Marion Dufresne. Elles ont été effectuées sur des échantillons monospécifiques de *G. ruber alba sensu stricto* (250 – 315 μm) provenant des sections 1.1 – 1.2 Ma BP et 1.8 – 2 Ma BP de cette carotte. Les valeurs de Mg/Ca obtenues ont été traduites en températures océaniques de surface en utilisant la calibration d'Anand et al. (2003) spécifique à *G. ruber alba* 250-350 μm .

La comparaison des reconstructions quantitatives de SST ainsi obtenues avec les reconstructions quantitatives de SST obtenues en appliquant une fonction de transfert aux assemblages de PF (déterminés dans les mêmes niveaux, mais avec une meilleure résolution temporelle) révèle une étonnante similitude (Figure 33). Cette similitude conforte la validité de la méthode « Mg/Ca sur PF » mise au point à EPOC dans le cadre de cette thèse.

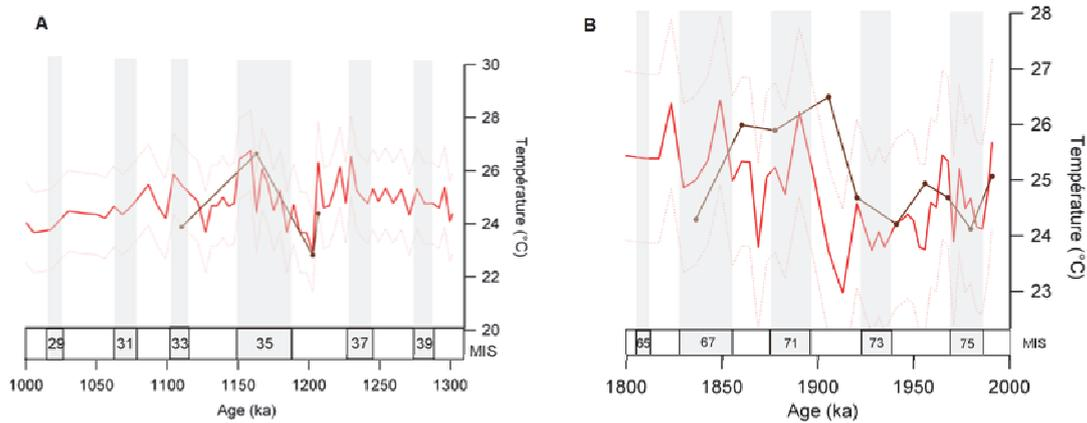


Figure 33 : Comparaison des signaux de température issus de la méthode Mg/Ca sur PF (courbes noires) et de la méthode fonction de transfert sur assemblages de PF (courbes rouges) sur les portions (a) 1 – 1.3 Ma BP et (b) 1.8 – 2 Ma BP de la carotte MD96-2048 (figure modifiée d’après Extier, 2015).

5. Résultats des mesures sur la carotte MD99-2285

Des mesures Mg/Ca sur *N. pachyderma* senestre (200-250 μm) ont été effectuées sur l’ensemble de la section étudiée de la carotte MD99-2285. Du fait de problèmes liés à la préparation chimique des échantillons, les mesures effectuées entre 0 et 290 cm (soit environ les derniers 25 ka cal BP) ne sont pas exploitables. Le reste des mesures (294 – 599 cm, soit ~ 25 – 41 ka cal BP) est toutefois exploitable. Ces résultats exploitables révèlent que sur de nombreux intervalles, souvent les GS et HS, les ratios Mg/Ca et températures équivalentes (calibration de Nürnberg et al., 1995) obtenus sont bien trop élevés sachant que les assemblages de PF de la carotte MD99-2285 sont composés à quasiment 100% de *N. pachyderma* senestre tout au long de la dernière période glaciaire (Figure 34). En effet, les mesures indiquent des températures Mg/Ca très souvent supérieures à 6 °C et pouvant même dépasser les 27°C comme à la fin de HS4, alors que les assemblages monospécifiques de PF indiquent plutôt des températures inférieures à 5 – 6 °C (cf. Figure 34d et références suivantes : Tolderlund & Bé, 1971 ; Carstens et al., 1997 ; Hillaire-Marcel & de Vernal, 2008). Ceci n’est pas surprenant dans la mesure où les mesures Mg/Ca peuvent être biaisées par de fortes dessalures et/ou de forts apports de particules détritiques (N. Caillon, *comm. pers.*). Les concentrations en éléments mineurs tendent d’ailleurs à prouver que les mesures Mg/Ca sont altérées sur ces intervalles. Ainsi, le signal de températures Mg/Ca obtenu sur cette carotte n’est pas exploitable, et ne sera donc pas utilisé dans la partie discussion de ce manuscrit.

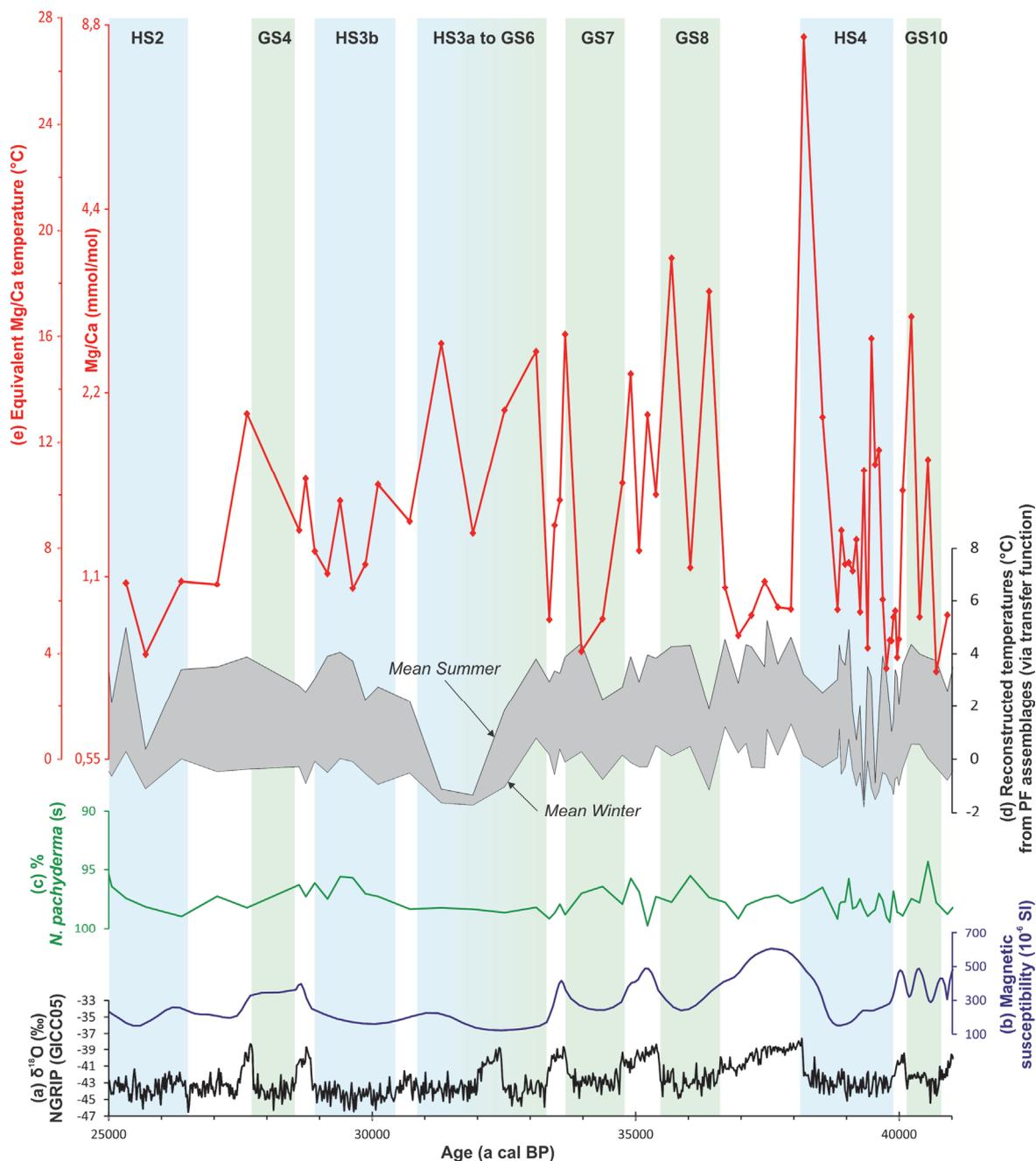


Figure 34 : Résultat des analyses Mg/Ca sur la carotte MD99-2285. (a) NGRIP $\delta^{18}O$. (b) Susceptibilité magnétique. (c) Abondance relative de *N. pachyderma senestre*. (d) Reconstitutions quantifiées des températures océaniques estivale et hivernale issues des assemblages de PF via l'application d'une fonction de transfert. (e) Ratio Mg/Ca mesuré sur *N. pachyderma senestre* et température équivalente d'après la calibration de Nürnberg et al. (1995).

Néanmoins, toujours dans l'optique de poursuivre le développement de méthode, et notamment d'étudier la possibilité de réduire les coûts d'analyse mais également le « temps technicien », l'ensemble de ces mesures a été réalisé en modifiant légèrement le protocole d'analyse pour le run 1 de telle sorte à pouvoir quantifier précisément les ratios Mg/Ca dès ce

run. Le protocole utilisé pour le run 2 est resté identique à celui défini initialement afin de pouvoir obtenir des mesures analytiquement exploitables. De cette façon, il est possible de comparer les ratios Mg/Ca issus de solutions de [Ca] plus ou moins différentes de 40 ppm (run 1) et de solutions de [Ca] ~ 40 ppm (run 2, considérées comme plus fiables), et ainsi estimer la nécessité (ou pas) d'effectuer deux runs de mesures (i.e. la possibilité de faire des économies en termes d'argon et de matériel consommable, et de réduire le temps d'analyse). Ces résultats n'ont pour l'instant pas été exploités dans cette optique, mais ils le seront prochainement. Ils devraient également permettre de mieux définir la méthode de calibration fournissant les résultats les plus justes et répétables.

6. Conclusion

- La méthode « Mg/Ca sur PF » mise au point à EPOC dans le cadre de cette thèse semble robuste :
 - ↳ Elle permet d'analyser des volumes suffisamment faibles / des solutions de concentration optimale.
 - ↳ Elle fournit des mesures répétables et justes.
- Les gammes étalon sont adaptées (sauf pour le Ba, mais cela vient vraisemblablement du protocole de chimie).
- La chimie semble également adaptée et « propre ».
- Les mesures sur la carotte MD99-2285 ne sont pas exploitables en termes de signal paléoclimatique, mais elles devraient permettre de poursuivre le développement de la méthode à EPOC.
- Le proxy Ba/Ca sur PF paraît très intéressant. Même si, en tant que proxy émergent, il ne fait pas l'unanimité de l'opinion scientifique, l'adaptation du protocole de chimie en vue de réaliser des analyses Ba/Ca à EPOC pourrait faire l'objet d'un développement futur.

Partie 3 : Outils complémentaires

Section 1. Assemblages de foraminifères planctoniques et reconstructions associées

Tout comme les dinokystes, les assemblages de PF constituent des indicateurs des conditions hydrologiques caractérisant la masse d'eau dans laquelle ils se développent. Et tout comme pour les dinokystes, l'application de fonctions de transfert « spéciales PF » permet d'obtenir des reconstructions quantifiées de ces paramètres hydrologiques.

Les assemblages de PF ont donc été déterminés (par Linda Rossignol) dans les fractions > 150 µm des deux carottes étudiées, dans les mêmes échantillons que ceux utilisés pour les analyses palynologiques. Les espèces dominantes et subordonnées majeures identifiées sont *Neogloboquadrina pachyderma* senestre, *Globigerina bulloides*, *Turborotalita quinqueloba*, *N. incompta* (forme dextre de *N. pachyderma*) et *Globigerinita glutinata*. D'après la littérature, ces espèces sont généralement considérées comme vivant potentiellement entre 0 et 300 m de profondeur (e.g. Schiebel et al., 2001 ; voir également Table 3 dans Staines-Urías et al., 2013 et références incluses).

Une fonction de transfert a alors été appliquée (par F. Eynaud) à ces assemblages de PF afin d'obtenir des reconstructions quantifiées de températures océaniques. Cette fonction de transfert a été développée par Eynaud et al. (2013). Comme pour les dinokystes, cette fonction de transfert utilise également la méthode MAT, elle est mise en œuvre avec le logiciel R en utilisant le script ReconstMAT développé par J. Guiot. La base de données modernes PF utilisée combine deux bases de données précédemment développées dans le cadre du projet MARGO (Kucera et al., 2005; Hayes et al., 2005). Elle réunit assemblages modernes et paramètres hydrologiques actuels issus de 1007 sites localisés dans l'Océan Atlantique Nord et la Mer Méditerranée. Parmi les paramètres hydrologiques reconstruits, nous utilisons dans le cadre de cette thèse les températures océaniques moyennes estivales (Juillet-Août-Septembre) et hivernales (Janvier-Février-Mars), dont les RMSEP sont respectivement de 1.3 °C et 1.2 °C.

En parallèle des comptages de PF, les foraminifères benthiques ont été dénombrés (par L. Rossignol) et leur concentration absolue déterminée. Ils ont également été identifiés sur une petite portion de la carotte MD99-2285 (444.5 – 549.5 cm, soit ~ 35.5 – 40 ka cal BP) par

C. Grimaldi lors d'un stage co-encadré avec J. Bonnin, mais les résultats issus de ces analyses n'ont finalement pas été exploités ici.

Section 2. IRD

Les grains détritiques grossiers ont été comptés dans la fraction $> 150 \mu\text{m}$ (sur les mêmes niveaux que ceux utilisés pour les analyses palynologiques et de PF) et leur concentration absolue déterminée. Comme dans de nombreux travaux menés dans la zone d'étude et focalisés sur la variabilité climatique rapide de la dernière période glaciaire, nous considérons que ces grains détritiques grossiers sont en grande partie composés d'IRD (e.g. Elliot et al., 1998, 2001 ; Rasmussen et al., 2002 ; Scourse et al., 2009), et donc que leur concentration absolue constitue un indicateur de la présence de glace flottante (icebergs ou glace de mer) sur la zone d'étude.

Section 3. Biomarqueurs : alcénones et IP25.

Afin d'obtenir des reconstructions quantifiées supplémentaires de SST et de glace de mer, des analyses de biomarqueurs (alcénones et IP25, respectivement) ont été réalisées sur la section 35-41 ka cal BP de la carotte MD99-2285 par M.-A. Sicre au LOCEAN.

Les alcénones sont des composés organiques lipidiques correspondant à de longues chaînes carbonées pouvant être mono-, di- ou tri-insaturées (i.e. avec une, deux, ou trois doubles liaisons carbone-carbone), principalement produites par les coccolithophoridées. Parmi ces molécules, celles composées de 37 atomes de carbone sont particulièrement utilisées en paléocéanographie car elles permettent de reconstituer les SST passées. En effet, ces alcénones en C_{37} sont principalement produites par deux espèces de coccolithophoridées : *Emiliana huxleyi* et *Gephyrocapsa oceanica* (Volkman et al., 1995). Ces organismes vont répondre aux changements de température de l'eau dans laquelle ils se développent en modifiant la proportion de C_{37} di- ($C_{37:2}$) et tri- ($C_{37:3}$) insaturées, selon une relation linéaire liant les SST au ratio U_{37}^K où $U_{37}^K = C_{37:2}/[C_{37:2}+C_{37:3}]$. Dans le cadre de cette thèse, les SST ont été reconstruites en utilisant la calibration de Prahl et al., (1998) : $SST_{\text{alk}} = [U_{37}^K - 0.039]/0.0034$.

Les IP25 sont des molécules lipidiques, appartenant à la famille des alcènes, composées de 25 atomes de carbone formant une chaîne ramifiée et mono-insaturée. Les IP25 sont produits par des diatomées vivant sous la glace de mer, principalement *Pleurosigma stuxbergii* var. *rhomboids*, *Haslea kjellmanii*, *H. crucigeroides* et/ou *H. spicula* (Brown et al., 2014). Les travaux successifs menés sur ce proxy ont montré que la présence d'IP25 dans les sédiments était indicatrice de présence de glace de mer saisonnière, cette molécule étant absente sous couvert de glace de mer pérenne (e.g. Belt et al., 2007 ; Belt & Müller, 2013 ; Weckström et al., 2013).

Par ailleurs, des analyses supplémentaires de quantification des stérols (molécules produites par des organismes phytoplanctoniques vivant dans des zones libres de glace au moins saisonnièrement) sont en cours (M.-A. Sicre). En attendant, les triènes, qui ont été quantifiés, et dont la présence traduirait également l'occurrence au moins saisonnière de conditions libres de glace (M.-A. Sicre, comm. pers.), ont été utilisés pour construire l'argumentation de l'article présenté en Chapitre 3, Partie 2, Section 1. Ces données ne sont toutefois pas montrées ici.

Section 4. Xrf

Des mesures de la composition élémentaire relative du sédiment ont été effectuées par fluorescence X (XRF). Ces mesures ont été réalisées par T. Richter avec une résolution de 2 cm en utilisant le scanner CORTEX du NIOZ. D'autres scans XRF ont été réalisés à EPOC par S. Zaragosi et les membres de la plate-forme analytique PAACS avec un Avaatech XRF Core Scanner ; ces mesures ont été effectuées de manière discontinue sur les carottes étudiées mais avec une résolution de 2 mm. Les deux jeux de données révèlent des résultats similaires sur les sections communes. Deux ratios élémentaires XRF ont principalement été utilisés dans le cadre de cette thèse :

- le ratio K/Ti, indicateur de la source dominante du sédiment puisque le K dérive principalement de l'érosion de roches continentales alors que le Ti est principalement issu de roches basaltiques (Richter et al., 2006).
- et le ratio Ca/Sr, qui fournit des informations sur l'origine des carbonates, le Sr étant exclusivement d'origine biogène alors que le Ca peut être d'origine biogène et terrigène (e.g. Mojtahid et al., 2005).

Chapitre 3 : Changements hydrographiques de part et d'autre de la Ride Islande-Ecosse au cours des derniers 45 ka

Le chapitre 3 regroupe l'ensemble des résultats obtenus dans le cadre de cette thèse.

La première partie (**Partie 1**) est consacrée à la **reconstitution des conditions hydrographiques** générales caractérisant les GS/HS et les GI de **part et d'autre de la Ride Féroé-Ecosse** (i.e. au Sud avec la carotte MD99-2281 – Section 1 –, et au Nord avec la carotte MD99-2285 – Section 2) au cours des derniers 45 ka, et leurs implications en termes de circulation océanique.

La seconde partie (**Partie 2**) traite plus particulièrement des enregistrements obtenus à très haute résolution sur la **période clé 35-41 ka autour de HS4**. Cette partie s'intéresse ainsi au séquençage détaillé des processus hydrographiques s'opérant tout au long des événements climatiques abrupts de cette période d'étude (i.e. GI, GS, HS4 et transitions – Section 1), ainsi qu'à l'extension spatiale (Sections 1 et 2) et temporelle (Sections 1, 2 et 3) de certains de ces processus clés.

Enfin, la dernière partie (**Partie 3**) traite plus spécifiquement des **mécanismes** associés à cette variabilité climatique millénaire. La première section (Section 1), qui combine paléoreconstructions régionales et expériences de modélisation, s'intéresse ainsi aux

mécanismes liés aux processus hydrographiques mis en évidence dans les deux précédentes parties de ce Chapitre 3. La deuxième section (Section 2) aborde quant à elle les mécanismes de déclenchement associés à ces événements climatiques abrupts via l'étude haute résolution de la période clé entourant l'évènement d'Heinrich 4.

Ce Chapitre 3 s'organise principalement sous forme d'articles :

- Partie 1 :
 - Section 1 : article sous presse dans *Climate of the Past*
 - Section 2 : article soumis à *Journal of Quaternary Science*
- Partie 2 :
 - Section 1 : article en préparation, soumission envisagée à *Quaternary Science Reviews*
 - Section 2 : article en préparation, soumission envisagée à *Earth and Planetary Science Letters*
- Partie 3 :
 - Section 1 : article en préparation, soumission envisagée à *Nature* (format *Letters*).
 - Section 2 : article en préparation pour *Heliyon*

Du fait de ce format, ce Chapitre 3 peut présenter certaines redondances avec les Chapitres 1 et 2 de ce manuscrit (i.e. au sein des sections « Introduction », « Contexte » et « Matériel et méthodes » des articles), dont la rédaction en français visait à fournir un état de l'art sur le contexte analytique de ce travail de doctorat et était donc cependant nécessaire.

Sommaire

PARTIE 1 : PALEOCEANOGRAPHIE DU POURTOUR DES ILES FEROE AU COURS DES DERNIERS

45 KA 83

Section 1. Stratification of surface waters during the last glacial millennial climatic events: a key factor in subsurface and deep water mass dynamics. 83

1. Introduction 86

2. Environmental setting and paleoceanographic interests 87

3. Material and methods 88

3.1. Stratigraphy of the core 88

3.2. Planktonic foraminifera 89

3.3. Dinocysts 91

3.4. Ecological indices 92

3.5. Sedimentological proxies 92

4. Results 93

4.1. Micropaleontological assemblages characteristics 93

4.2. Sea-surface hydrological parameters 94

4.3. Deep-water proxies 94

5. Discussion 95

5.1. A reworked signal? 95

5.2. Interpretation of proxies 96

5.2.1. Proxies of surface and subsurface hydrology 96

5.2.2. Proxies of deep water currents 98

5.3. Hydrological signature during Dansgaard-Oeschger events and implications 100

5.4. Different hydrological patterns during Heinrich stadials 103

6. Conclusion 106

Section 2. The Southern Norwegian Sea during the last 45 ka: hydrographical reorganizations under changing ice-sheet dynamics. 127

1. Introduction 130

2. Modern and past environmental settings 132

3. Stratigraphy	134
4. Materials and methods, proxy significance	137
4.1. Micropaleontological assemblages	137
4.2. Reconstructions of near-surface hydrological conditions	138
4.3. Sedimentological analyses	139
5. Results	141
5.1. Micropaleontological analyses	141
5.2. Near-surface and deep-water hydrological parameters	142
6. Discussion	144
6.1. A paradoxical hydrological scheme during the last glacial millennial events	144
6.2. Hydrological conditions during the last deglaciation and the Holocene	148
6.3. Implications on last glacial versus Holocene mode of deep water formation	150
7. Conclusion	151

PARTIE 2 : PROCESSUS HYDROGRAPHIQUES ET MECANISMES DE DECLENCHEMENT EN JEU LORS DES EVENEMENTS CLIMATIQUES ABRUPTS AVANT, PENDANT ET APRES UN HE : ZOOM SUR LA PERIODE 35-41 KA AUTOUR D'HE4.

<i>Section 1. Sea-surface warm pulses as the trigger of ice-sheet collapses: first evidence from paleodata</i>	163
1. Introduction	166
2. Environmental settings and paleoclimatic interests	167
2.1. Environmental settings	167
2.2. Paleoclimatic interests	169
3. Materials and methods	171
3.1. Stratigraphy	171
3.2. Sea ice reconstructions, sea-surface temperature and salinity estimates	171
3.3. Complementary tools	173
4. Results and discussion	175

4.1. Allochthonous vs autochthonous signals	175
4.2. General surface and subsurface in situ oceanic conditions during stadials and interstadials	177
4.3. Precise timing and interactions of hydrological processes during the millennial climatic events	179
4.4. Integrated regional view and implications	183
5. Conclusion.....	186

*Section 2. Surface and subsurface hydrographical reorganizations at the frontier
between Northeast Atlantic and Norwegian Sea basins around the Heinrich event 4 case
study period.....*

1. Introduction	204
2. Regional settings	205
3. Material and methods	206
4. Stratigraphy	207
5. Results and discussion.....	208
5.1. Surface/subsurface advection.....	208
5.1.1. Advection of warm Atlantic waters	208
5.1.2. Iceberg calving	210
5.2. Hydrological signals reflecting in situ conditions during stadials and interstadials	211
5.3. Zoom in on GI to GS/HS transitions.....	212
6. Conclusion.....	215

Section 3. Complément à l'étude de la carotte MD99-2285.....

223

PARTIE 3 : VUE SYNTHETIQUE ET SYNOPTIQUE DE LA PALEOCEANOGRAPHIE DE L'ATLANTIQUE
SUBBOREAL ET DE SES MERS BORDIERES AU COURS DES EVENEMENTS MILLENAIRES DE LA
DERNIERE PERIODE GLACIAIRE

227

Section 1. Warm and nearly ice-free Norwegian Sea during MIS3 Greenland stadials
.....

227

Section 2. On the triggering mechanisms of the last glacial millennial climatic events:
Heinrich event 4 as an outstanding case study..... 255

- 2.1. Introduction 258
- 2.2. Regional settings and chronostratigraphic framework..... 260
- 2.3. Material and methods, proxy significance 261
- 2.4. Results and discussion..... 262
 - 2.4.1. Triggering mechanisms of AMOC slowdowns 262
 - 2.4.1.1. Variations of AMOC strength over the 35-41 ka cal time period
..... 262
 - 2.4.1.2. Implications 263
 - 2.4.2. Triggering mechanisms of ice-sheet destabilizations 265
 - 2.4.2.1. Interpretation of $\delta^{18}\text{O}_{\text{NPS}}$ in core MD99-2281..... 265
 - 2.4.2.2. Implications 266
 - 2.4.3. Mechanisms responsible for the abrupt atmospheric warmings at the
onset of GI..... 268
- 2.5. Synthesis and conclusions: hydrographical scheme and processes during the
abrupt millennial climatic events of the last glacial period..... 271

Partie 1 : Paléocéanographie du pourtour des Iles Féroé au cours des derniers 45 ka

Section 1. Stratification of surface waters during the last glacial millennial climatic events: a key factor in subsurface and deep water mass dynamics.

*Article sous presse dans **Climate of the Past** (vol. 11, 1507-1525, doi:10.5194/cp-11-1507-2015), publié dans **Climate of the Past Discussion**.*

Wary Mélanie¹, Eynaud Frédérique¹, Sabine Marjolaine¹, Zaragosi Sébastien¹, Rossignol Linda¹, Malaizé Bruno¹, Palis Edouard^{1,*}, Zumaque Jena^{1,**}, Caille Clémence^{1,***}, Penaud Aurélie², Michel Elisabeth³, Charlier Karine¹

[1]{UMR 5805, EPOC (Environnements et Paléoenvironnements Océaniques et Continentaux), Université de Bordeaux, 33615 Pessac, France}

[2]{UMR 6538, Domaines Océaniques, IUEM-UBO, F-29280 Plouzané, France}

[3]{UMR 8212, LSCE (Laboratoire des Sciences du Climat et de l'Environnement), CEA/CNRS-INSU/UVSQ, 91198 Gif-sur-Yvette cedex, France}

[*]{now at: UMR 7329, Géoazur, Université de Sophia Antipolis, 06560 Valbonne, France}

[**]{now at: UQAM, Université du Québec à Montreal, Montréal, Québec H3C 3P8, Canada}

[***]{now at: Laboratory of Recent and Fossil Bio-Indicators, CNRS UMR6112 LPG-BIAF, Angers, France}

Correspondence to: M. Wary. (UMR 5805 EPOC – Université de Bordeaux. Bât. B18, Allée Geoffroy St Hilaire. 33615 Pessac Cedex) melanie.wary@u-bordeaux.fr

Résumé

La dernière période glaciaire a été ponctuée d'évènements climatiques abrupts dont les extrêmes sont connus sous les noms d'évènements d'Heinrich et évènements de Dansgaard-Oeschger. Ces variations millénaires ont fait l'objet de nombreuses paléoreconstructions et expériences de modélisation au cours des dernières décennies. Néanmoins, les processus hydrologiques impliqués restent encore incertains. Dans le cadre de cette étude, différentes analyses (couplant outils micropaléontologiques, géochimiques et sédimentologiques) ont été menées à haute résolution sur la section 12-42 ka cal BP de la carotte MD99-2281 prélevée au Sud-Ouest des îles Féroé. Ces analyses sont ici combinées à d'autres analyses micropaléontologiques produites sur la même carotte dans le cadre de deux études précédentes (Zumaque et al., 2012 ; Cauille et al., 2013). Cette approche multi-proxy nous permet de retracer les processus hydrologiques de surface, de subsurface, et de fond, en jeu lors de ces évènements climatiques rapides. Nos enregistrements indiquent que les phases les plus froides de la période étudiée (i.e. les stadias de Dansgaard-Oeschger et d'Heinrich) sont marquées par une forte stratification des eaux de surface. Cette stratification semble avoir joué un rôle clé dans la dynamique des masses d'eau sous-jacentes. En effet, les périodes de forte stratification se caractérisent par un couplage des circulations de subsurface et de fond, où les courants associés s'affaiblissent rapidement au début de ces épisodes froids, alors que les conditions de surface se détériorent quant à elles de manière progressive tout au long de ces stadias. A l'inverse, les périodes marquées par une diminution de la stratification (interstadias) se caractérisent par un couplage des masses d'eau de surface et de fond, des conditions de surface qui s'améliorent progressivement et une circulation profonde qui s'intensifie de manière graduelle, contrairement à l'afflux d'eau atlantique en subsurface dont la vigueur reste quant à elle constante tout au long de ces épisodes chauds. Nos résultats suggèrent également différents schémas hydrologiques durant les stadias d'Heinrich (HS). En effet, alors que HS1 et HS4 affichent des signatures « classiques » où la circulation océanique méridienne est réduite, HS2 semble être marqué par une circulation Nord-Atlantique relativement active, et HS3 par une ré-intensification de cette circulation au cœur même de l'évènement. Notre travail fournit ainsi de précieuses informations permettant une meilleure compréhension des processus hydrologiques en jeu dans un secteur clé lors des bascules climatiques abruptes de la dernière période glaciaire.

Abstract

The last glacial period was punctuated by abrupt climatic events with extrema known as Heinrich events and Dansgaard-Oeschger cycles. These millennial events have been the subject of many paleoreconstructions and model experiments in the past decades, but yet the hydrological processes involved remain elusive. In the present work, high resolution analyses were conducted on the 12-42 ka BP section of core MD99-2281 retrieved Southwest off Faeroes, and combined with analyses conducted in two previous studies (Zumaque et al., 2012; Caille et al., 2013). Such a multiproxy approach, coupling micropaleontological, geochemical and sedimentological analyses, allows us to track surface, subsurface, and deep hydrological processes occurring during these rapid climatic changes. Records indicate that the coldest episodes of the studied period (Greenland stadials and Heinrich stadials) were characterized by a strong stratification of surface waters. This surface stratification seems to have played a key role in the dynamics of subsurface and deep water masses. Indeed, periods of high surface stratification are marked by a coupling of subsurface and deep circulations which sharply weaken at the beginning of stadials while surface conditions progressively deteriorate throughout these cold episodes; at the opposite, periods of decreasing surface stratification (Greenland interstadials) are characterized by a coupling of surface and deep hydrological processes, with progressively milder surface conditions and gradual intensification of the deep circulation while the vigor of the subsurface northward Atlantic flow remains constantly high. Our results also reveal different and atypical hydrological signatures during Heinrich stadials (HS): while HS1 and HS4 exhibit a “usual” scheme with reduced overturning circulation, a relatively active North Atlantic circulation seems to have prevailed during HS2, and HS3 seems to have experienced a re-intensification of this circulation at mid-event. Our findings thus bring valuable information to better understand hydrological processes occurring in a key area during the abrupt climatic shifts of the last glacial period.

Keywords

Dansgaard-Oeschger cycles, Heinrich events, surface stratification, halocline, North Atlantic Drift, Norwegian Sea Overflow water.

1. Introduction

The last glacial period is characterized by abrupt climate oscillations. This millennial to sub-millennial climatic variability was first evidenced in Greenland atmospheric temperature records as oscillations occurring every 1-4 ka and known as Dansgaard-Oeschger events (DO) (Dansgaard et al., 1993, Bond et al., 1993). DO are characterized by a rapid transition occurring in a few decades from cold (Greenland stadial – GS) to warm (Greenland interstadial – GI) conditions. These events have been widely identified in marine archives from the subpolar North Atlantic Ocean and adjacent seas as coeval changes in surface and deep hydrology (e.g. Rasmussen et al., 1996a,b; Kissel et al., 1999; Van Kreveld et al., 2000; Rahmstorf, 2002). Moreover, during GS (including the most massive, i.e. Heinrich stadials – HS), increases of iceberg and ice-rafted debris (IRD) delivery from the boreal ice-sheets are recorded (e.g. Heinrich, 1988; Bond et al., 1993; Bond and Lotti, 1995; Elliot et al., 2001). Despite a large number of paleoreconstructions and model experiments focusing on this millennial climatic variability, processes involved still remain elusive and different mechanisms are invoked. Most of the considered theories involve changes in the meridional overturning circulation, either as the cause (e.g. Alvarez-Solas et al., 2010) or the consequence (e.g. Manabe and Stouffer, 1995; Ganopolski and Rahmstorf, 2001; Levine and Bigg, 2008) of these periodic ice-sheet instabilities.

In order to better understand these phenomena, the importance of working on high resolution records coming from key locations has been highlighted. Previous studies of marine cores located around major sills in between the North Atlantic Ocean and the Nordic Seas have shown the strong potential of this buffer area to track this variability (see references herein). Most of these studies agree with coeval oscillations of the meridional overturning circulation, depicted as weaker loop of Atlantic inflow and deep overflow from the Nordic Seas during GS and HS and inversely during GI (e.g. Rasmussen et al., 1996a,b, 2002a; Moros et al., 1997, 2002; Kissel et al., 1999, 2008; Van Kreveld et al., 2000; Elliot et al., 2002; Rasmussen and Thomsen, 2004; Ballini et al., 2006; Dickson et al., 2008). Some of them (Rasmussen et al., 1996a,b; Rasmussen and Thomsen, 2004; Van Kreveld et al., 2000; Dokken et al., 2013), on the basis of indirect proxies of sea surface conditions, suggest a strong stratification of the water column and the presence of a halocline during GS, which might have affected the oceanic circulation at greater depths.

Our study uses proxies that give access to (sub)surface (foraminifera assemblages and geochemical analyses on their shells) and deep water mass dynamics (sediment grain-size measurements and magnetic susceptibility), coupled to previously published reconstructions of sea-surface *sensu stricto* conditions obtained from dinoflagellate cyst (dinocyst) assemblages (Zumaque et al., 2012, Caulle et al., 2013). All analyses were conducted at centennial to millennial time scales on core MD99-2281 located southwest off Faeroe Islands. This multiproxy approach allows us (i) to directly evidence the past structure of the upper water column and especially if stratification did occur, (ii) to track this stratification evolution during the millennial abrupt events, and (iii) to evaluate its interaction with subsurface and bottom circulations.

2. Environmental setting and paleoceanographic interests

Core MD99-2281 (60.3418°N, -9.4557°E, 1197 m water depth) was retrieved during the IMAGES V – GINNA cruise on the RV Marion Dufresne (Labeyrie et al., 1999). The coring site is located southwest off Faeroes, at the southern foot of the Faeroe Bank and north of the Rockall Trough (Fig. 1).

This area constitutes a nodal point regarding modern oceanic circulation, as it is influenced by (i) the warm and salty Atlantic surface waters ($T > 5$ °C, $S > 35.0$; Hansen and Osterhus, 2000) conveyed by the poleward current of the North Atlantic Drift (NAD), and (ii) the intermediate and deep, cold and less saline waters ($T < 3$ °C, $S < 35.0$; Hansen and Osterhus, 2000) overflowing from the Nordic Seas (e.g. Kuijpers et al., 1998a,b, 2002; Hansen and Osterhus, 2000) (Fig. 1). These intermediate and deep water masses are formed within the Nordic Seas and are usually grouped under the name of Iceland Scotland Overflow Water (ISOW; Borenäs and Lundberg, 2004). At present, a branch of ISOW exits the Norwegian Sea by flowing southward through the Faeroe-Shetland Channel and then is divided into two branches: a northern, major and permanent branch, and a southern, minor, and non-permanent one (Fig. 1b). Our site is located beneath the southern branch, which intermittently crosses the Wyville-Thompson Ridge (a topographic barrier culminating at around 600 meters water-depth) and flows southward (e.g. Boldreel et al., 1998; Kuijpers et al., 1998a,b, 2002; Hansen and Østerhus, 2000). Nevertheless, according to Boldreel et al. (1998), the coring site is

located within the area unaffected by strong current activities, with sedimentation resulting from pelagic sediments deposited in a low-energy, deep-water environment.

This system of water-mass exchange is known to have been very sensitive to the millennial-scale climatic variability of the last glacial period (e.g. Rasmussen et al., 1996a,b, 2002a; Moros et al., 1997, 2002; Kissel et al., 1999, 2008; Van Kreveld et al., 2000; Elliot et al., 2002; Eynaud et al., 2002; Rasmussen and Thomsen, 2004, 2008; Ballini et al., 2006; Dickson et al., 2008; Zumaque et al., 2012; Cauille et al., 2013). This is particularly true for the Faeroe region which was then under the direct influence of the proximal European ice-sheets (i.e. the Fennoscandian and the British-Irish ice-sheets; Fig. 1a) whose decays/built-up have modulated the oceanic and climatic dynamics. Therefore, core MD99-2281 is expected to have recorded changes in the vigor of the NAD penetration and ISOW overflow in relation to European ice-sheets history.

3. Material and methods

3.1. Stratigraphy of the core

The age model of core MD99-2281 conforms to the previous published one from Zumaque et al. (2012) and Cauille et al. (2013). As recommended by several paleoceanographic studies in this area (e.g. Kissel et al., 1999, 2008; Laj et al., 2000; Elliot et al., 2002; Eynaud et al., 2002; Ballini et al., 2006; Rasmussen and Thomsen, 2009; Dokken et al., 2013), the age model is constrained by AMS ^{14}C dates (in the case of our study, 10 dates measured on planktonic foraminifera monospecific samples), combined to additional tie-points (18 in our case) obtained by comparing the magnetic susceptibility record of core MD99-2281 to the $\delta^{18}\text{O}$ signal of NGRIP ice-core (GICC05 time scale; Andersen et al., 2006; Svensson et al., 2008; Wolff et al., 2010; see Figs. 2, 3, 4 and 5 where dates are illustrated by red stars and tie-points by blue stars along the age axis). The age model was finally established on the basis of a linear interpolation between ages and tie-points (see Zumaque et al., 2012 for further explanations). It is important to note that supplementary stratigraphic control points, independent from climate, were retrieved from the record of the changes in the Earth's magnetic field (analysis performed at the LSCE), namely the Mono Lake and the

Laschamps events. Those additional tie points give confidence in the established age model (see Fig. 4 in Zumaque et al., 2012).

The coring site experienced relatively high sedimentation rates during the last glacial period (between 23 and 408 cm.ka⁻¹, with a mean around 61 cm.ka⁻¹ for the studied section, i.e. 300-2090 cm or ~ 12-42 ka cal BP, cf. Fig. 4). These rates, combined to our sampling frequency (every ~ 10 cm on the studied section for all analyses except for grain size analyses on a short portion of the core and for magnetic susceptibility measurements, cf. Sect. 3.5.), lead to appropriate degrees of temporal resolution (between ~ 25 and ~ 525 years, with a mean of ~ 165 years) to study the last glacial rapid climatic variability at an infra-millennial scale.

3.2. Planktonic foraminifera

Planktonic foraminifera analyses were performed on the > 150 µm fraction, on the same samples as those used for dinocyst analyses. A minimum of 350 specimens per sample were counted, and thirteen taxa were identified in the studied section. The dominant and major subordinate species are usually classified as surface/mid- to mid/deep dwelling taxa (*Neogloboquadrina pachyderma* (sinistral coiling), *Globigerina bulloides*, *Turborotalita quinqueloba*, *N. incompta* and *Globigerinita glutinata*) potentially living between 0 and 300 meters water depths according to literature (e.g. Schiebel et al., 2001, Table 3 in Staines-Urías et al., 2013 and references therein). Abundances of each species were calculated relative to the total sum of planktonic foraminifera. Counts of total benthic foraminifera were also performed, and planktonic and benthic foraminifera total concentrations (number of specimen g⁻¹ of dried sediment) were calculated.

Quantitative reconstructions of foraminifera-derived temperatures (hereafter “F-Temp”) were obtained using a transfer function applied to planktonic foraminifera assemblages. This transfer function has been developed by Eynaud et al. (2013). It has already been described in several previous studies (e.g. Matsuzaki et al., 2011; Penaud et al., 2011; Sánchez Goñi et al., 2012, 2013; Mary et al., 2015), but hereafter is a brief summary of the technical aspects of this method. The modern analogue technique (MAT, see Guiot and de Vernal, 2007, 2011a,b for a review of this technique) was applied and performed with the R software (R version 2.7.0; <http://www.r-project.org/>), using the ReconstMAT script developed by J. Guiot

(BIOINDIC package, <https://www.eccorev.fr/spip.php?article389>). The modern planktonic foraminifera database used here combines two databases previously developed within the MARGO framework (Kucera et al., 2005; Hayes et al., 2005). It includes modern assemblages and modern hydrological parameters from 1007 sites distributed over the North Atlantic Ocean and Mediterranean Sea. Modern hydrological parameters are annual and seasonal (mean winter: January/February/March, mean spring: April/May/June, mean summer: July/August/September, and mean fall: October/November/December) oceanic temperatures extracted at 10 meters water depth (with the WOA Sample tool especially built for the MARGO exercise, i.e. Schäfer-Neth and Manschke, 2002). Statistical treatments rely on the calculation of dissimilarity indexes between the fossil and modern spectra, leading to the selection of the five best analogues. Quantifications rely on a weighted average of temperature values associated with the five best modern analogues. For the present study, we will use the mean summer and mean winter F-Temp reconstructed with RMSEP of 1.3 °C and 1.2 °C respectively.

Stable oxygen isotope measurements ($\delta^{18}\text{O}$) were also performed on monospecific samples of *Neogloboquadrina pachyderma* (some previously reported in Zumaque et al., 2012 and Caille et al., 2013, as well as new measurements). For each sample (the same as those used for F-Temp reconstructions), 5 to 6 specimens (i.e. $\sim 65 \mu\text{g}$ mean weight aliquots) were hand-picked from the 200-250 μm size fraction. From 300 to 1190 cm ($\sim 12\text{-}27$ ka BP, 90 samples) measurements were done at LSCE laboratory using a Finnigan MAT 251 mass spectrometer. The mean external reproducibility of carbonate standard NBS19 was $\pm 0.05\text{‰}$. From 1200 to 2090 cm ($\sim 27\text{-}42$ ka BP, 90 samples), measurements were performed at EPOC laboratory with an Optima Micromass mass spectrometer. Reproducibility of NBS19 was $\pm 0.03\text{‰}$. Those two spectrometers are inter-calibrated thus allowing us to directly compare both records. In both cases, values are given versus Vienna Pee Dee Belemnite (VPDB) standard.

To estimate past changes in seawater isotopic composition ($\delta^{18}\text{O}_{\text{SW}}$), we used the paleotemperature equation developed by Epstein and Mayeda (1953) and Shackleton (1974) which links the $\delta^{18}\text{O}_{\text{SW}}$, the isotopic composition of calcareous shells ($\delta^{18}\text{O}_{\text{C}}$) and the calcification temperature (T) as follows: $T = 16.9 - 4.38 (\delta^{18}\text{O}_{\text{C}} - \delta^{18}\text{O}_{\text{SW}}) + 0.13 (\delta^{18}\text{O}_{\text{C}} - \delta^{18}\text{O}_{\text{SW}})^2$. Following Duplessy et al. (1991), we used $\delta^{18}\text{O}$ measurements on *N. pachyderma* as $\delta^{18}\text{O}_{\text{C}}$, and mean summer F-Temp corrected by 2.5°C as T. We then followed the method recently described in Malaizé and Caley (2009) to extract the $\delta^{18}\text{O}_{\text{SW}}$ signal. Variations of this

signal depend on past fluctuations of local salinities as well as on the global isotopic signal related to changes in continental ice-sheet volume. We used the global $\delta^{18}\text{O}$ signal of [Waelbroeck et al. \(2002\)](#) to remove $\delta^{18}\text{O}$ variations due to glacial-interglacial ice volume changes. We thus obtained a local $\delta^{18}\text{O}_{\text{SW}}$ signal that can be used as an indicator of local salinities changes in the depth range where *N. pachyderma* calcifies, i.e. from a few tens of meters to around 250 meters water depth (e.g. [Carstens et al., 1997](#); [Simstich et al., 2003](#); [Peck et al., 2008](#); [Jonkers et al., 2010](#)). Nevertheless, it should be kept in mind that this signal is not corrected from the rapid ice volume fluctuations associated with Marine Isotopic Stage 3 (MIS3) collapse events, as those fluctuations still remain not fully understood and discrepancies still exist between the various sea-level reconstructions ([Siddall et al., 2008](#)). Quantitative estimations of salinities were not carried out as large uncertainties remain concerning the temporal stability of the relation linking local $\delta^{18}\text{O}_{\text{SW}}$ to salinity, even if a recent study, using atmospheric isotopic model, tends to minimize these uncertainties within our study area ([Caley and Roche, 2013](#)).

3.3. *Dinocysts*

Dinocyst specific determination, counting, and estimates of past sea-surface estimates (through transfer function applied to dinocyst assemblages) were performed within the framework of two previous studies: [Caulle et al. \(2013\)](#) for the 12-27 ka BP section of the studied core, and [Zumaque et al. \(2012\)](#) for the 27-42 ka BP section. Methods for palynological preparation, identification, counts, calculation of abundances, and dinocyst transfer function are described in these two studies. Data stemming from those analyses and reused in the present study are the concentration of modern (i.e. Quaternary) dinocysts (number of cysts cm^{-3} of dried sediment), the relative abundances of some selected dinocyst species, the concentration of coenobia of freshwater micro-algae *Pediastrum* spp. (number cm^{-3} of dried sediment), and quantitative reconstructions of mean summer (July-August-September) and mean winter (January-February-March) sea-surface temperatures (SST) (with root mean square errors of prediction – RMSEP – of 1.5 °C and 1.05 °C respectively), mean summer and mean winter sea-surface salinities (SSS; respective RMSEP of 2.4 and 2.3 psu; see [Caulle et al., 2013](#) and [Zumaque et al., 2012](#) for further details).

3.4. Ecological indices

Some ecological indices were calculated both on dinocyst and planktonic foraminifera assemblages. Diversity is represented by the H index: $-\sum_{i=1}^s [(n_i/N) \times \ln(n_i/N)]$, where n_i is the number of specimens recorded for taxa i , s the total number of taxa and N the total number of individuals counted for each sample (Shannon and Weaver, 1949). Dominance corresponds to $(n' + n'') / N$ where n' is the number of individuals of the more abundant species, n'' the number of individuals of the second more abundant species, and N the total number of specimens counted for each sample (cf. Goodman, 1979).

3.5. Sedimentological proxies

Grain-size measurements were performed on a Malvern MASTER SIZER S at EPOC laboratory (University of Bordeaux). Subsamples of bulk sediment were taken every ~ 10 cm between 40 and 2170 cm (~ 11-43 ka BP), except between 1791.5 and 1940.5 cm (~ 37-40 ka BP) where sampling was done every centimeter (371 samples in total); those subsamples did not receive any chemical pretreatment before being analyzed. But to ensure that results obtained from non-pretreated sediment adequately reflect grain-size variations of the terrigenous fraction in our study area, a second set of analyses was conducted on carbonate-free and organic-free subsamples (pretreatment with HCl 10% and H₂O₂ 35%) taken every ~ 10 cm from 1593 to 1791 cm (~ 33.6-37 ka BP, same depth as the non-pretreated subsamples). Results derived from the bulk subsamples will be further represented as a mapping of the relative percentages of the different grain-size fractions along core. Some grain-size parameters were additionally calculated: median (D50), percentiles 10 and 90 (D10 and D90), mean grain size of the 10-63 µm fraction, mode, and silt ratio. The mode corresponds to the mean diameter of the most abundant size fraction. The silt ratio, reflecting size variations in the silt fraction, corresponds to the ratio of the percentage of the coarse silt fraction (26-63 µm) over the percentage of the fine silt fraction (10-26 µm).

Large Lithic Grains (LLG) concentrations (nb. of grains g⁻¹ of dry sediment) were determined in the > 150 µm sediment fraction of the studied core, in the same samples as those used for foraminifera and dinocyst analyses. As in many works conducted in the study area (e.g. Elliot et al., 1998, 2001; Rasmussen et al., 2002a; Scourse et al., 2009), we assume

that LLG contain a large proportion of ice-rafted debris, and thus consider this proxy as an indicator of floating ice (i.e. icebergs or coastal sea-ice) delivery to the site.

Magnetic Susceptibility was measured onboard every 2 cm with a GEOTEK Multi-Sensor Core Logger (Labeyrie and Cortijo, 2005). More detailed magnetic analyses were performed at the LSCE with a 45-mm diameter MS2-C Bartington coil on the MIS 3 section (see Zumaque et al., 2012). However, as the present study also focuses on MIS 2, we chose to present the continuous onboard signal which is furthermore very similar to the low field magnetic susceptibility record obtained at the LSCE (see Fig. 3 in Zumaque et al., 2012).

4. Results

As the age model and some raw data have already been shown in Zumaque et al. (2012) and Caille et al. (2013), all data will be here presented and discussed according to a calendar BP age scale. Furthermore, those two previous studies already provided a detailed description of dinocyst assemblages and derived hydrological reconstructions. Therefore, except for the ecological indices and seasonality signals which are inherent to the present work, we will not describe these data here again.

4.1. Micropaleontological assemblages characteristics

Planktonic foraminifera concentrations vary from 0 to 2500 individuals/g of dry sediment, with a mean value of around 400, and highest values recorded during GI (Fig. 2c). Assemblages are clearly dominated by the polar taxon *N. pachyderma* (relative abundance ranging from 20 to nearly 100%, Fig. 2b), peaking during GS and HS. *G. bulloides*, *T. quinqueloba*, *N. incompta* and *G. glutinata* are major subordinate species in some intervals, in particular GI and the Last Glacial Maximum (LGM).

Dinocyst and foraminifera ecological indices fluctuate in phase with the abrupt climatic oscillations of the last glacial period (Figs. 2e and 2f). Planktonic foraminifera diversity and dominance are always negatively correlated, with low values of diversity and high values of dominance during GS and HS, and inversely during GI. Dinocysts diversity and dominance variations are mostly opposite, with generally higher values of diversity and lower values of

dominance during GS and HS compared to GI; they appear covariant only along three very short intervals during the LGM around 20.7, 21.2 and 22.9 ka BP.

4.2. Sea-surface hydrological parameters

Planktonic foraminifera-derived mean summer temperatures (or mean summer F-Temp; Fig. 3b) vary between 2.5 and 10 °C, on average around 7 °C, and mean winter F-Temp range from -0.6 to 6.1 °C with a mean around 3 °C. These reconstructed F-Temp are lower than modern SST over the studied area which are around 11.7 and 8.6 °C on average for summer and winter seasons respectively (WOA09 data; Locarnini et al., 2010). Despite the gap of nearly 4 °C between these two signals, they both show similar trends with higher F-Temp during GI and lower values during GS and HS (Fig. 3b).

Local $\delta^{18}\text{O}_{\text{sw}}$ signal derived from foraminifera (here used as an indicator of local salinity changes) also responded to the millennial-scale variability (Fig. 3g). Values vary between around -2 and 1‰, the lowest ones being recorded during HS1 and HS4 and the highest ones during GI, the LGM and towards the Holocene.

Seasonality signals derived from dinocysts and planktonic foraminifera (calculated as mean summer minus mean winter temperatures, Fig. 3c) are clearly different from each other. The dinocyst-derived seasonality record displays large variations, with higher values during GS and the LGM (maximum of 15.1 °C, for an average of 13.6 °C) and lower ones during GI (minimum of 5.7 °C). On the contrary, the foraminifera-derived seasonality signal does not exhibit any comparable variation throughout the studied period since values vary between 2.4 and 5.1 °C with a mean value of 4.1 °C.

LLG concentrations describe a general scheme rather similar to the local $\delta^{18}\text{O}_{\text{sw}}$ and F-Temp signals (Fig. 3). They are generally higher during GS and HS than during GI. Only two noticeable exceptions exist: a high LLG concentration during the second half of GI8, and very few LLG during most of HS3.

4.3. Deep-water proxies

The millennial-scale variability has also been well captured by proxies related to bottom conditions as shown in Fig. 4. Compared to stadials (i.e. GS and HS), GI are characterized by

higher sedimentation rates, coarser grain-sizes (marked by D50 values up to 5 phi and D90 values up to 2.5 phi, and also evidenced on the grain-size mapping in Fig. 4c through the displacement towards the right, i.e. towards coarser grain-sizes, of the most abundant grain-size fractions, i.e. the ones colored from light blue to red), a higher proportion of the coarse silt fraction relative to the fine silt fraction, a coarser dominant fraction, higher magnetic susceptibility values, and higher benthic foraminifera concentrations. Among stadials, only HS2 exhibits a signature comparable to GI one. Note that except for magnetic susceptibility (and sedimentation rate), all the other deep-sea proxies seem to increase gradually throughout GI. It is visible for GI 11, 10 and 7, and particularly noticeable for GI 8; for shorter GI, this progressive trend is hardly or not distinguishable.

5. Discussion

5.1. A reworked signal?

Considering the size of micro-organisms used in this study and the sedimentary processes occurring in the area, one could object that assemblages may not result from local deposition only but also from lateral advections including reworking of previously deposited material on proximal areas. In this case, our reconstructions would not reflect local surface and subsurface hydrology but a combination of allochthonous and autochthonous signals, furthermore mixed throughout time.

To identify and circumscribe these problems, we used the methodology recommended by [Londeix et al. \(2007\)](#) to identify reworked intervals in sedimentary records by combining diversity and dominance indices in microfossil communities. Indeed, according to these authors, ecologically inconsistent covariance between these two indices is attributed to mixing processes. In core MD99-2281, diversity and dominance are negatively correlated all along the 12-42 ka BP studied section regarding both planktonic foraminifera and dinocysts (except for three very short episodes during the LGM, a period not discussed in this study, and only for dinocysts, [Fig. 2e and 2f](#)), and so do not reveal any evidence of reworking.

5.2. Interpretation of proxies

5.2.1. Proxies of surface and subsurface hydrology

As shown in Fig. 3, hydrological signals derived from planktonic foraminifera (F-Temp and local $\delta^{18}\text{O}_{\text{SW}}$) and from dinocysts (SST and SSS) share common features but also differ in some points through the studied period. Firstly, winter SST, winter F-Temp and summer F-Temp display similar variations and similar amplitudes of variation (with nonetheless noticeable discrepancies, e.g. during the LGM and between 32 and 27 ka cal BP), but are clearly different from dinocyst-derived summer SST. Indeed, summer SST show a clear opposite trend to the three other reconstructed temperature signals (with higher values during GS and HS), and they display values well above the ones of the three other signals as well as above the modern mean ones. Secondly, at stadial-interstadial transitions, dinocyst-derived SST and SSS display gradual increases/decreases whereas foraminifera-derived temperatures and local $\delta^{18}\text{O}_{\text{SW}}$ show more abrupt variations despite identical resolutions (Figs. 3b and 6a). Lastly, dinocysts mainly recorded a large seasonality with significant variations over the studied period whereas planktonic foraminifera recorded a low seasonality with very low or even nil fluctuations (Fig. 3c). As suggested in previous studies (e.g. de Vernal et al., 2005, 2006; Penaud et al., 2011), such discrepancies may result from differences in depth habitat of these organisms. Indeed, dinoflagellates are restricted to the photic layer while planktonic foraminifera may live deeper. This is particularly true for the dominant and subordinate foraminifera species identified in this study, since they do not bear any symbiont. According to literature, the depth habitat of these species potentially ranges between 0 and 300 meters water depth (see Table 3 in Staines-Urías et al., 2013 and references therein). Besides, dinocyst-derived SSS are very low throughout most of the studied period (means of 31 and 32 psu for summer and winter SSS), and the main planktonic foraminifera species identified in our assemblages barely tolerate such salinities (Tolderlund and Bé, 1971). Therefore, we can reasonably consider here that dinocysts provide a record of the surface sensu stricto, whereas planktonic foraminifera recorded hydrological conditions of a larger section of the upper water column that we call hereafter the subsurface for simplicity. It is worth noting that F-Temp reconstructions cannot be considered as subsurface absolute reconstructions since temperatures in the modern database used for the transfer function are extracted at 10 meters water depth. However, interpreting them as subsurface relative estimations is coherent if we consider previous works focused on transfer functions applied to planktonic foraminifera assemblages (see Supplementary Information).

Seasonality values derived from dinocysts (averaged value over the studied period of ~ 13.6 °C, Fig. 3c) are ~ 4 times higher than the modern sea-surface seasonality value over the study area (~ 3.2 °C; calculated from WOA09 data as mean summer minus mean winter oceanic temperatures; Locarnini et al., 2010). It might seem surprising, but similar values are presently recorded in several areas around the world (at the outlet of the Gulf of St Lawrence, in the Baltic Sea and outlets of the bordering gulfs, in the Sea of Japan, the East China Sea, the Black Sea, and the Caspian Sea, according to WOA09 data, Locarnini et al., 2010). For some of these areas, such high seasonality contrasts are related to a stratification of the upper water column marked by the presence of a halocline (e.g. the Baltic Sea, Kullenberg, 1981; the outlet of the Gulf of St Lawrence, Banks, 1966). Indeed, the very low SSS recorded by dinocysts (which are well below the modern ones over the study area, equal to 35.3 psu according to WOA09 data, Antonov et al., 2010; Fig. 3d), as well as the presence of the freshwater micro-algae *Pediastrum* spp. (a marker of freshwater advection in surface; e.g. Eynaud et al., 2007), support the existence of a thin freshwater surface layer of low thermal inertia overlying the study area during most of the studied period. Similarly to present situations, this freshwater layer would have certainly been responsible for a strong stratification of the water column due to the presence of a halocline. Such a pattern is also qualitatively consistent since the most abundant dinocyst species is *B. tepikiense*, a taxon which displays a strong affinity for stratified surface waters characterized by a large seasonality (Rochon et al., 1999). Furthermore, this interpretation explains why dinocyst (i.e. surface) signals are noisier than planktonic foraminifera ones.

Iceberg calving and associated meltwater inputs are potential initiator and feeder of this halocline. Ice-rafted debris have mainly been used as tracers of these iceberg surges. Here, we use LLG concentrations and assume, as generally admitted, that LLG are mainly constituted of IRD. Our LLG signal is indeed very similar to IRD records coming from many studies and sites in North Atlantic (e.g. Bond and Lotti, 1995; Elliot et al., 1998, 2001; Van Kreveld et al., 2000; Rasmussen and Thomsen, 2004; Dickson et al., 2008) which described higher ice-rafted debris concentrations during GS and HS and variable concentrations during the LGM. This supports the assumption that our LLG signal can be used as an indicator of iceberg delivery to the studied site. In this case, the resemblance between LLG concentrations and local $\delta^{18}\text{O}_{\text{SW}}$ and subsurface temperature (F-Temp) signals suggests that these latter signals are at least partly forced by iceberg calving and melting and associated cold freshwater releases. However, variations in the warm and salty northward Atlantic flow could also play a major

role in the fluctuations of these signals. Many freshwater model experiments (e.g. [Manabe and Stouffer, 1995](#); [Ganopolski and Rahmstorf, 2001](#); [Levine and Bigg, 2008](#)) have indeed shown that these two processes are clearly linked, in the sense that (i) freshwater release weakens the Atlantic meridional overturning circulation and limits the northward extension of the NAD, and (ii) the larger the amount of released freshwater is, the more weakened the oceanic circulation is. Moreover, the correspondence between LLG and foraminifera-derived signals is only partial. Some delays (e.g. during H4, GS8, GS6) and incoherencies (e.g. the relatively long periods before and after HS2 with considerably low $\delta^{18}\text{O}_{\text{SW}}$ but almost no LLG) can indeed be noticed. This leads us to think that paleo-fluctuations of our foraminifera-derived signals are the result of the combined two phenomena: the warm and saline Atlantic water northward flow and its southward retreat, and the episodic cold and fresh water release associated with iceberg surges. Respective contributions of these two phenomena could seem difficult to dissociate, but in this study, dinocyst data provide valuable clues. Indeed, as mentioned above, dinocyst-derived SSS and seasonality signals are indicators of surface stratification. Then we can suppose that during periods of high surface stratification (i.e. periods when the halocline strongly hampers or even prevents mixing between surface and subsurface waters), variations of F-Temp and local $\delta^{18}\text{O}_{\text{SW}}$ should be principally due to variations in the NAD intensity. At the opposite, during periods of weaker surface stratification, and when iceberg calving occurred, variations of planktonic foraminifera-derived parameters should be the result of the combination of meltwater inputs from the surface and NAD variations; but during periods of low stratification and without iceberg calving, subsurface hydrological variations should be due to NAD fluctuations only.

5.2.2. Proxies of deep water currents

Reconstructing past variations of the ISOW dynamics deserves to be attempted in this study as our multi-proxy approach provides various indicators of bottom current activities ([Fig. 4](#)). The first type of bottom flow proxy corresponds to parameters derived from grain-size measurements. These parameters (listed in [Sect. 3.5](#) and below) have been widely employed in reconstructions of bottom current activity (e.g. [McCave et al., 1995a,b](#); [McCave, 2007](#); [Bianchi and McCave, 1999](#); [Hodell et al., 2009](#)). Their use is based on the fact that bottom currents preferentially affect the silt fraction (10-63 μm) by size-sorting, such as stronger currents induce a coarsening and an increase of the relative proportion of this size fraction. Basically, an intensification of the ISOW will be depicted as a coarsening of D10, D50, and D90 ([Fig. 4c](#)), an increase of the mean size of the 10-63 μm fraction ([Fig. 4d](#)) and of

the silt ratio (Fig. 4e), a coarsening of the dominant mode towards values corresponding to the silt fraction or even coarser (Fig. 4f), and a grain size distribution showing a coarsening and an increase of the relative proportion of this coarse fraction (Fig. 4c). It is important to note that in the glacial North Atlantic Ocean, IRD < 150 μm could constitute a potential source of silt-size particulates which could bias the use of these parameters as bottom flow proxies (Prins et al., 2002). Nevertheless, in our case, LLG concentrations are generally higher during GS, i.e. when grain-size distribution and parameters indicate a general finning of the total sediment fraction – including silt fraction – and a predominance of the < 10 μm fraction. As the supplies of IRD > 150 μm (i.e. LLG) and < 150 μm are supposed to be synchronous, the impact of IRD inputs (fine as well as coarse ones) on the grain-size distribution seems to be minor, and so do not seem to bias the use of grain-size parameters as indicators of the bottom current strength. In a similar way, biogenic inputs could also influence grain-size distribution and bias the grain-size proxies. However, Fig. 4d, e and f show that the calculated grain-size parameters for the bulk samples and for the pretreated ones exhibit the same variations in terms of timing as well as in amplitude. Besides, grain-size analyses on pretreated samples were conducted on the core section where the content of CaCO_3 (data not shown) displays the largest variations and attains its maximal value over the studied portion of the core. This confirms that in our study area, grain-size variations of bulk sediment almost exclusively reflect changes in the terrigenous fraction and so can be directly interpreted in terms of fluctuations of the bottom current intensity.

The second type of bottom flow proxy used in this study is the magnetic susceptibility (Fig. 4g). Kissel et al. (1999, 2009) have shown that, in areas distributed along the path of the deep water-masses feeding the North Atlantic Deep Water, magnetic susceptibility fluctuations are directly related to variations in the relative amount of magnetic particulates within the sediment; as those magnetic minerals principally originates from a unique source (the Nordic basaltic province), changes in magnetic susceptibility reflect changes in the efficiency of their transport mode from the source area to the study site, i.e. changes in the intensity of bottom currents. Hence, in our study area, higher values of magnetic susceptibility reflect higher ISOW energy.

Our last type of indicator of bottom flow activity corresponds to benthic foraminiferal concentrations (Fig. 4h). Indeed, in the study of different cores located in the study area, Rasmussen et al. (1997, 1999, 2002a) related this parameter to the activity of the ISOW, with

high concentrations of benthic foraminifera associated with relatively strong bottom current influence and increased ventilation and supply of food, and conversely low benthic abundances related to more quiet deep-sea conditions with reduced fluxes of organic matter.

When looking at the evolution of all these proxies in core MD99-2281, it clearly appears that they all tend to the same general scheme: the ISOW was relatively active during GI and relatively reduced during GS (Figs. 4 and 5). These results are in accordance with findings from previous studies (e.g. Moros et al., 1997, 2002; Van Kreveld et al., 2000; Elliot et al., 2002; Rasmussen and Thomsen, 2004; Ballini et al., 2006). Besides, the higher sedimentation rates recorded during GI (Fig. 4b) indicate that in our study area and during the studied period, the ISOW was responsible of a higher supply of sediment during episodes of high activity rather than of a winnowing of the clay fraction ($< 10 \mu\text{m}$).

One could argue that since the age model of the studied core is based on correlations between our magnetic susceptibility record and the $\delta^{18}\text{O}$ signal of NGRIP ice-core (i.e. on the assumption that the ISOW was reduced during GS), we cannot make any supposition about the timing of changes in deep current intensity. This would be obviously true in the case of studies intending to precisely compare the timing of these changes relatively to the timing of Greenland atmospheric variations. But this is not the case of our study, which aims to compare the timing of deep circulation changes with the one of surface and subsurface hydrological variations (as deduced from the same sedimentological archive), and to compare the trends of all those fluctuations (progressive *versus* abrupt).

5.3. Hydrological signature during Dansgaard-Oeschger events and implications

MD99-2281 records are in general agreement with the usual climatic scheme depicted in previous studies and described in the introduction of this paper, i.e. iceberg surges and a weaker or shallower Atlantic meridional overturning circulation during GS, and conversely warmer surface conditions linked to a more northerly inflow of Atlantic surface waters and associated active deep water convection in the Nordic Seas during GI (cf. Fig. 5). This is especially noticeable with the strong and striking correlation between dinocysts, planktonic and benthic foraminifera abundances throughout all the studied period, which furthermore suggests a coupling of the productivity at the different layers of the water column.

However our records also reveal unusual features, such as the strong stratification of surface waters during GS. Previous studies from the subpolar North Atlantic (e.g. Rasmussen et al., 1996a,b, Rasmussen and Thomsen, 2004 and Dokken et al., 2013 at study sites close to MD99-2281 site, Van Kreveld et al., 2000 in the Irminger Basin) already indirectly deduced from planktonic foraminifera data the presence of a halocline and a stratified water column during GS. In our study, dinocyst assemblages and dinocyst-derived surface hydrological parameters provide direct evidences of the presence of a thin freshwater surface layer and stratified surface waters during stadials, and therefore confirm the previous assumption based on indirect proxies (rather subsurface proxies).

Our records also show atypical progressive trends that can be depicted within GS and most of all within GI (Figs. 3, 5 and 6a). During GS, dinocyst data indicate a deterioration of surface conditions characterized by a more or less gradual decrease of winter SST (depending on the GS considered) while summer SST, surface stratification and seasonality remain high. Foraminifera-derived subsurface hydrological parameters and grain-size data show rapid transitions at the beginning of GS (especially noticeable for GS 10 and 8 for example) which denote an abrupt slowing down of the northward Atlantic flow (sharp decreases of F-Temp and local $\delta^{18}\text{O}_{\text{SW}}$) and of the deep ISOW (marked decreases in grain-sizes, silt ratio and mean size of the silt fraction) at that time. Throughout GI, dinocyst data reveal progressively milder surface conditions marked by a gradual increase of winter SST in parallel with a gradual decrease of stratification and seasonality. Grain-size data also indicate a gradual intensification of the ISOW flow with a maximal intensity at the end of these periods (particularly noticeable when looking at the silt ratio and the mean size of the 10-63 μm fraction, and highlighted by red arrows on Fig. 5). At the opposite, planktonic foraminifera data show that the subsurface reactivation of the NAD at the GS-GI transitions was more abrupt than shown within proxies of surface and deep-sea dynamics.

At first sight, our set of proxies thus denotes a decoupling between surface, subsurface, and deep-sea hydrological processes during DO. This is in agreement with previous studies which already suggested a decoupling between surface and subsurface (Moros et al., 2002) or subsurface and deep circulations (Rasmussen et al., 1996b). However, a detailed examination of our records reveals that subsurface and deep circulations are coupled during GS, i.e. when surface waters are highly stratified, and that surface and deep circulations are coupled during GI, i.e. when the stratification is reduced. This leads us to think that the surface stratification

is a determinant factor for hydrological processes occurring at greater depth around the study area. We can therefore propose the following scenario which conciliates our records and highlights the importance of the water-column organization during millennial scale climatic events (Fig. 6b):

At the end of GS, the NAD rapidly extends northward again. However, the water column is still highly stratified and the near-surface halocline prevents heat exchange towards the atmosphere; heat is thus stored in the subsurface layer below the halocline. Subsurface waters are consequently not dense enough because too warm to sink and deep convection is nil or very limited (at least north of our study site). Then, at the beginning of GI, the halocline starts to be unstable (probably because of the accumulation of heat below). The stratification is then progressively reduced, and heat exchange (between subsurface and surface, and surface and atmosphere) becomes possible again. Subsurface Atlantic waters progressively mix with low salinity surface waters which progressively get saltier. They become sufficiently dense to sink, and deep convection is thus re-activated and progressively intensifies throughout the GI. As a consequence, the ISOW activity progressively strengthens and reaches its maximal vigor at the end of this period. Then, at the beginning of GS, iceberg discharges occur. The associated meltwater has several consequences on the stadial hydrology. First, the freshwater input rapidly propagates in the mixed surface-subsurface layer, lowers its salinity, strongly reduces deep convection, and thus weakens the NAD and the ISOW flows. Secondly, it contributes to the re-establishment of the freshwater surface layer and the associated halocline, and to the progressive slight strengthening of the stratification. NAD and ISOW flows remain weak until the end of GS.

Rasmussen et al. (1996a,b) and Rasmussen and Thomsen (2004) proposed a similar scenario where an accumulation of heat below the fresh surface layer is responsible for the destabilization of the halocline and the abrupt release of a large amount of heat to the atmosphere, then causing the sudden Greenland atmospheric warming. On the basis of benthic assemblages from various cores located around Faeroe Islands (e.g. ENAM93-21; 62.7383°N; -3.9987°E; 1020 m water depth – ENAM33; 61.2647°N; -11.1609°E; 1217 m water depth), they suggested that relatively warm Atlantic intermediate waters keep on flowing into the Nordic Seas below the halocline during GS, and they attributed these warm Atlantic waters to the NAD. However, our results derived from planktonic foraminifera data do not indicate any significant flow of NAD directly below the halocline during GS (Rasmussen et al., 1996a,b and Rasmussen and Thomsen, 2004 recorded indeed a total dominance of *Neogloboquadrina*

pachyderma during stadials), but enables such a flow at deeper water depth. In this case, both the reactivation of the subsurface NAD at the end of GS and the continuous northward flow of Atlantic intermediate waters during GS may have participated in the accumulation of heat below the halocline, the destabilization of this latter, and then the sudden release of heat to the atmosphere at the GS-GI transition.

Dokken et al. (2013) also proposed a similar scenario for GS, with a fresh surface layer, a halocline, and an active Atlantic inflow just below it. This scenario was inferred from planktonic foraminifera data in core MD99-2284 (62.3747°N; -0.9802°E; 1500 m water depth). Considering the location of their study site close to the continental shelf edge, this shallow Atlantic inflow is not contradictory to our results which allow the presence of a narrow warm Atlantic inflow flattened against the shelf edge by the Coriolis force. Such a narrow flow would not be recorded in cores located further away from the shelf such as ours.

The observed gradual intensification of the ISOW flow during GI constitutes the most unusual and salient feature revealed by our data. However, a previous study from the Reykjanes Ridge (Snowball and Moros, 2003) also depicted a very similar pattern in magnetic susceptibility data and quartz to plagioclase ratio in cores LO09-18GC (58.9674°N; -30.6832°E; 1460 m water depth) and SO82-05GGC (59.1857°N; -30.9047°E; 1420 m water depth), with a progressive intensification of the Iceland-Scotland Overflow Water during GI followed by an abrupt reduction.

5.4. Different hydrological patterns during Heinrich stadials

Figure 5 clearly shows that the four HS recorded in the studied section of core MD99-2281 (HS1, HS2, HS3 (which can be divided in HS3a and HS3b, see below) and HS4) do not exhibit the same hydrological patterns. The only common feature corresponds to the harsh surface conditions deduced from dinocyst data and also depicted during GS, and characterized by the presence of a fresh water lid, a high seasonality and a relatively strong stratification of the water column. On the contrary, planktonic foraminifera data and deep-sea proxies show different signals, in amplitude or in trend, thus suggesting different subsurface and deep water mass dynamics (see Table 1).

HS1 and HS4 appear such as HS are usually described in the literature, i.e. with very low local $\delta^{18}\text{O}_{\text{SW}}$ values indicative of very low salinities in the subsurface layer, and strongly

reduced or even shut down northward Atlantic flow and deep-water overflow (according to foraminifera-derived data and grain-size data respectively). Compared to GS, our data indicate a more drastic reduction of the meridional overturning circulation and a more southerly location of the deep convection center during HS1 and HS4, in agreement with previous studies (e.g. Elliot et al., 2002; Rahmstorf, 2002).

At the opposite, HS2 presents a very atypical hydrological signature: grain-size data, in agreement with the magnetic susceptibility signal, indicate a relatively active ISOW; in parallel, subsurface records show F-Temp and local $\delta^{18}\text{O}_{\text{SW}}$ comparable to most of GS ones but higher than the “classical” HS1 and HS4 and even than some GS. These results indicate the presence of saltier (and so denser) and slightly warmer subsurface waters bathing our study site, and thus denotes a slightly more active meridional overturning circulation and a more northerly center of convection during HS2 compared to “classical” HS. This would be besides in agreement with previous paleoreconstructions: in core Na 87-22 (located on the eastern banks of the Rockall Plateau; 55.4833°N; -14.6833°E; 2161 m water depth), Elliot et al. (2002) found benthic $\delta^{13}\text{C}$ values during HS2 which are higher than HS1 and HS4 values and similar to GS values; according to the interpretation of this proxy made by the authors, it suggests that the reduction of deep-water formation and the northward migration of $\delta^{13}\text{C}$ depleted southern source deep waters were less important during HS2 and stadials than during HS1 and HS4. Much farther away from our study area, in the Gulf of Cadiz, core MD99-2339 (35.88°N, -7.53°E; 1170 m water depth; Voelker et al., 2006) also provides indirect evidence of a more active North Atlantic overturning circulation. Indeed, paleoreconstructions of the strength of the Mediterranean Outflow Water (or MOW, which overflows from the Mediterranean Sea to and within the Gulf of Cadiz) have shown that this bottom current has been particularly active during periods of weak Atlantic meridional overturning circulation such as GS and HS (e.g. Cacho et al., 2000; Voelker et al., 2006; Toucanne et al., 2007). Grain-size data of core MD99-2339 show indeed a clear intensification of the MOW during HS1, HS4, HS5, and most GS. However they do not indicate such a strengthening during HS2 (and HS3), and so could denote a more vigorous North Atlantic circulation. Furthermore, Scourse et al. (2009) evidenced higher IRD fluxes during HS2 (compared to other HS) in cores located west and north off Great Britain. According to the authors, these strong fluxes typify the maximal extent of the British Irish Ice-Sheet. In such a context, an Atlantic flow extending more northerly as compared to the other HS might have also contributed to enhance iceberg release from the British Irish Ice-Sheet.

Concerning HS3 (defined, as usually, as the interval starting at the end of GI 5 and ending at the start of GI 4), grain-size data tend to indicate a low ISOW activity throughout the interval. However, foraminifera-derived subsurface parameters show a tripartite structure with (i) low F-Temp and local $\delta^{18}\text{O}_{\text{SW}}$ values indicative of a weak NAD at the beginning and the end of the event and (ii) higher values pointing to a stronger NAD in the central part of the event. Besides, the magnetic susceptibility record shows two peaks around 29.5 and 30.5 ka BP coeval with high F-Temp and local $\delta^{18}\text{O}_{\text{SW}}$ values. Benthic foraminifera concentrations also display a peak concomitant with the first MS peak. Furthermore, [Elliot et al. \(2002\)](#) found a two-phased incursion of southern sourced waters (at the onset and the termination of the event) in core Na 87-22 from the Rockall Plateau and core SU90-24 from the Irminger Basin (62.0667°N; -37.0333°E; 2100 m water depth). Hence, all of these records suggest that HS3 might have been a three-phased event with classical disruptions of the overturning circulation at the beginning and the end of the event, interrupted by a significant resumption of this circulation. The beginning of the period of resumption of this circulation is concomitant with the short interstadial phase defined as GI 5.1 by [Rasmussen et al. \(2014\)](#). Since both intervals before and after GI 5.1 have previously been related to HS3 (e.g. [Sanchez Goñi and Harrison, 2010](#); [Hall et al., 2011](#)) we propose to follow [Rasmussen et al. \(2014\)](#) and to divide the usual HS3 period in three phases: HS3a, GI 5.1, and HS3b such as indicated in [Fig. 5](#). In this way, HS3a and HS3b can be considered as two periods of relatively weak Atlantic meridional overturning circulation, separated from each other by a phase of re-intensification of this circulation also detectable in Greenland ice core records as a milder phase (GI 5.1). The absence of clear evidence of ISOW reactivation in grain-size data during GI 5.1, and its discrete and arguable evidence in the magnetic susceptibility and benthic concentration records is puzzling if we consider, as advanced previously, that subsurface and deep circulations should be coupled due to the strong surface stratification. However, the Wyville-Thompson Ridge could have acted as a topographic barrier (even more than at present) that would have prevented a too weak deep flow to influence our study site by constraining it into the Faeroe Bank Channel (cf. [Fig. 1](#)).

6. Conclusion

Analyses carried out within the framework of this study confirm that the area southwest off Faeroe Islands has been very sensitive to the last glacial millennial-scale climatic variability. Our multiproxy approach allows us to track hydrological processes at different key water depths, and reveals a partly and episodically coupling of surface, subsurface and deep water mass dynamics controlled by surface stratification during rapid climatic shifts. Indeed, GI are characterized by a decreasing stratification and a coupling of surface and deep hydrological processes, with progressively milder surface conditions and gradual intensification of the ISOW while the activity of the subsurface NAD flow remains constantly high. At the opposite, GS experienced a high surface stratification and coupled subsurface and deep circulations marked by a sharp weakening of the NAD and the ISOW at the beginning of GS, while surface conditions progressively deteriorate throughout the GS. These results led us to propose a scenario describing the evolution and interactions of hydrological processes during DO and taking into account the determining role of the surface stratification. Our records also denote different hydrological signatures during Heinrich stadials. HS1 and HS4 appear as “classical” HS with strongly reduced Atlantic meridional overturning circulation. On the contrary, HS2 probably experienced a relatively active North Atlantic circulation. Finally, HS3 seems to be a three-phased event marked by a re-intensification of the overturning circulation in the middle of the event.

Our study highlights the importance of coupling near-surface reconstructions of oceanic conditions to avoid misinterpretation of data, particularly in areas affected by changes in the structure of the upper water column. It illustrates the potential of such high resolution multiproxy paleoreconstructions, especially in areas close to glacial ice-sheets when aiming to track hydrological processes occurring during the still so enigmatic rapid climatic oscillations of glacial periods. It also encourages model experiments to take into account stratification artifacts and 3D-oceanic scenarios, and to test the robustness of the hydrological mechanisms and interactions proposed in this work.

Acknowledgements.

Part of the analyses conducted on MD99-2281 was supported by the **French INSU (Institut National des Sciences de l'Univers) programme LEFE** (Les enveloppes fluides et l'environnement) within the frame of the *EVE (Evolution et variabilité du climat à l'échelle globale)* 2009-2011 project "RISCC: Rôle des Ice-Shelves dans le Changement Climatique" and of the *IMAGO (Interactions multiples dans l'atmosphère, la glace et l'océan)* 2013 project "ICE-BIO-RAM : Impact des Changements Environnementaux sur la Biodiversité marine lors des Réchauffements Abrupts du cliMat", this latter being also supported by the *INTERRVIE (Interactions Terre/Vie) - TS (Terre solide) INSU programme*. We also acknowledge financial supports and facilities of the **ARTEMIS ¹⁴C AMS French INSU project**. The research leading to these results also benefited from fundings from the **European Union's Seventh Framework programme (FP7/2007-2013)** under grant agreement no 243908, "Past4Future. Climate change - Learning from the past climate". This is Past4Future contribution no XX.

We thank M-H. Castera, I. Billy, P. Lebleu, O. Ther, M. Georget for invaluable technical assistance at EPOC laboratory. We also warmly thank L. Londeix, D. Swingedouw and M. Cremer for their precious advice and enriching discussions which contributed to greatly improve the present study. Data provided in this paper can be obtained through written request to M. Wary.

This is an U.M.R. EPOC 5805 (Université de Bordeaux – C.N.R.S.) contribution.

References

- Alvarez-Solas, J., Charbit, S., Ritz, C., Paillard, D., Ramstein, G., and Dumas, C.: Links between ocean temperature and iceberg discharge during Heinrich events, *Nature Geoscience*, 3, 122-126, 2010.
- Andersen, K. K., Svensson, A., Johnsen, S. J., Rasmussen, S. O., Bigler, M., Röthlisberger, R., Ruth, U., Siggaard-Andersen, M. L., Peder Steffensen, J., Dahl-Jensen, D., Vinther, B. M., and Clausen, H. B.: The Greenland Ice Core Chronology 2005, 15-42 ka. Part 1: constructing the time scale, *Quaternary Science Reviews*, 25, 3246-3257, 2006.
- Antonov, J. I., Seidov, D., Boyer, T. P., Locarnini, R. A., Mishonov, A. V., Garcia, H. E., Baranova, O. K., Zweng, M. M., and Johnson, D. R.: World Ocean Atlas 2009, Volume 2: Salinity, edited by: Levitus, S., NOAA Atlas NESDIS 69, U.S. Government Printing Office, Washington, D.C., 184 pp., 2010.
- Ballini, M., Kissel, C., Colin, C., and Richter, T.: Deep-water mass source and dynamic associated with rapid climatic variations during the last glacial stage in the North Atlantic : a multi-proxy investigation of the detrital fraction of deep-sea sediments., *Geochem. Geophys. Geosystems*, 7, Q02N01, doi:10.1029/2005GC001070, 2006.
- Banks, R. E.: The cold layer in the Gulf of St. Lawrence, *Journal of Geophysical Research*, 71, 1603-1610, 1966.
- Bianchi, G. G. and McCave, I. N.: Holocene periodicity in North Atlantic climate and deep-ocean flow south of Iceland, *Nature*, 397, 515-517, 1999.
- Boldreel, L. O., Andersen, M. S., and Kuijpers, A.: Neogene seismic facies and deep-water gateways in the Faeroe Bank area, NE Atlantic, *Marine Geology*, 152, 129-140, 1998.
- Bond, G., Broecker, W., Johnsen, S., McManus, J., Labeyrie, L., Jouzel, J., and Bonani, G.: Correlations between climate records from North Atlantic sediments and Greenland ice, *Nature*, 365, 143-147, 1993.
- Bond, G. C. and Lotti, R.: Iceberg discharges into the North Atlantic on millennial time scales during the last glaciation, *Science*, 267, 1005-1010, 1995.
- Borenäs, K. and Lundberg, P.: The Faroe-Bank Channel deep-water overflow, *Deep-Sea Research Part II: Topical Studies in Oceanography*, 51, 335-350, 2004.
- Cacho, I., Grimalt, J. O., Sierro, F. J., Shackleton, N., and Canals, M.: Evidence for enhanced Mediterranean thermohaline circulation during rapid climatic coolings, *Earth and Planetary Science Letters*, 183, 417-429, 2000.
- Caley, T. and Roche, D. M.: $\delta^{18}O$ water isotope in the LOVECLIM model (version 1.0)-Part 3: A palaeo-perspective based on present-day data-model comparison for oxygen stable isotopes in carbonates, *Geoscientific Model Development*, 6, 1505-1516, 2013.
- Carstens, J., Hebbeln, D., and Wefer, G.: Distribution of planktic foraminifera at the ice margin in the Arctic (Fram Strait), *Marine Micropaleontology*, 29, 257-269, 1997.
- Caulle, C., Penaud, A., Eynaud, F., Zaragosi, S., Roche, D. M., Michel, E., Boulay, S., and Richter, T.: Sea-surface hydrographical conditions off South Faeroes and within the North-Eastern North Atlantic through MIS 2: The response of dinocysts, *Journal of Quaternary Science*, 28, 217-228, 2013.
- Dansgaard, W., Johnsen, S. J., Clausen, H. B., Dahl-Jensen, D., Gundestrup, N. S., Hammer, C. U., Hvidberg, C. S., Steffensen, J. P., Sveinbjörnsdottir, A. E., Jouzel, J., and Bond, G.: Evidence for general instability of past climate from a 250-kyr ice-core record, *Nature*, 364, 218-220, 1993.
- de Vernal, A., Eynaud, F., Henry, M., Hillaire-Marcel, C., Londeix, L., Mangin, S., Matthiessen, J., Marret, F., Radi, T., Rochon, A., Solignac, S., and Turon, J. L.: Reconstruction of sea-surface conditions at middle to high latitudes of the Northern Hemisphere during the Last Glacial Maximum (LGM) based on dinoflagellate cyst assemblages, *Quaternary Science Reviews*, 24, 897-924, 2005.
- de Vernal, A., Rosell-Melé, A., Kucera, M., Hillaire-Marcel, C., Eynaud, F., Weinelt, M., Dokken, T., and Kageyama, M.: Comparing proxies for the reconstruction of LGM sea-surface conditions in the northern North Atlantic, *Quaternary Science Reviews*, 25, 2820-2834, 2006.
- Dickson, A. J., Austin, W. E. N., Hall, I. R., Maslin, M. A., and Kucera, M.: Centennial-scale evolution of Dansgaard-Oeschger events in the northeast Atlantic Ocean between 39.5 and 56.5 ka B.P., *Paleoceanography*, 23, PA3206, doi:10.1029/2008PA001595, 2008.
- Dokken, T. M., Nisancioglu, K. H., Li, C., Battisti, D. S., and Kissel, C.: Dansgaard-Oeschger cycles: Interactions between ocean and sea ice intrinsic to the Nordic seas, *Paleoceanography*, 28, 491-502, 2013.

- Duplessy, J. C., Labeyrie, L., Juillet-Leclerc, A., Maitre, F., Duprat, J., and Sarnthein, M.: Surface salinity reconstruction of the North Atlantic Ocean during the Last Glacial maximum, *Oceanologica Acta*, 14, 311-324, 1991.
- Ehlers, J. and Gibbard, P. L.: The extent and chronology of Cenozoic Global Glaciation, *Quaternary International*, 164-165, 6-20, 2007.
- Elliot, M., Labeyrie, L., Bond, G., Cortijo, E., Turon, J. L., Tisnerat, N., and Duplessy, J. C.: Millennial-scale iceberg discharges in the Irminger Basin during the last glacial period: Relationship with the Heinrich events and environmental settings, *Paleoceanography*, 13, 433-446, 1998.
- Elliot, M., Labeyrie, L., Dokken, T., and Manthe, S.: Coherent patterns of ice-rafted debris deposits in the Nordic regions during the last glacial (10-60 ka), *Earth and Planetary Science Letters*, 194, 151-163, 2001.
- Elliot, M., Labeyrie, L., and Duplessy, J. C.: Changes in North Atlantic deep-water formation associated with the Dansgaard - Oeschger temperature oscillations (60-10 ka), *Quaternary Science Reviews*, 21, 1153-1165, 2002.
- Epstein, S. and Mayeda, T.: Variation of O18 content of waters from natural sources, *Geochimica et Cosmochimica Acta*, 4, 213-224, 1953.
- Eynaud, F., Turon, J. L., Matthiessen, J., Kissel, C., Peypouquet, J. P., De Vernal, A., and Henry, M.: Norwegian sea-surface palaeoenvironments of marine oxygen-isotope stage 3: The paradoxical response of dinoflagellate cysts, *Journal of Quaternary Science*, 17, 349-359, 2002.
- Eynaud, F., Zaragosi, S., Scourse, J. D., Mojtabid, M., Bourillet, J. F., Hall, I. R., Penaud, A., Locascio, M., and Reijonen, A.: Deglacial laminated facies on the NW European continental margin: The hydrographic significance of British-Irish Ice Sheet deglaciation and Fleuve Manche paleoriver discharges, *Geochemistry, Geophysics, Geosystems*, 8, Q06019, doi:10.1029/2006GC001496, 2007.
- Eynaud, F., Rossignol, L., and Gasparotto, M.-C.: Planktic foraminifera throughout the Pleistocene: from cell to populations to past marine hydrology, in *Foraminifera: Classification, Biology, and Evolutionary Significance*, edited by: Georgescu, M. D., Nova Science Publishers, New York, NY, 2013.
- Ganopolski, A. and Rahmstorf, S.: Rapid changes of glacial climate simulated in a coupled climate model, *Nature*, 409, 153-158, 2001.
- Goodman, D. K.: Dinoflagellate "communities"; from the lower Eocene Nanjemoy formation of Maryland, U.S.A, *Palynology*, 3, 169-190, 1979.
- Guiot, J. and de Vernal, A.: Transfer functions: methods for quantitative paleoceanography based on microfossils, Chapt. thirteen, in: *Developments in Marine Geology*, edited by: Hillaire-Marcel, C. and De Vernal, A., Elsevier, 1, 523-563, 2007.
- Guiot, J. and de Vernal, A.: Is spatial autocorrelation introducing biases in the apparent accuracy of paleoclimatic reconstructions?, *Quaternary Science Reviews*, 30, 1965-1972, 2011a.
- Guiot, J. and de Vernal, A.: QSR Correspondence "Is spatial autocorrelation introducing biases in the apparent accuracy of paleoclimatic reconstructions?" Reply to Telford and Birks, *Quaternary Science Reviews*, 30, 3214-3216, 2011b.
- Hall, I. R., Colmenero-Hidalgo, E., Zahn, R., Peck, V. L., and Hemming, S. R.: Centennial- to millennial-scale ice-ocean interactions in the subpolar northeast Atlantic 18-41 kyr ago, *Paleoceanography*, 26, PA2224, doi:10.1029/2010PA002084, 2011.
- Hansen, B. and Osterhus, S.: North Atlantic-Nordic Sea exchanges, *Progress in Oceanography*, 45, 109-208, 2000.
- Hayes, A., Kucera, M., Kallel, N., Saffi, L., and Rohling, E. J.: Glacial Mediterranean sea surface temperatures based on planktonic foraminiferal assemblages, *Quaternary Science Reviews*, 24, 999-1016, 2005.
- Heinrich, H.: Origin and consequences of cyclic ice rafting in the Northeast Atlantic Ocean during the past 130,000 years, *Quaternary Research*, 29, 142-152, 1988.
- Hodell, D. A., Minth, E. K., Curtis, J. H., McCave, I. N., Hall, I. R., Channell, J. E. T., and Xuan, C.: Surface and deep-water hydrography on Gardar Drift (Iceland Basin) during the last interglacial period, *Earth and Planetary Science Letters*, 288, 10-19, 2009.
- Howe, J. A., Stoker, M. S., Masson, D. G., Pudsey, C. J., Morris, P., Larter, R. D., and Bulat, J.: Seabed morphology and the bottom-current pathways around Rosemary Bank seamount, northern Rockall Trough, North Atlantic, *Marine and Petroleum Geology*, 23, 165-181, 2006.
- Jonkers, L., Brummer, G. J. A., Peeters, F. J. C., Van Aken, H. M., and De Jong, M. F.: Seasonal stratification, shell flux, and oxygen isotope dynamics of leftcoiling *N. pachyderma* and *T. quinqueloba* in the western subpolar North Atlantic, *Paleoceanography*, 25, PA2204, doi:10.1029/2009PA001849, 2010.
- Kissel, C., Laj, C., Labeyrie, L., Dokken, T., Voelker, A., and Blamart, D.: Rapid climatic variations during marine isotopic stage 3: Magnetic analysis of sediments from Nordic Seas and North Atlantic, *Earth and Planetary Science Letters*, 171, 489-502, 1999.
- Kissel, C., Laj, C., Piotrowski, A. M., Goldstein, S. L., and Hemming, S. R.: Millennial-scale propagation of Atlantic deep waters to the glacial Southern Ocean, *Paleoceanography*, 23, PA2102, doi:10.1029/2008PA001624, 2008.
- Kissel, C., Laj, C., Mulder, T., Wandres, C., and Cremer, M.: The magnetic fraction: A tracer of deep water circulation in the North Atlantic, *Earth and Planetary Science Letters*, 288, 444-454, 2009.
- Kucera, M., Weinelt, M., Kiefer, T., Pflaumann, U., Hayes, A., Chen, M. T., Mix, A. C., Barrows, T. T., Cortijo, E., Duprat, J., Juggins, S., and Waelbroeck, C.: Reconstruction of sea-surface temperatures from assemblages of planktonic foraminifera: Multi-technique approach based on geographically constrained calibration data sets and its application to glacial Atlantic and Pacific Oceans, *Quaternary Science Reviews*, 24, 951-998, 2005b.
- Kuijpers, A., Andersen, M. S., Kenyon, N. H., Kunzendorf, H., and Van Weering, T. C. E.: Quaternary sedimentation and Norwegian Sea overflow pathways around Bill Bailey Bank, northeastern Atlantic, *Marine Geology*, 152, 101-127, 1998a.
- Kuijpers, A., Troelstra, S. R., Wisse, M., Nielsen, S. H., and Van Weering, T. C. E.: Norwegian Sea overflow variability and NE Atlantic surface hydrography during the past 150,000 years, *Marine Geology*, 152, 75-99, 1998b.
- Kuijpers, A., Hansen, B., Hühnerbach, V., Larsen, B., Nielsen, T., and Werner, F.: Norwegian Sea overflow through the Faroe-Shetland gateway as documented by its bedforms, *Marine Geology*, 188, 147-164, 2002.
- Kullenberg, G.: Physical Oceanography, Chapt. 3, in: *The Baltic Sea*, edited by: Voipio, A., Elsevier Oceanography Series, Elsevier, 135-181, Amsterdam, The Netherlands, 1981.
- Labeyrie, L. and Cortijo, E.: Physical properties of sediment core MD99-2281, doi:10.1594/PANGAEA.253612, 2005.
- Labeyrie, L., Cortijo, E., and Jansen, E.: Rapport scientifique de la mission INTERPOLE MD99-114/812 IMAGES V, in: *Les Rapports de Campagne à la Mer à bord du Marion Dufresne*, (IPEV, Ed.), Brest, 1999.
- Laj, C., Kissel, C., Mazaud, A., Channell, J. E. T., and Beer, J.: North Atlantic palaeointensity stack since 75 ka (NAPIS-75) and the duration of the Laschamp event, *Philosophical Transactions of the Royal Society A: Mathematical, Physical and Engineering Sciences*, 358, 1009-1025, 2000.
- Levine, R. C. and Bigg, G. R.: Sensitivity of the glacial ocean to Heinrich events from different iceberg sources, as modeled by a coupled atmosphere-iceberg-ocean model, *Paleoceanography*, 23, PA4213, doi:10.1029/2008PA001613, 2008.
- Locarnini, R. A., Mishonov, A. V., Antonov, J. I., Boyer, T. P., Garcia, H. E., Baranova, O. K., Zweng, M. M., and Johnson, D. R.: *World Ocean Atlas 2009, Volume 1: Temperature*, edited by : Levitus, S., NOAA Atlas NESDIS 68, U.S. Government Printing Office, Washington, D.C., 184 pp., 2010.
- Londeix, L., Benzakour, M., Suc, J. P., and Turon, J. L.: Messinian palaeoenvironments and hydrology in Sicily (Italy): The dinoflagellate cyst record, *Geobios*, 40, 233-250, 2007.

- Malaizé, B. and Caley, T.: Sea surface salinity reconstruction as seen with foraminifera shells: Methods and cases studies, *European Physical Journal*, 1, 177-188, 2009.
- Manabe, S. and Stouffer, R. J.: Simulation of abrupt climate change induced by freshwater input to the North Atlantic Ocean, *Nature*, 378, 165-167, 1995.
- Mary, Y., Eynaud, F., Zaragosi, S., Malaizé, B., Cremer, M., and Schmidt, S.: High frequency environmental changes and deposition processes in a 2 kyr-long sedimentological record from the Cap-Breton canyon (Bay of Biscay), *Holocene*, 25, 348-365, 2015.
- Matsuzaki, K. M. R., Eynaud, F., Malaizé, B., Grousset, F. E., Tisserand, A., Rossignol, L., Charlier, K., and Jullien, E.: Paleoceanography of the Mauritanian margin during the last two climatic cycles: From planktonic foraminifera to African climate dynamics, *Marine Micropaleontology*, 79, 67-79, 2011.
- McCave, I. N.: Deep-sea sediment deposits and properties controlled by currents, Chapt. One, in: *Developments in Marine Geology*, edited by: Hillaire-Marcel, C. and De Vernal, A., Elsevier, 1, 19-62, 2007.
- McCave, I. N., Manighetti, B., and Beveridge, N. A. S.: Circulation in the glacial North Atlantic inferred from grain-size measurements, *Nature*, 374, 149-152, 1995a.
- McCave, I. N., Manighetti, B., and Robinson, S. G.: Sortable silt and fine sediment size/composition slicing: parameters for palaeocurrent speed and palaeoceanography, *Paleoceanography*, 10, 593-610, 1995b.
- Moros, M., Endler, R., Lackschewitz, K. S., Wallrabe-Adams, H. J., Mienert, J., and Lemke, W.: Physical properties of Reykjanes Ridge sediments and their linkage to high-resolution Greenland Ice Sheet Project 2 ice core data, *Paleoceanography*, 12, 687-695, 1997.
- Moros, M., Kuijpers, A., Snowball, I., Lassen, S., Bäckström, D., Gingele, F., and McManus, J.: Were glacial iceberg surges in the North Atlantic triggered by climatic warming?, *Marine Geology*, 192, 393-417, 2002.
- Orvik, K. A. and Nilner, P.: Major pathways of Atlantic water in the northern North Atlantic and Nordic Seas toward Arctic, *Geophysical Research Letters*, 29, 2-1, 2002.
- Peck, V. L., Hall, I. R., Zahn, R., and Elderfield, H.: Millennial-scale surface and subsurface paleothermometry from the northeast Atlantic, 55-8 ka BP, *Paleoceanography*, 23, PA3221, doi:10.1029/2008PA001631, 2008.
- Penaud, A., Eynaud, F., Voelker, A., Kageyama, M., Marret, F., Turon, J. L., Blamart, D., Mulder, T., and Rossignol, L.: Assessment of sea surface temperature changes in the Gulf of Cadiz during the last 30 ka: Implications for glacial changes in the regional hydrography, *Biogeosciences*, 8, 2295-2316, 2011.
- Prins, M. A., Bouwer, L. M., Beets, C. J., Troelstra, S. R., Weltje, G. J., Kruk, R. W., Kuijpers, A., and Vroon, P. Z.: Ocean circulation and iceberg discharge in the glacial North Atlantic: Inferences from unmixing of sediment size distributions, *Geology*, 30, 555-558, 2002.
- Rahmstorf, S.: Ocean circulation and climate during the past 120,000 years, *Nature*, 419, 207-214, 2002.
- Rasmussen, T. L. and Thomsen, E.: The role of the North Atlantic Drift in the millennial timescale glacial climate fluctuations, *Palaeogeography, Palaeoclimatology, Palaeoecology*, 210, 101-116, 2004.
- Rasmussen, T. L. and Thomsen, E.: Warm Atlantic surface water inflow to the Nordic seas 34-10 calibrated ka B.P., *Paleoceanography*, 23, 2008.
- Rasmussen, T. L. and Thomsen, E.: Ventilation changes in intermediate water on millennial time scales in the SE Nordic seas, 65-14 kyr BP, *Geophysical Research Letters*, 36, L01601, doi:10.1029/2008GL036563, 2009.
- Rasmussen, T. L., Thomsen, E., Labeyrie, L., and Van Weering, T. C. E.: Circulation changes in the Faeroe-Shetland Channel correlating with cold events during the last glacial period (58-10 ka), *Geology*, 24, 937-940, 1996a.
- Rasmussen, T. L., Thomsen, E., Van Weering, T. C. E., and Labeyrie, L.: Rapid changes in surface and deep water conditions at the Faeroe Margin during the last 58,000 years, *Paleoceanography*, 11, 757-771, 1996b.
- Rasmussen, T. L., Van Weering, T. C. E., and Labeyrie, L.: Climatic instability, ice sheets and ocean dynamics at high northern latitudes during the last glacial period (58-10 KA BP), *Quaternary Science Reviews*, 16, 71-80, 1997.
- Rasmussen, T. L., Balbon, E., Thomsen, E., Labeyrie, L., and Van Weering, T. C. E.: Climate records and changes in deep outflow from the Norwegian Sea ~ 150-55 ka, *Terra Nova*, 11, 61-66, 1999.
- Rasmussen, T. L., Thomsen, E., Troelstra, S. R., Kuijpers, A., and Prins, M. A.: Millennial-scale glacial variability versus Holocene stability: Changes in planktic and benthic foraminifera faunas and ocean circulation in the North Atlantic during the last 60 000 years, *Marine Micropaleontology*, 47, 143-176, 2002a.
- Rasmussen, T. L., Bäckström, D., Heinemeier, J., Klitgaard-Kristensen, D., Knutz, P. C., Kuijpers, A., Lassen, S., Thomsen, E., Troelstra, S. R., and Van Weering, T. C. E.: The Faeroe-Shetland Gateway: Late Quaternary water mass exchange between the Nordic seas and the northeastern Atlantic, *Marine Geology*, 188, 165-192, 2002b.
- Rasmussen, S. O., Bigler, M., Blockley, S. P., Blunier, T., Buchardt, S. L., Clausen, H. B., Cvijanovic, I., Dahl-Jensen, D., Johnsen, S. J., Fischer, H., Gkinis, V., Guillevic, M., Hoek, W. Z., Lowe, J. J., Pedro, J. B., Popp, T., Seierstad, I. K., Steffensen, J. P., Svensson, A. M., Vallelonga, P., Vinther, B. M., Walker, M. J. C., Wheatley, J. J., and Winstrup, M.: A stratigraphic framework for abrupt climatic changes during the Last Glacial period based on three synchronized Greenland ice-core records: Refining and extending the INTIMATE event stratigraphy, *Quaternary Science Reviews*, 106, 14-28, 2014.
- Rochon, A., de Vernal, A., Turon, J.-L., Matthiessen, J., and Head, M. J. (Eds.): Distribution of dinoflagellate cysts in surface sediments from the North Atlantic Ocean and adjacent basins and quantitative reconstruction of sea-surface parameters, *AASP special pub.*, Dallas, Texas, 1999.
- Sanchez Goñi, M. F. and Harrison, S. P.: Millennial-scale climate variability and vegetation changes during the Last Glacial: Concepts and terminology, *Quaternary Science Reviews*, 29, 2823-2827, 2010.
- Sanchez Goñi, M. F., Bakker, P., Desprat, S., Carlson, A. E., Van Meerbeeck, C. J., Peyron, O., Naughton, F., Fletcher, W. J., Eynaud, F., Rossignol, L., and Renssen, H.: European climate optimum and enhanced Greenland melt during the last interglacial, *Geology*, 40, 627-630, 2012.
- Sanchez Goñi, M. F., Bard, E., Landais, A., Rossignol, L., and D'Errico, F.: Air-sea temperature decoupling in western Europe during the last interglacial-glacial transition, *Nature Geoscience*, 6, 837-841, 2013.
- Schäfer-Neth, C. and Manschke, A.: Available at: <http://www.geo.uni-bremen.de/geomod/staff/csn/woasample.html>, 2002.
- Schiebel, R., Waniek, J., Bork, M., and Hemleben, C.: Planktic foraminiferal production stimulated by chlorophyll redistribution and entrainment of nutrients, *Deep-Sea Research Part I: Oceanographic Research Papers*, 48, 721-740, 2001.
- Schlitzer, R.: Ocean Data View, available at: <http://odv.awi.de> (last access: 8 April 2014), 2012.
- Scourse, J. D., Haapaniemi, A. I., Colmenero-Hidalgo, E., Peck, V. L., Hall, I. R., Austin, W. E. N., Knutz, P. C., and Zahn, R.: Growth, dynamics and deglaciation of the last British-Irish ice sheet: the deep-sea ice-rafted detritus record, *Quaternary Science Reviews*, 28, 3066-3084, 2009.
- Shackleton, N. J.: Attainment of isotopic equilibrium between ocean water and the benthic foraminifera genus *Uvigerina*: isotopic changes in the ocean during the Last Glacial, in: *Methodes Quantitatives d'Étude des Variations du Climat au Cours du Pleistocène*, edited by: Labeyrie, L., *Colloques Internationaux du CNRS*, no. 219, Paris, 203-209, 1974.
- Shannon, C. E. and Weaver, W.: *The Mathematical Theory of Information*, University of Illinois Press, Urbana, 1949.
- Siddall, M., Rohling, E. J., Thompson, W. G., and Waelbroeck, C.: Marine isotope stage 3 sea level fluctuations: Data

- synthesis and new outlook, *Reviews of Geophysics*, 46, RG4003, doi:10.1029/2007RG000226, 2008.
- Simstich, J., Sarnthein, M., and Erlenkeuser, H.: Paired $\delta^{18}\text{O}$ signals of *Neogloboquadrina pachyderma* (s) and *Turborotalita quinqueloba* show thermal stratification structure in Nordic Seas, *Marine Micropaleontology*, 48, 107-125, 2003.
- Snowball, I. and Moros, M.: Saw-tooth pattern of North Atlantic current speed during Dansgaard-Oeschger cycles revealed by the magnetic grain size of Reykjanes Ridge sediments at 59°N, *Paleoceanography*, 18, 4-1, 2003.
- Staines-Urías, F., Kuijpers, A., and Korte, C.: Evolution of subpolar North Atlantic surface circulation since the early Holocene inferred from planktic foraminifera faunal and stable isotope records, *Quaternary Science Reviews*, 76, 66-81, 2013.
- Stanford, J. D., Rohling, E. J., Bacon, S., and Holliday, N. P.: A review of the deep and surface currents around Eirik Drift, south of Greenland: Comparison of the past with the present, *Global and Planetary Change*, 79, 244-254, 2011.
- Svensson, A., Andersen, K. K., Bigler, M., Clausen, H. B., Dahl-Jensen, D., Davies, S. M., Johnsen, S. J., Muscheler, R., Parrenin, F., Rasmussen, S. O., Röthlisberger, R., Seierstad, I., Steffensen, J. P., and Vinther, B. M.: A 60 000 year Greenland stratigraphic ice core chronology, *Climate of the Past*, 4, 47-57, 2008.
- Tolderlund, D. S. and Bé, A. W. H.: Seasonal Distribution of Planktonic Foraminifera in the Western North Atlantic, *Micropaleontology*, 17, 297-329, 1971.
- Toucanne, S., Mulder, T., Schönfeld, J., Hanquiez, V., Gonthier, E., Duprat, J., Cremer, M., and Zaragosi, S.: Contourites of the Gulf of Cadiz: A high-resolution record of the paleocirculation of the Mediterranean outflow water during the last 50,000 years, *Palaeogeography, Palaeoclimatology, Palaeoecology*, 246, 354-366, 2007.
- Van Kreveld, S., Sarnthein, M., Erlenkeuser, H., Grootes, P., Jung, S., Nadeau, M. J., Pflaumann, U., and Voelker, A.: Potential links between surging ice sheets, circulation changes, and the Dansgaard-Oeschger cycles in the Irmiger Sea, 60-80 kyr, *Paleoceanography*, 15, 425-442, 2000.
- Voelker, A. H. L., Lebreiro, S. M., Schönfeld, J., Cacho, I., Erlenkeuser, H., and Abrantes, F.: Mediterranean outflow strengthening during northern hemisphere coolings: A salt source for the glacial Atlantic?, *Earth and Planetary Science Letters*, 245, 39-55, 2006.
- Waelbroeck, C., Labeyrie, L., Michel, E., Duplessy, J. C., McManus, J. F., Lambeck, K., Balbon, E., and Labracherie, M.: Sea-level and deep water temperature changes derived from benthic foraminifera isotopic records, *Quaternary Science Reviews*, 21, 295-305, 2002.
- Wolff, E. W., Chappellaz, J., Blunier, T., Rasmussen, S. O., and Svensson, A.: Millennial-scale variability during the last glacial: The ice core record, *Quaternary Science Reviews*, 29, 2828-2838, 2010.
- Zumaque, J., Eynaud, F., Zaragosi, S., Marret, F., Matsuzaki, K. M., Kissel, C., Roche, D. M., Malaizé, B., Michel, E., Billy, I., Richter, T., and Palis, E.: An ocean-ice coupled response during the last glacial: a view from a marine isotopic stage 3 record south of the Faeroe Shetland Gateway, *Climate of the Past*, 8, 1997-2017, 2012.

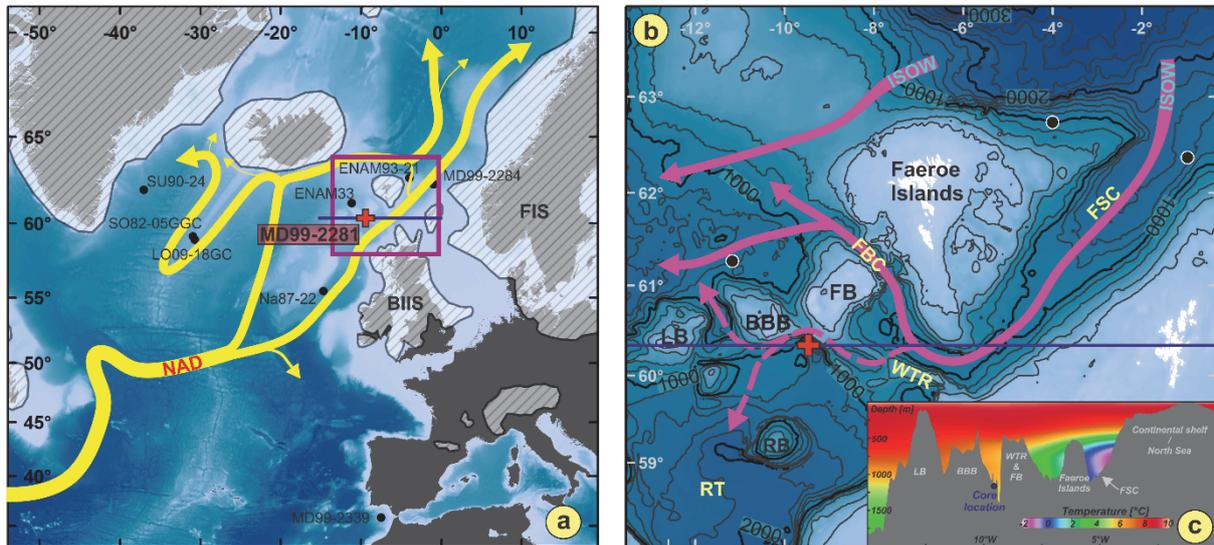
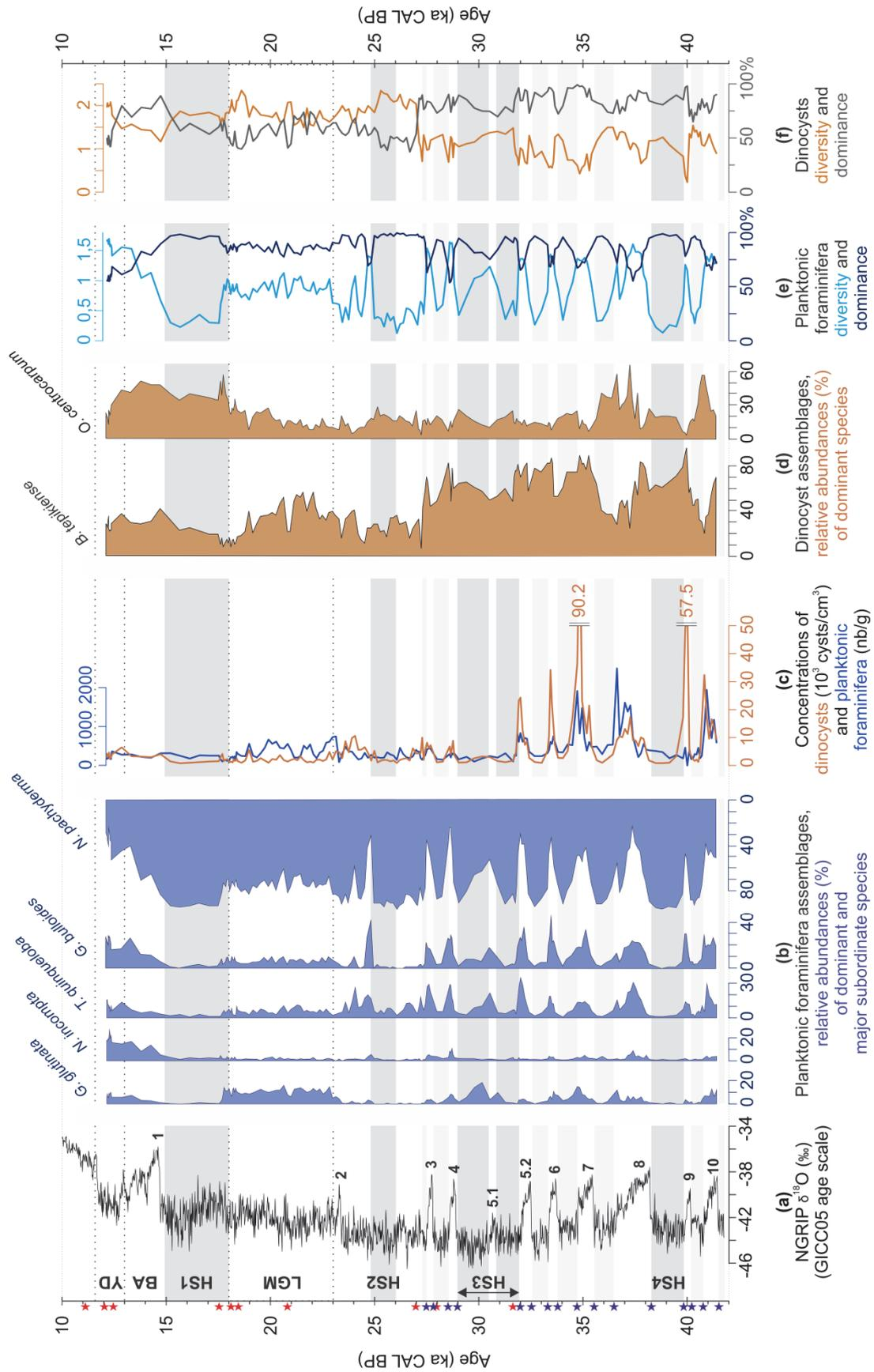


Figure 1: (a) General map of the studied area, showing the location of the studied core MD99-2281 (red cross) and of nearby cores referred to in the present study (black dots; ENAM93-21 and ENAM33, Rasmussen et al., 1996a,b, Rasmussen and Thomsen, 2004; MD99-2284, Dokken et al., 2013; LO09-18GC and SO82-05GGC, Snowball and Moros, 2003; Na87-22 and SU90-24, Elliot et al., 2002). The hatched areas represent the maximal last glacial extension of the proximal ice-sheets (after Ehlers and Gibbard, 2007; FIS: Fennoscandian Ice-Sheet; BIIS: British-Irish Ice-Sheet). The yellow arrows indicate the major pathways of the warm and saline surface water conveyed by the North Atlantic Drift (NAD, after Orvik and Niiler, 2002 and Stanford et al., 2011). Purple square indicates the area shown in Fig. 1b. Blue line indicates the location of the profile shown in Fig. 1c. (b) Detailed physiography of the studied area. Bathymetry is from GEBCO (www.gebco.net, isobaths every 200 m). Remarkable sub-marine structures are indicated (bathymetric heights: FB, Faeroe Bank; BBB, Bill Bailey Bank; LB, Lousy Bank; WTR, Wyville-Thompson Ridge – trough; RT, Rockall Trough – and channels: FSC, Faeroe-Shetland Channel; FBC, Faeroe Bank Channel). Purple arrows show the major (full lines) and intermittent (dotted lines) deep Iceland Scotland Overflow Water (ISOW) pathways, after Boldreel et al., (1998), Kuijpers et al. (1998b, 2002), and Howe et al. (2006). Blue line indicates the location of the profile shown in Fig. 1c. (c) East-west profile of oceanic temperatures. Temperature data are derived from WOA09 (Locarnini et al., 2010) and plot using Ocean Data View (Schlitzer, 2012); bathymetric data are from GEBCO (www.gebco.net). Locations of the studied core and of the main sub-marine structures are indicated. Geographic coordinate system: WGS 1984 – Projection: Mercator 55°N.

Figure 2: Evolution of index micro-planktonic assemblages compared to (a) NGRIP-GICC05 $\delta^{18}O$ record: (b) Relative abundances of the dominant planktonic foraminifera species – (c) Absolute abundances (nb. of specimen in the sediment) of dinocysts and planktonic foraminifera – (d) Relative abundances of dominant dinocyst species – (e) Planktonic foraminifera diversity and dominance (see calculations in Sect. 3.2.) – (f) Dinocyst diversity and dominance. Red stars indicate AMS 14C dates used, and blue stars show the tie-points obtained by comparing the MD99-2281 magnetic susceptibility record to the NGRIP $\delta^{18}O$ signal (see Zumaque et al., 2012). GS and HS are highlighted by light and dark grey bands respectively (age limits after Wolff et al., 2010). DO are numbered according to corresponding GI numbers in Dansgaard et al. (1993), except for GI 5 which was divided in GI 5.2 and GI 5.1 according to Rasmussen et al. (2014). LGM is for Last Glacial Maximum, BA for Bølling-Allerød, and YD for Younger Dryas.



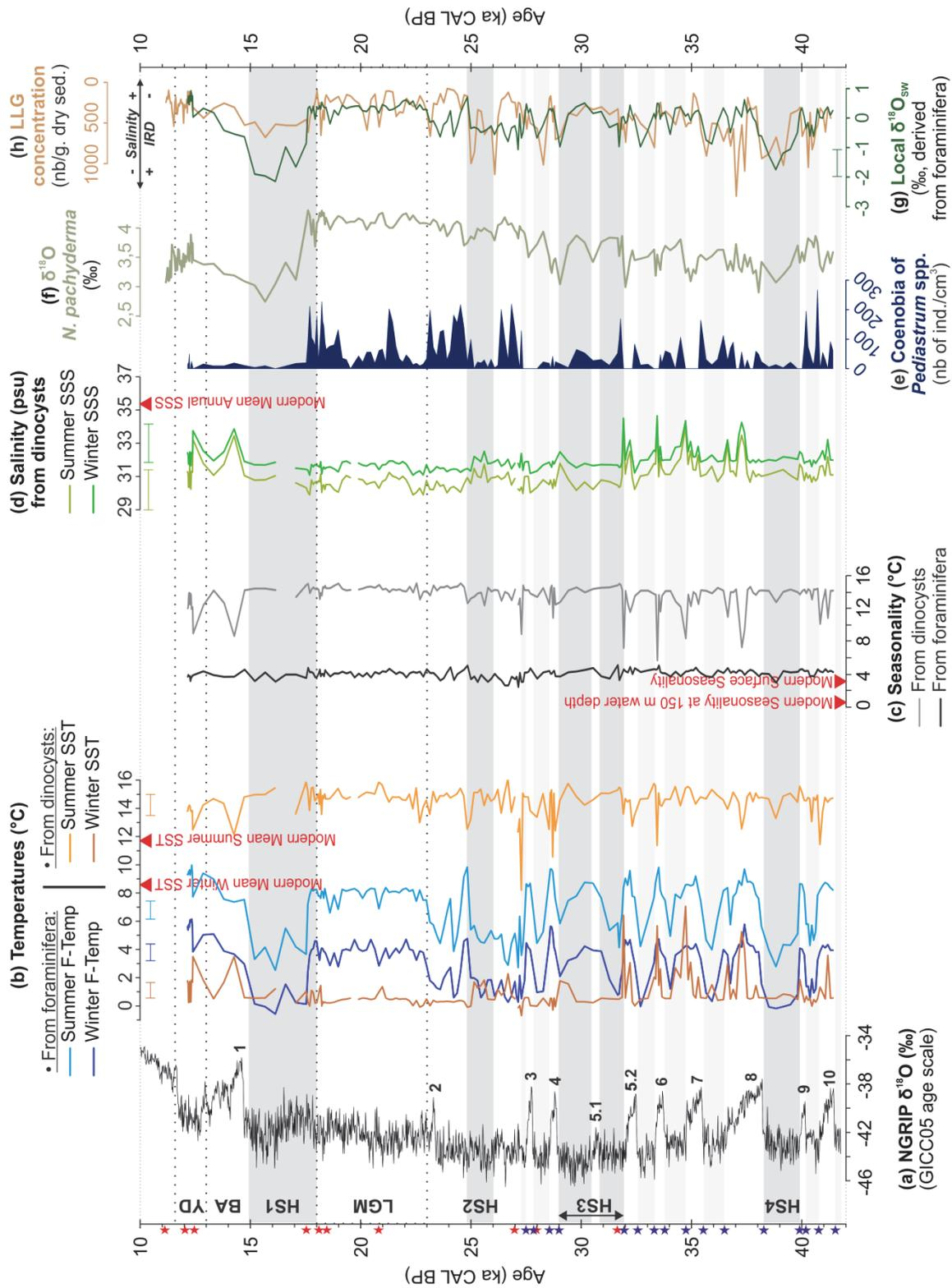
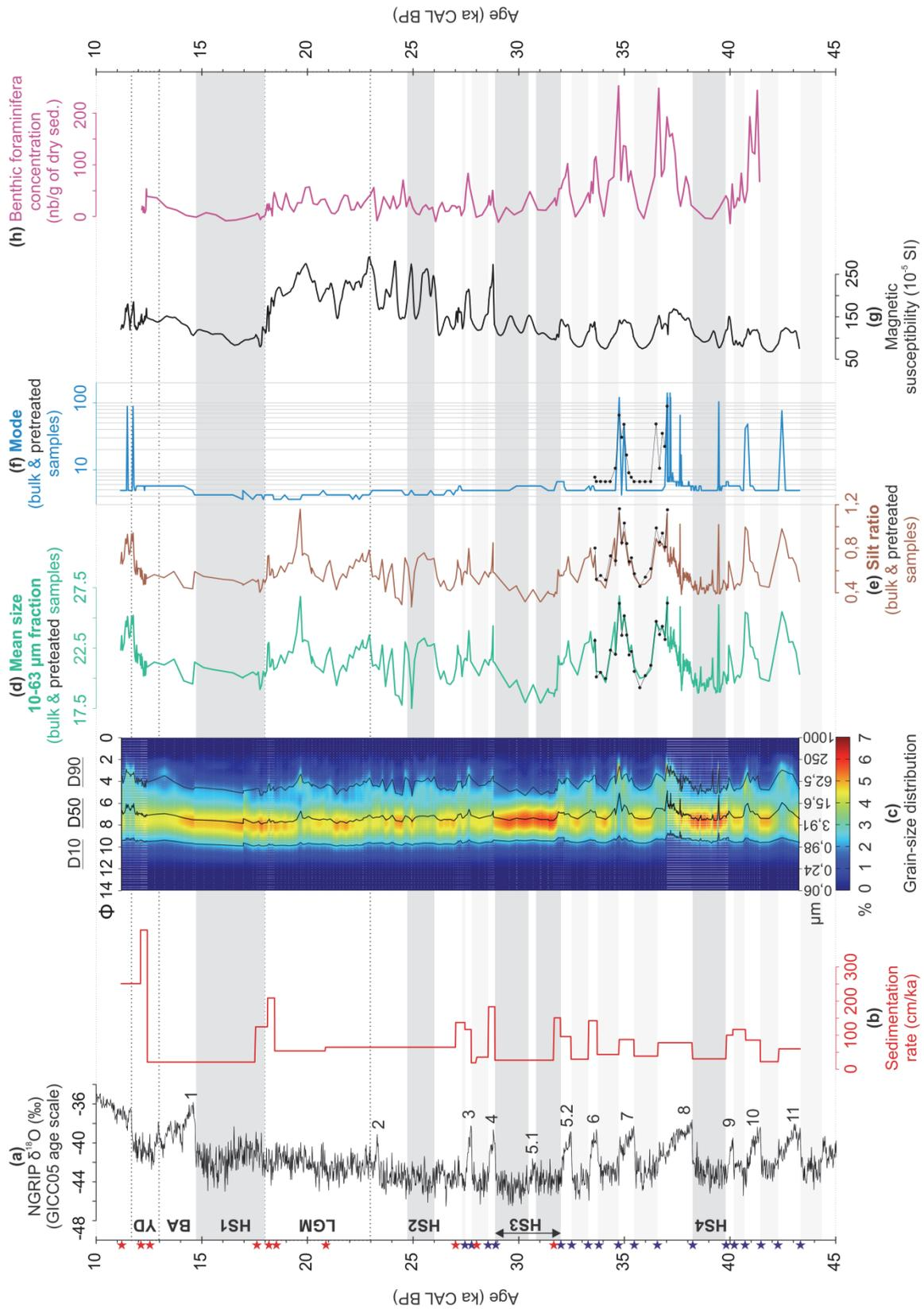


Figure 3: Reconstructed hydrological parameters derived from dinocyst and planktonic foraminifera assemblages compared to (a) NGRIP-GICC05 $\delta 18O$ record: – (b) Temperatures – (c) Seasonality (mean summer minus winter temperatures) – (d) SSS derived from dinocysts – (e) Abundances of *Coenobia* of the freshwater algae *Pediastrum* spp. – (f) $\delta 18O$ measured on *N. pachyderma* – (g) Local $\delta 18O_{sw}$ derived from $\delta 18O$ on *N. pachyderma* – (h) Large Lithic Grains (LLG) concentration, plotted on a reverse scale. Stars, bands, DO number and acronyms: same legend as Fig. 2.

Figure 4: Evolution of oceanic bottom conditions. (a) NGRIP-GICC05 $\delta^{18}O$ record – (b) Sedimentation rate (calculated between two consecutive tie-points) – (c) Grain-size distribution on the background, and D10, D50, and D90 represented as black curves in the foreground – (d) Mean size of the silt (10–63 μm) fraction for bulk samples and pretreated samples (carbonates and organic matter removed) – (e) Silt ratio between 26–63 μm and 10–26 μm fractions for bulk and pretreated samples – (f) Mean diameter of the dominant grain-size mode for bulk and pretreated samples – (g) Magnetic susceptibility record – (h) Absolute abundances of benthic foraminifera. Stars, bands, DO number and acronyms: same legend as Fig. 2.



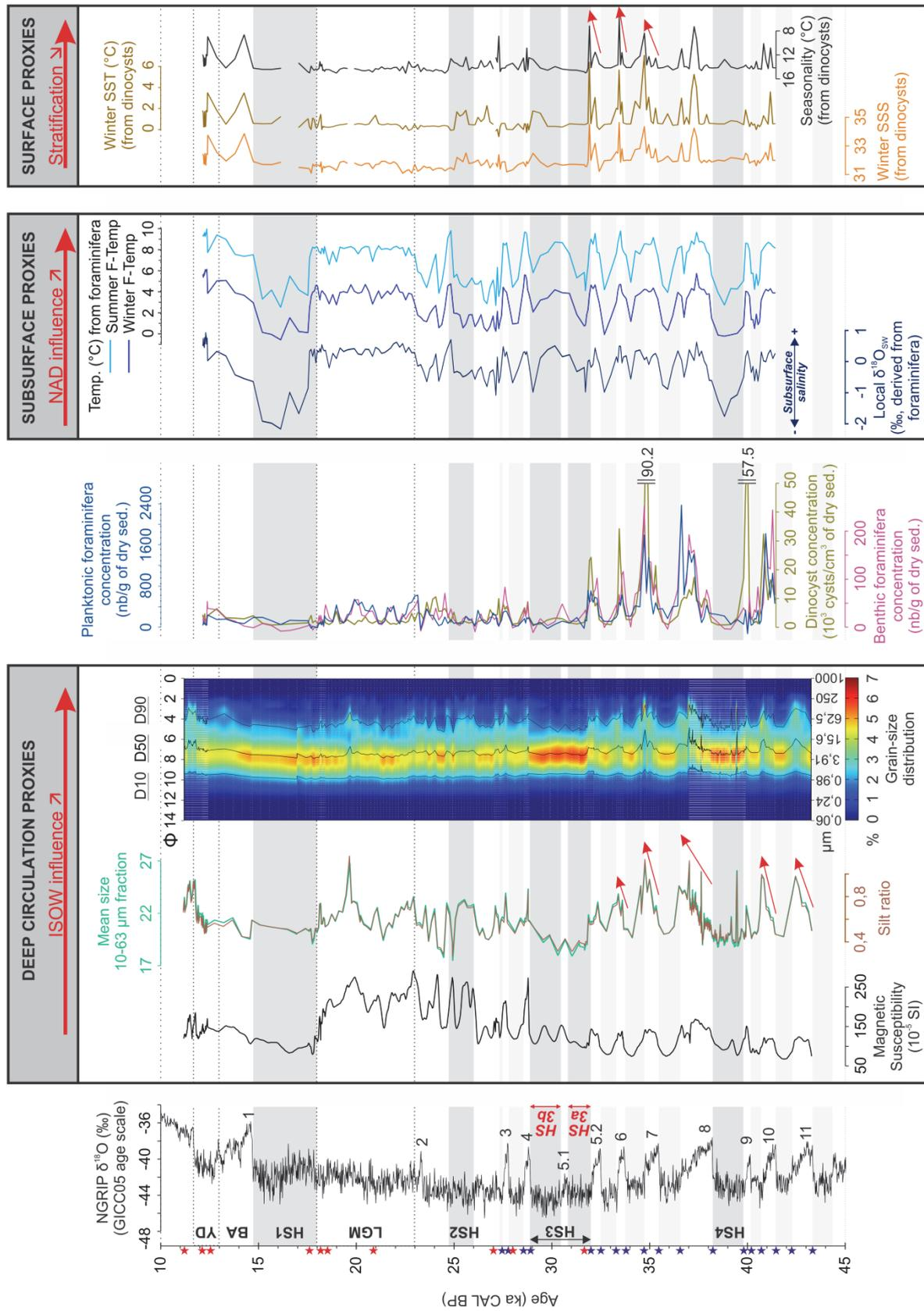


Figure 5: Comparative figure showing the evolution through time of proxies indicative of the ISOW bottom dynamics (left framed panel), the subsurface NAD intensity (middle framed panel), and the surface sensu stricto conditions (right framed panel). Absolute abundances of benthic foraminifera, planktonic foraminifera, and dinocysts are shown in the middle unframed panel. NGRIP $\delta^{18}\text{O}$ record is shown at the far left to illustrate the chronological framework. Stars, bands, DO number and acronyms: same legend as Fig. 2. Red arrows highlight the progressive trends.

Figure 6. Synthetic figure illustrating the hydrological processes occurring during Dansgaard-Oeschger cycles at the study site. (a) Zoom in on DO 8, 7, 6 and 5 showing the evolution of some selected proxies shown in Fig. 5, as well as the schematic evolution through DO of the ISOW activity, the NAD vigor, the intensity of mixing between surface and subsurface waters, and the degree of surface stratification. (b) Conceptual representation of the hydrological processes occurring during the different phases of DO as depicted in Fig. 6a.

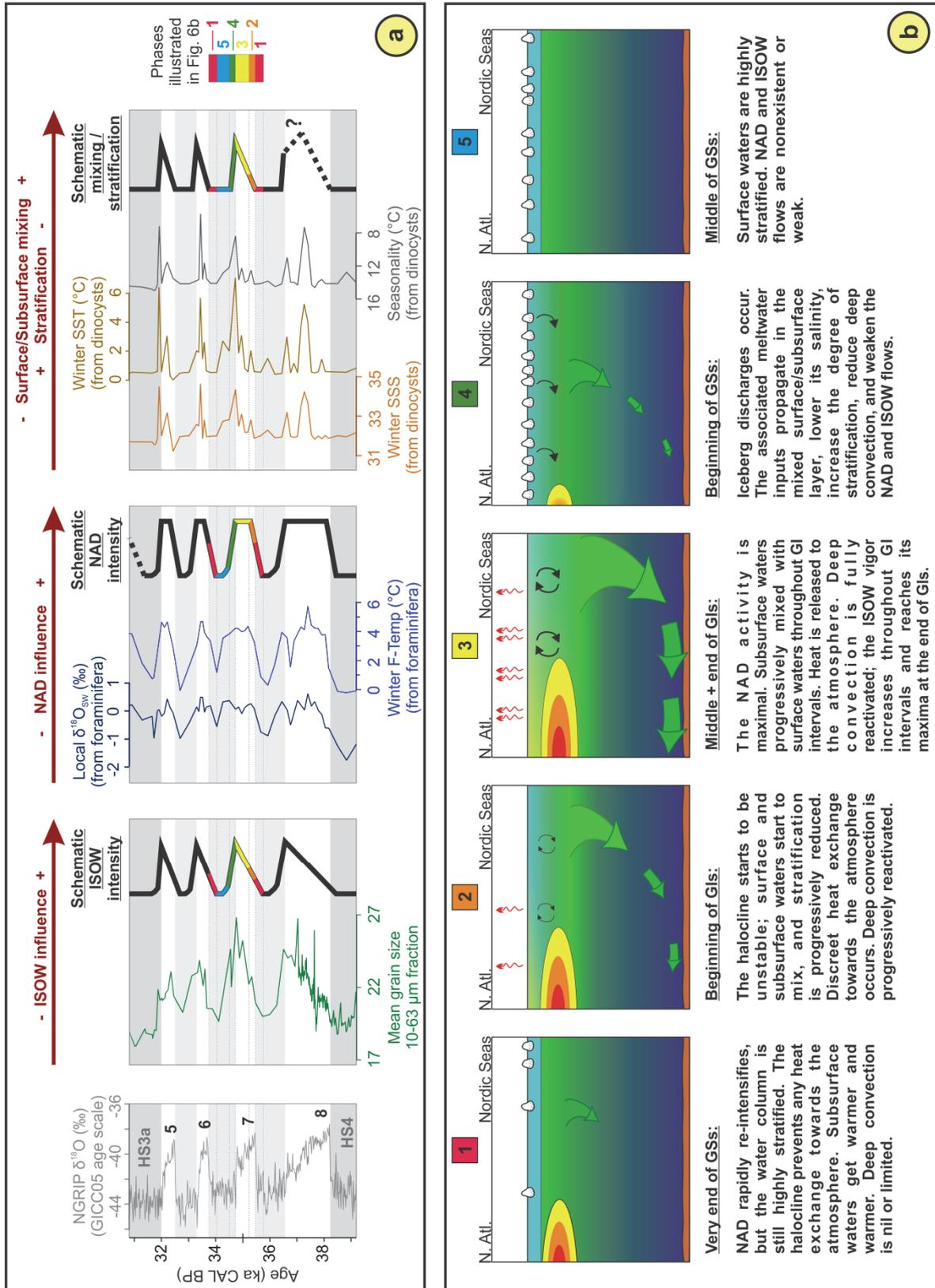


Table 1: Synthesis of the main hydrologic features depicted at the study site during Heinrich stadials (HS) 1 to 4.

Event	Bottom (ISOW)	Subsurface (NAD)	Surface	Interpretations
HS1 & HS4	Weak or stopped	Weak or stopped	High stratification	As usually described HS
HS2	Relatively active	More active than during HS1 & HS4	- No mixing between surface and subsurface waters	"Atypical" HS Relatively active overturning circulation, center of deep convection located more northerly
HS3	Three-phased or weak	Three-phased (↓↑↓)		Three-phased event (HS3a, GI 5.1, HS3b)

Supplementary Information and Material to:

“Stratification of surface waters during the last glacial millennial climatic events: a key factor in subsurface and deep water mass dynamics”

Wary Mélanie¹, Eynaud Frédérique¹, Sabine Marjolaine¹, Zaragosi Sébastien¹,
Rossignol Linda¹, Malaizé Bruno¹, Palis Edouard^{1,*}, Zumaque Jena^{1,**}, Caille Clémence^{1,***},
Penaud Aurélie², Michel Elisabeth³, Charlier Karine¹

¹ UMR 5805, EPOC (Environnements et Paléoenvironnements Océaniques et Continentaux), Université de Bordeaux, 33615 Pessac, France

² UMR 6538, Domaines Océaniques, IUEM-UBO, F-29280 Plouzané, France

³ UMR 8212, LSCE (Laboratoire des Sciences du Climat et de l'Environnement), CEA/CNRS-INSU/UVSQ, 91198 Gif-sur-Yvette cedex, France

* now at: UMR 7329, Géoazur, Université de Sophia Antipolis, 06560 Valbonne, France.

** now at: UQAM, Université du Québec à Montreal, Montréal, Québec H3C 3P8, Canada

*** now at: Laboratory of Recent and Fossil Bio-Indicators, CNRS UMR6112 LPG-BIAF, Angers, France

Why interpreting the reconstructed planktonic foraminiferal temperature signal as relative subsurface temperature variations is coherent in our study area?

In the present study, we reconstruct oceanic temperatures by applying a transfer function to planktonic foraminifera assemblages. This transfer function uses a modern database where annual and seasonal oceanic temperatures are extracted at 10 meters water depth. In such a configuration, the reconstructed temperatures are, or should be a priori, assumed to represent sea-surface temperatures (SST).

However, the comparison of our foraminifera-derived temperature (F-Temp) signals with our dinocyst-derived SST signals (reconstructed by applying a similar transfer function to dinocyst assemblages) shows strong discrepancies. Studies dealing with SST reconstructions obtained through different methods (e.g. Mg/Ca on planktonic foraminifera shells, relative abundance of planktonic foraminifera index species, alkenone index UK'37, transfer functions applied to assemblages of planktonic foraminifera, dinocysts, diatoms, coccoliths, etc.) are generally also confronted to similar discrepancies (e.g. Mazaud et al., 2002; Sicre et al., 2005; de Vernal et al., 2005, 2006; Peck et al., 2008; Penaud et al., 2011). To explain it, the authors usually call for differences in growth season and/or in depth habitat of the associated organisms, and/or for interannual variability, and/or for allochthonous advection. In the case of dinocyst-derived versus planktonic foraminifera-derived temperature reconstructions, many studies have mainly attributed these discrepancies to changes in depth habitat (e.g. de Vernal et al., 2005, 2006; Penaud et al., 2011).

In our case, such an explanation is strongly coherent from an ecological point of view, given that:

- 1) While dinoflagellates, as part of the phytoplankton, are restricted to the photic layer (Sarjeant, 1974), heterotrophic planktonic foraminifera may live deeper (e.g. Schiebel et al., 2001). This is particularly true for the main species composing our foraminiferal assemblages since they do not bear any symbiont.
- 2) Our dinocyst-derived SSS (sea-surface salinity) records indicate the presence of a low saline surface layer throughout the last glacial period (mean of 31 and 32 psu for summer and winter SSS respectively). However, the planktonic foraminifera species identified in our assemblages (Supplementary Table 1) barely tolerate such salinities (Tolderlund and Bé, 1971).

Hence, given the ecological tolerances of the identified planktonic foraminifera species, it seems consistent to relate planktonic foraminifera assemblages to a depth habitat deeper than the one of dinocysts.

However, as SST in the modern planktonic foraminifera database are extracted at 10 m water depth, it is a priori incoherent to interpret the reconstructed F-Temp as subsurface temperatures. Nonetheless, according to previous works focused on transfer functions (using the modern analog technique) applied to planktonic foraminifera assemblages, it seems reasonable to interpret the F-Temp signals as relative variations of subsurface temperatures in our study area.

Indeed, for transfer functions *sensu lato*, the reference living-depth of foraminifera to consider in modern SST training sets is really problematic and its definition not trivial. Numerous tests were previously done on this question. Among them, Pflaumann et al. (1996) have demonstrated that such a consideration does not provide significant differences in the reconstructed F-Temp. Telford et al. (2013) showed that “*For cores north of 25°N, the [paleo]reconstructions from different depths and seasons resemble one another, with an offset*”, implying that **even if we have chosen another extraction depth for SST, the relative variations of our signals would be very similar.**

Furthermore, even if Telford et al. (2013) evidenced that for sites in the North Atlantic drift (including the nearby site NA87-22; cf. page 862) paleoreconstructions at all depth are statistically significant, he also argue that “*the most ecologically relevant depth varies in space and time, and the assemblages will probably integrate the communities from several depths and seasons, so selecting a more appropriate fixed depth for temperature reconstructions for each location is probably not trivial and does not completely circumvent the problem.*”. This latter statement is also supported by Adloff et al. (2011): “*The currently used technique to reconstruct temperature from planktonic foraminifera [by extracting SST averaged over a depth interval depending on the living depth of the foraminifera species identified] is likely inadequate for time periods when the vertical temperature gradient was different from today*”. Hence, it appears that **there is no valuable reason to define a depth or a depth section (for the extraction of SST in the modern database) as more appropriate than another one, particularly because it must have evolved through time.**

Therefore, in our study area, it seems coherent to interpret the F-Temp signals – reconstructed from modern SST extracted at 10 m water depth – as relative variations of “subsurface” temperatures. The “subsurface” depth range is however difficult to define, but we can reasonably suppose that F-Temp signals are integrated over the potential depth range of the whole assemblage (i.e. 0-300 meters water depth here).

Such an assumption allows for the conciliation of our phytoplanktonic-derived versus zooplanktonic-derived signals, i.e. the reconstructed hydrological parameters as well as the environmental information carried by the respective assemblages (characterized by communities which ecologically do not sound as belonging to a common environment / water mass). Thus, it allows us to provide a constructive view of what can be interpreted from the strong difference calculated.

Supplementary references:

- Adloff, F., Mikolajewicz, U., Kučera, M., Grimm, R., Maier-Reimer, E., Schmiidl, G., and Emeis, K. C.: Upper ocean climate of the Eastern Mediterranean Sea during the Holocene Insolation Maximum - A model study, *Climate of the Past*, 7, 1103-1122, 2011.
- de Vernal, A., Eynaud, F., Henry, M., Hillaire-Marcel, C., Londeix, L., Mangin, S., Matthiessen, J., Marret, F., Radi, T., Rochon, A., Solignac, S., and Turon, J. L.: Reconstruction of sea-surface conditions at middle to high latitudes of the Northern Hemisphere during the Last Glacial Maximum (LGM) based on dinoflagellate cyst assemblages, *Quaternary Science Reviews*, 24, 897-924, 2005.
- de Vernal, A., Rosell-Melé, A., Kucera, M., Hillaire-Marcel, C., Eynaud, F., Weinelt, M., Dokken, T., and Kageyama, M.: Comparing proxies for the reconstruction of LGM sea-surface conditions in the northern North Atlantic, *Quaternary Science Reviews*, 25, 2820-2834, 2006.
- Mazaud, A., Sicre, M. A., Ezat, U., Pichon, J. J., Duprat, J., Laj, C., Kissel, C., Beaufort, L., Michel, E., and Turon, J. L.: Geomagnetic-assisted stratigraphy and sea surface temperature changes in core MD94-103 (Southern Indian Ocean): Possible implications for North-South climatic relationships around H4, *Earth and Planetary Science Letters*, 201, 159-170, 2002.
- Peck, V. L., Hall, I. R., Zahn, R., and Elderfield, H.: Millennial-scale surface and subsurface paleothermometry from the northeast Atlantic, 55-8 ka BP, *Paleoceanography*, 23, PA3221, doi:10.1029/2008PA001631, 2008.
- Penaud, A., Eynaud, F., Voelker, A., Kageyama, M., Marret, F., Turon, J. L., Blamart, D., Mulder, T., and Rossignol, L.: Assessment of sea surface temperature changes in the Gulf of Cadiz during the last 30 ka: Implications for glacial changes in the regional hydrography, *Biogeosciences*, 8, 2295-2316, 2011.
- Pflaumann, U., Duprat, J., Pujol, C., and Labeyrie, L. D.: SIMMAX: A modern analog technique to deduce Atlantic sea surface temperatures from planktonic foraminifera in deep-sea sediments, *Paleoceanography*, 11, 15-35, 1996.
- Sarjeant, W. A. S.: Fossil and living dinoflagellates, Elsevier, London, UK, 2013.
- Schiebel, R., Waniek, J., Bork, M., and Hemleben, C.: Planktic foraminiferal production stimulated by chlorophyll redistribution and entrainment of nutrients, *Deep-Sea Research Part I: Oceanographic Research Papers*, 48, 721-740, 2001.
- Sicre, M. A., Labeyrie, L., Ezat, U., Duprat, J., Turon, J. L., Schmidt, S., Michel, E., and Mazaud, A.: Mid-latitude Southern Indian Ocean response to Northern Hemisphere Heinrich events, *Earth and Planetary Science Letters*, 240, 724-731, 2005.
- Telford, R. J., Li, C., and Kucera, M.: Mismatch between the depth habitat of planktonic foraminifera and the calibration depth of SST transfer functions may bias reconstructions, *Climate of the Past*, 9, 859-870, 2013.
- Tolderlund, D. S. and Bé, A. W. H.: Seasonal Distribution of Planktonic Foraminifera in the Western North Atlantic, *Micropaleontology*, 17, 297-329, 1971.

Depth (cm)	Age (ka cal BP) - age model from Zumaque et al., 20102	<i>N. pachyderma</i>	<i>N. incompta</i>	<i>G. bulloides</i>	<i>G. quinqueloba</i>	<i>G. scitula</i>	<i>G. glutinata</i>	<i>G. inflata</i>	<i>H. aequilateralis</i>	<i>G. falconensis</i>	<i>G. hirsuta</i>	<i>G. truncatulinoides dextre</i>	<i>G. truncatulinoides senestre</i>	<i>O. universon</i>	<i>T. humilis</i>	<i>G. rubescens</i>	<i>G. ruber alba</i>	<i>G. ruber rosea</i>	<i>G. conglobatus</i>	<i>G. tenellus</i>	<i>G. calida</i>	<i>G. crassiformis</i>	<i>H. pelagica</i>	<i>G. digitata</i>	<i>G. trilobus</i>	<i>G. sacculiferus</i>	<i>N. duterrei</i>	<i>G. menardii</i>	<i>P. obliquiloculata</i>	<i>G. tumida</i>	<i>S. dehiscentis</i>	<i>C. nitida</i>	<i>T. hexagona</i>	<i>G. parkerae</i>	<i>G. theyeri</i>	<i>Praeobulina</i>	<i>O. suturalis</i>	<i>O. bilobata</i>	<i>G. conglomeraata</i>	<i>G. uvula</i>	<i>G. anfracta</i>	<i>H. adamsi</i>	Undetermined	Total											
1800	37146	170	18	70	83	4	26																																						371										
1810	37274	168	22	79	91	16	13	1																																				1	391										
1820	37402	192	36	96	123	24	25																																						396										
1830	37530	157	15	94	110	25	15	1																																					417										
1840	37658	151	16	82	70	18	16																																						2	355									
1850	37786	175	12	84	59	24	23																																						1	378									
1860	37914	259	9	73	38	15	8																																								402								
1870	38042	270	19	53	15	11	8																																							376									
1880	38170	330	5	16	8	1	4																																							1	365								
1890	38498	371	3	6	5	2																																									387								
1900	38826	350	5	4																																												359							
1910	39154	362	3	5	7	4																																										381							
1920	39482	382	3	4	10																																										1	400							
1930	39810	298	6	21	27	2																																											354						
1940	39910	184	8	114	54	7	14																																									381							
1950	40010	224	6	127	53	7	10																																										427						
1960	40110	295	2	42	46	4																																											389						
1970	40196	312	3	20	9	7																																											351						
1980	40281	318	4	22	12																																												356						
1990	40367	373	6	11	5	1																																											396						
2000	40453	328	5	14	16	1	2																																											366					
2010	40539	327	4	15	23	6																																												375					
2020	40624	324	5	23	17	2	3																																												374				
2030	40710	292	4	32	42	15																																															1	386	
2040	40827	203	10	107	21	5	26																																													1	373		
2050	40943	154	17	75	119	3	27																																														395		
2060	41060	184	8	76	71	6	24																																													369			
2070	41177	163	13	71	58	5	47																																													2	359		
2080	41293	194	14	105	43	3	25																																															384	
2090	41410	214	16	83	49	1	51																																																414

**Section 2. The Southern Norwegian Sea during the last 45 ka:
hydrographical reorganizations under changing ice-sheet dynamics**

*Article soumis à **Journal of Quaternary Science** depuis le 07/10/2015.*

Wary Mélanie¹, Eynaud Frédérique¹, Rossignol Linda¹, Zaragosi Sébastien¹, Sabine Marjolaine¹, Castera Marie-Hélène¹, Billy Isabelle¹

¹ UMR 5805, EPOC (Environnements et Paléoenvironnements Océaniques et Continentaux),
Université de Bordeaux, 33615 Pessac, France.

Corresponding author: M. Wary (melanie.wary@u-bordeaux.fr)

Résumé

Les événements climatiques millénaires de la dernière période glaciaire, i.e. les événements d'Heinrich et de Dansgaard-Oeschger, ont fait l'objet de nombreuses études au cours des dernières décennies. Cependant, des incertitudes notables demeurent encore, notamment à propos des mécanismes océaniques associés. Notre travail se propose d'étudier l'évolution des conditions hydrographiques enregistrées au cours de l'intervalle de temps 3 - 41 ka cal BP au sein de la carotte sédimentaire MD99-2285 prélevée au Sud de la Mer de Norvège. Nos résultats, basés sur une approche multi-indicateurs (reconstructions quantifiées issues des assemblages de dinokystes et de foraminifères planctoniques, IRD, granularité du sédiment, susceptibilité magnétique, analyses Xrf), révèlent un schéma relativement atypique dans cette région, où (i) lors des épisodes chauds enregistrés au Groenland (interstadias), la partie supérieure de la colonne d'eau apparaît comme relativement froide, homogène, et saisonnièrement couverte de glace de mer, avec pourtant l'évidence d'une circulation active d'eau profonde, (ii) lors des épisodes froids du Groenland (stadias), incluant ceux associés aux événements d'Heinrich, la colonne d'eau superficielle apparaît constituée d'un niveau de surface chaud (particulièrement en été), peu salé, presque entièrement libre de glace de mer où dérivait des icebergs, et séparé par une forte halocline d'un niveau de subsurface plus froid et plus salé, avec en parallèle une circulation profonde fortement réduite, et (iii) lors de l'Holocène, les conditions océaniques semblent similaires à celles caractérisant la période moderne mais significativement différentes de celles enregistrées au cours des interstadias. Ainsi, notre étude suggère fortement l'existence de différents modes de convection profonde au sein des Mers Nordiques, avec notamment, lors des interstadias, une formation d'eau profonde probablement principalement induite par le relargage de saumures en lien avec la présence de glace de mer sur une grande partie de l'année. D'après nos résultats, la transition entre ce mode glaciaire de formation d'eau profonde, et le mode moderne de convection en océan ouvert, pourrait s'être produite à la fin de la dernière déglaciation / début de l'Holocène, où les deux modes semblent avoir joué.

Abstract

The last glacial millennial Heinrich and Dansgaard-Oeschger events have been the subject of many studies in the past decades. However, significant uncertainties still remain, notably regarding associated oceanic mechanisms. Here we investigate the evolution of hydrographical conditions on the 3-41 ka cal BP interval of core MD99-2285 located in the Southern Norwegian Sea. Our results reveal an unusual scheme, with: (i) warm Greenland interstadials marked by a relatively cold and homogeneous upper water column seasonally ice-covered, with active deep water formation, (ii) cold Greenland and Heinrich stadials marked by a warm, low saline and nearly sea ice free surface layer with iceberg calving, separated by a strong halocline from a colder and saltier subsurface layer, as well as strongly reduced deep convection, and (iii) close to modern Holocene oceanic conditions but significantly different from interstadial ones. Hence, our work strongly suggests different deep water convection modes in the Nordic Seas, with especially interstadial deep water formation mainly forced by brine release. According to our results, the transition from the glacial mode of deep water formation, to the modern open ocean convection mode, might have occurred at the end of deglaciation / beginning of the Holocene, when both modes probably occurred.

Keywords

Dansgaard-Oeschger cycles, Heinrich events, Holocene, deep convection, sea-surface hydrological conditions.

1. Introduction

In Greenland ice core records, the Holocene appears as a relatively stable climatic period, whereas the last glacial period is punctuated by millennial climatic abrupt events (e.g. Dansgaard et al., 1993). These events correspond to high amplitude atmospheric temperature oscillations, occurring every 1-4 ka (Dansgaard et al., 1993; Bond et al., 1993). They are characterized by a rapid transition from a cold phase (Greenland Stadial, hereafter “GS”) to a warm phase (Greenland Interstadial, hereafter “GI”), and are known as Dansgaard-Oeschger events. Some of these GS are coeval with Heinrich events (and thus called Heinrich stadials, or “HS” hereafter), which were identified in marine archives from the North Atlantic Ocean as thick and ice-rafted debris-rich layers (Heinrich, 1988; Bond et al., 1992). These peculiar layers have been interpreted as the result of boreal ice-sheet collapses and subsequent massive iceberg calving episodes (Bond et al., 1992). Since then, both GS and HS have been widely identified in sedimentological archives from the subpolar North Atlantic Ocean and adjacent seas as pervasive iceberg calving episodes (e.g. Bond and Lotti, 1995; Elliot et al., 2001). Both have also been identified as pervasive changes in surface and deep hydrology, marked by cold sea-surface temperatures associated to the southward migration of polar waters, and reduced Atlantic Meridional Overturning Circulation (e.g. Bond et al., 1993; Rasmussen et al., 1996a,b; Kissel et al., 1999; Sachs and Lehman, 1999; Van Kreveld et al., 2000; Ganopolski and Rahmstorf, 2001; Rahmstorf, 2002).

In the present work we investigate variations of surface, subsurface, and deep hydrological conditions on the 3-41 ka cal BP section of core MD99-2285 located northeast off Faeroes. Numerous previous studies have shown the strong potential of this area to track hydrological changes related to the last glacial millennial climatic variability (e.g. Rasmussen et al., 1996a, b, 1997, 1999, 2002; Kissel et al., 1999; Dokken and Jansen, 1999; Elliot et al., 2001; Eynaud et al., 2002; Rasmussen and Thomsen, 2004, 2008, 2009; Dokken et al., 2013; Ezat et al., 2014). Most of these studies evidenced an oceanic circulation scheme and mode of deep water formation similar to the present one during GI, characterized by an active surface inflow of Atlantic waters in the Nordic Seas, deep convection occurring in the Nordic Seas, and active bottom circulation of waters overflowing from the Nordic Seas to the Atlantic Ocean (Rasmussen et al., 1996a,b, 1997, 1999, 2002; Dokken and Jansen, 1999; Kissel et al., 1999; Ballini et al., 2006; Rasmussen and Thomsen, 2009). At the opposite, during GS, most of them recorded a strongly reduced deep convection in the Nordic Seas and subsequent weaker deep overflow (Rasmussen et al., 1996a,b, 1997, 1999; Dokken and Jansen, 1999;

Kissel et al., 1999; Ballini et al., 2006; Rasmussen and Thomsen, 2009), as well as coeval enhanced iceberg delivery and associated meltwater input (Rasmussen et al., 1996a,b, 1997; Dokken and Jansen, 1999; Elliot et al., 2001; Eynaud et al., 2002; Rasmussen and Thomsen, 2009). Many model experiments support such a scheme, and indicate that the stadial oceanic circulation slow-down is very likely linked to the strong freshwater inputs due to iceberg release and melting (e.g. Manabe and Stouffer, 1995; Ganopolski and Rahmstorf, 2001; Bigg et al., 2011). Furthermore, Rasmussen and Thomsen (2009) and Wary et al. (CP, in press¹) suggested that the weaker meridional overturning circulation reported for GS might be related to a strong stratification of the water column due to the presence of a freshwater lid at that time. Besides, other studies denoted the presence of a halocline during GS (Rasmussen et al., 1996a, 1997, 2002; Rasmussen and Thomsen, 2004; Dokken et al., 2013). In parallel, several studies identified cold sea-surface temperature (SST) during GS, and inversely warmer SST during GI in the Nordic Seas (e.g. Rasmussen et al., 1996a,b, 1997; Rasmussen and Thomsen, 2004; Dickson et al., 2008; Van Kreveld et al., 2000; Dokken et al., 2013). Such a pattern is similar to the one detected in the North Atlantic Ocean (e.g. Bond et al., 1993; Sachs and Lehman, 1999), and is supported by freshwater hosing experiments (e.g. Stouffer et al., 2006). It also supports the assumption of an oceanic circulation scheme similar to the modern one during GI. However, it is worth noting that, in the Nordic Seas, this SST pattern has been deduced from near-surface proxies. Indeed, they are mainly based on assemblages and oxygen isotopes of planktonic foraminifera, which are known to migrate within a relatively large section of the upper water column during their life cycle (e.g. Schiebel et al., 2001) and can also adapt their living depth-habitat to sea-water conditions (e.g. Carstens et al., 1997; Simstich et al., 2003). Similarly, the cold stadial SST have regularly been associated with extensive sea-ice cover in the Nordic Seas (e.g. Rasmussen et al., 1999; Gildor and Tziperman, 2003; Rasmussen and Thomsen, 2004; Dokken et al., 2013). Such a pattern has been supported by model simulations (e.g. Li et al., 2010; Petersen et al., 2013; Singh et al., 2014) as well as by benthic and planktonic isotopic measurements (Dokken and Jansen, 1999; Dokken et al., 2013). However, Eynaud et al. (2002) evidenced an opposite and paradoxical pattern with warmer SST and shorter sea-ice cover duration during GS, and colder SST and longer sea-ice cover duration during GS. This scheme in fact reproduces the well-known existing meteorological balance between western and eastern North Atlantic sides i.e. "Greenland above / Oslo below normal" (Bromwich et al., 1999), linked to the North Atlantic

¹ cf. page 83 de ce manuscrit

Oscillation (NAO) seasonal/decadal modulations. Their findings are based on more direct proxies of sea-surface conditions: dinoflagellate cyst assemblages as well as quantitative sea-surface hydrological reconstructions obtained via transfer functions applied to dinocyst assemblages. Indeed, as dinoflagellates (phytoplankton) are mostly restricted to the photic layer (e.g. [Sarjeant, 1974](#)), dinocysts assemblages are assumed to reflect sea-surface conditions. Furthermore, recent freshwater hosing experiments could support [Eynaud et al.](#)'s scheme. Indeed, [Kleinen et al. \(2009\)](#) and [Swingedouw et al. \(2013\)](#)'s works suggest that high latitude freshwater release may be accompanied by enhanced northward advection of warm and saline Atlantic subsurface waters re-emerging in surface of the Nordic Seas, and also be responsible for a decrease in the strength of the Atlantic meridional overturning circulation. Such a scenario recalls [Rasmussen and Thomsen \(2004\)](#) and [Dokken et al. \(2013\)](#)'s works, where indices of Norwegian Sea intermediate-depth and/or subsurface warmings are reported during GS and attributed to a subduction of the Atlantic inflow.

Hence, despite numerous paleoceanographic studies and modelling experiments focused on the millennial climatic variability of the last glacial period, significant discrepancies and uncertainties still remain. Here, we use a large set of proxies indicative of (i) surface hydrographical conditions in terms of temperatures, salinities, and sea-ice cover duration (dinocyst assemblages), (ii) sub-surface hydrographical conditions (planktonic foraminifera assemblages), (iii) bottom flow activity (grain-size measurements, X-ray fluorescence analyses, magnetic susceptibility signal) and (iv) (sea-)ice drifting (ice-rafted debris concentration). We conduct those analyses on core MD99-2285 strategically retrieved at the northeastern foot of Faeroe Islands in the southern Norwegian Sea to track changes in past oceanic conditions in relation to the proximal European ice-sheet history over the last 45 ka .

2. Modern and past environmental settings

Core MD99-2285 (62.6938°N, -3.5723°E, 885 m water depth; [Fig. 1](#)) was retrieved on the slope of the northeastern margin of Faeroe Islands, during the IMAGES (International Marine Global Change study) V – MD99-114 (GINNA) cruise on the RV *Marion Dufresne* ([Labeyrie et al., 1999](#)). It is made of 46.92 meters of hemipelagic silty clays ([Labeyrie et al., 1999](#)).

Quaternary sedimentation on the Faeroe slopes is known to be primarily constrained by bottom currents through contouritic processes (van Weering et al., 1998; Andersen et al., 2000; Laberg et al., 2005). The bottom current flowing along the northeastern Faeroe margin transports water masses grouped under the name of Iceland Scotland Overflow Water (ISOW; e.g. Borenäs and Lundberg, 2004) to the Atlantic Ocean through the Faeroe Shetland Channel (Kuijpers et al., 1998; Borenäs and Lundberg, 2004; Mauritzen et al., 2005; Fig. 1b and 1d). ISOW is made of intermediate and deep water masses formed in the Nordic Seas. These water masses present temperatures below 5.5°C for the upper intermediate water (the Arctic Intermediate/North Iceland Water or Modified East Atlantic Water) and below 0.5°C for the deeper water masses (the Norwegian Sea Arctic Intermediate Water, and the Norwegian Sea Deep Water; Hansen and Østerhus, 2000; Mauritzen et al., 2005). The Faeroe-Shetland Channel is the deepest passage across the Greenland-Scotland Ridge, and this branch of ISOW acts as an important source water to the North Atlantic Deep Water (Borenäs and Lundberg, 2004).

Depending on their intensity, bottom flows may be depositional or erosive. On the Faeroe slopes, the last glacial sedimentation is characterized by high sedimentation rates of fine-grained sediments indicative of relatively weak bottom currents responsible for high sediment supply. On the contrary, interglacial deposits are generally strongly reduced due to intense winnowing by stronger bottom currents (Kuijpers et al., 1998; Nielsen et al., 2007). However, on the basis of seismic and side-scan sonar data, van Weering et al. (1998) showed that our core site is located (i) in the area where the sediment supply by ISOW deep current has been less important, i.e. where the bottom current strength is weaker, and (ii) above the erosional channel formed by the core of this deep current (Fig. 1c). In parallel, strong sediment supply during glacial periods has led to episodes of slope instability at the same time, including the last glacial period (van Weering et al., 1998; Kuijpers et al., 2001; Nielsen et al., 2007). However, seismic and side-scan sonar profiles (van Weering et al., 1998; Kuijpers et al., 2001) reveal that our core site is located well above the area affected by gravity-driven mass transport (called the North Faeroe Slide Complex; Fig. 1c), and thus that our core did not suffer from such reworking processes.

In addition to the deep current, the study area also constitutes a nodal point regarding the modern surface oceanic circulation. Indeed, it is under the dual influence of two different surface water masses: (i) the warm ($T > 8^{\circ}\text{C}$) and salty North Atlantic Water entrained

northward through the North Atlantic Current (Orvik and Niiler, 2002; Mauritzen et al., 2005), and (ii) the colder and fresher waters made of the mix between the North Atlantic Water and the cold polar waters ($< 0^{\circ}\text{C}$ to 2°C), transported from the Arctic to the southern Norwegian Sea through the southward East Greenland Current and its eastward extension called the East Icelandic Current (Valdimarsson and Malmberg, 1999; Fig. 1a and 1d). On the shallow parts of the Faeroe shelf, strong mixing occurs and generates a very homogeneous water mass, the Faeroe Shelf Water, separated from off-shelf waters by the Faeroe Shelf Front (Larsen et al., 2008, 2009).

Furthermore, during the last glacial period, the study site had very likely been under the direct influence of the European proximal ice-sheets, i.e. the Fennoscandian ice-sheet and the British-Irish ice-sheet. Indeed, both ice-sheets apparently got largely wider during this period (Svendsen et al., 2004; Fig. 1a). Moreover, the study site is located at the outlet of major paleo-ice streams having drained those ice-sheets (Sejrup et al., 2003; Bradwell et al., 2008; Fig. 1a), thus it is very likely that the site has been influenced by their ice discharges.

3. Stratigraphy

Seventeen radiocarbon ages were measured on mainly monospecific samples of planktonic foraminifera (Table 1) on the topmost four meters of core MD99-2285. Those AMS ^{14}C dates were converted to calendar ages using Calib 6 calibration program (Stuiver et al., 2010) and Marine09 calibration curve (Reimer et al., 2009) with a 400 year marine reservoir correction. A test was done with Calib 7 and the Marine13 calibration curve (Reimer et al., 2013) but no significant changes were detected on the retained datings (see below and Table 1). Actually, following many paleoceanographic studies conducted in the area (e.g. Rasmussen et al., 1996a,b; Kissel et al., 1999; Laj et al., 2000; Elliot et al., 2002; Ballini et al., 2006; Rasmussen and Thomsen, 2009), additional age-control points were obtained by correlating the magnetic susceptibility (MS) signal of the core to NGRIP $\delta^{18}\text{O}$ record (GICC05 time scale; Svensson et al., 2008; Wolff et al., 2010) i.e. the recommended regional stratotype (i.e. Austin and Hibbert, 2012; see Fig. 2a and 2b). The rationale is that, in the subpolar North Atlantic and adjacent seas, and along the path of bottom water masses feeding the North Atlantic Deep Water, low MS values are coincident with GS and HS, and inversely high MS values are synchronous with GI (Kissel et al., 1999). We thus obtained 19 age-

control points by correlating MS increases to the beginning of GI, and MS decreases to the end of GI. Ages associated to these tie-points conform to DO age limits defined by Wolff et al. (2010).

Considering all of these AMS ^{14}C dates and age-control points, it appeared that 9 AMS ^{14}C dates were not perfectly matching the NGRIP stratigraphy (see Table 1 and Fig. 2a). These dates, mainly the oldest, are probably related to ^{14}C dating limitations. Some of them, corresponding to HS sections, probably also reveal age reservoir artefacts, but in the absence of any comprehensive study documenting age reservoir delta for the area during these periods, we preferred to not consider them. The age model has thus been established on the basis of the remaining 8 AMS ^{14}C dates combined to the 19 age-control points. We chose to use a linear interpolation between the 27 tie-points since it offers a better fit between our MS record and the NGRIP regional stratotype (Fig. 2b). Our age model gives an average sediment rate of 18 cm.ka^{-1} for the upper six meters of the studied core (Fig. 2d).

It is worth noting that important uncertainties remain concerning our age model around the GS 6 / HS3 period. Indeed, in the current age model, GI 5 (according to Dansgaard et al. (1993)'s numbering) or GI 5.2 (according to Rasmussen et al. (2014)'s numbering, i.e. the interstadial event from 32450 to 31990 a cal BP after Rasmussen et al. (2014)'s age limits) is "missing": there is no MS peak coincident with GI 5.2 NGRIP event (Fig. 2b and 2c). However, one could argue that the MS peak located at around 370 cm depth, presently coincident with (but not manually tied to) GI 5.1 (Rasmussen et al. (2014)'s numbering), could have been correlated to GI 5.2. This could be particularly true if we consider that GI 5.1 is less marked than GI 5.2 in the NGRIP $\delta^{18}\text{O}$ record. Nonetheless, our choice of tie-points in this section relies on several elements:

- 1) In a few marine cores, MS events correlated/corresponding to GI 5.1 and to GI 5.2 present comparable amplitudes (see for example Caulle et al., 2013 or Kissel et al., 1999), thus this criterion does not appear discriminant. Moreover, in nearby core MD95-2009, GI 5.1 MS peak presents a relative amplitude comparable to MD99-2285 MS peak located around 370 cm (Fig. 2c).
- 2) Among the proxy records produced in our study, some of them have previously been used to establish age models of marine cores from the North Atlantic and Nordic Seas (e.g. relative abundance of *Neogloboquadrina pachyderma*, planktonic foraminifera

oxygen isotopic content) or to support/help to establish them (Xrf K/Ti ratio). Unfortunately, in our case, none of them allows us to confidently determine the best option of correlation in this section.

- 3) Two AMS ^{14}C dates were measured (layers 369.5 cm and 384.5 cm, see [Table 1](#)) in this problematic section of the core, but they surprisingly provided slightly too young ages in comparison to NGRIP and are thus also unhelpful.
- 4) Correlating the MS peak (located at ~ 370 cm depth in core) to GI 5.2 results in a HS3 thickness largely inferior to the one of three other HS recorded in our studied core section (i.e. 26 cm for HS3 against 43.5, 29.5 and 46 cm for HS1, HS2 and HS4 respectively, when using a linear interpolation). However, HS3 is known to be one of the longest stadials. At the opposite, not correlating it to any GI results in a larger thickness of the HS3 layer (at least 37 cm). It also makes the MS peak match GI 5.1 without any tuning. This option thus seems more reasonable, even if this implies the existence of a hiatus during GI 5.2.

Such a hiatus could be explained by a non-deposition/erosion by the deep current, but this seems unlikely given that the bottom current was weaker during GI than it is at present ([Kuijpers et al., 1998](#); [Nielsen et al., 2007](#)). It could also result from erosion by another sedimentary process, such as down-slope processes. However, as mentioned in Sect. 2, seismic and side-scan surveys revealed that the study area was *a priori* not affected by gravity-driven mass transport ([van Weering et al., 1998](#); [Kuijpers et al., 2001](#)). Indeed, neither X-ray images nor grain-size measurements reveal any erosional surface, but this is not sufficient to categorically exclude the occurrence of an erosional process over the study site in-between GS 6 and GI 5.1.

Following [Rasmussen et al. \(2014\)](#)'s subdivision of GI 5, and [Wary et al. \(CP, in press\)](#)'s subdivision of HS3, we thus divided the GS 6 / HS3 interval as follows: a first interval from 33290 to 30790 a cal BP representing the indistinct period spanning from GS 6 to HS3a, then GI 5.1 extending from 30790 to 30550 a cal BP (according to [Rasmussen et al., 2014](#)), and the last interval from 30550 to 28850 a cal BP corresponding to HS3b.

4. Materials and methods, proxy significance

Analyses were conducted on the 0 – 600 cm section of core MD99-2285. A panel of non-destructive analyses were first conducted (such as X-ray fluorescence and magnetic susceptibility measurements). Then, sediment samples were collected. Sampling frequency is not homogeneous along the core, varying in between 10 cm to 2 cm, i.e. from 35 to 1235 years (Fig. 2e). This reflects our efforts to increase the resolution on key portions of the studied period. A higher sampling frequency (up to 2 cm) has thus been used over the MIS 3 section (~ 275 – 600 cm, i.e. ~ 24 to 41 ka cal BP) and around Heinrich stadial 1 (from 100 to 210 cm, i.e. from ~ 13 to ~ 19 ka cal BP) to enable the effective study of the millennial climatic events. At each depth of sampling, two sediment samples were collected: one with no pre-treatment (used for grain-size measurements) and one wet sieved to separate fractions above and below 150 µm (both fractions used for micropaleontological analyses, as well as large lithic grain quantification in the > 150 µm fraction).

4.1. Micropaleontological assemblages

Determination and counting of Quaternary dinocysts were performed on the <150 µm fraction after palynological preparation of sediment samples (following the protocol of de Vernal et al., 1996, slightly modified at EPOC: http://www.epoc.u-bordeaux.fr/index.php?lang=fr&page=eq_paleo_pollens). Around 300 specimens were counted in each sample using a Leica Microscope at x400 magnification. Species identification follows Rochon et al. (1999), Head et al. (2001), and Radi et al. (2013). Relative abundances of each species were calculated relative to the total sum of individuals. Absolute concentration of modern dinocysts have also been calculated and expressed in cysts.cm⁻³ of dry sediment. As previously mentioned, variations in dinocyst assemblages are assumed to reflect changes in sea-surface hydrological conditions.

Planktonic foraminifera were counted (minimum of 350 specimens) in each sample > 150 µm within known aliquots of dried residues, in order to determine their concentration in terms of individuals.g⁻¹ of dry sediment. Species identification follows Hemleben et al. (1989) and Kennett and Srinivasan (1983). Foraminiferal assemblages are described by the relative percentages of each species, calculated relative to the total sum of planktonic foraminifera. In comparison to dinoflagellates and as already mentioned, planktonic foraminifera are known to

thrive in a larger section of the upper water column. This is especially true for symbiont-free taxa (such as the polar species *N. pachyderma* sinistral coiling) which may live below the photic layer (e.g. Carstens et al., 1997; Schiebel et al., 2001; Simstich et al., 2003) and constitutes the dominant species (even monospecific) over the record. Thus, planktonic foraminifera assemblages are assumed to reflect hydrological changes integrated over the depth range inhabited by the whole assemblage.

Diversity and dominance ecological indices were calculated both on dinocyst and planktonic foraminifera assemblages. Diversity is represented by the H index: $-\sum_{i=1}^s [(n_i/N) \times \ln(n_i/N)]$, where n_i is the number of specimens recorded for taxa i , s is the total number of taxa and N is the total number of individuals counted for each sample (Shannon and Weaver, 1949). Dominance corresponds to $(n' + n'') / N$ where n' is the number of individuals of the more abundant species, n'' is the number of individuals of the second more abundant species, and N is the total number of specimens counted for each sample (Goodman, 1979).

4.2. Reconstructions of near-surface hydrological conditions

Past sea-surface conditions were estimated using a transfer function applied to dinocyst assemblages. The modern analogue technique (MAT, see Guiot and de Vernal, 2007, 2011a,b for a review of this technique) was applied and performed with the R software (R version 2.7.0; <http://www.r-project.org/>), using the ReconstMAT script developed by J. Guiot (BIOINDIC package, <https://www.eccorev.fr/spip.php?article389>). The modern dinocyst database used here includes 1207 sites from North Atlantic Ocean, Arctic and sub-Arctic basins, Mediterranean Sea and North Pacific Ocean (database available from the DINO9 workshop, <http://pcwww.liv.ac.uk/~dino9/workshops.html>). This method provides quantitative reconstructions for mean summer (July-August-September) and mean winter (January-February-March) temperatures (hereafter “SST_{dino}”; with root mean square errors of prediction – RMSEP – of 1.5 °C and 1.05 °C respectively), mean summer and mean winter sea-surface salinity (SSS_{dino}; respective RMSEP of 2.4 and 2.3 psu), and mean annual sea-ice cover duration (SIC_{dino}; RMSEP of 1.2 month/year).

Past quantitative temperatures were also obtained from planktonic foraminifera (hereafter called “PF-Temp”) using a transfer function developed by Eynaud et al. (2013) and described in previous studies (Matsuzaki et al., 2011; Penaud et al., 2011; Sánchez Goñi al.,

2012, 2013; Mary et al., 2015; Wary et al., CP, in press). This transfer function is similar to the one used for dinocysts (MAT, same ReconstMAT script also performed with R). The modern planktonic foraminiferal database includes modern assemblages and modern hydrological parameters (extracted at 10 m water depth, as for the modern dinocyst database) from 1007 sites distributed over the North Atlantic Ocean and Mediterranean Sea. Statistical treatments provide quantitative reconstructions of annual and seasonal temperatures. Here, we will use mean summer and mean winter PF-Temp (RMSEP of 1.3 °C and 1.2 °C respectively).

Seasonality signals were reconstructed from temperature reconstructions derived from dinocyst and planktonic foraminifera assemblages, as well as from SSS_{dino} . In all cases, they were calculated as mean summer minus mean winter values.

4.3. Sedimentological analyses

Grain-size measurements were performed on samples of bulk sediments with a Malvern MASTER SIZER S at EPOC laboratory. Results will be further represented as a mapping of the relative percentages of the different grain-size fractions along core. Some grain-size parameters were additionally calculated: median (D50), percentiles 10 and 90 (D10 and D90), and mean grain size of the 0.5 – 10 µm and 0.5 – 20 µm fractions. The mean size of the 10-63 µm fraction is usually used as an indicator of bottom flow strength (e.g. McCave et al., 1995a,b; McCave, 2007; Hodell et al., 2009). However, Prins et al. (2002) have shown that, in the subpolar North Atlantic region influenced by bottom currents, the size distribution within the 10-63 µm fraction of glacial sediments is influenced not only by bottom flow speed but also by ice-rafted debris inputs. They have also shown that the well-sorted clay to fine silt fraction was a better proxy of the strength of low-energy bottom currents in such situations. Indeed, Snowball and Moros (2003) confirmed the suitability of the mean grain size of the 0.5 – 10 µm and 0.5 – 20 µm fractions as indicators of bottom current speed on the Reykjanes Ridge. Ballini et al. (2006) also supported the validity of the mean grain size of the 0.5 – 10 µm fraction as bottom flow proxy at a more regional scale, including the nearby MD95-2009 site. For all of these reasons, we will use the mean grain size of the 0.5 – 10 µm and 0.5 – 20 µm fractions to track the variability of the ISOW bottom flow strength over our study site, with coarser mean sizes of these fractions indicative of a stronger ISOW. It is worth noting that in some regions, the fact that sediment samples do not receive any chemical treatment to

remove carbonates and organic matter before being analysed could constitute a substantial bias. However, it is very likely that it does not have any incidence in our case. Indeed, the comparison of grain-size measurements between bulk samples and carbonate-free and organic-free samples from the core MD99-2281 (60.3418°N; -9.4557°E; 1197 m water depth; located around 500 km southwest from core MD99-2285, cf. [Fig. 1b](#)) does not reveal any significant differences ([Wary et al., CP, in press](#)). Besides, the CaCO₃ content of our core is less than half that of core MD99-2281 (maximal value over the studied sections: ~ 12% for MD99-2285, and ~ 28.5 % for core MD99-2281; data not shown). This strongly suggests that in our study core, results obtained from non-pretreated sediment also mainly reflect grain-size variations of the terrigenous fraction.

Magnetic susceptibility was measured onboard every 2 cm with a GEOTEK Multi-Sensor Core Logger ([Labeyrie and Cortijo, 2005](#)). This signal constitutes another record of changes in the strength of the ISOW bottom current. Indeed, [Kissel et al. \(1999\)](#) showed that, in cores located along the path of deep water masses feeding the North Atlantic Deep Water, magnetic susceptibility variations are due to changes in the amount of magnetic minerals transported and deposited by bottom currents. More precisely, higher magnetic susceptibility values are due to stronger inputs of magnetic particles by bottom current, that is to say to a stronger bottom current activity.

An X-ray fluorescence (Xrf) scan of the core was performed at a resolution of 2 cm using the CORTEX scanner at the NIOZ laboratory complemented by some higher resolution measurements on specific intervals at EPOC laboratory (not shown). For this article, we will specifically use the Xrf ratio K/Ti which can provide information on sediment sources, and by extension on the bottom current strength, in our study area (i.e. [Richter et al., 2006](#)). Indeed, low K/Ti values are indicative of enhanced supplies of basaltic material by the bottom current from the northern basaltic province (i.e. approximately, the Greenland-Scotland Ridge). At the opposite, high K/Ti values are indicative of enhanced supplies of continental material, possibly though ice-rafting transport.

Large Lithic Grains (LLG) concentrations (number per gram of dry sediment) were determined in each sample of the > 150 µm fraction. When it was possible, a minimum of 300 grains were counted; for samples with less than 300 grains, all the grains were counted. Following many works from the study area (e.g. [Elliot et al., 1998, 2001](#); [Rasmussen et al., 2002](#); [Scourse et al., 2009](#)), we assume that LLG contain a large proportion of ice-rafted

debris. We will thus use this proxy as an indicator of floating ice (i.e. icebergs or coastal sea ice) delivery to the site.

5. Results

5.1. Micropaleontological analyses

Forty-one taxa of modern dinocysts were identified in the studied section. Their concentration vary between ~ 175 and ~ 49500 cysts.cm⁻³, peaking during the Holocene (up to ~ 49500 cysts.cm⁻³) and at the end of GI (up to ~ 17650 cysts.cm⁻³; Fig. 3c). Assemblages are dominated by four species (Fig. 3b):

- *Islandinium minutum* (a polar taxon associated with cold surface waters seasonally covered by sea ice; Radi et al., 2013), peaking during GI and the Bølling-Allerød,
- *Pentapharsodinium dalei* (a subpolar species found in higher relative abundance in areas where large seasonality contrasts occur; Rochon et al., 1999), peaking during GS/HS, the Last Glacial Maximum (LGM, i.e. 19-23 ka cal BP sensu Mix et al., 2001), the Younger Dryas and the studied Holocene section.
- *Bitectatodinium tepikiense* (a temperate/subpolar taxon which displays a strong affinity for stratified surface waters characterized by a large seasonality; Rochon et al., 1999), showing its higher concentrations during GS/HS.
- and *Operculodinium centrocarpum* (a ubiquitous taxon characterized by a spatial distribution in the North Atlantic and adjacent seas tightly linked to the North Atlantic Drift pathways; Harland, 1983; Rochon et al., 1999), mostly abundant during GS/HS, the LGM and the base of the Holocene.

Dinocyst assemblages are also composed of major subordinate species/genera in some intervals (Fig. 3b): *Spiniferites ramosus* and more generally *Spiniferites* spp. during GS, the LGM and the base of the Holocene, *Nematosphaeropsis labyrinthus* during the deglaciation and early Holocene, *Brigantedinium* spp. during the Bølling-Allerød, and *Lingulodinium machaerophorum* during GS/HS and the LGM. Diversity and dominance indices calculated on dinocyst assemblages are negatively correlated (correlation coefficient of -0.96)

throughout the studied section of the core, with in general high diversity and low dominance during the cold episodes (GS/HS, LGM, Younger Dryas) and inversely during the warm intervals (Fig. 3d).

Eight planktonic foraminifera (PF) species were identified in the studied interval. Their concentration ranges from ~ 20 to ~ 2300 individuals.g⁻¹ of dry sediment, with maximal values recorded during GS, HS and intermittently during the LGM (Fig. 3f). Assemblages are poorly diversified throughout the last glacial period (Fig. 3e and 3g), with nearly monospecific assemblages dominated by the mid-dweller polar taxon *Neogloboquadrina pachyderma* (sinistral coiling form). Diversity significantly increases (and dominance decreases) since the beginning of Holocene, with *N. incompta* (syn. *N. pachyderma* dextral form), *Globigerina bulloides*, *Turborotalita quinqueloba*, and *Globigerinita glutinata* becoming major subordinate species from that moment on. As for dinocyst assemblages, planktonic foraminifera diversity and dominance indices are anti-correlated throughout the studied period (correlation coefficient of -0.96).

According to [Londeix et al. \(2007\)](#)'s methodology to identify reworked intervals, the ecologically consistent anti-correlation between diversity and dominance indices, visible all along the core and on both microfossil communities (Fig. 3d and 3g), suggests that those assemblages did not suffer from reworking processes (such as through bottom current transport for example) but reflect the composition of living biocenoses.

5.2. Near-surface and deep-water hydrological parameters

Fig. 4 shows hydrological parameters reconstructed on the studied section of core MD99-2285. Parameters related to the bottom current strength show coherent oscillations synchronous with the millennial climatic changes. Indeed, GI and the Bølling-Allerød are characterized by higher magnetic susceptibility values (Fig. 4b), a lower K/Ti ratio (Fig. 4c), and coarser mean sizes of the 0.5 – 10 μm and 0.5 – 20 μm size fractions (Fig. 4e and 4f), all indicative of a stronger ISOW. A reverse scheme is observable for GS/HS. The LGM is characterized by relatively high magnetic susceptibility values and relatively low K/Ti values, but fluctuating mean sizes of the clay to fine silt fractions. The Younger Dryas and the recorded Holocene section are marked by relatively low K/Ti values and coarse mean sizes of the 0.5 – 10 μm and 0.5 – 20 μm fractions, but also by a variable magnetic susceptibility signal. Along core mapping of grain-size distribution, D50 and D90 (Fig. 4d) do not illustrate

as clearly changes in the strength of ISOW since they mix the dual influence of this low-energy bottom current and of pelagic contribution including ice-rafted debris (>150 μm but also < 150 μm). Indeed, large lithic grain concentrations (equivalent to ice-rafted debris concentrations; Fig. 4g) are very low (almost nil) only during the Holocene, thus confirming that the study area was under the direct influence of proximal ice-sheets throughout the whole last glacial period and deglaciation. During this period of ice-sheet alternative build-ups and decays, LLG inputs were uninterrupted over the study area, generally peaking during GS/HS (except for GS4 and the HS3a to GS6 period) as well as during the LGM.

This background fluctuating signal is supported by SSS_{dino} , which, except for an increase from the base of the Holocene to mid-Holocene towards modern SSS values (equal to 35.2 psu for both seasons over the study area, WOA09 data, Antonov et al., 2010; Fig. 4h), do not seem to show peak to peak consistent variations with climatic changes. Indeed, during the last glacial period, SSS_{dino} are very low (mean of 31.4 psu for summer SSS_{dino} and of 32.7 psu for winter SSS_{dino}) and well below the modern values. They indicate the presence of more brackish surface waters over the study area during this period.

Similarly, temperature reconstructions from PF do not seem to display any consistency with the millennial climatic events of the last glacial period (Fig. 4i). Indeed, during this time interval, winter and summer PF-Temp records exhibit very low values (winter PF-Temp range from -1.8 to 2.1 $^{\circ}\text{C}$ with a mean of -0.2 $^{\circ}\text{C}$, and summer PF-Temp range from -1.5 to 5.4 $^{\circ}\text{C}$ with a mean of 3.2 $^{\circ}\text{C}$), well below the modern winter minima of 6.5 $^{\circ}\text{C}$ (WOA09 data, Locarnini et al., 2010). This clearly illustrates the very strong dominance of *N. pachyderma* (s) in PF assemblages, and highlights the limits of accuracy of transfer functions applied to monospecific polar PF assemblages. On the contrary, temperature reconstructions derived from the diversified dinocyst assemblages show quite different results (Fig. 4i), thus illustrating the complex and different ecological strategy of these planktonic populations. Indeed, on the same period, SST_{dino} exhibit strong fluctuations synchronous with millennial climatic events. Interestingly and paradoxically, SST_{dino} show higher values during cold periods (GS/HS, LGM, Younger Dryas): they nearly reach modern values up to 5.6 $^{\circ}\text{C}$ during winter, but surprisingly peak up to 17 $^{\circ}\text{C}$ for summer, thus well above the modern maxima values of 10.7 $^{\circ}\text{C}$ (WOA09 data, Locarnini et al., 2010). Inversely, SST_{dino} display lower values during GI and at the start of the Bølling-Allerød, with minimum summer SST_{dino} of 1.2 $^{\circ}\text{C}$ and minimum winter SST_{dino} of -1.3 $^{\circ}\text{C}$. These reconstructed SST large ranges logically

translate into seasonality signals (Fig. 4j). Indeed, on the basis of dinocyst populations, high temperature seasonality contrasts are recorded during cold periods, whereas low seasonality ones mark warm episodes (close to the modern seasonality value of 4.2 °C after WOA09 data; Locarnini et al., 2010). In parallel, PF recorded very low seasonality variations throughout the whole studied period (with a mean value close to the modern seasonality value of 4.2 °C). Nonetheless, it is worth noting, as mentioned above, that PF-Temp and their derived seasonality signal should be considered with caution during the last glacial period due to almost monospecific assemblages and related transfer function limitations. Reconstructions however seem to converge throughout the Holocene section (11.65 to 3.88 ka cal BP), with PF-Temp, SST_{dino} and seasonality signals tending towards modern values.

In concordance to SST_{dino}, sea-ice cover (SIC_{dino}) reconstructions also show an atypical pattern during the last glacial millennial climatic events. SIC_{dino} range from 0 to 8.8 months/year, with longer SIC_{dino} recorded during GI and at the beginning of the Bølling-Allerød, and shorter ones during GS/HS and the Holocene (Fig. 4k). Interestingly, the seasonality signal deduced from SSS_{dino} (Fig. 4l) follows a sensibly identical pattern, with GI marked by strong seasonal salinity contrasts probably reflecting mixed processes of winter brine release through sea ice formation and summer sea ice melting.

In relation to the method used for reconstructions (i.e. no calculation when fossil and modern assemblages are too dissimilar), the period between GS 4 and HS2 and the LGM interval offer a discontinuous signal. Given the large discontinuity of dinocyst-derived reconstructions for the LGM, we chose to not discuss this interval hereafter.

6. Discussion

6.1. A paradoxical hydrological scheme during the last glacial millennial events

As seen from our set of data, variations of the bottom current strength during the last glacial millennial climatic events conform to previous established schemes (e.g. Kissel, 1999; Ganopolski and Rahmstorf, 2001; Ballini et al., 2006; Böhm et al., 2015), i.e. with GI characterized by a relative strong bottom flow while GS/HS register weaker deep currents. It also reveals coherent hydrological variations throughout the whole water column, mainly

related to iceberg releases, with relatively low saline surface waters throughout the studied period (low SSS_{dino}), and GS/HS generally marked by higher LLG inputs. However, our study also reveals unusual near-surface hydrological features.

Firstly, in the study area, previous studies based on planktonic foraminifera analyses (e.g. Rasmussen et al., 1996a,b, 1997; Rasmussen and Thomsen, 2004) reported warmer near-surface temperatures during GI and colder ones during GS. In the present work, neither our temperature reconstructions nor our assemblages, neither derived from dinocyst nor planktonic foraminifera, evidence such a scheme. On the contrary, dinocyst analyses indicate paradoxical warm surface conditions during GS and HS (high relative percentage of *O. centrocarpum*, high summer and winter SST_{dino}) and cold ones during GI (assemblages dominated by *I. minutum*, low summer and winter SST_{dino}). In parallel, despite the potential limitations of the application of transfer function on planktonic foraminifera assemblages in polar environments, assemblages in themselves indicate cold subsurface conditions throughout the studied period. Indeed, they are clearly dominated by *N. pachyderma* (s), a taxon which presently thrives between a few tens of meters to around 250 meters water depth (e.g. Carstens et al., 1997; Simstich et al., 2003), and whose highest relative abundances are found in water masses with temperatures < 5-6 °C (e.g. Tolderlund and Bé, 1971; Carstens et al., 1997; Hillaire-Marcel and de Vernal, 2008). Such a scheme recalls the one evidenced by Eynaud et al. (2002) over the 30-48 ka cal BP section of the nearby core MD95-2009 (62.7375°N; -3.9977°E; 1027 m water depth) and of core MD95-2010 located on the Vøring Plateau (66.6842°N; 4.5662°E; 1226 m water depth; cf. Fig. 1). Indeed, in both cores, the authors also evidenced higher relative percentage of *O. centrocarpum*, lower relative abundance of *I. minutum*, and warmer SST_{dino} during GS and HS, and inversely during GI. In parallel, both cores also recorded relative percentage of *N. pachyderma* (s) ranging between 90 and 100% throughout the studied interval.

It is worth noting that the difference in interpretations derived from planktonic foraminifera assemblages in our study *versus* those from previous studies of nearby cores (Rasmussen et al., 1996a,b, 1997 in core ENAM93-21 (62.7383°N; -3.9987°E; 1020 m water depth; cf. Fig 1), and Rasmussen and Thomsen, 2004 and references therein in core ENAM93-21 and others) may be explained by the fact that planktonic foraminifera counts were not performed in the same size fraction. Indeed, in our study, counts were performed in the > 150 µm size fraction in order to apply the planktonic foraminifera transfer function. On

the contrary, in cores located in the southern Norwegian Sea published in Rasmussen et al. (1996a,b, 1997) and Rasmussen and Thomsen (2004), planktonic foraminiferal counts were performed in the $> 100 \mu\text{m}$ fraction. Assemblages in such a size fraction, even if also strongly dominated by *N. pachyderma* (s) during GI and GS/HS, might encounter overestimation of the small taxa *G. quinqueloba* (e.g. Nørgaard-Pedersen et al., 2007). However, their nearly monospecific character also indicates subsurface temperatures $< 5\text{-}6^\circ\text{C}$ during both GI and GS/HS, with apparently slightly warmer subsurface temperatures during GI.

Secondly, GS have usually been associated with extensive sea-ice cover in the Nordic Seas, either as a deduction of the assumed colder near-surface conditions, (e.g. Rasmussen et al., 1999; Gildor and Tziperman, 2003; Rasmussen and Thomsen, 2004), or on the basis of indirect proxies (i.e. foraminiferal isotopic content, Dokken and Jansen, 1999; Dokken et al., 2013). Here, similarly to Eynaud et al. (2002)'s findings, dinocyst assemblages and SIC_{dino} quantifications denote an opposite pattern, with longer sea-ice cover duration recorded during GI (high relative percentage of *I. minutum* and longer SIC_{dino}) and shorter one during GS/HS. The strong seasonal salinity contrast during GI also supports this pattern. In addition, sea ice proxy IP25 measurements have been conducted on the presently studied core over the 36-41 ka cal BP section spanning from GS 10 to GS 8 (yet unpublished); in coherence with dinocyst results, they reveal extensive sea ice formation during GI, and strongly reduced or even nil sea ice formation during GS and HS. Besides, in nearby cores ENAM93-21 (Rasmussen et al., 1996b) and MD95-2009 (Rasmussen et al., 1999), higher abundances of the benthic foraminifera taxon *Elphidium excavatum* are encountered during the second half of GI. According to the authors, the occurrence of this taxon may be related to polar conditions possibly with extensive sea-ice cover, which would support our findings. Moreover, Rasmussen et al. (1999) also reported higher relative abundance of *Islandiella norcrossi* during GI. This benthic foraminifera species is usually associated to cold environments seasonally ice-covered (e.g. Polyak et al., 2002), which also supports our results. Hence, the paradoxical hydrological scheme reported on the basis of dinocysts (in this work and in Eynaud et al., 2002), both in terms of SST and SIC, seems to be a robust feature.

In parallel, the different hydrological conditions depicted in surface (dinocysts) and in subsurface (planktonic foraminifera) denote the occurrence of a thermocline during GS, separating the warm surface waters from the colder subsurface waters (at least during summer). Moreover, *N. pachyderma* (s) barely tolerates salinities < 34 psu (e.g. Tolderlund and Bé, 1971; Carstens et al., 1997; Hillaire-Marcel and de Vernal, 2008). However, SSS_{dino}

are inferior to this value throughout the last glacial period, and especially during summer, i.e. the main production period of *N. pachyderma* (s) in the Nordic Seas (Kohfeld et al., 1996; von Gyldenfeldt et al., 2000). This indicates the additional occurrence of a halocline over the study area. Furthermore, this halocline seems to have been much stronger during GS. Indeed, planktonic foraminifera show higher absolute concentrations during these intervals. Since foraminifera assemblages are almost monospecific, this implies higher absolute concentrations of *N. pachyderma* (s), and thus more favorable conditions to the development of this taxon. Such a feature is supported by higher relative abundances of *B. tepikiense* during GS, a dinocyst taxa strongly related to stratified surface waters (Rochon et al., 1999). It is also supported by the strong surface temperature seasonality recorded at that time by dinocysts, which may be explained by the low thermal inertia of a relatively thin low saline surface layer. At the opposite, during GI, the apparent reduced temperature contrasts between surface and subsurface, the reduced surface temperature seasonality, and the lower absolute abundances of *N. pachyderma* (s) suggest a strongly reduced upper stratification, with reduced or even nil thermocline and halocline. Furthermore, the information carried by planktonic foraminiferal assemblages > 100 µm in nearby cores (Rasmussen et al., 1996a,b, 1997; Rasmussen and Thomsen, 2004 and references therein), with artificially slightly reduced relative abundances of *N. pachyderma* (s), could even imply the occurrence of a reverse thermocline during GI. However, the resemblance during GI 8, 7 and 6 between the relative abundance of *N. pachyderma* (s) > 100 µm in ENAM93-21 (see e.g. Figure 5c in Rasmussen and Thomsen, 2004) and summer SST_{dinos} in MD99-2285 (i.e. with GI values of relative abundance of *N. pachyderma* (s) > 100 µm getting lower and lower from GI 8 to 6, while GI summer SST_{dinos} gets higher and higher from GI 8 to 6) rather suggests a homogeneous upper water column during GI. These findings thus reconcile our study with previous conducted ones (e.g. Rasmussen et al., 1996a, 1997, 2002; Rasmussen and Thomsen, 2004, 2009; Wary et al., CP, in press) by testifying of a hydrological scheme characterized by the occurrence of a halocline during GS and HS and reduced upper stratification during GI.

Hence, in the study area, GI appear to be characterized by (i) a relatively strong bottom current activity, (ii) reduced iceberg calving, and (iii) a relatively homogeneous and cold upper water column, with extensive sea ice formation during winter, and summer sea ice melting probably hampering normal development of *N. pachyderma* (s). At the opposite, GS and HS seem to be marked by (i) a weaker bottom flow, (ii) intense iceberg calving, and (iii) a strong upper stratification, with a warm and low saline surface layer separated by a strong

halocline and (seasonal) thermocline from a colder and more saline subsurface layer favorable to *N. pachyderma* (s) development. Furthermore, given the resemblance of our signals with signals from nearby cores, and particularly with the ones from remote core MD95-2010 (in terms of surface, subsurface, as well as bottom hydrology; see e.g. Kissel et al., 1999; Rasmussen et al., 1999; Eynaud et al., 2002; Ballini et al., 2006), the particular hydrological scheme described in the present study might be representative of the whole Norwegian Sea.

6.2. Hydrological conditions during the last deglaciation and the Holocene

The interval presently spanning from 15.6 to 14 ka cal BP, i.e. just before and at the very beginning of the Bølling-Allerød (delimited by horizontal dashed lines on Fig. 4), is characterized by hydrological conditions similar to GI ones: active deep current, reduced iceberg calving, cold sea-surface conditions with extensive sea ice formation during winter and sea ice melting during summer, and probably also a reduced upper stratification (nearly 100% of *N. pachyderma* (s) but low concentration of planktonic foraminifera, reduced SST_{dino} seasonality, reduced temperature contrast between surface and subsurface). Since the Bølling-Allerød is often considered as a GI (GI 1, e.g. Rasmussen et al., 2014), such a similarity in hydrological signatures strongly suggests that this interval from 15.6 to 14 ka cal BP might correspond to the Bølling-Allerød in itself. In such a case, the stratigraphic lag could be explained by dating and age reservoir uncertainties, the age model being based only on AMS ¹⁴C dates on this section of the core.

Following this interval (and probably starting at 14 ka cal BP), the Younger Dryas, or GS 1, is marked by hydrological responses of GS-type but also of GI-type, depending on the water depth considered. Indeed, dinocyst-derived signals are comparable to GS ones: SST_{dino} are relatively high (comparable to minimal SST_{dino} recorded during GS of the last glacial period), SST_{dino} seasonality is also relatively high, and SIC_{dino} is comparable to maximal values reached during GS (low in comparison to GI). It thus denotes similar, or slightly damped, warm surface conditions with relatively reduced sea-ice cover. *B. tepikiense* is slightly peaking, and planktonic foraminifera assemblages are still monospecific, but the absolute abundance of planktonic foraminifera and thus of *N. pachyderma* (s) is relatively low. This suggests a relatively reduced upper stratification, with propagation of the low SSS_{dino} from surface to subsurface, making subsurface conditions too brackish and maybe also too warm for *N. pachyderma* (s) development. Proxies indicative of the bottom flow

strength do not reveal a coherent signature: magnetic susceptibility is decreasing, K/Ti is relatively low, and mean size of 0.5-10 and 0.5-20 fractions are relatively high even if slightly lower than during the Bølling-Allerød. This may reflect a moderate bottom current activity, weaker than during GI but very likely stronger than during GS. Hence, from a general point of view, the Younger Dryas seems to be characterized by “intermediate” hydrological conditions, or damped GS-type conditions.

Unsurprisingly, the studied Holocene section (~ 11.65 to 2.8 ka cal BP) is characterized by hydrological signals getting closer to the modern ones. Even if the lowest resolution of study for this period (marked by relatively low sedimentation rates around 8 cm.ka⁻¹, and mean temporal resolution around 1200 years, cf. Fig. 2) prevents us from a detailed discussion of the existing hydrological schemes, some features are worth to be pointed out.

Indeed, hydrological reconstructions derived from both dinocyst assemblages (SST_{dino}, SSS_{dino}, SIC_{dino}, temperature seasonality) and planktonic foraminifera assemblages (PF-Temp) tend towards modern values throughout the Holocene section (Fig. 4), and particularly at the core-top interval (0-1 cm, undated, see Fig. 4 and Table 2). It is worth mentioning that such features support the robustness of those reconstructions. Hence, these results denote milder surface and subsurface conditions compared to the last glacial period. Indeed, SST_{dino} are neither as cold as GI ones, nor as warm as GS ones. SST seasonal contrasts are also reduced, and surface waters become less brackish. SIC_{dino} indicate shorter or even nil sea-ice cover duration. Moreover, as indicated by foraminifera assemblages and PF-Temp, subsurface waters get also warmer than during the last glacial period. In parallel, except for the magnetic susceptibility signal, both the ratio K/Ti and mean size of 0.5-10 and 0.5-20 fractions indicate a relatively strong bottom current activity. Despite the absence of quantified modern value, it is very likely that these signals denote deep flow conditions similar to the modern ones, as near-surface conditions do. Hence, in a general way, these results indicate Holocene conditions similar to the modern ones, with a relatively homogenous upper water column characterized by milder conditions in surface as well as in subsurface, higher sea-surface salinity, reduced or even nil sea-ice cover, and active bottom current.

6.3. Implications on last glacial versus Holocene mode of deep water formation

The present study clearly shows that Holocene and GI are similar in terms of deep circulation since they are both characterized by relatively strong deep current activity, probably comparable to the modern one. However, these periods are significantly different in terms of near-surface hydrology: while the Holocene is marked by conditions similar to the modern ones, GI are marked by much colder conditions in surface and subsurface, more brackish upper water column, and the occurrence of sea ice during a great part of the year (up to 8.8 months/year). As already mentioned above, the resemblance of our signals with records coming from other Norwegian Sea cores (e.g. Kissel et al., 1999; Rasmussen et al., 1999; Eynaud et al., 2002; Ballini et al., 2006) strongly suggests that the peculiar hydrological conditions reported here for GI might be representative of the whole Norwegian Sea.

In such a case, this would have important consequences in terms of mode of deep water formation during the last glacial period. Indeed, since Holocene near-surface hydrological conditions seem to be similar to the modern ones, they suggest an open-ocean convection mode in the Nordic Seas, tightly linked to the Atlantic meridional overturning circulation, as in the present climate system (e.g. Hansen and Østerhus, 2000). However, the cold and intensively sea-ice covered near-surface conditions evidenced in the present study and by Eynaud et al. (2002) during GI prevents such a convection, and rather suggest deep water production through intense brine release at this time. This is in opposition with previous findings from Dokken and Jansen (1999), who reported open-ocean convection similar to the present one during GI, and deep water formation driven by sea ice formation and brine production during GS. Authors' interpretations are derived from analyses conducted in nearby core ENAM93-21 and remote core MD95-2010. However, they have been based on indirect proxies, i.e. benthic and planktonic foraminiferal $\delta^{18}\text{O}$ measurements. On the contrary, our work conducted on core MD99-2285, as well as Eynaud et al. (2002) and Kissel et al. (1999)'s works on core MD95-2010, provide more direct evidence of (i) strongly reduced deep current activity and strongly reduced sea-ice cover during GS, both of which do not support the occurrence of significant deep convection driven by brine release during GS, and (ii) cold near-surface conditions and extensive sea-ice cover during GI, both of which rule out the occurrence of open-ocean convection similar to the modern one during GI. Hence, the combination of our work to the ones of Eynaud et al. (2002) and Kissel et al. (1999) provides robust evidences of changes in the mode of deep water formation in the Norwegian Sea between the last glacial period and the Holocene. Given that deep convection was seemingly

of GI-type during the Bølling-Allerød, the transition from GI-type to modern-type convection probably occurred later. Furthermore, dinocyst-derived reconstructions indicate a sea-ice cover duration of 3 months/year during the Younger Dryas and beginning of Holocene (up to ~ 7 ka cal BP), with summer $SST_{\text{dino}} > 14$ °C. In parallel, the relative abundances of temperate planktonic foraminifera, and consequently PF-Temp, start to increase on this same time interval, around 11 ka cal BP. Therefore, both modes of convection might have occurred during this period, which could thus have constituted the transitional phase.

Hence, we propose that GI were characterized by intense deep convection mainly driven by seasonal sea ice formation and associated brine release in the Norwegian Sea. Additional contribution from open-ocean convection is possible but probably only south of the Greenland-Scotland Ridge given the nearly monospecific PF assemblages north of this sill (e.g. [Van Kreveld et al., 2000](#) in the southern Icelandic Sea; this study in the southern Norwegian Sea) and the intense sea-ice cover in the Norwegian Sea. At the opposite, GS were characterized by strongly reduced deep convection, and strongly reduced sea-ice cover in the Norwegian Sea, thus preventing any significant deep convection through brine release. The transition from GI-type convection to modern-type convection probably occurred during the time interval spanning the Younger Dryas and beginning of Holocene.

7. Conclusion

Our study combines surface, subsurface and deep hydrological records obtained over the 3-41 ka cal BP section of core MD99-2285 located in the Southern Norwegian Sea. Our results support the occurrence of an active deep convection in the Nordic Seas during GI, and the absence or strong reduction of deep water formation in the Nordic Seas during GS. However, they also depict an unusual near-surface hydrological scheme during the last glacial climatic events. Indeed, in the studied core, GI are marked by a relatively homogeneous and cold upper water column, with intensive sea ice formation during winter and sea ice melting during summer. At the opposite, GS and HS are characterized by the occurrence of a strong halocline and (seasonal) thermocline separating a warm, low saline and nearly sea ice free surface layer with iceberg calving, from a colder and more saline subsurface layer. The clear resemblance of these results with [Eynaud et al. \(2002\)](#)'s ones strongly suggests that this paradoxical scheme might have occurred in the whole Norwegian Sea. In such a case, the

similarity between Holocene and modern near-surface hydrological conditions, and their significant differences with GI ones, strongly suggest different modes of deep water formation during the last glacial period and during the Holocene/modern period. On the basis of our quantified reconstructions, we propose that, during GI, deep water formation occurred through seasonal sea ice formation and brine release in the Norwegian Sea. The transition from this glacial deep water formation mode, to the modern open ocean convection mode, might have occurred at the end of deglaciation / beginning of the Holocene, when both modes might have occurred. Our results suggest a more complex response of the Nordic Seas to the last glacial millennial climatic events than previously thought. They also suggest a striking decoupling between the Norwegian Sea and Greenland atmosphere, which would require further investigations through paleoclimatic studies and coupled ocean-atmosphere-cryosphere model experiments.

Acknowledgements

Analyses conducted on MD99-2285 were supported by the **French INSU (Institut National des Sciences de l'Univers) programme LEFE** (Les enveloppes fluides et l'environnement) within the frame of the *EVE (Evolution et variabilité du climat à l'échelle globale)* 2009-2011 project "RISCC: Rôle des Ice-Shelves dans le Changement Climatique" and of the *IMAGO (Interactions multiples dans l'atmosphère, la glace et l'océan)* 2013 project "ICE-BIO-RAM : Impact des Changements Environnementaux sur la Biodiversité marine lors des Réchauffements Abrupts du cliMat", this latter being also supported by the *INTERRVIE (Interactions Terre/Vie) - TS (Terre solide) INSU programme*. We also acknowledge financial supports and facilities of the **ARTEMIS ¹⁴C AMS French INSU project**. The research leading to these results also benefited from fundings from the **European Union's Seventh Framework programme (FP7/2007-2013)** under grant agreement no 243908, "Past4Future. Climate change - Learning from the past climate". We warmly thank T. Richter and the Royal Netherlands Institute for Sea Research (NIOZ) for providing Xrf data. We thank P. Lebleu, O. Ther for their assistance in core Imagery. We also warmly thank L. Londeix, D. Swingedouw and M. Cremer for their precious advices and enriching discussions which contributed to greatly improve the present study. Data provided in this paper will be available at <http://www.pangaea.de/>. This is an UMR EPOC contribution XXX.

References

- Andersen MS, Nielsen T, Sørensen AB, Boldreel LO, Kuijpers A. 2000. Cenozoic sediment distribution and tectonic movements in the Faroe region. *Global and Planetary Change* **24**: 239-259.
- Antonov JJ, Seidov D, Boyer TP, Locarnini RA, Mishonov AV, Garcia HE, Baranova OK, Zweng MM, Johnson DR. 2010. *World Ocean Atlas 2009, Volume 2: Salinity*.
- Austin WEN, Hibbert FD. 2012. Tracing time in the ocean: A brief review of chronological constraints (60-8 kyr) on North Atlantic marine event-based stratigraphies. *Quaternary Science Reviews* **36**: 28-37.
- Ballini M, Kissel C, Colin C, Richter T. 2006. Deep-water mass source and dynamic associated with rapid climatic variations during the last glacial stage in the North Atlantic: a multi-proxy investigation of the detrital fraction of deep-sea sediments. *Geochemistry Geophysics Geosystems* **7**: Q02N01.
- Bigg GR, Levine RC, Green CL. 2011. Modelling abrupt glacial North Atlantic freshening: Rates of change and their implications for Heinrich events. *Global and Planetary Change* **79**: 176-192.
- Böhm E, Lippold J, Gutjahr M, Frank M, Blaser P, Antz B, Fohlmeister J, Frank N, Andersen MB, Deininger M. 2015. Strong and deep Atlantic meridional overturning circulation during the last glacial cycle. *Nature* **517**: 73-76.
- Bond G, Broecker W, Johnsen S, McManus J, Labeyrie L, Jouzel J, Bonani G. 1993. Correlations between climate records from North Atlantic sediments and Greenland ice. *Nature* **365**: 143-147.
- Bond G, Heinrich H, Broecker W, Labeyrie L, McManus J, Andrews J, Huon S, Jantschik R, Glasen S, Simet C et al. 1992. Evidence for massive discharges of icebergs into the North Atlantic ocean during the last glacial period. *Nature* **360**: 245-XIII.
- Bond GC, Lotti R. 1995. Iceberg discharges into the North Atlantic on millennial time scales during the last glaciation. *Science* **267**: 1005-1010.
- Borenäs K, Lundberg P. 2004. The Faroe-Bank Channel deep-water overflow. *Deep-Sea Research Part II: Topical Studies in Oceanography* **51**: 335-350.
- Bradwell T, Stoker MS, Gollledge NR, Wilson CK, Merritt JW, Long D, Everest JD, Hestvik OB, Stevenson AG, Hubbard AL et al. 2008. The northern sector of the last British Ice Sheet: Maximum extent and demise. *Earth-Science Reviews* **88**: 207-226.
- Bromwich DH, Chen QS, Li Y, Cullather RI. 1999. Precipitation over Greenland and its relation to the North Atlantic Oscillation. *Journal of Geophysical Research: Atmospheres* **104**: 22103-22115.
- Carstens J, Hebbeln D, Wefer G. 1997. Distribution of planktic foraminifera at the ice margin in the Arctic (Fram Strait). *Marine Micropaleontology* **29**: 257-269.
- Caulle C, Penaud A, Eynaud F, Zaragosi S, Roche DM, Michel E, Boulay S, Richter T. 2013. Sea-surface hydrographical conditions off South Faeroes and within the North-Eastern North Atlantic through MIS 2: The response of dinocysts. *Journal of Quaternary Science* **28**: 217-228.
- Dansgaard W, Johnsen SJ, Clausen HB, Dahl-Jensen D, Gundestrup NS, Hammer CU, Hvidberg CS, Steffensen JP, Sveinbjörnsdóttir AE, Jouzel J et al. 1993. Evidence for general instability of past climate from a 250-kyr ice-core record. *Nature* **364**: 218-220.
- de Vernal A, Henry M, Bilodeau G. 1996. Techniques de préparation et d'analyse en micropaléontologie. *Les cahiers du GEOTOP* **3**: 1-29.
- Dickson AJ, Austin WEN, Hall IR, Maslin MA, Kucera M. 2008. Centennial-scale evolution of Dansgaard-Oeschger events in the northeast Atlantic Ocean between 39.5 and 56.5 ka B.P. *Paleoceanography* **23**: PA3206.
- Dokken TM, Jansen E. 1999. Rapid changes in the mechanism of ocean convection during the last glacial period. *Nature* **401**: 458-461.
- Dokken TM, Nisancioglu KH, Li C, Battisti DS, Kissel C. 2013. Dansgaard-Oeschger cycles: Interactions between ocean and sea ice intrinsic to the Nordic seas. *Paleoceanography* **28**: 491-502.
- Elliot M, Labeyrie L, Bond G, Cortijo E, Turon JL, Tisnerat N, Duplessy JC. 1998. Millennial-scale iceberg discharges in the Irminger Basin during the last glacial period: Relationship with the Heinrich events and environmental settings. *Paleoceanography* **13**: 433-446.
- Elliot M, Labeyrie L, Dokken T, Manthe S. 2001. Coherent patterns of ice-rafted debris deposits in the Nordic regions during the last glacial (10-60 ka). *Earth and Planetary Science Letters* **194**: 151-163.
- Elliot M, Labeyrie L, Duplessy JC. 2002. Changes in North Atlantic deep-water formation associated with the Dansgaard-Oeschger temperature oscillations (60-10 ka). *Quaternary Science Reviews* **21**: 1153-1165.
- Eynaud F, Rossignol L, Gasparotto M-C. 2013. Planktic foraminifera throughout the Pleistocene: from cell to populations to past marine hydrology. In *Foraminifera: Classification, Biology, and Evolutionary Significance*, Georgescu MD (ed). Nova Science Publishers, NY; 209-226.
- Eynaud F, Turon JL, Matthiessen J, Kissel C, Peyrouquet JP, De Vernal A, Henry M. 2002. Norwegian sea-surface palaeoenvironments of marine oxygen-isotope stage 3: The paradoxical response of dinoflagellate cysts. *Journal of Quaternary Science* **17**: 349-359.
- Ezat MM, Rasmussen TL, Groeneveld J. 2014. Persistent intermediate water warming during cold stadials in the southeastern Nordic seas during the past 65 k.y. *Geology* **42**: 663-666.
- Ganopolski A, Rahmstorf S. 2001. Rapid changes of glacial climate simulated in a coupled climate model. *Nature* **409**: 153-158.
- Gildor H, Tziperman E, Nienow PW, Shepherd JG, Alley RB, Lawton JH, Mahadevan A, Lenton TM. 2003. Sea-ice switches and abrupt climate change. *Philosophical Transactions of the Royal Society A: Mathematical, Physical and Engineering Sciences* **361**: 1935-1944.
- Goodman DK. 1979. Dinoflagellate "communities"; from the lower Eocene Nanjemoy formation of Maryland, U.S.A. *Palynology* **3**: 169-190.
- Guiot J, de Vernal A. 2007. Transfer Functions: Methods for Quantitative Paleoclimatology Based on Microfossils. In *Developments in Marine Geology*, Volume 1, Hillaire-Marcel C, de Vernal A (eds). Elsevier; 523-563.
- Guiot J, de Vernal A. 2011a. Is spatial autocorrelation introducing biases in the apparent accuracy of paleoclimatic reconstructions? *Quaternary Science Reviews* **30**: 1965-1972.
- Guiot J, de Vernal A. 2011b. QSR Correspondence "Is spatial autocorrelation introducing biases in the apparent accuracy of palaeoclimatic reconstructions?" Reply to Telford and Birks. *Quaternary Science Reviews* **30**: 3214-3216.
- Hansen B, Osterhus S. 2000. North Atlantic-Nordic Sea exchanges. *Progress in Oceanography* **45**: 109-208.
- Harland R. 1983. Distribution maps of recent dinoflagellate cysts in bottom sediments from the North-Atlantic Ocean and adjacent seas. *Palaeontology* **26**: 321-387.
- Head MJ, Harland R, Matthiessen J. 2001. Cold marine indicators of the late Quaternary: the new dinoflagellate cyst genus *Islandinium* and related morphotypes. *Journal of Quaternary Science* **16**: 621-636.
- Heinrich H. 1988. Origin and consequences of cyclic ice rafting in the Northeast Atlantic Ocean during the past 130,000 years. *Quaternary Research* **29**: 142-152.
- Hemleben C, Spindler M, Erson O. 1989. *Modern planktonic foraminifera*. Springer: Berlin.
- Hillaire-Marcel C, de Vernal A. 2008. Stable isotope clue to episodic sea ice formation in the glacial North Atlantic. *Earth and Planetary Science Letters* **268**: 143-150.

- Hodell DA, Minth EK, Curtis JH, McCave IN, Hall IR, Channell JET, Xuan C. 2009. Surface and deep-water hydrography on Gardar Drift (Iceland Basin) during the last interglacial period. *Earth and Planetary Science Letters* **288**: 10-19.
- Kennett JP, Srinivasan MS. 1983. *Neogene planktonic foraminifera: a phylogenetic atlas*. Hutchinson Ross Publishing Company: Stroudsburg.
- Kenyon NH. 1986. Evidence from bedforms for a strong poleward current along the upper continental slope of northwest Europe. *Marine Geology* **72**: 187-198.
- Kissel C, Laj C, Labeyrie L, Dokken T, Voelker A, Blamart D. 1999. Rapid climatic variations during marine isotopic stage 3: Magnetic analysis of sediments from Nordic Seas and North Atlantic. *Earth and Planetary Science Letters* **171**: 489-502.
- Kleinen T, Osborn TJ, Briffa KR. 2009. Sensitivity of climate response to variations in freshwater hosing location. *Ocean Dynamics* **59**: 509-521.
- Kohfeld KE, Fairbanks RG, Smith SL, Walsh ID. 1996. Neoglobobulimina papyroderma (sinistral coiling) as paleoceanographic tracers in polar oceans: Evidence from Northeast Water Polynya plankton tows, sediment traps, and surface sediments. *Paleoceanography* **11**: 679-699.
- Kuijpers A, Nielsen T, Akhmetzhanov A, De Haas H, Kenyon NH, Van Weering TCE. 2001. Late Quaternary slope instability on the Faeroe margin: Mass flow features and timing of events. *Geo-Marine Letters* **20**: 149-159.
- Kuijpers A, Troelstra SR, Wisse M, Nielsen SH, Van Weering TCE. 1998. Norwegian Sea overflow variability and NE Atlantic surface hydrography during the past 150,000 years. *Marine Geology* **152**: 75-99.
- Laberg JS, Stoker MS, Dahlgren KIT, de Haas H, Haflidason H, Hjelstuen BO, Nielsen T, Shannon PM, Vorren TO, van Weering TCE et al. 2005. Cenozoic alongslope processes and sedimentation on the NW European Atlantic margin. *Marine and Petroleum Geology* **22**: 1069-1088.
- Labeyrie L, Cortijo E. 2005. *Physical properties of sediment core MD99-2285*. DOI: 10.1594/PANGAEA.253616.
- Labeyrie L, Cortijo E, Jansen E. 1999. Rapport scientifique de la mission INTERPOLE MD99-114/812 IMAGES V. In *Les Rapports de Campagne à la Mer à bord du Marion Dufresne*, IPEV (eds). Brest.
- Laj C, Kissel C, Mazaud A, Channell JET, Beer J. 2000. North Atlantic palaeointensity stack since 75 ka (NAPIS-75) and the duration of the Laschamp event. *Philosophical Transactions of the Royal Society A: Mathematical, Physical and Engineering Sciences* **358**: 1009-1025.
- Larsen KMH, Hansen B, Svendsen H. 2008. Faroe Shelf Water. *Continental Shelf Research* **28**: 1754-1768.
- Larsen KMH, Hansen B, Svendsen H. 2009. The Faroe Shelf Front: Properties and exchange. *Journal of Marine Systems* **78**: 9-17.
- Li C, Battisti DS, Bitz CM. 2010. Can North Atlantic sea ice anomalies account for Dansgaard-Oeschger climate signals? *Journal of Climate* **23**: 5457-5475.
- Locarnini RA, Mishonov AV, Antonov JJ, Boyer TP, Garcia HE, Baranova OK, Zweng MM, Johnson DR. 2010. *World Ocean Atlas 2009, Volume 1: Temperature*.
- Londeix L, Benzakour M, Suc JP, Turon JL. 2007. Messinian palaeoenvironments and hydrology in Sicily (Italy): The dinoflagellate cyst record. *Geobios* **40**: 233-250.
- Manabe S, Stouffer RJ. 1995. Simulation of abrupt climate change induced by freshwater input to the North Atlantic Ocean. *Nature* **378**: 165-167.
- Mary Y, Eynaud F, Zaragosi S, Malaizé B, Cremer M, Schmidt S. 2015. High frequency environmental changes and deposition processes in a 2 kyr-long sedimentological record from the Cap-Breton canyon (Bay of Biscay). *Holocene* **25**: 348-365.
- Matsuzaki KMR, Eynaud F, Malaizé B, Grousset FE, Tisserand A, Rossignol L, Charlier K, Jullien E. 2011. Paleoclimatology of the Mauritanian margin during the last two climatic cycles: From planktonic foraminifera to African climate dynamics. *Marine Micropaleontology* **79**: 67-79.
- Mauritzen C, Price J, Sanford T, Torres D. 2005. Circulation and mixing in the Faroese Channels. *Deep-Sea Research Part I: Oceanographic Research Papers* **52**: 883-913.
- McCartney MS, Mauritzen C. 2001. On the origin of the warm inflow to the Nordic Seas. *Progress in Oceanography* **51**: 125-214.
- McCave IN. 2007. Chapter One Deep-Sea Sediment Deposits and Properties Controlled by Currents. In *Developments in Marine Geology*, Volume 1, Hillaire-Marcel C, de Vernal A (eds). Elsevier; 19-62.
- McCave IN, Manighetti B, Beveridge NAS. 1995a. Circulation in the glacial North Atlantic inferred from grain-size measurements. *Nature* **374**: 149-152.
- McCave IN, Manighetti B, Robinson SG. 1995b. Sortable silt and fine sediment size/composition slicing: parameters for palaeocurrent speed and palaeoceanography. *Paleoceanography* **10**: 593-610.
- Mix AE, Bard E, Schneider R. 2001. Environmental processes of the ice age: Land, Ocean, Glacier (EPILOG). *Quaternary Science Reviews* **20**: 627-657.
- Nielsen T, Rasmussen TL, Ceramicola S, Kuijpers A. 2007. Quaternary sedimentation, margin architecture and ocean circulation variability around the Faroe Islands, North Atlantic. *Quaternary Science Reviews* **26**: 1016-1036.
- Norgaard-Pedersen N, Mikkelsen N, Lassen SJ, Kristoffersen Y, Sheldon E. 2007. Reduced sea ice concentrations in the Arctic Ocean during the last interglacial period revealed by sediment cores off northern Greenland. *Paleoceanography* **22**: PA1218.
- Orvik KA, Niiler P. 2002. Major pathways of Atlantic water in the northern North Atlantic and Nordic Seas toward Arctic. *Geophysical Research Letters* **29**: 2-1.
- Penaud A, Eynaud F, Sánchez-Goñi M, Malaizé B, Turon JL, Rossignol L. 2011. Contrasting sea-surface responses between the western Mediterranean Sea and eastern subtropical latitudes of the North Atlantic during abrupt climatic events of MIS 3. *Marine Micropaleontology* **80**: 1-17.
- Petersen SV, Schrag DP, Clark PU. 2013. A new mechanism for Dansgaard-Oeschger cycles. *Paleoceanography* **28**: 24-30.
- Polyak L, Korsun S, Febo LA, Stanovoy V, Khusid T, Hald M, Paulsen BE, Lubinski DJ. 2002. Benthic foraminiferal assemblages from the southern Kara Sea, a river-influenced Arctic marine environment. *The Journal of Foraminiferal Research* **32**: 252-273.
- Prins MA, Bouwer LM, Beets CJ, Troelstra SR, Weltje GJ, Kruk RW, Kuijpers A, Vroon PZ. 2002. Ocean circulation and iceberg discharge in the glacial North Atlantic: Inferences from unmixing of sediment size distributions. *Geology* **30**: 555-558.
- Radi T, Bonnet S, Cormier MA, de Vernal A, Durantou L, Faubert É, Head MJ, Henry M, Pospelova V, Rochon A et al. 2013. Operational taxonomy and (paleo-)autecology of round, brown, spiny dinoflagellate cysts from the Quaternary of high northern latitudes. *Marine Micropaleontology* **98**: 41-57.
- Rahmstorf S. 2002. Ocean circulation and climate during the past 120,000 years. *Nature* **419**: 207-214.
- Rasmussen SO, Bigler M, Blockley SP, Blumier T, Buchardt SL, Clausen HB, Cvijanovic I, Dahl-Jensen D, Johnsen SJ, Fischer H et al. 2014. A stratigraphic framework for abrupt climatic changes during the Last Glacial period based on three synchronized Greenland ice-core records: Refining and extending the INTIMATE event stratigraphy. *Quaternary Science Reviews* **106**: 14-28.
- Rasmussen TL, Balbon E, Thomsen E, Labeyrie L, Van Weering TCE. 1999. Climate records and changes in deep outflow from the Norwegian Sea ~ 150-55 ka. *Terra Nova* **11**: 61-66.
- Rasmussen TL, Thomsen E. 2004. The role of the North Atlantic Drift in the millennial timescale glacial climate fluctuations. *Palaeogeography, Palaeoclimatology, Palaeoecology* **210**: 101-116.
- Rasmussen TL, Thomsen E. 2008. Warm Atlantic surface water inflow to the Nordic seas 34-10 calibrated ka B.P. *Paleoceanography* **23**: PA1201.
- Rasmussen TL, Thomsen E. 2009. Ventilation changes in intermediate water on millennial time scales in the SE Nordic seas, 65-14 kyr BP. *Geophysical Research Letters* **36**: L01601.
- Rasmussen TL, Thomsen E, Labeyrie L, Van Weering TCE. 1996a. Circulation changes in the Faeroe-Shetland Channel correlating with cold events during the last glacial period (58-10 ka). *Geology* **24**: 937-940.

- Rasmussen TL, Thomsen E, Troelstra SR, Kuijpers A, Prins MA. 2002. Millennial-scale glacial variability versus Holocene stability: Changes in planktic and benthic foraminifera faunas and ocean circulation in the North Atlantic during the last 60 000 years. *Marine Micropaleontology* **47**: 143-176.
- Rasmussen TL, Thomsen E, Van Weering TCE, Labeyrie L. 1996b. Rapid changes in surface and deep water conditions at the Faeroe Margin during the last 58,000 years. *Paleoceanography* **11**: 757-771.
- Rasmussen TL, Van Weering TCE, Labeyrie L. 1997. Climatic instability, ice sheets and ocean dynamics at high northern latitudes during the last glacial period (58-10 KA BP). *Quaternary Science Reviews* **16**: 71-80.
- Reimer PJ, Baillie MGL, Bard E, Bayliss A, Beck JW, Blackwell PG, Ramsey CB, Buck CE, Burr GS, Edwards RL et al. 2009. IntCal09 and Marine09 radiocarbon age calibration curves, 0-50,000 years CAL BP. *Radiocarbon* **51**: 1111-1150.
- Richter TO, Van Der Gaast S, Koster B, Vaars A, Gieles R, De Stigter HC, De Haas H, Van Weering TCE. 2006. The Avaatech XRF Core Scanner: Technical description and applications to NE Atlantic sediments. In *New Techniques in Sediment Core Analysis*, Rothwell RG (ed). Geological Society, London, Special Publications, 267; 39-50.
- Rochon A, de Vernal A, Turon J-L, Matthiessen J, Head MJ, ed. 1999. *Distribution of dinoflagellate cysts in surface sediments from the North Atlantic Ocean and adjacent basins and quantitative reconstruction of sea-surface parameters*. AASP special pub., Dallas, Texas.
- Sachs JP, Lehman SJ. 1999. Subtropical North Atlantic temperatures 60,000 to 30,000 years ago. *Science* **286**: 756-760.
- Sánchez Goñi MF, Bakker P, Desprat S, Carlson AE, Van Meerbeeck CJ, Peyron O, Naughton F, Fletcher WJ, Eynaud F, Rossignol L et al. 2012. European climate optimum and enhanced Greenland melt during the last interglacial. *Geology* **40**: 627-630.
- Sánchez Goñi MF, Bard E, Landais A, Rossignol L, D'Errico F. 2013. Air-sea temperature decoupling in western Europe during the last interglacial-glacial transition. *Nature Geoscience* **6**: 837-841.
- Sanchez Goñi MF, Harrison SP. 2010. Millennial-scale climate variability and vegetation changes during the Last Glacial: Concepts and terminology. *Quaternary Science Reviews* **29**: 2823-2827.
- Sarjeant WAS. 1974. *Fossil and living dinoflagellates*. Academic Press Inc.: London, UK.
- Schiebel R, Wanik J, Bork M, Hemleben C. 2001. Planktic foraminiferal production stimulated by chlorophyll redistribution and entrainment of nutrients. *Deep-Sea Research Part I: Oceanographic Research Papers* **48**: 721-740.
- Schlitzer R. 2012. *Ocean Data View*. <http://odv.awi.de> [8 April 2014]
- Scourse JD, Haapaniemi AI, Colmenero-Hidalgo E, Peck VL, Hall IR, Austin WEN, Knutz PC, Zahn R. 2009. Growth, dynamics and deglaciation of the last British-Irish ice sheet: the deep-sea ice-rafted detritus record. *Quaternary Science Reviews* **28**: 3066-3084.
- Sejrup HP, Larsen E, Hafliðason H, Berstad IM, Hjelstuen BO, Jonsdóttir HE, King EL, Landvik J, Longva O, Nygard A et al. 2003. Configuration, history and impact of the Norwegian Channel Ice Stream. *Boreas* **32**: 18-36.
- Shannon CE, Weaver W. 1949. *The Mathematical Theory of Information*. University of Illinois Press: Urbana.
- Simstich J, Sarnthein M, Erlenkeuser H. 2003. Paired $\delta^{18}O$ signals of *Neogloboquadrina pachyderma* (s) and *Turborotalita quinqueloba* show thermal stratification structure in Nordic Seas. *Marine Micropaleontology* **48**: 107-125.
- Singh HA, Battisti DS, Bitz CM. 2014. A heuristic model of dansgaard-oeschger cycles. Part I: Description, results, and sensitivity studies. *Journal of Climate* **27**: 4337-4358.
- Snowball I, Moros M. 2003. Saw-tooth pattern of North Atlantic current speed during Dansgaard-Oeschger cycles revealed by the magnetic grain size of Reykjanes Ridge sediments at 59°N. *Paleoceanography* **18**: 4-1.
- Stouffer RJ, Yin J, Gregory J, Dixon K, Spelman M, Hurlin W, Weaver A, Eby M, Flato G, Hasumi H. 2006. Investigating the causes of the response of the thermohaline circulation to past and future climate changes. *Journal of Climate* **19**: 1365-1387.
- Stuiver M, Reimer P, Reimer R. 2010. *CALIB 6.0, program*. Queens Univ, Belfast, UK. <http://radiocarbon.pa.qub.ac.uk/calib/>
- Reimer PJ, Bard E, Bayliss A, Beck JW, Blackwell PG, Bronk Ramsey C, Buck CE, Cheng H, Edwards RL, Friedrich M, Grootes PM, Guilderson TP, Hafliðason H, Hajdas I, Hatté C, Heaton TJ, Hogg AG, Hughen KA, Kaiser KF, Kromer B, Manning SW, Niu M, Reimer RW, Richards DA, Scott EM, Southon JR, Turney CSM, van der Plicht J. 2013. IntCal13 and MARINE13 radiocarbon age calibration curves 0-50000 years calBP. *Radiocarbon* **55**. DOI: 10.2458/azu_js_rc.55.16947
- Svensden JI, Alexanderson H, Astakhov VI, Demidov I, Dowdeswell JA, Funder S, Gataullin V, Henriksen M, Hjort C, Houmark-Nielsen M et al. 2004. Late Quaternary ice sheet history of northern Eurasia. *Quaternary Science Reviews* **23**: 1229-1271.
- Svensson A, Andersen KK, Bigler M, Clausen HB, Dahl-Jensen D, Davies SM, Johnsen SJ, Muscheler R, Parrenin F, Rasmussen SO et al. 2008. A 60 000 year Greenland stratigraphic ice core chronology. *Climate of the Past* **4**: 47-57.
- Swingedouw D, Rodehacke CB, Behrens E, Menary M, Olsen SM, Gao Y, Mikolajewicz U, Mignot J, Biastoch A. 2013. Decadal fingerprints of freshwater discharge around Greenland in a multi-model ensemble. *Climate Dynamics* **41**: 695-720.
- Tolderlund DS, Bé AWH. 1971. Seasonal Distribution of Planktonic Foraminifera in the Western North Atlantic. *Micropaleontology* **17**: 297-329.
- Valdimarsson H, Malmberg S-A. 1999. Near-surface circulation in Icelandic waters derived from satellite tracked drifters. *Rit Fiskideild* **16**: 23-40.
- Van Kreveld S, Sarnthein M, Erlenkeuser H, Grootes P, Jung S, Nadeau MJ, Pflaumann U, Voelker A. 2000. Potential links between surging ice sheets, circulation changes, and the Dansgaard-Oeschger cycles in the Irmiger Sea, 60-80 kyr. *Paleoceanography* **15**: 425-442.
- Van Weering TCE, Nielsen T, Kenyon NH, Akentieva K, Kuijpers AH. 1998. Sediments and sedimentation at the NE Faeroe continental margin; Contourites and large-scale sliding. *Marine Geology* **152**: 159-176.
- von Gyldenfeldt A-B, Carstens J, Meincke J. 2000. Estimation of the catchment area of a sediment trap by means of current meters and foraminiferal tests. *Deep Sea Research Part II: Topical Studies in Oceanography* **47**: 1701-1717.
- Wolff EW, Chappellaz J, Blunier T, Rasmussen SO, Svensson A. 2010. Millennial-scale variability during the last glacial: The ice core record. *Quaternary Science Reviews* **29**: 2828-2838.

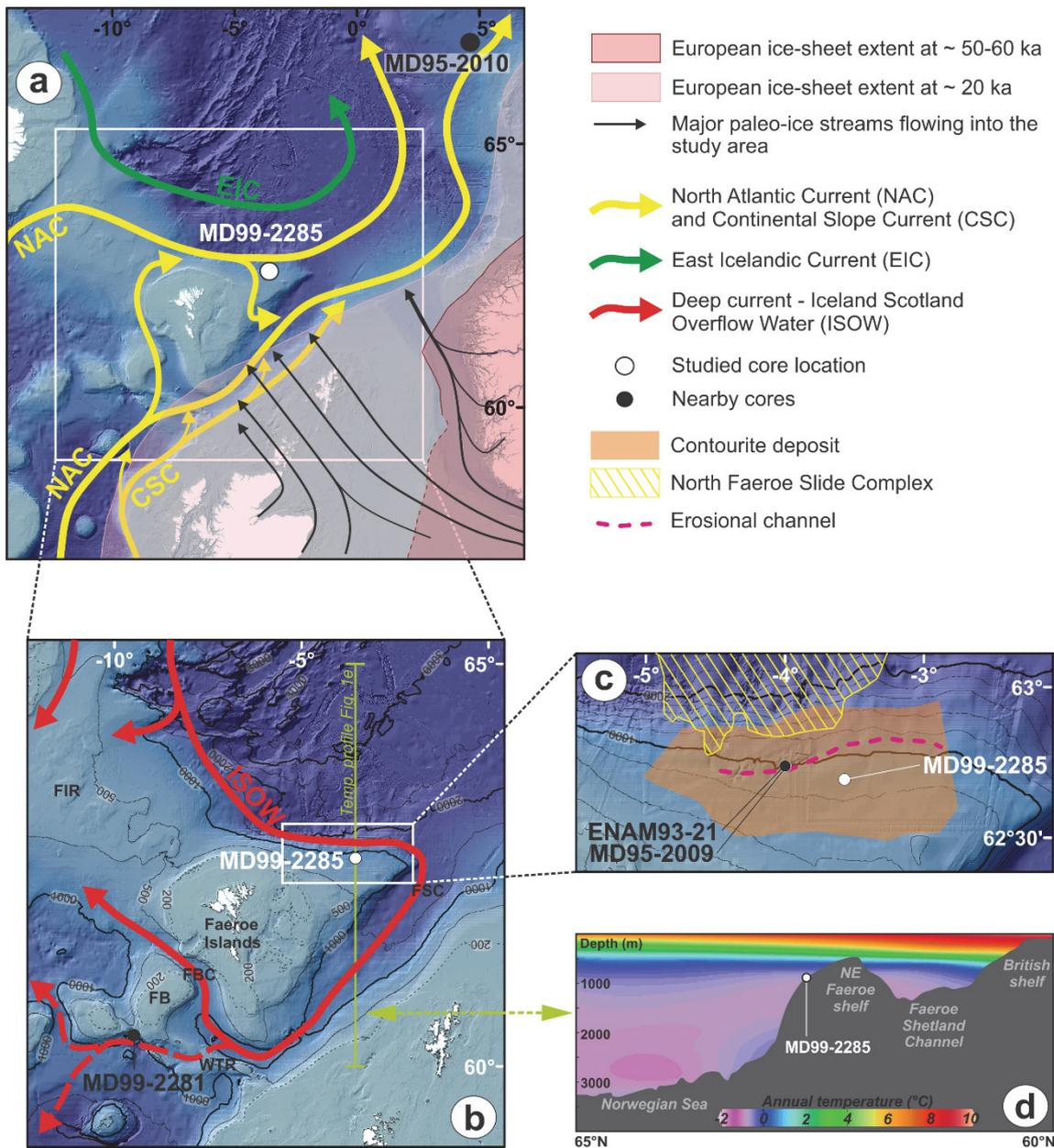


Figure 1: Map of the study area showing the locations of the studied core and of nearby cores referenced to in the present study, as well as past and modern environmental settings. (a) Surface hydrology (after Kenyon, 1986; Valdimarsson and Malmberg, 1999, Orvik and Niiler, 2002), last glacial ice-sheet extensions (after Svendsen et al., 2004) and major paleo-ice streams (after Sejrup et al., 2003 and Bradwell et al., 2008). (b) Detailed bottom physiography and deep Iceland Scotland Overflow Water (ISOW) major pathways across the Greenland Scotland Ridge via the bottom current (after Kuijpers et al., 1998). The first isobath (dotted) is at 200 m, then isobath interval is 500 m. Major bathymetric structures are indicated (FIR: Faeroe Iceland Ridge, FSC: Faeroe Shetland Channel, FBC: Faeroe Bank Channel; WTR: Wyville-Thomson Ridge, FB: Faeroe Bank). Location of the north-south temperature profile shown in Fig. 1d is indicated by the yellow line. (c) Modern sedimentary regimes, with indication of the area of contourite deposit (van Weering et al., 1998), the sector affected by down-slope mass transport (Kuijpers et al., 2001; Nielsen et al., 2007), and the location of the erosive channel formed through the bottom current action (van Weering et al., 1998). Isobath intervals is 200 m. (d) North-south temperature profile illustrating the structure of the water column over the study area. Temperature data are derived from WOA09 data (Locarnini et al., 2010) and plot using Ocean Data View (Schlitzer, 2012). Bathymetry is from EMODnet (www.emodnet.eu). Geographic coordinate system: WGS 1984 – Projection: Mercator 55°N.

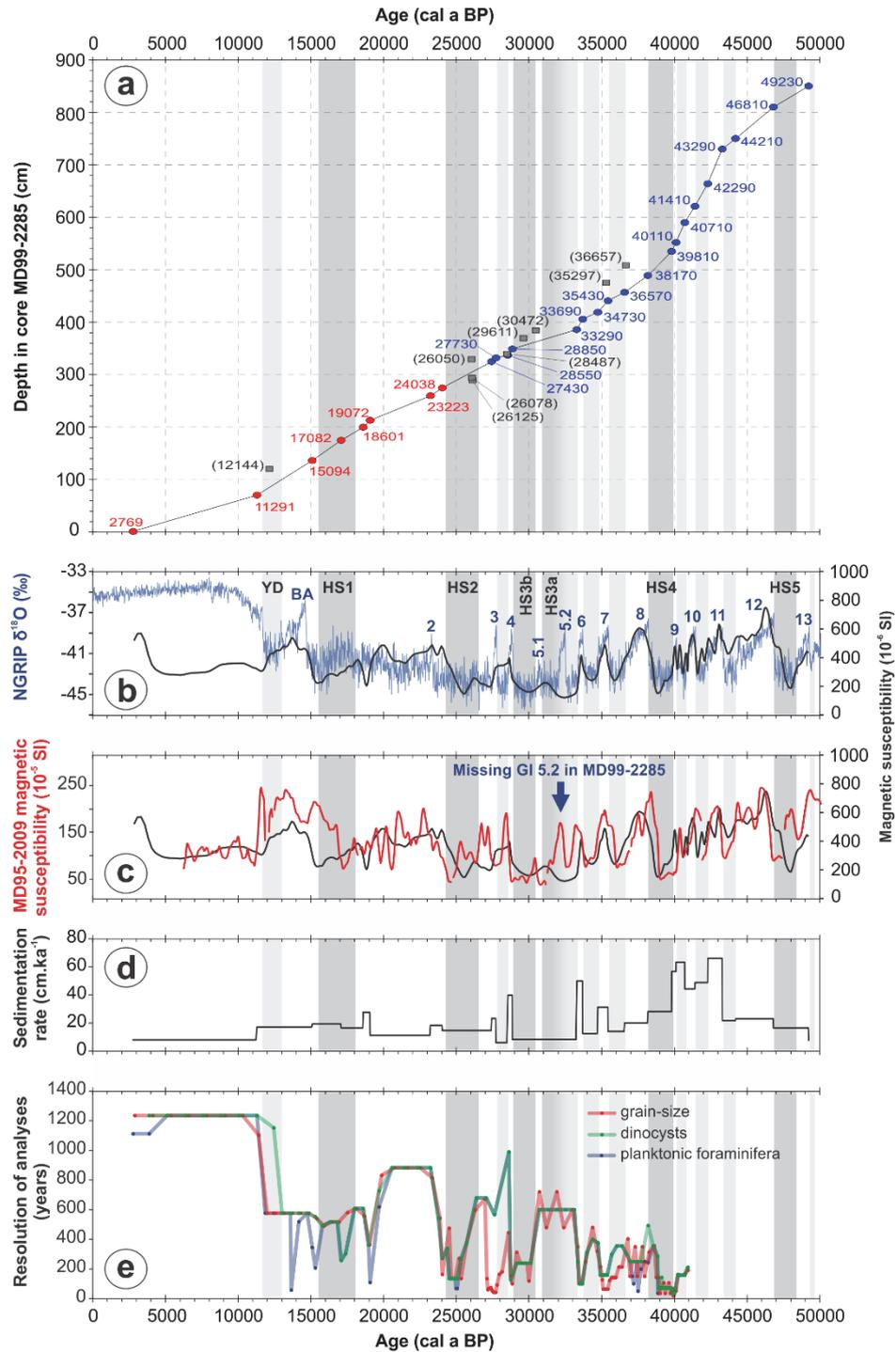
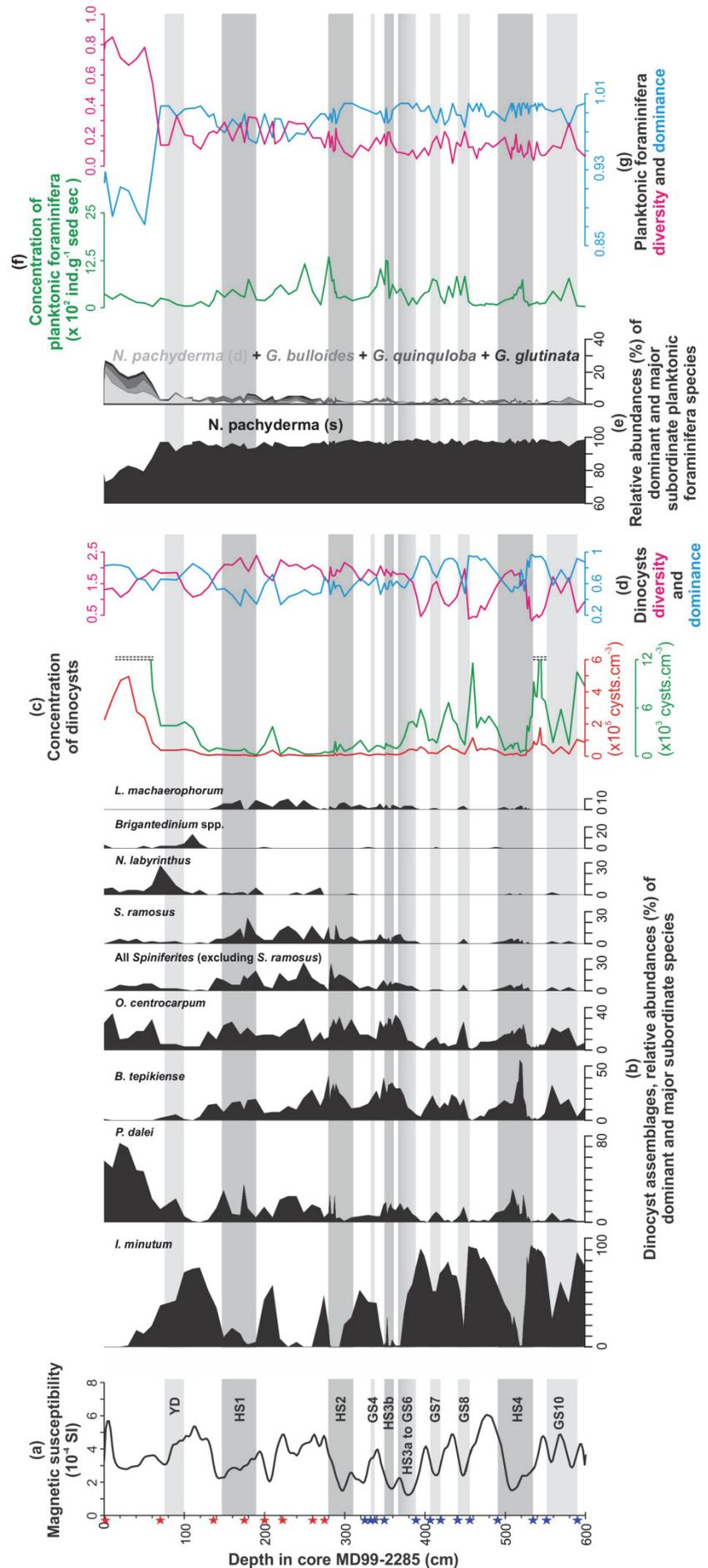


Figure 2: Age model, sedimentation rate and resolution of analyses on core MD99-2285 for the last 50 ka. (a) Linear interpolation (black curve) between tie-points, i.e. selected AMS14C dates (red dots) and age-control points (blue dots) obtained by correlation of the magnetic susceptibility signal of the core to the NGRIP $\delta^{18}O$ record (Wolff et al., 2010). Incoherent dates (unconsidered for the establishment of the age model) are also shown (grey squares with corresponding ages in brackets). (b) Graph showing the correspondence between the magnetic susceptibility signal of the core (plotted according to the resulting calendar BP age scale) and the NGRIP $\delta^{18}O$ record. (c) Comparison of MD99-2281 MS record with nearby core MD95-2009 (cf. Fig. 1c) MS signal from Kissel et al. (1999). (d) Evolution through time of sedimentation rates of the studied core. (e) Resolution of the three principal analyses conducted on core MD99-2285 for the present work.

Figure 3: Results from dinocyst and planktonic foraminifera assemblages over the section 0-600 cm of core MD99-2285. (a) Magnetic susceptibility signal, tie-points used to establish the age model (with blue stars = age control points obtained by correlating the core magnetic susceptibility signal to NGRIP $\delta 180$ record, and red stars = AMS 14C dates; cf. Figure 1 and Table 1) and chronostratigraphic framework. (b) Relative abundances of dominant and major subordinate modern dinocyst species. (c) Concentration of modern dinocysts. (d) Dinocyst diversity and dominance indices. (e) Relative abundances of dominant and major subordinate planktonic foraminifera species. (f) Concentration of planktonic foraminifera. (g) Planktonic foraminifera diversity and dominance indices. Key cold periods highlighted by grey bands (delimited according to our age model with age limits defined by Wolff et al., 2010, Sanchez-Goñi and Harrison, 2010, and Rasmussen et al., 2014; YD = Younger Dryas, HS# = Heinrich stadial number #, GS# = Greenland stadial number #).



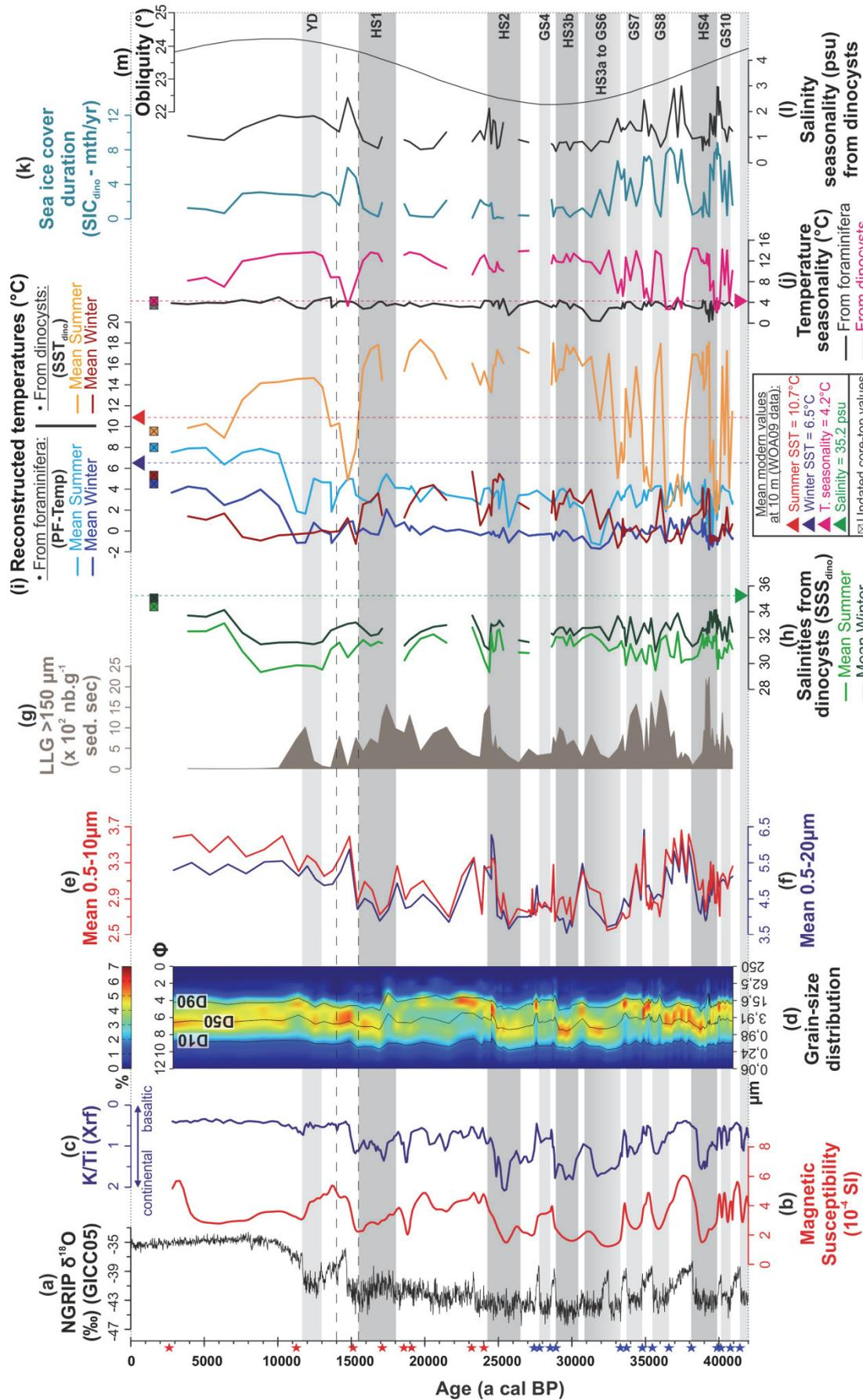


Figure 4: Age compilation of hydrological signals recorded on core MD99-2285. (a) NGRIP $\delta^{18}O$ regional stratotype. (b to e) Indicators of deep current activity, with (b) magnetic susceptibility, (c) Xrf K/Ti ratio, plotted on a reverse scale, (d) mapping of grain-size distribution, D10, D50, and D90, (e and f) mean sizes of the clay to silty clay size fractions. (g) Large Lithic Grains concentration, indicative of iceberg calving. (h to l) temperature seasonal contrast calculated from seasonal subsurface hydrological conditions, with (h) seasonal SSS_{dino} and PF-Temp, (i) seasonal SST $_{dino}$ and PF-Temp, (j) temperature seasonal contrast calculated from seasonal SST $_{dino}$ and PF-Temp, (k) SIC $_{dino}$, and (l) salinity seasonal contrast calculated from seasonal SSS $_{dino}$. (m) Obliquity signal, which displays relatively similar trends to some of our dinocyst-derived records and especially those related to sea ice. Stars and grey bands: same legend as Fig. 3. Mean modern hydrological values (after WOA09 data: Antonov et al., 2010; Locarnini et al., 2010) and undated core-top values are also indicated.

Table 1: Radiocarbon dates on MD99-2285 and age control points obtained by correlation of the magnetic susceptibility signal of core MD99-2285 to NGRIP $\delta^{18}O$ record (Svensson et al., 2008; Wolff et al., 2010). Selected and eliminated tie points are shown.

Level / Interval dated (cm)	Uncorrected AMS ¹⁴ C age (BP)	Lab. ID.	Corrected calendar age		1 σ ranges [start]	1 σ ranges [end]	Corrected		Tie points (age in cal a BP)	Dated material or event based stratigraphy
			(a cal BP) CALIB 6	(a cal BP) CALIB 7			Delta Catib version (7 minus 6)	calendar age (a cal BP) CALIB 7		
1.5	3005 ± 30	SacA 31203	2769	2769	2734	2804	0	2769	Bulk planktonic foraminifera, ARTEMIS 2013	
70.5	10335 ± 40	SacA 37852	11291	11291	11234	11348	28	11291	<i>N. pachyderma</i> (s), ARTEMIS 2014	
120.5	10740 ± 50	SacA 37853	12144	12144	12037	12251	19	**	<i>N. pachyderma</i> (s), ARTEMIS 2014	
136.5	13160 ± 45	SacA 31207	15094	15094	14941	15247	103	15094	<i>N. pachyderma</i> (s), ARTEMIS 2013	
175	14480 ± 50	SacA 31204	17082	17082	16943	17221	29	17082	<i>N. pachyderma</i> (s), ARTEMIS 2013	
200	15730 ± 50	SacA 37854	18600.5	18600.5	18548	18653	7	18600.5	<i>N. pachyderma</i> (s), ARTEMIS 2014	
213	16410 ± 50	SacA 31205	19071.5	19071.5	18986	19157	248	19071.5	<i>N. pachyderma</i> (s), ARTEMIS 2013	
260	19850 ± 200	SacA 37855	23222.5	23222.5	22927	23518	173	23222.5	<i>N. pachyderma</i> (s), ARTEMIS 2014	
275	20510 ± 90	SacA 37856	24037.5	24037.5	23868	24207	134	24037.5	<i>N. pachyderma</i> (s), ARTEMIS 2014	
289	22230 ± 90	SacA 31206	26125	26125	25925	26235	-74	*	<i>N. pachyderma</i> (s), ARTEMIS 2013	
294	22180 ± 100	SacA 37857	26077.5	26077.5	25900	26255	-80	*	<i>N. pachyderma</i> (s), ARTEMIS 2014	
325	22150 ± 120	SacA37858	26050	26050	25852	26248	-72	**	GI3 termination (duration 0.3 ka) after Wolff et al., 2010	
332									<i>N. pachyderma</i> (s), ARTEMIS 2014	
337								27730	GI3 warming after Wolff et al., 2010	
339.5	24150 ± 140	SacA37859	28486.5	28486.5	28263	28170	-677	28550	GI4 termination (duration 0.3 ka) after Wolff et al., 2010	
349								**	<i>N. pachyderma</i> (s), ARTEMIS 2014	
369.5	25180 ± 140	SacA37860	29611	29611	29401	29821	-811	28850	GI4 warming after Wolff et al., 2010	
384.5	26050 ± 160	SacA37861	30471.5	30471.5	30301	30642	-674	**	<i>N. pachyderma</i> (s), ARTEMIS 2014	
386								**	<i>N. pachyderma</i> (s), ARTEMIS 2014	
406								33290	GI6 termination (duration 0.4 ka) after Wolff et al., 2010	
419								33690	GI6 warming after Wolff et al., 2010	
441								34730	GI7 termination (duration 0.7 ka) after Wolff et al., 2010	
457								35430	GI7 warming after Wolff et al., 2010	
475.5	31380 ± 210	SacA 31209	35297	35297	35070	35524	-433	36570	GI8 termination (duration 1.6 ka) after Wolff et al., 2010	
489								**	Bulk planktonic foraminifera, ARTEMIS 2013	
508.5	32570 ± 230	SacA 31208	36657	36657	36466	36848	-602	38170	GI8 warming after Wolff et al., 2010	
535								**	<i>N. pachyderma</i> (s), ARTEMIS 2013	
552								39810	GI9 termination (duration 0.3 ka) after Wolff et al., 2010	
590								40110	GI9 warming after Wolff et al., 2010	
621								40710	GI10 termination (duration 0.7 ka) after Wolff et al., 2010	
664								41410	GI10 warming after Wolff et al., 2010	
730								42290	GI11 termination (duration 1 ka) after Wolff et al., 2010	
750								43290	GI11 warming after Wolff et al., 2010	
810								44210	GI12 termination (duration 2.6 ka) after Wolff et al., 2010	
850								46810	GI12 warming after Wolff et al., 2010	
								49230	GI13 warming after Wolff et al., 2010	

Radiocarbon dates unused for the age model: * too old ages, ** too young ages

Table 2: Modern hydrological conditions (WOA09 data, Locarnini et al., 2010; Antonov et al., 2010) and core-top (0-1 cm) reconstructed hydrological parameters at 10 m water depth.

	summer temperatures	winter temperatures	Seasonality	summer salinities	winter salinities
Modern values	10.7	6.5	4.2	35.2	35.2
core-top (0-1 cm) values derived from dinocyst assemblages	9.5	5.3	4.2	34.3	35.0
core-top (0-1 cm) values derived from planktonic foraminifera assemblages	8.0	4.4	3.6	/	/

Partie 2 : Processus hydrographiques et mécanismes de déclenchement en jeu lors des événements climatiques abrupts avant, pendant et après un HE : zoom sur la période 35-41 ka autour d'HE4.

Section 1. Sea-surface warm pulses as the trigger of ice-sheet collapses: first evidence from paleodata

*Article en préparation en vue d'une soumission à **Quaternary Science Reviews**.*

Wary Mélanie¹, Sicre Marie-Alexandrine², Eynaud Frédérique¹, Rossignol Linda¹, Lapuyade Joanna¹, Gasparotto Marie-Camille^{1,*}, Londeix Laurent¹, Malaize Bruno¹, Castera Marie-Hélène¹, Charlier Karine¹

¹ UMR 5805, EPOC (Environnements et Paléoenvironnements Océaniques et Continentaux), Université de Bordeaux, 33615 Pessac, France.

² LOCEAN (Laboratoire d'Océanographie et du Climat: Expérimentation et Approches Numériques), IPSL-UPMC/CNRS/IRD/MNHN, Paris, France.

* now at: UQAM, Université du Québec à Montréal, Montréal, Québec H3C 3P8, Canada.

Résumé

Les événements climatiques millénaires de la dernière période glaciaire (i.e. événements de Dansgaard-Oeschger et événements d'Heinrich) constituent des cas d'étude exceptionnels des interactions couplées océan-atmosphère-cryosphère. Notre travail se focalise ici sur l'évolution à très haute résolution des conditions océaniques de surface et de subsurface, en termes de températures, salinité, et couvert de glace de mer, enregistrées au sein d'une archive inédite, la carotte MD99-2285 (62.69 °N; -3.57 °E), durant la période 36 – 41 ka cal BP couvrant trois cycles de Dansgaard-Oeschger et incluant l'évènement d'Heinrich 4. Nous utilisons pour cela un large panel d'outils, combinant pour la première fois deux indicateurs indépendants de la présence de glace de mer : l'IP25 et les reconstructions quantifiées issues des assemblages de dinokystes. Le couplage approche multiproxies – haute résolution temporelle (résolution moyenne des analyses entre 55 et 155 ans en fonction des proxies) nous permet d'identifier le séquençage des processus hydrographiques et d'estimer les interactions océan-cryosphère s'opérant au cours de cette période d'instabilité récurrente des calottes de glace. Nos résultats mettent ainsi en évidence un schéma hydrologique paradoxal, où (i) les interstadias sont marqués par la présence d'une colonne d'eau supérieure relativement froide et homogène, avec un cycle saisonnier intense de formation / fonte de glace de mer, et (ii) les stadias (incluant aussi ceux associés aux événements d'Heinrich) se caractérisent par la présence d'une forte halocline séparant un niveau de surface chaud et peu salé, et où le vèlage d'icebergs inhibe la formation de glace de mer, d'un niveau de subsurface moins chaud et plus salé. Notre étude suggère également que le réchauffement de surface/subsurface enregistré en stadias, induit par l'advection d'eau chaude atlantique, ait commencé avant l'amorce de chaque débâcle d'icebergs. Ces résultats supportent ainsi l'hypothèse que ces épisodes de déstabilisation des glaciers aient pu être déclenchés par un réchauffement de l'océan. Par ailleurs, d'autres études conduites le long de la bordure des calottes européennes, sur le trajet de l'afflux d'eau atlantique, suggèrent qu'un tel processus puisse avoir eu lieu dans l'ensemble de cette zone. Néanmoins, de nouvelles paléoreconstructions à haute résolution seront nécessaires pour étayer ce schéma régional.

Abstract

The last glacial millennial climatic events (i.e. Dansgaard-Oeschger and Heinrich events) constitute outstanding case studies of coupled atmosphere-ocean-cryosphere interactions. Here, we investigate the evolution of sea-surface and subsurface conditions, in terms of temperature, salinity and sea-ice cover, at very high-resolution (mean resolution between 55 and 155 years depending on proxies) during the 36-41 ka cal BP interval covering three Dansgaard-Oeschger events and including Heinrich event 4, in a new and unpublished marine record, i.e. the MD99-2285 core (62.69 °N; -3.57 °E). We use a large panel of complementary tools, which includes for the first time coupled IP25 abundances and dinocyst-derived sea-ice cover duration quantifications. The high temporal resolution and multiproxy approach of this work allows us to identify the sequencing of processes and to assess ocean-cryosphere interactions occurring during these periodic ice-sheet collapse events. Our results evidence a paradoxical hydrological scheme where (i) Greenland interstadials are marked by a homogeneous and cold upper water column, with intensive winter sea ice formation and summer sea ice melting, and (ii) Greenland and Heinrich stadials are characterized by a very warm and low saline surface layer with iceberg calving and reduced sea ice formation, separated by a strong halocline from a less warm and saltier subsurface layer. Our work also suggests that this stadial surface/subsurface warming started before massive iceberg release, in relation with warm Atlantic water advection. These findings thus support the theory that upper ocean warming might have triggered European ice-sheet destabilization. Besides, previous paleoceanographic studies conducted along the Atlantic inflow pathways close to the edge of European ice-sheets suggest that such a feature might have occurred in this whole area. Nonetheless, additional high resolution paleoreconstructions are required to confirm such a regional scheme.

Keywords

Dansgaard-Oeschger events, Heinrich events, trigger mechanism, sea ice, surface/subsurface hydrological conditions, high resolution multiproxy approach.

1. Introduction

The last glacial period has been marked by two types of abrupt climatic events. The first ones, Dansgaard-Oeschger events, first evidenced in Greenland ice-cores, are characterized by a rapid transition from cold (Greenland stadial – GS) to warm (Greenland interstadial – GI) atmospheric conditions (Dansgaard et al., 1993). The second ones, Heinrich events, were identified in marine sediments from the North Atlantic Ocean as ice-rafted debris (IRD)-rich layers deposited during some GS (thus called Heinrich stadials – HS; e.g. Heinrich, 1988; Bond et al., 1992; Sanchez Goni and Harisson, 2010). In the subpolar North Atlantic, both GS and HS are associated with IRD deposits, which are interpreted as the result of ice-sheet collapses and subsequent iceberg calving (e.g. Bond and Lotti, 1995; Elliot et al., 2001). They are also both associated with significant slowdown of the Atlantic Meridional Overturning Circulation (e.g. Kissel et al., 1999; Rahmstorf, 2002). These similarities led to the theory that both GS and HS were triggered by the same processes, and that those processes involve changes in the meridional overturning circulation, either as the cause (e.g. Alvarez-Solas et al., 2010; Alvarez-Solas and Ramstein, 2011) or the consequence (e.g. Manabe and Stouffer, 1995; Ganopolski and Rahmstorf, 2001; Levine and Bigg, 2008) of these cyclic ice-sheet instabilities. In both cases, model experiments simulate coherent changes in Greenland atmospheric temperatures. Additionally, in both cases again, sea ice and ice shelves, located at the interface between ocean and ice-sheets, are assumed to play a key role in the processes involved (e.g. Li et al., 2010). However, the role and/or response of these important cryospheric components of the climate system during the last glacial millennial climatic events have been poorly investigated in paleoceanographic studies. Consequently, processes implied and dynamical interactions between ocean, cryosphere and atmosphere remain unclear. Yet a better understanding of these phenomena is crucial given the recent evolution of the Antarctic ice-sheet under the present climate change, i.e. the catastrophic breakdown of some ice-shelves and surrounding sea ice, and the subsequent ice stream acceleration and iceberg discharge.

To complement our knowledge on this subject, high resolution paleoceanographic studies conducted in key areas are needed. Several studies of marine cores located close to the Faeroe-Scotland Ridge, at the frontier between the North Atlantic Ocean and the Nordic Seas, have shown the strong potential of this area to track this millennial climatic variability (see references herein and Sect. 2.2). Here, we present a previously unpublished multiproxy record

from core MD99-2285 located Northeast off Faeroe Islands, a region located close to the edge of European ice-sheets during the last glacial period. Time series of proxies for surface and subsurface hydrological properties (temperatures, salinities) were developed together with two independent proxies of sea-ice cover: IP25 and dinocyst assemblages. Analyses were performed at high temporal resolution, and focused on the 35-41 ka cal BP period, i.e. from GI 10 to GS 8, including HS4 and Heinrich layer 4. Such an approach allows us to identify the sequence of processes at play at GI-GS/HS4 and GS/HS4-GI transitions, and to assess ocean-cryosphere interactions occurring during these millennial climatic events.

2. Environmental settings and paleoclimatic interests

2.1. Environmental settings

Core MD99-2285 (62.69 °N; -3.57 °E) was retrieved during the IMAGES (International Marine Global Change study) V – MD99-114 (GINNA) cruise on the RV *Marion Dufresne* (Labeyrie et al., 1999). It is made of 46.92 meters of hemipelagic silty clays (Labeyrie et al., 1999). It was collected at 885 m water depth, on the slope of the northeastern margin of Faeroe Islands (see Fig. 1 and Table 1 for site location).

Throughout the Cenozoic, this slope has been shaped by contourite deposits formed through the action of the local bottom flow, as well as by down-slope mass transport of sediment (van Weering et al., 1998; Andersen et al., 2000; Laberg et al., 2005). Presently, the bottom current flowing along this slope transports cold ($T < 5.5$ °C; e.g. Mauritzen et al., 2005) intermediate and deep water masses formed within the Nordic Seas (usually grouped under the name of Iceland Scotland Overflow Water or ISOW; e.g. Borenäs and Lundberg, 2004) to the Atlantic Ocean through the Faeroe Shetland Channel (Kuijpers et al., 1998; Borenäs and Lundberg, 2004; Mauritzen et al., 2005; Fig. 1b and 1d). During the last glacial period, this bottom flow has been responsible for high sediment supply in this area and subsequent large sedimentation rates (Nielsen et al., 2007). Nonetheless, this strong sediment supply has also led to concomitant episodes of slope instability (van Weering et al., 1998; Kuijpers et al., 2001; Nielsen et al., 2007). However, on the basis of seismic and side-scan sonar data, van Weering et al. (1998) showed that our core site is located in the area where the

sediment supply has been less important, and above the erosional channel formed by this deep current (Fig. 1c). These data and others of the same type (Kuijpers et al., 2001) also reveal that our core site is located well above the area affected by gravity-driven mass transport (called the North Faeroe Slide Complex, located on Fig. 1c), and thus that our core did not suffer from such reworking processes.

Above ISOW masses, the study area is currently under the dual influence of two different surface water masses (Fig. 1a and 1d). The first one is the warm ($T > 8\text{ °C}$) and salty North Atlantic Water, entrained northward through the North Atlantic Current and the joining Continental Slope Current which flows along the upper slope of Northwest Europe (e.g. Kenyon, 1986; McCartney and Mauritzen, 2001; Orvik and Niiler, 2002; Mauritzen et al., 2005). The second one is the colder and fresher water mass made from the mixing between the North Atlantic Water and the cold polar waters ($T < 0\text{ °C}$ to 2 °C), transported from the Arctic to the southern Norwegian Sea through the southward East Greenland Current and its eastward extension called the East Icelandic Current (Valdimarsson and Malmberg, 1999).

In addition to its location at a nodal point of the (modern) oceanic circulation, the study area was also, during the last glacial period, surrounded by proximal ice-sheets, i.e. the Fennoscandian ice-sheet, the British-Irish ice-sheet, and the Faeroe ice cap. During this period, the Fennoscandian and British-Irish ice-sheets became largely wider (Svendsen et al., 2004; Fig. 1a), while the Faeroe ice cap probably experienced smaller advances, extending to a maximal limit located at present water depth of around 200 m (Nielsen et al., 2007). The study site is located at the outlet of major paleo-ice streams having drained the Fennoscandian and British-Irish ice-sheets (Sejrup et al., 2003; Bradwell et al., 2008; Fig. 1a), thus it is very likely that this site has been influenced by their ice discharges. Indeed, several seismic and side-scan sonar data denote the presence of iceberg scouring down to maximal water depth around 800 m (i.e. above the study site) in the study area (e.g. around 30 km southeast of the study site: profile ISTRA280 in Nielsen et al., 2007; around 60 km west of the study site: Nielsen and van Weering, 1998 and van Weering et al., 1998; around 190 km southwest of the study site: Nielsen and Kuijpers, 2000). Nielsen et al. (2007) interpreted some of these features as the result of intense iceberg ploughing during the last glacial period and/or last deglaciation, by icebergs mainly originating from distant areas and not from the Faeroe ice cap. Despite changes in morphobathymetry since the last glacial period due to isostatic adjustments (Peltier, 2004), these fingerprints indicate the potential influence of massive

icebergs originating from the European ice-sheets over the study area during the studied period.

2.2. Paleoclimatic interests

Given its past and modern regional settings, this area appears as a key sector to study the last glacial millennial climatic variability since it coupled climatic, oceanic and cryospheric dynamics, and offers high sedimentation rates (e.g. Rasmussen et al., 1996b; Kissel et al., 1999; Nielsen et al., 2007) thanks to bottom flow sediment supplies. Five very nearby cores have indeed been previously studied with this focus: MD95-2009, ENAM93-21, ENAM93-20, JM11-FI-19PC and LINK16 (see Table 1 and Fig. 1c for cores location). Each of these five cores have evidenced the high sensitivity of this area to the last glacial rapid climatic variability. During GI, they all evidenced a circulation scheme similar to the present one, characterized by active Atlantic inflow, deep convection in the Nordic Seas and active bottom circulation of overflow water (Rasmussen et al., 1996a,b, 1997, 1999; Dokken and Jansen, 1999; Kissel et al., 1999; Rasmussen and Thomsen, 2004, 2009; Ballini et al., 2006; Ezat et al., 2014). During GS, they recorded enhanced iceberg calving and associated meltwater input (Rasmussen et al., 1996a,b, 1997; Dokken and Jansen, 1999; Elliot et al., 2001; Eynaud et al., 2002; Rasmussen and Thomsen, 2009), as well as a strongly reduced deep convection in the Nordic Seas and thus weaker deep circulation of ISOW (Rasmussen et al., 1996a,b, 1997, 1999; Dokken and Jansen, 1999; Kissel et al., 1999; Ballini et al., 2006; Rasmussen and Thomsen, 2004, 2009; Ezat et al., 2014).

Furthermore, based on benthic foraminifera assemblages and/or oxygen isotopic content in cores ENAM93-21 and ENAM93-20, Rasmussen and Thomsen (2004) suggested that Nordic Seas experienced a strong stratification and a reverse flow pattern during GS with intrusion of relatively warm intermediate-depth Atlantic water below the cold and low saline surface water (see also Rasmussen et al., 1996a,b, 1997). This hypothesis is supported by equivalent analyses on cores located in the Nordic Seas and North Atlantic Ocean (Rasmussen et al., 2002; Rasmussen and Thomsen, 2004), and by coupled Mg/Ca and $\delta^{18}\text{O}$ measurements on benthic foraminifera shells in core JM11-FI-19PC (Ezat et al., 2014). However, the origin of this intermediate Atlantic water-mass, and its presence in itself in the Norwegian Sea during GS, are still controversial (e.g. Rasmussen et al., 1996a, 2002; Dokken and Jansen, 1999; Lassen et al., 2002; Rasmussen and Thomsen, 2004; Dokken et al., 2013).

In parallel, in core ENAM93-21 (Rasmussen et al., 1996a,b, 1997) and other nearby cores (e.g. Rasmussen et al., 2004; Dickson et al., 2008), cold sea-surface temperatures (SST) were identified during GS, and inversely warmer SST during GI. Such a pattern is coherent with iceberg releases during GS, with SST changes recorded in the subtropical North Atlantic Ocean (Sachs and Lehman, 1999), and with atmospheric temperature changes depicted in ice-cores (Dansgaard et al., 1993). However, it is worth noting that, within the study area, they were deduced from subsurface (or “near-surface”) proxies. Indeed, they are mainly based on assemblages and oxygen isotopes of planktonic foraminifera, which are known to migrate in a relatively large section of the upper water column during their life cycle, and whose symbiont-free taxa (such as the polar species *N. pachyderma* sinistral coiling) may live below the photic layer (e.g. Schiebel et al., 2001; Simstich et al., 2003) and even deeper in case of low-salinity intrusions. Regularly, the cold stadial SST have been associated with extensive sea-ice cover within the Nordic Seas (e.g. Rasmussen et al., 1999; Gildor and Tziperman, 2003; Rasmussen and Thomsen, 2004). Such a pattern has been supported by benthic and planktonic isotopic records conducted on nearby cores ENAM93-21 (Dokken and Jansen, 1999) and MD99-2284 (Dokken et al., 2013; cf. Fig1b). Indeed, on the basis of those analyses, both studies evidenced extensive sea ice formation and reduced convection through brine extrusion during GS, and conversely open-ocean convection during GI. However, in cores MD95-2009 and MD95-2010 (cf. Fig. 1a), Eynaud et al. (2002) evidenced an opposite pattern with warmer SST and shorter sea-ice cover duration during GS, and colder SST and longer sea-ice cover duration during GI. Their findings are based on more direct proxies of sea-surface conditions: dinoflagellate cyst assemblages as well as quantitative sea-surface hydrological reconstructions obtained via transfer functions applied to dinocyst assemblages. Indeed, as dinoflagellates (phytoplankton) are restricted to the photic layer, they are assumed to track sea-surface *sensu stricto* conditions.

Hence, despite numerous paleoceanographic studies conducted within the study area and focused on the last glacial millennial climatic variability, discrepancies and uncertainties still remain. Furthermore, processes linking the cryospheric and oceanic components are still not fully understood. In this context, our work intends to improve our knowledge on the evolution and interaction of three key components of the climate system during the last glacial millennial climatic events: surface ocean, subsurface ocean, and cryosphere.

3. Materials and methods

3.1. Stratigraphy

MD99-2285 age model used in the present study conforms to the previously published one from Wary et al. (JQS, submitted¹). Following many paleoceanographic studies conducted in the area (e.g. Rasmussen et al., 1996a,b; Kissel et al., 1999; Laj et al., 2000; Elliot et al., 2002; Ballini et al., 2006; Rasmussen and Thomsen, 2009), it is constrained by 8 AMS ¹⁴C dates (measured on planktonic foraminifera) combined to 19 additional tie-points obtained by correlating the magnetic susceptibility signal of the core to NGRIP $\delta^{18}\text{O}$ record (GICC05 time scale; Svensson et al., 2008; Wolff et al., 2010) i.e. the recommended regional stratotype (Austin and Hibbert, 2012; see Fig. 2a and 2b). The age model was finally established by linear interpolation between all age control points.

It is worth noting that some uncertainties remain around the GS 6 / HS3 period. Indeed, in the current age model, GI 5 (according to Dansgaard et al. (1993)'s numbering, i.e. the interstadial event from 32450 to 31950 a cal BP after Wolff et al. (2010)'s age limits) is "missing": there is no MS peak coincident with GI 5 NGRIP event (Fig. 2b). However, this does not have any impact on the present study which focuses on the 35-41 ka cal BP (i.e. 444-600 cm core depth) interval and compare data within the same archive.

Based on this age model, an average sedimentation rate of 18 cm.ka⁻¹ is estimated for the upper six meters of the core, and of 30 cm.ka⁻¹ for the studied period (Fig. 2c). Sampling step (every 1 to 2 cm for biomarker analyses, and every 1 to 10 cm for other proxies) has been increased on key portions, particularly at the transition from GI9 to HS4 where the temporal resolution is less than 100 years for all proxies.

3.2. Sea ice reconstructions, sea-surface temperature and salinity estimates

For the first time, sea ice reconstructions were obtained from two methods which have never been confronted to each other up to now: transfer function applied to dinocyst assemblages, and IP25 analyses. Quantitative sea-surface temperatures (SST) were also estimated from two proxies: the transfer function applied to dinocysts and alkenone analyses.

¹ cf. page 127 de ce manuscrit

Alkenones were quantified following the procedures of Ternois et al. (1997), and IP25 following Massé et al. (2008). Briefly, biomarkers were extracted from freeze-dried sediments, and isolated from the total lipid extract by open silicagel column chromatography. Alkenones were then analyzed using a Varian CX3400 gas chromatograph (GC) coupled to a flame detector, and IP25 were quantified using an Agilent 7890 GC coupled to an Agilent 5975 mass spectrometer. SST_{alk} were calculated from the $U^{K'}_{37}$ index ($C37:2/[C37:2+C37:3]$) using the calibration of Prahl et al. (1988) ($SST_{alk} = [U^{K'}_{37} - 0.039]/0.0034$). Today, in subpolar/polar regions, spring/summer is the main season of alkenone production (e.g. Sikes et al., 1997; Ternois et al., 2000; Sicre et al., 2002, 2014). IP25 concentrations, indicative of the presence of seasonal sea ice (Weckström et al., 2013), are expressed in ng/g of dry sediment.

Quaternary dinocysts, as well as reworked dinocysts and freshwater algae *Pediastrum* spp. and *Halodinium* spp., were counted in the 10-150 μ m fraction after palynological preparation of sediment samples (following the protocol of de Vernal et al., 1996, slightly modified at EPOC laboratory: http://www.epoc.u-bordeaux.fr/index.php?lang=fr&page=eq_paleo_pollens). Around 300 Quaternary dinocysts were counted in each sample using a Leica Microscope at x400 magnification. Species identification follows Rochon et al. (1999), Head et al. (2001), and Radi et al. (2013). Relative abundances of each species were calculated relative to the total sum of Quaternary dinocysts. Past sea-surface conditions were obtained by applying a transfer function to those dinocyst assemblages. The modern analogue technique (MAT, see Guiot and de Vernal, 2007, 2011a,b for a review of this technique) was applied and performed with the R software (R version 2.7.0; <http://www.r-project.org/>), using the ReconstMAT script developed by J. Guiot (BIOINDIC package, <https://www.eccorev.fr/spip.php?article389>). The modern dinocyst database used here includes 1207 sites from North Atlantic Ocean, Arctic and sub-Arctic basins, Mediterranean Sea and North Pacific Ocean (database available from the DINO9 workshop, <http://pcwww.liv.ac.uk/~dino9/workshops.htm>). These statistical treatments provide quantitative reconstructions for mean summer (July-August-September) and mean winter (January-February-March) SST_{dino} (with root mean square errors of prediction – RMSEP – of 1.5 °C and 1.05 °C respectively), mean summer and mean winter sea-surface salinity (SSS_{dino} ; respective RMSEP of 2.4 and 2.3 psu), as well as mean annual sea-ice cover

duration (SIC_{dino}; RMSEP of 1.2 month/year), which represents the duration when sea-ice cover has a concentration superior to 50 %.

Among the species identified, three of them carry precious information given the topic of this study: (i) *Islandinium minutum*, whose highest abundances are found in cold polar waters seasonally covered by sea ice (Radi et al., 2013), (ii) *Bitectatodinium tepikiense*, which presents a strong affinity for stratified surface waters associated with high seasonal contrasts (Rochon et al., 1999), (iii) *Operculodinium centrocarpum*, a cosmopolitan taxon characterized by a spatial distribution in the North Atlantic and adjacent seas tightly linked to the North Atlantic Drift and extension pathways (Harland, 1983; Rochon et al., 1999). Their relative abundances will be used as indicators of these respective features.

Absolute concentrations of reworked (i.e. pre-Quaternary) dinocysts, *Halodinium* spp. and coenobia of *Pediastrum* spp., were also calculated and expressed in individuals.cm⁻³ of dry sediment. These palynomorphs are all indicative of allochthonous supplies from continental/fluvial origin (e.g. Matthiessen et al., 2000; Zaragosi et al., 2001; Eynaud et al., 2007; Penaud et al., 2009).

3.3. Complementary tools

Planktonic foraminifera and ice-rafted debris (IRD) were counted in the > 150 µm fraction after classical preparation of sediment samples (washed through a 150 µm sieve before being dried). A minimum of 300 specimens (of planktonic foraminifera and IRD respectively) was counted in each sample. IRD concentration, indicative of iceberg calving over the study area, was determined and expressed in number.g⁻¹ of dry sediment. The absolute concentration of planktonic foraminifera, and the relative abundance of the mesopelagic polar taxon *Neogloboquadrina pachyderma* sinistral coiling (NPS) were also calculated. As foraminiferal assemblages are nearly monospecific throughout the studied interval (with relative abundance of NPS ranging from 94.3 to 99.4 %), we chose to use the absolute concentration of NPS as an indicator of more favorable hydrological conditions for the development of this taxon in the depth range it thrives. Presently, its depth habitat is located near or below the pycnocline, ranging between a few tens of meters to around 250 meters water depth depending on local hydrological conditions (e.g. Carstens et al., 1997; Simstich et al., 2003). Optimal ecological conditions of this taxon can be found in water

masses with temperatures < 5-6 °C and salinity > 34 psu (e.g. Tolderlund and Bé, 1971; Carstens et al., 1997; Hillaire-Marcel and de Vernal, 2008). In the Nordic Seas, the main season of NPS production occurs in summer (Kohfeld et al., 1996; von Gyldenfeldt et al., 2000).

Stable isotope measurements ($\delta^{18}\text{O}$) were performed on monospecific samples of NPS ($\delta^{18}\text{O}_{\text{NPS}}$). For each sample, 6 to 8 specimens were hand-picked from the 200-250 μm size fraction. Measurements were performed with an Optima Micromass mass spectrometer at EPOC laboratory. The mean external reproducibility of carbonate standard NBS19 was ± 0.05 ‰. Values are given versus Vienna Pee Dee Belemnite (VPDB) standard. In the subpolar North Atlantic and adjacent seas, changes in $\delta^{18}\text{O}_{\text{NPS}}$ have usually been related to variations of meltwater input through iceberg releases in the near-surface layer (e.g. Bond et al., 1992, 1993, Cortijo et al., 1997). However, $\delta^{18}\text{O}_{\text{NPS}}$ is known to be also a function of ambient local temperature, and of continental ice volume (e.g. Shackleton, 1974; Malaizé and Caley, 2009). Recent studies (e.g. Dokken and Jansen, 1999; Hillaire-Marcel and de Vernal, 2008) have shown that $\delta^{18}\text{O}_{\text{NPS}}$ could be also influenced by the production of isotopically light brines during sea ice formation, and the release of isotopically heavier and low salinity waters during sea ice melting. Hence, the interpretation of $\delta^{18}\text{O}_{\text{NPS}}$ is not trivial in the framework of our study, but our other reconstructions of hydrological conditions will be used to assess the main factors impacting on this signal.

Diversity and dominance ecological indices were calculated on dinocyst assemblages. Diversity is represented by the H index: $-\sum_{i=1}^s [(n_i/N) \times \ln(n_i/N)]$, where n_i is the number of specimens recorded for taxa i , s is the total number of taxa and N is the total number of individuals counted for each sample (Shannon and Weaver, 1949). Dominance corresponds to $(n' + n'') / N$ where n' is the number of individuals of the more abundant species, n'' is the number of individuals of the second more abundant species, and N is the total number of specimens counted for each sample (Goodman, 1979).

4. Results and discussion

4.1. Allochthonous vs autochthonous signals

Surface proxies used here are related to nano- and micro-phytoplanktonic organisms (dinoflagellates for dinocysts, coccoliths for alkenones, and diatoms for IP25) which are potentially sensitive to advection by surface currents as well as reworking by bottom currents. This raises the critical question whether signals reconstructed from these proxies reflect autochthonous or allochthonous surface conditions. Thankfully, our multiproxy dataset offers the possibility to circumvent this crucial issue.

Reconstructions from dinocysts (SST_{dino} and SIC_{dino}) and IP25 show consistent variations, with warmer summer SST_{dino} coincident with longer SIC_{dino} and higher IP25, and *vice-versa* (Fig. 3c and 3e). By comparison, SST_{alk} exhibits similar variations, but consequently precede dinocyst and IP25 ones, a feature that is peculiarly noticeable between 480 and 545 cm (Fig. 3c). These results tend to suggest that dinocyst-derived and IP25 signals could reflect autochthonous regional signals whereas SST_{alk} could result from allochthonous inputs. As a matter of fact, according to Londeix et al. (2007), the negative correlation between diversity and dominance indices (correlation coefficient of -0.97; Fig. 3a) indicates that dinocyst assemblages are not biased by reworking processes. At the opposite, the striking phasing between SST_{alk} and the concentration of reworked dinocysts (except around 460 cm, but the resolution of palynological analyses is quite lower on this portion of the core; Fig. 3c) strongly suggests that alkenones might have been advected up to the study site. This is also supported by the coeval and strong increases of SST_{alk} , reworked dinocysts and concentrations of *Halodinium* spp. and *Pediastrum* spp. around 545 cm (Fig. 3b and 3c), as well as the coeval high SST_{alk} and high concentrations of advected palynomorphs on the 530-545 cm and 462-480 cm intervals. Hence, we can reasonably consider here that dinocyst-derived reconstructions and IP25 abundances reflect autochthonous regional signals, while reworked dinocysts, *Halodinium* spp., *Pediastrum* spp., and at least on some intervals SST_{alk} , reflect allochthonous advection. However, determining the origin of this advection and the processes of transport is not trivial. Yet, it could provide precious information, particularly for the periods where SST_{alk} remarkably precede SST_{dinos} such as on the 530-545 cm interval, and thus deserves to be attempted.

Reworked dinocysts can be supplied to the ocean through iceberg or fluvial transport (including glacier meltwater plumes, e.g. Rahman, 1995; Eynaud et al., 2007). Identification of reworked specimens in some horizons of the core indicated a Paleogene age but did not reveal any specific continental source area. Nonetheless, the similar scheme exhibited by reworked dinocysts, *Halodinium* spp. and *Pediastrum* spp, notably on the 530-545 cm interval, strongly suggests a common source area and transport mechanism, at least during such episodes. Freshwater algae such as *Halodinium* spp. and *Pediastrum* spp. are known to be supplied to coastal areas through (glacio)fluvial transport (e.g. Mudie, 1992), such as reworked dinocysts are. They can later be transported to deep-sea sites (such as ours) through various processes of reworking of coastal sediments: (i) brines released during sea ice formation may trigger coastal sediment resuspension and subsequent transport (Matthiessen et al., 2000), (ii) resuspended sediments may be also incorporated in the newly formed sea ice through basal freezing, and transported to deeper areas by drifting and melting of this sea ice (e.g. Mudie, 1992; Matthiessen et al., 2000), (iii) the Continental Slope Current flowing along the upper slope of Northwest Europe may also trigger sediment resuspension on this upper slope and subsequent transport before joining the North Atlantic Current flowing over our study site (cf. Fig. 1a). The first two options seem possible since, during the 462-580 cm and 530-545 cm intervals, SIC_{dinos} and IP25 concentration indicate intensive sea ice formation over the study area and probably also in a wider area including coastal zones, but it does not explain the warm SST_{alk} provenance. On the opposite, the last option, implying the warm and salty subsurface Continental Slope Current, does. Indeed, even if the high saline core of this slope current can be roughly located around 200 m water depth (at present), the warmest temperatures are recorded above, in the photic layer (e.g. Booth and Ellett, 1983; Hill and Mitchelson-Jacob, 1993), i.e. where coccoliths thrive. The Continental Slope Current could have thus incorporated reworked dinocysts and green algae (delivered through glaciofluvial export from the British Isles), and harboured warm alkenone producers. Throughout its northward propagation, it would have got colder through release of latent heat, and less saline through mixing with ambient waters; it would have kept on transporting reworked dinocysts, green algae, and no longer “warm coccoliths” but fossil “warm alkenones”, up to the study site. Similar interpretations have indeed already been used in the Southern Indian Ocean by Sicre et al. (2005) and at the Southeastern Greenland margin by Knutz et al. (2011). Indeed, both studies associated warmer than expected SST_{alk} with strong advection by the local warm

surface current (Agulhas Current and Irminger Current respectively) of alkenones produced in warmer upstream waters.

Hence, warmer SST_{alk} than summer SST_{dinos}, associated with high concentrations of reworked dinocyst and freshwater algae, could be assumed to track surface and/or subsurface advection of waters from Atlantic origin. In such a case, the fact that the increase in the relative abundance of *O. centrocarpum* (a dinocyst taxa strongly associated with the North Atlantic Drift pathways; Harland, 1983; Rochon et al., 1999) lags the increase of SST_{alk} (Fig. 3d) supports the idea of an *in situ* dinocyst production.

4.2. General surface and subsurface *in situ* oceanic conditions during stadials and interstadials

Fig. 4 shows the reconstructions of hydrological parameters and relative abundances of index dinocyst species. It reveals a general stadial/interstadial scheme somewhat surprising, with cold surface waters, extensive sea ice formation and longer duration during most part of GI and at the very beginning of GS, and inversely, warm SST and reduced sea-ice cover during most part of GS and at the very beginning of GI (Fig. 4b and 4c). However, this paradoxical scheme seems to be coherent in the Norwegian Sea, at least along the Atlantic inflow pathways, since Eynaud et al. (2002) evidenced a similar pattern in two other Norwegian Sea cores (MD95-2009 and MD95-2010; cf. Fig 1a) on the basis of dinocyst assemblages and derived hydrological reconstructions. Moreover, recent freshwater hosing experiments (Kleinen et al., 2009; Swingedouw et al., 2013) suggested that high latitude freshwater release might be accompanied by enhanced advection of warm and saline Atlantic-sourced waters up to the Nordic Seas, in addition to a decrease in the strength of the Atlantic meridional overturning circulation. In these model simulations, these advected warm waters propagate in subsurface in the North Atlantic and re-emerge in surface of the Nordic Seas where they consequently warm up surface waters. The present study thus brings new records which support such a paradoxical scheme during the last glacial millennial climatic events. In particular, the IP25 record indicates that the sea ice pattern previously and presently evidenced through dinocyst analyses in Norwegian Sea cores is not an artifact linked to the dinocyst proxy but seems to be a real feature.

The other analyses conducted in the present work complement our view of this hydrological scheme. SSS_{dino} are rather low throughout the studied period, averaging 31.3 psu in summer and 32.8 psu in winter (Fig. 4d). They are largely lower than modern values in the study area (~ 35.2 psu for both seasons; WOA09 data, Antonov et al., 2010), and therefore typify the presence of more brackish surface waters. Furthermore, most part of GI is characterized by a large difference between summer and winter SSS_{dino} (noticeable within GI9 and GI8 except for one point around 37.2 ka cal BP, but, as previously mentioned, the resolution of palynological analyses is quite lower on this portion of the core). This large seasonal difference of SSS_{dino} must be linked to the strong sea-ice cover characterizing these periods, with high winter SSS_{dino} owing to intense brine release through sea ice formation, and low summer SSS_{dino} reflecting sea ice melting. By comparison, both winter and summer SSS_{dino} are relatively high during the first part of GS, and then decrease during the second part. However, according to NPS ecological tolerances, SSS_{dino} are too low for the development of this taxon at this time. This is particularly true for summer reconstructions, i.e. during the main growing period of NPS in the Nordic Seas (Kohfeld et al., 1996; von Gyldenfeldt et al., 2000), when SSS_{dino} are ≤ 32.4 psu. Nonetheless, NPS concentration attains maximal values within GS (Fig. 4g), thus indicating the presence of relatively cold and salty subsurface waters. This antagonism suggests the occurrence of a strong stratification of the upper water column during most part of GS, with a halocline separating the very warm and low saline surface layer from the colder and saltier subsurface water mass. This hypothesis is supported by the higher relative abundances of the dinocyst taxon *B. tepikiense* (which has a strong affinity for stratified surface waters; Fig. 4g), and the strong seasonality contrast of surface temperatures recorded at this time. Indeed, during most part of GS, summer SST_{dino} are well above modern summer value (10.7 °C according to WOA09 data; Locarnini et al., 2010), while winter SST_{dino} remain below winter modern one (6.5 °C) throughout the studied period. At the opposite, NPS concentration is very low during GI and the onset of GS, when seasonal sea-ice cover is maximal. However, the presence of sea ice cannot explain such low concentrations. Indeed, Carstens et al. (1997) showed that planktonic foraminifera absolute abundances are very low in areas covered with sea ice in summer, but maximal at the sea ice margin and in the ice-free zone. SIC_{dino} duration is around 8 months/year at this time, implying the occurrence of ice-free conditions during summer months that should have been favorable to NPS development. Hence, these low concentrations might be related to a reduced

upper stratification allowing the downward propagation of the low saline surface waters, unfavorable to NPS blooming.

IRD concentration is maximal within GS, when minimal sea-ice cover conditions are recorded (Fig. 4e and 4b). This indicates intense iceberg calving that could have prevented sea ice formation. At this time, SSS_{dino} decrease, probably reflecting iceberg melting, and $\delta^{18}\text{O}_{\text{NPS}}$ is relatively low and/or decreasing (Fig. 4f). As mentioned in Sect. 3.3, most of previous studies have interpreted such low $\delta^{18}\text{O}_{\text{NPS}}$ values during GS and HS as low subsurface salinities due to iceberg melting, and/or as intense brine release due to sea-ice formation (e.g. Cortijo et al., 1997; Dokken and Jansen, 1999). However, due to the presence of a strong halocline preventing vertical water mass exchanges at this time, such a $\delta^{18}\text{O}_{\text{NPS}}$ signature cannot be explained neither by iceberg melting nor by *in situ* brine release. Moreover, the strongly reduced (and even non-existent sometimes) sea-ice cover recorded over the study area at that time suggests very few *in situ* brine production. Nonetheless, hypothetical occasional sea ice formation occurring above continental shelves unaffected by iceberg calving could partly contribute to the $\delta^{18}\text{O}_{\text{NPS}}$ signal. This would be possible if several specific features were encountered at that time: (i) the water column above those shelves must not have been stratified, (ii) after their release over the shelves, the brines produced must have propagated in the subsurface layer inhabited by NPS, and (iii) since the main season of NPS production occurs in summer and brine formation in winter, those brines must not have sunk to deep water depth but remained trapped in the subsurface layer. But, even if all of those features and processes did occur at that time, it seems very unlikely that this mechanism could explain the total decrease in the $\delta^{18}\text{O}_{\text{NPS}}$ signal (which can be up to 1.05 ‰ at GI9-HS4 transition). In parallel, the global sea-level increase recorded during those periods of ice-sheet destabilization (~ 20-30 m according to Siddall et al., 2008) can only account for a $\delta^{18}\text{O}_{\text{NPS}}$ diminution of ~ 0.2 to 0.3 ‰ (Fairbanks, 1989). The last factor able to explain the remaining part of this signal is an increase of subsurface temperatures. However, this subsurface warming probably had a relatively small amplitude since the high NPS concentration implies subsurface temperatures not exceeding 5-6 °C. This amplitude can be estimated < 3.2 °C if we assume no salinity changes, no brine influence, and a sea-level level contribution of 0.25 ‰, but was actually probably a little higher due to a necessary increase of salinity in the subsurface layer for NPS development (Epstein and Mayeda, 1954; Shackleton, 1974). Hence, the $\delta^{18}\text{O}_{\text{NPS}}$ decrease at GI-GS transition probably results from the combination of the global sea-level rise and a moderate increase of subsurface temperatures, with a very hypothetical

contribution of *ex situ* brine production. At the opposite, the heavy isotopic signature recorded during GI may be explained by summer sea ice melting over a non-stratified upper water column.

4.3. Precise timing and interactions of hydrological processes during the millennial climatic events

As described in the previous part, in core MD99-2285, mean GS (including HS4) conditions are characterized by a warm (strong signal during summer) and low saline surface layer with iceberg calving and reduced sea ice formation, separated by a strong halocline from a colder (but relatively warm) and more saline subsurface layer. Mean GI / very beginning of GS conditions are marked by a homogeneous and cold upper water column, with winter sea ice formation and summer sea ice melting preventing NPS development in subsurface. In addition, reworked palynomorphs and SST_{alk} suggest enhanced advection of Atlantic-sourced waters at GI-GS transitions, some hundred years before the strong warming of surface waters evidenced from dinocyst-derived data (Fig. 5e and 5g). The temporal resolution of analyses conducted in the present work offers the possibility to identify the sequencing of the processes occurring during these transitions and leading to the extreme conditions occurring at the heart of GS, and those allowing the termination of those drastic conditions towards mean GI conditions (cf. Fig. 5 and 6).

Starting from GI, the first phase (phase 1 on Fig. 5 and 6) corresponds to the scheme described for mean GI conditions: the study area is overlaid by a homogeneous and cold upper water column seasonally ice-covered (Fig. 5c and 5e). The amount and duration of sea-ice cover is relatively high and seem to increase more or less progressively throughout this interval (maybe depending on GI duration since the progressive trend is observable for GI8 but not for the short GI9). Sterols are often present during this phase, indicating open-ocean surface conditions during sea ice free months (Fig. 5b). The few NPS thriving in subsurface record summer sea ice melting (heavy $\delta^{18}\text{O}_{\text{NPS}}$) unfavorable to a strong development of this taxon (Fig. 5h and 5i). During winter, sea ice formation produces brines (cf. the high winter SSS_{dino} on Fig. 4d) which probably propagate at deeper depth and contribute to the formation of deep water masses in the Nordic Seas and *in fine* of the North Atlantic Deep Water. IRD concentration is very low, indicating very sparse iceberg calving over the study area (Fig. 5d).

Phase 2 starts around mid-GI, and marks the sharp beginning of Atlantic-sourced waters advection (Fig. 5g). Phase 2 is also characterized by a progressive increase in IRD concentration which denotes a progressive intensification of iceberg calving over the study area throughout this period. However, during the first part of this phase (phase 2a), hydrological conditions are almost the same than during phase 1. Indeed, the strong advection of initially warm and saline waters seems to not have any impact neither on salinity (Fig. 5f) nor temperatures, neither in surface nor in subsurface. For both parameters (temperature and salinity), this can be explained by the strong dilution of this advected water mass within the large volume of ambient waters, whatever the depth of the advected water mass (surface and/or subsurface). In parallel, if this water mass was in contact with the atmosphere, diffusion of heat at this interface could have consequently lowered its temperature. In such a case, latent heat emission could have occurred throughout the year (and probably mostly during winter) in the Atlantic sector, but only during summer (when sea ice is absent) in the Norwegian Sea. Indeed, sea ice formation is still intense during this phase and sea-ice cover duration relatively long (around 7 to 8 months/year). Relatively reduced iceberg calving occurs during summer months when sea ice is absent, but surface conditions are relatively close to an open-ocean situation since biomarker analyses reveal the presence of sterols.

The second part of this phase (phase 2b) marks the beginning of the impact of the warm and salty Atlantic-sourced advection on local hydrography. Indeed, while sea ice is still strongly present over the study area and sea ice melting still occurs during ~ 4 months/year, summer SSS_{dino} sharply increases of ~ 2 psu at the very beginning of phase 2b. This strong increase reflects the beginning of the dominance of advected saline waters over ambient surface waters, and attests that these advected water masses are present in surface at the study site. Besides, the absence of coeval effect on SST_{dino} (even during ice free summer months) suggests that these Atlantic-sourced waters are, at least from some upstream point, advected in contact with the atmosphere, with strong diffusion and loss of latent heat to the atmosphere still occurring during this phase. The upper stratification seems to be still reduced, and the absence of clear signature in $\delta^{18}O_{NPS}$ (or slight decrease) might suggest that the advected water mass is partly extending down to the subsurface layer since such a signal could result from the (almost) compensated effects of warming and salinity increase. However, despite such a salinity increase, subsurface salinities are still too low for the development of NPS. In parallel, coupled increase of IRD concentration and absence of sterols indicate more intense

iceberg calving during the ice-free summer months, associated with surface conditions which are no longer of open-ocean type but rather more chaotic.

During phase 2c, SST_{dino} and the relative percentage of *O. centrocarpum* (cf. Fig. 4c) start to increase while SSS_{dino} are still relatively high. This indicates that heat advected through Atlantic-sourced waters is no longer entirely released to the atmosphere, but that a part stays in the ocean. In parallel, both the duration of the sea ice free season (SIC_{dino}) and the rate of iceberg calving and melting (IRD concentration) moderately increase. During these months, surface conditions are still rather chaotic (sterols). Upper stratification is still reduced but seems to start to gently increase (NPS concentration and relative percentage of *B. tepikiense*). $\delta^{18}\text{O}_{\text{NPS}}$ keeps on decreasing, very probably as the result of moderate subsurface warming.

Phase 3 is characterized by the extreme GS conditions. SST_{dino} sharply increase at the beginning of this phase and attain values around 15 °C in summer and 2 °C in winter. Synchronously, IRD concentration sharply increases and attain maximal values while sea-ice cover formation and duration strongly decrease to become nil or strongly reduced. This points to intense iceberg calving over the study area strongly hampering or even preventing sea ice development. Besides, the absence of sterol denotes chaotic surface conditions at this time. In parallel, SST_{alk} and concentration of reworked dinocysts are high whereas concentrations of freshwater algae are now strongly reduced or even nil. This cannot be explained by a stop of Atlantic water advection as SST_{dino} and the relative percentage of *O. centrocarpum* are maximal and thus denote a maximum in this inflow at that time. However, this could result from changes in the source of production of these freshwater algae, but we cannot here be more precise about the nature of these changes. Hence, during this phase of maximal Atlantic inflow, the strong seasonal disparity in SST_{dino} (cf. Fig 4c) might reflect intense latent heat release during winter months, which are now (almost) sea ice free. SSS_{dino} decrease throughout this phase, probably as the result of iceberg melting. However, maximal NPS concentration and *B. tepikiense* relative abundance indicate the presence of a strong halocline separating the very warm and low saline surface layer from the subsurface layer characterized by favorable conditions for NPS blooming (i.e. temperature < 5-6 °C and salinity > 34). Hence, during summer, a strong thermocline must have also been present. $\delta^{18}\text{O}_{\text{NPS}}$ attains its minimal value, which due to the upper stratification cannot reflect iceberg melting but rather a combination of global sea-level rise and moderate subsurface warming. This moderate

subsurface warming might be directly related to Atlantic water advection, or, given the upper stratification at the study site, be rather indirectly related to the insulation of the subsurface layer by the North Atlantic meltwater lid evidenced in Kleinen et al. (2009) and Swingedouw et al. (2013), and as suggested by other previous modelling experiments (e.g. Shaffer et al., 2004).

Phase 4 marks the transition from extreme GS conditions (phase 3) to milder GI conditions (phase 1). Throughout this phase, several parameters exhibit a more or less progressive decrease (SSS_{dino}, SST_{alk} and concentration of reworked dinocysts, winter SST_{dino} and relative percentage of *O. centrocarpum* – cf. Fig. 4 –, and NPS concentration) or increase (relative percentage of *I. minutum* indicative of colder surface conditions – cf. Fig. 4 –, as well as $\delta^{18}\text{O}_{\text{NPS}}$). These signals might sign the decrease of the Atlantic inflow. However, the still high summer SST_{dino} is enigmatic. This feature is noticeable during the whole phase 4 of HS4, as well as on the studied section of phase 4 of GS8 but with only one point of measurement indicative of relatively high but decreasing summer SST_{dino}. Hence, the realization of similar analyses with similar resolution on other GS and/or HS periods would be useful to determine if this is a generic feature or not, and potentially to assess the processes behind. In addition, sea-level fall might also slightly contribute to the $\delta^{18}\text{O}_{\text{NPS}}$ signal. Indeed, IRD concentration is very low during this phase, which denotes very little iceberg calving over the study area and probable re-growth of proximal ice-sheets. IP25 abundances and SIC_{dino} indicate the relatively weak reappearance of sea ice, and the presence of sterols denotes the return to open-ocean surface conditions during sea ice free episodes. In parallel, upper stratification is still present but decreasing. Ultimately, this phase 4 leads to the milder GI conditions recorded during phase 1.

4.4. Integrated regional view and implications

Some of the hydrological parameters used in the present study to evidence such a sequencing of processes were previously analyzed (often at lower temporal resolutions) in four other Norwegian Sea cores located along the Atlantic inflow pathways (MD95-2009, ENAM93-21, LINK16 and MD95-2010; see Table 2 and references herein, and Fig. 1 and Table 1 for the location of the sites). In those cores, these proxies (dinocyst-derived data, IRD concentration, $\delta^{18}\text{O}_{\text{NPS}}$, and equivalent to NPS concentration) exhibit very similar general trends to the ones evidenced in core MD99-2285. Thus, according to our interpretation which

relies on the combination / reconciliation of the message brought by these proxies, those records also indicate (i) GS/HS characterized by a seasonally warm surface layer with iceberg calving and reduced sea ice formation, separated by a strong halocline from a colder saline subsurface layer favorable to NPS development, and (ii) GI marked by a cold and more homogeneous upper water column, with winter sea ice formation and summer sea ice melting preventing NPS development. Hence, all of these records denotes reproducible mean GI and GS/HS conditions over the whole last glacial period and in the whole Norwegian Sea area presently influenced by the Atlantic inflow.

Furthermore, other analyses conducted on these Norwegian Sea cores and others also support the occurrence of ocean warming at subsurface and intermediate depth along the Atlantic inflow pathways during GS/HS. First, on the basis of a transfer function applied to planktonic foraminifera assemblages, [Dokken et al. \(2013\)](#) evidenced a moderate subsurface warming throughout stadial intervals in core MD99-2284 (cf. [Fig. 1](#)). Their reconstructed subsurface temperatures rarely exceed 5-6 °C, getting higher generally only at the end of GS. Nonetheless, core MD99-2284 is located in the Faeroe Shetland Channel directly below the main northward pathway of the Atlantic water inflow. This site could have thus experienced slightly warmer subsurface temperatures than sites located further away from Atlantic water pathways. Indeed, contrary to site MD99-2284, those latter sites exhibit nearly monospecific planktonic foraminifera assemblages during GS/HS (see e.g. [Rasmussen et al., 1996b, 1997, 1999](#); [Eynaud et al., 2002](#); [Rasmussen and Thomsen, 2009](#)). Secondly, in the same core MD99-2284 and in cores ENAM93-21 and MD95-2010, [Dokken and Jansen \(1999\)](#) and [Dokken et al. \(2013\)](#) interpreted coeval oxygen isotopic depletion in tests of planktonic and benthic foraminifera at GS-GI transition as the result of brine rejection. However, as suggested from our data, sea-ice cover was apparently decreasing down to minimal value, and upper stratification increasing up to maximal value all over this region (including site MD95-2010) at this time, which does not support the brine rejection hypothesis. Moreover, other analyses conducted in some of these cores and others (all located at intermediate water depth, i.e. between ~ 850 m and 1760 m water depth) favor the alternative explanation of intermediate depth warming. Indeed, on the basis of Mg/Ca measurements on benthic foraminifera tests in core MD95-2010, [Marcott et al. \(2011\)](#) evidenced that the benthic $\delta^{18}\text{O}$ decrease recorded during HS1 at this site could be explained by a ~ 6 °C warming. Similarly, [Ezat et al. \(2014\)](#) showed a Mg/Ca-derived 2-5 °C bottom warming synchronous to light

benthic $\delta^{18}\text{O}$ excursions during GS/HS in core JM11-FI-19PC. Furthermore, [Rasmussen and Thomsen \(2004\)](#) and [Ezat et al. \(2014\)](#) reported the presence of warm Atlantic benthic foraminifera species during GS and/or HS intervals in cores NA81-10, NA81-04, ENAM93-21, MD95-2009, ENAM93-20 and JM11-FI-19PC (see also [Rasmussen et al., 1996a,b, 1999](#); see [Fig. 1](#) and [Table 1](#) for the location of these cores). The authors interpreted the presence of this “Atlantic species group” as the result of the intrusion of relatively warm intermediate waters. Hence, it seems that (i) the whole area located along the Atlantic inflow pathways experienced intermediate depth warming during GS, and (ii) the light benthic $\delta^{18}\text{O}$ excursions recorded during GS and HS in this area are related to this warming. Therefore, the similarity of planktonic and benthic $\delta^{18}\text{O}$ signals during the millennial climatic events of the last glacial period, coupled to the evidence of a strong upper stratification during GS/HS, both in the whole region along the Atlantic inflow pathways, support our interpretation of $\delta^{18}\text{O}_{\text{NPS}}$ and support [Dokken et al. \(2013\)](#)'s finding of moderate subsurface warming during GS/HS.

Therefore, all these data and cores support the occurrence of ocean warming in the whole water column of the discussed region during GS, marked by high summer temperatures in surface (up to 17°C; dinocyst-derived data; this study; [Eynaud et al., 2002](#)), temperatures generally $\leq 5\text{-}6$ °C in subsurface (planktonic foraminifera-derived data; this study; [Dokken et al., 2013](#)), and probably also $\leq 5\text{-}6$ °C at intermediate depth (according to Mg/Ca-derived bottom water temperatures from [Ezat et al., 2014](#)).

In parallel, the sequencing of processes leading to extreme GS conditions (phase 3), as evidenced in the present studied core, denotes a strong coupling between IRD concentration and surface advection of warm waters, as well as with the directly related, or not, subsurface (and probably also intermediate-depth) moderate warming. Indeed, IRD concentration starts to increase when advection of Atlantic water begins (phase 2a), then progressively increases throughout phase 2, and finally sharply increases when SST_{dino} also sharply increase and $\delta^{18}\text{O}_{\text{NPS}}$ keeps on decreasing or is minimal (beginning of phase 3). Such a coupling has up to now never been evidenced in paleoreconstructions but is observed along Greenland main glacier outlets (e.g. [Hanna et al. 2009](#)). Furthermore, the apparent reproducibility (during the whole last glacial period, and in the whole area presently influenced by the Atlantic inflow and located close to the edge of European ice-sheets) of mean GS/HS and GI conditions, and of water column warming during GS/HS, suggests that a similar sequencing of processes might have also occurred in this whole zone and during this whole period. In such a case, this

would suggest a strong coupling between the Atlantic inflow and European ice-sheet destabilization, and thus supports [Alvarez-Solas et al. \(2010\)](#)'s mechanism as the trigger of ice-sheet collapses. Indeed, such a surface and subsurface warming along the European ice-sheet edges could have induced sea ice and ice-shelf basal- and edge-melting, the subsequent collapse of those buttress areas, and finally iceberg release resulting from enhanced ice stream. Besides, a similar scenario have already been suggested for the Laurentide ice-sheet collapses, based on benthic Mg/Ca measurements and model simulations revealing a basin-wide subsurface warming prior to Heinrich layer deposition ([Marcott et al., 2011](#); [Alvarez-Solas and Ramstein, 2011](#)). Nonetheless, additional high resolution and multiproxy studies of other Norwegian Sea cores would be required to confirm such a feature in the Nordic Sea basin.

Furthermore, similarly to our findings, [Guillevic et al. \(2014\)](#) also evidenced a three-phase sequence during HS4 in Greenland ice cores. Surprisingly, the phase of HS4 when extreme GS conditions are recorded in our core (phase 3), i.e. when SST_{dino} and iceberg calving are peaking, is almost coeval with Guillevic et al.'s HS4 phase marked by a sharp change in Greenland moisture source area. Peculiarly, despite respective uncertainties of both age models, the distinct onset of changes in Greenland ice core are apparently concomitant with the sharp increase of SST and of seasonal SST difference (i.e. latent heat emission) recorded in our marine core. Guillevic et al. related this change as resulting from low-latitude change potentially induced by a southward shift of the Intertropical Convergence Zone. However, the striking apparent synchronicity between Greenland records and our SST_{dino} signal (and particularly the sharp onset of both records) suggests that the Norwegian Sea may have also played a key role in this infra-millennial variability.

5. Conclusion

The present study focuses on a previously unpublished core (MD99-2285), ideally located to track hydrological processes occurring during the last glacial millennial climatic events. It combines multiproxy analyses on the 35-41 ka cal BP section, i.e. spanning GI 10 to GS 8 including Heinrich event 4. Records derived from those analyses evidence a paradoxical hydrological scheme during the millennial climatic events. Indeed, GI are marked by an

homogeneous and cold upper water column, with intensive winter sea ice formation and summer sea ice melting. At the opposite, GS and HS4 are characterized by a warm and low saline surface layer with iceberg calving and reduced sea ice formation, separated from the subsurface layer by a strong halocline and seasonal thermocline. This subsurface layer is colder and more saline than the overlying surface layer, but experienced warmer temperatures than during GI. According to paleorecords obtained from other cores, this atypical scheme seems to have occurred all along the Atlantic inflow pathways in the Norwegian Sea and during the millennial climatic events of the whole last glacial period.

In parallel, our work also suggests warm Atlantic water advection starting before GS/HS inception and thus before the deposition of IRD-rich layers. For the first time, the high temporal resolution of our analyses allows us to identify the sequencing of processes leading to the extreme conditions occurring at the heart of GS, and those allowing the exit from those drastic conditions towards mean GI conditions. The most striking feature identified corresponds to a significant coupling between warm Atlantic water advection and iceberg calving. Given that surface and subsurface warming seems to have occurred during GS/HS all along the Atlantic inflow pathways close to the edge of European ice-sheets, such a coupling might be representative of this whole area. In such a case, this would strongly support [Alvarez-Solas et al. \(2010\)](#)'s mechanism as the trigger of ice-sheet collapses, where a subsurface warming is responsible for the destabilization of ice-shelves and subsequent collapses of the associated ice-sheet. However, additional high resolution and multiproxy studies of other cores would be required to (i) confirm such a feature at the scale of the whole Nordic Sea basin, (ii) precise its spatial pattern in the Atlantic sector and at the frontier between the Northeast Atlantic and Nordic Seas, and (iii) assess the relation between advection of warm waters and subsurface warming.

References

- Alvarez-Solas, J., Charbit, S., Ritz, C., Paillard, D., Ramstein, G., Dumas, C., 2010. Links between ocean temperature and iceberg discharge during Heinrich events. *Nature Geoscience* 3, 122-126.
- Alvarez-Solas, J., Ramstein, G., 2011. On the triggering mechanism of Heinrich events. *Proceedings of the National Academy of Sciences* 108, E1359-E1360.
- Andersen, M.S., Nielsen, T., Sørensen, A.B., Boldreel, L.O., Kuijpers, A., 2000. Cenozoic sediment distribution and tectonic movements in the Faroe region. *Global and Planetary Change* 24, 239-259.
- Antonov, J.I., Seidov, D., Boyer, T.P., Locarnini, R.A., Mishonov, A.V., Garcia, H.E., Baranova, O.K., Zweng, M.M., Johnson, D.R., 2010. *World Ocean Atlas 2009, Volume 2: Salinity*, Ed. NOAA Atlas NESDIS 69, U.S. Government Printing Office, Washington, D.C. ed.
- Austin, W.E.N., Hibbert, F.D., 2012. Tracing time in the ocean: A brief review of chronological constraints (60-8 kyr) on North Atlantic marine event-based stratigraphies. *Quaternary Science Reviews* 36, 28-37.
- Ballini, M., Kissel, C., Colin, C., Richter, T., 2006. Deep-water mass source and dynamic associated with rapid climatic variations during the last glacial stage in the North Atlantic: a multi-proxy investigation of the detrital fraction of deep-sea sediments. *Geochem. Geophys. Geosystems* 7.
- Bond, G., Broecker, W., Johnsen, S., McManus, J., Labeyrie, L., Jouzel, J., Bonani, G., 1993. Correlations between climate records from North Atlantic sediments and Greenland ice. *Nature* 365, 143-147.
- Bond, G., Heinrich, H., Broecker, W., Labeyrie, L., McManus, J., Andrews, J., Huon, S., Jantschik, R., Glasen, S., Simet, C., Tedesco, K., Klas, M., Bonanitt, G., Ivy, S., 1992. Evidence for massive discharges of icebergs into the North Atlantic ocean during the last glacial period. *Nature* 360, 245-XIII.
- Bond, G.C., Lotti, R., 1995. Iceberg discharges into the North Atlantic on millennial time scales during the last glaciation. *Science* 267, 1005-1010.
- Booth, D.A., Ellett, D.J., 1983. The Scottish continental slope current. *Continental Shelf Research* 2, 127-146.
- Borenäs, K., Lundberg, P., 2004. The Faroe-Bank Channel deep-water overflow. *Deep-Sea Research Part II: Topical Studies in Oceanography* 51, 335-350.
- Bradwell, T., Stoker, M.S., Gollledge, N.R., Wilson, C.K., Merritt, J.W., Long, D., Everest, J.D., Hestvik, O.B., Stevenson, A.G., Hubbard, A.L., Finlayson, A.G., Mathers, H.E., 2008. The northern sector of the last British Ice Sheet: Maximum extent and demise. *Earth-Science Reviews* 88, 207-226.
- Carstens, J., Hebbeln, D., Wefer, G., 1997. Distribution of planktic foraminifera at the ice margin in the Arctic (Fram Strait). *Marine Micropaleontology* 29, 257-269.
- Cortijo, E., Labeyrie, L., Vidal, L., Vautravers, M., Chapman, M., Duplessy, J.C., Elliot, M., Arnold, M., Turon, J.L., Auffret, G., 1997. Changes in sea surface hydrology associated with Heinrich event 4 in the North Atlantic Ocean between 40° and 60°N. *Earth and Planetary Science Letters* 146, 29-45.
- Dansgaard, W., Johnsen, S.J., Clausen, H.B., Dahl-Jensen, D., Gundestrup, N.S., Hammer, C.U., Hvidberg, C.S., Steffensen, J.P., Sveinbjörnsdóttir, A.E., Jouzel, J., Bond, G., 1993. Evidence for general instability of past climate from a 250-kyr ice-core record. *Nature* 364, 218-220.
- de Vernal, A., Henry, M., Bilodeau, G., 1996. Techniques de préparation et d'analyse en micropaléontologie. *Les cahiers du GEOTOP* 3, 1-29.
- Dickson, A.J., Austin, W.E.N., Hall, I.R., Maslin, M.A., Kucera, M., 2008. Centennial-scale evolution of Dansgaard-Oeschger events in the northeast Atlantic Ocean between 39.5 and 56.5 ka B.P. *Paleoceanography* 23.
- Dokken, T.M., Jansen, E., 1999. Rapid changes in the mechanism of ocean convection during the last glacial period. *Nature* 401, 458-461.
- Dokken, T.M., Nisancioglu, K.H., Li, C., Battisti, D.S., Kissel, C., 2013. Dansgaard-Oeschger cycles: Interactions between ocean and sea ice intrinsic to the Nordic seas. *Paleoceanography* 28, 491-502.
- Elliot, M., Labeyrie, L., Dokken, T., Manthe, S., 2001. Coherent patterns of ice-rafted debris deposits in the Nordic regions during the last glacial (10-60 ka). *Earth and Planetary Science Letters* 194, 151-163.
- Elliot, M., Labeyrie, L., Duplessy, J.C., 2002. Changes in North Atlantic deep-water formation associated with the Dansgaard-Oeschger temperature oscillations (60-10 ka). *Quaternary Science Reviews* 21, 1153-1165.
- Epstein, S., Mayeda, T., 1953. Variation of O18 content of waters from natural sources. *Geochimica et Cosmochimica Acta* 4, 213-224.
- Eynaud, F., Turon, J.L., Matthiessen, J., Kissel, C., Peypouquet, J.P., De Vernal, A., Henry, M., 2002. Norwegian sea-surface palaeoenvironments of marine oxygen-isotope stage 3: The paradoxical response of dinoflagellate cysts. *Journal of Quaternary Science* 17, 349-359.
- Eynaud, F., Zaragosi, S., Scourse, J.D., Mojtahid, M., Bourillet, J.F., Hall, I.R., Penaud, A., Locascio, M., Reijonen, A., 2007. Deglacial laminated facies on the NW European continental margin: The hydrographic significance of British-Irish Ice Sheet deglaciation and Fleuve Manche paleoriver discharges. *Geochemistry, Geophysics, Geosystems* 8.
- Ezat, M.M., Rasmussen, T.L., Groeneveld, J., 2014. Persistent intermediate water warming during cold stadials in the southeastern Nordic seas during the past 65 k.y. *Geology* 42, 663-666.
- Fairbanks, R.G., 1989. A 17,000-year glacio-eustatic sea level record: Influence of glacial melting rates on the Younger Dryas event and deep-ocean circulation. *Nature* 342, 637-642.
- Ganopolski, A., Rahmstorf, S., 2001. Rapid changes of glacial climate simulated in a coupled climate model. *Nature* 409, 153-158.
- Gildor, H., Tziperman, E., Nienow, P.W., Shepherd, J.G., Alley, R.B., Lawton, J.H., Mahadevan, A., Lenton, T.M., 2003. Sea-ice switches and abrupt climate change. *Philosophical Transactions of the Royal Society A: Mathematical, Physical and Engineering Sciences* 361, 1935-1944.
- Goodman, D.K., 1979. Dinoflagellate "communities"; from the lower Eocene Nanjemoy formation of Maryland, U.S.A. *Palynology* 3, 169-190.
- Guillevic, M., Bazin, L., Landais, A., Stowasser, C., Masson-Delmotte, V., Blunier, T., Eynaud, F., Falourd, S., Michel, E., Minster, B., Popp, T., Prié, F., Vinther, B.M., 2014. Evidence for a three-phase sequence during heinrich stadial 4 using a multiproxy approach based on Greenland ice core records. *Climate of the Past* 10, 2115-2133.
- Guiot, J., de Vernal, A., 2007. Transfer Functions: Methods for Quantitative Paleoceanography Based on Microfossils, In: Claude, H.M., Anne De, V. (Eds.), *Developments in Marine Geology*. Elsevier, pp. 523-563.
- Guiot, J., de Vernal, A., 2011a. Is spatial autocorrelation introducing biases in the apparent accuracy of paleoclimatic reconstructions? *Quaternary Science Reviews* 30, 1965-1972.
- Guiot, J., de Vernal, A., 2011b. QSR Correspondence "Is spatial autocorrelation introducing biases in the apparent accuracy of palaeoclimatic reconstructions?" Reply to Telford and Birks. *Quaternary Science Reviews* 30, 3214-3216.
- Hanna, E., Cappelen, J., Fettweis, X., Huybrechts, P., Luckman, A., Ribergaard, M.H., 2009. Hydrologic response of the Greenland ice sheet: The role of oceanographic warming. *Hydrological Processes* 23, 7-30.
- Head, M.J., Harland, R., Matthiessen, J., 2001. Cold marine indicators of the late Quaternary: the new dinoflagellate cyst

- genus *Islandinium* and related morphotypes. *Journal of Quaternary Science* 16, 621-636.
- Heinrich, H., 1988. Origin and consequences of cyclic ice rafting in the Northeast Atlantic Ocean during the past 130,000 years. *Quaternary Research* 29, 142-152.
- Hill, A.E., Mitchelson-Jacob, E.G., 1993. Observations of a poleward-flowing saline core on the continental slope west of Scotland. *Deep Sea Research Part I: Oceanographic Research Papers* 40, 1521-1527.
- Hillaire-Marcel, C., de Vernal, A., 2008. Stable isotope clue to episodic sea ice formation in the glacial North Atlantic. *Earth and Planetary Science Letters* 268, 143-150.
- Kenyon, N.H., 1986. Evidence from bedforms for a strong poleward current along the upper continental slope of northwest Europe. *Marine Geology* 72, 187-198.
- Kissel, C., Laj, C., Labeyrie, L., Dokken, T., Voelker, A., Blamart, D., 1999. Rapid climatic variations during marine isotopic stage 3: Magnetic analysis of sediments from Nordic Seas and North Atlantic. *Earth and Planetary Science Letters* 171, 489-502.
- Kleinen, T., Osborn, T.J., Briffa, K.R., 2009. Sensitivity of climate response to variations in freshwater hosing location. *Ocean Dynamics* 59, 509-521.
- Knutz, P.C., Sicre, M.A., Ebbesen, H., Christiansen, S., Kuijpers, A., 2011. Multiple-stage deglacial retreat of the southern Greenland Ice Sheet linked with Irminger Current warm water transport. *Paleoceanography* 26.
- Kohfeld, K.E., Fairbanks, R.G., Smith, S.L., Walsh, I.D., 1996. *Neoglobobulimina papyroderma* (sinistral coiling) as paleoceanographic tracers in polar oceans: Evidence from Northeast Water Polynya plankton tows, sediment traps, and surface sediments. *Paleoceanography* 11, 679-699.
- Kuijpers, A., Nielsen, T., Akhmetzhanov, A., De Haas, H., Kenyon, N.H., Van Weering, T.C.E., 2001. Late Quaternary slope instability on the Faeroe margin: Mass flow features and timing of events. *Geo-Marine Letters* 20, 149-159.
- Kuijpers, A., Troelstra, S.R., Wisse, M., Nielsen, S.H., Van Weering, T.C.E., 1998. Norwegian Sea overflow variability and NE Atlantic surface hydrography during the past 150,000 years. *Marine Geology* 152, 75-99.
- Laberg, J.S., Stoker, M.S., Dahlgren, K.I.T., de Haas, H., Hafliðason, H., Hjelstuen, B.O., Nielsen, T., Shannon, P.M., Vorren, T.O., van Weering, T.C.E., Ceramicola, S., 2005. Cenozoic alongslope processes and sedimentation on the NW European Atlantic margin. *Marine and Petroleum Geology* 22, 1069-1088.
- Labeyrie, L., Cortijo, E., Jansen, E., 1999. Rapport scientifique de la mission INTERPOLE MD99-114/812 IMAGES V, In: IPEV (Ed.), *Les Rapports de Campagne à la Mer à bord du Marion Dufresne*, Brest.
- Laj, C., Kissel, C., Mazaud, A., Channell, J.E.T., Beer, J., 2000. North Atlantic palaeointensity stack since 75 ka (NAPIS-75) and the duration of the Laschamp event. *Philosophical Transactions of the Royal Society A: Mathematical, Physical and Engineering Sciences* 358, 1009-1025.
- Lassen, S., Kuijpers, A., Kunzendorf, H., Lindgren, H., Heinemeier, J., Jansen, E., Knudsen, K.L., 2002. Intermediate water signal leads surface water response during Northeast Atlantic deglaciation. *Global and Planetary Change* 32, 111-125.
- Levine, R.C., Bigg, G.R., 2008. Sensitivity of the glacial ocean to Heinrich events from different iceberg sources, as modeled by a coupled atmosphere-iceberg-ocean model. *Paleoceanography* 23, PA4213.
- Li, C., Battisti, D.S., Bitz, C.M., 2010. Can North Atlantic sea ice anomalies account for Dansgaard-Oeschger climate signals? *Journal of Climate* 23, 5457-5475.
- Locarnini, R.A., Mishonov, A.V., Antonov, J.I., Boyer, T.P., Garcia, H.E., Baranova, O.K., Zweng, M.M., Johnson, D.R., 2010. *World Ocean Atlas 2009, Volume 1: Temperature*, Ed. NOAA Atlas NESDIS 68, U.S. Government Printing Office, Washington, D.C. ed.
- Londeix, L., Benzakour, M., Suc, J.P., Turon, J.L., 2007. Messinian palaeoenvironments and hydrology in Sicily (Italy): The dinoflagellate cyst record. *Geobios* 40, 233-250.
- Malaizé, B., Caley, T., 2009. Sea surface salinity reconstruction as seen with foraminifera shells: Methods and cases studies. *European Physical Journal* 1, 177-188.
- Manabe, S., Stouffer, R.J., 1995. Simulation of abrupt climate change induced by freshwater input to the North Atlantic Ocean. *Nature* 378, 165-167.
- Marcott, S.A., Clark, P.U., Padman, L., Klinkhammer, G.P., Springer, S.R., Liu, Z., Otto-Bliesner, B.L., Carlson, A.E., Ungerer, A., Padman, J., 2011. Ice-shelf collapse from subsurface warming as a trigger for Heinrich events. *Proceedings of the National Academy of Sciences* 108, 13415-13419.
- Massé, G., Rowland, S.J., Sicre, M.A., Jacob, J., Jansen, E., Belt, S.T., 2008. Abrupt climate changes for Iceland during the last millennium: Evidence from high resolution sea ice reconstructions. *Earth and Planetary Science Letters* 269, 564-568.
- Matthiessen, J., Kunz-Pirrung, M., Mudie, P.J., 2000. Freshwater chlorophycean algae in recent marine sediments of the Beaufort, Laptev and Kara Seas (Arctic Ocean) as indicators of river runoff. *International Journal of Earth Sciences* 89, 470-485.
- Mauritzen, C., Price, J., Sanford, T., Torres, D., 2005. Circulation and mixing in the Faeroe Channels. *Deep-Sea Research Part I: Oceanographic Research Papers* 52, 883-913.
- McCartney, M.S., Mauritzen, C., 2001. On the origin of the warm inflow to the Nordic Seas. *Progress in Oceanography* 51, 125-214.
- Mudie, P.J., 1992. Circum-Arctic Quaternary and Neogene marine palynofloras: paleoecology and statistical analysis. *Neogene and Quaternary dinoflagellate cysts and acritarchs* 10, 347-390.
- Nielsen, T., Kuijpers, A., 2000. Faeroe margin, In: Kenyon, N.H., Ivanov, M.K., Akhmetzhanov, A.M., Akhmanov, G.C. (Eds.), *Multidisciplinary Study of Geological Processes on the North East Atlantic and Western Mediterranean Margins*, UNESCO, pp. 9-26.
- Nielsen, T., Rasmussen, T.L., Ceramicola, S., Kuijpers, A., 2007. Quaternary sedimentation, margin architecture and ocean circulation variability around the Faeroe Islands, North Atlantic. *Quaternary Science Reviews* 26, 1016-1036.
- Nielsen, T., Van Weering, T.C.E., 1998. Seismic stratigraphy and sedimentary processes at the Norwegian Sea margin northeast of the Faeroe Islands. *Marine Geology* 152, 141-157.
- Orvik, K.A., Niiler, P., 2002. Major pathways of Atlantic water in the northern North Atlantic and Nordic Seas toward Arctic. *Geophysical Research Letters* 29, 2-1.
- Peltier, W.R., 2004. Global glacial isostasy and the surface of the ice-age earth: The ICE-5G (VM2) model and GRACE, *Annual Review of Earth and Planetary Sciences*, pp. 111-149.
- Penaud, A., Eynaud, F., Turon, J.L., Zaragosi, S., Malaizé, B., Toucanne, S., Bourillet, J.F., 2009. What forced the collapse of European ice sheets during the last two glacial periods (150 ka B.P. and 18 ka cal B.P.)? Palynological evidence. *Paleoceanography, Palaeoclimatology, Palaeoecology* 281, 66-78.
- Prahl, F.G., Muehlhausen, L.A., Zahnle, D.L., 1988. Further evaluation of long-chain alkenones as indicators of paleoceanographic conditions. *Geochimica et Cosmochimica Acta* 52, 2303-2310.
- Radi, T., Bonnet, S., Cormier, M.A., de Vernal, A., Durantou, L., Faubert, É., Head, M.J., Henry, M., Pospelova, V., Rochon, A., Van Nieuwenhove, N., 2013. Operational taxonomy and (paleo-)autecology of round, brown, spiny dinoflagellate cysts from the Quaternary of high northern latitudes. *Marine Micropaleontology* 98, 41-57.
- Rahman, A., 1995. Reworked nanofossils in the North Atlantic Ocean and subpolar basins: implications for Heinrich events and ocean circulation. *Geology* 23, 487-490.
- Rahmstorf, S., 2002. Ocean circulation and climate during the past 120,000 years. *Nature* 419, 207-214.
- Rasmussen, T.L., Balbon, E., Thomsen, E., Labeyrie, L., Van Weering, T.C.E., 1999. Climate records and changes in deep outflow from the Norwegian Sea ~ 150-55 ka. *Terra Nova* 11, 61-66.

Partie 2 : Processus hydrographiques et mécanismes de déclenchement en jeu lors des événements climatiques abrupts avant, pendant et après un HE : zoom sur la période 35-41 ka autour d'HE4.

- Rasmussen, T.L., Thomsen, E., 2004. The role of the North Atlantic Drift in the millennial timescale glacial climate fluctuations. *Palaeogeography, Palaeoclimatology, Palaeoecology* 210, 101-116.
- Rasmussen, T.L., Thomsen, E., 2009. Ventilation changes in intermediate water on millennial time scales in the SE Nordic seas, 65-14 kyr BP. *Geophysical Research Letters* 36.
- Rasmussen, T.L., Thomsen, E., Labeyrie, L., Van Weering, T.C.E., 1996a. Circulation changes in the Faeroe-Shetland Channel correlating with cold events during the last glacial period (58-10 ka). *Geology* 24, 937-940.
- Rasmussen, T.L., Thomsen, E., Troelstra, S.R., Kuijpers, A., Prins, M.A., 2002. Millennial-scale glacial variability versus Holocene stability: Changes in planktic and benthic foraminifera faunas and ocean circulation in the North Atlantic during the last 60 000 years. *Marine Micropaleontology* 47, 143-176.
- Rasmussen, T.L., Thomsen, E., Van Weering, T.C.E., Labeyrie, L., 1996b. Rapid changes in surface and deep water conditions at the Faeroe Margin during the last 58,000 years. *Paleoceanography* 11, 757-771.
- Rasmussen, T.L., Van Weering, T.C.E., Labeyrie, L., 1997. Climatic instability, ice sheets and ocean dynamics at high northern latitudes during the last glacial period (58-10 KA BP). *Quaternary Science Reviews* 16, 71-80.
- Rochon, A., de Vernal, A., Turon, J.-L., Matthiessen, J., Head, M.J., 1999. Distribution of dinoflagellate cysts in surface sediments from the North Atlantic Ocean and adjacent basins and quantitative reconstruction of sea-surface parameters. *AASP special pub.*, Dallas, Texas, p. 146.
- Sachs, J.P., Lehman, S.J., 1999. Subtropical North Atlantic temperatures 60,000 to 30,000 years ago. *Science* 286, 756-760.
- Sanchez Goñi, M.F., Harrison, S.P., 2010. Millennial-scale climate variability and vegetation changes during the Last Glacial: Concepts and terminology. *Quaternary Science Reviews* 29, 2823-2827.
- Schiebel, R., Waniek, J., Bork, M., Hemleben, C., 2001. Planktic foraminiferal production stimulated by chlorophyll redistribution and entrainment of nutrients. *Deep-Sea Research Part I: Oceanographic Research Papers* 48, 721-740.
- Schlitzer, R., 2012. *Ocean Data View*.
- Sejrup, H.P., Larsen, E., Hafliðason, H., Berstad, I.M., Hjelstuen, B.O., Jonsdottir, H.E., King, E.L., Landvik, J., Longva, O., Nygard, A., Ottesen, D., Raunholm, S., Rise, L., Stalsberg, K., 2003. Configuration, history and impact of the Norwegian Channel Ice Stream. *Boreas* 32, 18-36.
- Shackleton, N.J., 1974. Attainment of isotopic equilibrium between ocean water and the benthic foraminifera genus *Uvigerina*: isotopic changes in the ocean during the Last Glacial. In: Labeyrie, L. (Ed.), *Methodes quantitatives d'étude des variations du climat au cours du Pleistocène*, Editions du C.N.R.S., France ed, pp. 203-209.
- Shaffer, G., Olsen, S.M., Bjerrum, C.J., 2004. Ocean subsurface warming as a mechanism for coupling Dansgaard-Oeschger climate cycles and ice-rafting events. *Geophysical Research Letters* 31, 1-4.
- Shannon, C.E., Weaver, W., 1949. *The Mathematical Theory of Information*. University of Illinois Press, Urbana, Urbana.
- Sicre, M.A., Bard, E., Ezat, U., Rostek, F., 2002. Alkenone distributions in the North Atlantic and Nordic sea surface waters. *Geochemistry, Geophysics, Geosystems* 3, 1 of 13-13 of 13.
- Sicre, M.A., Labeyrie, L., Ezat, U., Duprat, J., Turon, J.L., Schmidt, S., Michel, E., Mazaud, A., 2005. Mid-latitude Southern Indian Ocean response to Northern Hemisphere Heinrich events. *Earth and Planetary Science Letters* 240, 724-731.
- Sicre, M.A., Weckström, K., Seidenkrantz, M.S., Kuijpers, A., Benetti, M., Masse, G., Ezat, U., Schmidt, S., Bouloubassi, I., Olsen, J., Khodri, M., Mignot, J., 2014. Labrador current variability over the last 2000 years. *Earth and Planetary Science Letters* 400, 26-32.
- Siddall, M., Rohling, E.J., Thompson, W.G., Waellbroeck, C., 2008. Marine isotope stage 3 sea level fluctuations: Data synthesis and new outlook. *Reviews of Geophysics* 46.
- Sikes, E.L., Volkman, J.K., Robertson, L.G., Pichon, J.-J., 1997. Alkenones and alkenes in surface waters and sediments of the Southern Ocean: Implications for paleotemperature estimation in polar regions. *Geochimica et Cosmochimica Acta* 61, 1495-1505.
- Simstich, J., Sarnthein, M., Erlenkeuser, H., 2003. Paired $\delta^{18}O$ signals of *Neoglobobulimina papyrifera* (s) and *Turborotalita quinqueloba* show thermal stratification structure in Nordic Seas. *Marine Micropaleontology* 48, 107-125.
- Svensen, J.I., Alexanderson, H., Astakhov, V.I., Demidov, I., Dowdeswell, J.A., Funder, S., Gataullin, V., Henriksen, M., Hjort, C., Houmark-Nielsen, M., Hubberten, H.W., Ingólfsson, O., Jakobsson, M., Kjær, K.H., Larsen, E., Lokrantz, H., Lunkka, J.P., Lyså, A., Mangerud, J., Matiouchkov, A., Murray, A., Möller, P., Niessen, F., Nikolskaya, O., Polyak, L., Saarnisto, M., Siegert, C., Siegert, M.J., Spielhagen, R.F., Stein, R., 2004. Late Quaternary ice sheet history of northern Eurasia. *Quaternary Science Reviews* 23, 1229-1271.
- Svensson, A., Andersen, K.K., Bigler, M., Clausen, H.B., Dahl-Jensen, D., Davies, S.M., Johnsen, S.J., Muscheler, R., Parrenin, F., Rasmussen, S.O., Röthlisberger, R., Seierstad, I., Steffensen, J.P., Vinther, B.M., 2008. A 60 000 year Greenland stratigraphic ice core chronology. *Climate of the Past* 4, 47-57.
- Swingedouw, D., Rodehacke, C.B., Behrens, E., Menary, M., Olsen, S.M., Gao, Y., Mikolajewicz, U., Mignot, J., Biastoch, A., 2013. Decadal fingerprints of freshwater discharge around Greenland in a multi-model ensemble. *Climate Dynamics* 41, 695-720.
- Ternois, Y., Sicre, M.A., Boireau, A., Conte, M.H., Eglinton, G., 1997. Evaluation of long-chain n-alkanes as paleotemperature indicators in the mediterranean sea. *Deep-Sea Research Part I: Oceanographic Research Papers* 44, 271-286.
- Tolderlund, D.S., Bé, A.W.H., 1971. Seasonal Distribution of Planktic Foraminifera in the Western North Atlantic. *Micropaleontology* 17, 297-329.
- Valdimarsson, H., Malmberg, S.-A., 1999. Near-surface circulation in Icelandic waters derived from satellite tracked drifters. *Rit Fiskideild* 16, 23-40.
- Van Weering, T.C.E., Nielsen, T., Kenyon, N.H., Akentjeva, K., Kuijpers, A.H., 1998. Sediments and sedimentation at the NE Faeroe continental margin; Contourites and large-scale sliding. *Marine Geology* 152, 159-176.
- von Gyldenfeldt, A.-B., Carstens, J., Meincke, J., 2000. Estimation of the catchment area of a sediment trap by means of current meters and foraminiferal tests. *Deep Sea Research Part II: Topical Studies in Oceanography* 47, 1701-1717.
- Weckström, K., Massé, G., Collins, L.G., Hanhijärvi, S., Bouloubassi, I., Sicre, M.A., Seidenkrantz, M.S., Schmidt, S., Andersen, T.J., Andersen, M.L., Hill, B., Kuijpers, A., 2013. Evaluation of the sea ice proxy IP25 against observational and diatom proxy data in the SW Labrador Sea. *Quaternary Science Reviews* 79, 53-62.
- Wolff, E.W., Chappellaz, J., Blunier, T., Rasmussen, S.O., Svensson, A., 2010. Millennial-scale variability during the last glacial: The ice core record. *Quaternary Science Reviews* 29, 2828-2838.
- Zaragosi, S., Eynaud, F., Pujol, C., Auffret, G.A., Turon, J.L., Garlan, T., 2001. Initiation of the European deglaciation as recorded in the northwestern Bay of Biscay slope environments (Meriadzek Terrace and Trevelyan Escarpment): A multi-proxy approach. *Earth and Planetary Science Letters* 188, 493-507.

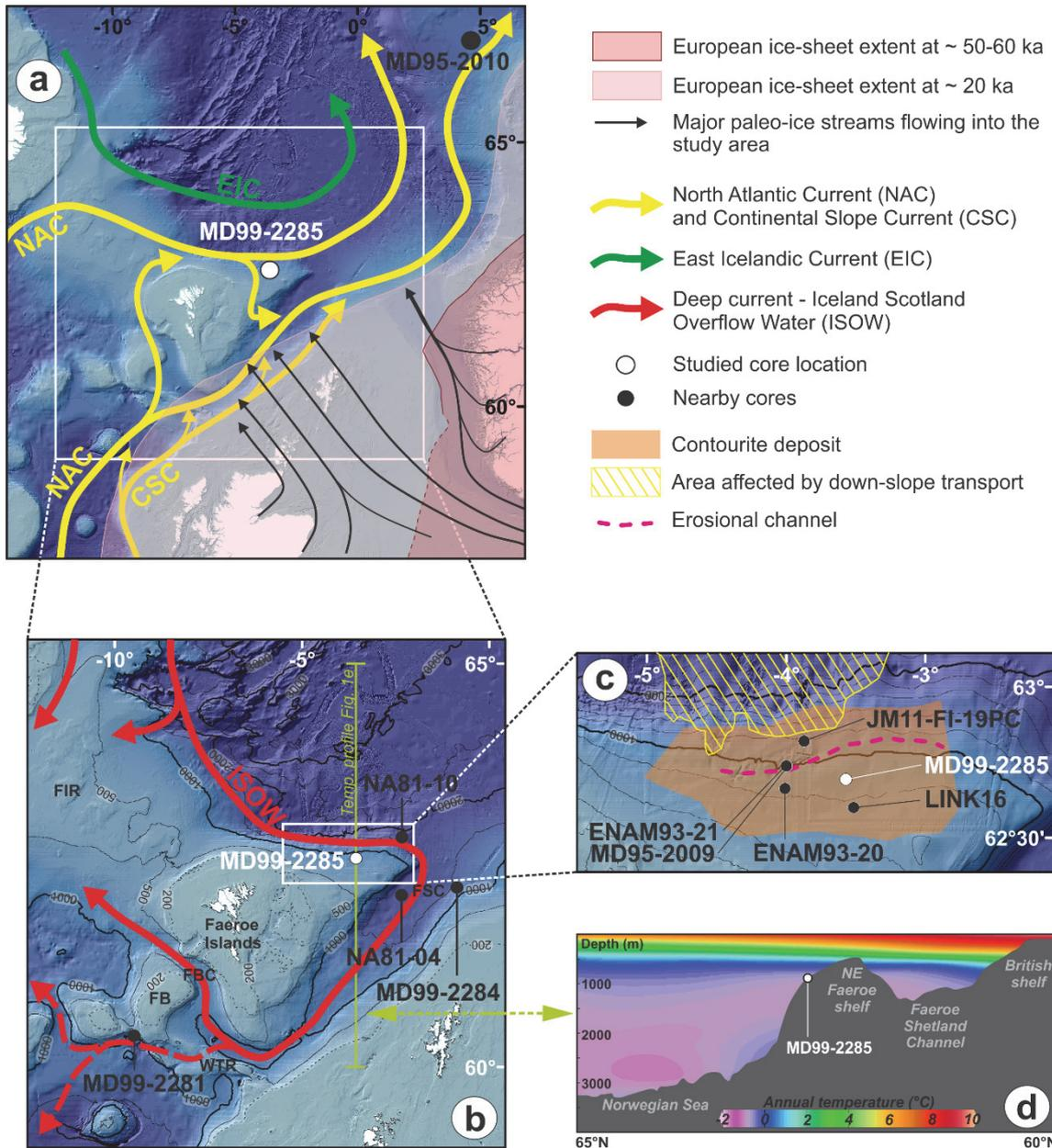


Figure 1: Map of the study area showing the locations of the studied core and of nearby cores referenced to in the present study, as well as past and modern environmental settings. (a) Surface hydrography (after Kenyon, 1986; Valdimarsson and Malmberg, 1999, Orvik and Niiler, 2002), last glacial ice-sheet extensions (after Svendsen et al., 2004) and major paleo-ice streams (after Sejrup et al., 2003 and Bradwell et al., 2008). (b) Detailed bottom physiography and deep Iceland Scotland Overflow Water (ISOW) major pathways across the Greenland Scotland Ridge via the bottom current (after Kuijpers et al., 1998). The first isobath (dotted) is at 200 m, then isobath interval is 500 m. Major bathymetric structures are indicated (FIR: Faeroe Iceland Ridge, FSC: Faeroe Shetland Channel, FBC: Faeroe Bank Channel; WTR: Wyville-Thomson Ridge, FB: Faeroe Bank). Location of the north-south temperature profile shown in Fig. 1d is indicated by the yellow line. (c) Modern sedimentary regimes, with indication of the area of contourite deposit (van Weering et al., 1998), the sector affected by down-slope mass transport (Kuijpers et al., 2001; Nielsen et al., 2007), and the location of the erosive channel formed through the bottom current action (van Weering et al., 1998). Isobath intervals is 200 m. (d) North-south temperature profile illustrating the structure of the water column over the study area. Temperature data are derived from WOA09 data (Locarnini et al., 2010) and plot using Ocean Data View (Schlitzer, 2012). Bathymetry is from EMODnet (www.emodnet.eu). Geographic coordinate system: WGS 1984 – Projection: Mercator 55°N.

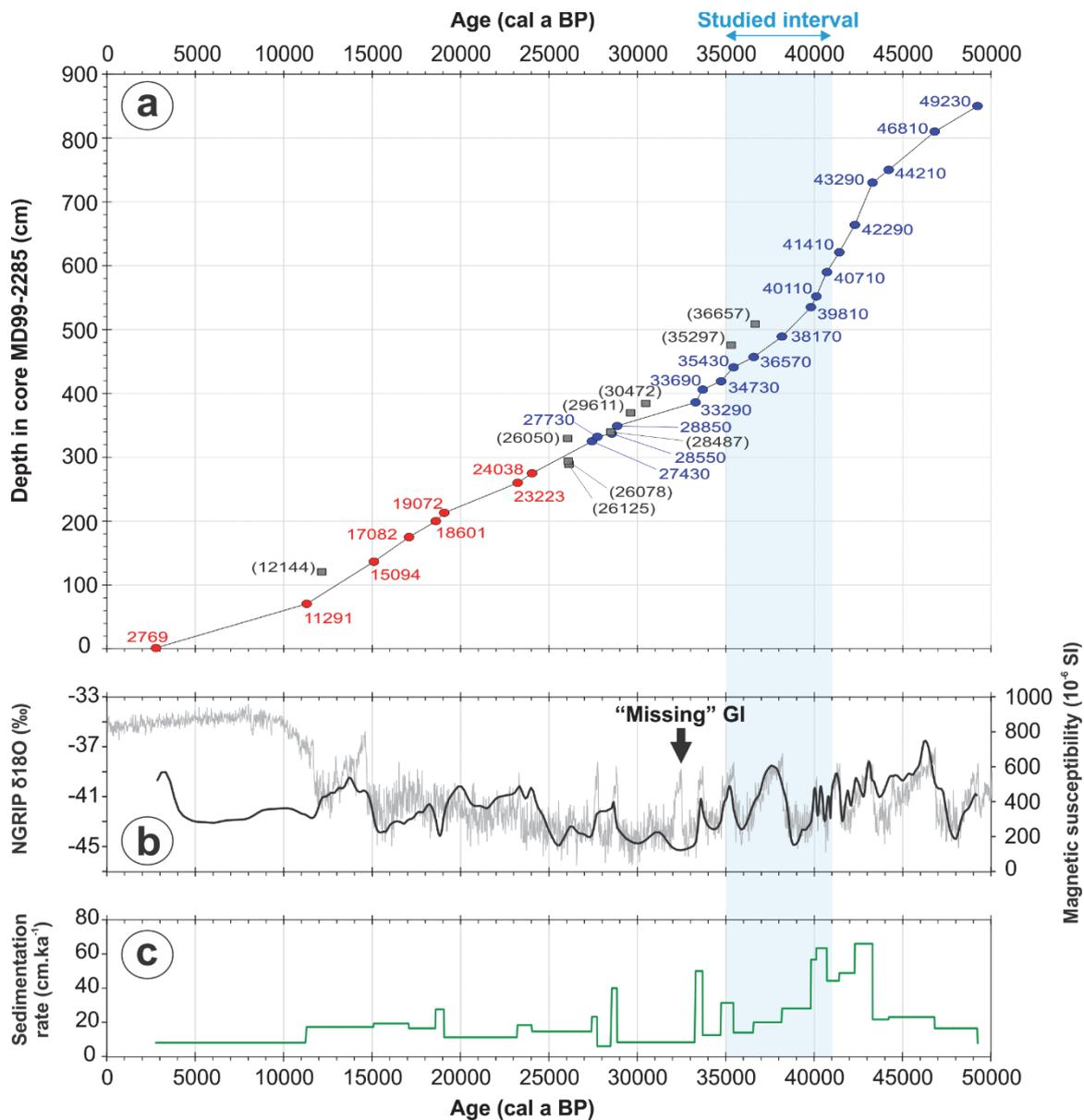


Figure 2: Age model and sedimentation rates of core MD99-2285 for the last 50 ka. (a) Linear interpolation (black curve) between tie-points, i.e. selected AMS¹⁴C dates (red dots) and age-control points (blue dots) obtained by correlation of the magnetic susceptibility signal of the core to the NGRIP $\delta^{18}O$ record (Wolff et al., 2010). Incoherent dates (unconsidered for the establishment of the age model) are also shown (grey squares with corresponding ages in brackets). (b) Graph showing the correspondence between the magnetic susceptibility signal of the core (plotted according to the resulting calendar BP age scale) and the NGRIP $\delta^{18}O$ record. (c) Evolution through time of sedimentation rates of the studied core.

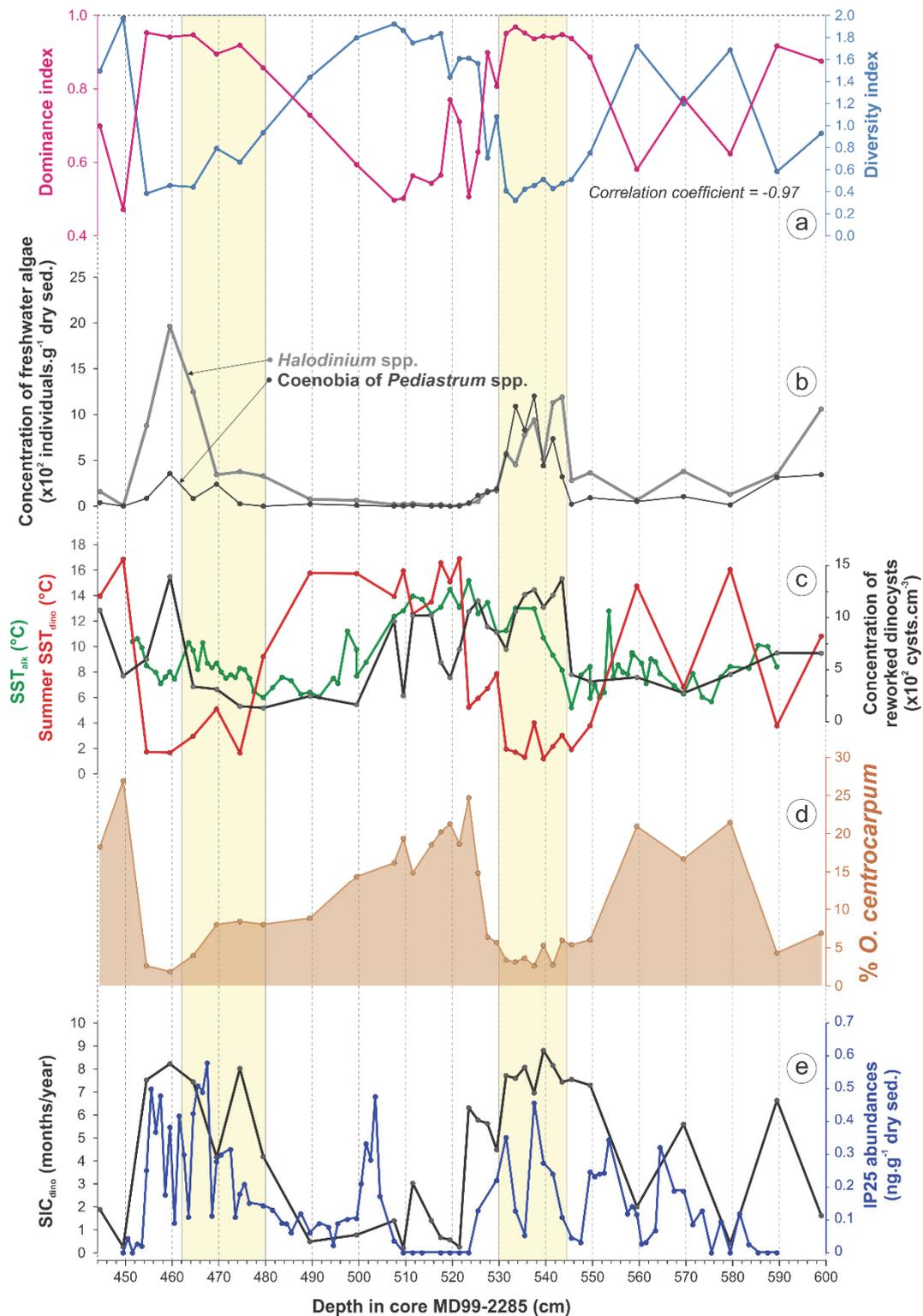


Figure 3: Evolution through depth on the studied interval (444-600 cm) of core MD99-2285 of selected parameters that enable the identification of allochthonous versus autochthonous signals. (a) Diversity and dominance indices calculated on dinocyst assemblages. (b) Concentrations of advected palynomorphs: *Halodinium* spp. and coenobia of *Pediastrum* spp. (c) SST stemming from dinocyst analyses (SST_{dino}) and from alkenones quantifications (SST_{alk}), compared to the concentration of advected pre-Quaternary dinocysts. (d) Relative abundance of *O. centrocarpum*, a dinocyst species related to the warm Atlantic inflow pathways. (e) Sea-ice cover duration derived from dinocyst analyses (SIC_{dino}) compared to IP25 abundances. The yellow bands highlight the intervals where coeval high SST_{alk} and high concentrations of advected palynomorphs are recorded.

Partie 2 : Processus hydrographiques et mécanismes de déclenchement en jeu lors des événements climatiques abrupts avant, pendant et après un HE : zoom sur la période 35-41 ka autour d'HE4.

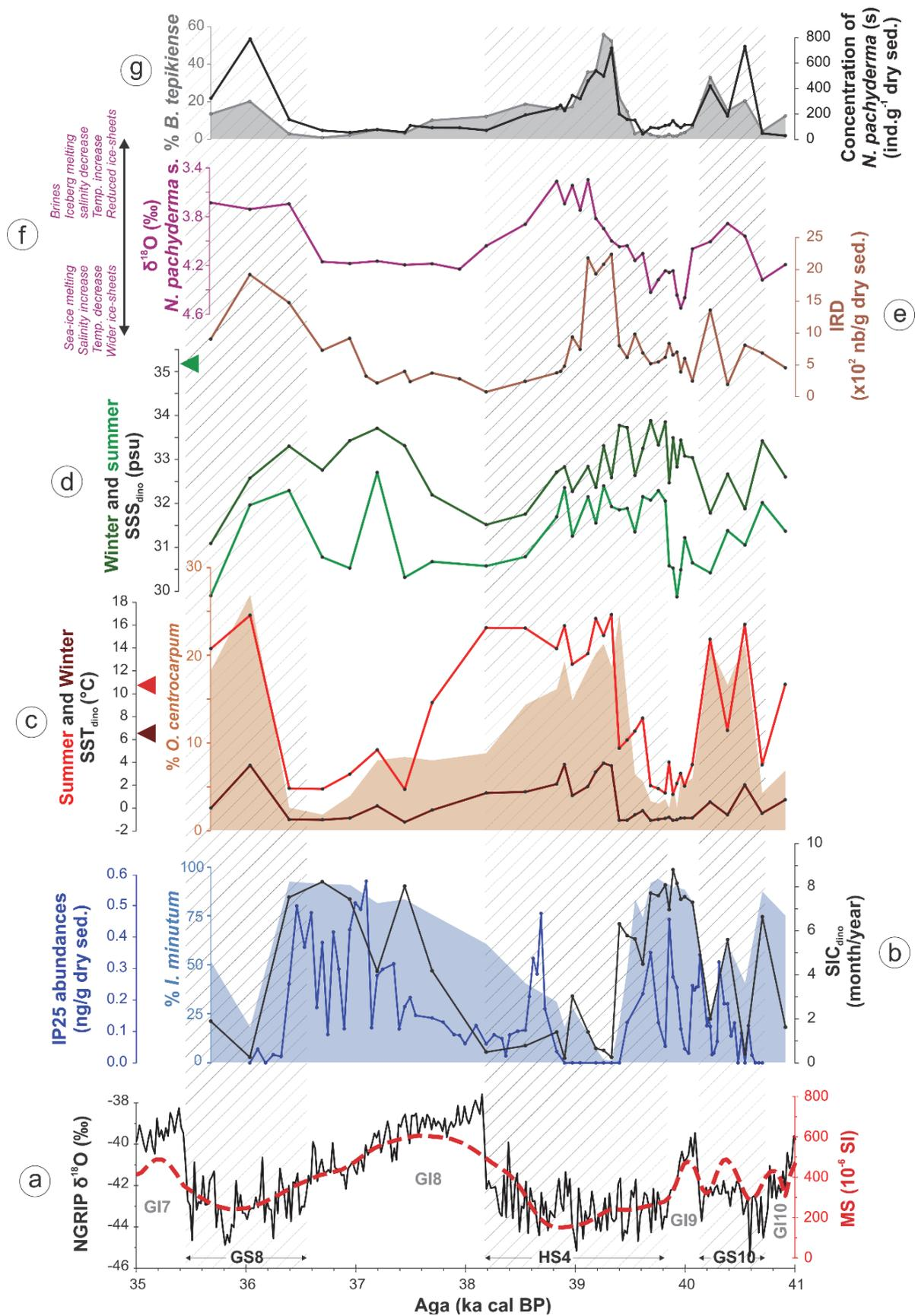


Figure 4

Figure 4: Compilation of autochthonous signals indicative of regional surface and subsurface hydrological conditions through time on the 35-41 ka cal BP section of core MD99-2285. (a) NGRIP $\delta^{18}\text{O}$ regional stratotype compared to the magnetic susceptibility signal of the studied core. (b) Sea-ice cover indicators: SIC_{dino} , IP25 abundances, and relative abundance of the dinocyst polar taxa *I. minutum*. (c) Seasonal SST_{dino} and relative abundance of *O. centrocarpum*, a dinocyst taxa associated to the warm Atlantic inflow pathways. Triangles indicate mean modern SST values in summer (light red) and winter (dark red), after WOA09 data (Locarnini et al., 2010). (d) Seasonal sea-surface salinities derived from dinocyst analyses (SSS_{dino}). The green triangle indicate mean modern SSS value (equal for both seasons) after WOA09 data (Antonov et al., 2010). (e) Ice-rafted debris (IRD) concentration. (f) $\delta^{18}\text{O}$ signal measured on *N. pachyderma* s. ($\delta^{18}\text{O}_{\text{NPS}}$) and its associated potential ways of interpretation. (g) Concentration of the planktonic foraminifera polar taxa *N. pachyderma* s. (NPS), and relative abundance of dinocyst taxa *B. tepikiense*, both indicative of upper stratification favorable to NPS development in subsurface. Hatched bands highlight stadial intervals (age limits after Wolff et al., 2010).

Figure 5: Selected hydrological parameters highlighting the sequencing of processes and ocean-cryosphere interactions occurring during Dansgaard-Oeschger and Heinrich events and associated ice-sheet collapses in core MD99-2285. (a) NGRIP $\delta^{18}\text{O}$ regional stratotype. (b) Indicator of (at least seasonally) open-ocean conditions (presence of sterols) versus more chaotic surface conditions (absence of sterols). (c) Sea-ice cover indicators. (d) Iceberg calving indicator. (e) Sea surface temperature record. (f) Sea surface salinity record. (g) Indirect indicators of warm Atlantic waters advection. (h) Indirect and relative indicator of subsurface warming versus propagation of sea-ice melting in subsurface, i.e. the two main factors impacting on local variations of $\delta^{18}\text{O}_{\text{NPS}}$. (i) Indirect indicator of upper stratification. Hatched bands highlight stadial intervals (age limits after Wolff et al., 2010). Colored bands highlight the different sequences of hydrological processes (numbered at the top of the graph, including the subphases of phase 2).

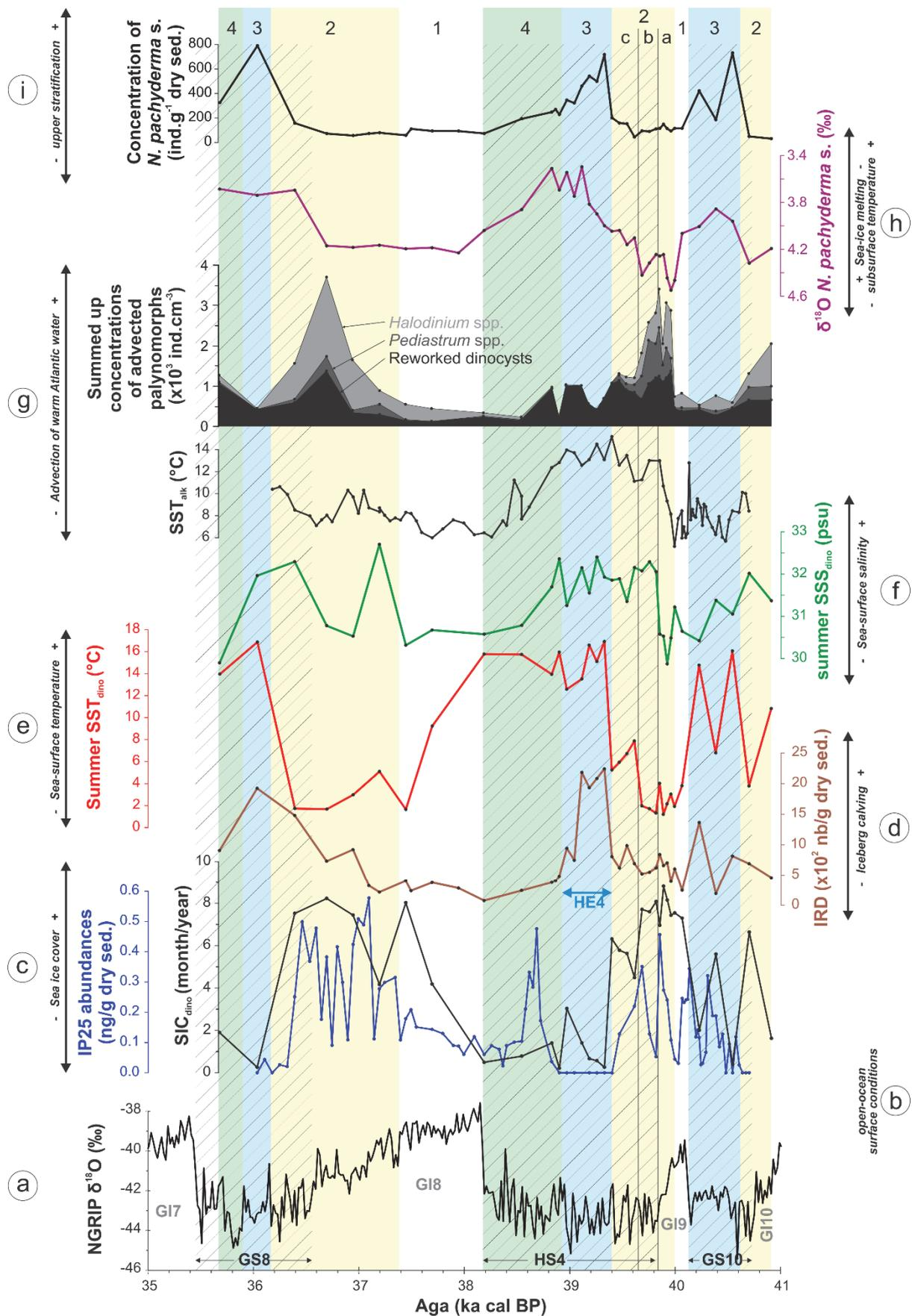


Figure 5

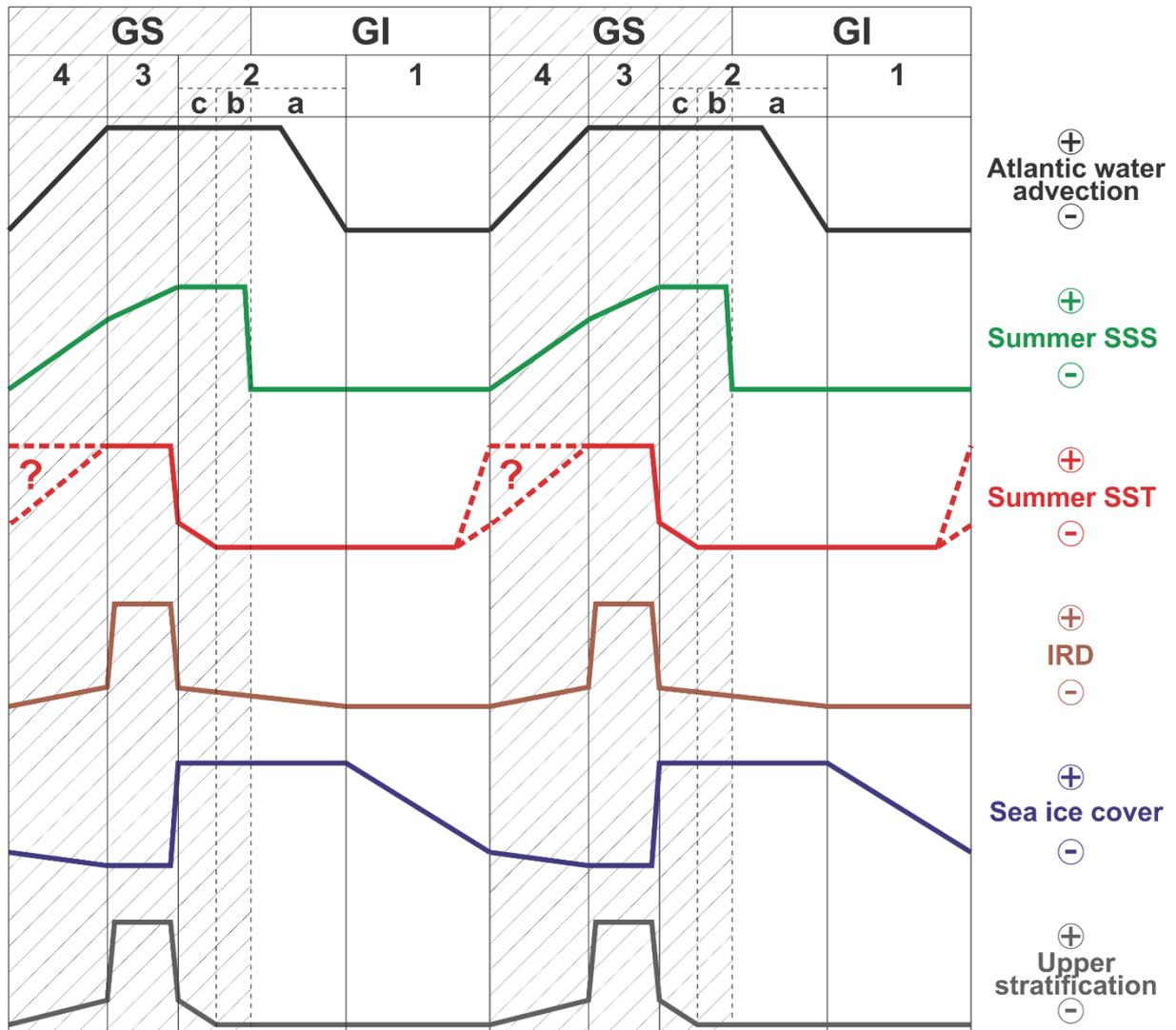


Figure 6: Conceptual scheme of the sequencing of hydrological processes occurring during Dansgaard-Oeschger and Heinrich events in the southern Norwegian Sea.

Table 1: Location and water depth of the studied core MD99-2285 and cores cited in the present study.

Core	latitude (°N)	longitude (°E)	water depth (m)
MD99-2285	62.6938	-3.5723	885
NA81-04	62.2333	-2.3333	1760
MD99-2284	62.3747	-0.9802	1500
LINK16	62.6002	-3.5160	773
ENAM 93-20	62.6700	-3.9967	853
MD95-2009	62.7375	-3.9977	1027
ENAM 93-21	62.7383	-3.9987	1020
JM11-FI-19PC	62.8167	-3.8667	1179
NA81-10	62.9667	-2.3667	1750
MD95-2010	66.6842	4.5662	1226

Table 2: Paleoceanographic studies conducted on Norwegian cores and using identical or equivalent analyses to some of those used in the present study.

Proxies	SST _{dino} , SIC _{dino} , relative percentages of <i>I. minutum</i> (% <i>Imin</i>), <i>O. centrocarpum</i> (% <i>Ocen</i>) and <i>B. tepikiense</i> (% <i>Btep</i>)	IRD concentration	$\delta^{18}\text{O}_{\text{NPS}}$	Concentration of planktonic foraminifera with nearly monospecific assemblages, i.e. that can be regarded as similar to NPS concentration
GS/HS signature	<ul style="list-style-type: none"> • High SST_{dino} + high %<i>Ocen</i> (warm surface conditions) • Low SIC_{dino} + low %<i>Imin</i> (reduced SIC duration) • High %<i>Btep</i> (upper stratification) 	High (intense iceberg calving)	Light (sea-level rise + moderate subsurface warming)	High (favorable subsurface conditions for NPS development)
GI signature	<ul style="list-style-type: none"> • Cold surface conditions • Longer SIC duration • Reduced upper stratification 	Low (reduced iceberg calving)	Heavy (sea ice melting + sea-level drop + temperature decrease)	Low (unfavorable subsurface conditions for NPS development)
MD95-2009 (62.7375°N; -3.9977°E)	Eynaud et al., 2002 ¹	Rasmussen et al., 1999 ³ Elliot et al., 2001 ² Eynaud et al., 2002 ¹	Rasmussen et al., 1999 ³ Elliot et al., 2001 ² Eynaud et al., 2002 ¹	Rasmussen et al., 1999 ³
ENAM93-21 (62.7383°N; -3.9987°E)		Elliot et al., 2001 ²	Rasmussen et al., 1996b ² Rasmussen et al., 1997 ⁵ Dokken and Jansen, 1999 ²	Rasmussen et al., 1996b ² Rasmussen et al., 1997 ⁵
MD95-2010 (66.6842°N; 4.5662°E)	Eynaud et al., 2002 ¹	Dokken and Jansen, 1999 ² Elliot et al., 2001 ²	Dokken and Jansen, 1999 ²	
LINK16 (60.6002°N; -3.5160°E)		Rasmussen and Thomsen, 2009 ⁴	Rasmussen and Thomsen, 2009 ⁴	Rasmussen and Thomsen, 2009 ⁴

¹MIS3, ²Last glacial period, ³MIS5 to MIS3, ⁴GI 18 to HS1, ⁵GI 9 to GS 8.

Partie 2 : Processus hydrographiques et mécanismes de déclenchement en jeu lors des événements climatiques abrupts avant, pendant et après un HE : zoom sur la période 35-41 ka autour d'HE4.

**Section 2. Surface and subsurface hydrographical reorganizations at the
frontier between Northeast Atlantic and Norwegian Sea basins around
the Heinrich event 4 case study period**

*Article en préparation en vue d'une soumission à **Earth and Planetary Science Letters***

Wary Mélanie¹, Eynaud Frédérique¹, Rossignol Linda¹, Kissel Catherine², Swingedouw
Didier¹, Lapuyade Joanna¹, Sicre Marie-Alexandrine³, Castera Marie-Hélène¹, Billy Isabelle¹

¹ UMR 5805, EPOC (Environnements et Paléoenvironnements Océaniques et Continentaux),
Université de Bordeaux, 33615 Pessac, France.

² UMR 8212, LSCE (Laboratoire des Sciences du Climat et de l'Environnement),
CEA/CNRS-INSU/UVSQ, 91198 Gif-sur-Yvette cedex, France

³ LOCEAN (Laboratoire d'Océanographie et du Climat: Expérimentation et Approches
Numériques), IPSL-UPMC/CNRS/IRD/MNHN, Paris, France.

Résumé

Les événements de Dansgaard-Oeschger et d'Heinrich font partie des anomalies climatiques les plus énigmatiques de la dernière période glaciaire. De nombreuses paléoreconstructions et expériences de modélisation se sont attachées à étudier leur variabilité climatique millénaire caractéristique, testant ainsi les couplages océan-atmosphère-cryosphère. Néanmoins, plusieurs incertitudes et incohérences majeures demeurent encore actuellement. De récents travaux de modélisation simulant l'impact d'un relargage d'eau douce en Atlantique Nord, similaire à ceux enregistrés lors des événements d'Heinrich, ont suggéré une advection accrue d'eaux chaudes atlantiques dans les Mers Nordiques, et ont ainsi mis en avant la nécessité d'effectuer de nouvelles reconstructions paléocéanographiques dans ce secteur. Notre étude se concentre ainsi sur l'évolution des conditions océaniques de surface et de subsurface, à très haute résolution temporelle, sur la section 37-40 ka cal BP de la carotte MD99-2281 localisée au Sud-Ouest des îles Féroé. Nous comparons ces signaux à des enregistrements haute résolution similaires obtenus sur la section 35-41 ka cal BP de la carotte MD99-2285 localisée au Nord-Est des Féroé. Cette comparaison multiproxies et multi-carottes appuie l'hypothèse d'une advection accrue d'eaux chaudes atlantiques dans les Mers Nordiques à une échelle régionale, et précise son schéma spatial. En effet nos résultats suggèrent que le site MD99-2281 se trouvait, au cours de l'évènement d'Heinrich 4, dans une zone de transition localisée à la jonction entre un bassin Atlantique Nord froid et un bassin nordique chaud. Ils suggèrent également que le flux d'eau douce initial soit le résultat d'apports glacio-fluviaux issus des calottes de glace européennes. Ils confortent ainsi l'hypothèse que cette advection d'eau chaude ait pu jouer un rôle déterminant sur la déstabilisation des calottes européennes, et font appel au concept de « précurseur européen ». Ils confirment également la signature laurentienne dominante de cet évènement d'Heinrich au sein de l'Atlantique Nord et au moins jusqu'au site MD99-2281, et suggèrent que les icebergs issus de cette calotte nord-américaine n'aient pu traverser la ride Islande-Ecosse au cours de cet épisode.

Abstract

Dansgaard-Oeschger and Heinrich events constitute ones of the most enigmatic features of the last glacial period. Many paleoreconstructions and model experiments have focused on their characteristic millennial climatic variability, testing atmospheric/cryospheric/oceanic couplings but major uncertainties and discrepancies still remain. Recently, some freshwater hosing experiments in the North Atlantic, simulating Heinrich event-type perturbations, suggested enhanced advection of warm Atlantic waters in the Nordic Seas thus urgently calling for additional paleoreconstructions in these domains. Here, we investigate at very high temporal resolution the evolution of sea-surface and subsurface conditions during the 37-40 ka cal BP interval in core MD99-2281 located southwest off Faeroes. We compare these records with similar high resolution records obtained on the 35-41 ka cal BP section of core MD99-2285 located northeast off Faeroes. This multiproxy and multicore comparison supports an enhanced advection of warm Atlantic waters at a regional scale, and outlines its spatial pattern. Indeed, our results strongly suggest that site MD99-2281 lies in a transitional zone between a cooled Atlantic Ocean and warmed-up Nordic Seas during Heinrich event 4, and that the initial freshwater flux might be the result of glacio-fluvial inputs from European ice-sheets. They thus suggest that enhanced advection of warm Atlantic waters played a key role on European ice-sheet destabilization and recalls for the “European precursor” concept. They also support the strong Laurentide signature of this event in the Atlantic Ocean as northeast as site MD99-2281, and suggest that most icebergs derived from the Laurentide ice-sheet did not cross the Iceland-Scotland Ridge at that time..

Keywords: Dansgaard-Oeschger events, Heinrich event 4, triggering mechanism, advection of warm Atlantic waters, freshwater flux.

1. Introduction

The last glacial millennial climatic events (i.e. Dansgaard-Oeschger and Heinrich events; Heinrich, 1988; Bond et al., 1992; Dansgaard et al., 1993) have been the subject of many paleoreconstructions and model experiments in the past decades. Despite some disagreements, most of them converge towards a scheme where the cold atmospheric phases of Dansgaard-Oeschger events (Greenland Stadials, hereafter GS), including the ones correlated with Heinrich events (called Heinrich Stadials, hereafter HS; Sanchez Goni and Harisson, 2010), are associated with: cold sea-surface temperatures (SST) in the North Atlantic Ocean and adjacent seas (e.g. Sachs and Lehman, 1999; Rasmussen and Thomsen, 2004), ice-rafted debris (IRD) deposits in the subpolar area resulting from ice-sheet collapses and subsequent iceberg calving (e.g. Bond and Lotti, 1995; Elliot et al., 2001), and a slowdown of the Atlantic Meridional Overturning Circulation (AMOC; e.g. Kissel et al., 1999; Rahmstorf, 2002; Böhm et al., 2015). Several paleoreconstructions from the Norwegian Sea support the SST pattern of this commonly accepted scheme (e.g. Rasmussen et al., 1996a,b,c, 1997; Rasmussen and Thomsen, 2004; Dokken et al., 2013). Nonetheless, it is worth mentioning that these Norwegian Sea cold stadial SST were deduced from indirect proxies mainly derived from planktonic foraminifera analyses (i.e. zooplanktonic organisms used in routine in paleoceanography but rather indicative of near-surface or even subsurface conditions, e.g. Telford and Kucera, 2013) or from benthic foraminiferal isotopes. At the opposite, other SST records from the Norwegian Sea, based on more direct proxies such as dinoflagellate cyst assemblages and alkenone analyses (i.e. derived from phytoplanktonic organisms), suggest a significantly different scheme for this adjacent basin, with GS characterized by a warm surface layer overlaying a colder subsurface layer (Eynaud et al., 2002; Wary et al., JQS, submitted¹, and Wary et al., QSR, to be submitted²). Recent freshwater hosing experiments lend support to this paradoxical scheme (Kleinen et al., 2009; Swingedouw et al., 2013). Indeed, in these modelling studies, a high latitude freshwater flux is responsible for a slowdown of the AMOC in parallel to enhanced subsurface advection of warm Atlantic waters up to the Nordic Seas where they re-emerge in surface, thus leading to surface cooling in the North Atlantic basin and surface warming in the Nordic Seas. Such an advection mechanism recalls Rasmussen and Thomsen (2004) and Dokken et al. (2013)'s

¹ cf. page 127 de ce manuscrit

² cf. page 163 de de ce manuscrit

works, where authors reported active Atlantic inflow in subsurface and/or at intermediate depth. Comparable evidences have furthermore been recently produced (Wary et al., QSR, to be submitted) on the basis of high resolution records bringing additional clues of enhanced surface (maybe extending to subsurface) advection of warm Atlantic waters in the southern Norwegian Sea at the end of Greenland interstadials (GI) and during much of GS/HS intervals. The authors also suggested that this advection might have played a key role on European ice-sheet destabilization. Hence, a new concept, which conciliates previous contradictory studies, is emerging but needs support from additional paleoreconstructions.

Here, we investigate at very high temporal resolution (from 4 to 38 years on average depending on proxies) the 37-40 ka cal BP section of core MD99-2281 located southwest off Faeroes. We use the same multiproxy analyses than those conducted on the 35-41 ka cal BP interval of core MD99-2285 (located northeast off Faeroes) by Wary et al. (QSR, to be submitted), as well as X-ray fluorescence data (unpublished in the case of core MD99-2285), and compare records from both cores. This methodological approach allows us to assess the spatial response of surface and subsurface oceanic conditions during the last glacial millennial climatic events, especially at the GI to GS-HS critical transitions and during HS4, and to relate them with the Laurentide and European ice-sheet histories of decays.

2. Regional settings

The studied cores MD99-2281 (60.3418 °N; -9.4557 °E; 1197 m water depth) and MD99-2285 (62.6938 °N; -3.5723 °E; 885 m water depth) are ideally located to track oceanic changes related to the millennial climatic variability (Fig. 1). They are both under the direct influence of the warm ($T > 8^{\circ}\text{C}$) and salty North Atlantic Water, entrained northward through the North Atlantic Current and the Continental Slope Current (e.g. Kenyon, 1986; McCartney and Mauritzen, 2001; Orvik and Niiler, 2002; Mauritzen et al., 2005) but are located on opposite sides of the Iceland-Scotland ridge thus offering contrasted oceanographical patterns. During the last glacial period, they were also under the direct influence of the proximal European ice-sheets (i.e. the Fennoscandian and the British-Irish ice-sheets; Svendsen et al., 2004; Sejrup et al., 2003; Bradwell et al., 2008) whose decays and built-up have modulated the oceanic and climatic dynamics. They both offer high sedimentation rates for the last glacial interval thanks to high sediment supply from relatively weak bottom currents

(Boldreel, 1998; Kuijpers et al., 1998a,b; Nielsen et al., 2007). These bottom currents transport deep and intermediate cold water masses from the Nordic Seas to the Atlantic Ocean, where they will feed the North Atlantic Deep Water (Hansen and Osterhus, 2000; Borenäs and Lundberg, 2004; Mauritzen et al., 2005).

3. Material and methods

The investigated cores were analyzed strictly using the same set of proxies (see Wary et al., QSR, to be submitted, for further analytical and technical details). We selected some key signals which include:

(1) Indices related to surface and/or subsurface advection:

- The absolute concentrations of advected palynomorphs, i.e. reworked (pre-Quaternary) dinocysts, and freshwater algae *Pediastrum* spp. and *Halodinium* spp. These palynomorphs are all related to allochthonous supplies from continental/(glacio)fluvial origin (e.g. Mudie, 1992; Matthiessen et al., 2000; Zaragosi et al., 2001; Eynaud et al., 2007; Penaud et al., 2009).
- Ice-rafted debris (IRD) concentration, indicative of iceberg calving over the study area.

(2) Signals reflecting autochthonous regional conditions, i.e.:

- Quantitative mean summer and mean winter sea-surface temperature and salinity reconstructions, obtained by applying the modern analogue technique to dinocyst assemblages after the n = 1207 modern database (hereafter called SST_{dino} and SSS_{dino} respectively).
- The relative abundance of the mesopelagic polar planktonic foraminifera taxon *N. pachyderma* sinistral coiling (NPS), which may be related to subsurface temperatures (see e.g. Wary et al., CP, in press³, and references therein).
- The absolute abundance of NPS, which may be considered as an indicator of more or less favorable hydrological conditions for the development of this taxon at its known depth habitat (from a few tens of meters to around 250 m water depth in the study area;

³ cf. page 83 de ce manuscrit

e.g. Carstens et al., 1997; Simstich et al., 2003), given that optimal ecological conditions of NPS are temperatures < 5-6 °C and salinity > 34 psu (e.g. Tolderlund and Bé, 1971; Carstens et al., 1997; Hillaire-Marcel and de Vernal, 2008).

In the present study we also use magnetic susceptibility (MS), low field magnetic susceptibility (κ), and X-ray fluorescence (Xrf) records from core MD99-2281 previously published in Zumaque et al. (2012; see this study for further technical details). We also use unpublished Xrf records from core MD99-2285, measured with the same Avaatech Xrf Core Scanner at EPOC laboratory. We specifically use the Ca/Sr Xrf ratio, which provides information on the carbonate origin (biogenic versus terrigenous, e.g. Mojtabid et al., 2005).

4. Stratigraphy

As already mentioned, the present study gathers MD99-2281 data with similar high resolution records obtained from core MD99-2285 on the 35-41 ka cal BP interval (Wary et al., QSR, to be submitted). The age model of core MD99-2281 conforms to the previous published one from Zumaque et al. (2012). Briefly, it is constrained by 10 AMS ^{14}C dates combined to 18 additional tie-points obtained by comparing the magnetic susceptibility record of core MD99-2281 to the $\delta^{18}\text{O}$ signal of NGRIP ice-core (GICC05 time scale; Andersen et al., 2006; Svensson et al., 2008; Wolff et al., 2010). Indeed, the rationale is that, along the path of bottom water masses feeding the North Atlantic Deep Water, low magnetic susceptibility values are coincident with GS and HS, and inversely high magnetic susceptibility values are synchronous with GI (Kissel et al., 1999). The age model was finally established by linear interpolation between ages and tie-points. It is important to note that supplementary stratigraphic control points, independent from climate, were retrieved from the record of the changes in the Earth's magnetic field (analysis performed at the LSCE). They correspond to the Mono Lake and the Laschamp events, dated from ~34 and ~41 ka cal BP respectively. Those additional tie points give confidence in the established age model, particularly for the presently studied section, spanning from 1792 to 1941 cm, i.e. time interval 37-40 ka cal BP covering GI9, HS4, and GI8. Based on this age model, an average sedimentation rate of 58 cm.ka^{-1} is estimated for the studied period. Sampling resolution depends on the proxies considered (from 0.2 to 2 cm), and leads to very high mean temporal resolutions varying from 4 to 38 years on the basis of this age model (Table 1).

MD99-2285 records are plotted according to the initial age model of this core, built similarly (same considerations) but independently from MD99-2281 age model (Wary et al., JQS, submitted). Fig. 2b shows the magnetic susceptibility signals of both cores, and the low field magnetic susceptibility record (κ) of MD99-2281, each plotted on their own age scale. The rather good correspondence of these signals (e.g. correlation coefficient of 0.76 between MS of MD99-2285 and MS of MD99-2281) lends support to both age models. Nonetheless, some minor lags can be noticed around 39 and 40 ka cal BP (with MD99-2285 signal preceding MD99-2281 ones by around 200 and 100 years respectively, cf. blue arrows on Fig 2b). Even if it could seem dangerous to compare timing from one core to the other, peculiarly at such high temporal resolution, the pretty good correspondence between these signals (which are commonly used to constrain age models in the study area) allows such a comparison, keeping in mind uncertainties, potential biases and the slight temporal lags apparent around GI9 and HS4.

5. Results and discussion

5.1. Surface/subsurface advection

5.1.1. Advection of warm Atlantic waters

Fig. 2e, f and g shows the evolution through time of the concentrations of advected palynomorphs on core MD99-2281, compared with the same records obtained from core MD99-2285. As in core MD99-2285, concentrations of these palynomorphs (related to glacio-fluvial inputs) display strong increases at the end of GI / onset of GS. In core MD99-2285, Wary et al. (QSR, to be submitted) related the synchronous increases in concentrations of those palynomorphs, coeval with warmer than expected SST reconstructions derived from alkenone analyses, to the beginning of advection of surface / subsurface warm Atlantic waters through the Continental Slope Current (yellow bands on Fig. 2) prior to ice-sheet collapses (blue bands on Fig. 2). Here, the strong similarity of MD99-2281 signals with MD99-2285 records, with only minor temporal lags which could be entirely due to age model uncertainties, lends support to this hypothesis at a more regional scale. This is particularly true when looking at the reworked dinocyst concentration signals, which display the same

fluctuations in both cores (green and yellow arrows on Fig. 2 highlight the corresponding lows).

However, it is worth noting that concentrations of these advected palynomorphs are lower in southern core MD99-2281 than in northern core MD99-2285. This result questions the origin and transport mechanism of these palynomorphs on both sites. As the concentration of each palynomorph exhibits similar and almost synchronous variations in both cores, common origin and transport are very likely. Two hypotheses can thus be proposed. First, as previously advanced by Wary et al. (QSR, to be submitted), reworked dinocysts, *Halodinium* spp and *Pediastrum* spp. are delivered from glacio-fluvial inputs mainly originating from the British-Irish ice-sheet and transported on both sites by the Continental Slope Current. This current could have had a greater influence on the northern site than on the southern one, which would explain the largest concentrations in core MD99-2285. Presently, this current joins the North Atlantic Current around Rockall Trough, and the downstream respective spatial contributions of these currents is not clearly identified (Hansen and Osterhus, 2000). Second hypothesis, these palynomorphs are solely related to the glacio-fluvial inputs. These inputs mainly come from the Fennoscandian ice-sheet rather than the British-Irish ice-sheet, and propagates into the Atlantic, thus explaining the largest concentrations in the northern core. As in the first hypothesis, this massive glacio-fluvial input is responsible for a slowdown of the AMOC in parallel to enhanced surface / subsurface advection of warm Atlantic waters in the Nordic Seas (which explains the warm SST from alkenones in core MD99-2285) as suggested by model experiments (Kleinen et al., 2009; Swingedouw et al., 2013). Indeed, Kleinen et al. (2009)'s experiments show that such an advection is independent of the exact location of the freshwater input. According to the duration of Kleinen et al. (2009) and Swingedouw et al. (2013)'s model experiments, the temporal lag between freshwater release and beginning of warm advection is less than 70-100 years (Kleinen et al., 2009), and 30-40 years (Swingedouw et al., 2013). Even if these simulations were performed under modern boundary conditions, such temporal lags evidence that the reaction of the system might have been very rapid, and maybe, could have not been caught by MD99-2285 reconstructions whose temporal resolution varies between 35 and 98 years at GI9/HS4 transition. However, as highlighted by Wary et al. (QSR, to be submitted), the good correspondence between SST signal derived from alkenones and reworked dinocysts concentration in core MD99-2285 suggests a common transport mechanism, which would support the first hypothesis.

Nonetheless, as things stand at present, we cannot confidently favor one hypothesis or the other.

5.1.2. Iceberg calving

IRD concentration records from both cores display similar and nearly synchronous variations (Fig. 2d). This is particularly noticeable around 39.2 ka cal BP (HE4 blue band on Fig. 2), where both cores exhibit their highest IRD concentrations, and where the respective sharp increases in IRD concentrations might be synchronous if we consider the temporal lags discussed in Sect. 4. However, the origin of the IRD composing these peaks seems to be different in each core. Indeed, in core MD99-2281, the IRD peak is associated with high Ca/Sr indicative of high detrital carbonate content. Previous studies from the North Atlantic already evidenced that IRD present in Heinrich layer 4 were mainly composed of detrital carbonate grains derived from the Hudson Strait (Snoeckx et al., 1999; Grousset et al., 2000; Hemming, 2004; Jullien et al., 2006). Furthermore, MD99-2281 IRD peak is also associated with a peak in magnetic susceptibility, usually considered as the typical signature of the Laurentide ice-sheet massive collapse events in the Atlantic Ocean (e.g. Grousset et al., 1993). At the opposite, MD99-2285 IRD peak is not associated with high Sr/Ca values nor magnetic susceptibility peak. This suggests a more proximal source, probably the European ice-sheets given site location at the outlet of major paleo ice streams which have drained the Fennoscandian and British-Irish ice-sheets (Sejrup et al., 2003; Bradwell et al., 2008; Fig. 1). Other studies have besides evidenced a strongly dominant European IRD source for Heinrich layer 4 in the Southern Norwegian Sea (Grousset et al., 2000; Snoeckx et al., 1999). Hence, these results lend support to the idea that in the Atlantic Ocean, including sites as northeast as site MD99-2281, Heinrich event 4 has a strong Laurentide imprint. At the opposite, the apparent absence of Laurentide signature during Heinrich event 4 in the Southern Norwegian Sea suggests that icebergs derived from the Laurentide ice-sheet might have been mostly restricted to the Atlantic sector during this event as already suggested by Grousset et al., 2000; the IRD delivered by the few icebergs which might have crossed the southeastern part of the Greenland-Scotland Ridge at that time are thus strongly diluted in the huge mass of European-sourced IRD. Furthermore, the possible synchronicity of both IRD peaks suggests that European and Laurentide ice-sheets might have collapsed at the same time.

Moreover, in the study area, and as observed in core MD99-2285, high IRD concentrations were often reported during GS8 interval (e.g. Elliot et al., 1998, 2001; Dokken and Jansen, 1999). Nonetheless, here, the Laurentide signature is absent from GS8 in both cores (absence of magnetic susceptibility peak and of high Sr/Ca values). This supports the idea that massive destabilization of the Laurentide ice-sheet were restricted to HS intervals, while proximal European ice sheets collapsed during both HS and GS (e.g. Elliot et al., 1998).

Furthermore, during the onset of warm advection in the Nordic Seas identified in core MD99-2285 by Wary et al. (QSR, to be submitted; yellow bands on Fig. 2), MD99-2281 IRD concentration also shows a progressive increase at GI8-GS8 transition (with nonetheless a different rate) and comparable moderate values at GI9-HS4 transition. In both cores, these periods are apparently not associated with Laurentide imprint in Xrf and magnetic susceptibility records, which suggests a European IRD source. This supports Wary et al. (QSR, to be submitted)'s hypothesis that warm Atlantic water advection plays an important role in the destabilization of proximal European ice-sheets. This also recalls for the "European precursor" concept usually mentioned for Heinrich event 4 (e.g. Snoeckx et al., 1999; Grousset et al., 2000) and other Heinrich events (e.g. Bond and Lotti, 1995; Grousset et al., 2000; Scourse et al., 2000).

5.2. Hydrological signals reflecting in situ conditions during stadials and interstadials

Contrary to advected signals, autochthonous hydrological records from the southern core MD99-2281 are rather different from those of the northern MD99-2285 site (Fig. 3). Indeed, summer SST_{dino} are relatively high (and winter SST_{dino} relatively low) throughout the whole 37-40 ka cal BP interval (Fig. 3c). However, during the phase of full advection of warm waters in the southern Norwegian Sea (blue bands on Fig. 3; cf. Wary et al., QSR, to be submitted), both SST_{dino} display comparable values in both cores. Despite the very noisy character of summer and winter SSS_{dino}, a comparable trend is observed for this hydrological parameter, with however noticeable values well below the modern one (i.e. 35.3 psu on site MD99-2281 after WOA09 data from Antonov et al., 2010; Fig. 3d). Relative and absolute abundances of *N. pachyderma* (s), indicative of subsurface hydrological conditions, also appear rather different in both cores (Fig. 3f and g). However, during GS, the nearly 100% of NPS, combined to a relatively high absolute concentration of this taxa (around 400 ind.g⁻¹ of dry sediment) and to SSS_{dino} values below the minimum requirement for optimal NPS

development (i.e. ~ 34 psu; e.g. Carstens et al., 1997; Hillaire-Marcel and de Vernal, 2008), could also be interpreted as in core MD99-2285, i.e. related to a low saline surface layer (with strong seasonal temperature contrasts) separated by a halocline from a more saline (and colder during summer) subsurface layer. During GI, the lower percentage of NPS portrays the influence of the North Atlantic Water at site MD99-2281 (cf. Wary et al., CP, in press). Such an influence is not detectable in core MD99-2285 where monospecific NPS values are still prevalent. From ~ 37.4 ka cal BP to the end of the studied interval, the percentage of NPS slightly increases at the southern site but stays relatively low ($< 70\%$). Concomitantly NPS concentration significantly increases while winter and summer SSS_{dino} exhibit higher (if even unstable) values, sometimes > 34 psu. This might be explained by a diminution of upper stratification and progressive mixing of surface and subsurface water masses, with a slight decrease of subsurface temperatures due to heat diffusion towards the topmost layers and the atmosphere. Such results support Wary et al. (CP, in press)'s findings, who reported a progressive decrease of upper stratification throughout GI intervals at a broader scale in the Nordic seas.

Hence, surface and subsurface hydrological conditions appear relatively similar in both cores during GS, with a low saline and high thermal inertia surface layer separated by a halocline and summer thermocline from a more saline (and colder during summer) subsurface layer. At the opposite, they are quite different during GI, with in core MD99-2281: (i) at a first stage, a low saline surface layer with strong thermal inertia separated by a halocline from a warm and saltier subsurface layer (made of North Atlantic Water), and (ii) at a second stage, a more homogeneous upper water column made of relatively salty and warm waters, with intense latent heat emission during winter. In core MD99-2285, GI conditions are marked by a homogeneous and cold upper water column, with winter sea ice formation (and brine extrusion responsible for the high SSS_{dino}) and summer sea ice melting (low summer SSS_{dino} ; cf. Wary et al., QSR, to be submitted).

5.3. Zoom in on GI to GS/HS transitions

While advected palynomorphs strongly suggest allochthonous advection of warm Atlantic waters on both sites at GI to GS/HS transitions (in tight relation with glacio-fluvial inputs; cf. Sect. 5.1.1), *in situ* past hydrological conditions appear completely different from

one site to the other. Indeed, the sequencing identified by Wary et al. (QSR, to be submitted) in core MD99-2285 is not detectable in core MD99-2281, where almost no change occurs in surface hydrological conditions. Conversely, while almost no change occurs in subsurface conditions in core MD99-2285, site MD99-2281 experiences a subsurface cooling. This attests of a strong difference in the local sensitivity of hydrographical conditions. However, these opposite features may be reconciled thanks to some freshwater hosing experiments conducted under modern boundary conditions (Kleinen et al., 2009; Swingedouw et al., 2013) and under glacial boundary conditions (Meniel et al., 2014; Bagniewski et al., 2015). Indeed, all these model simulations depict surface warming in the Nordic Seas and surface cooling in the North Atlantic subsequently to high latitude freshwater input. Depending on the model simulation considered, the location of the limit between the cooled area and the warmed area varies from $\sim 60^{\circ}\text{N}$ (Swingedouw et al., 2013, EC-Earth model) to $\sim 80^{\circ}\text{N}$ (Meniel et al., 2014, LOVECLIM model, see Fig. 4F in Bagniewski et al., 2015). The spatial response of subsurface temperature to the induced freshwater flux is even more heterogeneous than the surface response. When presented, the SSS response does not display a homogeneous pattern in the different models used (Swingedouw et al., 2013) or displays a scheme similar to the SST one with higher SSS in the Nordic Seas and lower ones in the North Atlantic basin (Kleinen et al., 2009). Hence, we can reasonably state that our data support and complement the scheme evidenced in these model simulations, with core MD99-2281 located in the transitional area between a cooled and less saline North Atlantic ocean, and warmed up and saltier Nordic Seas. In this transitional zone, the freshwater flux released at GI to GS/HS transition, i.e. the glacio-fluvial inputs from proximal ice-sheets, has an immediate neutral apparent impact on SST and SSS conditions (or at least, the induced change and return to similar conditions is too rapid to be caught by our dinocyst-derived records for which the temporal resolution is as “low” as 66 years on GI9-HS4 transition).

Furthermore, the GI8-GS8 transition period (from ~ 37.4 ka cal BP to the end of the studied interval) is identified by a progressive decrease of upper stratification at site MD99-2281 with also a progressive increase in IRD concentration and likely higher SSS_{dino} (Fig. 3). In core MD99-2285, this time interval is related to the onset of warm Atlantic water advection in the Norwegian Sea (cf. Fig. 2 and Wary et al., QSR, to be submitted). Hence, we can hypothesize that this change in upper stratification at site MD99-2281 constitutes the imprint of this advection of warm and saline waters, and that site MD99-2281 lies in the area where these subsurface advected waters re-emerge to the surface / near-surface and mix with

ambient brackish waters. Upper stratification would have later set up again at this site as soon as freshwater inputs from iceberg melting would have become sufficient (during GS), while advection of warm Atlantic waters would have continued, with a resurgence center probably slightly moving South(west). Nonetheless, in this area, the subsurface impact of these warm advected and upwelled waters is apparently undetectable during these transitions because “hidden” by the concomitant and stronger subsurface cooling due to a weakening of the North Atlantic Current (NAC). This latter subsurface cooling is, conversely, imperceptible at site MD99-2285, apparently located north of the NAC glacial northward limit. This NAC weakening echoes the AMOC slowdown evidenced in model simulations in response to the freshwater flux. It is worth noting that this decrease of upper stratification is not recorded at GI9-HS4 transition, maybe in relation with insufficient temporal resolution of analyses.

Moreover, according to [Wary et al. \(CP, in press\)](#)'s data and interpretations from core MD99-2281, the upper stratification progressively decreases throughout GI8, 7, 6 and 5, and seems to decrease more drastically to minimal values at the end of these periods. If our hypotheses prove to be correct, such recurring drastic decrease of upper stratification at the end of GI would support the idea that the hydrological processes evidenced in model simulations ([Kleinen et al., 2009](#); [Swingedouw et al., 2013](#)), in [Wary et al. \(QSR, to be submitted\)](#), and in the present study, occurred at each GI to GS/HS transition. In such a case, these decreases of upper stratification at the end of GI could be due to the combined effect of (i) upward destabilization of the halocline by warmer subsurface waters, and (ii) onset of advection and upwelling of warm and salty Atlantic surface waters.

Furthermore, coeval to the main IRD peak (around 39.2 ka cal BP), NPS concentration exhibits a significant decrease in core MD99-2281 but not in core MD99-2285. Such a feature might be explained by a sudden rupture of upper stratification at site MD99-2281 caused by iceberg calving derived from the Laurentide ice-sheet. Indeed, initial iceberg thickness may be as high as 600 m (see [Dowdeswell and Ottesen, 2013](#) and references therein), which is amply sufficient to break a halocline located above 250 m water depth (i.e. the downward limit of the mean depth range inhabited by NPS in the study area, e.g. [Carstens et al., 1997](#); [Simstich et al., 2003](#)). These icebergs would have crossed the cooled Atlantic Ocean, and kept a sufficient thickness to break the halocline at site MD99-2281. At the opposite, icebergs derived from the European ice-sheets would have crossed areas with warm SST. These high SST could have considerably reduced their size to thickness inferior to the halocline water

depth, and European icebergs would have thus not broken the halocline neither on site MD99-2285 nor on site MD99-2281. Such a feature could furthermore explain the spatial distribution of European *versus* Laurentian IRD, with massive Laurentian icebergs mostly unable to cross the Greenland-Scotland Ridge, contrary to the smaller European icebergs.

6. Conclusion

The present study investigates at very high temporal resolution the hydrological surface and subsurface conditions prevailing at site MD99-2281 (southwest off Faeroes) on the 35-40 ka cal BP time interval (spanning GI9, HS4 and GI8). Our multiproxy records are compared with similar high resolution records obtained on the 35-41 ka cal BP section of core MD99-2285 located northeast off Faeroes. Our results support and complement the scheme previously evidenced in model simulations (Kleinen et al., 2009; Swingedouw et al., 2013) and in Wary et al. (QSR, to be submitted) where high latitude freshwater inputs induce enhanced advection of warm Atlantic waters in the Nordic Seas at GI to GS/HS transitions. In model simulations, such processes lead to a surface cooling in the North Atlantic Ocean and to surface warming in the Nordic Seas, this latter feature being supported by MD99-2285 data and Eynaud et al. (2002)'s data. Our results strongly suggest that site MD99-2281 lies in the transitional zone in-between the cooled-down and warmed-up areas, where subsurface advected Atlantic waters re-emerge to the surface. They also strongly suggest that the initial freshwater flux might be the result of glacio-fluvial inputs from European ice-sheets, but do not exclude a potential contribution from the other pan-Atlantic ice-sheets (Greenland and Laurentide ones). More specifically to Heinrich event 4, our study supports the strong Laurentide signature of this event in the Atlantic Ocean as northeast as site MD99-2281, and suggests that icebergs derived from the Laurentide ice-sheet did not cross the Iceland-Scotland Ridge during this event. It also supports the idea that Laurentide massive collapse episodes might have been restricted to HS intervals, while European ice-sheets apparently collapsed during both GS and HS. Our results also support the idea that enhanced advection of warm Atlantic waters at the end of GI played an important role on European ice-sheet destabilization, including GI9 before Heinrich event 4 which recalls for the "European precursor" concept.

Furthermore, some discrete evidences suggest that the hydrological mechanisms discussed here might have occurred at each GI to GS/HS transitions of the last glacial period. However, new high resolution multiproxy reconstructions focused on other time intervals are needed to confirm such a scheme. Moreover, additional SST reconstructions are needed in the subpolar North Atlantic Ocean to confirm the surface cooling evidenced in model simulations. But, contrary to what was usually done previously, they should not be based on planktonic foraminifera analyses which could rather reflect subsurface conditions, particularly if these low SST are associated with low SSS as suggested by [Kleinen et al. \(2009\)](#)'s simulations. SST derived from dinocyst assemblages or alkenone analyses thus constitute potential alternative methods.

References

- Andersen, K.K., Svensson, A., Johnsen, S.J., Rasmussen, S.O., Bigler, M., Röthlisberger, R., Ruth, U., Siggaard-Andersen, M.L., Peder Steffensen, J., Dahl-Jensen, D., Vinther, B.M., Clausen, H.B., 2006. The Greenland Ice Core Chronology 2005, 15-42 ka. Part 1: constructing the time scale. *Quaternary Science Reviews* 25, 3246-3257.
- Antonov, J.I., Seidov, D., Boyer, T.P., Locarnini, R.A., Mishonov, A.V., Garcia, H.E., Baranova, O.K., Zweng, M.M., Johnson, D.R., 2010. *World Ocean Atlas 2009, Volume 2: Salinity*, Ed. NOAA Atlas NESDIS 69, U.S. Government Printing Office, Washington, D.C. ed.
- Bagniewski, W., Meissner, K.J., Menviel, L., Brennan, C.E., 2015. Quantification of factors impacting seawater and calcite $\delta^{18}O$ during Heinrich Stadials 1 and 4. *Paleoceanography* 30, 895-911.
- Böhm, E., Lippold, J., Gutjahr, M., Frank, M., Blaser, P., Antz, B., Fohlmeister, J., Frank, N., Andersen, M.B., Deininger, M., 2015. Strong and deep Atlantic meridional overturning circulation during the last glacial cycle. *Nature* 517, 73-76.
- Boldreel, L.O., Andersen, M.S., Kuijpers, A., 1998. Neogene seismic facies and deep-water gateways in the Faeroe Bank area, NE Atlantic. *Marine Geology* 152, 129-140.
- Bond, G., Heinrich, H., Broecker, W., Labeyrie, L., McManus, J., Andrews, J., Huon, S., Jantschik, R., Glasen, S., Simet, C., Tedesco, K., Klas, M., Bonanitt, G., Ivy, S., 1992. Evidence for massive discharges of icebergs into the North Atlantic ocean during the last glacial period. *Nature* 360, 245-XLIII.
- Bond, G.C., Lotti, R., 1995. Iceberg discharges into the North Atlantic on millennial time scales during the last glaciation. *Science* 267, 1005-1010.
- Borenäs, K., Lundberg, P., 2004. The Faeroe-Bank Channel deep-water overflow. *Deep-Sea Research Part II: Topical Studies in Oceanography* 51, 335-350.
- Bradwell, T., Stoker, M.S., Golledge, N.R., Wilson, C.K., Merritt, J.W., Long, D., Everest, J.D., Hestvik, O.B., Stevenson, A.G., Hubbard, A.L., Finlayson, A.G., Mathers, H.E., 2008. The northern sector of the last British Ice Sheet: Maximum extent and demise. *Earth-Science Reviews* 88, 207-226.
- Carstens, J., Hebbeln, D., Wefer, G., 1997. Distribution of planktic foraminifera at the ice margin in the Arctic (Fram Strait). *Marine Micropaleontology* 29, 257-269.
- Dansgaard, W., Johnsen, S.J., Clausen, H.B., Dahl-Jensen, D., Gundestrup, N.S., Hammer, C.U., Hvidberg, C.S., Steffensen, J.P., Sveinbjörnsdóttir, A.E., Jouzel, J., Bond, G., 1993. Evidence for general instability of past climate from a 250-kyr ice-core record. *Nature* 364, 218-220.
- Dokken, T.M., Jansen, E., 1999. Rapid changes in the mechanism of ocean convection during the last glacial period. *Nature* 401, 458-461.
- Dokken, T.M., Nisancioglu, K.H., Li, C., Battisti, D.S., Kissel, C., 2013. Dansgaard-Oeschger cycles: Interactions between ocean and sea ice intrinsic to the Nordic seas. *Paleoceanography* 28, 491-502.
- Dowdeswell, J.A., Ottesen, D., 2013. Buried iceberg ploughmarks in the early Quaternary sediments of the central North Sea: A two-million year record of glacial influence from 3D seismic data. *Marine Geology* 344, 1-9.
- Elliot, M., Labeyrie, L., Bond, G., Cortijo, E., Turon, J.L., Tisnerat, N., Duplessy, J.C., 1998. Millennial-scale iceberg discharges in the Irminger Basin during the last glacial period: Relationship with the Heinrich events and environmental settings. *Paleoceanography* 13, 433-446.
- Elliot, M., Labeyrie, L., Dokken, T., Manthe, S., 2001. Coherent patterns of ice-rafted debris deposits in the Nordic regions during the last glacial (10-60 ka). *Earth and Planetary Science Letters* 194, 151-163.
- Eynaud, F., Turon, J.L., Matthiessen, J., Kissel, C., Peypouquet, J.P., De Vernal, A., Henry, M., 2002. Norwegian sea-surface palaeoenvironments of marine oxygen-isotope stage 3: The paradoxical response of dinoflagellate cysts. *Journal of Quaternary Science* 17, 349-359.
- Eynaud, F., Zaragosi, S., Scourse, J.D., Mojtahid, M., Bourillet, J.F., Hall, I.R., Penaud, A., Locascio, M., Reijonen, A., 2007. Deglacial laminated facies on the NW European continental margin: The hydrographic significance of British-Irish Ice Sheet deglaciation and Fleuve Manche paleoriver discharges. *Geochemistry, Geophysics, Geosystems* 8.
- Grousset, F.E., 1993. Patterns of ice-rafted detritus in the glacial North Atlantic (40- 55°N). *Paleoceanography* 8, 175-192.
- Grousset, F.E., Pujol, C., Labeyrie, L., Auffret, G., Boelaert, A., 2000. Were the North Atlantic Heinrich events triggered by the behavior of the European ice sheets? *Geology* 28, 123-126.
- Hansen, B., Osterhus, S., 2000. North Atlantic-Nordic Sea exchanges. *Progress in Oceanography* 45, 109-208.
- Heinrich, H., 1988. Origin and consequences of cyclic ice rafting in the Northeast Atlantic Ocean during the past 130,000 years. *Quaternary Research* 29, 142-152.
- Hemming, S.R., 2004. Heinrich events: Massive late Pleistocene detritus layers of the North Atlantic and their global climate imprint. *Reviews of Geophysics* 42, RG1005 1001-1043.
- Hillaire-Marcel, C., de Vernal, A., 2008. Stable isotope clue to episodic sea ice formation in the glacial North Atlantic. *Earth and Planetary Science Letters* 268, 143-150.
- Jullien, E., Grousset, F.E., Hemming, S.R., Peck, V.L., Hall, I.R., Jeantet, C., Billy, I., 2006. Contrasting conditions preceding MIS3 and MIS2 Heinrich events. *Global and Planetary Change* 54, 225-238.
- Kenyon, N.H., 1986. Evidence from bedforms for a strong poleward current along the upper continental slope of northwest Europe. *Marine Geology* 72, 187-198.
- Kissel, C., Laj, C., Labeyrie, L., Dokken, T., Voelker, A., Blamart, D., 1999. Rapid climatic variations during marine isotopic stage 3: Magnetic analysis of sediments from Nordic Seas and North Atlantic. *Earth and Planetary Science Letters* 171, 489-502.
- Kleinen, T., Osborn, T.J., Briffa, K.R., 2009. Sensitivity of climate response to variations in freshwater hosing location. *Ocean Dynamics* 59, 509-521.
- Kuijpers, A., Andersen, M.S., Kenyon, N.H., Kunzendorf, H., Van Weering, T.C.E., 1998a. Quaternary sedimentation and Norwegian Sea overflow pathways around Bill Bailey Bank, northeastern Atlantic. *Marine Geology* 152, 101-127.
- Kuijpers, A., Troelstra, S.R., Wisse, M., Nielsen, S.H., Van Weering, T.C.E., 1998b. Norwegian Sea overflow variability and NE Atlantic surface hydrography during the past 150,000 years. *Marine Geology* 152, 75-99.
- Locarnini, R.A., Mishonov, A.V., Antonov, J.I., Boyer, T.P., Garcia, H.E., Baranova, O.K., Zweng, M.M., Johnson, D.R., 2010. *World Ocean Atlas 2009, Volume 1: Temperature*, Ed. NOAA Atlas NESDIS 68, U.S. Government Printing Office, Washington, D.C. ed.
- Matthiessen, J., Kunz-Pirrung, M., Mudie, P.J., 2000. Freshwater chlorophycean algae in recent marine sediments of the Beaufort, Laptev and Kara Seas (Arctic Ocean) as indicators of river runoff. *International Journal of Earth Sciences* 89, 470-485.
- Mauritzen, C., Price, J., Sanford, T., Torres, D., 2005. Circulation and mixing in the Faroese Channels. *Deep-Sea Research Part I: Oceanographic Research Papers* 52, 883-913.
- McCartney, M.S., Mauritzen, C., 2001. On the origin of the warm inflow to the Nordic Seas. *Progress in Oceanography* 51, 125-214.
- Menviel, L., Timmermann, A., Friedrich, T., England, M.H., 2014. Hindcasting the continuum of Dansgaard-Oeschger variability: mechanisms, patterns and timing. *Clim. Past* 10, 63-77.
- Mojtahid, M., Eynaud, F., Zaragosi, S., Scourse, J., Bourillet, J.F., Garlan, T., 2005. Palaeoclimatology and palaeohydrography of the glacial stages on Celtic and Armorican margins over the last 360 000 yrs. *Marine Geology* 224, 57-82.
- Mudie, P.J., 1992. Circum-Arctic Quaternary and Neogene marine palynofloras: paleoecology and statistical analysis.

- Neogene and Quaternary dinoflagellate cysts and acritarchs 10, 347-390.
- Nielsen, T., Rasmussen, T.L., Ceramicola, S., Kuijpers, A., 2007. Quaternary sedimentation, margin architecture and ocean circulation variability around the Faroe Islands, North Atlantic. *Quaternary Science Reviews* 26, 1016-1036.
- Orvik, K.A., Niiler, P., 2002. Major pathways of Atlantic water in the northern North Atlantic and Nordic Seas toward Arctic. *Geophysical Research Letters* 29, 2-1.
- Penaud, A., Eynaud, F., Turon, J.L., Zaragosi, S., Malaizé, B., Toucanne, S., Bourillet, J.F., 2009. What forced the collapse of European ice sheets during the last two glacial periods (150 ka B.P. and 18 ka cal B.P.)? Palynological evidence. *Palaeogeography, Palaeoclimatology, Palaeoecology* 281, 66-78.
- Rahmstorf, S., 2002. Ocean circulation and climate during the past 120,000 years. *Nature* 419, 207-214.
- Rasmussen, T.L., Thomsen, E., 2004. The role of the North Atlantic Drift in the millennial timescale glacial climate fluctuations. *Palaeogeography, Palaeoclimatology, Palaeoecology* 210, 101-116.
- Rasmussen, T.L., Thomsen, E., Labeyrie, L., Van Weering, T.C.E., 1996a. Circulation changes in the Faeroe-Shetland Channel correlating with cold events during the last glacial period (58-10 ka). *Geology* 24, 937-940.
- Rasmussen, T.L., Thomsen, E., Van Weering, T.C.E., Labeyrie, L., 1996b. Rapid changes in surface and deep water conditions at the Faeroe Margin during the last 58,000 years. *Paleoceanography* 11, 757-771.
- Rasmussen, T.L., Van Weering, T.C.E., Labeyrie, L., 1996c. High resolution stratigraphy of the Faeroe-Shetland Channel and its relation to North Atlantic paleoceanography: The last 87 kyr. *Marine Geology* 131, 75-88.
- Rasmussen, T.L., Van Weering, T.C.E., Labeyrie, L., 1997. Climatic instability, ice sheets and ocean dynamics at high northern latitudes during the last glacial period (58-10 KA BP). *Quaternary Science Reviews* 16, 71-80.
- Sachs, J.P., Lehman, S.J., 1999. Subtropical North Atlantic temperatures 60,000 to 30,000 years ago. *Science* 286, 756-760.
- Sanchez Goñi, M.F., Harrison, S.P., 2010. Millennial-scale climate variability and vegetation changes during the Last Glacial: Concepts and terminology. *Quaternary Science Reviews* 29, 2823-2827.
- Scourse, J.D., Hall, I.R., McCave, I.N., Young, J.R., Sugdon, C., 2000. The origin of Heinrich layers: evidence from H2 for European precursor events. *Earth and Planetary Science Letters* 182, 187-195.
- Sejrup, H.P., Larsen, E., Hafliðason, H., Berstad, I.M., Hjelstuen, B.O., Jonsdottir, H.E., King, E.L., Landvik, J., Longva, O., Nygard, A., Ottesen, D., Raunholm, S., Rise, L., Stalsberg, K., 2003. Configuration, history and impact of the Norwegian Channel Ice Stream. *Boreas* 32, 18-36.
- Simstich, J., Sarnthein, M., Erlenkeuser, H., 2003. Paired $\delta^{18}O$ signals of *Neogloboquadrina pachyderma* (s) and *Turborotalita quinqueloba* show thermal stratification structure in Nordic Seas. *Marine Micropaleontology* 48, 107-125.
- Snoeckx, H., Grousset, F., Revel, M., Boelaert, A., 1999. European contribution of ice-rafted sand to Heinrich layers H3 and H4. *Marine Geology* 158, 197-208.
- Svendsen, J.I., Alexanderson, H., Astakhov, V.I., Demidov, I., Dowdeswell, J.A., Funder, S., Gataullin, V., Henriksen, M., Hjort, C., Houmark-Nielsen, M., Hubberten, H.W., Ingólfsson, O., Jakobsson, M., Kjær, K.H., Larsen, E., Lokrantz, H., Lunkka, J.P., Lyså, A., Mangerud, J., Matoriouchkov, A., Murray, A., Möller, P., Niessen, F., Nikolskaya, O., Polyak, L., Saarnisto, M., Siegert, C., Siegert, M.J., Spielhagen, R.F., Stein, R., 2004. Late Quaternary ice sheet history of northern Eurasia. *Quaternary Science Reviews* 23, 1229-1271.
- Svensson, A., Andersen, K.K., Bigler, M., Clausen, H.B., Dahl-Jensen, D., Davies, S.M., Johnsen, S.J., Muscheler, R., Parrenin, F., Rasmussen, S.O., Röthlisberger, R., Seierstad, I., Steffensen, J.P., Vinther, B.M., 2008. A 60 000 year Greenland stratigraphic ice core chronology. *Climate of the Past* 4, 47-57.
- Swingedouw, D., Rodehacke, C.B., Behrens, E., Menary, M., Olsen, S.M., Gao, Y., Mikolajewicz, U., Mignot, J., Biastoch, A., 2013. Decadal fingerprints of freshwater discharge around Greenland in a multi-model ensemble. *Climate Dynamics* 41, 695-720.
- Telford, R.J., Li, C., Kucera, M., 2013. Mismatch between the depth habitat of planktonic foraminifera and the calibration depth of SST transfer functions may bias reconstructions. *Climate of the Past* 9, 859-870.
- Tolderlund, D.S., Bé, A.W.H., 1971. Seasonal Distribution of Planktonic Foraminifera in the Western North Atlantic. *Micropaleontology* 17, 297-329.
- Wolff, E.W., Chappellaz, J., Blunier, T., Rasmussen, S.O., Svensson, A., 2010. Millennial-scale variability during the last glacial: The ice core record. *Quaternary Science Reviews* 29, 2828-2838.
- Zaragosi, S., Eynaud, F., Pujol, C., Auffret, G.A., Turon, J.L., Garlan, T., 2001. Initiation of the European deglaciation as recorded in the northwestern Bay of Biscay slope environments (Meriadzek Terrace and Trevelyan Escarpment): A multi-proxy approach. *Earth and Planetary Science Letters* 188, 493-507.
- Zumaque, J., Eynaud, F., Zaragosi, S., Marret, F., Matsuzaki, K.M., Kissel, C., Roche, D.M., Malaizé, B., Michel, E., Billy, I., Richter, T., Palis, E., 2012. An ocean-ice coupled response during the last glacial: a view from a marine isotopic stage 3 record south of the Faeroe Shetland Gateway. *Climate of the Past* 8, 1997-2017.

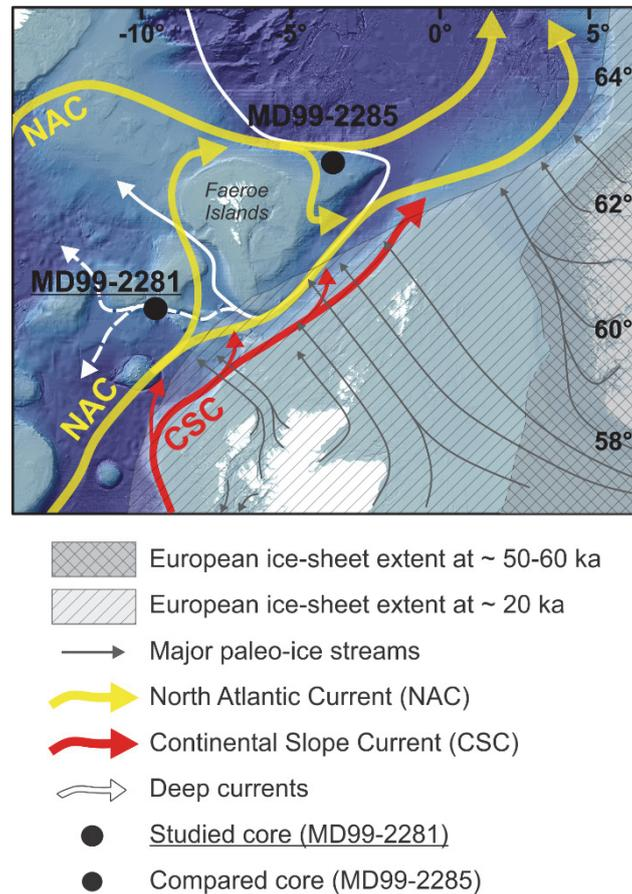


Figure 1: Map of the study area showing the location of the studied core (MD99-2281) and of the compared core (MD99-2285), the modern surface currents (after Kenyon, 1986; Orvik and Niiler, 2002) and deep currents (after Boldreel, 1998; Kuijpers et al., 1998a,b), the last glacial ice-sheet extensions (after Svendsen et al., 2004) and locations of major paleo-ice streams (after Sejrup et al., 2003 and Bradwell et al., 2008).

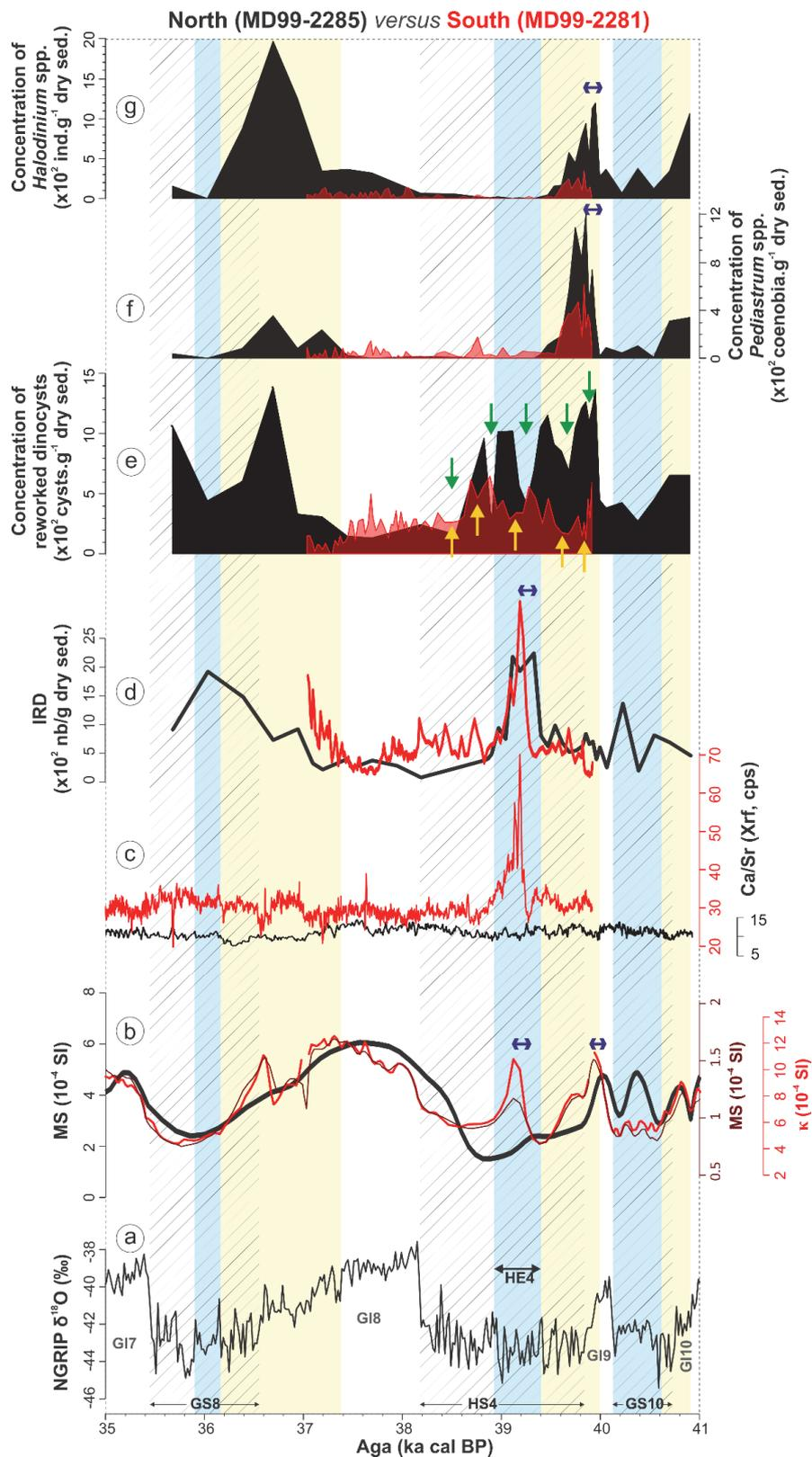


Figure 2: Age compilation of proxies indicative of surface advection and chronological framework for cores MD99-2281 (red) and MD99-2285 (black). (a) NGRIP $\delta^{18}\text{O}$ record. (b) Magnetic susceptibility (MS) and low field magnetic susceptibility (κ). (c) Ca/Sr Xrf ratio. (d) Ice-rafted debris concentration. (e) Reworked dinocyst concentration. (f) Concentration of Coenobia of Pediastrum spp. (g) Concentration of Halodinium spp.

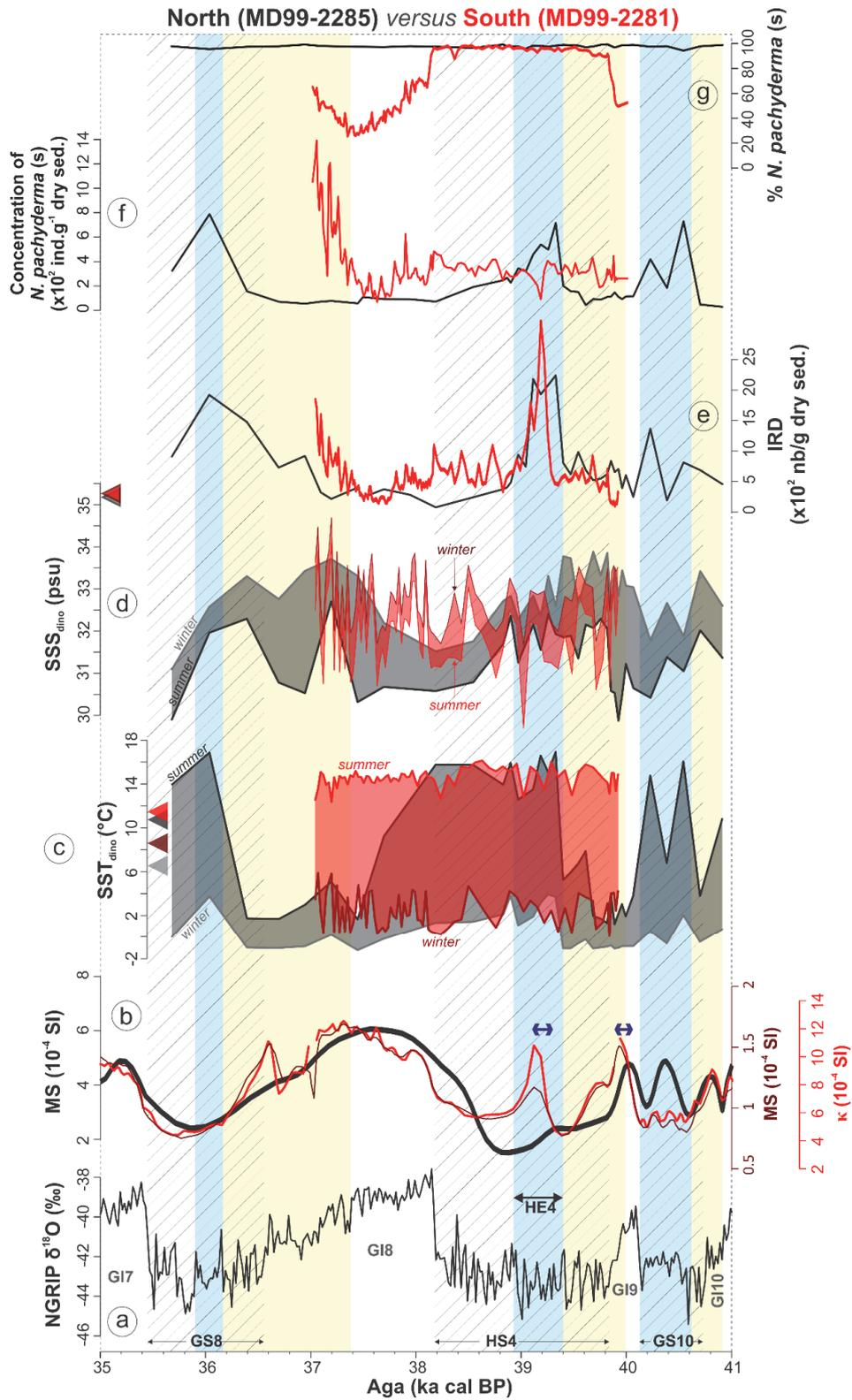


Figure 3: Age compilation of proxies indicative of in situ hydrological conditions and chronological framework for cores MD99-2281 (red) and MD99-2285 (black). (a) NGRIP $\delta^{18}O$ record. (b) Magnetic susceptibility (MS) and low field magnetic susceptibility (κ). (c) SST stemming from dinocyst analyses. (d) SSS stemming from dinocyst analyses. (e) Ice-rafted debris concentration. (f) Concentration of *N. pachyderma* sinistral coiling. (g) Relative abundance of *N. pachyderma* sinistral coiling.

Partie 2 : Processus hydrographiques et mécanismes de déclenchement en jeu lors des événements climatiques abrupts avant, pendant et après un HE : zoom sur la période 35-41 ka autour d'HE4.

Table 1: Temporal resolution of the different analyses conducted on section 1792-1941 cm (i.e. ~ 37-40 ka cal BP) of core MD99-2281.

Sampling frequency		0.2 cm	1 cm	2 cm
Proxies		Xrf	Planktonic foraminifera analyses, IRD	Magnetic susceptibility, palynological analyses
Temporal resolution (years)	minimal	2	10	20
	maximal	7	33	66
	mean	4	19	38

Section 3. Complément à l'étude de la carotte MD99-2285

Les paramètres hydrologiques de surface et de subsurface utilisés pour mettre en évidence le séquençage des processus hydrologiques au cours des événements de Dansgaard-Oeschger 10 à 8 et d'Heinrich 4 montrent des tendances similaires (à plus basse résolution) sur l'ensemble de la section glaciaire de la carotte MD99-2285 (Figure 35). En effet :

- Comme précédemment illustré dans Wary et al. (JQS¹, submitted), les conditions hydrologiques de surface atypiques mises en évidence sur l'intervalle 35-41 ka cal BP sont similaires pour l'ensemble des événements climatiques millénaires de la dernière période glaciaire. Ainsi, chaque GS/HS se caractérise par des SST_{dino} élevées, un couvert de glace réduit, et des débâcles d'icebergs soutenues. A l'inverse, les GI sont marqués par des conditions de surface froides, avec un couvert de glace de mer important et peu de vêlage d'icebergs (Figure 35b, c, et d).
- Les paramètres précédemment reliés à l'advection d'eaux chaudes atlantiques (concentrations en dinokystes remaniés et algues d'eau douce ; Figure 35e, f et g) montrent également des valeurs élevées juste avant chaque GS et HS de la dernière période glaciaire (exceptés HS3b, et éventuellement HS1 où le pic de palynomorphes advectés est enregistré environ 200 ans avant le début de l'évènement). Malgré l'absence d'enregistrement SST issu des alcénones sur cette section, et malgré une plus faible résolution, ceci pourrait là encore traduire l'arrivée d'eaux atlantiques sur la zone d'étude quelques siècles avant le réchauffement *in situ* des eaux de surface.
- La concentration absolue en *N. pachyderma* senestre (Figure 35i), ainsi que l'abondance relative de *B. tepikiense* (cf. Wary et al., JQS, submitted), sont relativement élevées lors de chaque GS et HS (excepté sur l'intervalle GS6 à HS3a, et lors du GS4). Ceci tend également à indiquer une stratification plus importante du sommet de la colonne d'eau lors de ces épisodes, isolant la subsurface des faibles salinités de surface (cf. enregistrement des SSS_{dino} dans Wary et al., JQS, submitted), et permettant ainsi le développement de *N. pachyderma* senestre en subsurface.

¹ cf. page 127 de ce manuscrit

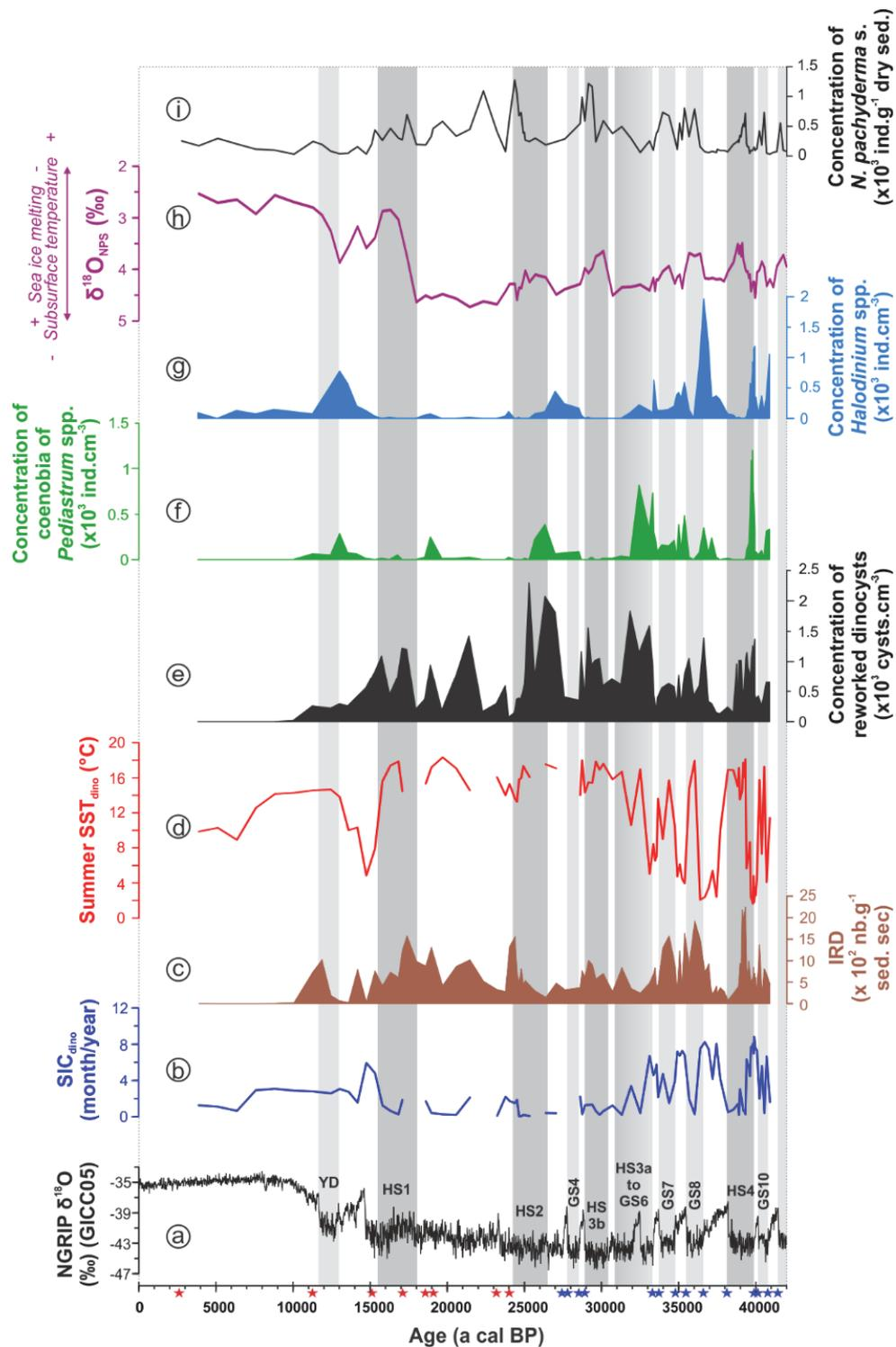


Figure 35 : Evolution temporelle sur la section 3-41 ka cal BP de la carotte MD99-2285 de certains paramètres hydrologiques de surface et subsurface utilisés pour mettre en évidence le séquençage des processus hydrologiques au cours des événements de Dansgaard-Oeschger 10 à 8 incluant l'évènement d'Heinrich 4. (a) Enregistrement du $\delta^{18}\text{O}$ de NGRIP, et cadre chrono-stratigraphique. (b) SIC_{dino} . (c) Concentration en IRD $> 150 \mu\text{m}$. (d) SST_{dino} pour la période estivale. (e) Concentration en dinokystes remaniés. (f) Concentration des colonies de *Pediastrum* spp. (g) Concentration en *Halodinium* spp. (h) $\delta^{18}\text{O}$ mesuré sur *N. pachyderma senestre*. (i) Concentration absolue en *N. pachyderma senestre*.

- Le signal de $\delta^{18}\text{O}$ mesuré sur *N. pachyderma* senestre montre également des valeurs plus lourdes lors des GI, et plus légères lors des GS et HS (Figure 35h). L'amplitude des variations est similaire à celle mise en évidence sur la section 35-41 ka cal BP, excepté au cours de HS1. Lors de cet épisode, la diminution en $\delta^{18}\text{O}$ est plus importante, de l'ordre de 1.6 ‰. Cette forte diminution pourrait englober à la fois le changement local de $\delta^{18}\text{O}$ enregistré ici lors des transitions GI à GS/HS, et la variation globale de $\delta^{18}\text{O}$ classiquement enregistrée lors des transitions glaciaire à interglaciaire (i.e. 1.05 ‰, Waelbroeck et al., 2002). Par ailleurs, du fait de l'apparente stratification de la colonne d'eau en GS/HS, les faibles valeurs de $\delta^{18}\text{O}$ enregistrées lors de ces épisodes sont probablement également liées à la combinaison entre élévation de quelques mètres du niveau marin et réchauffement de quelques degrés des eaux de subsurface.

Cette étroite similitude entre les enregistrements haute résolution de la section 35-41 ka cal BP et les enregistrements « basse résolution » sur l'ensemble de la section glaciaire de la carotte MD99-2285 supporte l'hypothèse avancée dans Wary et al. (QSR, to be submitted, et EPSL, to be submitted) suggérant que la séquence hydrologique mise en évidence pour les événements de Dansgaard-Oeschger 10 à 8 (incluant HS4) puisse également caractériser l'ensemble des événements de Dansgaard-Oeschger et d'Heinrich de la dernière période glaciaire sur la zone d'étude.

Partie 3 : Vue synthétique et synoptique de la paléocéanographie de l'Atlantique subboréal et de ses mers bordières au cours des événements millénaires de la dernière période glaciaire

Section 1. Warm and nearly ice-free Norwegian Sea during MIS3 Greenland stadials

*Article en préparation en vue d'une soumission à **Nature**.*

Wary Mélanie¹, Eynaud Frédérique¹, Swingedouw Didier¹, Rossignol Linda¹, Zumaque Jéna¹,
Masson-Delmotte Valérie², Kissel Catherine², Jouzel Jean², Matthiessen Jens³, Roche
Didier^{2,4}

¹UMR5805, EPOC (Environnements et Paléoenvironnements Océaniques), Université de
Bordeaux, 33615 Pessac, France.

²UMR8212, LSCE (Laboratoire des Sciences du Climat et de l'Environnement), CEA/CNRS-
INSU/UVSQ, 91191 Gif-sur-Yvette CEDEX, France.

³AWI (Alfred Wegener Institute), Helmholtz Centre for Polar and Marine Research, 27568
Bremerhaven, Germany.

⁴Earth and Climate Cluster, Faculty of Earth and Life Sciences, Vrije Universiteit Amsterdam,
Amsterdam, The Netherlands.

Résumé

Les données issues des carottes de glace du Groenland ont révélé l'existence, durant la dernière période glaciaire, de variations climatiques abruptes où alternent périodes chaudes (interstadias) et périodes froides (stadias) à une échelle millénaire¹. Diverses archives marines de l'Atlantique Nord et expériences de modélisation ont montré que, comparé aux interstadias, les stadias étaient également caractérisés par d'importantes décharges d'icebergs et d'eau de fonte², une circulation océanique méridienne en Atlantique Nord affaiblie³⁻⁵, et des températures océaniques de surface (SST) plus froides⁶. Certaines études de modélisation^{4,7} ont suggéré que les Mers Nordiques étaient englacées lors des stadias, contribuant ainsi aux fortes amplitudes thermiques enregistrées au Groenland. Cette hypothèse a été appuyée par quelques études paléoclimatiques⁸⁻¹¹ basées sur des proxys indirects, mais n'a toujours pas été confirmée au travers de reconstructions directes du couvert de glace de mer. Notre étude, qui s'appuie sur des reconstructions quantifiées issues des assemblages de dinokystes et obtenues sur quatre carottes sédimentaires prélevées en Atlantique Nord-Est et Mer de Norvège, suggère au contraire que les Mers Nordiques ont connu un schéma tout autre durant le MIS 3 (30-48 ka BP). En effet, durant les stadias, ce bassin était marqué par des SST plus chaudes, un contraste saisonnier plus fort, et un couvert de glace réduit. Pour étayer ces résultats, nous les comparons à des expériences de type « *freshwater hosing* » conduites avec cinq modèles climatiques de dernière génération. En accord avec nos observations, ces simulations montrent un réchauffement dans les Mers Nordiques en réponse à un apport d'eau douce en Atlantique Nord tel qu'enregistré lors des stadias. Par ailleurs, les données issues d'un taxon polaire mésopélagique de foraminifère planctonique indiquent des variations de la circulation océanique en Atlantique Nord cohérentes avec la littérature. Nous proposons ainsi un nouveau paradigme où, lors des stadias, la circulation océanique méridienne est réduite du fait de fortes décharges d'icebergs et d'eau douce, et les SST sont plus froides en Atlantique Nord, excepté dans les Mers Nordiques où un afflux réduit d'eau atlantique se répand en surface, se mélange avec les eaux polaires ambiantes, et réchauffe ainsi les niveaux supérieurs de la colonne d'eau tout en limitant l'expansion de la glace de mer. Ce nouveau paradigme pourrait avoir d'importantes conséquences en termes d'estimation de l'impact climatique de la fonte actuelle de la calotte groenlandaise.

Greenland ice core data first revealed the existence during the last glacial period of millennial abrupt climatic variations between warm (interstadial) and cold (stadial) conditions¹. Marine archives from the North Atlantic and model experiments showed that, compared to interstadials, stadials were also marked by iceberg melting², a weaker North Atlantic meridional circulation³⁻⁵, and colder sea-surface temperatures (SST)⁶. A few modeling studies^{4,7} have up to now also suggested that Nordic Seas were ice-covered during stadials, contributing to the large temperature signature offset recorded over Greenland. This hypothesis has been supported by some paleoclimatic studies⁸⁻¹¹ based on indirect proxies, but has still not been confirmed through direct reconstructions of sea-ice cover. Here we show, using quantitative sea-surface reconstructions derived from dinocyst assemblages and conducted on four sediment cores from the northern North Atlantic and southern Norwegian Sea, that, on the contrary, Nordic Seas experienced a different scheme during Marine Isotopic Stage 3 (48,000 to 30,000 years before present). Indeed, during stadials, they recorded warmer SST marked by stronger seasonal contrasts and a shorter seasonal sea-ice cover duration. To support these results, we compare them with freshwater hosing experiments from five state-of-the-art climate models. Consistently with our observations, the simulations do show a large warming in the Nordic Seas in response to freshwater input in the North Atlantic as experienced during stadials. In addition, data acquired from a mesopelagic foraminifera species indicate variations of the oceanic meridional circulation coherent with literature, i.e. signaling a southward migration of polar waters during stadials. Our new paradigm therefore proposes that stadials encountered reduced Atlantic overturning due to large iceberg and meltwater fluxes, colder SST in the North Atlantic, except in the Nordic Seas where a small flow of Atlantic waters, mixed with polar waters, spreads in surface, warms up the topmost layer and limits sea-ice extent. This new paradigm may have important consequences concerning estimation of climatic impact of on-going Greenland melting.

High resolution reconstructions of sea-surface *sensu stricto* conditions focused on Greenland stadial (GS) / interstadial (GI) variability are very sparse within the subpolar North Atlantic and adjacent Nordic Seas. Cold sea-surface temperatures (SST) during GS were inferred from indirect evidence, such as the relative abundance of the planktonic foraminifera species *Neogloboquadrina pachyderma* sinistral coiling (NPS) – whose the preferential depth habitat

lies from a few dozens of meters to around 250 meters water depth^{12,13} – coupled to the significant increases in ice-rafted debris indicative of broad iceberg releases^{2,10,14,15}.

Here we investigate variations of sea-surface *sensu stricto* conditions within a new regional compilation regrouping three Norwegian Sea cores and one northern North Atlantic core (Fig. 1a) over the 30-48 ka cal BP period. Quantitative SST and sea-ice cover (SIC) duration were estimated from transfer functions applied to dinocysts assemblages using the modern analogue technique¹⁶. For cores MD99-2281, MD99-2285 and MD95-2009, age models were established on the basis of radiocarbon AMS ¹⁴C dates coupled to additional tie-points obtained by correlating the magnetic susceptibility (MS) records with the NGRIP $\delta^{18}\text{O}$ signal (GICC05 time scale¹⁷), in line with the current consensus that increases (respectively decreases) in MS are synchronous with abrupt warmings (respectively beginning of stadials; Methods)^{5,18}. For core MD95-2010, we used the initially published age model⁸ made of ¹⁴C dates combined to climate-independent control point (tephrochronology), keeping in mind that this method can lead to stratigraphical discrepancies compared to NGRIP GICC05 age scale and hence to the three other cores.

Previous paleoceanographic studies^{19,20} have shown that this study area recorded very sensitive sea-surface responses to the millennial climatic variability over the Marine Isotopic Stage (MIS) 3 period, probably in relation to its modern nodal oceanic position (Fig. 1). Our results highlight such a sensitivity (Fig. 2), and reveal different responses of the Nordic Seas and the Atlantic sector. Indeed, the Atlantic core MD99-2281 exhibits warmer SST during GI compared to GS, and a strongly reduced SIC duration throughout the MIS3. On the contrary, and in opposition to the general agreement, the three Norwegian cores are characterized by warmer SST and shorter SIC during the cold GS, and colder SST and longer SIC during the warm GI. This scheme is less obvious in core MD95-2010 where the amplitudes of SIC variations and the resolution are lower, but is clearly visible at the scale of dinocyst assemblages with higher relative percentages of *Islandinium minutum* (% I.MIN; Methods) – a polar taxon associated with cold surface waters seasonally covered by sea-ice²¹ – during GI (high MS values), and inversely during GS (Extended Data Figs 2 and 3). This atypical pattern is thus observable whatever the site considered within the Norwegian Sea and in spite of their distinct physiographical contexts, and especially well expressed in the 63°N cores. There, all parameters converge to indicate conditions which are nearly peak to peak (i.e. event to event) anti-correlated to the North Atlantic and Greenland climatic variability as deduced from $\delta^{18}\text{O}$ ice core records.

To evidence mechanisms potentially explaining this feature, we compare this pattern to the spatial fingerprints of 40 years long freshwater hosing experiments conducted using five models under preindustrial conditions²² (Methods). Consistently with our observations, the five-member ensemble mean of the differences between hosing and control experiments shows that the Nordic Seas experienced a large surface warming while the rest of the North Atlantic is strongly cooled in response to a freshwater input in the North Atlantic (Fig. 1). SST anomalies calculated from dinocyst reconstructions (as GS minus GI mean annual SST; Methods) confirms such a pattern, with the Atlantic core recording a slightly negative SST anomaly of -0.2 °C and the 63°N cores displaying strong positive anomalies of +2.1 °C (MD95-2009) and +3.7 °C (MD99-2285). Despite clear relative increases of % I.MIN during periods of high MS values (i.e. clear coolings during interstadials), core MD95-2010 exhibits a negative anomaly of -1 °C, a value that seems to be unrepresentative, mainly due to low temporal resolution and stratigraphical discrepancies (Methods). Another modelling study²³ also evidenced such a warming in the Nordic Seas in response to a freshwater perturbation, independently from the location of the freshwater input. Both studies^{22,23} attributed this surface warming to subsurface propagation of warm Atlantic water masses beneath the North Atlantic meltwater lid (resulting from the freshwater input) and up to the Nordic Seas where it re-emerged and mixed with ambient surface waters. Our model simulations show indeed a subsurface positive heat anomaly south of the Greenland-Scotland sill, located below the North Atlantic freshwater cap (Fig. 1b). This freshwater cap plays a key role by preventing oceanic vertical mixing which normally transfers winter surface cooling (through atmospheric heat fluxes) in subsurface. Hence, these simulations suggest a process that might have occurred during stadials and provide an explanation for the pattern found in our new dinocyst-derived sea-surface reconstructions.

However, and in agreement with previous paleoceanographic studies within the Nordic Seas¹⁰ and the North Atlantic^{10,14}, all of our cores also reveal the occurrence of monospecific planktonic foraminifera assemblages characterized by nearly 100% of the mesopelagic taxon NPS during GS (Fig. 3; Methods). This indicates the presence of cold waters from polar origin²⁴ in subsurface of the study area.

Hence, we propose that stadials encountered a reduced overturning circulation due to large meltwater fluxes (initiated and/or sustained by iceberg releases within the North Atlantic), a southward migration of subsurface polar waters, and colder SST within the North Atlantic, with, in parallel, a small flow of Atlantic waters propagating northward, below the North

Atlantic surface meltwater lid where it joined and partially mixed with the cold polar waters, before reemerging at the surface when entering the Nordic Seas (Fig. 4). There, this slightly mixed water-mass occupies the upperpart of the water column. The topmost tens of meters of this layer present relatively high SST due to the heat transport associated with the Atlantic waters (isolated from the atmosphere by the meltwater cap throughout their northward transport across the North Atlantic). As indicated by dinocyst-derived sea-surface salinities (SSS; Extended Data Table 3), they also present relatively low SSS (around 31.6 psu over the entire study area) probably due to the additional mixing with surface meltwater produced within the Nordic Seas by iceberg releases (indicated through ice-rafted peaks during GS²⁵) and the seasonal melting of (reduced) sea ice. Model simulations show indeed a very slight decrease of SSS in the Norwegian Sea (Extended data Fig. 4). In opposition, at the base of the mixed layer, the nearly 100% NPS indicate colder and at least slightly saltier waters than in the topmost tens of meters (according to the ecological tolerances of NPS²⁶). Hence, a thick and progressive pycnocline existed between the very-surface warm and low SSS waters, and the subsurface cold and saltier waters. This large and gradual pycnocline was also probably sustained by brine extrusion occurring on the continental shelves during occasional sea-ice formation, those brines being stored at the base of the relatively mixed layer²⁷. Based on indirect proxies, previous studies^{9,28} suggested the existence of a strong halocline separating cold and low SSS surface waters from warm and salty Atlantic subsurface waters during stadials. Here, based on direct sea-surface reconstructions, we show a somewhat reverse scheme where a halocline, even if thick and progressive, also exists. This stratification of the upper water column resulted in strong sea-surface seasonality contrasts as depicted by dinocysts (Fig. 3; Methods), explained by the relatively low thermal inertia of the low SSS very-surface waters and to the sea-ice extent (although limited) during winter. Despite these low SSS in the first tens of meters of the water column, the sea-ice cover was indeed reduced in comparison to GI and only few sea-ice formation occurred during GS (SIC duration inferior to 4 month/year at the study sites) because of the heat flux provided by the Atlantic waters and probably sustained by relatively high June insolation at 65°N²⁹.

During GI (Fig. 4), sea-surface conditions derived from dinocysts and subsurface conditions deduced from planktonic foraminifera (Fig. 2 and Fig. 3) reveal similar and coherent trends within each of the four cores, indicative of the disappearance/deepening of the pycnocline. The Norwegian Sea is indeed characterized by colder SST, reduced seasonal SST contrasts, and 100% NPS, typifying the presence of a homogenous mixed layer made of cold polar

waters, as well as longer sea-ice cover durations. Core MD99-2281, in the Atlantic sector, exhibits less than 50% NPS, warmer SST and reduced seasonal SST contrasts, indicating here again the occurrence of a weakly stratified mixed layer where polar waters and Atlantic waters mix together.

The new paradigm proposed here does not rule out the “brine hypothesis”^{8,9} employed to explain the isotopically light $\delta^{18}\text{O}$ values measured on NPS during GS within cores from the southern Nordic Seas (including core MD95-2010⁸). Taking into account the changes of upper stratification in the Nordic Seas during GS/GI as evidenced in the present study, as well as the fact that the main production period of NPS occurs in summer within the Nordic Seas^{30,31}, we suggest that: (i) during GS (thick and progressive pycnocline), the $\delta^{18}\text{O}$ NPS could capture the reduced winter shelf brine production – stored within the subsurface waters inhabited by NPS – and not the seasonal melting trapped in very-surface, (ii) during GI (low stratification), it could only capture the large seasonal melting of sea ice occurring directly above during summer and which produces isotopically heavy waters²⁷, whereas the isotopically light brine extrusion – produced during winter, i.e. when NPS is nearly absent – would directly convect to form bottom waters, without stagnating at the base of the mixed layer.

Our findings and the new interpretations we propose thus conciliate most of the proxies used to study the MIS3 millennial climate variability within the North Atlantic and the Nordic Seas. Based on paleo-data and model simulations, we develop a new feature where a large surface warming occurs within the Nordic Seas in response to meltwater inputs in the North Atlantic. This warming might have contributed to enhanced iceberg calving within the Nordic Seas, and might have therefore constituted a positive feedback for the destabilization of the bordering ice-sheets. Furthermore, the scheme depicted in the Norwegian Sea SST signals recalls the antiphased temperature changes detected in between central Greenland (GRIP site) and the modern evaporative moisture source region (North Atlantic; Fig. 2)^{32,33}. The re-emergence of warm Atlantic waters depicted here within the Nordic Seas could hence constitute a possible alternative moisture source for Greenland during GS.

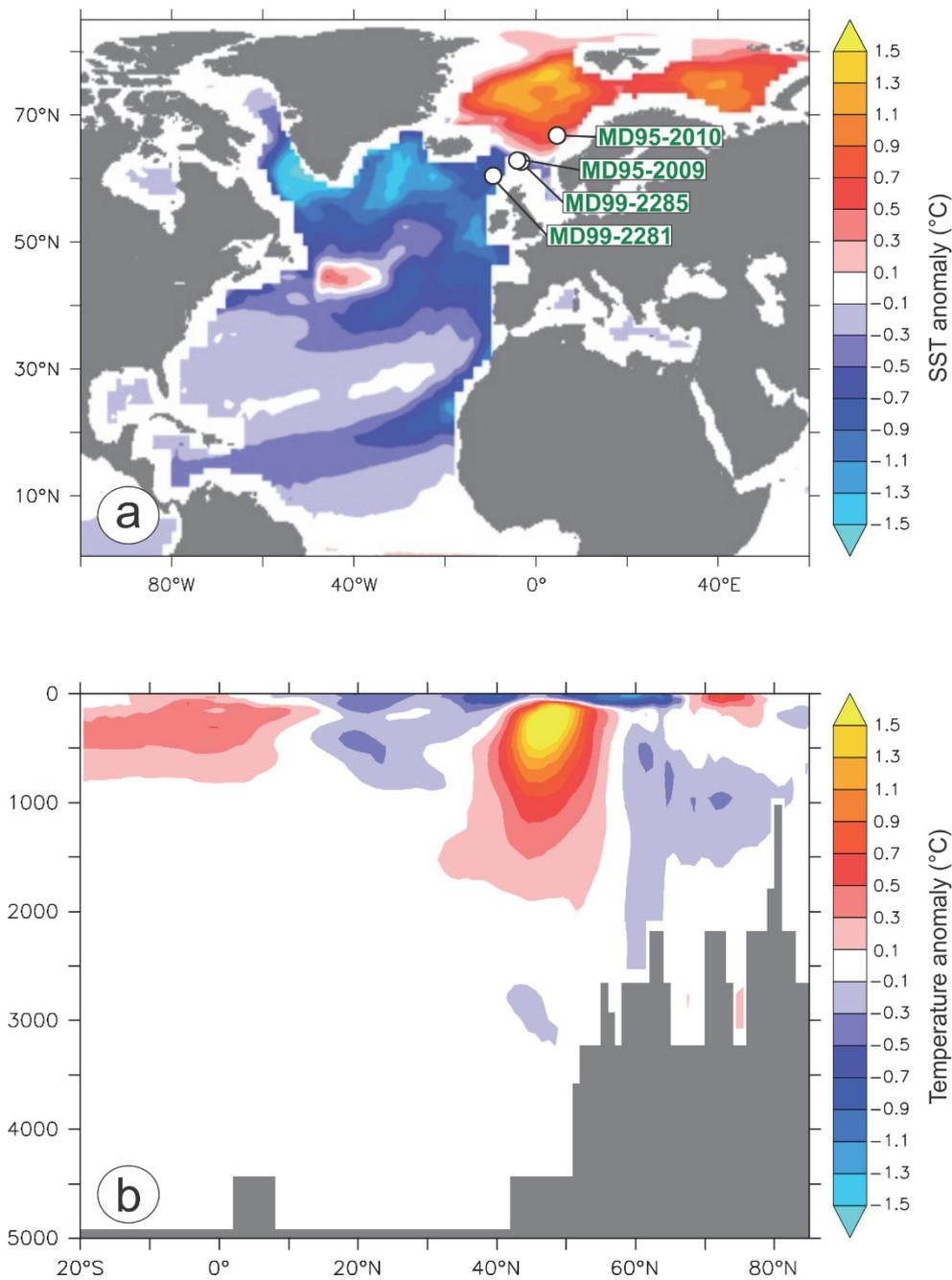


Figure 1: Five-member ensemble mean of temperature differences. a, Map showing the cores location (from north to south: MD95-2010, 66.68°N, 4.57°E, 1,226 m depth; MD95-2009, 62.74°N, -4.00°E, 1,027 m depth; MD99-2285, 62.69°N, -3.57°E, 885 m depth; MD99-2281, 60.34°N, -9.46°E, 1,197m depth) as well as SST differences (°C) between hosing and control experiments averaged over the 4th decade. The study area constitutes a nodal point regarding the modern surface oceanic circulation. It is indeed located at the convergence of (i) the northward warm North Atlantic water inflow and (ii) the southward polar water outflow through the East Greenland current terminal limb, i.e. the East Icelandic Current. Previous paleoclimatic studies^{34,35} evidenced that this area was also a key sector during the Last Glacial Maximum when, similarly to the SST pattern shown on the present map, warmer SST were recorded within the Nordic Seas and colder ones within the North Atlantic. This suggests that such a situation might represent a regular feature, at least for glacial periods. b, Latitude-depth section of the temperature differences (in °C, averaged over the whole Atlantic basin) between hosing and control experiments averaged over the 4th decade.

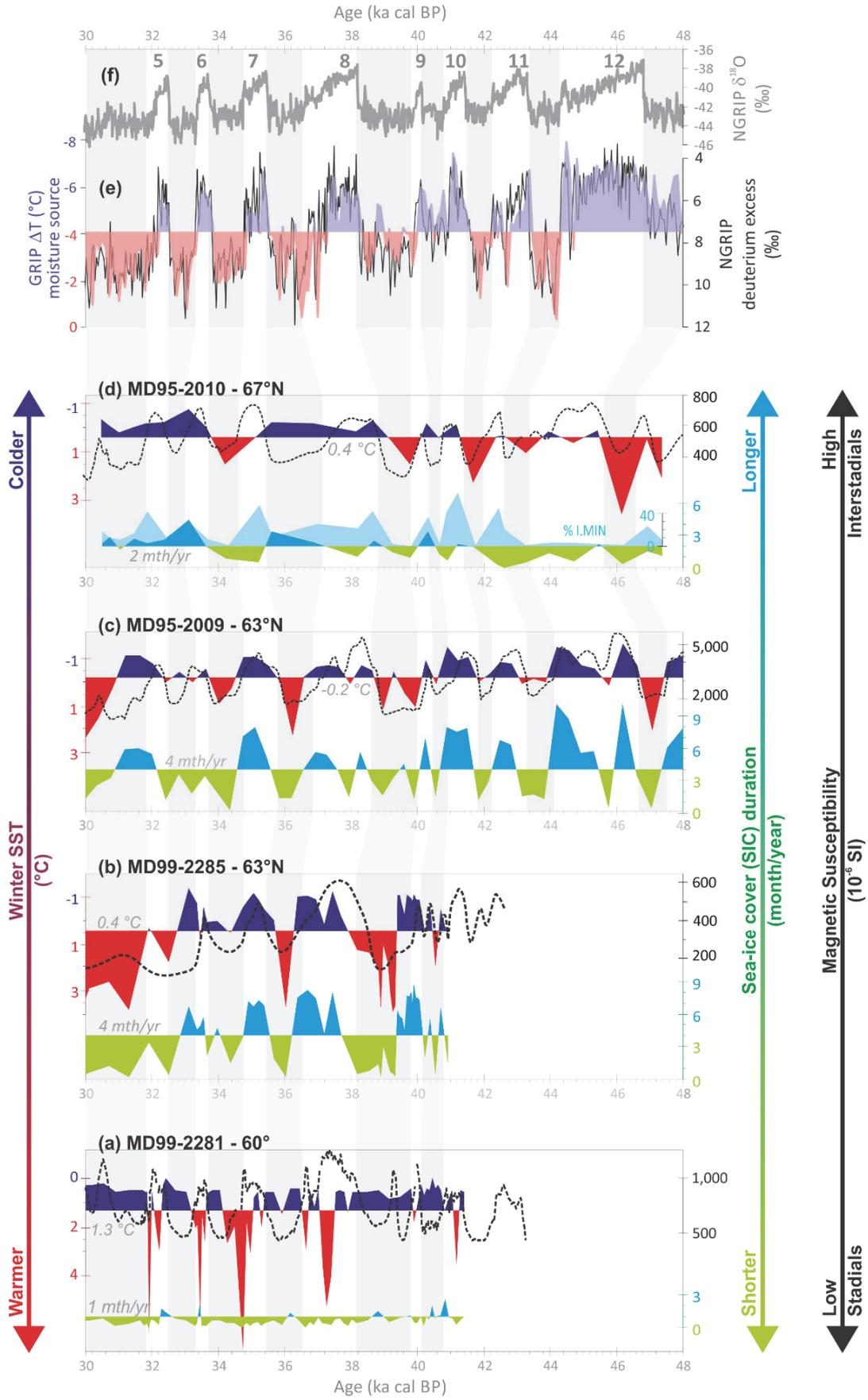


Figure 2

Figure 2: SST and SIC records from the four studied cores, with from the south to the north of the considered area: (a) core MD99-2281, (b) core MD99-2285, (c) core MD95-2009 and (d) core MD95-2010. To highlight the phase/antiphase of signals, SST and SIC signals have been shaded relatively to a threshold that corresponds to the mean value of the parameter over the studied period (red / dark blue for SST, and green / light blue for SIC). The value of this threshold is indicated in grey next to each signal. Worth is noting the latitudinal gradient expressed in the SIC mean values and especially the discrepancy between Norwegian Sea versus Atlantic sites. Magnetic susceptibility (MS) signals (black dotted curves) have been added for each core as they can be directly related to (f) the NGRIP $\delta^{18}O$ record⁵ (GICC05 age scale). Results are also compared to (e) the temperature anomaly (compared to modern value of ~ 20 °C) of the evaporative moisture source region for Greenland precipitation (shaded relatively to its mean value over 30-48 ka cal BP) deduced from GRIP deuterium excess signal, and superposed to the NGRIP deuterium excess record (black curve). Grey bands highlight low NGRIP $\delta^{18}O$ and low MS values, i.e. stadial periods. Their position is highly coherent in core sections constrained by the MS/ $\delta^{18}O$ tuning but appears shifted when it is not the case (see methods). For core MD95-2010, the %I.MIN, indicative of colder SST and longer SIC duration, is also shown.

Figure 3: Polar water protrusions vs sea-surface seasonality contrasts. Indices of subsurface migration of polar waters (a), as deduced from the NPS abundances in the respective cores (with a shading in core MD99-2281 thanks to an arbitrary threshold of 75 % used to better evidence changes), are here plotted against the seasonality ranges calculated in the different cores (from b to e) as Summer SST minus Winter SST and compared to the reference (f) NGRIP $\delta^{18}O$ (GICC05 age scale) stratotype. Sea-surface seasonality values are shaded relatively to the mean value obtained over the studied period within each core (threshold value indicated in grey next to each record). Triangles indicate modern values of summer SST (red), winter SST (blue), and seasonality (black) for each study site (WOA09 data³⁶). As in Fig. 2, grey bands highlight low NGRIP $\delta^{18}O$ and low MS values, i.e. stadial periods.

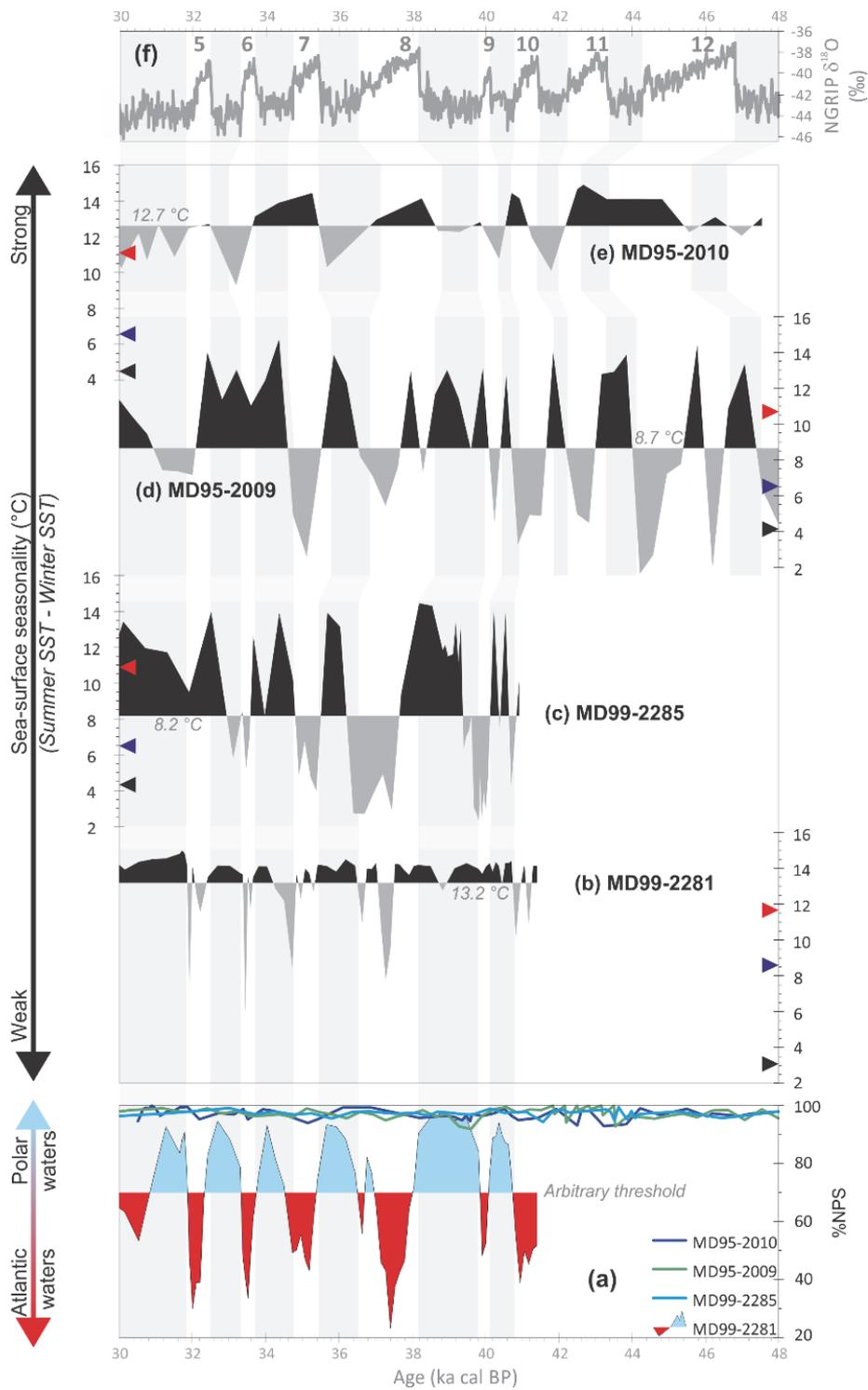


Figure 3

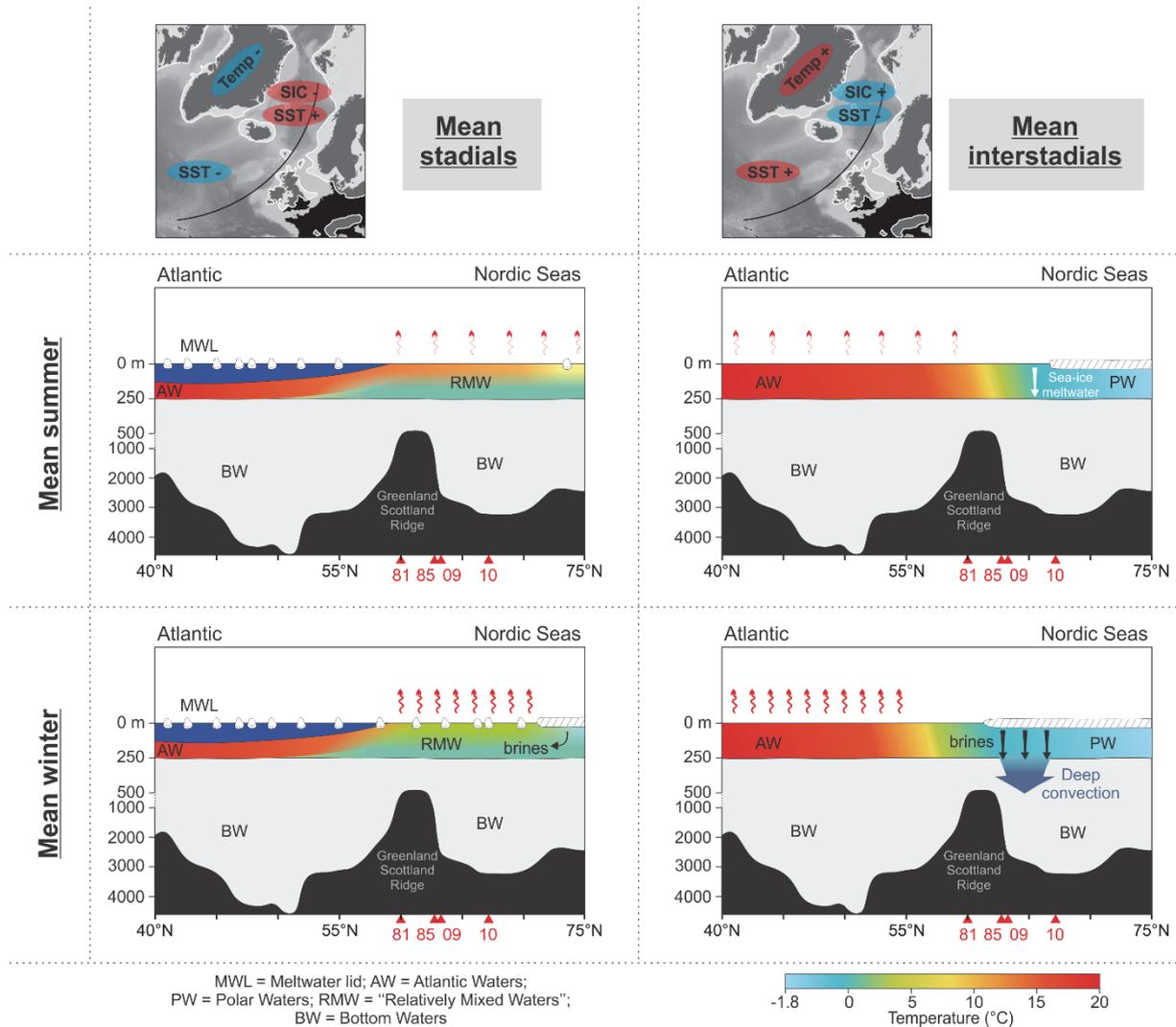


Figure 4: Conceptual hydrological scheme. The diagrams depict the mean conditions in the suboreal Atlantic area during stadials/interstadials, and summer/winter. Section location is indicated on the top maps. Bathymetry is from GEBCO (www.gebco.net), and has been simplified for sections. Ice-sheet extent on maps corresponds to the last glacial maximal extension, after³⁷. Colors indicate temperature range, as indicated by the bottom scale.

METHODS

Stratigraphy. For each of the studied sediment cores, radiocarbon (AMS ^{14}C) datings (Supplementary Information Table 1), when insufficiently dense over the studied interval, have been completed by event-based tie-points derived from the correlation of magnetic concentration data to the NGRIP-GICC05 $\delta^{18}\text{O}$ record³⁸ (i.e. the recommended North Atlantic regional stratotype after¹⁸). The rationale is that marine records of magnetic concentration parameters from MIS 3 are consistent across the North Atlantic basin on the path of different overflow branches of the North Atlantic Deep Water and can be tied on the high frequency climatic variability (Dansgaard-Oeschger – DO – cycles) characteristic of this period⁵. Stratigraphies of cores MD95-2009, MD99-2281 and MD99-2285 have been constructed using this DO event chronostratigraphy after dates from¹⁷ (NGRIP-GICC05 derived, see Supplementary Information Table 1 and Extended data Fig. 1). The age models however differ in their final construction. A linear regression was chosen for cores MD99-2281³⁹ and MD99-2285 to best fit all the tie-points during MIS3, whereas a polynomial regression was used for MD95-2009 in order to generate a unique age model for the whole core. This later choice induces some minor deviations from the DO events / MS peak to peak correlation (Extended data Fig. 1) that should be kept in mind for further interpretations.

Core MD95-2010 age model conforms to the initially published one⁸ (<http://doi.pangaea.de/10.1594/PANGAEA.735730>). This record benefits from the recovery of ash-layer well-dated horizons (Supplementary Information Table1). A polynomial regression (order 5) has been applied to generate the age model⁸. As no additional tie points were generated, phasing issues do occur almost all along the record regarding the NGRIP-GICC05 record (see Fig. 2; Extended data Fig. 1).

Supplementary tie-points, independent from climate, are also retrieved from the record of the changes in the Earth's magnetic field intensity, in particular the two prominent lows attributed to the Mono Lake and to the Laschamp excursions⁴⁰. They have been identified within MD95-2009, MD95-2010 and MD99-2281 records^{5,20}.

Dinocyst counts, transfer function and seasonality signals. Dinocysts – or dinoflagellate cysts – were counted in the 10-150 μm fraction after palynological preparation of sediment samples (http://www.epoc.u-bordeaux.fr/index.php?lang=fr&page=eq_paleo_pollens).

Around 300 dinocysts were counted in each sample using a Leica Microscope at x400 magnification. Species identification follows^{21,41,42}. Relative abundances of each species were calculated relative to the total sum of Quaternary modern dinocysts. Among the dominant species of the four studied cores, one deserves here a special attention – *Islandinium minutum* – as it is strongly related to cold and seasonally sea-ice covered surface environments (maximum abundance observed in areas covered by sea ice between 8 and 12 months/yr⁴²; [Extended Data Figs 2](#)), the two hydrological parameters mainly discussed in this paper. Within the Norwegian Sea cores, records of %I.MIN ([Extended Data Fig. 3](#)) clearly indicate colder SST and longer SIC during GI, and milder surface conditions during GS. In the Atlantic core MD99-2281, the %I.MIN signal shows low values throughout the studied period indicative of a strongly reduced SIC duration; the very slight increase of %I.MIN during GS indicates relatively colder sea-surface conditions, thus confirming the difference of pattern observed in-between the Nordic Seas and the North Atlantic Ocean.

Past sea-surface conditions were derived from a transfer function applied to dinocyst assemblages, using the modern analogue technique (see ref.⁴³⁻⁴⁵ for a review of this technique). Briefly, calculation relies on a statistical comparison of fossil samples to a large set of modern (surface sediment) samples. The five best analogues (i.e. minimal statistical dissimilarity between the species spectra) are selected for the reconstructions. The hydrographic data corresponding to these analogues, compiled from the 2001 version of the World Ocean Atlas, are then used to calculate weighted (inversely to the dissimilarity of the analogues) averaged past sea-surface parameters.

Former studies previously published such quantified reconstructions for three of the studied cores: cores MD95-2009 and MD95-2010 using a modern dinocyst database including 677 samples¹⁹, core MD99-2281 using the 1189 modern sample database²⁰.

For the present study, new (and even unpublished in the case of MD99-2285 core) calculations have been done using an extended modern database composed of 1207 sites from North Atlantic Ocean, Arctic and sub-Arctic basins, Mediterranean Sea and North Pacific Ocean (database available from the DINO9 workshop, <http://pcwww.liv.ac.uk/~dino9/workshops.htm>). These statistical treatments provide quantitative reconstructions for various hydrological parameters, among which are mean summer (July-August-September) and mean winter (January-February-March) SST (with root mean square errors of prediction – RMSEP – of 1.5 °C and 1.05 °C respectively), mean

summer and mean winter sea-surface salinities (SSS; respective RMSEP of 2.4 and 2.3 psu), and mean annual SIC duration (RMSEP of 1.2 month/year). Seasonality signals were then determined by subtracting mean winter SST to mean summer SST.

Model simulations. Freshwater hosing experiments were conducted using five state-of-the-art climate models²². Four of them are coupled ocean-atmosphere models (HadCM3, IPSLCM5A, MPI-ESM, EC-Earth) and one is ocean-only model (ORCA05; [Extended Data Table 1](#)). Two types of simulations are considered: (i) the transient control simulations, corresponding to historical simulations without any additional freshwater input, and (ii) the hosing simulations, corresponding to historical simulations with an additional freshwater input of 0.1 Sv released on all the coastal grid points around Greenland with a homogenous rate during 40 years (over the historical era 1965–2004, except for HadCM3 and MPI-ESM for which the experiments were performed over the periods 1960–1999 and 1880–1919, respectively). Two parameters were regarded: temperatures ([Fig. 1](#)) and salinities ([Extended Data Fig. 4](#)). BCM2 model is not used considered here while present in the original study²². Indeed, it showed a very different behavior as compared to the five models considered here, and was therefore considered as an outlier in the former ensemble²². Nevertheless, its inclusion in the ensemble only slightly change the pattern of the response and its amplitude. In addition, the use of an ocean-only model allows to attribute the observed changes to oceanic processes and weakly to atmospheric feedbacks.

SST and SSS anomalies. Mean annual SST and SSS anomalies were calculated for each core ([Extended Data Table 2](#) and [Extended Data Table 3](#)) as follows: mean winter and mean summer SST (SSS) were determined over (i) the stadial period, comprising GS 10, 9, 8, 7 and 6, and (ii) the interstadial period, comprising GI 10, 9, 8, 7, 6, and 5, using the GICC05 age limits of each GS/GI¹⁷. Then, mean annual SST (SSS), for GS and for GI periods, were determined by averaging mean winter and mean summer SST (SSS). Finally, mean annual SST (SSS) anomalies were obtained by subtracting mean annual GI SST to mean annual GS SST (i.e. GS minus GI).

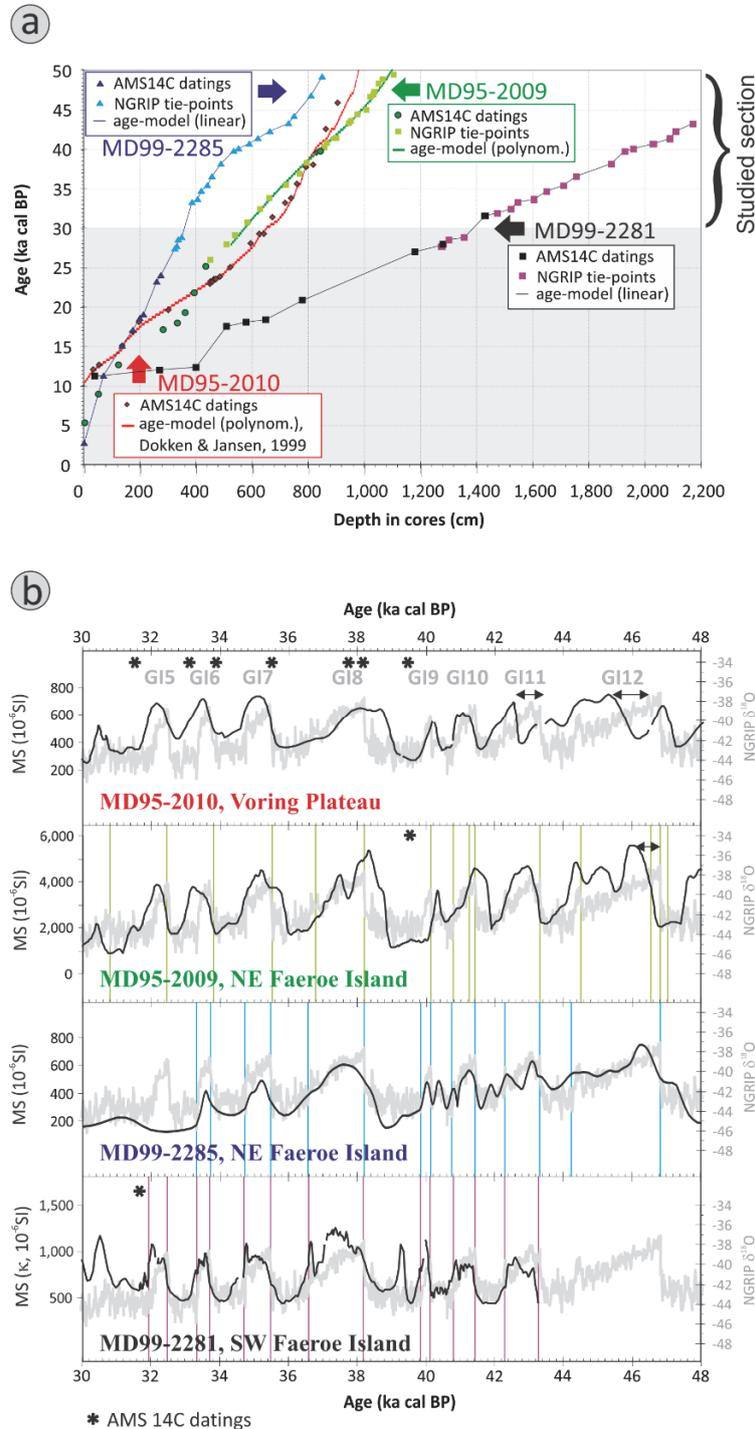
We chose to use common age limits of GS and GI for each core in order to be consistent over the entire study area. We chose the GICC05 age limits¹⁷ since age models of cores MD95-2009, MD99-2281 and MD99-2285 are partly based on this GICC05 age scale. However, this

approach lacks precision in the case of core MD95-2010 for which the stratigraphy is not tied to the GICC05 age scale; this, combined to the lower temporal resolution of this core, leads to inaccurate mean GI and mean GS annual SST, largely explaining the slightly negative and unrepresentative SST anomaly calculated for this site. In addition, dinocyst assemblages are highly diversified in all cores (with at least 30 taxa identified within each core), but the structure of dinocyst assemblages is significantly different in core MD95-2010 compared to the three other ones. Indeed, while assemblages are strongly dominated by one or two taxa in cores MD99-2281 (see Fig. 5 in ref. ²⁰), MD99-2285 and MD95-2009 (see [Extended Data Fig. 3](#)), five dominant taxa with comparable relative abundances are present within core MD95-2010 (see Figure 3 in ref. ¹⁹). This peculiar assemblage structure might have contributed to dampen the GS / GI contrasts within SST and SIC quantitative reconstructions obtained with the new modern database. Hence, these dampened SST reconstructions might also partly explain the slightly negative SST anomaly calculated for this site.

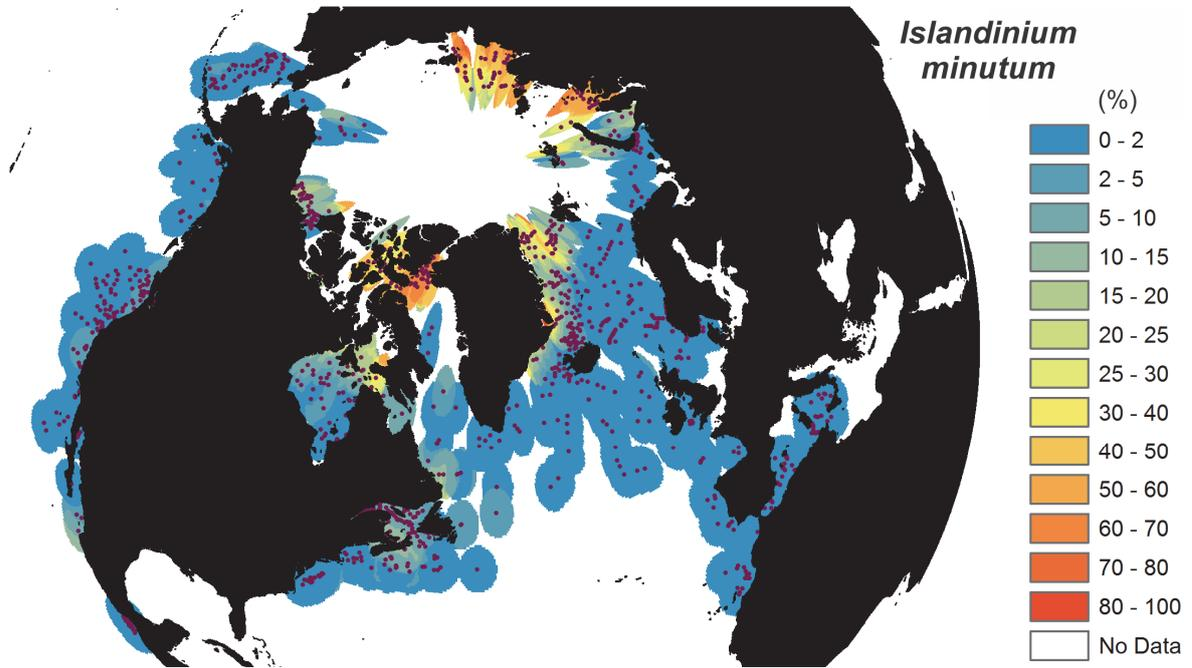
Relative percentages of *Neogloboquadrina pachyderma* sinistral coiling (%NPS). Planktonic foraminifera were counted in the > 150 µm fraction after classical preparation of sediment samples (washed through a 150 µm sieve before being dried). Around 300 specimens were counted in each sample, and relative abundances of each species were determined. We focus here on the relative percentage of NPS, a taxon usually used to track the migration of the cold polar waters²⁴.

Dinoflagellates versus NPS depth habitats. We insist here on the fact that noticeable differences exist in the depth habitats of dinoflagellates and NPS, which, if not taken into account, can lead to inaccurate interpretations. Indeed, dinoflagellates are known to be mainly restricted to the uppermost 50 meters of the water column⁵⁶, implying that dinocysts are tracers of sea-surface *sensu-stricto* conditions. On the contrary, growing evidences of the mesopelagic affinity characterizing the planktonic foraminifera NPS have emerged during the last decades^{12,13,46-50}. This involves that dinocysts and NPS may not track the same water mass, i.e. that NPS may not track sea-surface conditions as often admitted but rather subsurface or near-surface conditions. The present study well illustrates this possibility of decoupling, with (i) in the case of a strong stratification of the upper few hundred meters of the water column (GS), dinocyst and NPS displaying opposite signals, i.e. tracking different water masses (the surface and subsurface, respectively), and (ii) in the case of reduced/nil

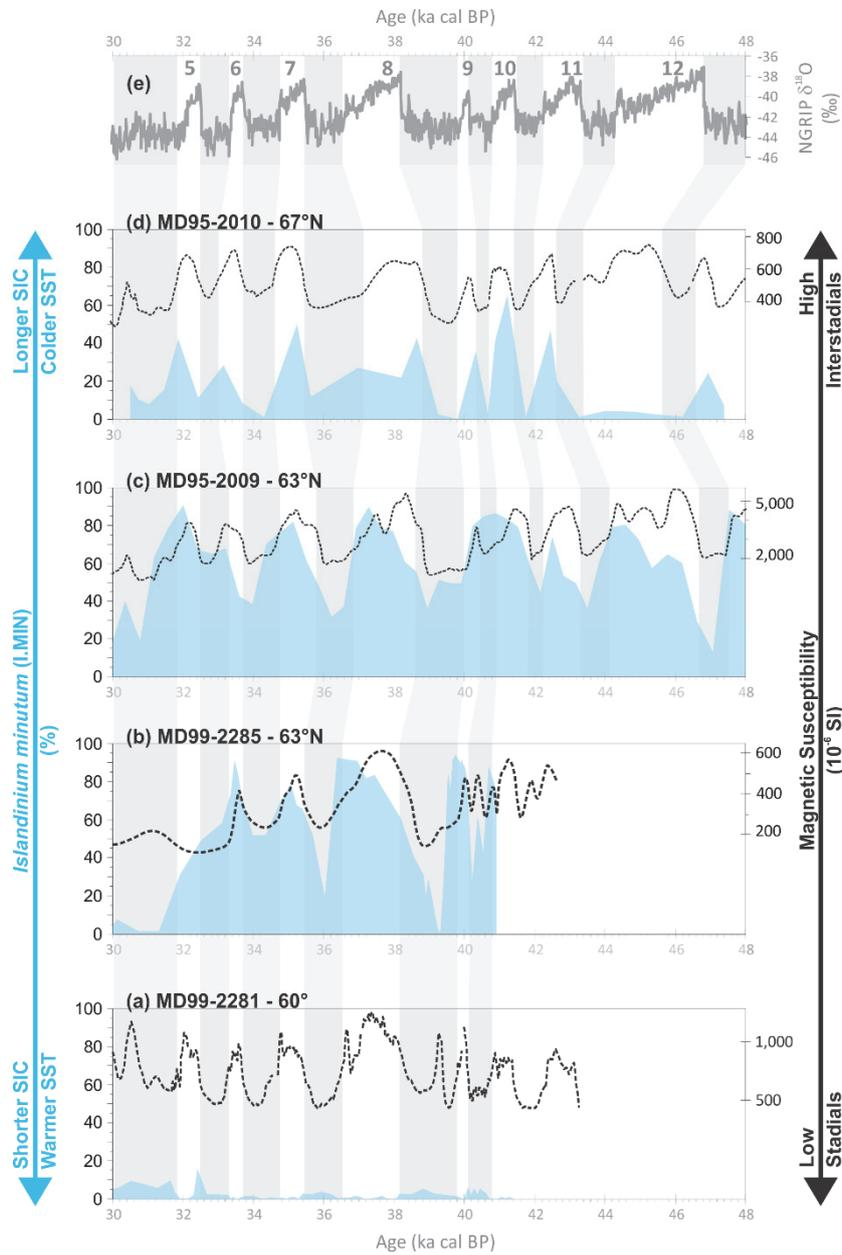
stratification, dinocyst and NPS displaying concordant signals, i.e. tracking the same homogeneous upper water mass.



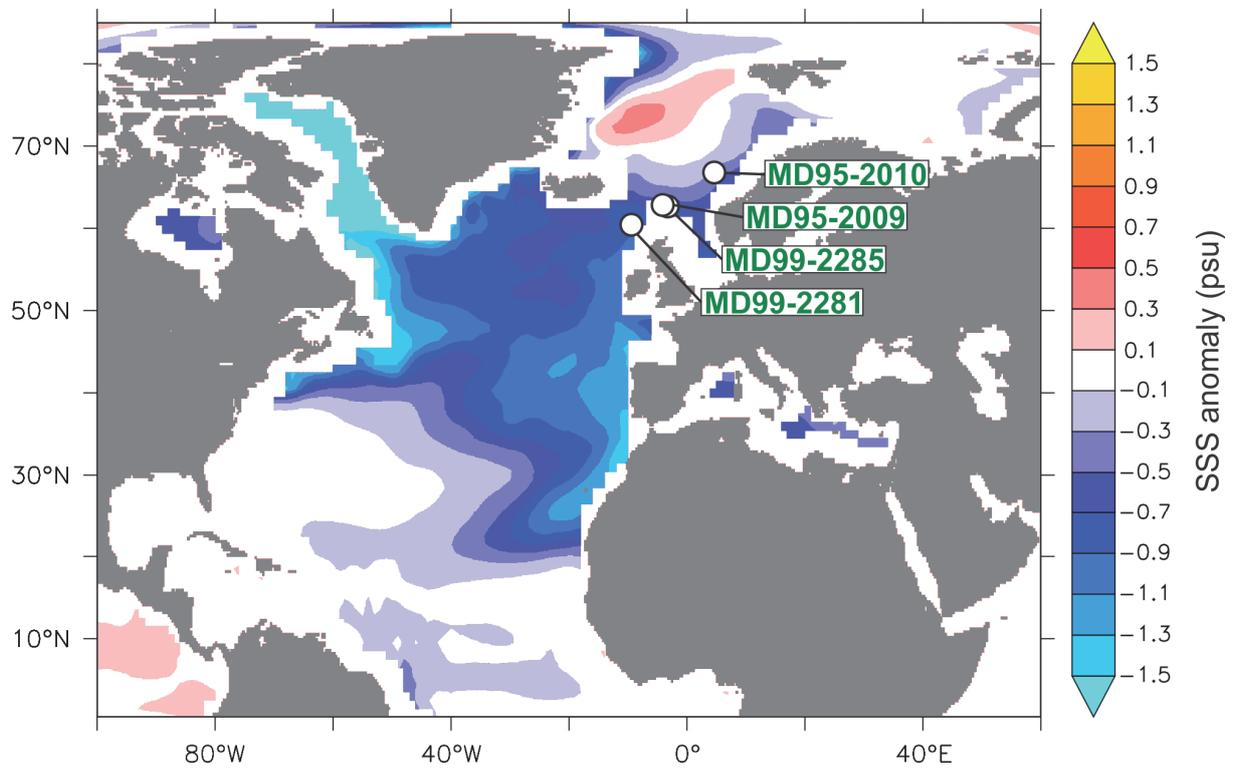
Extended data Figure 1: Information regarding the age model construction of the studied cores. a, age versus depth plots of the respective chronological constrains used to built the chronology (see Supplementary Information Table 1). b, Correlation of the NGRIP GICC05 $\delta^{18}O$ record³⁸ (a thick grey line has been chosen to circumscribe issues due to the b2k versus BP age scaling) to the magnetic susceptibility records of the respective studied cores.



Extended Data Figure 2: Islandinium minutum distribution within the modern dinocyst database made of 1207 points. This map clearly shows that this dinocyst taxon is strongly linked to cold and seasonally sea-ice covered surface environments.



Extended Data Figure 3: Records of the relative percentage of *Islandinium minutum* within the four studied cores. For each core (from a to d) the %I. MIN records, indicative of colder SST and longer SIC, are compared to the magnetic susceptibility signals which can be directly correlated to Greenland climate variability as detected within the NGRIP $\delta^{18}O$ record (e). Grey bands highlight low NGRIP $\delta^{18}O$ and low MS values, i.e. stadial periods. It is worth noting the opposite scheme described by %I. MIN variations within the Nordic Seas versus in the Atlantic sector, which again illustrates the different patterns observed within the Nordic Seas and within the North Atlantic Ocean.



Extended Data Figure 4: Five-member ensemble mean of SSS differences. Anomalies between hosing and control experiments averaged over the 4th decade.

Extended Data Table 1: Characteristics of the five models considered.

Model	Institute	Type*	Ocean	Atmosphere	Reference
HadCM3	Hadley Centre	OAGCM	No name 1.25 x 1.25, L20	HadAM3 91 x 76, L19	51
IPSLCM5A	Institut Pierre Simon Laplace	OAGCM	NEMO 2°, L31	LMD5 96 x 96, L39	52
MPI-ESM	MPI	OAGCM (ESM)	MPI-OM 1.5°, L40	ECHAM6 T63-L47	53
ORCA05	GEOMAR	OGCM	NEMO 0.5°, L46	CORE.v2 Forcing	54
EC-Earth	DMI	OAGCM	NEMO 1°, L42	IFS T159-L31	55

* OAGCM: Ocean-Atmosphere General Circulation Model; OGCM: Ocean General Circulation Model; ESM: Earth System Model

Extended Data Table 2: SST anomalies.

Core	Number of samples		GS SST			GI SST			Mean annual SST anomalies (GS-GI)
	GS	GI	mean winter	mean summer	mean annual	mean winter	mean summer	mean annual	
MD99-2281	25	37	0.9	14.6	7.8	1.6	14.4	8.0	-0.2
MD99-2285	26	22	0.9	10.9	5.9	-0.6	4.9	2.2	3.7
MD95-2009	14	13	0.1	11.2	5.7	-0.3	7.5	3.6	2.1
MD95-2010	9	6	0.0	12.1	6.1	0.3	13.8	7.1	-1.0

Extended Data Table 3: SSS anomalies.

Core	Number of samples		GS SST			GI SST			Mean annual SST anomalies (GS-GI)
	GS	GI	mean winter	mean summer	mean annual	mean winter	mean summer	mean annual	
MD99-2281	25	37	32.1	31.2	31.7	32.5	31.7	32.1	-0.4
MD99-2285	26	22	32.7	31.6	32.1	32.9	31.0	31.9	0.2
MD95-2009	14	13	31.7	30.6	31.2	32.4	31.3	31.8	-0.7
MD95-2010	9	6	31.9	30.9	31.4	31.8	30.3	31.1	0.3

REFERENCES

1. Dansgaard, W. *et al.* Evidence for general instability of past climate from a 250-kyr ice-core record. *Nature* **364**, 218-220 (1993).
2. Bond, G. C. & Lotti, R. Iceberg discharges into the North Atlantic on millennial time scales during the last glaciation. *Science* **267**, 1005-1010 (1995).
3. Böhm, E. *et al.* Strong and deep Atlantic meridional overturning circulation during the last glacial cycle. *Nature* **517**, 73-76, doi:10.1038/nature14059 (2015).
4. Ganopolski, A. & Rahmstorf, S. Rapid changes of glacial climate simulated in a coupled climate model. *Nature* **409**, 153-158 (2001).
5. Kissel, C. *et al.* Rapid climatic variations during marine isotopic stage 3: Magnetic analysis of sediments from Nordic Seas and North Atlantic. *Earth and Planetary Science Letters* **171**, 489-502, doi:10.1016/S0012-821X(99)00162-4 (1999).
6. Sachs, J. P. & Lehman, S. J. Subtropical North Atlantic temperatures 60,000 to 30,000 years ago. *Science* **286**, 756-760, doi:10.1126/science.286.5440.756 (1999).
7. Li, C., Battisti, D. S. & Bitz, C. M. Can North Atlantic sea ice anomalies account for Dansgaard-Oeschger climate signals? *Journal of Climate* **23**, 5457-5475, doi:10.1175/2010JCLI3409.1 (2010).
8. Dokken, T. M. & Jansen, E. Rapid changes in the mechanism of ocean convection during the last glacial period. *Nature* **401**, 458-461 (1999).
9. Dokken, T. M., Nisancioglu, K. H., Li, C., Battisti, D. S. & Kissel, C. Dansgaard-Oeschger cycles: Interactions between ocean and sea ice intrinsic to the Nordic seas. *Paleoceanography* **28**, 491-502 (2013).
10. Rasmussen, T. L. & Thomsen, E. The role of the North Atlantic Drift in the millennial timescale glacial climate fluctuations. *Palaeogeography, Palaeoclimatology, Palaeoecology* **210**, 101-116, doi:10.1016/j.palaeo.2004.04.005 (2004).
11. Rasmussen, T. L. & Thomsen, E. Pink marine sediments reveal rapid ice melt and Arctic meltwater discharge during Dansgaard-Oeschger warmings. *Nature Communications* **4** (2013).
12. Carstens, J., Hebbeln, D. & Wefer, G. Distribution of planktic foraminifera at the ice margin in the Arctic (Fram Strait). *Marine Micropaleontology* **29**, 257-269 (1997).
13. Simstich, J., Sarnthein, M. & Erlenkeuser, H. Paired $\delta^{18}O$ signals of *Neogloboquadrina pachyderma* (s) and *Turborotalita quinqueloba* show thermal stratification structure in Nordic Seas. *Marine Micropaleontology* **48**, 107-125 (2003).
14. Dickson, A. J., Austin, W. E. N., Hall, I. R., Maslin, M. A. & Kucera, M. Centennial-scale evolution of Dansgaard-Oeschger events in the northeast Atlantic Ocean between 39.5 and 56.5 ka B.P. *Paleoceanography* **23**, doi:10.1029/2008PA001595 (2008).
15. Van Kreveld, S. *et al.* Potential links between surging ice sheets, circulation changes, and the Dansgaard-Oeschger cycles in the Irmiger Sea, 60-80 kyr. *Paleoceanography* **15**, 425-442 (2000).
16. De Vernal, A. & Rochon, A. 1 edn. (2011).
17. Wolff, E. W., Chappellaz, J., Blunier, T., Rasmussen, S. O. & Svensson, A. Millennial-scale variability during the last glacial: The ice core record. *Quaternary Science Reviews* **29**, 2828-2838 (2010).
18. Austin, W. E. N. & Hibbert, F. D. Tracing time in the ocean: A brief review of chronological constraints (60-8 kyr) on North Atlantic marine event-based stratigraphies. *Quaternary Science Reviews* **36**, 28-37, doi:10.1016/j.quascirev.2012.01.015 (2012).
19. Eynaud, F. *et al.* Norwegian sea-surface palaeoenvironments of marine oxygen-isotope stage 3: The paradoxical response of dinoflagellate cysts. *Journal of Quaternary Science* **17**, 349-359, doi:10.1002/jqs.676 (2002).
20. Zumaque, J. *et al.* An ocean-ice coupled response during the last glacial: a view from a marine isotopic stage 3 record south of the Faeroe Shetland Gateway. *Climate of the Past* **8**, 1997-2017 (2012).
21. Radi, T. *et al.* Operational taxonomy and (paleo-)autecology of round, brown, spiny dinoflagellate cysts from the Quaternary of high northern latitudes. *Marine Micropaleontology* **98**, 41-57 (2013).
22. Swingedouw, D. *et al.* Decadal fingerprints of freshwater discharge around Greenland in a multi-model ensemble. *Climate Dynamics* **41**, 695-720, doi:10.1007/s00382-012-1479-9 (2013).
23. Kleinen, T., Osborn, T. J. & Briffa, K. R. Sensitivity of climate response to variations in freshwater hosing location. *Ocean Dynamics* **59**, 509-521, doi:10.1007/s10236-009-0189-2 (2009).
24. Eynaud, F. *et al.* Position of the Polar Front along the western Iberian margin during key cold episodes of the last 45 ka. *Geochemistry, Geophysics, Geosystems* **10**, doi:10.1029/2009GC002398 (2009).
25. Elliot, M., Labeyrie, L., Dokken, T. & Manthe, S. Coherent patterns of ice-rafted debris deposits in the Nordic regions during the last glacial (10-60 ka). *Earth and Planetary Science Letters* **194**, 151-163, doi:10.1016/S0012-821X(01)00561-1 (2001).
26. Bé, A. W. H. An ecological, zoogeographic and taxonomic review of Recent planktonic foraminifera. In: Ramsay, A.T.S. (Ed.), *Oceanic Micropaleontology*, vol. 1. Academic Press, London, pp. 1-100. (1977).
27. Hillaire-Marcel, C. & de Vernal, A. Stable isotope clue to episodic sea ice formation in the glacial North Atlantic. *Earth and Planetary Science Letters* **268**, 143-150, doi:10.1016/j.epsl.2008.01.012 (2008).
28. Ezat, M. M., Rasmussen, T. L. & Groeneveld, J. Persistent intermediate water warming during cold stadials in the southeastern Nordic seas during the past 65 k.y. *Geology* **42**, 663-666, doi:10.1130/G35579.1 (2014).
29. Berger, A. & Loutre, M. F. Insolation values for the climate of the last 10 million years. *Quaternary Science Reviews* **10**, 297-317, doi:10.1016/0277-3791(91)90033-Q (1991).
30. Kohfeld, K. E., Fairbanks, R. G., Smith, S. L. & Walsh, I. D. *Neogloboquadrina pachyderma* (sinistral coiling) as paleoceanographic tracers in polar oceans: Evidence from Northeast Water Polynya plankton tows, sediment traps, and surface sediments. *Paleoceanography* **11**, 679-699 (1996).
31. von Gyldenfeldt, A.-B., Carstens, J. & Meincke, J. Estimation of the catchment area of a sediment trap by means of current meters and foraminiferal tests. *Deep Sea Research Part II: Topical Studies in Oceanography* **47**, 1701-1717, doi:10.1016/S0967-0645(00)00004-7 (2000).
32. Jouzel, J. *et al.* The GRIP deuterium-excess record. *Quaternary Science Reviews* **26**, 1-17, doi:10.1016/j.quascirev.2006.07.015 (2007).
33. Masson-Delmotte, V. *et al.* Atmospheric science: GRIP deuterium excess reveals rapid and orbital-scale changes in Greenland moisture origin. *Science* **309**, 118-121, doi:10.1126/science.1108575 (2005).
34. de Vernal, A. *et al.* Comparing proxies for the reconstruction of LGM sea-surface conditions in the northern North Atlantic. *Quaternary Science Reviews* **25**, 2820-2834 (2006).

35. Waelbroeck, C. *et al.* Constraints on the magnitude and patterns of ocean cooling at the Last Glacial Maximum. *Nature Geoscience* **2**, 127-132, doi:10.1038/ngeo411 (2009).
36. Locarnini, R. A. *et al.* *World Ocean Atlas 2009, Volume 1: Temperature*. Ed. NOAA Atlas NESDIS 68, U.S. Government Printing Office, Washington, D.C. edn, (2010).
37. Ehlers, J. & Gibbard, P. L. The extent and chronology of Cenozoic Global Glaciation. *Quaternary International* **164-165**, 6-20 (2007).
38. Svensson, A. *et al.* A 60 000 year Greenland stratigraphic ice core chronology. *Climate of the Past* **4**, 47-57, doi:10.1126/science.305.5690.1567a (2008).
39. Caille, C. *et al.* Sea-surface hydrographical conditions off South Faeroes and within the North-Eastern North Atlantic through MIS 2: The response of dinocysts. *Journal of Quaternary Science* **28**, 217-228, doi:10.1002/jqs.2601 (2013).
40. Laj, C., Kissel, C., Mazaud, A., Channell, J. E. T. & Beer, J. North Atlantic palaeointensity stack since 75 ka (NAPIS-75) and the duration of the Laschamp event. *Philosophical Transactions of the Royal Society A: Mathematical, Physical and Engineering Sciences* **358**, 1009-1025 (2000).
41. Head, M. J., Harland, R. & Matthiessen, J. Cold marine indicators of the late Quaternary: the new dinoflagellate cyst genus *Islandinium* and related morphotypes. *Journal of Quaternary Science* **16**, 621-636, doi:10.1002/jqs.657 (2001).
42. Rochon, A., de Vernal, A., Turon, J.-L., Matthiessen, J. & Head, M. J. 146 (AASP special pub., Dallas, Texas, 1999).
43. Guiot, J. & de Vernal, A. in *Developments in Marine Geology* Vol. Volume 1 (eds Hillaire-Marcel Claude & Vernal Anne De) 523-563 (Elsevier, 2007).
44. Guiot, J. & de Vernal, A. QSR Correspondence "Is spatial autocorrelation introducing biases in the apparent accuracy of palaeoclimatic reconstructions?" Reply to Telford and Birks. *Quaternary Science Reviews* **30**, 3214-3216, doi:10.1016/j.quascirev.2011.07.023 (2011).
45. Guiot, J. & de Vernal, A. Is spatial autocorrelation introducing biases in the apparent accuracy of paleoclimatic reconstructions? *Quaternary Science Reviews* **30**, 1965-1972, doi:10.1016/j.quascirev.2011.04.022 (2011).
46. Carstens, J. & Wefer, G. Recent distribution of planktonic foraminifera in the Nansen Basin, Arctic Ocean. *Deep Sea Research Part A, Oceanographic Research Papers* **39**, S507-S524, doi:10.1016/S0198-0149(06)80018-X (1992).
47. Bauch, D., Carstens, J. & Wefer, G. Oxygen isotope composition of living *Neogloboquadrina pachyderma* (sin.) in the Arctic Ocean. *Earth and Planetary Science Letters* **146**, 47-58 (1997).
48. Volkmann, R. & Mensch, M. Stable isotope composition ($\delta^{18}O$, $\delta^{13}C$) of living planktic foraminifers in the outer Laptev Sea and the Fram Strait. *Marine Micropaleontology* **42**, 163-188, doi:10.1016/S0377-8398(01)00018-4 (2001).
49. Kozdon, R., Eisenhauer, A., Weinelt, M., Meland, M. Y. & Nürnberg, D. Reassessing Mg/Ca temperature calibrations of *Neogloboquadrina pachyderma* (sinistral) using paired $\delta^{44}Ca/^{40}Ca$ and Mg/Ca measurements. *Geochemistry, Geophysics, Geosystems* **10**, doi:10.1029/2008GC002169 (2009).
50. Jonkers, L., Brummer, G. J. A., Peeters, F. J. C., Van Aken, H. M. & De Jong, M. F. Seasonal stratification, shell flux, and oxygen isotope dynamics of leftcoiling *N. pachyderma* and *T. quinqueloba* in the western subpolar North Atlantic. *Paleoceanography* **25**, doi:10.1029/2009PA001849 (2010).
51. Gordon, C. *et al.* The simulation of SST, sea ice extents and ocean heat transports in a version of the Hadley Centre coupled model without flux adjustments. *Climate Dynamics* **16**, 147-168, doi:10.1007/s003820050010 (2000).
52. Dufresne, J. L. *et al.* Climate change projections using the IPSL-CM5 Earth System Model: from CMIP3 to CMIP5. *Climate Dynamics* **40**, 2123-2165, doi:10.1007/s00382-012-1636-1 (2013).
53. Jungclauss, J. H. *et al.* Characteristics of the ocean simulations in the Max Planck Institute Ocean Model (MPIOM) the ocean component of the MPI-Earth system model. *Journal of Advances in Modeling Earth Systems* **5**, 422-446, doi:10.1002/jame.20023 (2013).
54. Biastoch, A., Böning, C. W., Getzlaff, J., Molines, J.-M. & Madec, G. Causes of Interannual-Decadal Variability in the Meridional Overturning Circulation of the Midlatitude North Atlantic Ocean. *Journal of Climate* **21**, 6599-6615, doi:10.1175/2008JCLI2404.1 (2008).
55. Sterl, A. *et al.* A look at the ocean in the EC-Earth climate model. *Climate Dynamics* **39**, 2631-2657, doi:10.1007/s00382-011-1239-2 (2012).
56. Sarjeant, W. A. S. Fossil and living dinoflagellates. 1-12 (Academic Press Inc., 1974).

SUPPLEMENTARY INFORMATION

Supplementary Information Table 1: Age constrains for each of the studied cores. Lab. ID.: KIA – Tandetron AMS facility at Kiel Leibniz Laboratory (Germany); GifA – Tandetron AMS facility at Gif-sur-Yvette (France); SacA– ARTEMIS Tandetron AMS facility at Saclay (France).

Core	Level /Interval dated (cm)	AMS14C ages (AR = -400yr)	Error (+/-) yr	Dated material or event based stratigraphy	Lab. ID.	Calendar age (yr)	Age model construction / Reference (if any)
MD95-2009	0	4,610	70	N. pachyderma (s)	?	5,319	Polynomial regression (order 5), this work
MD95-2009	50	8,240	100	N. pachyderma (s)	?	9,034	Polynomial regression (order 5), this work
MD95-2009	120	10,530	100	N. pachyderma (s)	?	12,594	Polynomial regression (order 5), this work
MD95-2009	280	14,190	130	N. pachyderma (s)	?	16,893	Polynomial regression (order 5), this work
MD95-2009	330	15,020	130	N. pachyderma (s)	?	17,848	Polynomial regression (order 5), this work
MD95-2009	360	16,320	140	N. pachyderma (s)	?	19,344	Polynomial regression (order 5), this work
MD95-2009	390	18,360	160	N. pachyderma (s)	?	21,692	Polynomial regression (order 5), this work
MD95-2009	430	21,360	200	N. pachyderma (s)	?	25,166	Polynomial regression (order 5), this work
MD95-2009	449			MS event (low) cor. analyseries		25,840	Polynomial regression (order 5), this work
MD95-2009	506			GI3 onset cor. analyseries		27,760	Polynomial regression (order 5), this work
MD95-2009	536			GI4 onset cor. analyseries		28,880	Polynomial regression (order 5), this work
MD95-2009	581			MS event (low) cor. analyseries		30,760	Polynomial regression (order 5), this work
MD95-2009	626			GI5 onset cor. analyseries		32,420	Polynomial regression (order 5), this work
MD95-2009	659			GI6 onset cor. analyseries		33,800	Polynomial regression (order 5), this work
MD95-2009	718			GI7 onset cor. analyseries		35,480	Polynomial regression (order 5), this work
MD95-2009	767			MS event cor. analyseries		36,800	Polynomial regression (order 5), this work
MD95-2009	793			GI8 onset cor. analyseries		38,180	Polynomial regression (order 5), this work
MD95-2009	840	34,160	500	N. pachyderma (s)	?	39,532	Polynomial regression (order 5), this work
MD95-2009	854			GI9 onset cor. analyseries		40,160	Polynomial regression (order 5), this work
MD95-2009	863			MS event (low) cor. analyseries		40,800	Polynomial regression (order 5), this work
MD95-2009	887			MS event cor. analyseries		41,240	Polynomial regression (order 5), this work

MD95-2009	900			GI10 warming after Wolff et al., 2010	41,410	Polynomial regression (order 5), this work
MD95-2009	942			GI11 warming after Wolff et al., 2010	43,290	Polynomial regression (order 5), this work
MD95-2009	947			MS event cor. analyseries	43,600	Polynomial regression (order 5), this work
MD95-2009	976			MS event cor. analyseries	44,480	Polynomial regression (order 5), this work
MD95-2009	1004			MS event cor. analyseries	44,920	Polynomial regression (order 5), this work
MD95-2009	1018			MS event cor. analyseries	46,560	Polynomial regression (order 5), this work
MD95-2009	1030			GI12 warming after Wolff et al., 2010	46,810	Polynomial regression (order 5), this work
MD95-2009	1036			MS event cor. analyseries	47,000	Polynomial regression (order 5), this work
MD95-2009	1049			MS event cor. analyseries	48,180	Polynomial regression (order 5), this work
MD95-2009	1061			MS event cor. analyseries	48,920	Polynomial regression (order 5), this work
MD95-2009	1102			GI13 warming after Wolff et al., 2010	49,230	Polynomial regression (order 5), this work
MD95-2009	1149			MS event cor. analyseries	53,580	Polynomial regression (order 5), this work
MD95-2009	1160			GI14 warming after Wolff et al., 2010	54,170	Polynomial regression (order 5), this work
MD95-2010	34-35	10,300		Vedde ash – base	11,980	Original age-model after Dokken & Jansen (1999)
MD95-2010	54-55	11,015	55	KIA 6551	12,790	Original age-model after Dokken & Jansen (1999)
MD95-2010	136-137	12,850	60	KIA 6552	15,080	Original age-model after Dokken & Jansen (1999)
MD95-2010	173-174	14,350	110	KIA 6553	16,930	Original age-model after Dokken & Jansen (1999)
MD95-2010	197-198	15,220	70	KIA 6554	17,990	Original age-model after Dokken & Jansen (1999)
MD95-2010	300-301	16,590	110	KIA 6555	19,640	Original age-model after Dokken & Jansen (1999)
MD95-2010	449-450	19,430	130	GifA 96476	22,990	Original age-model after Dokken & Jansen (1999)
MD95-2010	450-451	19,630	110	GifA 96477	23,220	Original age-model after Dokken & Jansen (1999)
MD95-2010	459-460	19,530	120	GifA 96487	23,110	Original age-model after Dokken & Jansen (1999)
MD95-2010	464-465	19,940	120	GifA 96489	23,580	Original age-model after Dokken & Jansen (1999)
MD95-2010	469-470	19,940	130	GifA 96490	23,580	Original age-model after Dokken & Jansen (1999)
MD95-2010	470-471	19,990	160	GifA 96684	23,640	Original age-model after Dokken & Jansen (1999)
MD95-2010	484-485	20,050	120	GifA 96492	23,710	Original age-model after Dokken & Jansen (1999)
MD95-2010	521-522	21,190	190	GifA 96685	25,020	Original age-model after Dokken & Jansen (1999)
MD95-2010	594-595	23,930	220	GifA 96686	28,110	Original age-model after Dokken & Jansen (1999)
MD95-2010	624-625	25,140	200	GifA 96493	29,440	Original age-model after Dokken & Jansen (1999)

Partie 3 : Vue synthétique et synoptique de la paléocéanographie de l'Atlantique subboréal et de ses mers bordières au cours des évènements millénaires de la dernière période glaciaire

MD95-2010	640-641	25,120	240		KIA 6557	29,420	Original age-model after Dokken & Jansen (1999)
MD95-2010	670-671	27,050	200		GifA 96496	31,510	Original age-model after Dokken & Jansen (1999)
MD95-2010	716-717	28,540	240		GifA 96497	33,100	Original age-model after Dokken & Jansen (1999)
MD95-2010	736-738	29,270	260		GifA 96687	33,870	Original age-model after Dokken & Jansen (1999)
MD95-2010	757-758	30,840	300		GifA 96688	35,500	Original age-model after Dokken & Jansen (1999)
MD95-2010	790-791	33,020	370		GifA 96494	37,710	Original age-model after Dokken & Jansen (1999)
MD95-2010	816-817	33,420	390		GifA 96689	38,110	Original age-model after Dokken & Jansen (1999)
MD95-2010	827-828	35,080	550		GifA 96690	39,420	Original age-model after Dokken & Jansen (1999)
MD95-2010	903-904	45,540	-1,31		KIA 6559	46,000	Original age-model after Dokken & Jansen (1999)
MD95-2010	1000-1001			Ash-layer II - base		53,000	Original age-model after Dokken & Jansen (1999)

MD99-2281	40	9,860	100	G. bulloides	Gif	11,165	Linear regression, Zumaque et al., 2012
MD99-2281	270	10,400	100	G. bulloides	Gif	12,081	Linear regression, Zumaque et al., 2012
MD99-2281	400	10,660	110	G. bulloides	Gif	12,400	Linear regression, Zumaque et al., 2012
MD99-2281	510	14,890	130	N. pachyderma (s)	Gif	17,529	Linear regression, Zumaque et al., 2012
MD99-2281	580	15,360	170	N. pachyderma (s)	Gif	18,092	Linear regression, Zumaque et al., 2012
MD99-2281	650	15,640	140	N. pachyderma (s)	Gif	18,427	Linear regression, Zumaque et al., 2012
MD99-2281	780	17,660	160	N. pachyderma (s)	Gif	20,830	Linear regression, Zumaque et al., 2012
MD99-2281	1180	22,940	240	N. pachyderma (s)	Gif	26,993	Linear regression, Zumaque et al., 2012
MD99-2281	1240			GI3 termination (duration 0.3 ka) after Wolff et al., 2010		27,430	Linear regression, Zumaque et al., 2012
MD99-2281	1275			GI3 warming after Wolff et al., 2010		27,730	Linear regression, Zumaque et al., 2012
MD99-2281	1280-1281	23,810	140	N. pachyderma (s)	SacA 19117	27,992	Linear regression, Zumaque et al., 2012
MD99-2281	1300			GI4 termination (duration 0.3 ka) after Wolff et al., 2010		28,550	Linear regression, Zumaque et al., 2012
MD99-2281	1355			GI4 warming after Wolff et al., 2010		28,850	Linear regression, Zumaque et al., 2012
MD99-2281	1430-1431	27,030	140	N. pachyderma (s)	SacA 19118	31,652	Linear regression, Zumaque et al., 2012
MD99-2281	1475			GI5 termination (duration 0.5 ka) after Wolff et al., 2010		31,950	Linear regression, Zumaque et al., 2012
MD99-2281	1523			GI5 warming after Wolff et al., 2010		32,450	Linear regression, Zumaque et al., 2012
MD99-2281	1548			GI6 termination (duration 0.4 ka) after Wolff et al., 2010		33,290	Linear regression, Zumaque et al., 2012
MD99-2281	1605			GI6 warming after Wolff et al., 2010		33,690	Linear regression, Zumaque et al., 2012
MD99-2281	1650			GI7 termination (duration 0.7 ka) after Wolff et al., 2010		34,730	Linear regression, Zumaque et al., 2012

MD99-2281	1711			GI7 warming after Wolff et al., 2010		35,430	Linear regression, Zumaque et al., 2012
MD99-2281	1755			GI8 termination (duration 1.6 ka) after Wolff et al., 2010		36,570	Linear regression, Zumaque et al., 2012
MD99-2281	1880			GI8 warming after Wolff et al., 2010		38,170	Linear regression, Zumaque et al., 2012
MD99-2281	1930			GI9 termination (duration 0.3 ka) after Wolff et al., 2010		39,810	Linear regression, Zumaque et al., 2012
MD99-2281	1960			GI9 warming after Wolff et al., 2010		40,110	Linear regression, Zumaque et al., 2012
MD99-2281	2030			GI10 termination (duration 0.7 ka) after Wolff et al., 2010		40,710	Linear regression, Zumaque et al., 2012
MD99-2281	2090			GI10 warming after Wolff et al., 2010		41,410	Linear regression, Zumaque et al., 2012
MD99-2281	2110			GI11 termination (duration 1 ka) after Wolff et al., 2010		42,290	Linear regression, Zumaque et al., 2012
MD99-2281	2170			GI11 warming after Wolff et al., 2010		43,290	Linear regression, Zumaque et al., 2012
MD99-2285	1,5	2,605	30	Bulk planktonic foraminifera	SacA 31203	2,769	Linear regression, this study
MD99-2285	70,5	9,935	40	N. pachyderma (s)	SacA 37852	11,291	Linear regression, this study
MD99-2285	136,5	12,760	45	N. pachyderma (s)	SacA 31207	15,094	Linear regression, this study
MD99-2285	175	14,080	50	N. pachyderma (s)	SacA 31204	17,082	Linear regression, this study
MD99-2285	200	15,330	50	N. pachyderma (s)	SacA 37854	18,600.5	Linear regression, this study
MD99-2285	213	16,010	50	N. pachyderma (s)	SacA 31205	19,071.5	Linear regression, this study
MD99-2285	260	19,450	200	N. pachyderma (s)	SacA 37855	23,222.5	Linear regression, this study
MD99-2285	275	20,110	90	N. pachyderma (s)	SacA 37856	24,037.5	Linear regression, this study
MD99-2285	325			GI3 termination (duration 0.3 ka) after Wolff et al., 2010		27,430	Linear regression, this study
MD99-2285	332			GI3 warming after Wolff et al., 2010		27,730	Linear regression, this study
MD99-2285	337			GI4 termination (duration 0.3 ka) after Wolff et al., 2010		28,550	Linear regression, this study
MD99-2285	349			GI4 warming after Wolff et al., 2010		28,850	Linear regression, this study
MD99-2285	386			GI6 termination (duration 0.4 ka) after Wolff et al., 2010		33,290	Linear regression, this study
MD99-2285	406			GI6 warming after Wolff et al., 2010		33,690	Linear regression, this study
MD99-2285	419			GI7 termination (duration 0.7 ka) after Wolff et al., 2010		34,730	Linear regression, this study
MD99-2285	441			GI7 warming after Wolff et al., 2010		35,430	Linear regression, this study
MD99-2285	457			GI8 termination (duration 1.6 ka) after Wolff et al., 2010		36,570	Linear regression, this study
MD99-2285	489			GI8 warming after Wolff et al., 2010		38,170	Linear regression, this study
MD99-2285	535			GI9 termination (duration 0.3 ka) after Wolff et al., 2010		39,810	Linear regression, this study
MD99-2285	552			GI9 warming after Wolff et al., 2010		40,110	Linear regression, this study

Partie 3 : Vue synthétique et synoptique de la paléocéanographie de l'Atlantique subboréal et de ses mers bordières au cours des évènements millénaires de la dernière période glaciaire

MD99-2285	590	GI10 termination (duration 0.7 ka) after Wolff et al., 2010	40,710	Linear regression, this study
MD99-2285	621	GI10 warming after Wolff et al., 2010	41,410	Linear regression, this study
MD99-2285	664	GI11 termination (duration 1 ka) after Wolff et al., 2010	42,290	Linear regression, this study
MD99-2285	730	GI11 warming after Wolff et al., 2010	43,290	Linear regression, this study
MD99-2285	750	GI12 termination (duration 2,6 ka) after Wolff et al., 2010	44,210	Linear regression, this study
MD99-2285	810	GI12 warming after Wolff et al., 2010	46,810	Linear regression, this study
MD99-2285	850	GI13 warming after Wolff et al., 2010	49,230	Linear regression, this study

Section 2. On the triggering mechanisms of the last glacial millennial climatic events: Heinrich event 4 as an outstanding case study

*Article en préparation en vue d'une soumission à **Heliyon**.*

Wary Mélanie¹, Eynaud Frédérique¹, Rossignol Linda¹, Zaragosi Sébastien¹, Malaize Bruno¹, Sicre Marie-Alexandrine², Swingedouw Didier¹, Londeix Laurent¹, Lapuyade Joanna¹, Kissel Catherine³, Gasparotto Marie-Camille^{1,*}, Castera Marie-Hélène¹, Charlier Karine¹

¹ UMR 5805, EPOC (Environnements et Paléoenvironnements Océaniques et Continentaux), Université de Bordeaux, 33615 Pessac, France.

² LOCEAN (Laboratoire d'Océanographie et du Climat: Expérimentation et Approches Numériques), IPSL-UPMC/CNRS/IRD/MNHN, Paris, France.

³ UMR8212, LSCE (Laboratoire des Sciences du Climat et de l'Environnement), CEA/CNRS-INSU/UVSQ, 91191 Gif-sur-Yvette CEDEX, France.

* now at: UQAM, Université du Québec à Montréal, Montréal, Québec H3C 3P8, Canada.

Résumé

Les événements climatiques millénaires de la dernière période glaciaire (i.e. les événements de Dansgaard-Oeschger et d'Heinrich) ont fait l'objet de nombreuses reconstructions paléocéanographiques et expériences de modélisation. Cependant, des incertitudes et incohérences notables demeurent, notamment à propos des mécanismes de déclenchement associés, et tout particulièrement ceux liés aux changements de circulation océanique en Atlantique (i.e. l'AMOC), à la dynamique des calottes de glace boréales, et aux variations abruptes de température atmosphérique. Nous combinons ici des enregistrements très haute résolution issus des sections 35-41 ka cal BP de deux carottes (MD99-2281 et MD99-2285) prélevées de part et d'autre de la ride Islande-Ecosse, i.e. deux sites antagonistes idéaux pour retracer les changements hydrographiques en lien avec la variabilité climatique millénaire de la dernière période glaciaire. Ces enregistrements sont documentés par le biais d'un large panel d'outils indicateurs de la vigueur de l'AMOC (à la fois la branche de surface pénétrant dans les Mers Nordiques, i.e. la Dérive Nord Atlantique – NAD – et ses extensions, et la branche profonde sortant des Mers Nordiques, i.e. l'*Iceland Scotland Overflow Water* – ISOW), des températures de surface et de subsurface, des décharges d'icebergs, des apports glacio-fluviaux, et des fluctuations de la couverture de glace de mer. L'intégration de l'ensemble de ces signaux suggèrent fortement que (i) les ralentissements de la NAD sont principalement dus aux apports glacio-fluviaux, alors que les ralentissements de l'AMOC semblent quant à eux être essentiellement liés à de fortes réductions de la couverture de glace en Mer de Norvège, (ii) l'advection accrue d'eaux chaudes atlantiques en surface des Mers Nordiques et le réchauffement de subsurface semblent tous deux avoir joué un rôle clé dans la déstabilisation des calottes de glace européennes, le déclenchement des effondrements de la Laurentide semblant quant à lui être plus spécifiquement lié au réchauffement de subsurface, et (iii) les réchauffements atmosphériques abrupts semblent être étroitement liés à une ré-intensification abrupte de la NAD en lien avec une réorganisation rapide des gyres et de la circulation Nord-atlantiques, cette réorganisation se produisant suite à une diminution significative des flux d'eau douce associés à la fonte d'icebergs. Ainsi, sur la base de ces résultats et de ceux émanant de précédentes études, nous proposons un scénario hydrographique permettant d'expliquer les événements climatiques abrupts de la dernière période glaciaire.

Abstract

The last glacial millennial climatic events (i.e. Dansgaard-Oeschger and Heinrich events) have been the subject of many paleoceanographical reconstructions and model experiments. However, large uncertainties and discrepancies remain, peculiarly about the associated triggering mechanisms and especially those related to the Atlantic Meridional Overturning Circulation (AMOC) changes, ice-sheet dynamics, and abrupt atmospheric temperature changes. Here, we combine very high resolution records recovered from the 35-41 ka cal BP interval of two cores (MD99-2281 and MD99-2285) retrieved from each sides of the Iceland-Scotland ridge, i.e. at key antagonist locations to track hydrographical changes related to the millennial climatic variability of the last glacial period. These records are documented by a large set of proxies indicative of AMOC (upper inflow branch, i.e. North Atlantic Drift – NAD – northward extensions, and deep outflow branch, i.e. Iceland Scotland Overflow Water – ISOW) strength, surface and subsurface temperatures, glacio-fluvial freshwater and iceberg calving discharges, and sea-ice cover fluctuations. The integration of these indices strongly suggests that (i) NAD slowdowns are mainly due to glacio-fluvial inputs while ISOW slowdowns seem to be mainly due to strong reductions of Norwegian Sea ice cover, (ii) both enhanced surface advection of warm Atlantic waters in the Nordic Seas and subsurface warming play a key role in the destabilization of European ice-sheets, the Laurentide collapse being apparently mainly triggered by subsurface warming, and (iii) the abrupt atmospheric warmings seem to be mainly due to an abrupt NAD re-intensification related to a rapid reorganization of the North Atlantic gyres and circulation subsequently to a significant decrease of meltwater inputs from icebergs. On the basis of these results and of those stemming from previous studies, we thus propose a new hydrographical scenario to explain the abrupt climate events of the last glacial period.

Keywords: Dansgaard-Oeschger events, Heinrich events, triggering mechanisms, AMOC slowdowns, ice-sheet collapses, abrupt atmospheric warming.

1. Introduction

Dansgaard-Oeschger events and Heinrich events constitute ones of the most emblematic and enigmatic features of the last glacial period. Despite many paleoreconstructions and model experiments focused on this subject, large uncertainties and discrepancies remain about their internal and individual dynamics. Nonetheless, it is commonly admitted that the cold atmospheric phases of Dansgaard-Oeschger events (Greenland Stadials, hereafter GS), including the ones correlated with Heinrich events (called Heinrich Stadials, hereafter HS; Sanchez Goni and Harisson, 2010), are associated with ice-rafted debris (IRD) deposits in the subpolar area resulting from ice-sheet collapses and subsequent iceberg calving (e.g. Bond and Lotti, 1995; Elliot et al., 2001). Their systematic occurrence during phases of significant reduction of the Atlantic Meridional Overturning Circulation (AMOC; e.g. Kissel et al., 1999; Rahmstorf, 2002; Böhm et al., 2015) suggests that these cyclic ice-sheet instabilities were triggered by processes involving AMOC changes, either as the cause (e.g. Alvarez-Solas et al., 2010; Alvarez-Solas and Ramstein, 2011) or the consequence (e.g. Manabe and Stouffer, 1995; Ganopolski and Rahmstorf, 2001; Levine and Bigg, 2008).

While most studies converge towards a similar hydrographical scheme in the North Atlantic Ocean during these millennial changes (with e.g. cold sea-surface temperatures – SST – during GS and HS; e.g. Sachs and Lehman, 1999), hydrographical conditions in the Norwegian Sea are more subject to discussion since significant discrepancies exist between the different paleoreconstructions and model experiments (see references herein). Recent studies conducted on two cores retrieved southwest (MD99-2281; 60.3418 °N; -9.4557 °E; 1197 m water depth) and northeast (MD99-2285; 62.6938 °N; -3.5723 °E; 885 m water depth) off Faeroes (i.e. Zumaque et al., 2012; Caille et al., 2013; Wary et al., CP, in press¹, JQS, submitted², QSR, to be submitted³, EPSL, to be submitted⁴, and Nature, to be submitted⁵; cf Fig. 1), with support from other paleoreconstructions and model experiments (see particularly Eynaud et al., 2002, Rasmussen and Thomsen, 2004, Kleinen et al., 2009, Swingedouw et al., 2013, and references below), have brought evidence for a new hydrographical scenario in the NE Atlantic Ocean and SE Nordic Seas during the last glacial millennial climatic events.

¹ cf. page 83 de ce manuscrit

² cf. page 127 de ce manuscrit

³ cf. page 163 de ce manuscrit

⁴ cf. page 201 de ce manuscrit

⁵ cf. page 227 de ce manuscrit

These new hydrographical scheme and processes, which conciliate many paleodata coming from previous studies, imply:

- During GI, an active AMOC (e.g. Kissel et al., 1999; Ganopolski and Rahmstorf, 2001; Bigg et al., 2011; Böhm et al., 2015), with deep water formation mainly driven by intense seasonal sea-ice formation in the cold Norwegian Sea, and possible contribution from open-ocean convection south of the Greenland-Scotland Ridge.
- At the end of GI, the occurrence of a significant glacio-fluvial freshwater flux, and the subsequent beginning of advection of warm Atlantic waters in the Norwegian Sea (with these advected waters seemingly propagating in subsurface in the Atlantic basin, and re-emerging in surface at the entrance of the Norwegian Sea around site MD99-2281).
- During GS and HS, reduced AMOC, enhanced iceberg calving (e.g. Elliot et al., 1998, 2001), strongly reduced or even nil sea-ice cover in the Norwegian sea, very warm summer sea-surface temperatures (SST) in the Norwegian Sea (up to 17°C), as well as moderate subsurface and intermediate-depth warming (see Shaffer et al., 2004) in the Norwegian Sea (Rasmussen and Thomsen, 2004 and references therein; Marcott et al., 2011; Dokken et al., 2013; Ezat et al., 2014) and in the NW Atlantic (Marcott et al., 2011).

This new hydrographical scenario thus highlights the occurrence of several mechanisms susceptible to have triggered:

- AMOC slowdowns: the glacio-fluvial freshwater flux (end of GI) and its influence on the upper branch of the AMOC (i.e. the North Atlantic Drift – NAD – and its northward extensions) and/or the destabilization of the Norwegian Sea ice cover at the beginning of GS.
- Ice-sheet destabilizations: melting of buttress structures (i.e. sea ice and ice-shelves) due to strong surface warming in the Nordic Sea and/or to basin-wide subsurface warming.

However, some uncertainties remain, notably regarding the respective contribution of these triggering mechanisms. Here we present new high resolution records indicative of NAD strength and of subsurface warming at site MD99-2281 over the 37-40 ka cal BP interval. We compare them with previously published high resolution records from cores MD99-2281 and MD99-2285, spanning the 35-41 ka cal BP interval, which are indicative of glacio-fluvial freshwater inputs, iceberg calving, and strength of the lower branch of the AMOC at both

sites, as well as of advection of warm Atlantic waters, sea-ice cover, SST and subsurface warming in the Southern Norwegian Sea (site MD99-2285). This comparison allows us to go further in these hydrographical processes by assessing the role played by each potential triggering mechanisms of AMOC slowdowns and ice-sheet collapses during GI-HS and GI-GS transitions around the H4 case study period.

2. Regional settings and chronostratigraphic framework

Both sites are ideally located to track hydrographical changes related to the millennial ice-sheet collapse events and to AMOC fluctuations. Indeed, this area is presently under the dual influence of (i) the warm and salty Atlantic waters of the northward extensions of the NAD, and of the Continental Slope Current whose geographical origin is debated (e.g. Kenyon, 1986; McCartney and Mauritzen, 2001; Orvik and Niiler, 2002; Mauritzen et al., 2005), and (ii) the deep and intermediate cold waters overflowing from the Nordic Seas (Iceland Scotland Overflow Water, ISOW) to the North Atlantic where they will feed the North Atlantic Deep Water (see Fig. 1; Boldreel et al., 1998; Kuijpers et al., 1998; Hansen and Osterhus, 2000; Borenäs and Lundberg, 2004; Mauritzen et al., 2005). During the last glacial period, it was also under the direct influence of the proximal European ice-sheets (i.e. the Fennoscandian and the British-Irish ice-sheets; cf. Fig. 1; Svendsen et al., 2004; Sejrup et al., 2003; Bradwell et al., 2008) whose decays and built-up have modulated the regional oceanic and climatic dynamics.

Both cores are chrono-stratigraphically constrained by AMS ^{14}C datings and tied to the NGRIP GICC05 time scale (Andersen et al., 2006; Svensson et al., 2008; Wolff et al., 2010) thanks to a peak to peak correlation between their magnetic susceptibility records and the NGRIP $\delta^{18}\text{O}$ signal (cf. Zumaque et al., 2012; Wary et al., JQS, submitted) as recommended in the study area (e.g. Rasmussen et al., 1996a,b; Kissel et al., 1999; Laj et al., 2000; Elliot et al., 2002; Ballini et al., 2006; Rasmussen and Thomsen, 2009). The present study focuses on the 37-40 ka cal BP interval of core MD99-2281, and on the 35-41 ka cal BP interval of core MD99-2285. The high sedimentation rates of the presently studied sections (on average 58 cm.k^{-1} for core MD99-2281, and 30 cm.k^{-1} for core MD99-2285) provide sufficient temporal resolutions (mean resolutions between 4 and 38 years for core MD99-2281, and between 55 and 155 years for core MD99-2285, depending on proxies) to resolve the abrupt

hydrographical changes of the last glacial millennial climatic variability throughout the H4 case study period. Moreover, temporal comparison between these two cores is reasonable on the studied period as long as we keep in mind age model uncertainties and the slight temporal lags evidenced around GI9 and HS4 (cf. Fig. 2b, see Wary et al., EPSL, to be submitted for further details).

3. Material and methods, proxy significance

The new high resolution records recovered from the ~37-40 ka cal BP section of core MD99-2281 are derived from planktonic foraminifera (PF) analyses (see e.g. Wary et al., CP, in press for further analytical and technical details), with here exploited:

- The relative abundances of dominant and index species in PF assemblages > 150 μm (polar taxon *Neogloboquadrina pachyderma* sinistral form – hereafter NPS –, and temperate species *Globigerina bulloides* and *Turborotalita quinqueloba*).
- The quantified mean summer and mean winter temperature reconstructions (hereafter PF-Temp) obtained by applying a transfer function to PF assemblages developed by Eynaud et al. (2013) and based on the Modern Analogue Technique (method also described in e.g. Matsuzaki et al., 2011; Penaud et al., 2011; Sánchez Goñi et al., 2012, 2013; Mary et al., 2015).
- The $\delta^{18}\text{O}$ measurements performed on monospecific samples of NPS (200-250 μm , hereafter $\delta^{18}\text{O}_{\text{NPS}}$).

In core MD99-2281, variations in the relative abundances of the dominant PF species (polar *versus* temperate taxa) and in PF-Temp have been previously related at lowest temporal resolutions to relative variations of subsurface hydrological conditions tightly linked to the NAD strength (cf. Wary et al., CP, in press). The same study has shown that, in this core, $\delta^{18}\text{O}_{\text{NPS}}$ variations recorded during the last glacial millennial events are mainly due to temperature effects related to variations in the NAD strength. However, HS4 is characterized by a peculiar $\delta^{18}\text{O}_{\text{NPS}}$ signature whose interpretation will be further discussed in Sect. 4.2.1.

Here, we compare these signals with previously published high resolution records from cores MD99-2281 and MD99-2285. These published records are listed in Table 1 which includes their provenance (see these studies for further methodological details) and their main

interpretation in the corresponding studied core(s). It is worth mentioning that reconstructions stemming from dinocysts in core MD99-2285 (SST_{dino} and SIC_{dino}) are considered as very likely representative of surface conditions in the whole Norwegian Sea since Eynaud et al. (2002) found similar results in core MD95-2010 located on the Vøring Plateau (66.6842°N; 4.5662°E).

Furthermore, we extend our new PF derived records over the ~ 35-37 ka cal BP and ~ 40-41 ka cal BP intervals with previously published lower resolution records obtained from the same core (Zumaque et al., 2012; Wary et al., CP, in press). Such extension appears meaningful as both sets of measurements (“low” and high resolution) were acquired under the exact same conditions (i.e. PF assemblages counted by the same person and with the same binocular magnifier, and $\delta^{18}O_{NPS}$ measured with the same Optima Micromass mass spectrometer at EPOC laboratory). We do not do the same for other lower resolution records available from Zumaque et al. (2012, i.e. concentrations of IRD and reworked dinocysts) or from Wary et al. (CP, submitted, i.e. concentration of *Pediastrum* spp.) as they were not acquired under the same conditions which could lead to some minor biases (e.g. Mertens et al., 2009).

4. Results and discussion

4.1. Triggering mechanisms of AMOC slowdowns

4.1.1. Variations of AMOC strength over the 35-41 ka cal time period

Records indicative of AMOC strength clearly reveal different dynamics of slowdown between the upper inflow branch (NAD, Fig. 2d and e) and the deep outflow branch (ISOW, Fig. 2c) at GI to GS/HS transitions, such that AMOC slowdowns can be divided into two phases.

The first phase (phase 1, green bands on Fig. 2) is characterized by an important decrease in the relative abundances of temperate PF taxa (%PF temperate) in relation to a concomitant significant increase in the relative abundance of the polar taxa NPS (%NPS), and a slight decrease of PF-Temp. These features typify of a relative slowdown of the NAD. In

the meantime, mean size of 10-63 μm , 0.5-10 μm and 0.5-20 μm fractions are maximal or relatively high, which indicates strong ISOW bottom flow.

In the second phase (phase 2, blue bands on Fig. 2), %PF temperate keep on increasing and %NPS keeps on decreasing (at lower rates), PF-Temp strongly decrease, and mean size of the 10-63 μm , 0.5-10 μm and 0.5-20 μm fractions generally strongly decrease as well. These features thus denote significant slowdowns of the NAD and of ISOW bottom flow, i.e. significant slowdowns of the whole AMOC.

It is worth noting that phase 2 of GI9 to HS4 transition appears slightly different from the one of GI10 to GS10 and GI8 to GS8 transitions. Indeed, during phase 2 of GI10 to GS10 and GI8 to GS8 transitions, NAD and ISOW strengths seem to decrease almost perfectly synchronously. This is clearly not the case during phase 2 of GI9 to HS4 transition, which can be subdivided into two sub-phases. During the first one (sub-phase 2.1, light blue band on Fig. 2), PF-derived data indicate a decrease of NAD strength to minimal (nil) activity. Grain-size records of ISOW activity are more ambiguous to interpret, peculiarly in core MD99-2285 where no trend clearly appears. In core MD99-2281, they seem to denote an apparent decrease of ISOW strength, which would be very coherent with the scheme depicted during the second phase of GI10 to GS10 and GI8 to GS8 transitions. Hence, sub-phase 2.1 would be equivalent to phase 2 of GI10 to GS10 and GI8 to GS8 transitions. During the second sub-phase (sub-phase 2.2, dark blue band on Fig. 2), while records indicate that NAD is already strongly reduced, ISOW strength signals exhibit significant decrease and attain their minimal values in both cores (except for mean size of 10-63 μm fraction in core MD99-2281 which displays moderate values at this time, but these moderate values are very likely due to IRD inputs given their occurrence during the main IRD peak recorded in this core – cf. Fig. 3c – and given the minimal values exhibited by mean size of 0.5-20 μm fraction in this same core). Hence, contrary to GI10 to GS10 and GI8 to GS8 transitions, ISOW strength keeps on decreasing after NAD slowdown during GI9 to HS4 transition.

4.1.2. Implications

The comparison of these signals of AMOC strength with the ones indicative of glacio-fluvial inputs clearly reveals that these freshwater inputs had a direct impact on the NAD strength. Indeed, NAD strength seems to decrease throughout time intervals when glacio-fluvial inputs are recorded (i.e. higher concentrations of reworked dinocysts, *Pediastrum* spp.

and *Halodinium* spp., highlighted by green horizontal double arrows on Fig.2f). However, their impact on ISOW strength is not obvious, since ISOW strength starts to decrease only when glacio-fluvial inputs are already lowering (i.e. when the concentrations of advected palynomorphs are decreasing). On the contrary, the strong decreases of ISOW strength (phase 2, and sub-phase 2.2) appear to be concomitant with strong reduction of sea-ice cover in the Norwegian Sea, expressed in terms of sea-ice cover duration (SIC_{dino}) as well as sea ice formation (IP25, Fig. 2g). Similarly, the moderate ISOW strength decreases recorded during sub-phase 2.1 appears to be concomitant with a moderate reduction of sea-ice cover in the Norwegian Sea. Furthermore, it is worth noting that both mean size of the 10-63 µm fraction (MD99-2281) and IP25 abundances (MD99-2285) seem to exhibit progressive increasing trends throughout GI8. Progressive increase of ISOW strength during GI8, and abrupt decrease at the beginning of GS8, have also been recorded in other cores from the Reykjanes Ridge (Snowball and Moros, 2003). Such a coupling supports Wary et al. (JQS, submitted)'s hypothesis that sea-ice formation is a significant motor of deep convection in the Norwegian Sea.

Hence, these results suggest that:

- NAD and ISOW slowdowns are surprisingly not fully coupled.
- NAD slowdowns at investigated GI to GS/HS transitions are mainly due to glacio-fluvial inputs from the European ice-sheets (and maybe also from additional concomitant contributions other pan-Atlantic ice-sheets, cf. Wary et al., EPSL, to be submitted)
- The impact of these freshwater inputs on ISOW strength seems not to be significative.
- Sea-ice formation in the Norwegian Sea seems to be the main driver of deep convection during GI, and ISOW slowdowns at GI to GS/HS transitions appear to be mainly due to strong reduction in this sea-ice cover. Wary et al. (QSR, to be submitted) related these strong reduction of Norwegian Sea ice cover to intense iceberg calving implying chaotic surface conditions where sea ice formation is prevented.

4.2. Triggering mechanisms of ice-sheet destabilizations

4.2.1. Interpretation of $\delta^{18}\text{O}_{\text{NPS}}$ in core MD99-2281

$\delta^{18}\text{O}_{\text{NPS}}$ signals are remarkably similar in both cores during HS4: they decrease up to ~ 39 ka cal BP, and then increase again (Fig. 3f). However, it is worth mentioning that such a signature must be exceptional in core MD99-2281. Indeed, in this core (Fig. 3f, see also Fig. 3f in Wary et al., CP, in press), and seemingly in cores located along the Atlantic pathway of the NAD extensions (such as core MD95-2006 in Rockall Trough, cf. Figure 3 from Dickson et al., 2008), lower resolution $\delta^{18}\text{O}_{\text{NPS}}$ signals were shown to be generally higher during GS and lower during GI. Both studies interpreted these $\delta^{18}\text{O}_{\text{NPS}}$ variations as mainly due to subsurface temperature changes related to weaker (GS) *versus* stronger (GI) NAD flow. Furthermore, in core MD99-2281, $\delta^{18}\text{O}_{\text{NPS}}$ first starts to increase at the very beginning of HS4 (up to ~ 39.6 ka cal BP). Nonetheless, very slight decreases are also depicted during GS10, 8, 7 and 6 despite the general high values, and an even stronger decrease is recorded during HS1 (cf. Fig. 3 in the present study for GS10 and 8, and Fig. 3f in Wary et al., CP, in press for GS7, GS6 and HS1). Besides, similarly to the exceptionally low $\delta^{18}\text{O}_{\text{NPS}}$ values recorded in core MD99-2281 during HS4 and HS1, Dickson et al. (2008) recorded a significant $\delta^{18}\text{O}_{\text{NPS}}$ decrease during HS5 (the only investigated HS in their study). Conversely, in the Norwegian Sea, $\delta^{18}\text{O}_{\text{NPS}}$ records exhibit significant decreases during both GS and HS (e.g. Dokken and Jansen, 1999; Rasmussen and Thomsen, 2004).

In core MD99-2281, and as in core MD99-2285, due to the presence of a strong halocline isolating the surface layer (inhabited by dinoflagellates, i.e. the photic layer) from the subsurface layer (inhabited by PF, i.e. from a few tens of meters to ~ 300 m water depth) during GS and HS (cf. Wary et al., CP, submitted and EPSL, to be submitted), these stadial $\delta^{18}\text{O}_{\text{NPS}}$ decreases can only be explained by: (i) a slight contribution from the sea-level rises recorded during these periods (e.g. Siddall et al., 2008), but which cannot explain the whole amplitude of HS4 signal, and (ii) a moderate subsurface warming, with subsurface temperatures $< 5-6$ °C according to the strong dominance of NPS at that time and to the reconstructed PF-Temp (Fig. 2d and e) (see Wary et al., QSR, to be submitted and references therein for further details). The only exception concerns the low $\delta^{18}\text{O}_{\text{NPS}}$ peak recorded around 39.2 ka cal BP and which interrupts the progressive decrease. Indeed, this peak occurs coevally to the main IRD peak identified in core MD99-2281 (Fig. 3c), during a short episode related to decreasing upper stratification by Wary et al. (EPSL, to be submitted).

4.2.2. Implications

Two potential triggering mechanisms of ice sheet destabilization and collapse (recorded through IRD concentrations; Fig. 3c) are here considered through their impact on buttress structures, i.e. sea ice and ice-shelves: (i) subsurface warming, recorded by $\delta^{18}\text{O}_{\text{NPS}}$ (Fig. 3f), and (ii) Norwegian Sea surface warming, recorded by summer SST_{dino} (Fig. 3e), which is due to enhanced warm Atlantic water advection, recorded by SST_{alk} (Fig. 3d). Furthermore, it is important to mention that Wary et al. (EPSL, to be submitted) suggested that MD99-2285 IRD signal mainly reflects European ice-sheets dynamic, while in core MD99-2281, the main IRD peak recorded during HS4 (~ from 39.3 to 38.9 ka cal BP) has a strong Laurentide signature whereas the rest of the IRD signal is seemingly mainly related to European ice-sheets dynamic.

In both cores, European-derived IRD concentrations start to increase when surface advection of warm Atlantic waters also starts to increase and starts to impact on summer Norwegian Sea SST, while $\delta^{18}\text{O}_{\text{NPS}}$ is still relatively high (green bands and arrows on Fig. 3). This clearly suggests that advection of Atlantic waters and subsequent Norwegian Sea surface warming play a key role on European ice-sheets initial destabilization.

Nonetheless, during GS and HS maxima IRD peaks, which occur coevally to maxima summer SST_{dino} peaks and high SST_{alk} values, $\delta^{18}\text{O}_{\text{NPS}}$ values are low or decreasing (blue bands and arrows on Fig. 3). During these peaks, it seems difficult to differentiate the contribution of both mechanisms (i.e. surface *versus* subsurface warming). Indeed, due to the strong upper halocline and summer thermocline evidenced at that time in the study area (e.g. Wary et al., QSR, to be submitted), Norwegian Sea summer SST increases are very likely due to enhanced surface advection of warm Atlantic waters rather than upwelling of subsurface heat. Thus, the striking synchronicity between MD99-2285 IRD peaks and SST_{dino} maxima, in parallel to high SST_{alk} , strongly suggests an important contribution of enhanced Atlantic water advection to the final collapse of European ice sheets. However, even if MD99-2281 HS4 IRD peak also appears to be potentially relatively synchronous with the sudden increase in summer SST_{dino} recorded at that time, it seems impossible that Norwegian Sea surface warming triggered Laurentide massive collapse. Nonetheless, the possible synchronicity between HS4 IRD peaks from both cores strongly suggests the occurrence of a common triggering mechanism to the final massive collapse of European and Laurentide ice-sheets. The similarity between $\delta^{18}\text{O}_{\text{NPS}}$ signals from both cores during HS4 strongly suggests that a

subpolar North Atlantic basin-wide subsurface warming could be this common triggering mechanism, as previously advanced from modelling experiments (e.g. Shaffer et al., 2004; Alvarez-Solas et al., 2010, 2011).

Furthermore, the Hudson Strait imprint is inexistent or very weak in IRD layers associated to non-HS stadials (e.g. Bond and Lotti, 1995; Wary et al., EPSL, to be submitted). In parallel, none, or only weak, subsurface warmings are recorded by $\delta^{18}\text{O}_{\text{NPS}}$ signals from Atlantic cores MD99-2281 and MD95-2006 (Dickson et al., 2008) during these non-HS stadials. Moreover, based on Mg/Ca measurements conducted on NPS from core DS97-2P located on the Reykjanes Ridge, Jonkers et al. (2010) also evidenced moderate subsurface warming during stadials, with especially weaker subsurface warmings during GI8, 7, and 6 than during HS4. In this core, these planktonic Mg/Ca rises are concomitant with $\delta^{18}\text{O}_{\text{NPS}}$ decreases of similar relative amplitude, i.e. weaker decrease during GS than HS4. In addition, in core MD99-2285, $\delta^{18}\text{O}_{\text{NPS}}$ decreases also seem to be slightly weaker during GS8 and 10 than during HS4. Similarly, in Norwegian Sea cores ENAM93-21 and MD95-2010, $\delta^{18}\text{O}_{\text{NPS}}$ decreases are generally much stronger during HS than GS over the 10-60 ka cal BP studied interval (Dokken and Jansen, 1999; Rasmussen and Thomsen, 2004). Such findings support the hypothesis that Laurentide ice-sheet collapses during HS are triggered by subsurface warming (see also Marcott et al., 2011). They also lend support to Alvarez-Solas et al. (2013)'s modeling study, where HS are associated with strong subsurface warming in the Labrador Sea while non-HS stadials are associated with smaller subsurface warming in this basin, and suggest that these features might be characteristic of the whole subpolar North Atlantic basin and adjacent seas.

Hence, on the basis of these results, we propose that:

- During HS4 (and maybe other HS), enhanced surface advection of warm Atlantic waters in the Nordic Seas first starts to destabilize European ice sheets, leading to the so-called "European precursor". Later, the massive destabilization and subsequent collapse of the Laurentide ice sheet was seemingly due to a strong subpolar North Atlantic basin-wide subsurface warming. In parallel, the probably almost synchronous collapse of European ice-sheets was likely due to the combination of both this subsurface warming and Norwegian Sea surface warming linked to enhanced Atlantic water advection.

- In comparison during GS, the subsurface warming seems to be weaker, both in the North Atlantic basin and adjacent seas, which could explain the absence of strong evidence of Laurentide ice-sheet collapse during these stadials. However, in the Norwegian Sea, this reduced subsurface warming was reinforced by enhanced surface advection of warm Atlantic waters. These combined processes were likely responsible for the triggering of European ice-sheet collapses during GS.

Furthermore, it is worth mentioning that such scenarios of triggering of ice-sheet collapse do not preclude a potential additional contribution from subsequent sea-level rise, as suggested by previous studies (e.g. Chappell, 2002; Shaffer et al., 2004).

4.3. Mechanisms responsible for the abrupt atmospheric warmings at the onset of GI

Most works studying the millennial climatic variability of the last glacial periods have focused on the cold and catastrophic phases rather than on the abrupt atmospheric warmings following them. Nonetheless, some studies have suggested that these strong atmospheric warmings might originate from the abrupt destabilization of the upper halocline due to the accumulation of subsurface heat below (e.g. Rasmussen and Thomsen, 2004, Dokken et al., 2013; Wary et al., 2015). However, $\delta^{18}\text{O}_{\text{NPS}}$ records from both MD99-2281 and MD99-2285 cores indicate that subsurface temperatures start to decrease well before the abrupt warming of GI8 (Fig. 3f), which does not favor such an hypothesis. Moreover, while abrupt atmospheric warmings of similar amplitude are recorded at the onset of each GI, our work suggests that subsurface warming was strongly reduced in the subpolar North Atlantic basin during non-HS stadials, which here again does not favor such an hypothesis.

On the contrary, our reconstructed PF-Temp exhibit a more than striking resemblance with NGRIP $\delta^{18}\text{O}$ record, particularly noticeable on the 37-40 ka cal BP high resolution section if we account for age model uncertainties (Fig. 4a and b; correlation coefficient of 0.81 and 0.85 for mean summer and mean winter PF-Temp respectively, with the present age models). Most remarkably, the abrupt warming recorded in NGRIP $\delta^{18}\text{O}$ signal at the onset of GI8 is peculiarly well reproduced in PF-Temp record. Furthermore, Fig. 4 (b and c) also highlights the remarkable anti-phase between PF-Temp, i.e. NAD strength, and SST_{alk}, i.e. advection of warm and saline water through the Continental Slope Current to the Norwegian Sea (correlation coefficient of -0.55 and -0.56 for mean summer and mean winter PF-Temp

respectively). This feature recalls the one evidenced by Hátún et al. (2005), who showed that when the subpolar gyre (SPG) circulation is relatively strong (which can be considered as the “classical” situation), the transport from the SPG to the Nordic Seas through the NAD is high, while the transport from the subtropical gyre (STG) to the Nordic Seas, seemingly through the Continental Slope Current (cf. McCartney and Mauritzen, 2001; Hátún et al., 2005), is low. Inversely, when SPG circulation is relatively weak (which is expected subsequently to the freshwater input at the end of GI, cf. Kleinen et al., 2009), the transport from the SPG to the Nordic Seas through the NAD is reduced, while the transport from the STG to the Nordic Seas through the Continental Slope Current is high, leading to an enhanced and more saline Atlantic inflow in the Nordic Seas across the Iceland-Scotland Ridge.

Hence, we rather propose that the abrupt atmospheric warmings recorded at the onset of GI are due to an abrupt reorganization of the North Atlantic gyres and circulation, characterized by a rapid return to a “classical” circulation configuration where the NAD suddenly becomes more active while the Continental Slope Current strength strongly decreases. The triggering mechanism of this abrupt hydrographic reorganization is more enigmatic. We can hypothesize that after iceberg calving episodes, the North Atlantic meltwater cap is not fed anymore by meltwater inputs and abruptly disintegrates, thus enabling the abrupt re-intensification of the SPG circulation. The NAD could then cross the North Atlantic Ocean directly in surface in contact with the atmosphere, and dive to subsurface around site MD99-2281 (cf. Wary et al., CP, in press) as presently in the Arctic (e.g. Aagard et al., 1981). Such an hypothesis could be supported by the significant and abrupt decrease recorded in IRD concentration from core MD99-2281 (from ~ 1100 to ~ 400 IRD.g⁻¹ of dry sediment) coevally to the strong and abrupt increase of PF-Temp at the onset of GI8 (Fig. 3c).

Nonetheless, it is worth noting that while SST_{alk} abruptly decrease at the onset of GI9, and PF-Temp abruptly increase at the onset on GI9 and 8, which all support our hypothesis, the progressive decrease of SST_{alk} recorded during the second half of HS4 would rather favor a progressive re-intensification of the SPG. Wary et al. (QSR, to be submitted) already mentioned the curious character of this time interval, when local Norwegian Sea summer SST stay high whereas SST_{alk} / advection of warm Atlantic waters decrease. A change in upstream alkenone production (e.g. in terms of seasonality) could maybe explain this conflicting signal.

Moreover, it is also worth mentioning that in core MD99-2284, Dokken et al. (2013)'s PF-derived reconstructed temperatures generally display a slight but abrupt increase at the onset of GS, then a more or less progressive increase throughout GS, and finally an abrupt decrease at the onset of GI, almost in anti-phase with NGRIP $\delta^{18}\text{O}$ signal. The authors, and Wary et al. (QSR, to be submitted), previously related this signal to subsurface stadial warming, which is in contradiction with our $\delta^{18}\text{O}_{\text{NPS}}$ records and thus with our hypothesis. Nonetheless, as mentioned in Sect. 4.2.1., the increase of $\delta^{18}\text{O}_{\text{NPS}}$ recorded in our cores during the second half of HS4 undeniably reflects a decrease of subsurface temperatures. It cannot be an artifact related to a rupture of the upper stratification, since (i) Wary et al. (EPSL, to be submitted) showed that a halocline was undeniably present throughout the whole HS4 interval at least at site MD99-2281, and (ii) given sea surface conditions recorded at that time in both cores (low salinities and high summer SST, cf. Wary et al., EPSL, to be submitted), such a rupture of the halocline would not explain this increase of $\delta^{18}\text{O}_{\text{NPS}}$. Furthermore, site MD99-2284 is located very close to the Continental Slope Current pathway (cf. Fig. 1). Hence, we can reasonably hypothesize that Dokken et al. (2013)'s PF-derived temperature reconstructions rather reflect the strength of the Continental Slope Current. Indeed, despite significant differences between our SST_{alk} signal and Dokken et al.'s PF-derived temperature signal (which could possibly be explained by different temporal resolution on the common time interval), both signals share common trends, particularly the atypical warm stadial temperatures *versus* cold interstadial temperatures. Such an alternative interpretation would thus explain the atypical character of Dokken et al.'s reconstructions, and would be in better agreement with our data and hypotheses.

Furthermore, if we consider that NGRIP $\delta^{18}\text{O}$ variations are due to changes in NAD strength, i.e. that PF-Temp may be tuned NGRIP $\delta^{18}\text{O}$, this would have significant impact in terms of timing of hydrographical variations identified at GI9 to HS4 transition. Firstly, the glacio-fluvial input, decrease of NAD strength, enhancement of Atlantic water advection through the Continental Slope Current, and moderate/progressive increase of iceberg calving would start not at the end but in the middle of GI9, such as during GI8. Secondly, the subsurface warming would start at the end of GI. And thirdly, the abrupt Norwegian Sea surface warming and ice cover decline, ISOW slowdown, and massive iceberg calving episode would occur at the beginning of HS4, such as for GS8.

5. Synthesis and conclusions: hydrographical scheme and processes during the abrupt millennial climatic events of the last glacial period

On the basis of the results stemming from the present study, and from previous ones (Eynaud et al., 2002; Kleinen et al., 2009; Swingedouw et al., 2013; Wary et al., CP, in press, JQS, submitted, QSR, to be submitted, EPSL, to be submitted, and Nature, to be submitted, and references below), we can thus propose the following hydrographical scenario:

- During the whole GI and onset of GS/HS, the Norwegian Sea is marked by cold sea surface conditions seasonally covered with sea-ice. The seasonal formation of sea-ice seems to be the main driver of deep convection in the Norwegian Sea, while open-ocean convection might have also occurred south of the Greenland-Scotland Ridge.
- During the second half of GI, a significant freshwater flux, very likely related to glacio-fluvial inputs from the European ice-sheets (i.e. the Fennoscandian and/or the British-Irish ice-sheets) and maybe also from the other pan-Atlantic ice-sheets, is responsible for the creation of a cold meltwater lid in surface of the North Atlantic Ocean.
- These freshwater flux and subsequent North Atlantic meltwater lid reduce the SPG circulation, which in turn first leads to enhanced propagation of warm Atlantic waters from the STG to the Nordic Seas, and secondly induces a NAD slowdown (and subsequent Greenland atmospheric cooling) that persists throughout GS/HS (see Hátún et al., 2005). The propagation of advected Atlantic waters very likely occurs in subsurface in the Atlantic basin before re-emerging to the surface around site MD99-2281 at the entrance of the Nordic Seas, and probably in surface along the present path of the Continental Slope Current (cf. McCartney and Mauritzen, 2001; Hátún et al., 2005; Peck et al., 2008; Dokken et al., 2013). This surface warm Atlantic water mass mixes with Nordic Sea ambient surface waters, and progressively warms up Nordic Sea surface, peculiarly during summer season.
- In parallel during GS and HS, the insulation of the subsurface layer by the North Atlantic meltwater lid induces a moderate warming of the subsurface and intermediate-depth layers (Shaffer et al., 2004). These relatively warm subsurface and intermediate water masses propagates into the Norwegian Sea (with temperatures remaining $\leq 5-6$ °C; Rasmussen and Thomsen, 2004; Marcott et al., 2011; Ezat et al., 2014), maybe partly entrained by the enhanced Continental Slope Current, and seemingly also in the whole subpolar North Atlantic basin, including NW Atlantic (Marcott et al., 2011).

- At the beginning of GS and HS, the strong Nordic Sea surface warming (increase of summer SST up to 17 °C at site MD99-2285), combined to the moderate subsurface and intermediate-depth warming, significantly destabilize the sea-ice cover of the Norwegian Sea and the bordering ice-shelves. During GS, this subpolar North Atlantic basin-wide subsurface warming seems to be weaker and apparently insufficient to strongly destabilize the Laurentian ice-shelves. Conversely during HS(4), a much stronger subsurface warming occurs and is likely responsible for the significant destabilization of the Laurentian ice-shelves.
- This has two major hydrographic impacts: (i) the significant size reduction of these buttress structures *in fine* induces ice stream acceleration and iceberg surges (Alvarez-Solas et al., 2010) from European ice-sheets during GS, and from both European and Laurentide ice-sheets during HS, and (ii) the relatively warm winter Norwegian Sea SST (Wary et al., QST, to be submitted) combined to intense iceberg calving prevent sea-ice formation in the Norwegian, the main motor of deep convection during the last glacial period. Consequently, ISOW flow, and thus the whole AMOC, slow down.
- Finally, when iceberg discharges end up, the North Atlantic freshwater cap is not fed by meltwater anymore, and is suddenly destabilized. This allows the abrupt re-intensification of the SPG circulation and subsequent abrupt re-intensification of NAD while the Continental Slope Current strength abruptly decreases. This also induces the abrupt atmospheric warming recorded in Greenland ice cores.
- In parallel, the return to cold and non-chaotic surface conditions in the Norwegian Sea at GS/HS to GI transition enables sea ice formation again, and subsequent deep convection and reactivation of ISOW and thus of the whole AMOC.

Our study thus provides new insights about the dynamical interactions between ocean, cryosphere and atmosphere, and most particularly about the hydrographical mechanisms triggering AMOC slowdowns, ice-sheets destabilization and final collapse, and abrupt atmospheric warmings during the last glacial millennial climatic events. However, new paleoreconstructions and model experiments are needed to confirm our hypotheses at greater spatial and temporal scales, and to support the physics behind the proposed mechanisms. Furthermore, some uncertainties still remain, and our proposed hydrographical scenario raises further questions, that would need to be assessed through new studies, such as for example:

- What is the origin of the initial freshwater flux, in terms of source area (only European ice-sheets or also Laurentide and/or Greenland ice-sheets? Mainly Fennoscandian or British-Irish Ice-sheet?) and of triggering mechanism(s) (the warm interstadial atmospheric temperatures? A more direct impact of the active NAD on ice-sheets/ice-shelves? Other?)
- Are the SST and SIC patterns identified in the Norwegian Sea characteristic of the whole Nordic Seas?
- Did the subsurface warming really occur in the whole subpolar North Atlantic basin and adjacent seas during GS and HS as suggested by model experiments and data from the Northeast Atlantic Ocean and Norwegian Sea? Why was it weaker during GS than HS?
- What is the impact of surface warming on sea ice and ice-shelves in models?
- What is the system reaction to sea-ice retreat in models?

Despite such uncertainties, our results and hypotheses suggest that the millennial glacial oscillations are self-sustained and due to an apparent natural instability of glacial climate, rather than forced by a preferred external or internal forcing. However, it is probable that the system reactions were sensitive to orbital conditions, such as suggested by the fact that major Heinrich events occurred during maximal high latitude summer insolation ([Rasmussen and Thomsen, 2004](#)), or by the similarity between Norwegian Sea ice cover maximal extension and obliquity signal ([Wary et al., JQS, submitted](#)).

References

- Aagaard K., Coachman L.K. and Carmack E. (1981). On the halocline of the Arctic Ocean. *Deep Sea Research Part A, Oceanographic Research Papers* 28(6): 529-545.
- Alvarez-Solas J., Charbit S., Ritz C., Paillard D., Ramstein G. and Dumas C. (2010). Links between ocean temperature and iceberg discharge during Heinrich events. *Nature Geoscience* 3(2): 122-126.
- Alvarez-Solas J. and Ramstein G. (2011). On the triggering mechanism of Heinrich events. *Proceedings of the National Academy of Sciences* 108(50): E1359-E1360.
- Alvarez-Solas J., Robinson A., Montoya M. and Ritz C. (2013). Iceberg discharges of the last glacial period driven by oceanic circulation changes. *Proceedings of the National Academy of Sciences of the United States of America* 110(41): 16350-16354.
- Álvarez-Solas J., Montoya M., Ritz C., Ramstein G., Charbit S., Dumas C., Nisancioglu K., Dokken T. and Ganopolski A. (2011). Heinrich event 1: An example of dynamical ice-sheet reaction to oceanic changes. *Climate of the Past* 7(4): 1297-1306.
- Andersen K.K., Svensson A., Johnsen S.J., Rasmussen S.O., Bigler M., Röthlisberger R., Ruth U., Siggaard-Andersen M.L., Peder Steffensen J., Dahl-Jensen D., Vinther B.M. and Clausen H.B. (2006). The Greenland Ice Core Chronology 2005, 15-42 ka. Part 1: constructing the time scale. *Quaternary Science Reviews* 25(23-24): 3246-3257.
- Ballini M., Kissel C., Colin C. and Richter T. (2006). Deep-water mass source and dynamic associated with rapid climatic variations during the last glacial stage in the North Atlantic: a multi-proxy investigation of the detrital fraction of deep-sea sediments. *Geochem Geophys Geosystems* 7(Q02N01).
- Bigg G.R., Levine R.C. and Green C.L. (2011). Modelling abrupt glacial North Atlantic freshening: Rates of change and their implications for Heinrich events. *Global and Planetary Change* 79(3-4): 176-192.
- Böhm E., Lippold J., Gutjahr M., Frank M., Blaser P., Antz B., Fohlmeister J., Frank N., Andersen M.B. and Deininger M. (2015). Strong and deep Atlantic meridional overturning circulation during the last glacial cycle. *Nature* 517(7532): 73-76.

- Boldreel L.O., Andersen M.S. and Kuijpers A. (1998). Neogene seismic facies and deep-water gateways in the Faeroe Bank area, NE Atlantic. *Marine Geology* 152(1-3): 129-140.
- Bond G.C. and Lotti R. (1995). Iceberg discharges into the North Atlantic on millennial time scales during the last glaciation. *Science* 267(5200): 1005-1010.
- Borenäs K. and Lundberg P. (2004). The Faeroe-Bank Channel deep-water overflow. *Deep-Sea Research Part II: Topical Studies in Oceanography* 51(4-5): 335-350.
- Bradwell T., Stoker M.S., Golledge N.R., Wilson C.K., Merritt J.W., Long D., Everest J.D., Hestvik O.B., Stevenson A.G., Hubbard A.L., Finlayson A.G. and Mathers H.E. (2008). The northern sector of the last British Ice Sheet: Maximum extent and demise. *Earth-Science Reviews* 88(3-4): 207-226.
- Caulle C., Penaud A., Eynaud F., Zaragosi S., Roche D.M., Michel E., Boulay S. and Richter T. (2013). Sea-surface hydrographical conditions off South Faeroes and within the North-Eastern North Atlantic through MIS 2: The response of dinocysts. *Journal of Quaternary Science* 28(3): 217-228.
- Chappell J. (2002). Sea level changes forced ice breakouts in the Last Glacial cycle: New results from coral terraces. *Quaternary Science Reviews* 21(10): 1229-1240.
- Dickson A.J., Austin W.E.N., Hall I.R., Maslin M.A. and Kucera M. (2008). Centennial-scale evolution of Dansgaard-Oeschger events in the northeast Atlantic Ocean between 39.5 and 56.5 ka B.P. *Paleoceanography* 23(3): PA3206.
- Dokken T.M. and Jansen E. (1999). Rapid changes in the mechanism of ocean convection during the last glacial period. *Nature* 401(6752): 458-461.
- Dokken T.M., Nisancioglu K.H., Li C., Battisti D.S. and Kissel C. (2013). Dansgaard-Oeschger cycles: Interactions between ocean and sea ice intrinsic to the Nordic seas. *Paleoceanography* 28(3): 491-502.
- Elliot M., Labeyrie L., Bond G., Cortijo E., Turon J.L., Tisnerat N. and Duplessy J.C. (1998). Millennial-scale iceberg discharges in the Irminger Basin during the last glacial period: Relationship with the Heinrich events and environmental settings. *Paleoceanography* 13(5): 433-446.
- Elliot M., Labeyrie L., Dokken T. and Manthe S. (2001). Coherent patterns of ice-rafted debris deposits in the Nordic regions during the last glacial (10-60 ka). *Earth and Planetary Science Letters* 194(1-2): 151-163.
- Elliot M., Labeyrie L. and Duplessy J.C. (2002). Changes in North Atlantic deep-water formation associated with the Dansgaard - Oeschger temperature oscillations (60-10 ka). *Quaternary Science Reviews* 21(10): 1153-1165.
- Eynaud F., Turon J.L., Matthiessen J., Kissel C., Peypouquet J.P., De Vernal A. and Henry M. (2002). Norwegian sea-surface palaeoenvironments of marine oxygen-isotope stage 3: The paradoxical response of dinoflagellate cysts. *Journal of Quaternary Science* 17(4): 349-359.
- Eynaud F., Rossignol L. and Gasparotto M.-C. (2013). Planktic foraminifera throughout the Pleistocene: from cell to populations to past marine hydrology. In In : "Foraminifera: Classification, Biology, and Evolutionary Significance", (ed. ed. M.D.G.), pp. 209-226. Nova Science Publishers, NY.
- Ezat M.M., Rasmussen T.L. and Groeneveld J. (2014). Persistent intermediate water warming during cold stadials in the southeastern Nordic seas during the past 65 k.y. *Geology* 42(8): 663-666.
- Ganopolski A. and Rahmstorf S. (2001). Rapid changes of glacial climate simulated in a coupled climate model. *Nature* 409(6817): 153-158.
- Hansen B. and Osterhus S. (2000). North Atlantic-Nordic Sea exchanges. *Progress in Oceanography* 45: 109-208.
- Hátún H., Sande A.B., Drange H., Hansen B. and Valdimarsson H. (2005). Influence of the atlantic subpolar gyre on the thermohaline circulation. *Science* 309(5742): 1841-1844.
- Hodell D.A., Minth E.K., Curtis J.H., McCave I.N., Hall I.R., Channell J.E.T. and Xuan C. (2009). Surface and deep-water hydrography on Gardar Drift (Iceland Basin) during the last interglacial period. *Earth and Planetary Science Letters* 288(1-2): 10-19.
- Jonkers L., Moros M., Prins M.A., Dokken T., Dahl C.A., Dijkstra N., Perner K. and Brummer G.J.A. (2010). A reconstruction of sea surface warming in the northern North Atlantic during MIS 3 ice-rafting events. *Quaternary Science Reviews* 29(15-16): 1791-1800.
- Kenyon N.H. (1986). Evidence from bedforms for a strong poleward current along the upper continental slope of northwest Europe. *Marine Geology* 72(1-2): 187-198.
- Kissel C., Laj C., Labeyrie L., Dokken T., Voelker A. and Blamart D. (1999). Rapid climatic variations during marine isotopic stage 3: Magnetic analysis of sediments from Nordic Seas and North Atlantic. *Earth and Planetary Science Letters* 171(3): 489-502.
- Kleinen T., Osborn T.J. and Briffa K.R. (2009). Sensitivity of climate response to variations in freshwater hosing location. *Ocean Dynamics* 59(3): 509-521.
- Kuijpers A., Andersen M.S., Kenyon N.H., Kunzendorf H. and Van Weering T.C.E. (1998). Quaternary sedimentation and Norwegian Sea overflow pathways around Bill Bailey Bank, northeastern Atlantic. *Marine Geology* 152(1-3): 101-127.
- Laj C., Kissel C., Mazaud A., Channell J.E.T. and Beer J. (2000). North Atlantic palaeointensity stack since 75 ka (NAPIS-75) and the duration of the Laschamp event. *Philosophical Transactions of the Royal Society A: Mathematical, Physical and Engineering Sciences* 358(1768): 1009-1025.
- Levine R.C. and Bigg G.R. (2008). Sensitivity of the glacial ocean to Heinrich events from different iceberg sources, as modeled by a coupled atmosphere-iceberg-ocean model. *Paleoceanography* 23(4): PA4213.
- Manabe S. and Stouffer R.J. (1995). Simulation of abrupt climate change induced by freshwater input to the North Atlantic Ocean. *Nature* 378(6553): 165-167.
- Marcott S.A., Clark P.U., Padman L., Klinkhammer G.P., Springer S.R., Liu Z., Otto-Bliesner B.L., Carlson A.E., Ungerer A. and Padman J. (2011). Ice-shelf collapse from subsurface warming as a trigger for Heinrich events. *Proceedings of the National Academy of Sciences* 108(33): 13415-13419.
- Mary Y., Eynaud F., Zaragosi S., Malaizé B., Cremer M. and Schmidt S. (2015). High frequency environmental changes and deposition processes in a 2 kyr-long sedimentological record from the Cap-Breton canyon (Bay of Biscay). *Holocene* 25(2): 348-365.
- Matsuzaki K.M.R., Eynaud F., Malaizé B., Grousset F.E., Tisserand A., Rossignol L., Charlier K. and Jullien E. (2011). Paleoenvironment of the Mauritanian margin during the last two climatic cycles: From planktonic foraminifera to African climate dynamics. *Marine Micropaleontology* 79(3-4): 67-79.
- Mauritzen C., Price J., Sanford T. and Torres D. (2005). Circulation and mixing in the Faroese Channels. *Deep-Sea Research Part I: Oceanographic Research Papers* 52(6): 883-913.
- McCartney M.S. and Mauritzen C. (2001). On the origin of the warm inflow to the Nordic Seas. *Progress in Oceanography* 51(1): 125-214.

- McCave I.N., Manighetti B. and Beveridge N.A.S. (1995). Circulation in the glacial North Atlantic inferred from grain-size measurements. *Nature* 374(6518): 149-152.
- Mertens K.N., Verhoeven K., Verleye T., Louwye S., Amorim A., Ribeiro S., Deaf A.S., Harding I.C., De Schepper S., González C., Kodrans-Nsiah M., De Vernal A., Henry M., Radi T., Dybkjaer K., Poulsen N.E., Feist-Burkhardt S., Chitolie J., Heilmann-Clausen C., Londeix L., Turon J.L., Marret F., Matthiessen J., McCarthy F.M.G., Prasad V., Pospelova V., Kyffin Hughes J.E., Riding J.B., Rochon A., Sangiorgi F., Welters N., Sinclair N., Thun C., Soliman A., Van Nieuwenhove N., Vink A. and Young M. (2009). Determining the absolute abundance of dinoflagellate cysts in recent marine sediments: The *Lycopodium* marker-grain method put to the test. Review of Palaeobotany and Palynology 157(3-4): 238-252.
- Orvik K.A. and Niiler P. (2002). Major pathways of Atlantic water in the northern North Atlantic and Nordic Seas toward Arctic. *Geophysical Research Letters* 29(19): 2-1.
- Peck V.L., Hall I.R., Zahn R. and Elderfield H. (2008). Millennial-scale surface and subsurface paleothermometry from the northeast Atlantic, 55-8 ka BP. *Paleoceanography* 23(3): PA3221.
- Penaud A., Eynaud F., Voelker A., Kageyama M., Marret F., Turon J.L., Blamart D., Mulder T. and Rossignol L. (2011). Assessment of sea surface temperature changes in the Gulf of Cadiz during the last 30 ka: Implications for glacial changes in the regional hydrography. *Biogeosciences* 8(8): 2295-2316.
- Prins M.A., Bouwer L.M., Beets C.J., Troelstra S.R., Weltje G.J., Kruk R.W., Kuijpers A. and Vroon P.Z. (2002). Ocean circulation and iceberg discharge in the glacial North Atlantic: Inferences from unmixing of sediment size distributions. *Geology* 30(6): 555-558.
- Rahmstorf S. (2002). Ocean circulation and climate during the past 120,000 years. *Nature* 419(6903): 207-214.
- Rasmussen T.L., Thomsen E., Labeyrie L. and Van Weering T.C.E. (1996a). Circulation changes in the Faeroe-Shetland Channel correlating with cold events during the last glacial period (58-10 ka). *Geology* 24(10): 937-940.
- Rasmussen T.L., Thomsen E., Van Weering T.C.E. and Labeyrie L. (1996b). Rapid changes in surface and deep water conditions at the Faeroe Margin during the last 58,000 years. *Paleoceanography* 11(6): 757-771.
- Rasmussen T.L. and Thomsen E. (2004). The role of the North Atlantic Drift in the millennial timescale glacial climate fluctuations. *Palaeogeography, Palaeoclimatology, Palaeoecology* 210(1): 101-116.
- (2009). Ventilation changes in intermediate water on millennial time scales in the SE Nordic seas, 65-14 kyr BP. *Geophysical Research Letters* 36(1): L01601.
- Sachs J.P. and Lehman S.J. (1999). Subtropical North Atlantic temperatures 60,000 to 30,000 years ago. *Science* 286(5440): 756-760.
- Sanchez Goñi M.F. and Harrison S.P. (2010). Millennial-scale climate variability and vegetation changes during the Last Glacial: Concepts and terminology. *Quaternary Science Reviews* 29(21-22): 2823-2827.
- Sánchez Goñi M.F., Bakker P., Desprat S., Carlson A.E., Van Meerbeeck C.J., Peyron O., Naughton F., Fletcher W.J., Eynaud F., Rossignol L. and Renssen H. (2012). European climate optimum and enhanced Greenland melt during the last interglacial. *Geology* 40(7): 627-630.
- Sánchez Goñi M.F., Bard E., Landais A., Rossignol L. and D'Errico F. (2013). Air-sea temperature decoupling in western Europe during the last interglacial-glacial transition. *Nature Geoscience* 6(10): 837-841.
- Sejrup H.P., Larsen E., Haflidason H., Berstad I.M., Hjelstuen B.O., Jonsdottir H.E., King E.L., Landvik J., Longva O., Nygard A., Ottesen D., Raunholm S., Rise L. and Stalsberg K. (2003). Configuration, history and impact of the Norwegian Channel Ice Stream. *Boreas* 32(1): 18-36.
- Shaffer G., Olsen S.M. and Bjerrum C.J. (2004). Ocean subsurface warming as a mechanism for coupling Dansgaard-Oeschger climate cycles and ice-rafter events. *Geophysical Research Letters* 31(24): 1-4.
- Siddall M., Rohling E.J., Thompson W.G. and Waellbroeck C. (2008). Marine isotope stage 3 sea level fluctuations: Data synthesis and new outlook. *Reviews of Geophysics* 46(4): RG4003.
- Snowball I. and Moros M. (2003). Saw-tooth pattern of North Atlantic current speed during Dansgaard-Oeschger cycles revealed by the magnetic grain size of Reykjanes Ridge sediments at 59°N. *Paleoceanography* 18(2): 4-1.
- Svensden J.I., Alexanderson H., Astakhov V.I., Demidov I., Dowdeswell J.A., Funder S., Gataullin V., Henriksen M., Hjort C., Houmark-Nielsen M., Hubberten H.W., Ingólfsson O., Jakobsson M., Kjær K.H., Larsen E., Lokrantz H., Lunkka J.P., Lyså A., Mangerud J., Matiouchkov A., Murray A., Möller P., Niessen F., Nikolskaya O., Polyak L., Saarnisto M., Siegert C., Siegert M.J., Spielhagen R.F. and Stein R. (2004). Late Quaternary ice sheet history of northern Eurasia. *Quaternary Science Reviews* 23(11-13): 1229-1271.
- Svensson A., Andersen K.K., Bigler M., Clausen H.B., Dahl-Jensen D., Davies S.M., Johnsen S.J., Muscheler R., Parrenin F., Rasmussen S.O., Röthlisberger R., Seierstad I., Steffensen J.P. and Vinther B.M. (2008). A 60 000 year Greenland stratigraphic ice core chronology. *Climate of the Past* 4(1): 47-57.
- Swingedouw D., Rodehacke C.B., Behrens E., Menary M., Olsen S.M., Gao Y., Mikolajewicz U., Mignot J. and Biastoch A. (2013). Decadal fingerprints of freshwater discharge around Greenland in a multi-model ensemble. *Climate Dynamics* 41(3-4): 695-720.
- Valdimarsson H. and Malmberg S.-A. (1999). Near-surface circulation in Icelandic waters derived from satellite tracked drifters. *Rit Fiskideild* 16: 23-40.
- Wary M., Eynaud F., Sabine M., Zaragosi S., Rossignol L., Malaizé B., Palis E., Zumaque J. and Caille C. (2015). Stratification of surface waters during the last glacial millennial climatic events: a key factor in subsurface and deep water mass dynamics. *Climate of the Past Discussion* 11: 2077-2119.
- Wolff E.W., Chappellaz J., Blunier T., Rasmussen S.O. and Svensson A. (2010). Millennial-scale variability during the last glacial: The ice core record. *Quaternary Science Reviews* 29(21-22): 2828-2838.
- Zumaque J., Eynaud F., Zaragosi S., Marret F., Matsuzaki K.M., Kissel C., Roche D.M., Malaizé B., Michel E., Billy I., Richter T. and Palis E. (2012). An ocean-ice coupled response during the last glacial: a view from a marine isotopic stage 3 record south of the Faeroe Shetland Gateway. *Climate of the Past* 8(6): 1997-2017.

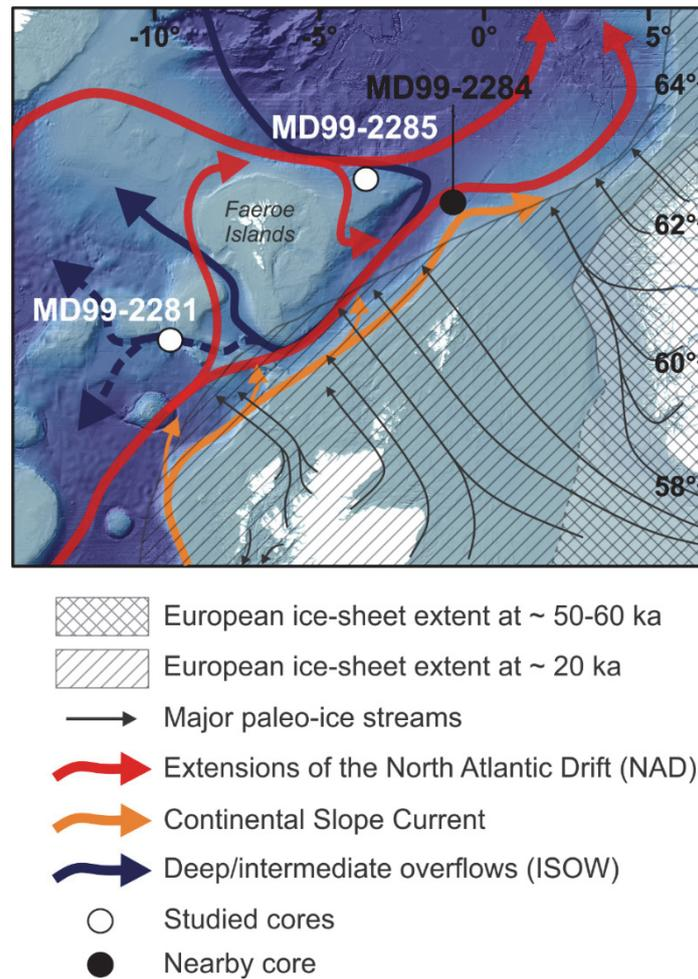


Figure 1: Map of the study area showing the locations of the studied cores (MD99-2281 and MD99-2285) and of nearby core (MD99-2284), as well as past and modern environmental settings. Last glacial ice-sheet extensions are from Svendsen et al. (2004). Major paleo-ice streams are from Sejrup et al. (2003) and Bradwell et al. (2008). Surface current pathways are from Kenyon (1986), Valdimarsson and Malmberg (1999) and Orvik and Niiler (2002). Deep bottom flow pathways of ISOW are from Kuijpers et al. (1998) and Boldreel et al. (1998). Bathymetry is from EMODnet (www.emodnet.eu). Geographic coordinate system: WGS 1984 – Projection: Mercator 55°N.

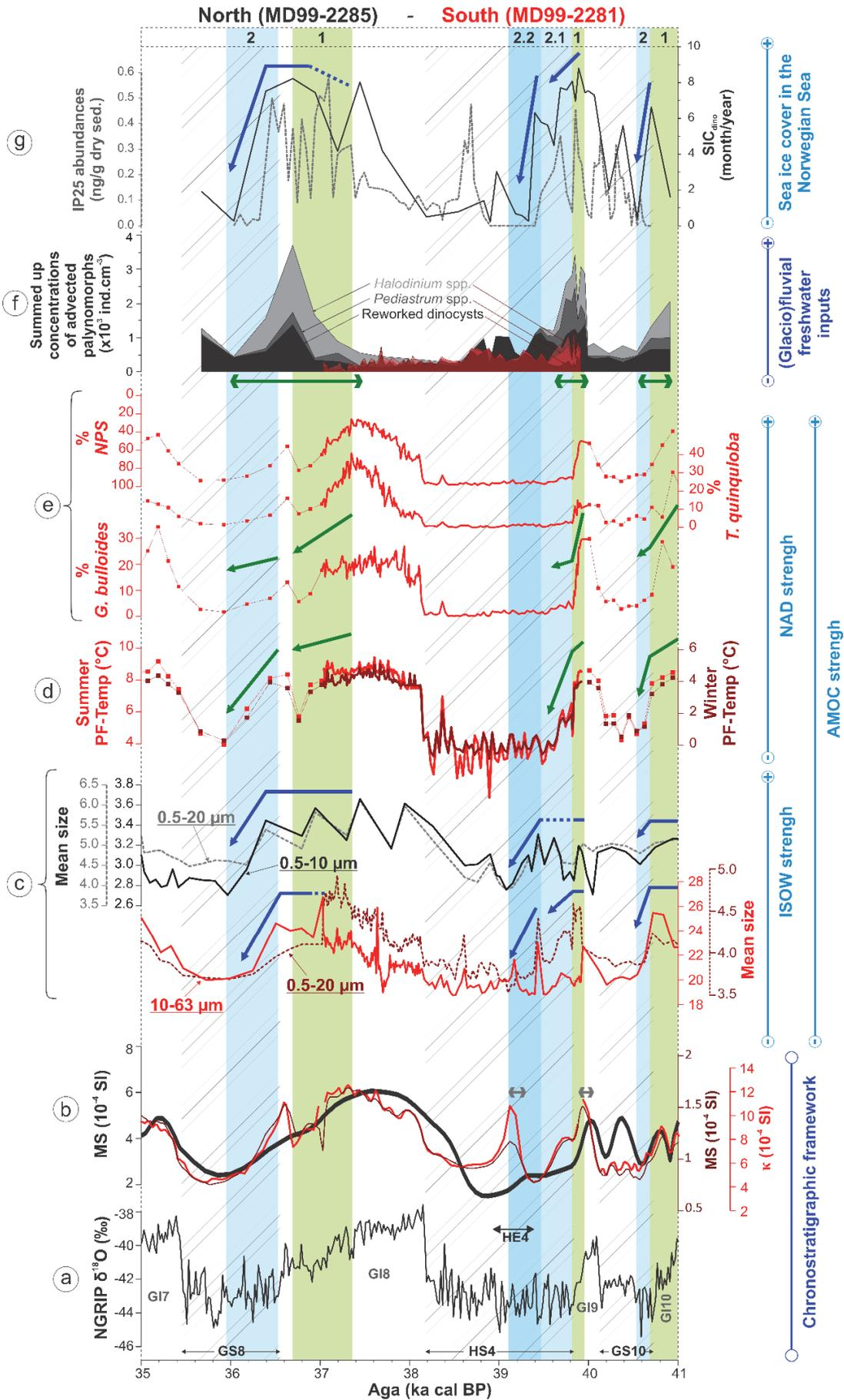


Figure 2

Figure 2: Age compilation of records from cores MD99-2281 (in red and dark red) and MD99-2285 (in black and gray) indicative of AMOC strength and potential triggering mechanisms of its slowdowns at GI to GS/HS transitions. (a) NGRIP $\delta^{18}\text{O}$ regional stratotype, compared to (b) the magnetic susceptibility (MS) and/or low field magnetic susceptibility (κ) of both cores. (c) ISOW strength indicators. (d and e) NAD strength indicators (after Wary et al., CP, in press), with PF-derived temperature reconstructions (d) and relative percentages of temperate and polar PF species (e). Note the reverse scale of the relative percentage of *N. pachyderma* sinistral form (NPS). (f) Summed up concentrations of *Halodinium* spp. (light gray and red), *Pediastrum* spp. (medium gray and red), and reworked dinocysts (black and dark red), indicative of glacio-fluvial inputs after Wary et al. (QSR, to be submitted, and EPSL, to be submitted). (g) Indicators of sea-ice cover in the Norwegian Sea, i.e. IP25 abundances indicative of sea ice formation, and sea-ice cover duration derived from dinocyst assemblages, from Wary et al. (QSR, to be submitted). Hatched bands indicate GS intervals (age limits after Wolff et al., 2010). Green bands highlight periods when NAD strength decreases while ISOW flow is strong (phase 1). Light blue bands highlight periods when both NAD and ISOW strength decrease (phase 2 and sub-phase 2.1). Dark blue band highlight the period when ISOW strength decreases while NAD strength is reduced (sub-phase 2.2). Green horizontal double arrows indicate time intervals when glacio-fluvial inputs occur. Green simple arrows indicate NAD strength decreases. Blue arrows indicate ISOW strength and Norwegian Sea ice cover dynamics at GI to GS/HS transitions.

Figure 3: Age compilation of records from cores MD99-2281 (in red and dark red) and MD99-2285 (in black) indicative of ice-sheet decays and potential triggering mechanisms of ice-sheet collapses at GI to GS/HS transitions. (a) NGRIP $\delta^{18}\text{O}$ regional stratotype, compared to (b) the magnetic susceptibility (MS) and/or low field magnetic susceptibility (κ) of both cores. (c) IRD concentrations indicative of iceberg calving, i.e. ice-sheet destabilization, after Wary et al. (QSR, to be submitted, and EPSL, to be submitted). (d) SST reconstructions derived from alkenone analyses, indicative of surface advection of warm Atlantic waters after Wary et al. (QSR, to be submitted). (e) summer SST reconstructions stemming from dinocyst analyses, indicative of in situ Norwegian Sea summer SST after Wary et al. (QSR, to be submitted). (f) $\delta^{18}\text{O}$ measured on *N. pachyderma* sinistral form, indicative of subsurface temperatures during GS and HS, according to the present study and to Wary et al. (QSR, to be submitted). (g) PF-derived temperature reconstructions. Hatched bands indicate GS intervals (age limits after Wolff et al., 2010). Green bands and arrows highlight the beginning of ice-sheet destabilization, of surface advection of warm Atlantic waters in the Nordic Seas, and of increase of Norwegian Sea summer SST. Blue bands and arrows highlight periods of massive ice-sheet collapse, maximal Norwegian Sea summer SST, strong surface advection of warm Atlantic waters in the Nordic Seas, and moderate subsurface warming.

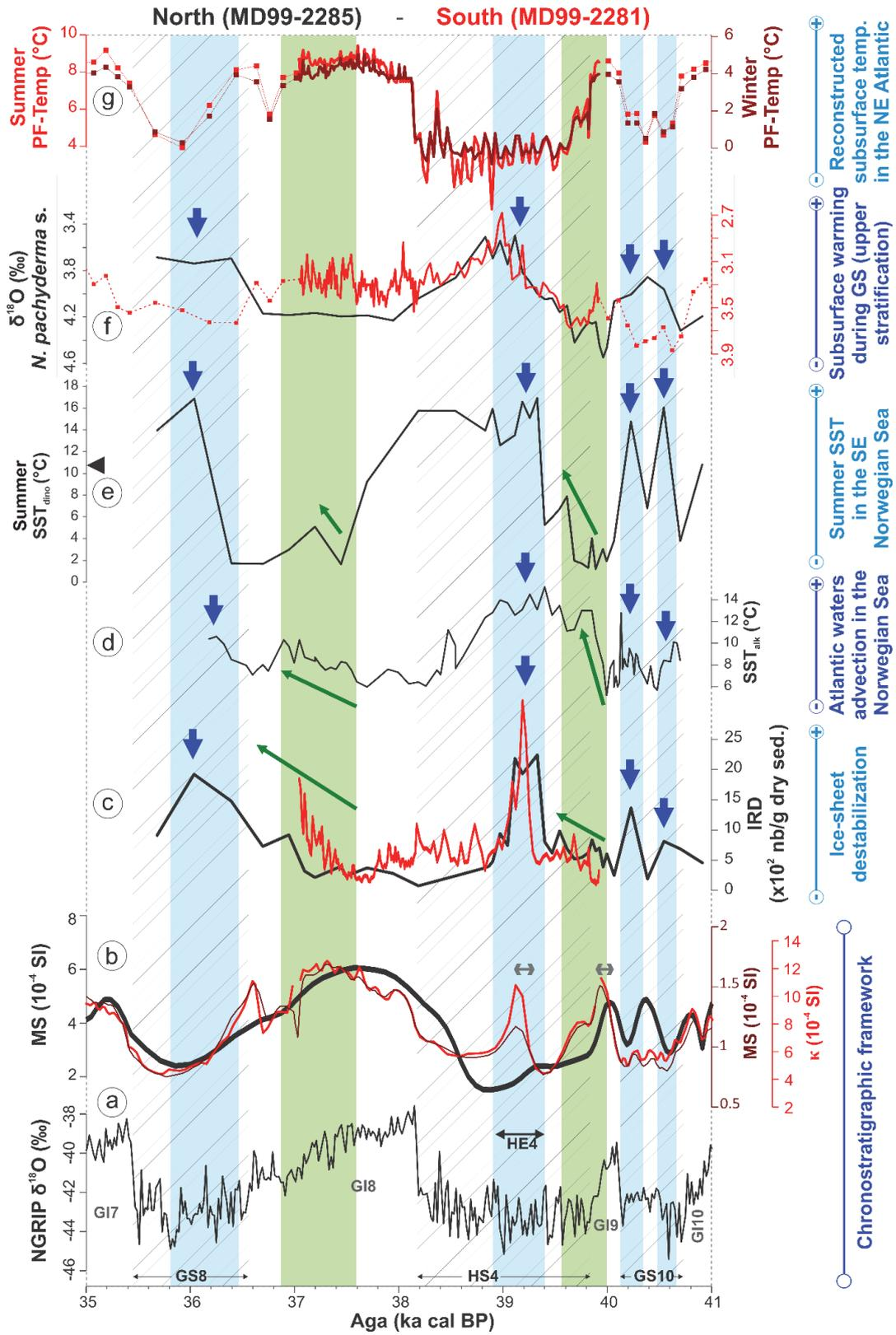


Figure 3

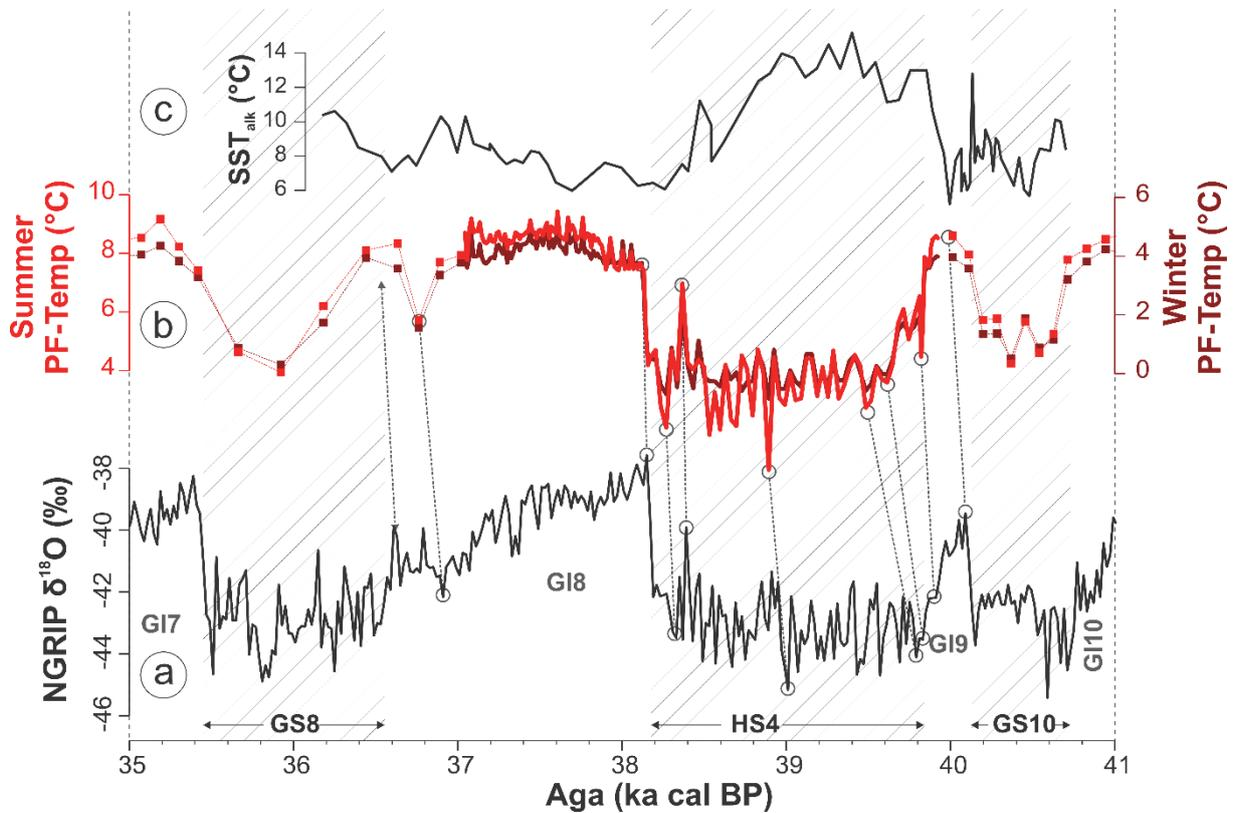


Figure 4: Comparison between (a) NGRIP $\delta^{18}O$ signal, indicative of atmospheric temperatures above Greenland ice-sheet, (b) PF-Temp record from core MD99-2281, indicative of NAD strength, and (c) SST_{alk} signal from core MD99-2285 indicative of enhanced advection of warm Atlantic waters seemingly through the Continental Slope Current. This figure highlights the more than striking resemblance between NGRIP $\delta^{18}O$ and PF-Temp signals, which suggests that a rapid re-intensification of the NAD might be the triggering mechanism of the abrupt atmospheric warming recorded in NGRIP at the onset of GI. It also highlights the remarkable anti-phase between PF-Temp and SST_{alk} records, which suggests that this rapid NAD re-intensification might be due to an abrupt re-organization of the North Atlantic gyres and circulation. Hatched bands indicate GS intervals (age limits after Wolff et al., 2010).

Table 1: List of previously published records used in the present study, their provenance, and their main interpretation in the related study(ies)/core(s).

Proxies	Main interpretation in studied core	MD99-2281	MD99-2285
IRD (>150µm) concentration	Iceberg calving	Wary et al., EPSL, to be submitted	Wary et al., QSR, to be submitted
Concentration of <i>Pediastrum</i> spp. and <i>Halodinium</i> spp.	Glacio-fluvial freshwater inputs from the European ice-sheets	Wary et al., EPSL, to be submitted	Wary et al., QSR, to be submitted
Concentration of reworked dinocysts	Glacio fluvial inputs + advection of warm Atlantic waters in the Norwegian Sea	Wary et al., EPSL, to be submitted	Wary et al., QSR, to be submitted
SST reconstructions stemming from alkenone analyses	Advection of warm Atlantic waters in the Norwegian Sea		Wary et al., QSR, to be submitted
Summer SST reconstructions stemming from dinocyst assemblages (SST_{dino})	<i>in situ</i> summer SST		Wary et al., QSR, to be submitted
Sea-ice cover reconstructions stemming from dinocyst assemblages (SIC_{dino})	<i>in situ</i> sea-ice cover duration		Wary et al., QSR, to be submitted
Sea-ice cover reconstructions stemming from IP25 analyses	<i>in situ</i> sea ice formation		Wary et al., QSR, to be submitted
Grain-size measurements¹	Strength of ISOW bottom flow	Wary et al., CP, in press (mean of 0.5-20 µm and 10-63 µm fraction)	Wary et al., JQS, submitted (mean of 0.5-10 µm and 0.5-20 µm fractions)
δ¹⁸O_{NPS}	moderate subsurface warming <i>versus</i> sea ice melting		Wary et al., QSR, to be submitted

¹ Mean size of 10-63 µm size fraction is a proxy widely used to estimate past changes of bottom current strength, including in the Rockall Trough close to MD99-2281 site (e.g. McCave et al., 1995; Hodell et al., 2009). Mean size of 0.5-10 µm and 0.5-20 µm size fractions appear as better proxies to track variations of the strength of low-energy bottom currents in glacial sediments influenced not only by bottom flow speed but also by IRD inputs (Prins et al., 2002), and have been proved to be suitable for the area around MD99-2285 site (Ballini et al., 2006). In the present study, we added the record of mean size of 0.5-20 µm fraction for site MD99-2281 to identify eventual variations in the mean size of 10-63 µm fraction due to IRD inputs.

Conclusions générales et perspectives

Cette thèse avait pour objectif principal d'étendre nos connaissances sur la variabilité climatique millénaire caractérisant la dernière période glaciaire à travers la reconstruction et l'analyse des changements hydrographiques enregistrés dans deux archives sédimentaires (carottes MD99-2281 et MD99-2285) prélevées de part et d'autre de la ride Islande-Ecosse, une zone dont la forte sensibilité à la variabilité climatique rapide avait déjà été démontrée par de précédentes études. Ces changements hydrographiques ont été documentés à travers une approche multiproxies (couplant analyses micropaléontologiques – dinokystes et autres palynomorphes, foraminifères planctoniques et benthiques –, géochimiques – $\delta^{18}\text{O}$, biomarqueurs, Xrf –, et sédimentologiques – granularité du sédiment et IRD) et à haute résolution temporelle (résolution moyenne minimale d'environ 350 ans, et maximale d'environ 30 ans), permettant de retracer la dynamique des masses d'eau de surface, de subsurface, et de fond, ainsi que la dynamique des calottes de glace et de la glace de mer. Notre étude s'est concentrée sur trois problématiques principales :

- Les conditions caractérisant les GS/HS et les GI de part et d'autre de la Ride Islande-Ecosse, et leurs implications en termes de circulation océanique (Chapitre 3, Partie 1)
- Les processus hydrographiques en jeu, incluant notamment, pour les processus majeurs, leurs dimensions spatiale et temporelle (Chapitre 3, Partie 2).
- Les interactions océan-atmosphère-cryosphère, et les mécanismes de déclenchement impliqués (Chapitre 3, Partie 3).

A l'échelle des derniers 45 ka, nos résultats mettent en avant une configuration relativement classique dans le secteur Atlantique (MD99-2281), où, malgré une stratification quasi-permanente durant la dernière période glaciaire (ne diminuant que progressivement au cours des GI pour devenir minimale à la fin de ces épisodes chauds), la dynamique générale de la circulation océanique méridienne en Atlantique Nord (AMOC) apparaît cohérente avec la littérature, i.e. plus intense en GI (avec notamment une intensification progressive de la branche profonde débordant des Mers Nordiques) et réduite en GS/HS. Côté Mers Nordiques (MD99-2285), nos résultats mettent en évidence un schéma paradoxal, où (i) lors des GI, la partie supérieure de la colonne d'eau apparaît relativement froide et homogène, la durée du couvert de glace de mer est relativement longue, mais la formation d'eau profonde reste intense, et (ii) lors des GS et HS, la convection profonde est fortement réduite, et la colonne d'eau supérieure apparaît stratifiée, constituée d'un niveau de surface chaud en été, peu salé, presque entièrement libre de glace mais (car) subissant un vêlage d'icebergs intense, et séparé par une forte halocline d'un niveau de subsurface plus froid et plus salé. Ces résultats ont

d'importantes implications en termes de circulation océanique. En effet, la stratification côté Atlantique semble jouer un rôle majeur sur la dynamique des masses d'eau sous-jacentes, puisqu'en période de forte stratification (GS/HS), les branches profonde (ISOW) et de subsurface (Dérive Nord Atlantique – NAD) de l'AMOC semblent dynamiquement couplées, alors que lors des périodes où la stratification diminue (GI) un tel couplage s'opère entre les masses d'eau de surface et de fond. Côté Mers Nordiques, le facteur clé ne semble pas être la stratification mais plutôt la glace de mer, qui paraît être le moteur principal de formation d'eau profonde en période glaciaire via la libération de saumures. Une seconde source, *a priori* mineure, d'eau profonde et/ou modale est toutefois possible côté Atlantique, formée par refroidissement des eaux chaudes et salées de subsurface transportées par la NAD lors des périodes de diminution de la stratification de la colonne d'eau supérieure.

Il est important de noter que l'approche multiproxies qui nous a permis d'obtenir ces résultats a mis en avant (i) le fort potentiel des reconstructions quantifiées issues des dinokystes, dont les assemblages sont nettement plus diversifiés que ceux des foraminifères planctoniques (PF) en domaine subpolaire à polaire, et (ii) les limites des reconstructions quantifiées issues des assemblages de PF dans ce type d'environnements, ces limites étant ici reliées au caractère monospécifique de ces assemblages et/ou à la profondeur de vie de ces organismes zooplanctoniques.

A haute résolution sur l'intervalle de temps 35 – 41 ka cal BP, nos analyses nous ont permis d'identifier le séquençage des processus hydrologiques s'opérant au cours des événements climatiques abrupts de la dernière période glaciaire. Ils révèlent notamment qu'à la fin des GI (i.e. avant l'amorce de chaque débâcle d'icebergs), en réponse à un flux d'eau douce probablement lié à des apports glacio-fluviaux issus des calottes européennes, les Mers Nordiques ont été affectées par une advection accrue d'eaux chaudes et salées en provenance de l'Atlantique. Cette masse d'eau advectée semble s'être propagée en subsurface dans le bassin atlantique, avoir ré-émergé en surface au niveau du site MD99-2281, puis s'être propagée en surface de la Mer de Norvège où, en se mélangeant à la masse d'eau ambiante, elle a induit un réchauffement des eaux de surface locales lors des GS et d'HS4. En parallèle, nos deux sites ont enregistré un réchauffement des eaux de subsurface lors de ces épisodes froids. Ce réchauffement de surface/subsurface semble avoir joué un rôle prépondérant dans la déstabilisation des calottes européennes, y compris au début d'HS4, i.e. avant l'évènement d'Heinrich 4 (HE4) *sensu stricto*, rappelant ainsi le concept de « précurseur européen ». Par ailleurs, les enregistrements « basse résolution » 0 – 45 ka de la carotte MD99-2285, couplés

aux résultats d'autres études conduites le long de la bordure des calottes européennes sur le trajet de l'afflux d'eau atlantique, suggèrent qu'un tel processus d'advection puisse avoir eu lieu dans l'ensemble de cette zone et pour l'ensemble des événements rapides de la dernière période glaciaire. Enfin, nos résultats confirment la signature laurentienne dominante d'HE4 au sein de l'Atlantique Nord et au moins jusqu'au site MD99-2281, et suggèrent cependant que les icebergs issus de cette calotte nord-américaine n'aient pu traverser la ride Islande-Ecosse au cours de cet épisode.

Du point de vue des **mécanismes impliqués**, notre comparaison conceptuelle données – modèles supporte l'hypothèse d'une advection accrue d'eau atlantique couplée à un réchauffement de subsurface, en réponse à un flux d'eau douce initial localisé alors qu'en parallèle à une échelle plus régionale s'enregistre un ralentissement de l'AMOC. Les résultats des simulations numériques mettent en évidence le rôle clé joué par le flux d'eau douce initial : celui-ci se traduit par la mise en place d'une couverture dessalée en Atlantique Nord, qui va isoler la masse d'eau de subsurface de l'atmosphère, et induire alors à la fois un réchauffement des eaux de subsurface et une propagation accrue d'eau chaude et salée (en subduction) vers les Mers Nordiques. Par ailleurs, l'intégration de plusieurs enregistrements issus des deux carottes étudiées dans la cadre de cette thèse nous permet d'estimer les **mécanismes de déclenchement** dominants et les **interactions océan-glace-atmosphère** liés à ces événements climatiques abrupts. Les résultats issus de cette intégration suggèrent en effet que : (i) les ralentissements de la NAD sont principalement dus aux apports glacio-fluviaux, alors que les ralentissements de l'AMOC semblent être quant à eux essentiellement liés à de fortes réductions de la couverture de glace de mer en Mer de Norvège, (ii) l'advection accrue d'eaux chaudes atlantiques en surface des Mers Nordiques et le réchauffement de subsurface semblent tous deux avoir joué un rôle clé dans la déstabilisation des calottes de glace européennes, le déclenchement des effondrements de la Laurentide semblant quant à lui être plus spécifiquement lié au réchauffement de subsurface généralisé à l'ensemble du bassin atlantique, et (iii) les réchauffements atmosphériques abrupts semblent être étroitement liés à une ré-intensification abrupte de la NAD en lien avec une réorganisation rapide des gyres et de la circulation Nord-atlantiques, cette réorganisation se produisant suite à une diminution significative des flux d'eau douce associés à la fonte d'icebergs. Ainsi, sur la base de ces résultats et de ceux émanant de précédentes études, nous proposons un scénario hydrographique permettant d'expliquer les événements climatiques abrupts de la dernière période glaciaire.

Notre travail a ainsi fourni plusieurs éléments de réponse à la problématique étudiée, tout en démontrant le fort potentiel des approches multiproxies. Néanmoins, il met également en avant des voies de recherches, actuelles ou nouvelles, qui nécessitent d'être abordées, approfondies et/ou validées.

A l'échelle **régionale**, de nouvelles paléoreconstructions multiproxies et haute résolution seront nécessaires pour (i) valider le schéma hydrographique et les hypothèses proposées dans le cadre de cette thèse, (ii) estimer les dimensions spatiale et temporelle des processus/mécanismes suggérés ici, et notamment (iii) déterminer si le schéma hydrographique paradoxal (SST et de couvert de glace) mis en évidence en Mer de Norvège est caractéristique de l'ensemble du bassin des Mers Nordiques ou présente un gradient Est-Ouest et/ou Nord-Sud.

A l'échelle **du bassin Nord Atlantique**, il serait intéressant de mener de nouvelles études pour estimer :

(i) l'origine géographique précise du flux d'eau douce à la fin des GI (apports glacio-fluviaux issus seulement des calottes fennoscandienne et/ou britannique ? synchrones / asynchrones de ceux des calottes laurentienne et groenlandaise ?),

(ii) le mécanisme à l'origine de ces apports glacio-fluviaux (les températures atmosphériques élevées caractéristiques des GI ? un impact plus direct de la NAD sur les calottes et/ou les *ice-shelves* ? autres ?),

(iii) si le réchauffement de subsurface a réellement affecté l'ensemble du bassin Nord Atlantique subpolaire et ses mers bordières (y compris la Mer du Labrador) durant les GS et HS tel que suggéré par diverses expériences de modélisation (e.g. [Shaffer et al., 2004](#) ; [Marcott et al., 2011](#)) ainsi que par plusieurs reconstructions paléoenvironnementales principalement issues de l'Atlantique Nord Est et de la Mer de Norvège ([Dokken & Jansen, 1999](#) ; [Rasmussen & Thomsen, 2004](#) ; [Jonkers et al., 2010a](#) ; [Marcott et al., 2011](#) ; [Dokken et al., 2013](#) ; [Ezat et al., 2014](#) ; cette thèse),

(iv) si ce réchauffement de subsurface a réellement été plus fort en HS qu'en GS (e.g. [Alvarez-Solas et al., 2013](#)), et si oui,

(v) la raison pour laquelle cela a été le cas, et enfin,

(vi) si ce réchauffement a réellement constitué l'élément déclencheur des débâcles de la Laurentide en HS comme suggéré par e.g. [Marcott et al. \(2011\)](#), [Alvarez-Solas et al. \(2013\)](#).

Il serait également utile d'estimer l'impact du réchauffement de surface (mis en évidence par nos assemblages de dinokystes) sur la glace de mer et les *ice-shelves* au sein de modèles couplés océan-glace(-atmosphère).

Enfin, il apparaît nécessaire de comprendre comment des Mers Nordiques libres de glace en GS peuvent être accompagnées de températures atmosphériques froides au-dessus du Groenland alors que certains modèles (e.g. Li et al., 2010), mais pas tous (e.g. Swingedouw et al., 2013), suggèrent plutôt une relation inverse. Il sera pour cela important de prendre en considération les éventuelles connexions atmosphériques Mers Nordiques – Groenland suggérées dans le cadre de cette thèse, ainsi que les processus atmosphériques en jeu à l'actuel en Atlantique Nord, et notamment l'Oscillation Nord Atlantique tel que suggéré par Eynaud et al. (2002).

A l'échelle **inter-hémisphérique**, le réchauffement de subsurface plus fort en HS suggéré par nos résultats et par Alvarez-Solas et al. (2013) pourraient constituer le paramètre clé dans la dynamique bipolaire de l'AMOC et *in fine* dans les processus à l'origine des « *Antarctic warm events* ». Par ailleurs, il serait également intéressant d'estimer l'impact de la dynamique de la glace de mer et son développement spécifique au sein des Mers Nordiques, tels que mis en évidence dans le cadre de cette thèse, à une échelle plus globale, via notamment son impact potentiel sur les téléconnexions intra- et inter-hémisphériques et son rôle dans les couplages océan-atmosphère.

A l'échelle **actuelle**, il apparaît nécessaire de prendre en considération le découplage Atlantique Nord – Mers Nordiques mis en avant dans cette thèse, et précédemment mis en évidence pour la période du Dernier Maximum Glaciaire dans le cadre du programme MARGO (e.g. de Vernal et al., 2005, 2006), dans nos estimations futures concernant l'évolution des Mers Nordiques et de la calotte groenlandaise, et plus largement de l'évolution paléoenvironnementale de l'Atlantique Nord et de ses impacts sur le climat des continents alentours. Par ailleurs, il serait intéressant d'estimer quel peut être le rôle d'un tel découplage dans le phénomène d'amplification polaire pour lequel des incertitudes demeurent encore.

Enfin, d'un point de vue **analytique**, le travail de développement de méthode géochimique sur ICP-OES mené dans le cadre de cette thèse offre de nouvelles perspectives d'analyse à EPOC avec les mesures Mg/Ca sur foraminifères planctoniques. Il encourage également un nouveau développement de méthode, le Ba/Ca sur foraminifères planctoniques,

qui constitue un proxy émergeant de salinité. Par ailleurs, notre travail a montré le fort potentiel des analyses couplées dinokystes – biomarqueurs, notamment concernant les reconstitutions de glace de mer qui sont relativement rares dans les études paléocéanographiques, et encourage ainsi de telles approches.

Références bibliographiques (hors articles)

- Alley R.B., Mayewski P.A., Sowers T., Stuiver M., Taylor K.C. and Clark P.U. (1997). Holocene climatic instability: A prominent, widespread event 8200 yr ago. *Geology* **25**(6): 483-486.
- Alvarez-Solas J., Charbit S., Ritz C., Paillard D., Ramstein G. and Dumas C. (2010). Links between ocean temperature and iceberg discharge during Heinrich events. *Nature Geoscience* **3**(2): 122-126.
- Alvarez-Solas J. and Ramstein G. (2011). On the triggering mechanism of Heinrich events. *Proceedings of the National Academy of Sciences* **108**(50): E1359-E1360.
- Alvarez-Solas J., Robinson A. and Ritz C. (2012). Brief communication "can recent ice discharges following the Larsen-B ice-shelf collapse be used to infer the driving mechanisms of millennial-scale variations of the Laurentide ice sheet?". *Cryosphere* **6**(3): 687-693.
- Alvarez-Solas J., Robinson A., Montoya M. and Ritz C. (2013). Iceberg discharges of the last glacial period driven by oceanic circulation changes. *Proceedings of the National Academy of Sciences of the United States of America* **110**(41): 16350-16354.
- Anand P., Elderfield H. and Conte M.H. (2003). Calibration of Mg/Ca thermometry in planktonic foraminifera from a sediment trap time series. *Paleoceanography* **18**(2): 28-21.
- Andersen M.S., Nielsen T., Sørensen A.B., Boldreel L.O. and Kuijpers A. (2000). Cenozoic sediment distribution and tectonic movements in the Faroe region. *Global and Planetary Change* **24**(3-4): 239-259.
- Andrews J., Jennings A.E., Kerwin M., Kirby M., Manley W., Miller G., Bond G. and MacLean B. (1995). A Heinrich-like event, H-0 (DC-0): Source (s) for detrital carbonate in the North Atlantic during the Younger Dryas Chronozone. *Paleoceanography* **10**(5): 943-952.
- Austin W.E.N. and Hibbert F.D. (2012). Tracing time in the ocean: A brief review of chronological constraints (60-8 kyr) on North Atlantic marine event-based stratigraphies. *Quaternary Science Reviews* **36**: 28-37.
- B**allini M., Kissel C., Colin C. and Richter T. (2006). Deep-water mass source and dynamic associated with rapid climatic variations during the last glacial stage in the North Atlantic: a multi-proxy investigation of the detrital fraction of deep-sea sediments. *Geochem Geophys Geosystems* **7**(Q02N01).
- Barker S., Greaves M. and Elderfield H. (2003). A study of cleaning procedures used for foraminiferal Mg/Ca paleothermometry. *Geochemistry, Geophysics, Geosystems* **4**(9).
- Belt S.T., Massé G., Rowland S.J., Poulin M., Michel C. and LeBlanc B. (2007). A novel chemical fossil of palaeo sea ice: IP25. *Organic Geochemistry* **38**(1): 16-27.
- Belt S.T. and Müller J. (2013). The Arctic sea ice biomarker IP25: a review of current understanding, recommendations for future research and applications in palaeo sea ice reconstructions. *Quaternary Science Reviews* **79**(0): 9-25.
- Berger A. and Loutre M.F. (1991). Insolation values for the climate of the last 10 million years. *Quaternary Science Reviews* **10**(4): 297-317.
- Bianchi G.G. and McCave I.N. (1999). Holocene periodicity in North Atlantic climate and deep-ocean flow south of Iceland. *Nature* **397**(6719): 515-517.
- Bigg G.R., Levine R.C. and Green C.L. (2011). Modelling abrupt glacial North Atlantic freshening: Rates of change and their implications for Heinrich events. *Global and Planetary Change* **79**(3-4): 176-192.
- Böhm E., Lippold J., Gutjahr M., Frank M., Blaser P., Antz B., Fohlmeister J., Frank N., Andersen M.B. and Deininger M. (2015). Strong and deep Atlantic meridional overturning circulation during the last glacial cycle. *Nature* **517**(7532): 73-76.
- Boldreel L.O., Andersen M.S. and Kuijpers A. (1998). Neogene seismic facies and deep-water gateways in the Faeroe Bank area, NE Atlantic. *Marine Geology* **152**(1-3): 129-140.
- Bond G., Heinrich H., Broecker W., Labeyrie L., McManus J., Andrews J., Huon S., Jantschik R., Glasen S., Simet C., Tedesco K., Klas M., Bonanitt G. and Ivy S. (1992). Evidence for massive discharges of icebergs into the North Atlantic ocean during the last glacial period. *Nature* **360**(6401): 245-XIII.
- Bond G., Broecker W., Johnsen S., McManus J., Labeyrie L., Jouzel J. and Bonani G. (1993). Correlations between climate records from North Atlantic sediments and Greenland ice. *Nature* **365**(6442): 143-147.
- Bond G.C. and Lotti R. (1995). Iceberg discharges into the North Atlantic on millennial time scales during the last glaciation. *Science* **267**(5200): 1005-1010.
- Borenäs K. and Lundberg P. (2004). The Faeroe-Bank Channel deep-water overflow. *Deep-Sea Research Part II: Topical Studies in Oceanography* **51**(4-5): 335-350.

- Bradwell T., Stoker M.S., Golledge N.R., Wilson C.K., Merritt J.W., Long D., Everest J.D., Hestvik O.B., Stevenson A.G., Hubbard A.L., Finlayson A.G. and Mathers H.E. (2008). The northern sector of the last British Ice Sheet: Maximum extent and demise. *Earth-Science Reviews* **88**(3-4): 207-226.
- Broecker W., Bond G., Klas M., Clark E. and McManus J. (1992). Origin of the northern Atlantic's Heinrich events. *Climate Dynamics* **6**(3-4): 265-273.
- Broecker W.S. (1991). The great ocean conveyor. *Oceanography* **4**(2): 79-89.
- Brown T.A., Belt S.T., Tatarek A. and Mundy C.J. (2014). Source identification of the Arctic sea ice proxy IP 25. *Nature Communications* **5**: 4197.
- C**arstens J., Hebbeln D. and Wefer G. (1997). Distribution of planktic foraminifera at the ice margin in the Arctic (Fram Strait). *Marine Micropaleontology* **29**(3-4): 257-269.
- Caulle C., Penaud A., Eynaud F., Zaragosi S., Roche D.M., Michel E., Boulay S. and Richter T. (2013). Sea-surface hydrographical conditions off South Faeroes and within the North-Eastern North Atlantic through MIS 2: The response of dinocysts. *Journal of Quaternary Science* **28**(3): 217-228.
- Clark C.D., Hughes A.L.C., Greenwood S.L., Jordan C. and Sejrup H.P. (2012). Pattern and timing of retreat of the last British-Irish Ice Sheet. *Quaternary Science Reviews* **44**: 112-146.
- Comiso J.C., Parkinson C.L., Gersten R. and Stock L. (2008). Accelerated decline in the Arctic sea-ice cover. *Geophysical Research Letters* **35**(1).
- Cook A.J. and Vaughan D.G. (2010). Overview of areal changes of the ice shelves on the Antarctic Peninsula over the past 50 years. *The Cryosphere* **4**(1): 77.
- Cortijo E., Labeyrie L., Vidal L., Vautravers M., Chapman M., Duplessy J. C., Elliot M., Arnold M., Turon J.-L. and Auffret, G. (1997). Changes in sea surface hydrology associated with Heinrich event 4 in the North Atlantic Ocean between 40 and 60 N. *Earth and Planetary Science Letters*, **146**(1): 29-45.
- D**ale B. (1976). Cyst formation, sedimentation, and preservation: Factors affecting dinoflagellate assemblages in recent sediments from trondheimsfjord, Norway. *Review of Palaeobotany and Palynology* **22**(1): 39-60.
- Dansgaard W., Johnsen S.J., Clausen H.B., Dahl-Jensen D., Gundestrup N.S., Hammer C.U., Hvidberg C.S., Steffensen J.P., Sveinbjörnsdóttir A.E., Jouzel J. and Bond G. (1993). Evidence for general instability of past climate from a 250-kyr ice-core record. *Nature* **364**(6434): 218-220.
- De Vernal A., Eynaud F., Henry M., Hillaire-Marcel C., Londeix L., Mangin S., Matthiessen J., Marret F., Radi T., Rochon A., Solignac S. and Turon J.L. (2005). Reconstruction of sea-surface conditions at middle to high latitudes of the Northern Hemisphere during the Last Glacial Maximum (LGM) based on dinoflagellate cyst assemblages. *Quaternary Science Reviews* **24**(7-9 SPEC. ISS.): 897-924.
- de Vernal A., Rosell-Melé A., Kucera M., Hillaire-Marcel C., Eynaud F., Weinelt M., Dokken T. and Kageyama M. (2006). Comparing proxies for the reconstruction of LGM sea-surface conditions in the northern North Atlantic. *Quaternary Science Reviews* **25**(21-22): 2820-2834.
- De Vernal A. and Marret F. (2007). Organic-walled dinoflagellate cysts: tracers of sea-surface conditions. In *Developments in Marine Geology*, Vol 1 (ed. Hillaire-Marcel C. and de Vernal A.), pp. 371-408.
- de Villiers S., Greaves M. and Elderfield H. (2002). An intensity ratio calibration method for the accurate determination of Mg/Ca and Sr/Ca of marine carbonates by ICP-AES. *Geochemistry, Geophysics, Geosystems* **3**(1): 1001.
- Dickson A.J., Austin W.E.N., Hall I.R., Maslin M.A. and Kucera M. (2008). Centennial-scale evolution of Dansgaard-Oeschger events in the northeast Atlantic Ocean between 39.5 and 56.5 ka B.P. *Paleoceanography* **23**(3): PA3206.
- Dokken T.M. and Jansen E. (1999). Rapid changes in the mechanism of ocean convection during the last glacial period. *Nature* **401**(6752): 458-461.
- Dokken T.M., Nisancioglu K.H., Li C., Battisti D.S. and Kissel C. (2013). Dansgaard-Oeschger cycles: Interactions between ocean and sea ice intrinsic to the Nordic seas. *Paleoceanography* **28**(3): 491-502.
- Dove D., Arosio R., Finlayson A., Bradwell T. and Howe J.A. (2015). Submarine glacial landforms record Late Pleistocene ice-sheet dynamics, Inner Hebrides, Scotland. *Quaternary Science Reviews* **123**: 76-90.
- Duplessy J.C., Labeyrie L., Juillet-Leclerc A., Maitre F., Duprat J. and Sarnthein M. (1991). Surface salinity reconstruction of the North Atlantic Ocean during the Last Glacial maximum. *Oceanologica Acta* **14**(4): 311-324.
- E**hlers J. and Gibbard P.L. (2007). The extent and chronology of Cenozoic Global Glaciation. *Quaternary International* **164-165**: 6-20.

- Elderfield H. and Ganssen G. (2000). Past temperature and $\delta^{18}\text{O}$ of surface ocean waters inferred from foraminiferal Mg/Ca ratios. *Nature* **405**(6785): 442-445.
- Ellegaard M., Figueroa R. and Versteegh G. (2013). Dinoflagellate life cycles, strategy and diversity: key foci for future research. *Biological and Geological Perspectives of Dinoflagellates* 5: 249.
- Elliot M., Labeyrie L., Bond G., Cortijo E., Turon J.L., Tisnerat N. and Duplessy J.C. (1998). Millennial-scale iceberg discharges in the Irminger Basin during the last glacial period: Relationship with the Heinrich events and environmental settings. *Paleoceanography* **13**(5): 433-446.
- Elliot M., Labeyrie L., Dokken T. and Manthe S. (2001). Coherent patterns of ice-rafted debris deposits in the Nordic regions during the last glacial (10-60 ka). *Earth and Planetary Science Letters* **194**(1-2): 151-163.
- Elliot M., Labeyrie L. and Duplessy J.C. (2002). Changes in North Atlantic deep-water formation associated with the Dansgaard - Oeschger temperature oscillations (60-10 ka). *Quaternary Science Reviews* **21**(10): 1153-1165.
- Epstein S. and Mayeda T. (1953). Variation of O18 content of waters from natural sources. *Geochimica et Cosmochimica Acta* **4**(5): 213-224.
- Extier T. (2015). Etude d'un enregistrement paleoceanographique dans l'océan indien sud-ouest et conséquences climatiques sur l'Afrique du sud entre -0,8 et -2 ma d'années. p. 29. Mémoire de Master 1 (Master Océanographie). Université de Bordeaux.
- Eynaud F., Turon J.L., Matthiessen J., Kissel C., Peypouquet J.P., De Vernal A. and Henry M. (2002). Norwegian sea-surface palaeoenvironments of marine oxygen-isotope stage 3: The paradoxical response of dinoflagellate cysts. *Journal of Quaternary Science* **17**(4): 349-359.
- Eynaud F., Zaragosi S., Scourse J.D., Mojtahid M., Bourillet J.F., Hall I.R., Penaud A., Locascio M. and Reijonen A. (2007). Deglacial laminated facies on the NW European continental margin: The hydrographic significance of British-Irish Ice Sheet deglaciation and Fleuve Manche paleoriver discharges. *Geochemistry, Geophysics, Geosystems* **8**(6): Q06019.
- Eynaud F., Rossignol L. and Gasparotto M.-C. (2013). Planktic foraminifera throughout the Pleistocene: from cell to populations to past marine hydrology. In *In : "Foraminifera: Classification, Biology, and Evolutionary Significance"*, (ed. ed. M.D.G.), pp. 209-226. Nova Science Publishers, NY.
- Ezat M.M., Rasmussen T.L. and Groeneveld J. (2014). Persistent intermediate water warming during cold stadials in the southeastern Nordic seas during the past 65 k.y. *Geology* **42**(8): 663-666.
- G**anopolski A. and Rahmstorf S. (2001). Rapid changes of glacial climate simulated in a coupled climate model. *Nature* **409**(6817): 153-158.
- Gildor H., Tziperman E., Nienow P.W., Shepherd J.G., Alley R.B., Lawton J.H., Mahadevan A. and Lenton T.M. (2003). Sea-ice switches and abrupt climate change. *Philosophical Transactions of the Royal Society A: Mathematical, Physical and Engineering Sciences* **361**(1810): 1935-1944.
- Greaves M., Caillon N., Rebaubier H., Bartoli G., Bohaty S., Cacho I., Clarke L., Cooper M., Daunt C., Delaney M., deMenocal P., Dutton A., Eggins S., Elderfield H., Garbe-Schoenberg D., Goddard E., Green D., Groeneveld J., Hastings D., Hathorne E., Kimoto K., Klinkhammer G., Labeyrie L., Lea D.W., Marchitto T., Martínez-Botí M.A., Mortyn P.G., Ni Y., Nuernberg D., Paradis G., Pena L., Quinn T., Rosenthal Y., Russell A., Sagawa T., Sosdian S., Stott L., Tachikawa K., Tappa E., Thunell R. and Wilson P.A. (2008). Interlaboratory comparison study of calibration standards for foraminiferal Mg/Ca thermometry. *Geochemistry, Geophysics, Geosystems* **9**(8): Q08010.
- Grousset F.E., Pujol C., Labeyrie L., Auffret G. and Boelaert A. (2000). Were the North Atlantic Heinrich events triggered by the behavior of the European ice sheets? *Geology* **28**(2): 123-126.
- Guiot J. and de Vernal A. (2007). Transfer Functions: Methods for Quantitative Paleoclimatology Based on Microfossils. In *Developments in Marine Geology*, Vol Volume 1 (ed. Claude H.M. and Anne De V.), pp. 523-563. Elsevier.
- Guiot J. and de Vernal A. (2011a). Is spatial autocorrelation introducing biases in the apparent accuracy of paleoclimatic reconstructions? *Quaternary Science Reviews* **30**(15-16): 1965-1972.
- (2011b). QSR Correspondence "Is spatial autocorrelation introducing biases in the apparent accuracy of palaeoclimatic reconstructions?" Reply to Telford and Birks. *Quaternary Science Reviews* **30**(21-22): 3214-3216.
- H**all J.M. and Chan L.H. (2004). Ba/Ca in Neogloboquadrina pachyderma as an indicator of deglacial meltwater discharge into the western Arctic Ocean. *Paleoceanography* **19**(1): PA1017.

- Hansen B. and Osterhus S. (2000). North Atlantic-Nordic Sea exchanges. *Progress in Oceanography* **45**: 109-208.
- Harland R. (1983). Distribution maps of recent dinoflagellate cysts in bottom sediments from the North Atlantic Ocean and adjacent seas. *Palaeontology* **26**(2): 321-387.
- Hayes A., Kucera M., Kallel N., Sbaifi L. and Rohling E.J. (2005). Glacial Mediterranean sea surface temperatures based on planktonic foraminiferal assemblages. *Quaternary Science Reviews* **24**(7-9 SPEC. ISS.): 999-1016.
- Head M.J., Harland R. and Matthiessen J. (2001). Cold marine indicators of the late Quaternary: the new dinoflagellate cyst genus *Islandinium* and related morphotypes. *Journal of Quaternary Science* **16**(7): 621-636.
- Heinrich H. (1988). Origin and consequences of cyclic ice rafting in the Northeast Atlantic Ocean during the past 130,000 years. *Quaternary Research* **29**(2): 142-152.
- Hemming S.R. (2004). Heinrich events: Massive late Pleistocene detritus layers of the North Atlantic and their global climate imprint. *Reviews of Geophysics* **42**(1): RG1005 1001-1043.
- Hillaire-Marcel C., de Vernal A. and Piper D.J.W. (2007). Lake Agassiz Final drainage event in the northwest North Atlantic. *Geophysical Research Letters* **34**(15): L15601.
- Hillaire-Marcel C. and de Vernal A. (2008). Stable isotope clue to episodic sea ice formation in the glacial North Atlantic. *Earth and Planetary Science Letters* **268**(1-2): 143-150.
- Hjulström F. (1935). *Studies of the morphological activity of rivers as illustrated by the River Fyris: Inaugural Dissertation*. Almqvist & Wiksells.
- Hodell D.A., Minth E.K., Curtis J.H., McCave I.N., Hall I.R., Channell J.E.T. and Xuan C. (2009). Surface and deep-water hydrography on Gardar Drift (Iceland Basin) during the last interglacial period. *Earth and Planetary Science Letters* **288**(1-2): 10-19.
- Hughes A.L.C., Clark C.D. and Jordan C.J. (2014). Flow-pattern evolution of the last British Ice Sheet. *Quaternary Science Reviews* **89**: 148-168.
- J**ohnsen S., Clausen H.B., Dansgaard W., Fuhrer K., Gundestrup N., Hammer C.U., Iversen P., Jouzel J., Stauffer B. and Steffensen J.P. (1992). Irregular glacial interstadials recorded in a new Greenland ice core. *Nature* **359**(6393): 311-313.
- Jonkers L., Brummer G.J.A., Peeters F.J.C., Van Aken H.M. and De Jong M.F. (2010a). Seasonal stratification, shell flux, and oxygen isotope dynamics of leftcoiling *N. pachyderma* and *T. quinqueloba* in the western subpolar North Atlantic. *Paleoceanography* **25**(2): PA2204.
- Jonkers L., Moros M., Prins M.A., Dokken T., Dahl C.A., Dijkstra N., Perner K. and Brummer G.J.A. (2010b). A reconstruction of sea surface warming in the northern North Atlantic during MIS 3 ice-rafting events. *Quaternary Science Reviews* **29**(15-16): 1791-1800.
- K**enyon N.H. (1986). Evidence from bedforms for a strong poleward current along the upper continental slope of northwest Europe. *Marine Geology* **72**(1-2): 187-198.
- Kissel C., Laj C., Labeyrie L., Dokken T., Voelker A. and Blamart D. (1999). Rapid climatic variations during marine isotopic stage 3: Magnetic analysis of sediments from Nordic Seas and North Atlantic. *Earth and Planetary Science Letters* **171**(3): 489-502.
- Kleinen T., Osborn T.J. and Briffa K.R. (2009). Sensitivity of climate response to variations in freshwater hosing location. *Ocean Dynamics* **59**(3): 509-521.
- Knutz P.C., Sicre M.A., Ebbesen H., Christiansen S. and Kuijpers A. (2011). Multiple-stage deglacial retreat of the southern Greenland Ice Sheet linked with Irminger Current warm water transport. *Paleoceanography* **26**(3): Pa3204.
- Kucera M., Weinelt M., Kiefer T., Pflaumann U., Hayes A., Chen M.T., Mix A.C., Barrows T.T., Cortijo E., Duprat J., Juggins S. and Waelbroeck C. (2005b). Reconstruction of sea-surface temperatures from assemblages of planktonic foraminifera: Multi-technique approach based on geographically constrained calibration data sets and its application to glacial Atlantic and Pacific Oceans. *Quaternary Science Reviews* **24**(7-9 SPEC. ISS.): 951-998.
- Kuijpers A. and Party S.S. (1997). Deep-tow side scan sonar study of Norwegian Sea Overflow pathways off the Faeroe Islands. *DANA* **97**(9): 1-14.
- Kuijpers A., Andersen M.S., Kenyon N.H., Kunzendorf H. and Van Weering T.C.E. (1998a). Quaternary sedimentation and Norwegian Sea overflow pathways around Bill Bailey Bank, northeastern Atlantic. *Marine Geology* **152**(1-3): 101-127.
- Kuijpers A., Troelstra S.R., Wisse M., Nielsen S.H. and Van Weering T.C.E. (1998b). Norwegian Sea overflow variability and NE Atlantic surface hydrography during the past 150,000 years. *Marine Geology* **152**(1-3): 75-99.

- Kuijpers A., Nielsen T., Akhmetzhanov A., De Haas H., Kenyon N.H. and Van Weering T.C.E. (2001). Late Quaternary slope instability on the Faeroe margin: Mass flow features and timing of events. *Geo-Marine Letters* **20**(3): 149-159.
- Kuijpers A., Hansen B., Hühnerbach V., Larsen B., Nielsen T. and Werner F. (2002). Norwegian Sea overflow through the Faroe-Shetland gateway as documented by its bedforms. *Marine Geology* **188**(1-2): 147-164.
- L**aberg J.S., Stoker M.S., Dahlgren K.I.T., de Haas H., Haflidason H., Hjelstuen B.O., Nielsen T., Shannon P.M., Vorren T.O., van Weering T.C.E. and Ceramicola S. (2005). Cenozoic alongslope processes and sedimentation on the NW European Atlantic margin. *Marine and Petroleum Geology* **22**(9-10): 1069-1088.
- Labeyrie L., Cortijo E. and Jansen E. (1999). Rapport scientifique de la mission INTERPOLE MD99-114/812 IMAGES V. In *Les Rapports de Campagne à la Mer à bord du Marion Dufresne*, (ed. IPEV), Brest.
- Labeyrie L. and Cortijo E. (2005a). Physical properties of sediment core MD99-2281.
- (2005b). Physical properties of sediment core MD99-2285.
- Laj C., Kissel C., Mazaud A., Channell J.E.T. and Beer J. (2000). North Atlantic palaeointensity stack since 75 ka (NAPIS-75) and the duration of the Laschamp event. *Philosophical Transactions of the Royal Society A: Mathematical, Physical and Engineering Sciences* **358**(1768): 1009-1025.
- Lang C., Leuenberger M., Schwander J. and Johnsen S. (1999). 16°C rapid temperature variation in Central Greenland 70,000 years ago. *Science* **286**(5441): 934-937.
- Larsen K.M.H., Hansen B. and Svendsen H. (2008). Faroe Shelf Water. *Continental Shelf Research* **28**(14): 1754-1768.
- (2009). The Faroe Shelf Front: Properties and exchange. *Journal of Marine Systems* **78**(1): 9-17.
- Lassen S., Kuijpers A., Kunzendorf H., Lindgren H., Heinemeier J., Jansen E. and Knudsen K.L. (2002). Intermediate water signal leads surface water response during Northeast Atlantic deglaciation. *Global and Planetary Change* **32**(2-3): 111-125.
- Levine R.C. and Bigg G.R. (2008). Sensitivity of the glacial ocean to Heinrich events from different iceberg sources, as modeled by a coupled atmosphere-iceberg-ocean model. *Paleoceanography* **23**(4): PA4213.
- Li C., Battisti D.S. and Bitz C.M. (2010). Can North Atlantic sea ice anomalies account for Dansgaard-Oeschger climate signals? *Journal of Climate* **23**(20): 5457-5475.
- Lisiecki L. and Raymo M. (2005). LR04 global Pliocene-Pleistocene benthic $\delta^{18}O$ stack. *IGBP PAGES/World Data Center for Paleoclimatology Data Contribution Series* **8**.
- Locarnini R.A., Mishonov A.V., Antonov J.I., Boyer T.P., Garcia H.E., Baranova O.K., Zweng M.M. and Johnson D.R. (2010). *World Ocean Atlas 2009, Volume 1: Temperature*.
- M**acAyeal D. (1993). Binge/purge oscillations of the Laurentide ice sheet as a cause of the North Atlantic's Heinrich events. *Paleoceanography* **8**(6): 775-784.
- Malaizé B. and Caley T. (2009). Sea surface salinity reconstruction as seen with foraminifera shells: Methods and cases studies. *European Physical Journal* **1**: 177-188.
- Manabe S. and Stouffer R.J. (1995). Simulation of abrupt climate change induced by freshwater input to the North Atlantic Ocean. *Nature* **378**(6553): 165-167.
- Mann M.E. (2002a). Little ice age. *Encyclopedia of global environmental change* **1**: 504-509.
- (2002b). Medieval climatic optimum. *Encyclopedia of Global environmental change* **1**: 514-516.
- Marcott S.A., Clark P.U., Padman L., Klinkhammer G.P., Springer S.R., Liu Z., Otto-Bliesner B.L., Carlson A.E., Ungerer A. and Padman J. (2011). Ice-shelf collapse from subsurface warming as a trigger for Heinrich events. *Proceedings of the National Academy of Sciences* **108**(33): 13415-13419.
- Marret F. and Zonneveld K.A.F. (2003). Atlas of modern organic-walled dinoflagellate cyst distribution. *Review of Palaeobotany and Palynology* **125**(1-2): 1-200.
- Matsuoka K., Kawami H., Nagai S., Iwataki M., Takayama H. (2009). Re-examination of cyst-motile relationships of *Polykrikos kofoidii* Chatton and *Polykrikos schwartzii* Bütschli (Gymnodiniales, Dinophyceae). *Review of Palaeobotany and Palynology* **154**(1-4): 79-90.
- Matthiessen J., Kunz-Pirring M. and Mudie P.J. (2000). Freshwater chlorophycean algae in recent marine sediments of the Beaufort, Laptev and Kara Seas (Arctic Ocean) as indicators of river runoff. *International Journal of Earth Sciences* **89**(3): 470-485.

- Mauritzen C., Price J., Sanford T. and Torres D. (2005). Circulation and mixing in the Faroese Channels. *Deep-Sea Research Part I: Oceanographic Research Papers* **52**(6): 883-913.
- Mayewski P.A., Rohling E.E., Stager J.C., Karlén W., Maasch K.A., Meeker L.D., Meyerson E.A., Gasse F., van Kreveld S., Holmgren K., Lee-Thorp J., Rosqvist G., Rack F., Staubwasser M., Schneider R.R. and Steig E.J. (2004). Holocene climate variability. *Quaternary Research* **62**(3): 243-255.
- McCartney M.S. and Mauritzen C. (2001). On the origin of the warm inflow to the Nordic Seas. *Progress in Oceanography* **51**(1): 125-214.
- McCave I.N., Manighetti B. and Beveridge N.A.S. (1995a). Circulation in the glacial North Atlantic inferred from grain-size measurements. *Nature* **374**(6518): 149-152.
- McCave I.N., Manighetti B. and Robinson S.G. (1995b). Sortable silt and fine sediment size/composition slicing: parameters for palaeocurrent speed and palaeoceanography. *Paleoceanography* **10**(3): 593-610.
- McCave I.N. (2007). Chapter One Deep-Sea Sediment Deposits and Properties Controlled by Currents. In *Developments in Marine Geology*, Vol Volume 1 (ed. Hillaire-Marcel C. and De Vernal A.), pp. 19-62. Elsevier.
- Mertens K.N., Bringué M., Van Nieuwenhove N., Takano Y., Pospelova V., Rochon A., De Vernal A., Radi T., Dale B., Patterson R.T., Weckström K., Andrén E., Louwey S. and Matsuoka K. (2012). Process length variation of the cyst of the dinoflagellate *Protoceratium reticulatum* in the North Pacific and Baltic-Skagerrak region: Calibration as an annual density proxy and first evidence of pseudo-cryptic speciation. *Journal of Quaternary Science* **27**(7): 734-744.
- Milankovitch M. (1941). *Kanon der Erdebestrahlung und seine Anwendung auf das Eiszeitenproblem*. Königlich Serbische Akademie.
- Mojtahid M., Eynaud F., Zaragosi S., Scourse J., Bourillet J.F. and Garlan T. (2005). Palaeoclimatology and palaeohydrography of the glacial stages on Celtic and Armorican margins over the last 360 000 yrs. *Marine Geology* **224**(1-4): 57-82.
- Moros M., Endler R., Lackschewitz K.S., Wallrabe-Adams H.J., Mienert J. and Lemke W. (1997). Physical properties of Reykjanes Ridge sediments and their linkage to high-resolution Greenland Ice Sheet Project 2 ice core data. *Paleoceanography* **12**(5): 687-695.
- Mudie P.J. (1992). Circum-Arctic Quaternary and Neogene marine palynofloras: paleoecology and statistical analysis. *Neogene and Quaternary dinoflagellate cysts and acritarchs* **10**: 347-390.
- Nielsen T. and Van Weering T.C.E. (1998). Seismic stratigraphy and sedimentary processes at the Norwegian Sea margin northeast of the Faeroe Islands. *Marine Geology* **152**(1-3): 141-157.
- Nielsen T. and Kuijpers A. (2000). Faeroe margin. In *Multidisciplinary Study of Geological Processes on the North East Atlantic and Western Mediterranean Margins*, Vol IOC Technical Series No. 56 (ed. Kenyon N.H., Ivanov M.K., Akhmetzhanov A.M. and Akhmanov G.C.), pp. 9-26, UNESCO.
- Nielsen T., Rasmussen T.L., Ceramicola S. and Kuijpers A. (2007). Quaternary sedimentation, margin architecture and ocean circulation variability around the Faeroe Islands, North Atlantic. *Quaternary Science Reviews* **26**(7-8): 1016-1036.
- Nuernberg D. (1995). Magnesium in tests of *Neoglobobulimina papyrifera* sinistral from high northern and southern latitudes. *Journal of Foraminiferal Research* **25**: 350-368.
- Nürnberg D., Bijma J. and Hemleben C. (1996). Assessing the reliability of magnesium in foraminiferal calcite as a proxy for water mass temperatures. *Geochimica et Cosmochimica Acta* **60**(5): 803-814.
- Orvik K.A. and Niiler P. (2002). Major pathways of Atlantic water in the northern North Atlantic and Nordic Seas toward Arctic. *Geophysical Research Letters* **29**(19): 2-1.
- Peck V.L., Hall I.R., Zahn R. and Elderfield H. (2008). Millennial-scale surface and subsurface paleothermometry from the northeast Atlantic, 55-8 ka BP. *Paleoceanography* **23**(3): PA3221.
- Peltier W.R. (2004). Global glacial isostasy and the surface of the ice-age earth: The ICE-5G (VM2) model and GRACE. In *Annual Review of Earth and Planetary Sciences*, Vol 32, pp. 111-149.
- Penaud A. (2009). *Interactions climatiques et hydrologiques du système Méditerranée / Atlantique au Quaternaire*. Thèse. Université Bordeaux 1. pp. 372.
- Penaud A., Eynaud F., Turon J.L., Zaragosi S., Malaizé B., Toucanne S. and Bourillet J.F. (2009). What forced the collapse of European ice sheets during the last two glacial periods (150 ka B.P. and 18 ka cal B.P.)? Palynological evidence. *Palaeogeography, Palaeoclimatology, Palaeoecology* **281**(1-2): 66-78.

- Petersen S.V., Schrag D.P. and Clark P.U. (2013). A new mechanism for Dansgaard-Oeschger cycles. *Paleoceanography* **28**(1): 24-30.
- Pillans B. and Naish T. (2004). Defining the Quaternary. *Quaternary Science Reviews* **23**(23-24): 2271-2282.
- Prahl F.G., Muehlhausen L.A. and Zahnle D.L. (1988). Further evaluation of long-chain alkenones as indicators of paleoceanographic conditions. *Geochimica et Cosmochimica Acta* **52**(9): 2303-2310.
- Prins M.A., Bouwer L.M., Beets C.J., Troelstra S.R., Weltje G.J., Kruk R.W., Kuijpers A. and Vroon P.Z. (2002). Ocean circulation and iceberg discharge in the glacial North Atlantic: Inferences from unmixing of sediment size distributions. *Geology* **30**(6): 555-558.
- R**adi T., Bonnet S., Cormier M.A., de Vernal A., Durantou L., Faubert É., Head M.J., Henry M., Pospelova V., Rochon A. and Van Nieuwenhove N. (2013). Operational taxonomy and (paleo-)autecology of round, brown, spiny dinoflagellate cysts from the Quaternary of high northern latitudes. *Marine Micropaleontology* **98**: 41-57.
- Rahman A. (1995). Reworked nannofossils in the North Atlantic Ocean and subpolar basins: implications for Heinrich events and ocean circulation. *Geology* **23**(6): 487-490.
- Rahmstorf S. (2002). Ocean circulation and climate during the past 120,000 years. *Nature* **419**(6903): 207-214.
- Rahmstorf S. (2003). Thermohaline circulation: The current climate. *Nature* **421**(6924): 699-699.
- Rasmussen T.L., Thomsen E., Labeyrie L. and Van Weering T.C.E. (1996a). Circulation changes in the Faeroe-Shetland Channel correlating with cold events during the last glacial period (58-10 ka). *Geology* **24**(10): 937-940.
- Rasmussen T.L., Thomsen E., Van Weering T.C.E. and Labeyrie L. (1996b). Rapid changes in surface and deep water conditions at the Faeroe Margin during the last 58,000 years. *Paleoceanography* **11**(6): 757-771.
- Rasmussen T.L., Van Weering T.C.E. and Labeyrie L. (1996c). High resolution stratigraphy of the Faeroe-Shetland Channel and its relation to North Atlantic paleoceanography: The last 87 kyr. *Marine Geology* **131**(1-2): 75-88.
- Rasmussen T.L., Van Weering T.C.E. and Labeyrie L. (1997). Climatic instability, ice sheets and ocean dynamics at high northern latitudes during the last glacial period (58-10 KA BP). *Quaternary Science Reviews* **16**(1): 71-80.
- Rasmussen T.L., Balbon E., Thomsen E., Labeyrie L. and Van Weering T.C.E. (1999). Climate records and changes in deep outflow from the Norwegian Sea ~ 150-55 ka. *Terra Nova* **11**(2-3): 61-66.
- Rasmussen T.L., Thomsen E., Troelstra S.R., Kuijpers A. and Prins M.A. (2002). Millennial-scale glacial variability versus Holocene stability: Changes in planktic and benthic foraminifera faunas and ocean circulation in the North Atlantic during the last 60 000 years. *Marine Micropaleontology* **47**(1-2): 143-176.
- Rasmussen T.L. and Thomsen E. (2004). The role of the North Atlantic Drift in the millennial timescale glacial climate fluctuations. *Palaeogeography, Palaeoclimatology, Palaeoecology* **210**(1): 101-116.
- (2009). Ventilation changes in intermediate water on millennial time scales in the SE Nordic seas, 65-14 kyr BP. *Geophysical Research Letters* **36**(1): L01601.
- Reid J.L. (1979). On the contribution of the Mediterranean Sea outflow to the Norwegian-Greenland Sea. *Deep Sea Research Part A Oceanographic Research Papers* **26**(11): 1199-1223.
- Richter T.O., Van Der Gaast S., Koster B., Vaars A., Gieles R., De Stigter H.C., De Haas H. and Van Weering T.C.E. (2006). The Avaatech XRF Core Scanner: Technical description and applications to NE Atlantic sediments. Vol 267 (ed. Rothwell R.G.), pp. 39-50.
- Rochon A., de Vernal A., Turon J.-L., Matthiessen J. and Head M.J., ed (1999). *Distribution of dinoflagellate cysts in surface sediments from the North Atlantic Ocean and adjacent basins and quantitative reconstruction of sea-surface parameters*. AASP special pub., Dallas, Texas.
- Rochon A., Eynaud F. and de Vernal A. (2008). Dinocysts as tracers of hydrographical conditions and productivity along the ocean margins: Introduction. *Marine Micropaleontology* **68**(1): 1-5.
- Ruddiman W.F. (1977). Late Quaternary deposition of ice-rafted sand in the subpolar North Atlantic (lat 40 to 65 N). *Geological Society of America Bulletin* **88**(12): 1813-1827.
- (2001). *Earth's Climate: past and future*. Macmillan.
- S**achs J.P. and Lehman S.J. (1999). Subtropical North Atlantic temperatures 60,000 to 30,000 years ago. *Science* **286**(5440): 756-760.
- Sanchez Goñi M.F. and Harrison S.P. (2010). Millennial-scale climate variability and vegetation

- changes during the Last Glacial: Concepts and terminology. *Quaternary Science Reviews* **29**(21-22): 2823-2827.
- Sarjeant W.A.S. (1974). *Fossil and living dinoflagellates*. Academic Press Inc., London, UK.
- Schiebel R., Waniek J., Bork M. and Hemleben C. (2001). Planktic foraminiferal production stimulated by chlorophyll redistribution and entrainment of nutrients. *Deep-Sea Research Part I: Oceanographic Research Papers* **48**(3): 721-740.
- Schlitzer R. (2012). Ocean Data View. <http://odv.awi.de> [8 April 2014]
- Schmitz W.J. and McCartney M.S. (1993). On the north Atlantic circulation. *Reviews of Geophysics* **31**(1): 29-49.
- Scourse J.D., Haapaniemi A.I., Colmenero-Hidalgo E., Peck V.L., Hall I.R., Austin W.E.N., Knutz P.C. and Zahn R. (2009). Growth, dynamics and deglaciation of the last British-Irish ice sheet: the deep-sea ice-rafted detritus record. *Quaternary Science Reviews* **28**(27-28): 3066-3084.
- Sejrup H.P., Larsen E., Haflidason H., Berstad I.M., Hjelstuen B.O., Jonsdottir H.E., King E.L., Landvik J., Longva O., Nygard A., Ottesen D., Raunholm S., Rise L. and Stalsberg K. (2003). Configuration, history and impact of the Norwegian Channel Ice Stream. *Boreas* **32**(1): 18-36.
- Sejrup H.P., Nygård A., Hall A.M. and Haflidason H. (2009). Middle and Late Weichselian (Devensian) glaciation history of south-western Norway, North Sea and eastern UK. *Quaternary Science Reviews* **28**(3-4): 370-380.
- Shackleton N.J. (1974). Attainment of isotopic equilibrium between ocean water and the benthic foraminifera genus *Uvigerina*: isotopic changes in the ocean during the Last Glacial. In *Methodes quantitatives d'étude des variations du climat au cours du Pleistocène*, Vol 219 (ed. Labeyrie L.), pp. 203-209.
- Shaffer G., Olsen S.M. and Bjerrum C.J. (2004). Ocean subsurface warming as a mechanism for coupling Dansgaard-Oeschger climate cycles and ice-rafting events. *Geophysical Research Letters* **31**(24): 1-4.
- Shepherd A., Wingham D., Payne T. and Skvarca P. (2003). Larsen ice shelf has progressively thinned. *Science* **302**(5646): 856-859.
- Sicre M.A., Khodri M., Mignot J., Eiriksson J., Knudsen K.L., Ezat U., Closset I., Nogues P. and Massé G. (2013). Sea surface temperature and sea ice variability in the subpolar North Atlantic from explosive volcanism of the late thirteenth century. *Geophysical Research Letters* **40**(20): 5526-5530.
- Simstich J., Sarnthein M. and Erlenkeuser H. (2003). Paired $\delta^{18}\text{O}$ signals of *Neogloboquadrina pachyderma* (s) and *Turborotalita quinqueloba* show thermal stratification structure in Nordic Seas. *Marine Micropaleontology* **48**(1-2): 107-125.
- Singh H.A., Battisti D.S. and Bitz C.M. (2014). A heuristic model of dansgaard-oeschger cycles. part i: Description, results, and sensitivity studies. *Journal of Climate* **27**(12): 4337-4358.
- Snoeckx H., Grousset F., Revel M. and Boelaert A. (1999). European contribution of ice-rafted sand to Heinrich layers H3 and H4. *Marine Geology* **158**(1-4): 197-208.
- Snowball I. and Moros M. (2003). Saw-tooth pattern of North Atlantic current speed during Dansgaard-Oeschger cycles revealed by the magnetic grain size of Reykjanes Ridge sediments at 59°N. *Paleoceanography* **18**(2): 4-1.
- Staines-Urías F., Kuijpers A. and Korte C. (2013). Evolution of subpolar North Atlantic surface circulation since the early Holocene inferred from planktic foraminifera faunal and stable isotope records. *Quaternary Science Reviews* **76**: 66-81.
- Stanford J.D., Rohling E.J., Bacon S. and Holliday N.P. (2011). A review of the deep and surface currents around Eirik Drift, south of Greenland: Comparison of the past with the present. *Global and Planetary Change* **79**(3-4): 244-254.
- Stokes C.R. and Clark C.D. (2001). Palaeo-ice streams. *Quaternary Science Reviews* **20**(13): 1437-1457.
- Stouffer R.J., Yin J., Gregory J., Dixon K., Spelman M., Hurlin W., Weaver A., Eby M., Flato G. and Hasumi H. (2006). Investigating the causes of the response of the thermohaline circulation to past and future climate changes. *Journal of Climate* **19**(8): 1365-1387.
- Svendsen J.I., Alexanderson H., Astakhov V.I., Demidov I., Dowdeswell J.A., Funder S., Gataullin V., Henriksen M., Hjort C., Houmark-Nielsen M., Hubberten H.W., Ingólfsson O., Jakobsson M., Kjær K.H., Larsen E., Lokrantz H., Lunkka J.P., Lyså A., Mangerud J., Matiouchkov A., Murray A., Möller P., Niessen F., Nikolskaya O., Polyak L., Saarnisto M., Siegert C., Siegert M.J., Spielhagen R.F. and Stein R. (2004). Late Quaternary ice sheet history of northern Eurasia. *Quaternary Science Reviews* **23**(11-13): 1229-1271.
- Svensson A., Andersen K.K., Bigler M., Clausen H.B., Dahl-Jensen D., Davies S.M., Johnsen S.J., Muscheler R., Parrenin F., Rasmussen S.O., Röthlisberger R., Seierstad I., Steffensen J.P. and

- Vinther B.M. (2008). A 60 000 year Greenland stratigraphic ice core chronology. *Climate of the Past* **4**(1): 47-57.
- Swingedouw D., Rodehacke C.B., Behrens E., Menary M., Olsen S.M., Gao Y., Mikolajewicz U., Mignot J. and Biastoch A. (2013). Decadal fingerprints of freshwater discharge around Greenland in a multi-model ensemble. *Climate Dynamics* **41**(3-4): 695-720.
- Swingedouw D., Ortega P., Mignot J., Guilyardi E., Masson-Delmotte V., Butler P.G., Khodri M. and Séférian R. (2015). Bidecadal North Atlantic ocean circulation variability controlled by timing of volcanic eruptions. *Nature Communications* **6**: 6545.
- T**olderlund D.S. and Bé A.W.H. (1971). Seasonal Distribution of Planktonic Foraminifera in the Western North Atlantic. *Micropaleontology* **17**(3): 297-329.
- Toucanne S., Zaragosi S., Bourillet J.F., Marieu V., Cremer M., Kageyama M., Van Vliet-Lanoë B., Eynaud F., Turon J.L. and Gibbard P.L. (2010). The first estimation of Fleuve Manche palaeoriver discharge during the last deglaciation: Evidence for Fennoscandian ice sheet meltwater flow in the English Channel ca 20-18 ka ago. *Earth and Planetary Science Letters* **290**(3-4): 459-473.
- Turon J.L. (1984). Le palynoplankton dans l'environnement actuel de l'Atlantique nord-oriental. Evolution climatique et hydrologique depuis le dernier maximum glaciaire. *Mémoires - Institut de Géologie du Bassin d'Aquitaine* **17**.
- V**aldimarsson H. and Malmberg S.-A. (1999). Near-surface circulation in Icelandic waters derived from satellite tracked drifters. *Rit Fiskideild* **16**: 23-40.
- Van Kreveld S., Sarnthein M., Erlenkeuser H., Grootes P., Jung S., Nadeau M.J., Pflaumann U. and Voelker A. (2000). Potential links between surging ice sheets, circulation changes, and the Dansgaard-Oeschger cycles in the Irmiger Sea, 60-80 kyr. *Paleoceanography* **15**(4): 425-442.
- Van Weering T.C.E., Nielsen T., Kenyon N.H., Akentieva K. and Kuijpers A.H. (1998). Sediments and sedimentation at the NE Faeroe continental margin; Contourites and large-scale sliding. *Marine Geology* **152**(1-3): 159-176.
- Vidal L., Labeyrie L., Cortijo E., Arnold M., Duplessy J. C., Michel E., Becqué S. and Van Weering, T. C. E. (1997). Evidence for changes in the North Atlantic Deep Water linked to meltwater surges during the Heinrich events. *Earth and Planetary Science Letters*, **146**(1): 13-27.
- Voelker A.H. (2002). Global distribution of centennial-scale records for Marine Isotope Stage (MIS) 3: a database. *Quaternary Science Reviews* **21**(10): 1185-1212.
- Volkman J.K., Barrerr S.M., Blackburn S.I. and Sikes E.L. (1995). Alkenones in *Gephyrocapsa oceanica*: Implications for studies of paleoclimate. *Geochimica et Cosmochimica Acta* **59**(3): 513-520.
- W**aelbroeck C., Labeyrie L., Michel E., Duplessy J.C., McManus J.F., Lambeck K., Balbon E. and Labracherie M. (2002). Sea-level and deep water temperature changes derived from benthic foraminifera isotopic records. *Quaternary Science Reviews* **21**(1-3): 295-305.
- Wagner A.J., Morrill C., Otto-Bliesner B.L., Rosenbloom N. and Watkins K.R. (2013). Model support for forcing of the 8.2 ka event by meltwater from the Hudson Bay ice dome. *Climate Dynamics* **41**(11-12): 2855-2873.
- Walker M., Johnsen S., Rasmussen S.O., Popp T., Steffensen J.P., Gibbard P., Hoek W., Lowe J., Andrews J. and Björck S. (2009). Formal definition and dating of the GSSP (Global Stratotype Section and Point) for the base of the Holocene using the Greenland NGRIP ice core, and selected auxiliary records. *Journal of Quaternary Science* **24**(1): 3-17.
- Wall D. and Dale B. (1968). Modern dinoflagellate cysts and evolution of the Peridinales. *Micropaleontology*: 265-304.
- Wall D., Dale B., Lohmann G. and Smith W.K. (1977). The environmental and climatic distribution of dinoflagellate cysts in modern marine sediments from regions in the North and South Atlantic Oceans and adjacent seas. *Marine Micropaleontology* **2**: 121-200.
- Weckström K., Massé G., Collins L.G., Hanhijärvi S., Bouloubassi I., Sicre M.A., Seidenkrantz M.S., Schmidt S., Andersen T.J., Andersen M.L., Hill B. and Kuijpers A. (2013). Evaluation of the sea ice proxy IP25 against observational and diatom proxy data in the SW Labrador Sea. *Quaternary Science Reviews* **79**: 53-62.
- Williams D. (1971). The distribution of marine dinoflagellates in relation to physical and chemical conditions. *The Micropalaeontology of Oceans*: 91-95.
- Wolff E.W., Chappellaz J., Blunier T., Rasmussen S.O. and Svensson A. (2010). Millennial-scale variability during the last glacial: The ice core record. *Quaternary Science Reviews* **29**(21-22): 2828-2838.

Woodgate R.A., Weingartner T. and Lindsay R. (2010). The 2007 Bering Strait oceanic heat flux and anomalous Arctic sea-ice retreat. *Geophysical Research Letters* **37**(1).

Zaragosi S., Eynaud F., Pujol C., Auffret G.A., Turon J.L. and Garlan T. (2001). Initiation of the European deglaciation as recorded in the northwestern Bay of Biscay slope environments (Meriadzek Terrace and Trevelyan Escarpment): A multi-proxy approach. *Earth and Planetary Science Letters* **188**(3-4): 493-507.

Zenk W. (2008). Abyssal and Contour Currents. In *Developments in Sedimentology*, Vol 60, pp. 37-57.

Zonneveld K.A., Versteegh G.J. and de Lange G.J. (1997). Preservation of organic-walled dinoflagellate cysts in different oxygen regimes: a 10,000 year natural experiment. *Marine micropaleontology* **29**(3): 393-405.

Zonneveld K.A.F., Marret F., Versteegh G.J.M., Bogus K., Bonnet S., Bouimetarhan I., Crouch E., de Vernal A., Elshanawany R., Edwards L., Esper O., Forke S., Grøsfjeld K., Henry M., Holzwarth U., Kieft J.F., Kim S.Y., Ladouceur S., Ledu D., Chen L., Limoges A., Londeix L., Lu S.H., Mahmoud M.S., Marino G., Matsouka K., Matthiessen J., Mildenhall D.C., Mudie P., Neil H.L., Pospelova V., Qi Y., Radi T., Richerol T., Rochon A., Sangiorgi F., Solignac S., Turon J.L., Verleye T., Wang Y., Wang Z. and Young M. (2013). Atlas of modern dinoflagellate cyst distribution based on 2405 data points. *Review of Palaeobotany and Palynology* **191**: 1-197.

Zumaque J., Eynaud F., Zaragosi S., Marret F., Matsuzaki K.M., Kissel C., Roche D.M., Malaizé B., Michel E., Billy I., Richter T. and Palis E. (2012). An ocean-ice coupled response during the last glacial: a view from a marine isotopic stage 3 record south of the Faeroe Shetland Gateway. *Climate of the Past* **8**(6): 1997-2017.

Annexes

Annexe 1 : Zumaque et al., 2012

“An ocean–ice coupled response during the last glacial: a view from a marine isotopic stage 3 record south of the Faeroe Shetland Gateway”

Zumaque J., Eynaud F., Zaragosi S., Marret F., Matsuzaki K.M., Kissel C., Roche D.M., Malaizé B., Michel E., Billy I., Richter T. and Palis E.

(2012), *Climate of the Past* 8(6): 1997-2017.



An ocean–ice coupled response during the last glacial: a view from a marine isotopic stage 3 record south of the Faeroe Shetland Gateway

J. Zumaque^{1,*}, F. Eynaud¹, S. Zaragosi¹, F. Marret², K. M. Matsuzaki^{1,**}, C. Kissel³, D. M. Roche^{3,4}, B. Malaizé¹, E. Michel³, I. Billy¹, T. Richter⁵, and E. Palis¹

¹EPOC – Environnements et Paléoenvironnements Océaniques, UMR5805, Université Bordeaux I, Talence, France

²School of Environmental Sciences, University of Liverpool, Liverpool, L69 7ZT, UK

³Laboratoire des Sciences du Climat et de l'Environnement (LSCE), CEA/CNRS-INSU/UVSQ – UMR8212, 91191 Gif s/s Yvette, France

⁴Vrije Universiteit Amsterdam, de Boelelaan 1085, 1081 HV Amsterdam, The Netherlands

⁵NIOZ Royal Netherlands Institute for Sea Research, P.O. Box 59, 1790 AB Den Burg (Texel), The Netherlands

* present address: GEOTOP, Montréal, Canada

** present address: Institute of Geology and Paleontology, Graduate School of Science, Tohoku University, Aramaki 6-3, Sendai, 980-8578, Japan

Correspondence to: F. Eynaud (f.eynaud@epoc.u-bordeaux1.fr)

Received: 17 July 2012 – Published in Clim. Past Discuss.: 1 August 2012

Revised: 5 November 2012 – Accepted: 14 November 2012 – Published: 7 December 2012

Abstract. The rapid climatic variability characterising the Marine Isotopic Stage (MIS) 3 (~ 60–30 cal ka BP) provides key issues to understand the atmosphere–ocean–cryosphere dynamics. Here we investigate the response of sea-surface paleoenvironments to the MIS3 climatic variability through the study of a high resolution oceanic sedimentological archive (core MD99-2281, 60°21' N; 09°27' W; 1197 m water depth), retrieved during the MD114-IMAGES (International Marine Global Change Study) cruise from the southern part of the Faeroe Bank. This sector was under the proximal influence of European ice sheets (Fennoscandian Ice Sheet to the East, British Irish Ice Sheet to the South) during the last glacial and thus probably responded to the MIS3 pulsed climatic changes.

We conducted a multi-proxy analysis of core MD99-2281, including magnetic properties, x-ray fluorescence measurements, characterisation of the coarse (> 150 µm) lithic fraction (grain concentration) and the analysis of selected biogenic proxies (assemblages and stable isotope ratio of calcareous planktonic foraminifera, dinoflagellate cyst – e.g. dinocyst – assemblages). Results presented here are focussed on the dinocyst response, this proxy providing the reconstruction of past sea-surface hydrological conditions, qualitatively as well as quantitatively (e.g. transfer function

sensu lato). Our study documents a very coherent and sensitive oceanic response to the MIS3 rapid climatic variability: strong fluctuations, matching those of stadial/interstadial climatic oscillations as depicted by Greenland ice cores, are recorded in the MD99-2281 archive. Proxies of terrigenous and detrital material suggest increases in continental advection during Greenland Stadials (including Heinrich events), the latter corresponding also to southward migrations of polar waters. At the opposite, milder sea-surface conditions seem to develop during Greenland Interstadials. After 30 ka, reconstructed paleohydrological conditions evidence strong shifts in SST: this increasing variability seems consistent with the hypothesised coalescence of the British and Fennoscandian ice sheets at that time, which could have directly influenced sea-surface environments in the vicinity of core MD99-2281.

1 Introduction

The alternation of glacial/interglacial periods that defines the Quaternary is thought to be mainly triggered by changes in orbital parameters (e.g. Imbrie et al., 1993; Berger, 2006). However, a higher frequency in climatic variability is

detected during glacial periods and appears to have no direct orbital forcing origin. This millennial-scale climatic variability was observed for the first time in the oxygen isotope records from Greenland ice cores (Dansgaard et al., 1993) and is expressed through significant and rapid changes in atmospheric temperatures, especially during the Marine Isotope Stage (MIS) 3 (e.g. Dansgaard et al., 1993; Kiefer et al., 2002; Wolff et al., 2010; Austin and Hibbert, 2012). These oscillations switching between warm (GIs for Greenland interstadials) and cold (GSs for Greenland Stadials) climatic phases are known as the Dansgaard-Oeschger (DO) cycles (e.g. Bond et al., 1993; Dansgaard et al., 1993). These cycles are punctuated by abrupt ice-sheet discharge events, the so-called Heinrich Events (HEs), corresponding to some of the DO coldest phases, and are illustrated in the North Atlantic sediments by layers rich in silico-clastic coarse particles (ice-rafted debris – IRD; e.g. Bond et al., 1992). IRD are transported by floating ice and preferentially deposited in the Ruddiman Belt (Ruddiman, 1977), a latitudinal belt (40 to 50° N) identified as the preferential area of melting for icebergs during these discharge periods. Study of these IRD particles allowed the characterisation of sources involved in these events with great influence of the Laurentide ice sheet during HE1, HE2, HE4 and HE5, and a greater influence of European ice sheets during HE3 and HE6 (cf. Hemming, 2004 and references therein). At the same time, the North Atlantic basin recorded large changes in hydrological conditions, corresponding to temperature and salinity decreases in sea-surface waters and changes in the meridional overturning circulation (MOC), with peculiar consequences on the North Atlantic Drift (NAD) and on the formation of North Atlantic Deep Waters (NADW) (e.g. Bond et al., 1992; Bond and Lotti, 1995; Broecker, 1997; Kissel et al., 1999a; Alley et al., 1999; Clark et al., 2002; Ramhstorf, 2002; Broecker, 2003; Hemming, 2004). Even though these phenomena are now relatively well identified, the causes and consequences of such climatic changes and dynamic interactions between ice, ocean and atmosphere remain uncertain. For instance, the role of ice shelves developed at the margins of European ice sheets during the last glacial period has probably been underestimated, as suggested by recent works (Hulbe et al., 2004; Alvarez-Solas et al., 2010). There is also a need for a better definition of the geographical fingerprint of such events to help identifying the likely source regions and perturbation mechanisms (Roche et al., 2010).

Here we propose to reconstruct the paleoclimatic and paleoceanographic setting of the southern Faeroe Islands during MIS3 in order to explore the evolution of the surface Atlantic Ocean under the influence of growing European ice sheets. To reach this goal, analysis of organic-walled dinoflagellate cyst (dinocyst) assemblages was undertaken on core MD99-2281, retrieved off SW Faeroe, and quantifications of surface hydrological parameters were obtained from ecological transfer functions (the modern analogue technique – MAT, e.g. Guiot and de Vernal, 2007) applied to these

assemblages. Dinocysts have long since been used as sea-surface paleohydrological proxies, as their modern biogeographical distribution in surface sediments appears to be tied to ecological parameters of the overlying surface water masses (e.g. Harland, 1983; Rochon et al., 1999a,b, 2008; Marret and Zonneveld, 2003; de Vernal and Marret, 2007). Dinocysts are organic microfossils and derive from the sexual reproduction of dinoflagellates. The wall of dinocysts, comparable to the sporopollenin of pollen grains, has been called dinosporin (e.g. De Leeuw et al., 2006) and confers to dinocysts a strong resistance to dissolution, and a good fossilization potential (e.g. Evitt, 1985; Rochon et al., 1999a,b; Marret and Zonneveld, 2003). Recent studies however suggest that this compound is in fact closer to cellulose than to sporopollenin (e.g. Versteegh et al., 2012), but their preservation potential is still high, even if the assemblages can be altered by oxidation processes in some specific environments (e.g. Zonneveld et al., 2007; Bogus et al., 2012). They are among the rare proxies offering access to past hydrological conditions of polar and/or glacial extreme environments (e.g. de Vernal and Rochon, 2011).

In addition, our study compiles a set of multi-proxy data (x-ray fluorescence – XRF – core scanning, magnetic properties, abundances of the polar planktonic foraminifera *Neogloboquadrina pachyderma* s and IRD concentrations) that contributes to document and discuss the response of the ocean during MIS3.

2 Environmental setting

2.1 Modern oceanic and sedimentological setting

2.1.1 Physiography

Core MD99-2281 (60°21' N, 09°27' W) was retrieved by the RV *Marion-Dufresne* during the IMAGES (International Marine Global Change Study) V – MD99-114 cruise (Labeyrie et al., 1999). It is made of 29 meters of hemipelagic silty clays (Labeyrie et al., 1999; Boulay, 2000). The core was collected at 1197 m deep at the foot of the Faeroe Bank located at the northern end of the Rockall Trough (Figs. 1 and 2). It has been retrieved at a location where seismic continuous parallel draping internal reflectors (see seismic section C in Boldreel et al., 1998) have been attributed to pelagic sediments deposited in a low-energy, deep-water environment, unaffected by the strong current activity (Boldreel et al., 1998).

Sediment accumulation in the Rockall Trough is primarily constrained by bottom currents (Kuijpers et al., 2002). This trough extends from 53° to 60° N west of the UK, with water depths ranging from 4000 m (southern part) to 1000 m (northern part). The topography is relatively complex (Masson et al., 2002). The northwest margin is bordered by three separate seamounts (George Bligh, Lousy and Bill Bailey's)

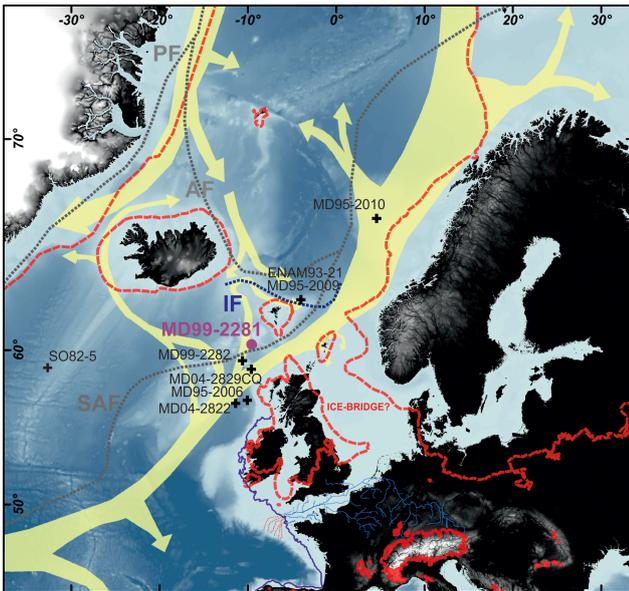


Fig. 1. Location of the studied core (MD99-2281: this work) and other cores discussed in the paper (MD95-2009; MD95-2010 – Eynaud et al., 2002; ENAM93-21 – Rasmussen and Thomsen, 2004; core SO82-5 – Van Kreveld et al., 2000; MD04-2822; MD95-2006 – Knutz et al., 2001; Hibbert et al., 2010; MD04-2829CQ – Hall et al., 2011). The yellow arrows depict the pathway of the main modern surface currents (Fogelqvist et al., 2003). Dotted grey lines locate major modern hydrographic fronts: PF= Polar Front, AF= Arctic Front, SAF: Sub-Arctic Front (Dickson et al., 1988). The IF= Iceland Faeroe Front is indicated by the dark blue dotted line (Rasmussen et al., 2002b). The palaeogeography of the adjacent European continent during the Last Glacial Maximum with the hydrographic system/paleovalleys of the Manche River (Lericolais et al., 2003) and the paleo-coastline (bold blue line) at 21 ka BP (Bourillet et al., 2003) are also depicted. The full glacial extension of the North Hemispheric ice sheets (Grosswald and Hughes, 2002, and Ehlers and Gibbard, 2004) is schematized by the red dotted-line.

culminating at more than 500 m water depth. The merging of the different deep channels between these seamounts forms a connection between the Rockall Trough and the Iceland Basin (Fig. 2).

In the northeastern part, the Rockall Trough is bordered by the Faeroe Bank (FB) and the Wyville-Thompson ridge culminating at less than 100 and 500 m water depths, respectively (Bett, 2001, Fig. 2). The barrier, which separates the Faeroe Bank Channel and the Faeroe Shetland Channel, plays an essential role in the distribution of water masses and the dynamic of bottom currents (Kuijpers et al., 2002). These landforms are the result of the opening of the North Atlantic basin during the Lower Eocene, and post-rift tectonic events that followed (Howe et al., 2006).

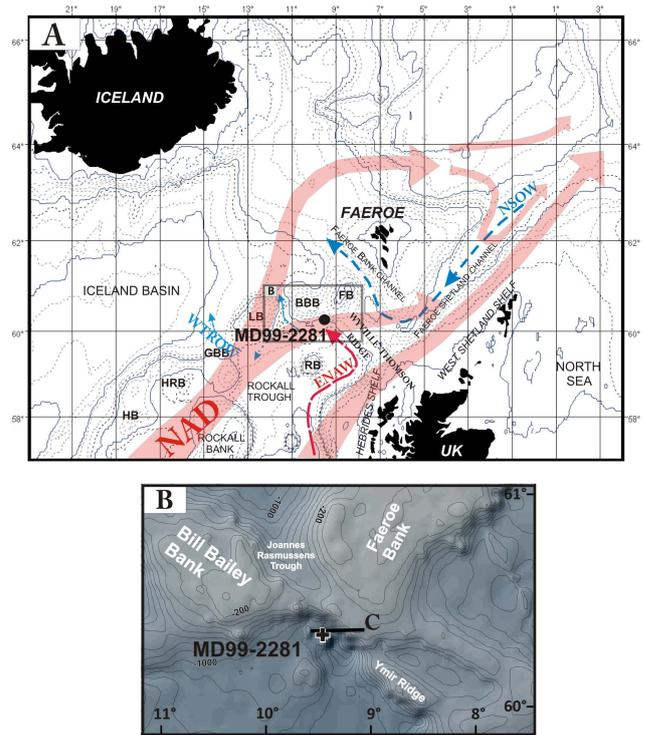


Fig. 2. Detailed physiography of the studied area. (A) Isobath: the first depth contour represents the 200 m isobar on the shelf. The next depth contour is the 1000 m isobar. At water depths greater than 1000 m, the distance between the isobars is 1000 m. Bill Bailey’s Bank (BBB), Faeroe Bank (FB), George Bligh Bank (GBB), Hatton Bank (HB), Hatton-Rockall Basin (HRB), Lousy Bank (LB), Rosemary Bank (RB) (Howe et al., 2006). Surface and sub-surface Currents: North Atlantic Drift (NAD), East North Atlantic Water (ENAW). Bottom currents: Norwegian Sea Overflow Water (NSOW), North East Atlantic Deep Water, Wyville-Thompson Ridge Overflow Water (WTROW) (Kuijpers et al., 1998, 2002; Holiday et al., 2000; New and Smythe-Wright, 2001; Howe et al., 2006). (B) Bathymetric map (contour interval 100 m) zooming on the core site with location of the C seismic section documented by Boldreel et al. (1998), who identified pelagic deposits unaffected by currents in the coring area.

2.1.2 Hydrographic and oceanographic setting

The dynamic of surface currents in the Rockall Trough area is primarily driven by the influence of two major gyres: the subtropical anticyclonic and subpolar cyclonic North Atlantic gyres. The latter is characterised by numerous streams, including the well-known poleward current of the NAD, which defines a peculiar distribution pattern of fronts and water masses in the area. The topography of the region, and more specifically the presence of Iceland, forces the penetration of the NAD across the “Iceland–Faeroe–Scotland” ridge where our study site is located. The NAD splits into two branches in the vicinity of the Faeroe Islands (Figs. 1 and 2; Larsen et al., 2008, 2009).

Core MD99-2281 is presently located under the influence of the modified North Atlantic surface waters, between the Arctic Front (AF) to the north and the sub-Arctic Front (SAF) to the south (Fig. 1). The modern sea-surface temperature (SST) in the area varies from 8 °C during winter to 12 °C during summer (WOA, 1998). Below the surface, the water-mass distribution and deep circulation are governed by the bathymetric complexity of the sector (Fig. 2, Holliday et al., 2000).

The first 1000 m of the water column are occupied by a relatively homogeneous body of water whose temperature and salinity ranges characterise the East North Atlantic Water (ENAW, Holliday et al., 2000; New and Smythe-Wright, 2001). Below dominates the North East Atlantic Deep Water (NEADW). A core of this water enters the Trough from the south and, trapped by the topography to the north, makes a cyclonic gyre, joining the Wyville-Thompson Ridge Overflow Water (WTROW) to continue its trajectory into the Iceland Basin (Howe et al., 2006). North of the Wyville-Thompson Ridge, the Norwegian Sea Overflow Water (NSOW) migrates southward across the Faeroe Shetland Channel and then turns west to enter the Faeroe Bank channel (Kuijpers et al., 2002) to join the southern flank of the Iceland–Faeroe Ridge. The NSOW intermittently crosses the Wyville-Thompson Ridge to join the LSW, then reaching our core location (Holliday et al., 2000; New and Smythe-Wright, 2001; Kuijpers et al., 1998, 2002; Rasmussen et al., 2002b).

2.2 Paleoclimatic interest

Previous paleoceanographic studies have demonstrated the high sensitivity of the Faeroe area to millennial-scale climatic variability and its intimate relation to the MOC dynamics (Rasmussen et al., 1996a, b, 2002a, b, 2008; Rasmussen and Thomsen, 2004, 2008; Eynaud et al., 2002; Voelker, 2002). During the last glacial period, the southern part of the Faeroe Islands was under the direct influence of the proximal European ice sheets (Fennoscandian ice sheet: FIS and the British–Irish ice sheet: BIIS) (Fig. 1). Therefore, core MD99-2281 has likely recorded the history of these ice sheets at a millennial scale, especially episodes of decay (including those of HEs) which occurred during MIS3, together with changes in the penetration and vigour of the NAD current, and in the latitude of the Arctic Front. In addition, our site may have recorded instabilities of the marine extensions of the ice sheets, i.e. ice shelves that are up to now poorly considered in HE dynamics (Hulbe et al., 2004; Alvarez-Solas et al., 2010). Another point concerns the potential existence of an “ice bridge” in the North Sea joining the BIS to the FIS between 30 and 25 cal ka BP. The presence of this ice bridge is still strongly debated, even if this hypothesis has gained increasing acceptance in recent years (Bradwell et al., 2008; Scourse et al., 2009; Hibbert et al., 2010; Chiverrell and Thomas, 2010; Toucanne et al., 2010).

Instabilities of proximal glaciers have had a major impact on the surface hydrology of the region and have strongly influenced the NAD, and, consequently, the NADW overflow from the Nordic Seas (e.g. Bond et al., 1992; Bond and Lotti, 1995; Broecker, 1997, 2003; Hemming, 2004).

3 Material and methods

Core MD99-2281 has been sampled every 10 cm between 2090 and 1200 cm. The 90 samples were then wet sieved to separate fractions above and below 150 µm. Both fractions were analyzed separately. Planktonic foraminiferal assemblages and ice rafted detritus (IRD) concentrations were determined on the > 150 µm fraction, whereas palynological analyses (dinocyst assemblages, freshwater algae) were conducted on the < 150 µm one.

3.1 Dinoflagellate cysts (dinocysts)

3.1.1 Dinocyst assemblage analysis

Palynological preparations follow the protocol described by de Vernal et al. (1996), slightly modified at EPOC laboratory (cf. http://www.epoc.u-bordeaux.fr/index.php?lang=fr&page=eq-paleo_protocoles for details). The dinocyst specific determination was done with a Leica Microscope at a X400 magnification. Around 300 dinocysts were counted in each sample to obtain a good statistical representation of the assemblage. Species identification follows Rochon et al. (1999b). Relative abundances were calculated relative to the total sum of Quaternary dinoflagellate cysts and absolute abundances (concentration cysts/cm³ of dried sed.) were obtained thanks to the marker grain method (*Lycopodium* tablets, de Vernal et al., 1996; Mertens et al., 2009). Counts of non-Quaternary reworked dinocysts were done in order to evaluate the ratio Rd/Md [reworked dinocysts/modern dinocysts] which along the western European margin could provide a proxy of terrigenous advection (e.g. Zaragosi et al., 2001; Eynaud et al., 2007; Penaud et al., 2009).

3.1.2 Transfer functions

An ecological transfer function has been applied to the raw data derived from the counts (relative abundances) to quantitatively reconstruct the sea-surface paleohydrological parameters. The transfer function was performed with the R software (“R” version 2.7.0, R Development Core Team, 2008) using a script developed by Guiot and Brewer (www.cerege.fr/IMG/pdf/formationR08.pdf) for the modern analogue technique (MAT, e.g. Guiot and de Vernal, 2007). This statistical tool principally uses the statistic distance between fossil (paleoceanographic record) and current (modern database) assemblages. Modern dinocyst assemblages are compiled in a geo-referenced database of marine surface sediment samples. The database we used here is that

of de Vernal et al. (2008) with 1189 stations from North Atlantic, Arctic and North Pacific oceans and their adjacent seas (see recurrent updates at <http://www.geotop.ca/fr/bases-de-donnees/dinokystes.html>). Calculations rely on a weighted average of SST values (compiled from the 2001 version of the World Ocean Atlas) from the best five modern analogues, with a maximum weight given for the closest analogue in terms of statistical distance, i.e. dissimilarity minimum (e.g. Kucera et al., 2005; Guiot and de Vernal, 2007). Among the sea-surface parameters that we can reconstruct on the basis of dinocysts are SSTs and sea-surface salinities (SSSs) for the warm season, i.e. mean summer (June–July–August average), the cold season, i.e. mean winter (January–February–March average), the warmest (August) and the coldest (February) months of the year, but also the sea-ice cover duration (months per year). The reader is referred to Guiot and de Vernal (2007, 2011a,b) for a review of the theory of transfer functions, and to de Vernal et al. (2001, 2005) for a step-by-step description of the application of transfer functions to dinocysts, including discussion about the degree of accuracy of the method.

Standard deviations must be taken into account in the reconstituted hydrological parameters because of the accuracy of the database calibration. They have been established by comparing the predictions provided by the transfer function and direct instrumental measurements made on surface waters. The root mean square errors of prediction (RMSEP) for the parameters presented in this paper are $\pm 1.1^\circ\text{C}$ and $\pm 1.6^\circ\text{C}$ for SST of February and August, respectively, and ± 1.1 months per year for the ice cover duration (Penaud, 2009). They are ± 2.2 and ± 2.5 psu for February and August SSS, and ± 2.3 and ± 2.4 psu for mean winter and mean summer SSSs, respectively. The relatively large error for salinity prediction is due to the inclusion of Arctic sites characterised by low and highly variably salinities (down to 11). In the > 30 salinity domain, the error of prediction is 0.63 (Eynaud et al., 2012). Associated and additional information is listed on the GEOTOP website (<http://www.geotop.ca/>).

3.2 Magnetic properties

The core has been sub-sampled using u-channels to perform detailed magnetic analyses. In order to complement on-board susceptibility measurements made with a large diameter coil (low resolution), magnetic susceptibility has been repeated at the LSCE with a 45-mm diameter MS2-C Bartington coil. The data were generated every 2 cm on the u-channels and they were normalized by the volume to get the volume susceptibility (κ). The natural remanent magnetization (NRM) was measured using a 755-R 2G cryogenic pass-through magnetometer, equipped with a high resolution set of coils and placed in the μ -metal shielded room of LSCE (see Kissel et al., 1999b for detailed laboratory procedures). An in-line alternating field (AF) demagnetization unit was used for the stepwise demagnetization at 5, 10, 15, 20, 25, 30, 35,

40, 45, 50, 60 and 80 mT. After demagnetization at 80 mT, 87 to 97 % of the initial magnetization was removed. The anhysteretic remanent (ARM) and isothermal remanent (IRM) magnetizations were acquired and demagnetized also on u-channels using the same method and instruments. ARM was acquired along the vertical geographical axis in a peak alternating field of 100 mT and a steady bias field of 50 μT . During acquisition, the samples were translated through the coils at a speed of about 1 cm s^{-1} (Brachfeld et al., 2004). After acquisition, the ARM was then progressively demagnetized using 10 steps at 10, 15, 20, 25, 30, 35, 40, 50, 60, and 80 mT. Saturated IRM (SIRM) was then acquired, also along the vertical geographical axis in six steps (0.05, 0.1, 0.2, 0.3, 0.5 and 1 T) using a 2G 1.6 m long pulsed solenoid and stepwise demagnetized using the same 10 steps as for the ARM. During the demagnetization of NRM, ARM and IRM, the u-channels were translated at a speed of about 4 cm s^{-1} through the demagnetization coils. All the data were acquired using software developed at LSCE, which allow to considerably reduce the translation speed during the measurements while the u-channel passes through the pick-up coil. This is particularly adapted to the measurements of very high magnetizations as the ones of core MD99-2281 because the reduced translation speed allows to reliably count the flux jumps. Previous works already conducted in the area established that the main magnetic mineral is magnetite (Kissel et al., 1999a; Ballini et al., 2006). The co-variations obtained between the low field magnetic susceptibility, the ARM and the IRM data therefore indicate that these parameters are only concentration dependent in this sediment (except during HE4, see below).

3.3 XRF (x-ray fluorescence) elementary analyses

A non-destructive X-ray fluorescence (XRF) scan of the core was done using the CORTEX scanner at a resolution of 2 cm (Richter et al., 2006). To complement these data, a high resolution scan (every 2 mm) was done at EPOC laboratory with the Avaatech XRF Core Scanner on the sections (990–2100 cm) investigated for dinocysts. This provides us with a semi-quantitative approach of the sediment chemical composition (for major and some minor chemical elements), and thus permits estimation of changes in the nature of sediments along time. Richter et al. (2006) demonstrated on the basis of the low resolution XRF scan of a proximal core MD99-2282 ($59^\circ 29' \text{N}$; $10^\circ 34' \text{W}$) that the abundance of some elements, such as Ca, or the ratio K/Ti, provides information about glacial–interglacial alternances. It was also observed by Ballini et al. (2006) at the DO scale. Among other applications of the XRF tool, the ratio K/Ti could provide information about lithic grain sources, and the $(\text{Fe} + \text{Ti})/(\text{Ca} + \text{Sr})$ ratio further gives access to the proportion of lithogenic versus biogenic components within the sediments. The variations in Fe, Mn and S abundances further help to identify early diagenesis processes (Mojtahid et al., 2005; Richter et al., 2006).

3.4 Analysis of the coarse fraction > 150 μm

3.4.1 Planktonic foraminifera

These calcareous-walled protists form part of the zooplankton, and their geographical distribution covers almost all oceans (e.g. Kucera, 2007). There are currently about forty species in the modern assemblage of planktonic foraminifera. One of the mesopelagic species well known and frequently used in paleoclimatology and biostratigraphy is the polar taxon, *Neogloboquadrina pachyderma* sinistral (NPS) coiled form. Quantification of this taxon abundance (%) in the planktonic assemblages provides access to a qualitative estimate of surface water temperatures, and depending on the areas, directly follows the Polar Front migrations (e.g. Ericson, 1959; Eynaud et al., 2009). Counts of the relative abundances of this species have been made on known aliquots of the dried > 150 μm residues (total sum of planktonic foraminifera of minimum 300 specimens) from the same samples studied for dinocyst assemblages.

In addition, stable isotope measurements were done on NPS shells. Specimens were picked out from the 200–250 μm fraction and analysed at EPOC using an Optima Micromass mass spectrometer. For each measurement, 80 μg mean weight aliquots (5 to 6 specimens) were treated with individual acid baths. The extracted CO_2 gas was analyzed versus a laboratory reference gas calibrated with respect to VPDB (Vienna Pee Dee Belemnite) using the international standard NBS 19. For this paper, only $\delta^{18}\text{O}$ data will be discussed.

3.4.2 Ice-rafted debris

In hemipelagic cores, ice rafted detritus (IRD) are generally determined in the coarse lithic > 150 μm grain fraction. These large lithic grains (LLG) are actually torn-off bedrock under ice sheet dynamic processes. They were disseminated by icebergs throughout the North Atlantic Ocean during ice-sheet calving events, as for instance during Heinrich events (Heinrich, 1988; Bond et al., 1992; Bond and Lotti, 1995; Elliot et al., 2001; Broecker, 2003; Hemming, 2004). The study of IRD concentrations (number of LLG > 150 μm g^{-1} dry sediment) thus provides a way to document ice-sheet dynamics throughout time. The LLG were counted in the same samples as those used for NPS relative abundance characterisation. Their raw number per samples varies from 64 to 955 grains per g of dry sediment.

4 Stratigraphy of the core

Nine AMS ^{14}C dates measured on planktonic foraminifera monospecific samples (cf. Table 1) have been obtained on the topmost eleven meters of core MD99-2281 (Table 1, Boulay, 2000), providing a first stratigraphic frame between 10 and 24 ka cal BP. For this work, four supplementary AMS ^{14}C

dates were obtained between 12 and 19 m in the core. Regarding the time period we consider for this paper, radiocarbon dates were calibrated using the “glacial polynomial” from Bard (1998) and Bard et al. (1998), which provides calibration up to 36 ^{14}C ka BP (Table 1).

Following several paleoceanographic studies in the area (Rasmussen et al., 1996b, 1997; Kissel et al., 1999a; Eynaud, 1999; Stoner et al., 2000; Laj et al., 2000), these age control points were combined to tie-points generated by the comparison of the record of magnetic concentration parameters to the NGRIP-GICC05 $\delta^{18}\text{O}$ record (Svensson et al., 2008), i.e. the recommended North Atlantic regional stratotype (Austin and Hibbert, 2012). The rationale is that marine records of magnetic concentration parameters from MIS3 are consistent across the North Atlantic Basin on the path of different overflow branches of the NADW and could be tied on the high frequency climatic variability (DO cycles, e.g. Sanchez-Goñi and Harrison, 2010; Wolff et al., 2010) characteristic of this period (e.g. Kissel et al., 1999a). This approach is comparable to an event-based stratigraphy and has recently been acknowledged as one of the most robust ways to establish age models for marine sediments (Austin and Hibbert, 2012).

Our stratigraphy has thus been constructed by linking the magnetic concentration increases to the beginning of Greenland interstadial (GIs) warmings (Austin and Hibbert, 2012 recommended protocol) and conversely, the magnetic concentration decreases to Greenland stadial (GS) coolings (Fig. 3). The chronostratigraphic ages used for this work conform to the recent update done by Wolff et al. (2010) on DO events. As a result, 18 stratigraphic control points have been added to the AMS ^{14}C dates (Table 1, Fig. 3). The age model has been constructed on the basis of a linear interpolation between tie points (Table 1, Fig. 4) giving an average sedimentation rate of about 80 cm ka^{-1} for the studied period.

Additional tie points, independent from climate, are also retrieved from the record of the changes in the Earth's magnetic field intensity, namely the two prominent lows attributed to the Mono Lake (MLE) and to the Laschamp (LE) excursion (Laj et al., 2000). Due to the modulation of cosmogenic isotopes production by the dipolar Earth magnetic field, these two excursions have their counterpart in the ^{10}Be and ^{36}Cl records from ice (Wagner et al., 2000). Therefore, they allow a robust correlation between ice and sediment climatic records. In both archives, the MLE occurred during GS7 and the LE is centered on GI10. We observe that both are at the right place in core MD99-2281 (Figs. 3 and 4), giving confidence on the correlation discussed above.

Table 1. Radiocarbon dates for core MD99-2281 and age-control points derived from the correlation of the MS signal with the NGRIP GICC05 $\delta^{18}\text{O}$ record (Svensson et al., 2008; Wolff et al., 2010). See also Fig. 3.

Depth (cm) in core MD99-2281	LAB_ID	AMS ^{14}C age uncorrected (BP)	Calendar age corrected (cal BP) (Bard, 1998)	Calendar age corrected (cal BP) CALIB 6.0	1σ ranges: [start]	1σ ranges: [end]	Coherency of the two calibration method [Δ]	Tie points (age in cal BP)	Dated material/age control points/references
40	GifA 100405	10 260 ± 100	11 165	11 261	11 137	11 384	95	11 165	<i>G. bulloides</i> , Boulay (2000)
170	GifA 100406	12 970 ± 110	14 729*	14 657	14 156	15 158	72		<i>G. bulloides</i> , Boulay (2000)
270	GifA 100407	10 800 ± 100	12 081	12 229	12 070	12 388	148	12 081	<i>G. bulloides</i> , Boulay (2000)
400	GifA 100408	11 060 ± 110	12 400	12 431	12 478	12 517	31	12 400	<i>G. bulloides</i> , Boulay (2000)
510	GifA 100409	15 290 ± 130	17 529	18 037	17 931	18 142	507	17 529	<i>N. pachyderma</i> s., Boulay (2000)
580	GifA 100410	15 760 ± 170	18 092	18 219	18 261	18 490	126	18 092	<i>N. pachyderma</i> s., Boulay (2000)
650	GifA 100411	16 040 ± 140	18 427	18 777	18 651	18 902	349	18 427	<i>N. pachyderma</i> s., Boulay (2000)
780	GifA 100412	18 060 ± 160	20 830	20 630	20 562	20 697	200	20 830	<i>N. pachyderma</i> s., Boulay (2000)
1180	GifA 100414	23 340 ± 240	26 993	27 144	20 903	21 361	151	26 993	<i>N. pachyderma</i> s., Boulay (2000)
1240					27 037	27 251			Correlation NGRIPGICC05, G13 termination, Wolff et al. (2010)
1275					24 522	28 087			Correlation NGRIPGICC05, G13 warming, Wolff et al. (2010)
1280	SacA 19117	24 210 ± 140	27 992	28 567	28 326	28 807	574	27 992	<i>N. pachyderma</i> s., ARTEMIS 2010
1300									Correlation NGRIPGICC05, G14 termination, Wolff et al. (2010)
1355									Correlation NGRIPGICC05, G14 warming, Wolff et al. (2010)
1430	SacA 19118	27 430 ± 140	31 652	31 306	31 211	31 400	346	31 652	<i>N. pachyderma</i> s., ARTEMIS 2010
1440	SacA 19119	27 940 ± 140	32 226*	31 576	31 411	31 740	650		<i>N. pachyderma</i> s., ARTEMIS 2010
1475									Correlation NGRIPGICC05, G15 termination, Wolff et al. (2010)
1523									Correlation NGRIPGICC05, G15 warming, Wolff et al. (2010)
1548									Correlation NGRIPGICC05, G16 termination, Wolff et al. (2010)
1605									Correlation NGRIPGICC05, G16 warming, Wolff et al. (2010)
1650									Correlation NGRIPGICC05, G17 termination, Wolff et al. (2010)
1711									Correlation NGRIPGICC05, G17 warming, Wolff et al. (2010)
1755									Correlation NGRIPGICC05, G18 termination, Wolff et al. (2010)
1820	SacA 19121	34 610 ± 290	39 586*	39 105	38 722	39 488	481		<i>N. pachyderma</i> s., ARTEMIS 2010
1880									Correlation NGRIPGICC05, G18 warming, Wolff et al. (2010)
1930									Correlation NGRIPGICC05, G19 termination, Wolff et al. (2010)
1960									Correlation NGRIPGICC05, G19 warming, Wolff et al. (2010)
2030									Correlation NGRIPGICC05, G110 termination, Wolff et al. (2010)
2090									Correlation NGRIPGICC05, G110 warming, Wolff et al. (2010)
2110									Correlation NGRIPGICC05, G111 termination, Wolff et al. (2010)
2170									Correlation NGRIPGICC05, G111 warming, Wolff et al. (2010)

Bold characters: age values used for the interpolation. * Age reversals removed.

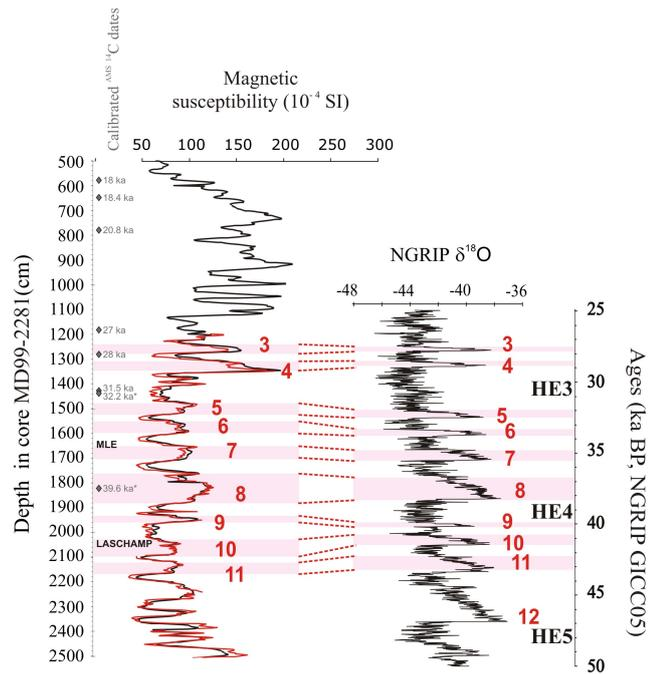


Fig. 3. Magnetic susceptibility (MS) record from core MD99-2281 (dark line = onboard data versus red line = low field magnetic susceptibility) and its correlation to the NGRIP GICC05 $\delta^{18}\text{O}$ record (Svensson et al., 2008) to define supplementary age control-points over the MIS3 period. See also Table 1. Pink bars underline GIs, labels and limits after Wolff et al. (2010). The horizons having recorded the geomagnetic excursions (MLE for Mono Lake excursion and Laschamp) are also indicated.

5 Results

5.1 Dinocyst data

Thirty dinocyst taxa were identified in the MIS3 assemblages. Their absolute abundances in the sediment (concentrations) are high and vary between 1000 and 90 000 cysts/cm³ along the studied section, with a mean value around 10 000 cysts/cm³ (Fig. 5). As a whole the dinocyst concentrations follow the MS properties data, thus indicating maximum dinocyst production and/or deposition and/or preservation to the studied site during warm GIs, and conversely during cold GSs. Some strong excursions were recorded over the studied interval, with especially two peaks in concentrations of about 90 000 and 57 000 cysts/cm³ at 1660 and 1950 cm depths, respectively.

The assemblages are dominated by five species (Fig. 5, Table 2), which are: *Bitectatodinium tepikiense* (largely dominates the assemblages), *Operculodinium centrocarpum*, *Brigantedinium* spp., *Islandinium minutum* (upper part of the section), and *Pentapharsodinium dalei* (lower part of the section). Table 2 summarizes the most salient features recorded for the encountered species both at present and along the studied section of core MD99-2281. The

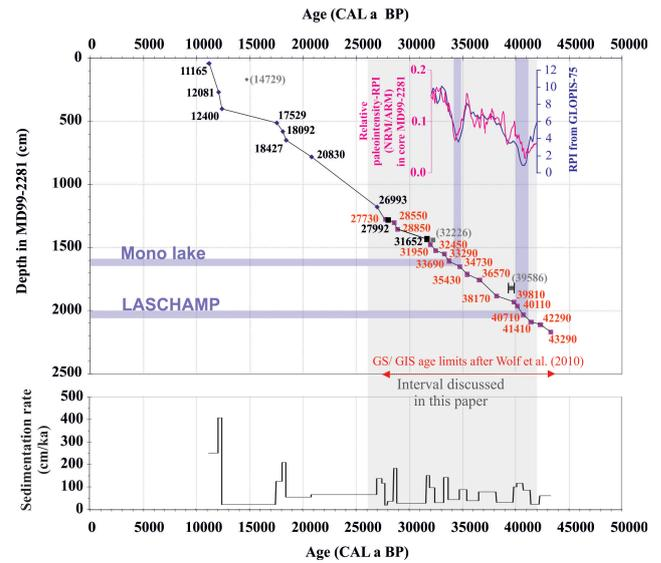


Fig. 4. Age model and sedimentation rates for the last 50 ka BP in core MD99-2281 (see also Table 1). Dates in red are those deduced from the correlation (see also Fig. 3) of the MS record and the NGRIP GICC05 $\delta^{18}\text{O}$ (Wolff et al., 2010). A comparison of the relative paleointensity (RPI) record from core MD99-2281 with the reference RPI curve of GLOPIS-75 is shown for the 32–42 ka interval.

continuous presence along the record of specimens from the genus *Brigantedinium*, with occurrence of other peridinioid-species, indicate that the alteration of the assemblage by oxygenation processes (e.g. Zonneveld et al., 2007) was not intense. This is also supported by high dinocyst concentrations in the sediments during GIs which record active deep-sea circulation (e.g. Kissel et al., 1999a), and thus better ventilation.

5.2 Sea-surface paleohydrology (from dinocyst transfer function) during MIS3

The sea-surface paleohydrological conditions quantified on the basis of the dinocyst MAT transfer function (database 1189) are shown in Fig. 5 (right panel).

In the studied section, August SSTs vary between 8.5 and 17 °C, with a mean around 16 °C, and February SST between 6 and –1 °C. The reconstructed February SSTs are considerably lower than the modern ones over the area, which fluctuate around an average of 8.7 °C (WOA, 1998). In contrast, the reconstructed August SSTs are well above the modern averages of 12.1 °C (WOA, 1998). Our reconstructions indicate that a positive anomaly of nearly 4 °C (in comparison to the modern conditions) was recorded over the area during MIS3 in summer.

Sea-ice cover duration varies between 0 and 2 months/year along the main part of the section, except in the topmost part of the studied section where it reaches values up to 5 months per year. These values are above the modern ones, the area being presently free of sea-ice even in winter, but are still

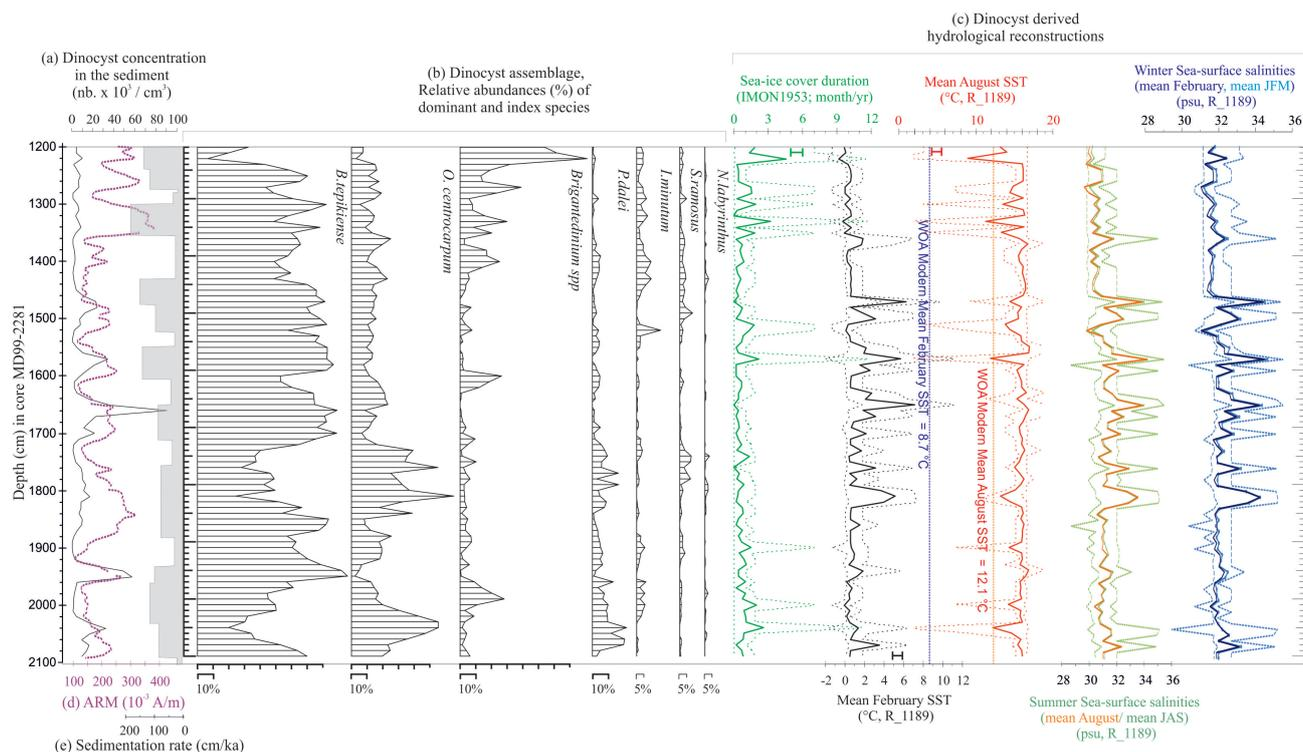


Fig. 5. Results from dinocyst analyses (see also Table 2) over the section 1200–2100 cm in core MD99-2281, with (a) dinocyst total concentrations in the sediment (nb. of cyst/cm³ of dry sed.); (b) relative abundances of some selected species; (c) Dinocyst derived reconstructions (modern analogue technique) of sea-surface conditions (sea-ice cover duration \pm 1.1 months per year; February SST \pm 1.1 °C; August SST \pm 1.6 °C; February SSS \pm 2.2; August SSS \pm 2.5; mean winter SSS \pm 2.3; mean summer \pm 2.4 psu). The dotted lines surrounding each reconstructed parameter correspond to minima and maxima values found in the set of the 5 selected analogues. Modern values of SSTs after WOA (1998). These results are compared to (d) the ARM (for anhysteretic remanent magnetization) data and (e) the sedimentation rate calculated from our age model (see Fig. 4).

very low. They should be considered rather as an index of the intermittent presence of ice, regarding the RMSEP of 1.1 months per year.

Paleosalinity reconstructions show variations within a range of 4 psu, from 30 to 34 in summer (during mean summer months, i.e. July-August-September, and mean August only) and 31 to 35 in winter (during mean winter months, i.e. January-February-March as well as February only). SSS oscillations are recorded synchronously during both seasons (same trends along our record), even if summer SSSs tend to be less saline than during winters. This is probably due to the influence of the summer melting of proximal ice sheets. Mean annual modern values over the area are of 35.3, with a positive Δ 0.07 psu difference between winter and summer seasons (WOA 2009, http://www.nodc.noaa.gov/OC5/WOA09/netcdf_data.html). Sea-surface waters were thus sensibly more brackish in the area during MIS3.

5.3 Multiproxy compilation

Figure 6 compiles the multiproxy dataset we obtained on core MD99-2281 between 1100 and 2100 cm, i.e. 26.5 and 41.5 ka cal BP (\pm 1.6 ka considering the GICC05 chronological uncertainty, Svensson et al., 2008). High-resolution XRF data are compared to MS data, planktonic foraminifera data and to large lithic grain (LLG > 150 μ m) concentration in the sediment, this latter indicating IRD arrivals on site.

The XRF data show a high variability in correlation with changes in magnetic records (Fig. 6) with each minimum in magnetic concentration corresponding to a minimum in the XRF calcium detection curve (^{XRF}Ca), and conversely maxima in magnetic concentration matching maxima in ^{XRF}Ca. This indicates that the magnetic concentration record does not result from a dilution effect by calcium carbonate and really illustrates changes in the input of magnetites by overflow water, as for the other cores distributed along the path of the NADW. This correlation also suggests relatively low biogenic calcareous inputs (Richter et al., 2006) during stadial periods, alternating with higher inputs during interstadials. At the opposite, interstadials record increases in the ^{XRF}Ca

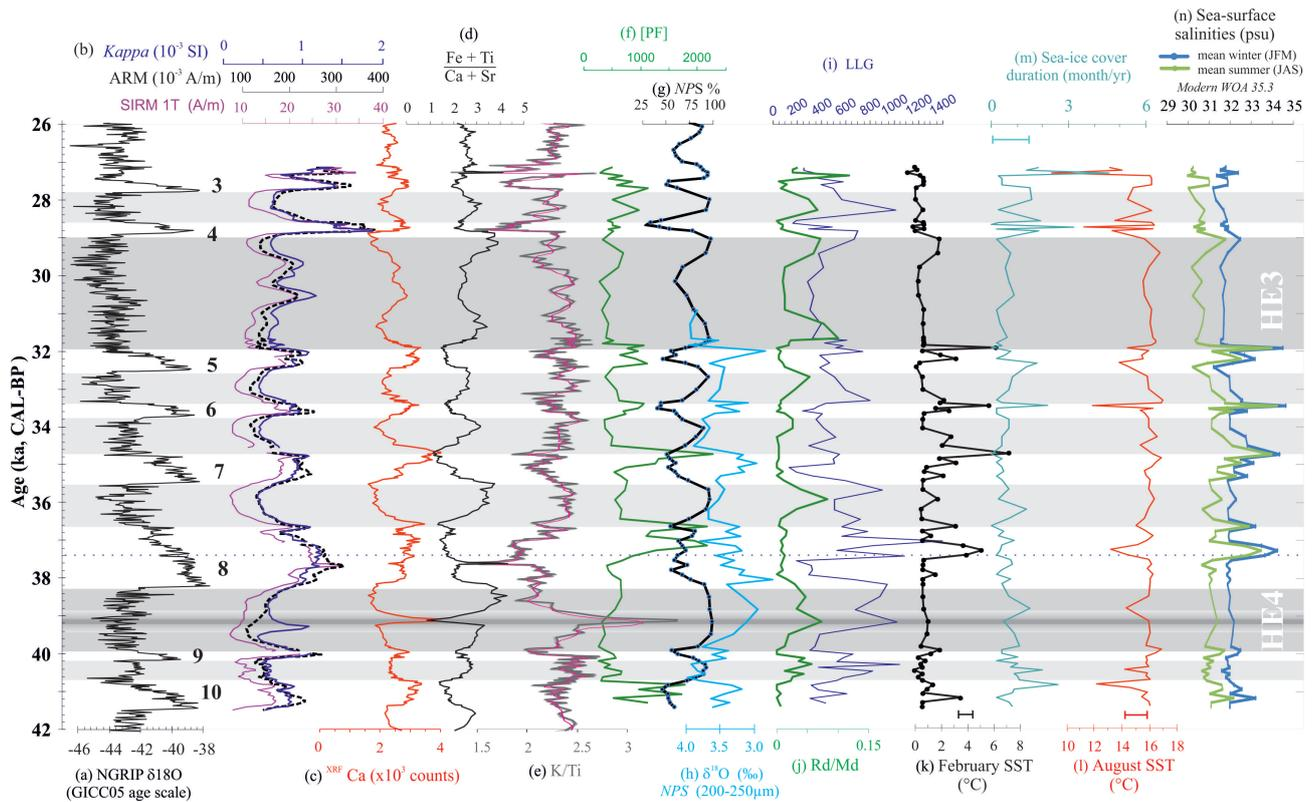


Fig. 6. Multiproxy results obtained on the MIS3 section of core MD99-2281 compared to the (a) $\delta^{18}\text{O}$ NGRIP GICC05 record (Svensson et al., 2008), with: (b) Magnetic properties (volume susceptibility – *Kappa* – ARM; Isothermal Remanent – IRM – magnetizations); XRF data with (c) Ca raw counts, (d) ratio (Fe + Ti)/(Ca + Sr) and (e) ratio K/Ti (pink curve: smoothed 3 points running average); (f) planktonic foraminifera absolute concentration in the sediment ([PF]=Nb. of shells > 150 μm per g of dry sed.); (g) relative abundances (%) of the polar taxon *N. pachyderma sin.* (NPS); (h) $\delta^{18}\text{O}$ measurements on monospecific samples of NPS shells (200–250 μm); (i) Large lithic grain concentration in the sediment (LLG = Nb. of grain > 150 μm per g of dry sed.); (j) Reworked dinocyst versus modern dinocyst concentrations, i.e. Rd/Md ratio; (k)–(n) dinocyst derived reconstructions of sea-surface conditions with (k) February SST ± 1.1 $^{\circ}\text{C}$; (l) August SST ± 1.6 $^{\circ}\text{C}$; (m) sea-ice cover duration ± 1.1 months per year, (n) sea-surface salinities ± 2.5 psu. Greenland stadials (light grey bands), including Heinrich events (dark grey bands) are defined in agreement with the stratigraphic synthesis of Wolff et al. (2010). Within HE4, the 39 ka event (see text) is highlighted.

content occurring in concordance with higher concentration of planktonic foraminifera shells in the sediment and lower NPS $\delta^{18}\text{O}$ values. It is worth noting that these conditions are particularly characteristic of the interstadial terminal parts in our record.

The $^{\text{XRF}}\text{Ca}$ is corroborated by the ratios (Ti + Fe)/(Ca + Sr), K/Ti and the LLG concentration in the sediment, which together indicate strong terrigenous input preferentially during stadials, but poor in magnetic content. The K/Ti XRF intensity ratio reflects changing provenance of the terrigenous fraction, with an enhanced ice-rafted continental crust (high K) contribution during stadials vs. relatively more bottom current derived basaltic input (high Ti) during interstadials (cf. Ballini et al., 2006; Richter et al., 2006; Grützner and Higgins, 2010). Considerable short-term variability is superimposed upon the general stadial–interstadial pattern.

6 Towards an integrated view of the response of sea-surface paleoenvironments south of the Faeroe Islands during MIS3

The Marine Isotopic Stage 3 covers more than 30 000 yr. Its lower stratigraphic limit is located at around 59 ka BP (e.g. Martinson et al., 1987) and its upper stratigraphic boundary has recently been revised by Wolff et al. (2010) and positioned at the transition between GS4 and GI3 around 27.73 ka cal BP. Other previous work considered MIS3 termination at the end of HE3 after 29 ka cal BP (Voelker, 2002; Bradwell et al., 2008; Hibbert et al., 2010).

Figure 6, integrating the most significant results of our study, summarizes salient features detected during MIS3 in core MD99-2281. If the DO structure (cold GSs versus warm GIs) is clearly recognizable in this multiproxy dataset, it is worth noting the good consistency between the different studied paleoenvironmental proxies. The highlighted

Table 2. Summary of the ecology of the main species recorded over the studied section of core MD99-2281.

Dinocyst specie	Modern bioprovinces (Rochon et al., 1999b)	Known ecological preferences (Rochon et al., 1999b; Marret and Zonneveld, 2003; de Vernal and Marret, 2007)	Presence in core MD99-2281
<i>B. tepikiense</i>	– temperate to subarctic (high abundance spots at the St. Laurence and Baltic Sea outlets)	– tolerates a wide range of SST and salinities, but most represented in areas when summer SST exceed 10 °C – strong affinity for stratified surface waters characterised by a large seasonality (Rochon et al., 1999b)	– dominates the assemblages along most of the MIS3 section with percentages sometimes reaching 95 %. These atypical high values are not observed at present in the North Atlantic ocean surface sediments (max. of 30 %).
<i>O. centrocarpum</i>	– observed from mid to high latitudes – associated with the North Atlantic Drift (NAD) pathway	– tolerates a wide range of temperatures and salinities	– second most abundant species encountered, especially at the base of the section
<i>Brigantedinium</i> spp.	– ubiquitous, often dominant in upwelling zones – also associated with sub-arctic and arctic water masses	– tolerates a wide range of temperatures, salinities and sea-ice cover duration – heterotrophic taxa, has been related to its main food source, diatoms.	– well represented at the top of the section – Relatively difficult to identify at the species level due to the crumbled aspect of the cyst
<i>I. minutum</i>	– sub-polar to polar	– associated with long sea-ice cover duration (from 8 to 12 months)	– poorly represented in our sequence, except in the upper part of the section
<i>P. dalei</i>	– sub-polar to polar environments in North Atlantic basins, north of the NAD	– tolerates a wide range of SSSs, SSTs, and sea-ice cover duration – requires a 4 °C SST minimum during summer – abundant in regions with a large seasonal gradient of SSTs	– low abundances in the sequence; presence most noticeable at the base of the section

variability is well defined through qualitative data as well as through quantitative ones, with a pattern which reveals the sequencing of MIS3 millennial scale events over the area. The following discussion has been structured on this basis, considering separately GSs and GIs in order to better discriminate their specific paleoenvironments.

6.1 Interstadials (GIs)

The pattern detected for GIs on the basis of our study (Fig. 6) appears to be reproducible for almost all the recovered

GIs and reveals milder climatic and sea-surface conditions. $^{22}\text{RfCa}$, $\delta^{18}\text{O}$ low values (signing a warm and/or meltwater advection) and the absolute abundance of planktonic foraminifera, appear together in close agreement with the reconstructed February SSTs. They all converge to indicate mean sea-surface conditions which were probably nearly as warm as the modern ones. However, detailing the internal structure of the GIs reveals pulsed warm excursions (especially well expressed in February SSTs) that are detected late during GIs, at the transition towards GSs. This is quite

atypical considering the abruptness classically attributed to DO atmospheric warmings (Severinghaus and Brook, 1999; Lang et al., 1999; Schulz, 2002). These late events also coincide with brief decreases in summer SSTs and positive excursions in salinity, together expressing conditions closely similar to the modern ones. Other proxies reveal GIs marked by lower IRD inputs, together occurring with reduced advection of terrigenous material (i.e. low values of the ratios $[\text{Ti} + \text{Fe}]/[\text{Ca} + \text{Sr}]$ and K/Ti , also probably linked to a dilution by an enhanced carbonate biogenic productivity), and a ratio of Rd/Md close to zero. This suggests reduced calving from the surrounding ice sheets. The magnetic content is high at the same time as bottom currents are enhanced, transporting magnetite-rich sediments from the basaltic sill. The reconstructed sea-ice cover duration indicates GIs mostly sea-ice free. This is coherent with warmer SSTs recorded during winter (February) and summer (August) for most of the duration of these warm events (except within events of larger sea-ice duration excursions, see below). However, during GIs, our reconstructions argue for very different sea-surface conditions than the modern ones, especially because strong SST anomalies (modern versus GIs) are detected (Fig. 5): winters appear to be colder compared to modern ones (-6°C) whereas summers record positive anomalies of nearly 4°C . These anomalies are strongly reduced during warm winter excursions that mark the end of the GIs; SSTs thus tend very briefly to mirror modern conditions. Transient sea-ice cover development accompanies these peculiar events.

High relative abundances of NPS ($> 80\%$) in the North Atlantic modern sediments mark the presence of the polar front (PF) (e.g. Eynaud et al., 2009). A shift is observed concerning this species in the vicinity of Faeroes with abundances sharply increasing north of these islands and reaching monospecific values in the Greenland Sea. Percentages up to 40% can be recorded in modern sediment of the area. The signal reconstructed in MD99-2281 during MIS3 could thus provide a record of the evolution of the PF position over the area. The pattern identified within this proxy follows the DO oscillations with GIs recording percentages close to their modern values, i.e. conditions which characterise a northern position of the PF. Along the studied section, relative abundances of NPS mirror the evolution of the ^{XRF}Ca signal (Fig. 6).

GI8

The GI8 records atypical conditions. It is considered as one of the warmer MIS3 interstadials (Sanchez-Goni et al., 2008) and is marked by a gradual cooling in ice records; its occurrence in our archive evidences at least two distinct phases. The reconstructed sea-surface conditions characterise a GI8 recording warm August SST of nearly 16°C during the first centuries, followed by a sharp cooling at about 37.4 ka BP , which instead corresponds to warmer February SSTs and to an abrupt increase (the largest in our record) in the detrital

material as documented by the LLG concentrations (Fig. 6). However, it should be noted that this transition is not accompanied by any increase in the $[\text{Ti} + \text{Fe}]/[\text{Ca} + \text{Sr}]$ or K/Ti ratios or any change in the ^{XRF}Ca or magnetic concentration. $\delta^{18}\text{O}$ values indicate rapid minor oscillations within GI8, with a trend toward higher values recorded precisely when the LLG peak occurred. We also note that percentages of NPS are then relatively high compared to the other GIs, with also high absolute abundances of planktonic foraminifera shells in the sediment. This terminal phase probably relates to milder conditions (especially during the winter months, as detected by dinocysts).

6.2 Stadials (GSs and Heinrich Events HEs)

In our record, all GSs (underlined by grey bands on Fig. 6), except HE3, are characterised by high LLG concentrations and high abundances of NPS, coupled with high values of the ratios Rd/Md , $[\text{Ti} + \text{Fe}]/[\text{Ca} + \text{Sr}]$ and K/Ti . Conversely, both ^{XRF}Ca content and planktonic foraminiferal abundances significantly decrease. This reflects important terrigenous advections (Matthiessen et al., 2000; Zaragosi et al., 2001; Richter et al., 2006; Ménot et al., 2006; Penaud et al., 2009). However, there are less magnetic particles than during GIs. This is related to the calving of the proximal ice sheets that does not bring magnetic particles at that time, and is combined with a reduced bottom current, while, during GIs, stronger deep currents bring magnetic particles from the Iceland plateau. The high percentages of NPS (between 80 and 100%), accompanied by high $\delta^{18}\text{O}$ values, further indicate a marked southward migration of polar waters.

These discharges are accompanied by SST approaching 0°C in February. However, a strong seasonality is observed during these periods as SSTs are still high in August. Such a strong seasonality occurring during GSs is at the opposite of what is at present characteristic of the area. Modern sea-surface environments are indeed strongly influenced by the penetration of the NAD, reducing the SST difference between winter and summer (3°C only). Conditions recorded during MIS3 could then be due to a globally reduced NAD influence over the site of study. The increase in seasonality we find could also be related to sea-surface conditions marked by the presence of proximal ice sheets that may have maintained cold atmospheric situations during winters. Additionally, another scenario could imply the development during summers of a thin, low salinity surface layer in relation to the seasonal melting of local ice sheets, which could be rapidly warmed up during the warm season. This atypical warm summer signal could also be related to the formation of polynyas, which could have constituted patchy “hot spots” free of ice. Actually, such phenomema are observed at present in the modern Arctic Ocean, where strong winds associated or not to the upwelling of warm waters, create holes in the sea-ice cover (e.g. Platov, 2011).

6.2.1 Heinrich event 4 (HE4)

Known as the largest amplitude cooling event over HEs (e.g. Cortijo et al., 1997), with in particular a very strong Laurentide ice-sheet (LIS) signature, HE4 can be divided into three phases in some parts of the Northeast Atlantic (e.g. Hemming, 2004), with a first European phase, a second longest Canadian phase, and then a terminal European phase (Snoeckx et al., 1999; Grousset et al., 2000). Multiphasing within HE4, with especially a mid-event warming, was recently reported from the central North Atlantic (Reykjanes Ridge, Jonkers et al., 2010a).

In our multiproxy dataset, a typical GSs signature is recorded for HE4, with indices suggesting ice-sheet collapse (high LLG concentrations, low $\delta^{18}\text{O}$ values). Interestingly, a major peak in the ^{XRF}Ca content is recorded in the middle of HE4 (around 39 ka). This peak is quite atypical regarding other GSs that otherwise record low ^{XRF}Ca values. It also differs from interstadial ^{XRF}Ca maxima with respect to shape, amplitude and duration, as well as in its relationship to proxies of terrigenous input. The ^{XRF}Ca peak displays a sharp onset and termination but lacks an intermittent “plateau” of roughly constant or slightly variable values; it is inverse V-shaped rather than inverse U-shaped, corresponding to a pulse rather than a period of high ^{XRF}Ca . The Ca peak during HE4 coincides with a maximum of the K/Ti intensity ratio (highest values of the entire record), while there is little if any relationship between both XRF parameters for the remainder of MIS3. Regarding data of magnetic properties, it finds echoes only in the low field magnetic susceptibility (κ , Fig. 6), suggesting advection of large-sized magnetic grains. The pulse-like structure combined with the bulk terrigenous and magnetic signatures suggest that this anomaly may reflect an ice-rafting event, hence a detrital origin of carbonates. Relatively low ^{XRF}Sr with respect to ^{XRF}Ca provides further circumstantial evidence for this hypothesis, as detrital carbonates are generally depleted in Sr compared to biogenic ones (Hodell et al., 2008). According to Hemming (2004), high proportions of detrital carbonates characterise IRD sourced from Hudson Strait and Laurentide ice sheet. This signal might then have overlapped the European ice sheets one. In this case, changes due to local ice sheets instabilities have probably occurred before the signal that characterises the destabilization of the LIS, as featured in our record. However, this is not sufficient to suggest a precursor role of the European system (e.g. Scourse et al., 2000) for HE4. It must indeed be noted that European ice sheets finally have had the same behaviour for each GSs throughout MIS3, which attests to their sensitivity, with no evidence of asynchronicity with the LIS. Taking into account the distance between the core MD99-2281 and the Laurentide source, few IRD may have reached the area after crossing the North Atlantic, and are therefore only recorded as exceptional outburst events. This is also observed in the proximal core MD04-2829CQ further south (Fig. 1) that only

records LIS-sourced IRD during a 200–300 yr period within HE4 (for the section studied in this work), which might argue for this first hypothesis (Hall et al., 2011). Another possible explanation for the peak of ^{XRF}Ca could also be related to calcite secondary precipitation under anoxic bottom conditions, as suggested by some authors in the atypical sedimentological facies of HEs (Auffret et al., 1996; Zaragosi et al., 2001).

An interesting feature during HE4, but also during the others GSs, is the high SSTs during summer (August), up to 4 °C more than modern values, contrasting with the percentages of NPS that then reach nearly 100 % (Fig. 6). This could suggest a strong stratification of the water masses but also emphasizes ecological strategy differences between planktonic foraminifera and dinoflagellates, the later living in the 50 upper meters of the water column while NPS can be mesopelagic (de Vernal et al., 2006; Jonkers et al., 2010b).

6.2.2 Heinrich event 3 (HE3)

HE3 is one of the most contentious HEs, especially from a stratigraphic point of view (e.g. Sanchez-Goni and Harrison, 2010), but also because of its atypical low IRD rate (e.g. Bond and Lotti, 1995; Grousset et al., 2001) and its strong European geochemical signature (Snoeckx et al., 1999; Grousset et al., 2000).

Our data reveal a low concentration of IRD during HE3 with two LLG peaks bracketing the event (Fig. 6), at its onset (32 ka BP) and at its termination (29 ka BP). These two low amplitude peaks correspond also to increases in the Rd/Md and $[\text{Ti} + \text{Fe}]/[\text{Ca} + \text{Sr}]$ ratios and to minima in the ^{XRF}Ca , thus reflecting advection of terrigenous material probably related to proximal ice-sheet dynamics. Abundances of NPS follow this bimodal pattern, with two periods marked by quasi-monospecific values. Conversely, dinocyst derived sea-surface conditions show no characteristic excursions at this time, but rather out of phase: sea-ice cover duration increases briefly before the first IRD pulse, and just after the last one, i.e. respectively within GI5 and 4.

A clear rise in the ^{XRF}Ca content is noted in the second part of HE3, coeval with two minor peaks in magnetic concentration. However, ^{XRF}Ca values remain under previous GI values. As already introduced for HE4, it is possible that such a rise characterises LIS preferentially detrital-sourced material advection. Bond et al. (1992) hypothesised warmer SSTs in the North Atlantic during HE3, leading to an accelerated melting of icebergs, which thus cannot fully reach the eastern basins of the North Atlantic. This longitudinal “barrier” was also mentioned by Hemming (2004). If so, the late arrival of this collapse from the North American ice sheets could have led to further destabilization of the European ice sheets (second peak recorded by proxies at the transition to GI4).

From the end of HE3, some changes are taking place. Sea-surface conditions seem to record higher amplitude changes between GIs and GSs, as shown for example in the

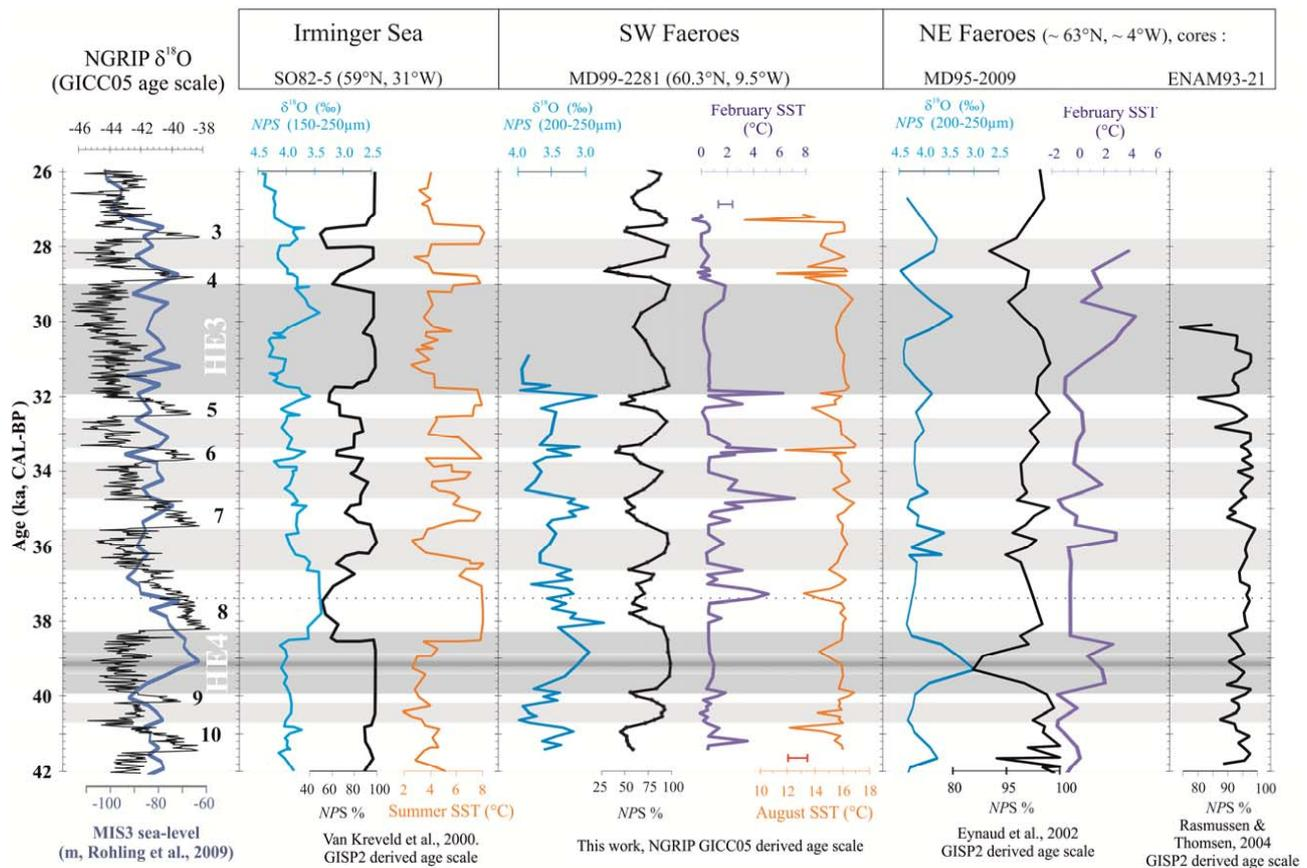


Fig. 7. Compilation of comparable MIS3 marine records from the subpolar North Atlantic (see Fig. 1 for the location of the cores), including core SO82-5 (Van Kreveland et al., 2000), core MD99-2281 (this work), core MD95-2009 (Eynaud et al., 2002) and core ENAM93-21 (Rasmussen and Thomsen, 2004). Proxies from the same nature are shown with the same colour. A reconstruction of the MIS3 sea-level (m) is also shown on the left (Rohling et al., 2009; Siddall et al., 2006). Grey bands: same legend as Fig. 6.

percentages of NPS or in the MS record. This is also attested by the reconstructed SSTs with extreme oscillations recorded in August and in the sea-ice duration as well.

7 Heterogeneity of the climatic response of the North Atlantic basin during MIS3

Our dataset constitutes one of the first multiproxy datasets detailing MIS3 sea-surface paleoenvironments south of the Norwegian Sea. Some detailed reconstructions of MIS3 exist further north or further south (e.g. Rasmussen et al., 1996a,b, 1997, 2002a,b; Rasmussen and Thomsen, 2004, 2008) but only a few have been using the same multiproxy approach. Figure 7 tentatively compiles high resolution MIS3 data comparable to the dataset generated for MD99-2281. Despite some differences in the chronology (compiled records other than MD99-2281 derive from the GISP2 chronology) and resolution, it illustrates hydrographical gradients, and thus zonal responses within the same subboreal latitudinal band.

MD99-2281 reconstructions could be compared to those previously produced by Eynaud et al. (2002), who used the same set of proxies in two marine cores retrieved from the southern Norwegian Sea (north of the Faeroe Islands – MD95-2009 and on the Voring plateau – MD95-2010, Fig. 1). Intriguingly, Eynaud et al. (2002) observed an antiphase between sea-surface paleoenvironments (sea ice cover duration, February SST) of the Norwegian Sea and the GIs/GSs atmospheric conditions registered above Greenland (e.g. Dansgaard et al., 1993). Their records demonstrated the establishment of low February SSTs accompanied by a longer sea-ice cover duration in the Norwegian Sea during GIs, whereas the Greenland ice-records testify warm interstadial atmospheric conditions (and vice-versa during GSs, see Fig. 7). According to Eynaud et al. (2002), this paradox pointed to a decoupling between the North Atlantic eastern and western parts during MIS3, involving past climatic phenomena comparable to the modern North Atlantic Oscillation (“Greenland above/Oslo below normal”, e.g. Bromwich et al., 1999).

Low concentrations of IRD were observed by these authors during HE4, in sharp contrast with what was observed in the temperate North Atlantic (e.g. Cortijo et al., 1997; Hemming, 2004). It further suggests isolation of the Norwegian Sea in terms of response to the climatic variability.

Similar results were obtained by de Vernal et al. (2000, 2001, 2005, 2006) for the Nordic Seas with positive SST anomalies (SST above the modern ones) detected during the Last Glacial Maximum. The reconstructed August SSTs on core MD99-2281 during MIS3 show comparable positive anomalies (up to 4 °C) dominating the whole studied period (Fig. 5). These observations could be due to peculiar oceanic conditions developing during MIS3 and strongly related to the dynamics of the proximal ice-sheets. A strong stratification of the water column could have been favoured by partial melting of the ice sheets and thus advection of fresh waters, preferentially during summers. The existence of a strong stratification could justify a rapid warming of “a brackish superficial water lens” generating such an anomaly.

The anomalous August SSTs testified a “Norwegian Sea type response” for the summer months (see Eynaud et al., 2002). Late increases of February SST during each GIs furthermore underline some kind of inertia in the sea-surface response of the southern Faeroe domain, thus arguing for a potential influence of the Norwegian sector. However, the high concentrations of IRD observed in core MD99-2281 during HE4 (Fig. 6) suggest that our site also responds synchronously to the temperate North Atlantic, and is thus outside the paradoxical “Nordic Seas” type response.

GI6, 5 and 4 are also paradoxically marked by a higher sea-ice cover duration roughly in antiphase with the percentages of NPS. The same anomaly is observed in the northern core MD95-2010 where interstadial phases over Greenland correspond to a longer sea-ice cover development (Eynaud et al., 2002). We can suggest that from GI6 to GI3, the conditions are so drastic, with proximal European ice sheets reaching their critical maximum size that “our region adopts the same behaviour as the Nordic seas do”. The IRD signal recorded in core MD99-2281 during these last GIs could thus correspond to the one also recorded in core MD95-2010 and could therefore be related to the destabilization of the FIS. It is also worth noting that the ice cover in core MD95-2010 varies between 5 and 8 months/year for the GIs, while our core does not record an ice cover exceeding 2 months/year during the whole MIS3. It is conceivable however that from GI6, a change in the local sea-surface conditions may have been initiated due to the gradual development of the proximal ice-sheets.

8 The role of European ice sheets on proximal sea-surface paleoenvironments during MIS3

8.1 Ice-sheet dynamics: the MIS3 marine record

In the Faeroe Island area, arrivals of detrital material (IRD) to the ocean were interpreted as proximal European ice sheets sourced: their record throughout MIS3 is continuous and highly sensitive to millennial climatic variability as shown by our data and also by previous studies in the same sector (e.g. Scourse et al., 2009; Hibbert et al., 2010; Chiverell and Thomas, 2010; Hall et al., 2011). Continental data from the proximal British Isles have shown “ice-free” conditions during MIS3, as well as in central Scotland, Northern Ireland and the Isle of Man. The BIIS extension was then reduced in latitude at that time and mainly located in the north of Scotland, probably with an advance northward and northwestward (Scourse et al., 2009; Chiverell and Thomas, 2010). This configuration could have promoted the development of an ice shelf, feeding a quite constant icebergs calving and contributing to the observed IRD input record in the area. It is not possible from our data to pinpoint the exact source of IRD; however, the large size of the FIS compared to the British one suggests a preferential Fennoscandian source for IRD. Nevertheless, Hall et al. (2011) pointed to a major BIIS contribution in IRD fluxes recorded in core MD04-2829CQ. This latter being located only 100 km (nearly one degree in latitude) southward of core MD99-2281 (Figs. 1 and 8), and furthermore responding in the same way during GSs, i.e. recording higher IRD concentrations, it is thus likely that BIIS derived products may also have reached the site of core MD99-2281.

8.2 The MIS3/MIS2 transition

The MIS3 termination and the beginning of MIS2 are worth discussion considering our results. Indeed, changes are taking place at the transition between HE3 and GI4 at 28.9 cal ka BP where alternating GIs/GSs sea-surface conditions seem to be more extreme, with marked shifts in SSTs (August especially) and in the sea-ice cover duration. Generally, the MIS3 to MIS2 transition marks conditions that seem progressively more severe in the area, also registering higher instability. Even if only observed in the last 2000 yr of the sequence, it is clearly expressed throughout all our proxies and could be due to growing European ice sheets, with maybe the development of ice shelves on the continental shelf. In fact, the maximum ice volume, which marks the Last Glacial Maximum between 19 and 23 cal ka BP (sensu Mix et al., 2001), does not necessarily correspond to the maximum geographical extension of each ice sheet, which also evolved independently (e.g. Chiverell and Thomas, 2010). Indeed, some previous studies have suggested that the BIS advanced between 30 and 25 cal ka BP. Hibbert et al. (2010) show that the core MD04-2822 (Fig. 8), located

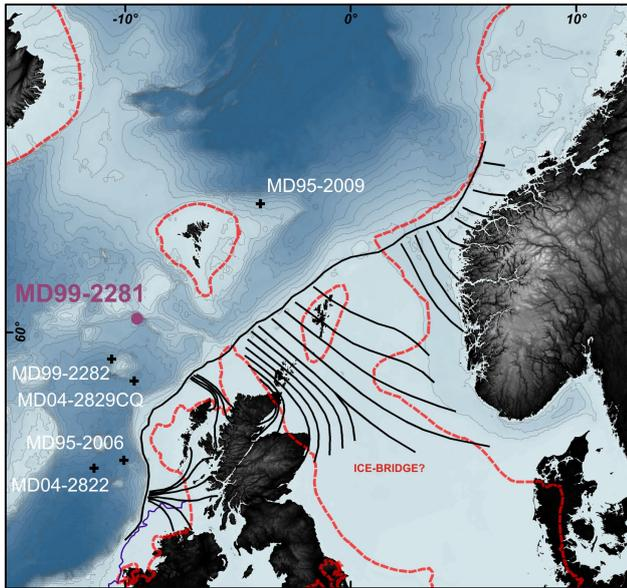


Fig. 8. BIIS-FIS ice sheets and their associated paleo-ice-stream main directions (black solid line, Bradwell et al., 2008). The full glacial extension of the North Hemispheric ice sheets is schematized by the red dotted-line (Grosswald and Hughes, 2002); Ehlers and Gibbard, 2004). Palaeo-coastline at 21 ka BP in blue (Bourillet et al., 2003). The studied core (MD99-2281: this work) and other cores discussed in the paper (MD95-2009; Eynaud et al., 2002; MD04-2822; MD95-2006; Knutz et al., 2001; Hibbert et al., 2010; MD04-2829CQ; Hall et al., 2011) are also located.

west of the Barra-Donegal Fan, has recorded an increase in IRD at 27.4 cal ka BP. The same is observed by Hall et al. (2011) in core MD04-2829CQ, located southeast of the Rosemary Bank, pointing to an increase of the BIIS size after ~ 28 ka BP. Similarly, Knutz et al. (2001) observed in core MD95-2006 (Fig. 8), located in the heart of Barra-Donegal Fan, increases of IRD concentrations (coming from the Tertiary basaltic provinces involving a British source) at about 30 ka, which coincide with the MIS3/MIS2 transition (Hibbert et al., 2010). Scourse et al. (2009) also illustrate an advance in the west of the British ice sheet (BIS) at the Bench level and Rosemary Barra-Donegal Fan just after HE3, at about 29 ka. IRD concentration increases at 27 ka on the Irish western margin and at 25 ka on the Goban Spur, characterising a progressive southward ice-sheet development (Scourse et al., 2009). This progression also affected the northeastern British ice margin. Actually, geomorphological studies conducted in the North Sea Basin and Norwegian Channel (Bradwell et al., 2007, 2008) have suggested confluent British and Fennoscandian ice sheets during this period. This coalescence associated to a major paleo-ice-stream system purging the “ice-bridge” (Fig. 8, Bradwell et al., 2008) might have alimented one of the most important ice shelves of the European margin. Core MD99-2281, which is located in the axis of two of these ice streams (Fig. 8, Bradwell et al.,

2008), the Minch paleo-ice stream and the North Sea paleo-ice stream, may have thus recorded destabilizations of this system.

9 Conclusions

The present multiproxy study, conducted on the MIS3 section of core MD99-2281 located off SW Faeroes, provides a new and unique set of data, expanding our knowledge about the evolution of NW Europe oceanic palaeoenvironments during the last glacial. Our results demonstrate that the marine reservoir echoes directly to the rapid climate changes detected in the atmosphere (Greenland $\delta^{18}\text{O}$ records). Deep-sea parameters (deduced from magnetic properties) show the same general pattern as along the main path of the NADW in the subpolar North Atlantic (e.g. Kissel et al., 1999a). These parameters were therefore used to tie the surface multi-proxy records on the millennial climatic variability that characterises the MIS3. Results demonstrate that the surface oceanic response of the area was strongly influenced by the dynamics of the proximal ice sheets. Data identify a much more important calving of European ice sheets during GSs and milder conditions during GIs, with however late and terminal warmings (rather occurring at the transition towards GSs). Large amounts of detrital material (including IRD) are recovered for each GSs and are likely to have a European origin, and more precisely a BIS source. Sea-surface palaeoenvironmental conditions during HEs are quite similar to those recorded during other GSs, except for some indices of a probable larger Laurentide influence (both within HE4 and HE3).

Marked palaeoenvironmental changes seem to occur after 28.9 cal ka BP (post-HE3 record). This reinforces previous findings which hypothesise the existence of an ice bridge between the British and the Fennoscandian ice sheets, which would have potentially directly influenced our site of study after HE3. The coalescence of the FIS and BIS could have fed an ice shelf proximal to the site of core MD99-2281; the high variability of sea-surface palaeoenvironments detected in our data could support the presence of such a structure. This implies that the glacial advance of the British ice sheet toward its maximum extension was probably reached before the Last Glacial Maximum. Further studies are needed to better constrain this late history of the British ice sheet and its relation to the dynamics of its surrounding ice shelves.

Acknowledgements. The authors are grateful to IPEV, the captain and the crew of the *Marion-Dufresne* and the scientific team of the GINNA cruise (Labeyrie et al., 1999). We wish to thank Y. Balut for his assistance at sea. J. St Paul, O. Ther, M.-H. Castera and M. Georget provided invaluable technical assistance. We acknowledge financial support by the ARTEMIS ^{14}C Accelerator Mass Spectrometry French project. Part of the analyses conducted on MD99-2281 was supported by the French INSU (Institut

National des Sciences de l'Univers) program LEFE/EVE (Les enveloppes fluides et l'environnement/Evolution et variabilité du climat à l'échelle globale) "RISCC: Rôle des Ice-Shelves dans le Changement Climatique". The magnetic analyses at LSCE were made with the help of Camille Wandres from laboratory funds from the French Atomic Energy Commission and from the CNRS. This is an U.M.R./EPOC 5805 (Université Bordeaux I – C.N.R.S.) contribution.

Edited by: M. Siddall



The publication of this article is financed by CNRS-INSU.

References

- Alley, R. B., Clark, P. U., Keigwin, L. D., and Webb, R. S.: Making sense of millennial-scale climate change, in: Mechanisms of global climate change at millennial time scales, edited by: Clark, P. U., Webb, R. S., and Keigwin, L. D., *Geophys. Monogr.*, 385–394, 1999.
- Alvarez-Solas, J., Charbit, S., Ritz, C., Paillard, D., Ramstein, G., and Dumas, C.: Links between ocean temperature and iceberg discharge during Heinrich events, *Nat. Geosci.*, 3, 122–126, 2010.
- Auffret, G. A., Boelaert, A., Vergnaud-Grazzini, C., Müller, C., and Kerbrat, R.: Identification of Heinrich layers in core ks 01 north-eastern Atlantic (46° N, 17° W), implications for their origin, *Mar. Geol.*, 131, 5–20, 1996.
- Austin, W. E. N. and Hibbert, F. D.: Tracing time in the ocean: A brief review of chronological constraints (60–8 kyr) on north atlantic marine event-based stratigraphies, *Quaternary Sci. Rev.*, 36, 28–37, 2012.
- Ballini, M., Kissel, C., Colin, C., and Richter, T.: Deep-water mass source and dynamic associated with rapid climatic variations during the last glacial stage in the north Atlantic: a multi-proxy investigation of the detrital fraction of deep-sea sediments, *Geochim. Geophys. Geos.*, 7, Q02N01, doi:10.1029/2005GC001070, 2006.
- Bard, E.: Geochemical and geophysical implications of the radiocarbon calibration, *Geochim. Cosmochim. Acta*, 62, 2025–2038, 1998.
- Bard, E., Arnold, M., Hamelin, B., Tisnerat-Laborde, N., and Cabioch, G.: Radiocarbon calibration by means of mass spectrometric $^{230}\text{Th}/^{234}\text{U}$ and ^{14}C ages of corals. An updated data base including samples from Barbados, Mururoa and Tahiti, *Radiocarbon*, 40, 1085–1092, 1998.
- Berger, A.: Les causes astronomiques des grandes variations du climat au Quaternaire, *C. R. Palevol.*, 5, 21–26, 2006.
- Bett, B. J.: UK atlantic margin environmental survey: introduction and overview of bathyal benthic ecology, *Cont. Shelf Res.*, 21, 917–956, 2001.
- Bogus, K. A., Zonneveld, K. A. F., Fischer, D., Kasten, S., Bohrmann, G., and Versteegh, G. J. M.: The effect of meter-scale lateral oxygen gradients at the sediment-water interface on selected organic matter based alteration, productivity and temperature proxies, *Biogeosciences*, 9, 1553–1570, doi:10.5194/bg-9-1553-2012, 2012.
- Boldreel, L. O., Andersen, M. S., and Kuijpers, A.: Neogene seismic facies and deep-water gateways in the faeroe bank area, ne atlantic, *Mar. Geol.*, 152, 129–140, 1998.
- Bond, G. and Lotti, R.: Iceberg discharges into the north Atlantic on millennial time scales during the last glaciation, *Science*, 267, 1005–1010, 1995.
- Bond, G., Heinrich, H., Broecker, W., Labeyrie, L., McManus, J., Andrews, J., Huon, S., Jantschik, R., Clasen, S., Simet, C., Tedesco, C., Klas, M., Bonani, G., and Ivy, S.: Evidence for massive discharges of icebergs into the north Atlantic ocean during the last glacial period, *Nature*, 360, 246–249, 1992.
- Bond, G., Broecker, W., Johnsen, S., McManus, J., Labeyrie, L., Jouzel, J., and Bonani, G.: Correlations between climate records from North Atlantic sediments and Greenland ice, *Nature*, 365, 143–147, 1993.
- Boulay, S.: Variabilité climatique rapide en atlantique nord - un potentiel de réponses: La carotte MD99-2281 (sud des îles faeroes), MASTER Université Paris-Sud, Orsay, 2000.
- Bourillet, J.-F., Reynaud, J. Y., Baltzer, A., and Zaragosi, S.: The "fleuve manche": The sub-marine sedimentary features from the outer shelf to the deep-sea fans, *J. Quaternary Sci.*, 18, 261–282, 2003.
- Brachfeld, S., Kissel, C., Laj, C., and Mazaud, A.: Behavior of u-channels during acquisition and demagnetization of remanence: Implications for paleomagnetic and rock-magnetic measurements, *Phys. Earth Planet. Int.*, 145, 1–8, 2004.
- Bradwell, T., Stoker, M., and Larter, R.: Geomorphological signature and flow dynamics of the minch palaeo-ice stream, north-west Scotland, *J. Quaternary Sci.*, 22, 609–617, 2007.
- Bradwell, T., Stoker, M., Golledge, N. R., Wilson, C. K., Merritt, J. W., Long, D., Everest, J. D., Hestvik, O. B., Stevenson, A. G., Hubbard, A. L., Finlayson, A. G., and Mathers, H. E.: The northern sector of the last British ice sheet: Maximum extent and demise, *Earth-Sci. Rev.*, 88, 207–226, 2008.
- Broecker, W. S.: Thermohaline circulation, the Achilles heel of our climate system: Will man-made CO_2 upset the current balance?, *Science*, 278, 1582–1588, 1997.
- Broecker, W. S.: Does the trigger for abrupt climate change reside in the ocean or in the atmosphere?, *Science*, 300, 1519–1522, 2003.
- Bromwich, D. H., Chen, Q.-S., Li, Y., and Cullather, R. I.: Precipitation over Greenland and its relation to the north Atlantic oscillation, *J. Geophys. Res.*, 104, 22103–22115, 1999.
- Chiverrell, R. C. and Thomas, G. S. P.: Extent and timing of the last glacial maximum (LGM) in Britain and Ireland: A review, *J. Quaternary Sci.*, 25, 535–549, 2010.
- Clark, P. U., Pisias, N. G., Stocker, T. F., and Weaver, A. J.: The role of the thermohaline circulation in abrupt climate change, *Nature*, 415, 863–869, 2002.
- Cortijo, E., Labeyrie, L., Vidal, L., Vautravers, M., Chapman, M., Duplessy, J. C., Elliot, M., Arnold, M., Turon, J. L., and Auffret, G. A.: Changes in sea surface hydrology associated with Heinrich event 4 in the north Atlantic ocean between 40° and 60° N, *Earth Planet. Sc. Lett.*, 146, 29–45, 1997.

- Dansgaard, W., Johnsen, S. J., Clausen, H. B., Dahl-Jensen, D., Gundestrup, N. S., Hammer, C. U., Hvidberg, C. S., Steffensen, J. P., Sveinbjörnsdóttir, A. E., Jouzel, J., and Bond, G.: Evidence for general instability of past climate from 250-kyr ice-core record, *Nature*, 364, 218–220, 1993.
- De Leeuw, J. W., Versteegh, G. J. M., and Van Bergen, P. F.: Biomacromolecules of algae and plants and their fossil analogues, *Plant Ecol.*, 182, 209–233, 2006.
- de Vernal, A.: Dino8 workshop: Quantitative treatments for paleoceanographical reconstructions based on dinocyst assemblages, Dino8 conference, Montréal, 2008.
- de Vernal, A. and Marret, F.: Chapter nine : Organic-walled dinoflagellate cysts: tracers of sea-surface conditions, in: Developments in marine geology, edited by: Hillaire-Marcel, C. and de Vernal, A., Elsevier, 371–408, 2007.
- de Vernal, A. and Rochon, A.: Dinocysts as tracers of sea-surface conditions and sea-ice cover in polar and subpolar environments, IOP Conference Series: Earth and Environmental Science, 2011.
- de Vernal, A., Henry, M., and Bilodeau, G.: Techniques de préparation et d'analyse en micropaléontologie, *Les cahiers du GEOTOP*, 3, 1–29, 1996.
- de Vernal, A., Hillaire-Marcel, C., Turon, J. L., and Matthiessen, J.: Reconstruction of sea-surface temperature, salinity, and sea-ice cover in the northern north Atlantic during the last glacial maximum based on dinocyst assemblages, *Can. J. Earth Sci.*, 37, 725–750, 2000.
- de Vernal, A., Henry, M., Matthiessen, J., Mudie, P. J., Rochon, A., Boessenkool, K. P., Eynaud, F., Gräsfjeld, K., Guiot, J., Hamel, D., Harland, R., Head, M. J., Kunz-Pirrung, M., Levac, E., Loucheur, V., Peyron, O., Pospelova, V., Radi, T., Turon, J. L., and Voronina, E.: Dinoflagellate cyst assemblages in surface sediments of the Laptev sea region (Arctic Ocean) and their relationship to hydrographic conditions, *J. Quaternary Sci.*, 16, 637–649, 2001.
- de Vernal, A., Eynaud, F., Henry, M., Hillaire-Marcel, C., Londeix, L., Mangin, S., Matthiessen, J., Marret, F., Radi, T., Rochon, A., Solignac, S., and Turon, J. L.: Reconstruction of sea-surface conditions at middle to high latitudes of the northern hemisphere during the last glacial maximum (LGM) based on dinoflagellate cyst assemblages, *Quaternary Sci. Rev.*, 24, 897–924, 2005.
- de Vernal, A., Rosell-Melé, A., Kucera, M., Hillaire-Marcel, C., Eynaud, F., Weinelt, M., Dokken, T., and Kageyama, M.: Comparing proxies for the reconstruction of LGM sea-surface conditions in the northern north Atlantic, *Quaternary Sci. Rev.*, 25, 2820–2834, 2006.
- Dickson, R. R., Meincke, J., Malmberg, S.-A., and Lee, A. J.: The “Great salinity anomaly” in the northern north Atlantic 1968–1982, *Prog. Oceanogr.*, 20, 103–151, 1988.
- Ehlers, J. and Gibbard, P.: Quaternary glaciations - extent and chronology part I: Europe, in: Developments in quaternary science, no. 2, Publisher Elsevier, Amsterdam, p. 488, 2004.
- Elliot, M., Labeyrie, L., Dokken, T., and Manthe, S.: Coherent patterns of ice-rafted debris deposits in the Nordic regions during the last glacial (10–60 ka), *Earth Planet. Sc. Lett.*, 194, 151–163, 2001.
- Ericson, D. B.: Coiling direction of *Globigerina pachyderma* as a climatic index, *Science*, 130, 219–220, 1959.
- Evitt, W. R.: Sporopollenin dinoflagellate cysts: their morphology and interpretation, AASP Foundation – American Association of Stratigraphic Palynologists, Dallas, 1985.
- Eynaud, F.: Kystes de dinoflagellés et evolution paléoclimatique et paléohydrologique de l'atlantique nord au cours du dernier cycle climatique du quaternaire, Université de Bordeaux I, 291 pp., 1999.
- Eynaud, F., Turon, J. L., Matthiessen, J., Kissel, C., Peypouquet, J. P., De Vernal, A., and Henry, M.: Norwegian sea-surface palaeoenvironments of marine oxygen-isotope state 3: the paradoxical response of dinoflagellate cysts, *J. Quaternary Sci.*, 17, 349–359, 2002.
- Eynaud, F., Zaragosi, S., Scourse, J. D., Mojtahid, M., Bourillet, J. F., Hall, I. R., Penaud, A., Locascio, M., and Reijonen, A.: Deglacial laminated facies on the NW European continental margin: The hydrographic significance of British-Irish Ice Sheet deglaciation and Fleuve Manche paleoriver discharges, *Geochem. Geophys. Geosy.*, 8, Q06019, doi:10.1029/2006GC001496, 2007.
- Eynaud, F., De Abreu, L., Voelker, A., Schönfeld, J., Salgueiro, E., Turon, J. L., Penaud, A., Toucanne, S., Naughton, F., Sanchez Goni, M. F., Malaizé, B., and Cacho, I.: Position of the polar front along the western Iberian margin during key cold episodes of the last 45 ka, *Geochem. Geophys. Geosy.*, 10, Q07U05, doi:10.1029/2009GC002398, 2009.
- Eynaud, F., Malaizé, B., Zaragosi, S., de Vernal, A., Scourse, J., Pujol, C., Cortijo, E., Grousset, F. E., Penaud, A., Toucanne, S., Turon, J. L., and Auffret, G.: New constraints on European glacial freshwater releases to the North Atlantic Ocean, *Geophys. Res. Lett.*, 39, L15601, doi:10.1029/2012GL052100, 2012.
- Fogelqvist, E., Blindheim, J., Tanhua, T., Østerhus, S., Buch, E., and Rey, F.: Greenland-Scotland overflow studied by hydro-chemical multivariate analysis, *Deep-Sea Res. Pt. I*, 50, 73–102, 2003.
- Grosswald, M. G. and Hughes, T. J.: The russian component of an arctic ice sheet during the last glacial maximum, *Quaternary Sci. Rev.*, 21, 121–146, 2002.
- Grousset, F., Pujol, C., Labeyrie, L., Auffret, G. A., and Boelaert, A.: Were the North Atlantic Heinrich events triggered by the behavior of the European ice sheet?, *Geology*, 28, 123–126, 2000.
- Grousset, F. E., Cortijo, E., Huon, S., Hervé, L., Richter, T., Burdloff, D., Duprat, J., and Weber, O.: Zooming in on Heinrich layers, *Paleoceanography*, 16, 240–259, 2001.
- Grützner, J. and Higgins, S. M.: Threshold behavior of millennial scale variability in deep water hydrography inferred from a 1.1 Ma long record of sediment provenance at the southern Gardar Drift, *Paleoceanography*, 25, PA4204, doi:10.1029/2009PA001873, 2010.
- Guiot, J. and de Vernal, A.: Chapter thirteen transfer functions: Methods for quantitative paleoceanography based on microfossils, in: Developments in marine geology, edited by: Hillaire-Marcel, C. and de Vernal, A., Elsevier, Amsterdam, 523–563, 2007.
- Guiot, J. and de Vernal, A.: Is spatial autocorrelation introducing biases in the apparent accuracy of paleoclimatic reconstructions?, *Quaternary Sci. Rev.*, 30, 1965–1972, 2011a.
- Guiot, J. and de Vernal, A.: QSR correspondence “Is spatial autocorrelation introducing biases in the apparent accuracy of paleoclimatic reconstructions?” Reply to Telford and Birks, *Quaternary Sci. Rev.*, 30, 3214–3216, 2011b.

- Hall, I. R., E. Colmenero-Hidalgo, R. Zahn, V. L. Peck, and S. R. Hemming: Centennial- to millennial-scale ice-ocean interactions in the subpolar northeast Atlantic 18–41 kyr ago, *Paleoceanography*, 26, PA2224, doi:10.1029/2010PA002084, 2011.
- Harland, R.: Distribution maps of recent dinoflagellate cysts in bottom sediments from the north Atlantic Ocean and adjacent seas, *Palaeontology*, 26, 321–387, 1983.
- Heinrich, H.: Origin and consequences of cyclic ice rafting in the northeast Atlantic Ocean during the past 130,000 years, *Quaternary Res.*, 29, 142–152, 1988.
- Hemming, S. R.: Heinrich events: massive late Pleistocene detritus layers of the north Atlantic and their global climate imprint, *Rev. Geophys.*, 42, 1001–1043, 2004.
- Hibbert, F. D., Austin, W. E. N., Leng, M. J., and Gatliff, R. W.: British ice sheet dynamics inferred from north Atlantic ice-rafted debris records spanning the last 175 000 years, *J. Quaternary Sci.*, 25, 461–482, 2010.
- Hodell, D. A., Channell, J. E. T., Curtis, J. H., Romero, O. E., and Röhl, U.: Onset of “Hudson Strait” Heinrich events in the eastern North Atlantic at the end of the middle Pleistocene transition (~640 ka)?, *Paleoceanography*, 23, PA4218, doi:10.1029/2008PA001591, 2008.
- Holliday, N. P., Pollard, R. T., Read, J. F., and Leach, H.: Water mass properties and fluxes in the Rockall trough, 1975–1998, *Deep-Sea Res. Pt. I*, 47, 1303–1332, 2000.
- Howe, J. A., Stoker, M. S., Masson, D. G., Pudsey, C. J., Morris, P., Larter, R. D., and Bulat, J.: Seabed morphology and the bottom-current pathways around rosemary bank seamount, northern Rockall trough, north Atlantic, *Mar. Petrol. Geol.*, 23, 165–181, 2006.
- Hulbe, C. L., MacAyeal, D. R., Denton, G. H., Kleman, J., and Lowell, T. V.: Catastrophic ice shelf breakup as the source of Heinrich event icebergs, *Paleoceanography*, 19, 711–717, 2004.
- Imbrie, J., Berger, A., Boyle, E. A., Clemens, S. C., Duffy, A., Howard, W. R., Kukla, G., Kutzbach, J., Martinson, D. G., McIntyre, A., Mix, A. C., Molfino, B., Morley, J. J., Peterson, L. C., Pisias, N. G., Prell, W. L., Raymo, M. E., Shackleton, N. J., and Toggweiler, J. R.: On the structure and origin of major glaciation cycles: 2. The 100,000 year cycle, *Paleoceanography*, 8, 699–735, 1993.
- Jonkers, L., Moros, M., Prins, M. A., Dokken, T., Andersson Dahl, C., Dijkstra, N., Perner, K., and Brummer, G.-J. A.: A reconstruction of sea surface warming in the northern north Atlantic during MIS3 ice-rafting events, *Quaternary Sci. Rev.*, 29, 1791–1800, 2010a.
- Jonkers, L., Brummer, G. J. A., and De Jong, M. F.: Seasonal stratification, shell flux, and oxygen isotope dynamics of left coiling *N. pachyderma* and *T. quinqueloba* in the western subpolar north Atlantic, *Paleoceanography*, 25, PA2204, doi:10.1029/2009PA001849, 2010b.
- Kiefer, T., Lorenz, S., Schulz, M., Lohmann, G., Sarnthein, M., and Elderfield, H.: Response of precipitation over Greenland and the adjacent ocean to the north Pacific warm spells during Dansgaard-Oeschger stadials, *Terra Nova*, 14, 295–300, 2002.
- Kissel, C., Laj, C., Labeyrie, L., Dokken, T., Voelker, A., and Blamart, D.: Rapid climatic variations during marine isotopic stage 3: Magnetic analysis of sediments from Nordic seas and north Atlantic, *Earth Planet. Sc. Lett.*, 171, 489–502, 1999a.
- Kissel, C., Laj, C., Labeyrie, L., Dokken, T., Voelker, A., and Blamart, D.: Magnetic signature of rapid climatic variations in North Atlantic sediments, in: *Reconstructing Ocean History: A Window Into the Future*, edited by: Abrantes, F. and Mix, A., Springer, New York, 419–437, 1999b.
- Knutz, P. C., Austin, W. E. N., and Jones, E. J. W.: Millennial-scale depositional cycles related to British ice sheet variability and north Atlantic paleocirculation since 45 kyr B.P., *Barra fan, U.K. Margin, Paleoceanography*, 16, 53–64, 2001.
- Kucera, M.: Chapter six: planktonic foraminifera as tracers of past oceanic environments, in: *Developments in Marine Geology*, Elsevier, Amsterdam, 213–262, 2007.
- Kucera, M., Rosell-Melé, A., Schneider, R., Waelbroeck, C., and Weinelt, M.: Multiproxy approach for the reconstruction of the glacial ocean surface (MARGO), *Quaternary Sci. Rev.*, 24, 813–819, 2005.
- Kuijpers, A., Andersen, M. S., Kenyon, N. H., Kunzendorf, H., and van Weering, T. C. E.: Quaternary sedimentation and Norwegian sea overflow pathways around bill bailey bank, northeastern Atlantic, *Mar. Geol.*, 152, 101–127, 1998.
- Kuijpers, A., Hansen, B., Huhnerbach, V., Larsen, B., Nielsen, T., and Werner, F.: Norwegian sea overflow through the Faeroe-Shetland gateway as documented by its bedforms, *Mar. Geol.*, 188, 147–164, 2002.
- Labeyrie, L., Cortijo, E., and Jansen, E.: Rapport scientifique de la mission INTERPOLE MD99-114/812 IMAGES V, Brest, 1999.
- Laj, C., Kissel, C., Mazaud, A., Channell, J. E. T., and Beer, J.: North Atlantic Paleointensity Stack since 75 ka (NAPIS-75) and the duration of the Laschamp event, *Philos. T. Roy. Soc. Lond.*, 358, 1009–1025, 2000.
- Lang, C., Leuenberger, M., Schwander, J., and Johnsen, S.: 16 °C rapid temperature variation in central Greenland 70,000 years ago, *Science*, 1286, 934–937, 1999.
- Larsen, K. M. H., Hansen, B., and Svendsen, H.: Faeroe shelf water, *Cont. Shelf Res.*, 28, 1754–1768, 2008.
- Larsen, K. M. H., Hansen, B., and Svendsen, H.: The Faeroe shelf front: Properties and exchange, *J. Mar. Syst.*, 78, 9–17, 2009.
- Lericolais, G., Auffret, J.-P., and Bourillet, J.-F.: The Quaternary Channel River: seismic stratigraphy of its palaeo-valleys and deeps, *J. Quaternary Sci.*, 18, 245–260, 2003.
- Marret, F. and Zonneveld, K. A. F.: Atlas of modern organic-walled dinoflagellate cyst distribution, *Rev. Palaeobot. Palynol.*, 125, 1–200, 2003.
- Martinson, D. G., Pisias, N. G., Hays, J. D., Imbrie, J., Moore Jr., T. C., and Shackleton, N. J.: Age dating and the orbital theory of the ice ages: Development of a high-resolution 0 to 300,000-year chronostratigraphy, *Quaternary Res.*, 27, 1–29, 1987.
- Masson, D. G., Howe, J. A., and Stoker, M. S.: Bottom-current sediment waves, sediment drifts and contourites in the northern Rockall trough, *Mar. Geol.*, 192, 215–237, 2002.
- Matthiessen, J., Kunz-Pirrung, M., and Mudie, P. J.: Freshwater chlorophycean algae in recent marine sediments of the Beaufort, Laptev and Kara seas (Arctic ocean) as indicators of river runoff, *Int. J. Earth Sci.*, 89, 470–485, 2000.
- Ménot, G., Bard, E., Rostek, F., Weijers, J. W. H., Hopmans, E. C., Schouten, S., and Sinninghe-Damsté, J. S.: Early reactivation of European rivers during the last deglaciation, *Science*, 313, 1623–1625, 2006.

- Mertens, K. N., Verhoeven, K., Verleye, T., Louwye, S., Amorim, A., Ribeiro, S., Deaf, A. S., Harding, I., De Schepper, S., Kodrans-Nsiah, M., de Vernal, A., Radi, T., Dybkjaer, K., Poulsen, N. E., Feist-burkhardt, S., Chitolie, J., González Arango, C., Heilmann-Clausen, C., Londeix, L., Turon, J.-L., Marret, F., Matthiessen, J., McCarthy, F. M. G., Prasad, V., Pospelova, V., Kyffin Hughes, J. E., Riding, J. B., Rochon, A., Sangiorgi, F., Welters, N., Sinclair, N., Thun, C., Soliman, A., Van Nieuwenhove, N., Vink, A., and Young, M.: Determining the absolute abundance of dinoflagellate cysts in recent marine sediments: The *Lycopodium* marker-grain method put to the test, *Rev. Palaeobot. Palynol.*, 157, 238–252, 2009.
- Mix, A. E., Bard, E., and Schneider, R.: Environmental processes of the ice age: Land, ocean, glacier (EPILOG), *Quaternary Sci. Rev.*, 20, 627–657, 2001.
- Mojtahid, M., Eynaud, F., Zaragosi, S., Scourse, J., Bourillet, J. F., and Garlan, T.: Palaeoclimatology and palaeohydrography of the glacial stages on Celtic and Armorican margins over the last 360 000 yrs, *Mar. Geol.*, 224, 57–82, 2005.
- New, A. L. and Smythe-Wright, D.: Aspects of the circulation in the Rockall trough, *Cont. Shelf Res.*, 21, 777–810, 2001.
- Penaud, A.: Interactions climatiques et hydrologiques du système Méditerranée/Atlantique au Quaternaire, PhD thesis, Bordeaux, 2009.
- Penaud, A., Eynaud, F., Turon, J. L., Zaragosi, S., Malaizé, B., Toucanne, S., and Bourillet, J. F.: What forced the collapse of European ice sheets during the last two glacial periods (150 ka B.P. and 18 ka cal B.P.)? Palynological evidence, *Palaeogeogr. Palaeoclimatol.*, 281, 66–78, 2009.
- Platov, G. A.: Numerical modeling of the arctic ocean deepwater formation: Part II. Results of regional and global experiments, *Izvestiya, Atmos. Ocean. Phys.*, 47, 377–392, 2011.
- Rahmstorf, S.: Ocean circulation and climate during the past 120,000 years, *Nature*, 419, 207–214, 2002.
- Rasmussen, S. O., Seierstad, I. K., Andersen, K. K., Bigler, M., Dahl-Jansen, D., and Johnsen, S. J.: Synchronization of the NGRIP, GRIP, and GISP2 ice cores across MIS 2 and palaeoclimatic implications, *Quaternary Sci. Rev.*, 27, 18–28, 2008.
- Rasmussen, T. L. and Thomsen, E.: The role of the north Atlantic drift in the millennial timescale glacial climate fluctuations, *Palaeogeogr. Palaeoclimatol.*, 210, 101–116, 2004.
- Rasmussen, T. L. and Thomsen, E.: Warm Atlantic water inflow to the Nordic seas 34–10 ka calibrated ka BP, *Paleoceanography*, 23, PA1201, doi:10.1029/2007PA001453, 2008.
- Rasmussen, T. L., Vanweering, T. C. E., and Labeyrie, L.: High resolution stratigraphy of the Faeroe-Shetland channel and its relation to north Atlantic paleoceanography: The last 87 kyr, *Mar. Geol.*, 131, 75–88, 1996a.
- Rasmussen, T. L., Thomsen, E., Vanweering, T. C. E., and Labeyrie, L.: Rapid changes in surface and deep water conditions at the Faeroe margin during the last 58,000 years, *Paleoceanography*, 11, 757–771, 1996b.
- Rasmussen, T. L., Van weering, T. C. E., and Labeyrie, L.: Climatic instability, ice sheets and ocean dynamics at high northern latitudes during the last glacial period (58–10 ka BP), *Quaternary Sci. Rev.*, 16, 71–80, 1997.
- Rasmussen, T. L., Thomsen, E., Troelstra, S. R., Kuijpers, A., and Prins, M. A.: Millennial-scale glacial variability versus Holocene stability: Changes in planktic and benthic foraminifera faunas and ocean circulation in the north Atlantic during the last 60000 years, *Mar. Micropaleontol.*, 47, 143–176, 2002a.
- Rasmussen, T. L., Bäckström, D., Heinemeier, J., Klitgaard-Kristensen, D., Knutz, P. C., Kuijpers, A., Lassen, S., Thomsen, E., Troelstra, S. R., and van Weering, T. C. E.: The faeroe-shetland gateway: Late quaternary water mass exchange between the nordic seas and the northeastern atlantic, *Mar. Geol.*, 188, 165–192, 2002b.
- Richter, T. O., Van Der Gaast, S., Koster, B., Vaars, A., Gieles, R., de Stigter, H. C., de Haas, H., and Van Weering, T. C. E.: The AVAATECH XRF core scanner: Technical description and applications to NE Atlantic sediments, in: *New techniques in sediment core analysis*, edited by: Rothwell, R. G., Geological Society Special Publications, London, 39–50, 2006.
- Roche, D. M., Wiersma, A. P., and Renssen, H.: A systematic study of the impact of freshwater pulses with respect to different geographical locations, *Clim. Dynam.*, 34, 997–1013, 2010.
- Rochon, A., de Vernal, A., Turon, J.-L., Matthiessen, J., and Head, M. J.: Recent dinoflagellate cysts of the north Atlantic ocean and adjacent seas in relation to sea-surface parameters, edited by: Ser, A. C., AASP – American Association of Stratigraphic Palynologists, Contrib. Ser., Dallas, 1–152, 1999a.
- Rochon, A., de Vernal, A., Turon, J.-L., Matthiessen, J., and Head, M. J.: Distribution of dinoflagellate cysts in surface sediments from the north Atlantic ocean and adjacent basins and quantitative reconstruction of sea-surface parameters, AASP special pub., p. 146, 1999b.
- Rochon, A., Eynaud, F., and de Vernal, A.: Dinocysts as tracers of hydrographical conditions and productivity along the ocean margins: Introduction, *Mar. Micropaleontol.*, 68, 1–5, 2008.
- Rohling, E. J., Grant, K., Bolshaw, M., Roberts, A. P., Siddall, M., Hemleben, C., and Kucera, M.: Antarctic temperature and global sea level closely coupled over the past five glacial cycles, *Nat. Geosci.*, 2, 7, 500–504, 2009.
- Ruddiman, W. F.: Late Quaternary deposition of ice-rafted sand in the subpolar North Atlantic (lat 40° to 65° N), *GSA Bulletin*, 88, 1813–1827, 1977.
- Sánchez Goñi, M. F. and Harrison, S. P.: Global patterns of vegetation response to millennial-scale variability and rapid climate change during the last glacial period, *Quaternary Sci. Rev.*, 29, 2957–2980, 2010.
- Sánchez-Goñi, M. F., Landais, A., Fletcher, W. J., Naughton, F., Desprat, S., and Duprat, J.: Contrasting impacts of dansgaard-oeschger events over a western european latitudinal transect modulated by orbital parameters, *Quaternary Sci. Rev.*, 27, 1136–1151, 2008.
- Schulz, M.: On the 1470-year pacing of Dansgaard-Oeschger warm events, *Paleoceanography*, 17, 1014, doi:10.1029/2000PA000571, 2002.
- Scourse, J. D., Hall, I. R., McCave, I. N., Young, J. R., and Sugdon, C.: The origin of Heinrich layers: Evidence from h2 for European precursor events, *Earth Planet. Sc. Lett.*, 182, 187–195, 2000.

- Scourse, J. D., Haapaniemi, A. L., Colmenero-Hidalgo, E., Peck, V. L., Hall, I. R., Austin, W. E. N., Knutz, P. C., and Zahn, R.: Growth, dynamics and deglaciation of the last British-Irish ice sheet: The deep-sea ice rafted detritus record, *Quaternary Sci. Rev.*, 28, 3066–3084, 2009.
- Severinghaus, J. P. and Brook, E. J.: Abrupt climate change at the end of the last glacial period inferred from trapped air in polar ice, *Science*, 286, 930–934, 1999.
- Siddall, M. et al.: Red Sea Sea Level Reconstruction, IGBP PAGES/World Data Center for Paleoclimatology Data Contribution Series # 2006-063, NOAA/NCDC Paleoclimatology Program, Boulder CO, USA, 2006.
- Snoeckx, H., Grousset, F. E., Revel, M., and Boelaert, A.: European contribution of ice-rafted sand to Heinrich layers H3 and H4, *Mar. Geol.*, 158, 197–208, 1999.
- Stoner, J. S., Channell, J. E. T., Hillaire-Marcel, C., and Kissel, C.: Geomagnetic paleointensity and environmental record from Labrador sea core MD95-2024: Global marine sediment and ice core chronostratigraphy for the last 110 kyr, *Earth Planet. Sc. Lett.*, 183, 161–177, 2000.
- Svensson, A., Andersen, K. K., Bigler, M., Clausen, H. B., Dahl-Jensen, D., Davies, S. M., Johnsen, S. J., Muscheler, R., Parrenin, F., Rasmussen, S. O., Röthlisberger, R., Seierstad, I., Steffensen, J. P., and Vinther, B. M.: A 60 000 year Greenland stratigraphic ice core chronology, *Clim. Past*, 4, 47–57, doi:10.5194/cp-4-47-2008, 2008.
- Toucanne, S., Zaragosi, S., Bourillet, J. F., Marieu, V., Cremer, M., Kageyama, M., Van Vliet-Lanoé, B., Eynaud, F., Turon, J. L., and Gibbard, P. L.: The first estimation of fleuve manche palaeoriver discharge during the last deglaciation: Evidence for Fennoscandian ice sheet meltwater flow in the English channel ca 20–18 ka ago, *Earth Planet. Sc. Lett.*, 290, 459–473, 2010.
- Van Kreveld, S., Sarnthein, M., Erlenkeuser, H., Grootes, P., Jung, S., Nadeau, M. J., Pflaumann, U., and Voelker, A.: Potential links between surging ice sheets, circulation changes, and the Dansgaard-Oeschger cycles in the Irmiger Sea, 60–80 kyr, *Paleoceanography*, 15, 425–442, 2000.
- Versteegh, G. J. M., Blokker, P. K. B., Harding, I., Lewis, J., Oltmanns, S., Rochon, A., and Zonneveld, K. A. F.: Infra red spectroscopy, flash pyrolysis, thermally assisted hydrolysis and methylation (THM) in the presence of tetramethylammonium hydroxide (TMAH) of cultured and sediment-derived *Lingulodinium polyedrum* (Dinoflagellata) cyst walls, *Org. Geochem.*, 43, 92–102, 2012.
- Voelker, A. H. L.: Global distribution of centennial-scale records for marine isotope stage (MIS) 3: a database, *Quaternary Sci. Rev.*, 21, 1185–1212, 2002.
- Wagner, G., Beer, J., Laj, C., Kissel, C., Mazarik, J., Muscheler, R., and Synal, H.-A.: Chlorine-36 evidence for the mono lake event in the summit grip ice core, *Earth Planet. Sc. Lett.*, 181, 1–6, 2000.
- WOA – World Ocean Atlas: general information available at: <http://www.nodc.noaa.gov/OC5/>, sampling tool: <http://www.geo.uni-bremen.de/geomod/staff/csn/woasample.html> (last access: 31 July 2012), 1998.
- Wolff, E. W., Chappellaz, J., Blunier, T., Rasmussen, S. O., and Svensson, A.: Millennial-scale variability during the last glacial: The ice core record, *Quaternary Sci. Rev.*, 29, 2828–2838, 2010.
- Zaragosi, S., Eynaud, F., Pujol, C., Auffret, G. A., Turon, J. L., and Garlan, T.: Initiation of the European deglaciation as recorded in the north-western Bay of Biscay slope environments (Meriadzek terrace and Trevelyan escarpment): A multi-proxy approach, *Earth Planet. Sc. Lett.*, 188, 493–507, 2001.
- Zonneveld, K. A. F., Bockelmann, F., and Holzwarth, U.: Selective preservation of organic-walled dinoflagellate cysts as a tool to quantify past net primary production and bottom water oxygen concentrations, *Mar. Geol.*, 237, 109–126, 2007.

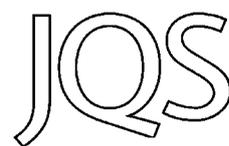
Annexe 2 : Caulle et al., 2013

“Sea-surface hydrographical conditions off South Faeroes and within the North-Eastern North Atlantic through MIS 2: The response of dinocysts”

Caulle C., Penaud A., Eynaud F., Zaragosi S., Roche D.M., Michel E., Boulay S. and Richter T.

(2013), *Journal of Quaternary Science* 28(3): 217-228.

Sea-surface hydrographical conditions off South Faeroes and within the North-Eastern North Atlantic through MIS 2: the response of dinocysts



CLÉMENCE CAULLE,^{1,2†} AURÉLIE PENAUD,¹ FRÉDÉRIQUE EYNAUD,^{2*} SÉBASTIEN ZARAGOSI,² DIDIER M. ROCHE,^{3,4} ELIZABETH MICHEL,³ SÉBASTIEN BOULAY³ and THOMAS RICHTER⁵

¹UMR 6538 Domaines Océaniques, IUEM-UBO, Plouzané, France

²UMR 5805, EPOC (Environnements et Paléoenvironnements Océaniques), Université de Bordeaux I, 33405 Talence, France

³UMR 8212, LSCE (Laboratoire des Sciences du Climat et de l'Environnement), CEA/CNRS-INSU/UVSQ, Gif s/sYvette, France

⁴Vrije Universiteit Amsterdam, Amsterdam, The Netherlands

⁵NIOZ Royal Netherlands Institute for Sea Research, AB Den Burg (Texel), The Netherlands

Received 25 May 2012; Revised 17 September 2012; Accepted 8 October 2012

ABSTRACT: The last glacial period, showing the progressive development of large boreal ice sheets, was punctuated by large climatic excursions. These excursions were triggered mainly by atmosphere–ocean–ice coupled dynamics and are thus exemplary case studies of natural climate variability. To characterize the sea-surface palaeohydrographical changes accompanying these oscillations along the European margin, we have integrated new palynological data (dinocysts) acquired on core MD99-2281 (60°N, Faeroe Margin) during Marine Isotope Stage 2 in a latitudinal transect including published cores MD95-2002 (47°N, Celtic Margin) and MD95-2010 (66°N, Vöring Plateau). This transect is superimposed on the modern North Atlantic Drift pathway, but also at the outskirts of glacial European ice sheets, thus ideally located to track sea-ice extent and ice-sheet instabilities through time. The results show a coherent and sensitive response of sea-surface environments to the complex chain of abrupt events that punctuated the end of the last glacial period. The Last Glacial Maximum was marked by large seasonal contrasts of temperatures, whereas Heinrich events (HE) were characterized by a sharp cooling and sea-ice development. A tripartite structure is identified within HE1, with indices of melting at 19k cal a BP, followed by a temperate phase synchronous of a relative stability of ice sheets, and a terminal phase (17.5–15k cal a BP) characteristic of the ‘conventional Laurentian’ HE1. Copyright © 2013 John Wiley & Sons, Ltd.

KEYWORDS: dinoflagellate cysts; European ice sheets; Faeroe Margin; Last Glacial Maximum; sea-surface parameters.

Introduction

Accurate characterization of climate dynamics requires understanding the earth system as a whole and especially the interaction between its main components. Among them, ice sheets and sea ice constitute key elements whose roles need to be better documented under different climatic boundary conditions. This is especially true given the recent catastrophic breakdowns of parts of ice shelves in Antarctica revealing: (1) the instability of sea-ice platforms in the context of the present-day climate change, and (2) their impact on the accelerated break-up of upstream glaciers (e.g. Rignot *et al.*, 2004; Domack *et al.*, 2005). Interfaced between the ocean, the atmosphere and glaciers (hereafter ice shelves, e.g. Alvarez-Solas *et al.*, 2010), sea ice is actually an important component of the polar climate systems. Recent studies (e.g. Li *et al.*, 2005, 2010) have demonstrated that the displacement of its edge could have been responsible for past ice-sheet rapid collapses, notably for Heinrich events (HEs).

HEs are clearly identified in North Atlantic sediments by layers rich in silicoclastic coarse particles, marking abrupt iceberg discharge events from the surrounding ice sheets during the last glacial (e.g. Heinrich, 1988). HEs are included in a cycle of recurrent global climate degradations (i.e. stadial conditions, Bond and Lotti, 1995; Elliot *et al.*, 2001; Sánchez Goñi and Harrison, 2010). Synchronously with HEs, the whole North Atlantic basin recorded large changes in hydrological conditions, resulting in temperature and salinity decreases in

sea-surface waters, with drastic consequences for the Atlantic Meridional Overturning Circulation (AMOC) and thus for global climate (e.g. Vidal *et al.*, 1997; Rahmstorf, 2002; McManus *et al.*, 2004; Roche *et al.*, 2010; Stanford *et al.*, 2011). The terminology used to describe HEs therefore often ambiguously confuses processes and impacts (reviewed by Sánchez Goñi and Harrison, 2010).

Here we explore the sensitivity of the sea-surface north-eastern North Atlantic (NNA) Ocean, documenting hydrographical changes and their phase relationships to the European ice-sheet dynamics at the southern Faeroe Margin. This area is presently located on the North Atlantic Drift (NAD) pathway and was under the direct influence of the proximal European ice sheets, i.e. the Fennoscandian ice sheet (FIS) and the British–Irish ice sheet (BIIS) during the last glacial period (Fig. 1). Previous studies have suggested that the area was affected by major sea-surface changes during the last glacial, and especially during Marine Isotope Stage (MIS) 3 (e.g. Rasmussen *et al.*, 1996a,b; Eynaud *et al.*, 2002; Rasmussen and Thomsen, 2008; Zumaque *et al.*, 2012). Here we focus on MIS2, including HE2 and 1, and the Last Glacial Maximum (LGM), a key snapshot of the late Quaternary (e.g. CLIMAP Project Members, 1981; Kutzbach and Wright, 1986; Sarnthein *et al.*, 2003; MARGO Project Members, 2009; Kageyama *et al.*, 2010).

Our work is based on the multiproxy investigation of core MD99-2281, recovered from the foot of the Faeroe Bank, and includes micropalaeontological [dinoflagellate cyst (dinocyst) assemblages and relative abundances of the polar planktonic foraminifera *Neogloboquadrina pachyderma* sinistral (*Nps*) form], sedimentological [lithic grain concentrations, X-ray fluorescence (XRF) scanning] and geochemical (stable isotopes of oxygen and carbon) analyses. Furthermore, we

*Correspondence: F. EYNAUD, as above.

E-mail: f.eynaud@epoc.u-bordeaux1.fr

† Present address: UMR 6112, BIAF (Bio-Indicateurs Actuels et Fossiles), Université d'Angers, 49045 Angers, France

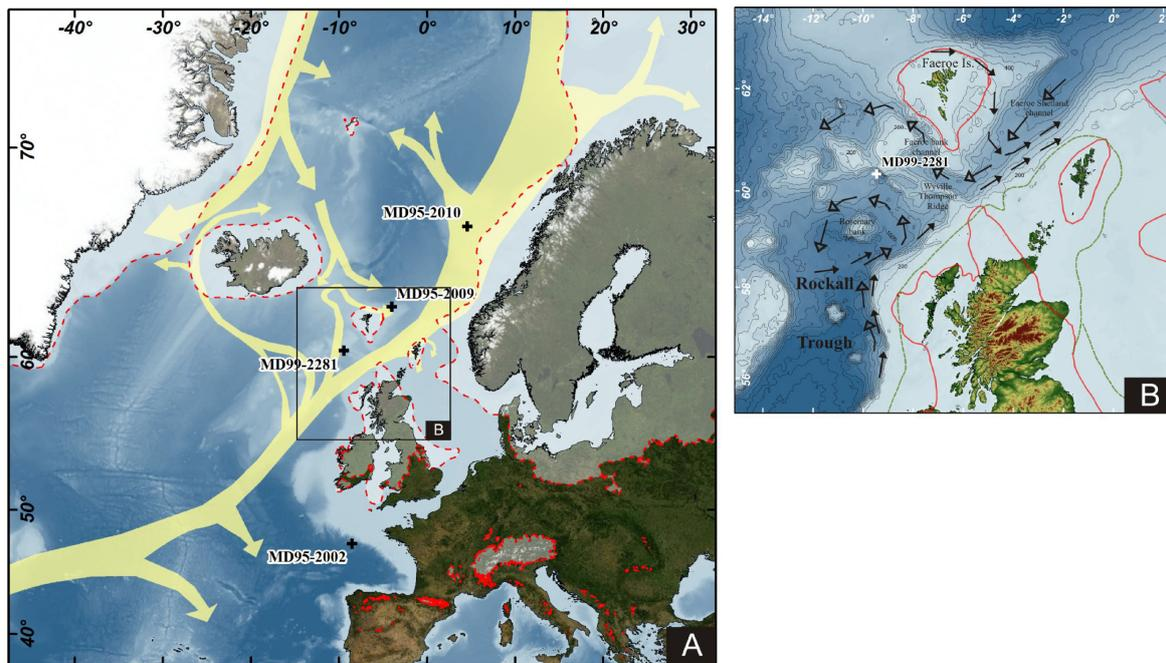


Figure 1. (A) Location of core MD99-2281 and of other cores discussed in this paper. Yellow arrows indicate modern oceanic surface circulation (after Fogelqvist *et al.*, 2003). The dashed line shows the limit of the full glacial extension of the northern hemispheric ice sheets during the LGM (after Grosswald and Hughes, 2002; Ehlers and Gibbard, 2004). (B) Detailed location of MD99-2281 in the Rockall Trough; schematic representation of the superficial oceanic circulation is indicated by black full arrows and the deep circulation by the black empty arrows (modified from Masson *et al.*, 2002). The dashed line locates the BIIS limits after modelling and compilation from Boulton and Hagdorn (2006) together with the full glacial extension (continuous unbroken line) of the northern hemispheric ice sheets based on field studies (after Grosswald and Hughes, 2002; Ehlers and Gibbard, 2004). This figure is available in colour online at wileyonlinelibrary.com.

derived sea-surface conditions from a transfer function applied to dinocyst assemblages, thus providing quantitative estimates of winter and summer sea-surface temperature (SST) and of sea-ice cover duration, a crucial parameter of the climatic system rarely quantified in palaeoceanographic studies.

Modern regional setting

The CALYPSO core MD99-2281 (60°21'N, 09°27'W; 1197 m water depth, 28.77 m length) was retrieved during the IMAGES V-GINNA cruise on the RV *Marion Dufresne* (Labeyrie *et al.*, 1999; Table 1). The coring site is located at the northern end of the Rockall Trough (Fig. 1), an area where the sedimentation is known to be controlled by geostrophic currents (especially contouritic processes, Boldreel *et al.*, 1998; Stoker *et al.*, 1998; Masson *et al.*, 2002). Core MD99-2281 has, however, been retrieved at a location where pelagic sediments were deposited in a deep-water environment unaffected by strong current activities (Boldreel *et al.*, 1998).

Watermasses in the Rockall Trough are mainly characterized by Eastern North Atlantic Waters (ENAW) in the upper thousand meters and by North Atlantic Deep Waters (NADW) at the bottom (e.g. Ellet *et al.*, 1986; Turrell *et al.*, 1999; Hansen and Østerhus, 2000). The upper part of the ENAW (first 500 m) flows across the Wyville–Thompson ridge and contributes to the NAD (Turrell *et al.*, 1999). The deep and cold NADW is mainly composed of Labrador Sea Waters with some contributions of Norwegian Sea Deep Waters, and of Antarctic Bottom Waters (e.g. Masson *et al.*, 2002). North of the Rockall Trough, the Wyville–Thompson ridge is 400–500 m in height and forms an important oceanographic barrier. Consequently, at the front of the Faeroe Islands, the NAD surface current splits into two branches flowing eastward and westward of the islands (Larsen *et al.*, 2008) and diverging then within two different channels (Faroe Bank Channel and Faroe Shetland Channel; Fig. 1). The eastern NAD branch flows northward along the British Isles (Hansen and Østerhus, 2000; Orvik and Niiler, 2002). The western NAD branch flows north-west of the

Table 1. Geographical references of the discussed cores.

Core	Latitude	Longitude	Water depth (m)	Core length (m)	CRUISE	References for MIS2
MD95-2002	47.45	−8.53	2174	29.99	MD 101 - IMAGES (International Marine Global Change Study) I	Eynaud, 1999; Zaragosi <i>et al.</i> , 2001; Eynaud <i>et al.</i> , 2007; Penaud <i>et al.</i> , 2009
MD95-2009	62.74	−4.00	1027	32.43	MD 101 - IMAGES (International Marine Global Change Study) I	Eynaud, 1999; de Vernal <i>et al.</i> , 2005
MD95-2010	66.68	4.57	1226	32.53	MD 101 - IMAGES (International Marine Global Change Study) I	Eynaud, 1999; de Vernal <i>et al.</i> , 2005; de Vernal <i>et al.</i> , 2006
MD99-2281	60.34	−9.46	1197	28.77	MD114 - IMAGES (International Marine Global Change Study) V	Labeyrie <i>et al.</i> , 1999; Boulay, 2000; This work

Table 2. Radiocarbon dates for the first 12 m of core MD99-2281 (see also Zumaque *et al.*, 2012).

Depth (cm) in core MD99-2281	Uncorrected AMS ^{14}C age (a BP)	Corrected calendar age (cal a BP)	Dated material/age control points/references
40	10 260 ± 100	11 165	<i>G. bulloides</i> , Boulay (2000), Zumaque <i>et al.</i> (2012)
170	12 970 ± 110	14 729*	<i>G. bulloides</i> , Boulay (2000), Zumaque <i>et al.</i> (2012)
270	10 800 ± 100	12 081	<i>G. bulloides</i> , Boulay (2000), Zumaque <i>et al.</i> (2012)
400	11 060 ± 110	12 400	<i>G. bulloides</i> , Boulay (2000), Zumaque <i>et al.</i> (2012)
510	15 290 ± 130	17 529	<i>N. pachyderma</i> s., Boulay (2000), Zumaque <i>et al.</i> (2012)
580	15 760 ± 170	18 092	<i>N. pachyderma</i> s., Boulay (2000), Zumaque <i>et al.</i> (2012)
650	16 040 ± 140	18 427	<i>N. pachyderma</i> s., Boulay (2000), Zumaque <i>et al.</i> (2012)
780	18 060 ± 160	20 830	<i>N. pachyderma</i> s., Boulay (2000), Zumaque <i>et al.</i> (2012)
1180	23 340 ± 240	26 993	<i>N. pachyderma</i> s., Boulay (2000), Zumaque <i>et al.</i> (2012)
1280	24 210 ± 140	27 992	<i>N. pachyderma</i> s., ARTEMIS- SacA 19117, Zumaque <i>et al.</i> (2012)

*Age reversals removed.

Faeroe Islands and is affected by cold and fresh waters derived from the East Icelandic Current.

Material and methods

Chronology

The age model of core MD99-2281 was published in Zumaque *et al.* (2012). It is constrained from 13 accelerator mass spectrometry (AMS) ^{14}C dates obtained on monospecific samples of planktonic foraminifera between 11 and 32k cal a BP (Table 2). In the older part of the record, 18 complementary tie-points have been obtained by comparing the magnetic susceptibility signal of core MD99-2281 with the $\delta^{18}\text{O}$ signal of the NGRIP ice core (GICC05 time scale; Svensson *et al.*, 2008). The final age model was then established by linear interpolation between ages and pointers (see Zumaque *et al.*, 2012, for further details). Core MD99-2281 exhibits a mean sedimentation rate of 80 cm ka^{-1} .

Palynological analyses

Qualitative analyses

Palynological preparation was conducted on core MD99-2281 between 300 and 1190 cm (90 slides, 12–27k cal a BP interval), following the standard palynological protocol of de Vernal *et al.* (1996) slightly modified at EPOC (see details on http://www.epoc.u-bordeaux.fr/index.php?lang=fr&page=eq_paleo_protocoles). Acetolysis was not employed in order to avoid destruction of heterotrophic species such as *Polykrikaceae* and *Brigantedinium* cysts as suggested by Marret (1993). Palynological remains were then analysed by focusing on Quaternary dinocyst assemblages at the species level. An average of 300 dinocysts per sample were identified and counted using an Olympus optical microscope at $\times 400$ magnification. Taxonomic identification conforms to Fensome *et al.* (1998), Rochon *et al.* (1999), de Vernal *et al.* (2001), Head *et al.* (2001) and Fensome and Williams (2004). Dinocyst assemblages are described with the abundances of each species relative to the total number of dinocysts including unidentified taxa (fewer than four specimens per sample) and excluding reworked (pre-Quaternary) specimens. Reworked taxa were easily identified due to their general aspect (thick coloured wall and relative large size compared with Quaternary dinocysts). They were counted, as well as coenobia of *Pediastrum* spp., separately on each slide. Palynomorph absolute concentrations were calculated using the marker-grain method (e.g. Stockmarr, 1971; Mertens *et al.*, 2009). Calculation of the counting

error was done thanks to the Stockmarr method (Stockmarr, 1971); it is plotted for each dinocyst discussed species. The ratio 'Reworked (pre-Quaternary) to Modern (Quaternary)' dinocysts (Rd/Md) was also calculated to trace allochthonous supplies to the open ocean by continental erosion and fluvial transport (e.g. Zaragosi *et al.*, 2001; Lézine *et al.*, 2005; Eynaud *et al.*, 2007; Penaud *et al.*, 2009).

Quantitative analyses

Past sea-surface parameters were estimated using the Modern Analogue Technique (MAT) applied to dinocyst assemblages (cf. Guiot and de Vernal, 2007, 2011a,b). Statistical treatments were performed under the 'R' software (R version 2.7.0; R Development Core Team, 2008) using a script developed by Guiot and Brewer (www.cerege.fr/IMG/pdf/formationR08.pdf). Modern dinocyst assemblages are compiled in a geo-referenced database of marine surface sediment samples including 1189 modern samples from the North Atlantic, Arctic and sub-Arctic basins, the Mediterranean Sea and the North Pacific (Radi *et al.*, 2009; cf. <http://www.geotop.ca/>). MAT uses the statistical distance between fossil (palaeoceanographic record) and current (modern database) assemblages. Calculations of sea-surface parameters rely on a weighted average of the hydrographical values associated with the five closest analogues (i.e. dissimilarity minimum). The reader is referred to Guiot and de Vernal (2007, 2011a,b) for a review of the theory of transfer functions, and to de Vernal *et al.* (2001, 2005) for a step-by-step description of the application of MAT to dinocysts, including discussion about the degree of accuracy. Regarding the parameters presented here, root mean square errors of prediction are $\pm 1.05^\circ\text{C}$ for winter SST, $\pm 1.5^\circ\text{C}$ for summer SST and ± 1.1 months per year for sea-ice cover duration.

Complementary tools

1. Relative abundances (%) of *Nps* were calculated versus the total planktonic foraminiferal fauna on the $> 150\text{-}\mu\text{m}$ fraction of core MD99-2281 (Boulay, 2000). Abundances of *Nps* were used to trace southward excursions of polar waters during glacial episodes (e.g. Ericson, 1959; Eynaud *et al.*, 2009).
2. Coarse lithic grain (CLG) concentrations [no. of grains (g dry sediment) $^{-1}$] from core MD99-2281 were calculated on the $> 150\text{-}\mu\text{m}$ sediment fraction (Boulay, 2000). CLGs document ice-sheet collapses throughout time and are mainly composed of quartz and volcanic elements (particles of glass and basalt), that constitute common components of the surrounding continents.

- Stable isotope measurements ($\delta^{13}\text{C}$, $\delta^{18}\text{O}$) were done on monospecific samples of *Nps*. Six specimens (i.e. $\sim 80\ \mu\text{g}$ mean weight aliquots) were picked out from the 200- to 250- μm fraction and analysed at the LSCE laboratory using a Finnigan MAT 251 mass spectrometer coupled to an automated carbonate preparation device (external reproducibility of $\pm 0.05\text{‰}$ for oxygen and $\pm 0.03\text{‰}$ for carbon, values given versus Pee Dee Belemnite standard, Boulay, 2000).
- A non-destructive XRF scan of core MD99-2281 was performed using the CORTEX scanner at a low resolution of 2 cm at the NIOZ laboratory, and at a high resolution of 2 mm at EPOC using the Avaatech XRF Core Scanner. In this study, we use the ratio $(\text{Fe} + \text{Ti})/(\text{Ca} + \text{Sr})$ and the individual counts of Ca-XRF to quantify terrigenous supply and bio-productivity, respectively (e.g. Jansen *et al.*, 1998; Richter *et al.*, 2006).

Multi-proxy observations on core MD99-2281

Dinocyst assemblages

Thirty Quaternary species were recognized in the studied section. Mean absolute concentrations are c. 2900 cysts cm^{-3} with a maximum observed around 1000 cm ($\sim 24\text{k}$ cal a BP). Assemblages are dominated by: *Bitectatodinium tepikiense*, *Operculodinium centrocarpum*, *Islandinium minutum*, *Nematosphaeropsis labyrinthus* and round brown *Brigantedinium* species (Fig. 2). Secondary species consist of: cysts of *Pentaparsodinium dalei*, *Lingulodinium machaerophorum*, *Selenopemphix quanta*, *Impagidinium sphaericum* and *Spiniferites ramosus*. Several broken *Spiniferites* species, supposed to mainly represent *S. ramosus*, were grouped under *Spiniferites* spp.

Maximal abundances of *O. centrocarpum* ($\sim 50\%$) are found in the upper part of the section between 550 and 400 cm (17.5–12.5k cal a BP). Conversely, *O. centrocarpum* is poorly represented between 1050 and 650 cm (25–18k cal a BP), while *B. tepikiense* show maximum abundances (20–50%). This opposite pattern between *O. centrocarpum* and *B. tepikiense* is observable along the entire record (Fig. 2). Higher percentages of *I. minutum* are recorded twice: between 1050 and 850 cm (25–21k cal a BP) and between 650 and 450 cm (18.5–15k cal a BP). *N. labyrinthus* shows maximum abundances in the topmost part of the record (after 12.5k cal a BP).

Sea-ice cover extent through time

Along the studied section, *I. minutum* percentages remain relatively high (mean 10%). At present, this species dominates dinocyst assemblages from arctic/sub-arctic regions, where sea-ice cover can persist year-round. It is thus a robust proxy of sea-ice cover extent through time (de Vernal *et al.*, 2000, 2001; Kunz-Pirring *et al.*, 2001). Sea-ice cover duration fluctuates between 0 and 2 months a^{-1} with an average of 0.7 months a^{-1} (Fig. 3). The significance of these low values has to be considered carefully due to the 1.1 month a^{-1} error bar in our reconstruction. They can, however, be considered as valuable indices of ice presence (either short expansion or drifting) as, at present, sea-ice cover does not develop on site (World Ocean Atlas, WOA, 1998).

Highest values of *I. minutum* percentages (25%) and sea-ice cover estimates (1–2 months a^{-1}) are observed concomitantly during HE1 and from 24 to 22k cal a BP (Fig. 3), just prior to the LGM *sensu stricto* (i.e. after Mix *et al.*, 2001; 19–23k cal a BP). HE2 has low percentages of *I. minutum* but is marked by seasonal sea-ice presence.

Shorter sea-ice cover durations (0–1 month a^{-1}) are recorded twice in the studied section: during the LGM and during the

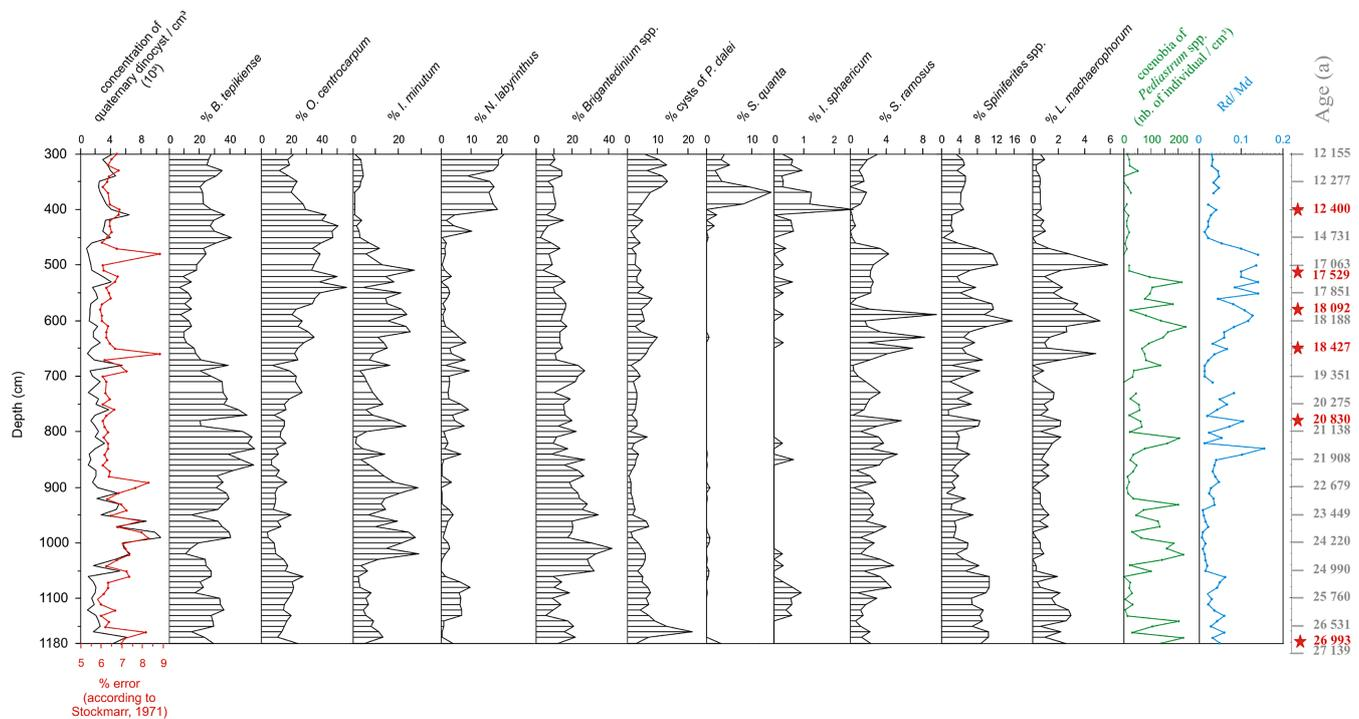


Figure 2. Palynological diagram representing the raw relative abundances (%) of the Quaternary dinocyst assemblages recovered within core MD99-2281 (section 1180–300 cm). The error on the counts, calculated according to Stockmarr (1971), is plotted on the left. On the right are also shown the coenobia of *Pediastrum* spp. Concentration observed in the samples (no. of individuals cm^{-3}) and the Rd/Md ratio of reworked non-Quaternary dinocyst (Rd) versus modern dinocyst (Md). The age scale on the right is calculated according to Zumaque *et al.* (2012). The stars indicate the AMS ^{14}C dates (see Table 2). This figure is available in colour online at wileyonlinelibrary.com.

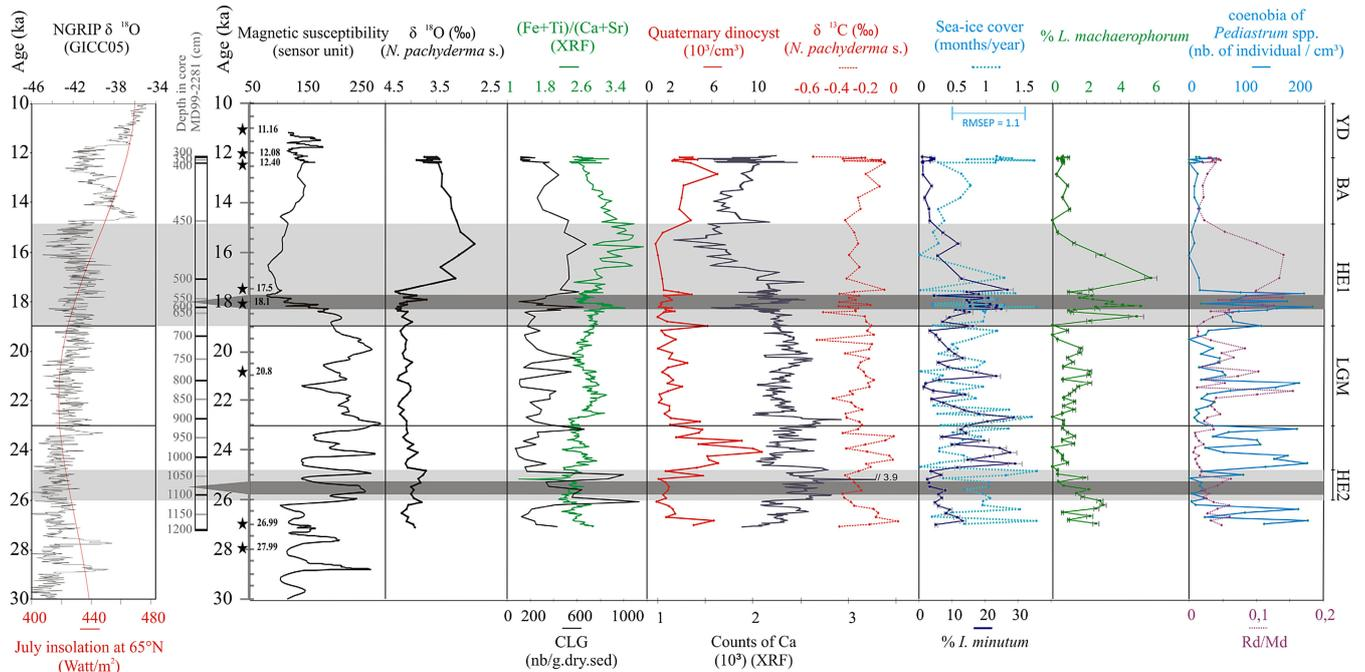


Figure 3. Multi-proxy age compilation (k cal a BP) on core MD99-2281. Stars on the age scale indicate AMS ^{14}C -dated samples. NGRIP $\delta^{18}\text{O}$ (GICC05, b2k) after Svensson *et al.* (2008). Summer (July) insolation values at 65°N after Berger and Loutre (1991). Grey bands indicate the tri-partite phases of HEs. The LGM is delimited by the black lines (19–23k cal a BP) *sensu* Mix *et al.* (2001). CLG, coarse lithic grains; Rd/Md, ratio of reworked (Rd) to modern dinocysts (Md). This figure is available in colour online at wileyonlinelibrary.com.

warm pause of the Bölling–Alleröd (B/A) (Fig. 3). Our results thus demonstrate, similarly to MARGO (e.g. MARGO Project Members, 2009), that the north European margin was ice-free a large part of the year during the LGM, and furthermore that sea-surface conditions were then close to those recorded during the B/A.

Primary productivity

Primary productivity patterns can be deduced from Quaternary dinocyst absolute concentrations, planktonic $\delta^{13}\text{C}$ and individual counts of Ca (XRF) that mainly reflect biogenic productivity of calcareous microfossils. Maximum dinocyst concentrations are observed just prior to the LGM *sensu stricto*, between 24.7 and 23k cal a BP (Fig. 3). This high productivity peak is validated by globally higher values in planktonic $\delta^{13}\text{C}$. Maximum values of Ca characterize the interval encompassing HE2 to HE1. These latter events record low dinocyst concentrations (fewer than 2000 cysts cm^{-3}) and slightly lighter values of planktonic $\delta^{13}\text{C}$ (well marked for HE2) compared with the surrounding sections. Ca (XRF) counts are variable during HEs.

Terrigenous and fluvial input

The reverse correlation between Fe and Ti (terrigenous continental source) with Ca and Sr (biogenic origin) enabled us to establish the ratio $(\text{Fe} + \text{Ti})/(\text{Ca} + \text{Sr})$ to trace increasing transport of detrital material and/or decreasing biogenic input towards our oceanic site (Fig. 3). This ratio generally increases from HE2 to the end of HE1 and decreases rapidly at the start of the B/A, with a slight recovery during the Younger Dryas (YD). This general trend of increasing detrital input through MIS2 is also clear through CLG concentrations and Rd/Md ratio. This latter ratio implies continental erosion of pre-Quaternary sedimentary bedrock and then fluvial transport and/or ice rafting, which would allow pre-Quaternary dinocysts to settle at our study site among *in situ* Quaternary species. It is also

possible to trace this fluvial transport via coenobia of the freshwater micro-algae *Pediastrum* spp. and increasing percentages of the dinocyst species *L. machaerophorum* (e.g. Eynaud *et al.*, 2007; Penaud *et al.*, 2009).

When considering HEs in detail, both HE1 and HE2 show a tripartite structure with higher terrigenous advection during the first and third phases, and a second phase without any strong evidence of terrigenous input and fluvial discharge. Furthermore, continental supplies during HE2 are less severe than those occurring during HE1. HE1 is also characterized by the highest terrigenous signature of the whole studied section.

SST estimates

Quantitative estimates of past summer and winter SST reveal important contrasts in palaeohydrographical changes through MIS2 (Fig. 4). In the studied section, winter and summer SSTs fluctuate between 0 and 3.5°C and between 12 and 16°C , respectively. Modern winter SSTs are roughly 8.3°C , i.e. 8°C higher than those reconstructed for MIS2. Interestingly, mean MIS2 summer SSTs are 3°C higher than present-day conditions (11.6°C). These results suggest that the seasonal contrast (summer minus winter SST) was far larger during MIS2 (around 14°C) than today (around 4°C). Lowest winter SSTs (-0.2°C) and highest summer SSTs (16°C) are recorded during the LGM (Fig. 4), underlining the prevalence of an atypical sea-surface hydrographical scheme during this period.

Sea-surface currents

Sea-surface circulation features can be accessed with two dinocyst species: *O. centrocarpum* and *N. labyrinthus*. A link between *O. centrocarpum* and the NAD has been suggested from its modern distribution in the North Atlantic sediments as maximum occurrence of this species follows the NAD pathway (e.g. Rochon *et al.*, 1999). In the subboreal Atlantic, *N. labyrinthus* occurs today in the vicinity of oceanic fronts and is mainly abundant where the cold West Greenland

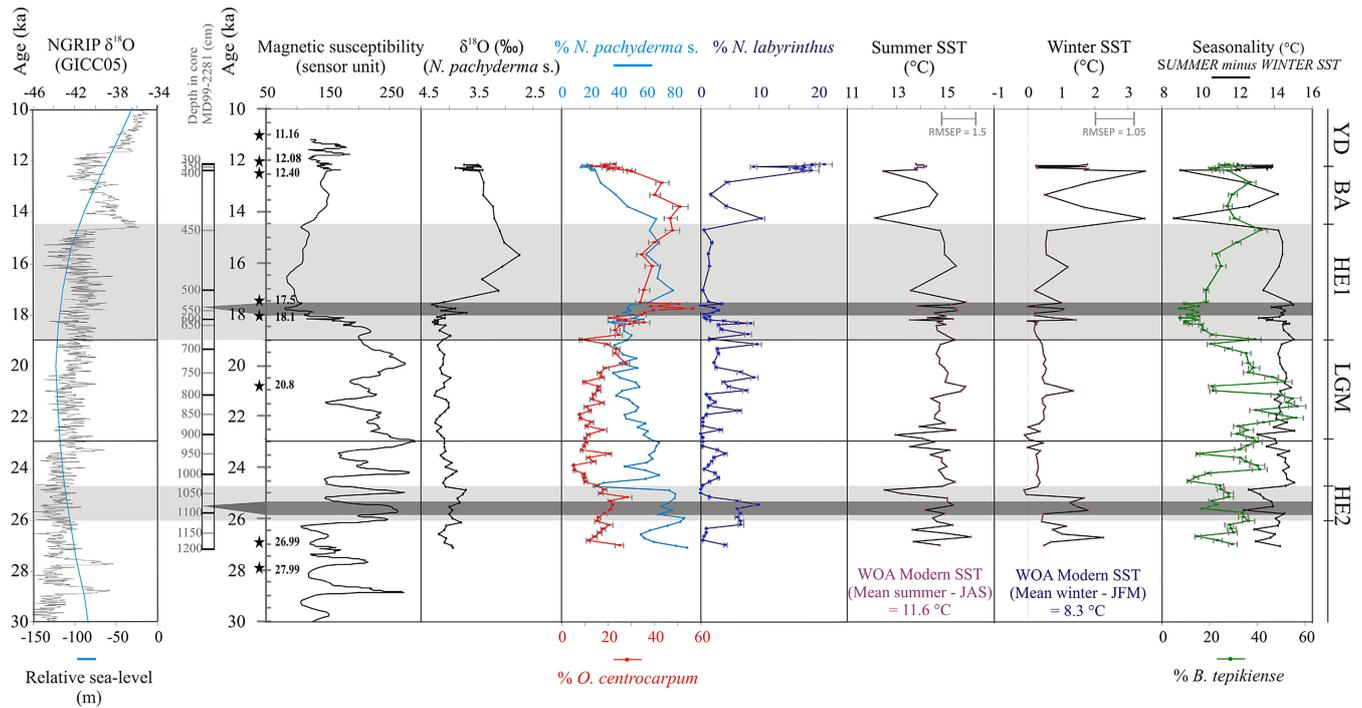


Figure 4. Multi-proxy age compilation (k cal a BP) on core MD99-2281. Stars on the age scale indicate AMS ^{14}C -dated samples. NGRIP $\delta^{18}\text{O}$ (GICC05, b2k) after Svensson *et al.* (2008). The relative sea level conforms to the published reconstruction of Waelbroeck *et al.* (2002). Grey bands indicate the tri-partite phases of HEs. The LGM is delimited by the black lines (19–23 ka a BP) *sensu* Mix *et al.* (2001). This figure is available in colour online at wileyonlinelibrary.com.

Current and the warm Irminger Current converge, south of Greenland (e.g. Marret *et al.*, 2004).

It is interesting to note that percentages of *O. centrocarpum* increase from the base of the studied section to the end of HE1 (Fig. 4). Minor peaks of *N. labyrinthus* (4–8%) are synchronous with peaks of *O. centrocarpum* except for the large last peaks encompassing the onsets of the B/A and YD. These two dinocyst species show an opposite trend to the polar planktonic foraminifera *Nps*, percentages of which progressively decrease with time (except for HE1, Fig. 4). Within the context of a glacial termination, it would thus imply a northward shift of the Polar Front to higher latitudes (except during HE1) in parallel with increasing influence of warmer waters with an NAD signature.

Discussion

LGM in the NNA

Seasonal contrasts

The LGM period is characterized by high relative abundances of *B. tepikiense* (40%) in core MD99-2281. The occurrence of this species suggests a strong seasonal contrast (e.g. Rochon *et al.*, 1999), and its weight in the assemblages during this period is logically transferred to the derived SST estimates (Fig. 4). Mean LGM SSTs obtained on core MD99-2281 thus reveal cold winters around 0–1 °C and warm summers around 15–16 °C. Since the pioneering works of CLIMAP Project Members (1981), several studies have attempted to reconstruct sea-surface conditions in the North Atlantic based on various sets of microfossils (e.g. Weinelt *et al.*, 1996; van Kreveld *et al.*, 2000; de Vernal *et al.*, 2000, 2001; Sarthein *et al.*, 2003; Rosell-Melé *et al.*, 2004; Rasmussen and Thomsen, 2008). The recent re-evaluation of LGM SSTs by the MARGO project improved reconstructions by combining multiproxy-derived

estimates and by delimiting a better temporal definition and geographical coverage (e.g. Kucera *et al.*, 2005a,b; Meland *et al.*, 2005; de Vernal *et al.*, 2005, 2006; MARGO Project Members, 2009). MARGO results have highlighted the prevalence of atypical LGM sea-surface conditions in Nordic seas, especially during summer. Positive summer SST anomalies (LGM minus modern-WOA, SST extracted with <http://www.geo.uni-bremen.de/geomod/staff/csn/woasample.html>), in the same range as those we have reconstructed, were also detected (Kucera *et al.*, 2005b; de Vernal *et al.*, 2005). They reflect very different sea-surface conditions from today. A noticeable pattern during this period is that reconstructed summer SSTs are higher than modern values while winter SSTs are lower, thus producing extreme values of seasonal contrast. Such a contrast could result from specific LGM conditions, with, in particular, the possible development of a thin melt-water lens in summer, promoting a strong water column stratification (as already suggested and emphasized by de Vernal *et al.*, 2006) and thus a rapid sea-surface warming.

The comparison of our dinocyst data with those previously acquired at the same time resolution on two other cores from the NW European margin highlights some significant similarities/dissimilarities along a north–south gradient (encompassing 20 degree in latitude, Fig. 5). Core MD95-2002, located on the Celtic margin at the outlet of the Fleuve Manche palaeoriver, and core MD99-2281 show a similar trend during MIS2 with the highest percentages of *B. tepikiense* recorded during the LGM (Fig. 5b). *B. tepikiense* percentages recorded during the LGM also fluctuate around 15% in core MD95-2010 (Vøring plateau). Therefore, our results reveal that the LGM, often considered as a uniform cold period through the North Atlantic (CLIMAP Project Members, 1981), in fact shows a much more complex and patchy pattern (Sarthein *et al.*, 2003; Kucera *et al.*, 2005a; de Vernal *et al.*, 2005, 2006; Kageyama *et al.*, 2006; MARGO Project Members, 2009) with significant

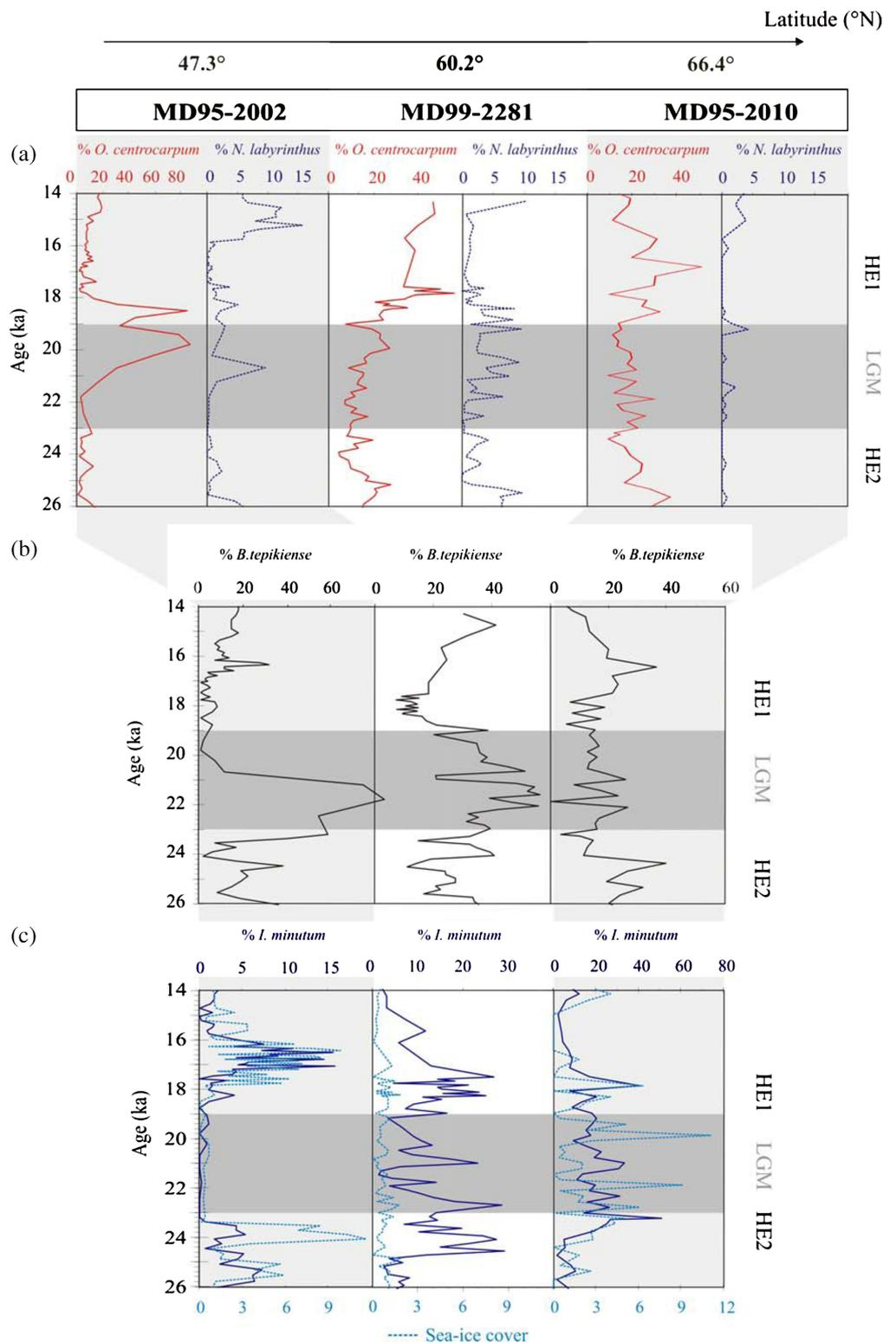


Figure 5. Multicore compilation (MD95-2002, MD95-2010 after Eynaud *et al.*, 2002, 2007; MD99-2281, this work) and comparison of the relative abundances of some selected dinocyst species over the interval 14–26 ka BP. (a) Relative abundance of the dinocyst species *O. centrocarpum* (full line) and *N. labyrinthus* (dotted line); (b) relative abundances of the dinocyst species *B. tepikiense*; (c) relative abundance of the dinocyst species *I. minutum* (full line) and estimated duration of sea-ice cover (months a⁻¹; dotted line). LGM limits *sensu* Mix *et al.* (2001). This figure is available in colour online at wileyonlinelibrary.com.

differences observed within the same region (Eynaud *et al.*, 2002; Rasmussen and Thomsen, 2008).

Sea-ice cover and terrigenous supplies

Sea-ice cover is a crucial parameter within the climate system given the radiative budget of the earth's surface (albedo, heat, salinity and moisture transfer, etc.). Sea-ice development also plays an essential role regarding the density and stratification of the water column. Furthermore, sea-ice cover duration is

closely associated with ice-sheet dynamics. However, few proxies are able to quantify this parameter robustly, leaving a gap in data model comparisons (e.g. Byrkjedal *et al.*, 2006; Li *et al.*, 2010).

According to the MD99-2281 record, the LGM was characterized by a short seasonal sea-ice cover duration compared with the surrounding HEs. Terrigenous advection also appears to have been moderate, although fluctuating significantly (Fig. 3). Indeed, the high resolution of core MD99-2281 emphasizes a strong variability during the LGM

underlined by several peaks (at least three) of CLG concentrations supported by synchronous peaks of (Fe + Ti)/(Ca + Sr) and Rd/Md (Fig. 3). This internal variability within the LGM can also be observed through increasing *Nps* and *I. minutum* percentages, and minor planktonic $\delta^{18}\text{O}$ fluctuations probably revealing intermittent advection of freshwater and/or meltwater from the proximal BIIS. Recent studies support that this ice-sheet reached its maximum extent earlier than the LGM *sensu stricto* (Peltier and Fairbanks, 2006; Scourse *et al.*, 2009). High abundances of *I. minutum* (>20%) at the bottom of our record are consistent with early growth of the BIIS. According to Scourse *et al.* (2009), the BIIS experienced a rapid retreat at 23k cal a BP followed by a broad re-advance between 22 and 16k cal a BP, during a period of weak summer insolation (Fig. 3).

Large palaeo-ice streams may have contributed to terrigenous supplies in core MD99-2281. These palaeo-ice streams could have included the ice stream off Scotland flowing to the west of Scotland, the Minch palaeo-ice stream flowing through the Hebrides and a north-east flow from the BIIS and FIS flowing across Shetland and the Orkney islands (Chiverrell and Thomas, 2010). Asymmetrical behaviour for the BIIS retreat controlled sedimentary supply and may have influenced ice streams draining the main dome of the ice sheet (Scourse *et al.*, 2009; Clark *et al.*, 2010). Indeed, new evidence suggests that the BIIS reached its maximum extent at 30–27k cal a BP on the west side and at 25–17k cal a BP in the south (Clark *et al.*, 2010).

When integrating the other cores, reconstructions of sea-ice cover duration during the LGM show increasing values towards northern latitudes: from less than 1 month a^{-1} on cores MD95-2002 and MD99-2281, to about peaks of nearly 9 months a^{-1} on core MD95-2010 (Fig. 5c). This gradient confirms the development of patchy sea-ice cover in the NNA during the LGM (e.g. de Vernal *et al.*, 2001). Only our northernmost site, close to the Arctic Circle, experienced episodic sea-ice development over this 4000-year period.

At 19k cal a BP, significant terrigenous advection is recorded in core MD99-2281, possibly linked to major ice-sheet instabilities. Indeed, higher Rd/Md and *L. machaerophorum* percentages mark an increase in detrital advection (Fig. 3). Synchronously, fluvial discharges and terrigenous supplies via the Fleuve Manche palaeo-river were observed at core site MD95-2002, attributed to the early retreat and collapse of European ice sheets and continental glaciers (e.g. Toucanne *et al.*, 2009), and in agreement with the Kilkeel meltwater pulse identified along the Irish coast at this time (i.e. Clark *et al.*, 2004).

MIS2 ice-sheet instabilities and oceanic circulation

Co-occurrences of *O. centrocarpum* and *N. labyrinthus* in MD99-2281 assemblages (Fig. 5a) during the LGM suggest active penetration of the NAD at that time. Dinocyst data from cores MD95-2002 and MD95-2010 also support persistence of the NAD with high percentages of *O. centrocarpum*. Therefore, this drift may have flowed eastward and westward of the Faeroes, similarly to the present-day circulation pattern. However, modern abundances of *O. centrocarpum* at the Faeroe Islands reach 40–60% (Rochon *et al.*, 1999), i.e. twice the values recorded in MD99-2281 during the LGM, thus suggesting less vigorous penetration than today. Persistence of the NAD in the South Norwegian Sea is not contradictory with a maximum development of ice sheets during the LGM as the build-up of a boreal ice sheet requires snowfall, which is dependent on humidity and thus frequency of westerly

depressions (Winograd, 2001; Byrkjedal *et al.*, 2006). Recovery of westerly depressions is promoted when thermal contrasts between the Nordic domains and temperate latitudes is weak, i.e. when the AMOC is efficient enough to transfer heat towards high latitudes (e.g. Johnsen *et al.*, 1989; Winograd, 2001).

Increasing percentages of *O. centrocarpum* over the LGM (maximum of 50% at 18k cal a BP) at the South Faeroe Island suggest a growing influence of the NAD before the HE1 collapse. Intensification of this warm water inflow is coherent with data acquired in the Bay of Biscay from core MD95-2002 (Zaragosi *et al.*, 2001; Fig. 5) and the proximal MD03-2692 sequence (Penaud *et al.*, 2009). Therefore, NAD inflow along the Britannic and Fennoscandic coasts could have contributed to destabilize European ice sheets. This confirms, in our study area and potentially in the whole NNA, that oceanic heat transfer may have played a major role in the initiation of ice-sheet collapses (e.g. Moros *et al.*, 2002).

Occurrences of *N. labyrinthus* from core MD99-2281 also suggest active inflow of the cold East Icelandic Current (EIC) towards the Faeroe Islands area. *N. labyrinthus* is presently associated in the vicinity of Iceland with strong current frontal systems characterized by high productivity (Marret *et al.*, 2004) and could thus indicate the expression of comparable hydrographical structures along the NAD and the EIC at our site. Core MD99-2281 is indeed located today at the convergence point between these two surface currents. Further north (core MD95-2010) and further south (core MD95-2002), *N. labyrinthus* is poorly represented during the LGM (Fig. 5a), showing that core MD99-2281 was thus located at a particular point regarding sea-surface circulation at that time.

Heinrich events

HE1 and HE2: convergences and discrepancies

HE2 and HE1 occurred, respectively, during periods of transition from MIS3 to MIS2 and from MIS2 to MIS1 (i.e. Termination 1). In our study, HE2 and HE1 have been delimited at 26–24.7 and 19–14.5k cal a BP, respectively, according to maximum CLG concentrations and high percentages of *Nps* (>60%). These ages agree well with those compiled by Sánchez-Goñi and Harrison (2010) and with the recent study of Stanford *et al.* (2011) that considers a longer interval of HE1 of approximately 4000 years between 19 and 15k cal a BP.

These two events show several similarities in core MD99-2281. Melting of icebergs during ice-sheet collapses are recorded in both cases by high CLG concentrations and low isotopic values of planktonic $\delta^{18}\text{O}$. Both HEs also exhibit high abundances of *Nps* (maximum values of 80% versus 30% today at the South Faeroe Islands), suggesting southward migration of the polar front. These drastic sea-surface conditions were not favourable for marine primary productivity as seen by lower dinocyst concentrations and slightly lighter planktonic $\delta^{13}\text{C}$ values. Several discrepancies are, however, visible between HE1 and HE2. Dilution processes appear to be much more important during HE1 than during HE2, these events being marked by a decrease of planktonic $\delta^{18}\text{O}$ values of 1.5 and 0.4‰, respectively. Finally, HE2 and HE1 both display a multiphase structure with a relatively temperate median phase marked by lower percentages of *Nps* and higher relative abundances of *N. labyrinthus* and *O. centrocarpum*. The observed poly-phase structure of both HEs is consistent with previous observations made from the Nordic Basins to the Iberian Margin (e.g. Grousset *et al.*, 2000; Zaragosi *et al.*, 2001; Naughton *et al.*, 2009; Stanford *et al.*, 2011). The tri-partite structure of HE1 is worthy of detailed discussion (Fig. 6).

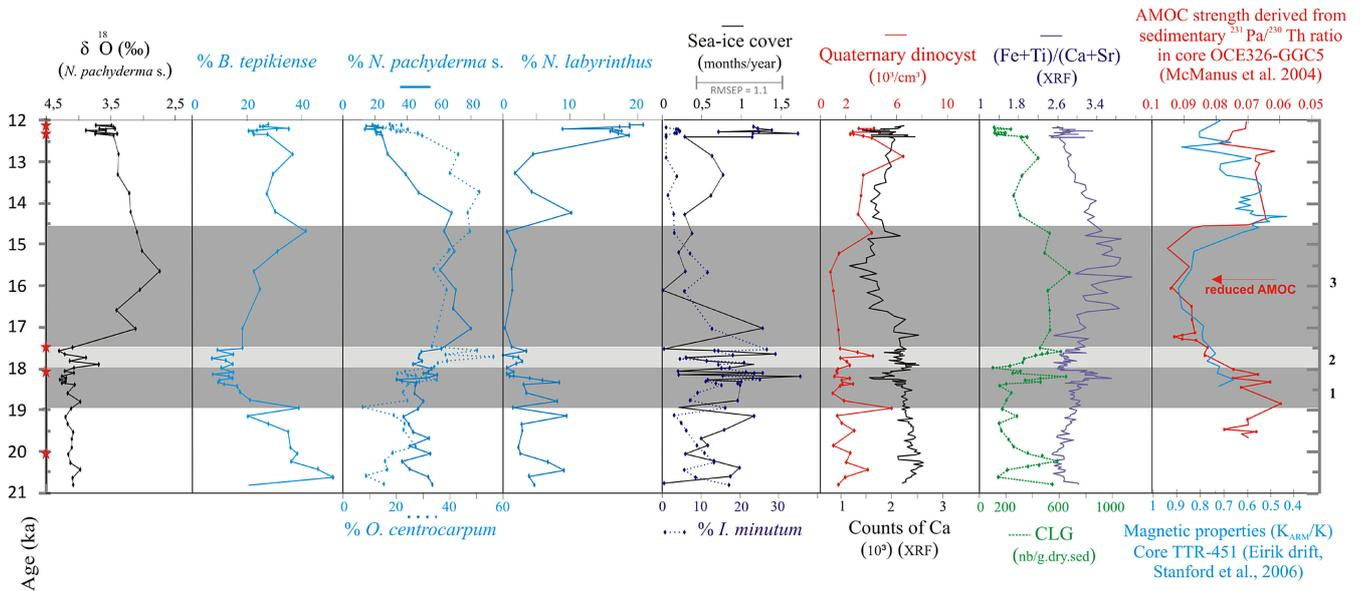


Figure 6. Multi-proxy age compilation (k cal a BP) on core MD99-2281 focusing on HE 1. Grey bands and associated numbers (1, 2 and 3) indicate the tri-partite phases of HE1. On the left are two records documenting the AMOC strength: the Pa/Th record from Bermuda Rise (after McManus *et al.*, 2004) and the ratio of susceptibility of anhysteretic remanent magnetization (kARM) to low-field magnetic susceptibility (k) from Eirik Drift (after Stanford *et al.*, 2006). The stars on the right scale indicate AMS ^{14}C dates (see Table 2). This figure is available in colour online at wileyonlinelibrary.com.

Tri-partite structure of HE1

Phase 1 (19–18k cal a BP). At 19k cal a BP, a sharp decrease of *B. tepikiense* percentages is recorded (Figs 5b and 6) synchronously with increasing *Nps* abundances. Sea-surface environments then abruptly experienced severe cold conditions, as also indicated by an increase in *I. minutum* abundances and longer durations of sea-ice cover (mean of 1 month a^{-1}). In parallel, dinocyst concentrations as well as the Ca-XRF signal decrease significantly, suggesting a pause in marine primary productivity. This latest observation is coherent with conclusions deduced from models showing a decline of the marine ecosystem during phases of AMOC reduction, including HEs (e.g. Schmittner, 2005), but could also be the result of dilution by terrigenous supplies. Terrigenous advection is maximal between 18.3 and 18k cal a BP, as seen in CLG concentrations and the ratio $(\text{Fe} + \text{Ti})/(\text{Ca} + \text{Sr})$. This pulse, recorded in the first part of HE1, may result from the onset of European ice-sheet collapses (Icelandic ice sheet, BIIS or FIIS) (e.g. Hemming, 2004). Meltwater may then sustain the slow-down of the AMOC intensity observed at 19k cal a BP on the Bermuda rise (McManus *et al.*, 2004; Fig. 6).

Phase 2 (18–17.5k cal a BP). The interval 18–17.5k cal a BP is marked by a drop of 10% in *Nps* percentages and a synchronous positive excursion in *O. centrocarpum* abundances (Figs 5a and 6), suggesting milder conditions with active penetration of the NAD toward the Faeroes. This 500-year phase may, however, be too short to suppose a renewal of the AMOC circulation at its modern rate. Finally, this second phase of HE1 is characterized by a lowering of terrigenous supplies.

Phase 3 (17.5–15k cal a BP). The last phase of HE1 (17.5–15k cal a BP) is marked by a drop of 1‰ in planktonic $\delta^{18}\text{O}$ values (Fig. 6) while Stanford *et al.* (2011), based on Dokken and Jansen's (1999) original data, document a drop of 2‰ of the planktonic $\delta^{18}\text{O}$ signal in core MD95-2010. This reflects a massive input of freshwater from ice-sheet melting observed synchronously in the Fram Strait (Weinelt *et al.*, 1991), in the Greenland Sea (Stanford *et al.*, 2011) or around the Faeroes (Rasmussen *et al.*, 1996a). Moreover, comparison

between the planktonic $\delta^{18}\text{O}$ signals from Eirik drift and the Nordic seas shows similar values, suggesting a synchronicity in sea-surface hydrographical changes between the East and West basins of the North Atlantic (Stanford *et al.*, 2011). It suggests that major iceberg discharges were principally sourced from collapse of the Laurentide ice sheet at and after 17k cal a BP (Rasmussen *et al.*, 1996a; Scourse *et al.*, 2000; Zaragosi *et al.*, 2001; Penaud *et al.*, 2009). The early retreat of European ice sheets and the associated increase in sea level may, however, have contributed to destabilization of the Laurentide ice sheet (e.g. Grousset *et al.*, 2000; Scourse *et al.*, 2000, 2009).

Sediment supplies are maximal during this 17.5–15k cal a BP interval. The strong terrigenous advection is synchronous with the paroxysmal phase of the Laurentide ice-sheet collapse. At the same time, *O. centrocarpum* percentages decrease sharply, probably indicating a reduced influence of the NAD over the area. *Nps* percentages reach 80% (Fig. 6), values recorded today in the vicinity of the Northern Polar Front, up to 70°N . The 17.5–14.5k cal a BP interval corresponds to the so-called HE1 *sensu stricto* defined as the significant retreat of the pan-Atlantic ice sheets (e.g. Dyke *et al.*, 2002). High sedimentation rates are recorded at the outlet of glacial areas, consistent with global ice-sheet retreat (e.g. Lekens *et al.*, 2005). Climatic perturbations associated with iceberg discharges in the North Atlantic reduce northern hemispheric temperatures significantly.

After 15.5k cal a BP, the terrigenous supply from BIIS and FIS decreases. A progressive recovery of the AMOC (e.g. McManus *et al.*, 2004) is thus observed. This interval records higher SSTs, higher primary productivity and increasing percentages of *O. centrocarpum*, suggesting a vigorous NAD (Fig. 6).

Conclusion

Our study demonstrates that the NNA has displayed a complex evolution of sea-surface conditions during MIS2 (LGM, HE1 and 2). By combining multiproxy information obtained on core MD99-2281 (60°N , this study) and on previously published cores MD95-2002 and MD95-2010, a robust scenario retracing

pan-north European sea-surface palaeoenvironments can be built up millennium after millennium.

Dinocyst data obtained for the LGM reveal a coherent regional pattern over the NNA from 47 to 66°N. Strong seasonal contrasts, marked by higher summer SSTs and winter SSTs lower than today, are recorded throughout this period. Furthermore, our study reveals only episodic sea-ice cover in the Nordic Seas. In parallel, proxies of terrigenous advection attest to instability of the BIIS through the LGM.

Surrounding the LGM, HE1 and HE2 depict a tripartite internal structure in core MD99-2281. Following previous observations done within and without the Ruddiman belt (Ruddiman, 1977), it confirms a multi-step pattern within HEs that has been poorly tackled by modellers to date. HE1 (19–14.5k cal a BP) accurately records the last deglaciation and the melting of pan-Atlantic ice sheets and notably BIIS collapse. Additional analyses on the terrigenous material could help to trace the origin of the continental material to our study area. This perspective would help to establish a chronology of continental supplies according to their sources throughout the last deglaciation.

Acknowledgements. We are grateful to IPEV, the captain and crew of the *Marion Dufresne* and the scientific team of the GINNA cruise. We thank Mr Y. Balut for his assistance at sea. J. St Paul, O. Ther, M-H. Castera, I. Billy and M. Georget provided invaluable technical assistance, and we thank D. Urrego for reviewing the language. We acknowledge financial support by the ARTEMIS ¹⁴C AMS French project. Part of the analyses conducted on MD99-2281 was supported by the French INSU (Institut National des Sciences de l'Univers) programme LEFE/EVE (Les enveloppes fluides et l'environnement/Evolution et variabilité du climat à l'échelle globale) 'RISCC: Rôle des Ice-Shelves dans le Changement Climatique'. We also thank the European Union's Seventh Framework programme "Past4Future. Climate change-Learning from the past climate." The authors declare no conflict of interest. This is U.M.R./EPOC 5805 (Université Bordeaux I-C.N.R.S.) contribution.

Abbreviations. AMOC, Atlantic Meridional Overturning Circulation; AMS, accelerator mass spectrometry; B/A, Bölling–Alleröd; BIIS, British–Irish ice sheet; CLG, coarse lithic grains; EIC, East Icelandic Current; ENAW, Eastern North Atlantic Waters; FIS, Fennoscandian ice sheet; HE, Heinrich event; LGM, Last Glacial Maximum; MAT, Modern Analogue Technique; MIS, Marine Isotope Stage; NAD, North Atlantic Drift; NADW, North Atlantic Deep Waters; NNA, north-eastern North Atlantic; Nps, *Neogloboquadrina pachyderma sinistral*; Rd/Md, 'Reworked (pre-Quaternary) to Modern (Quaternary)' dinocysts; SST, sea surface temperature; XRF, X-ray fluorescence; YD, Younger Dryas.

References

- Alvarez-Solas J, Charbit S, Ritz C, *et al.* 2010. Links between ocean temperature and iceberg discharge during Heinrich events. *Nature Geoscience* **3**: 122–126.
- Berger A, Loutre M-F. 1991. Insolation values for the climate of the last 10 millions years. *Quaternary Science Review* **10**: 297–317.
- Blindheim J, Borovkov V, Hansen B, *et al.* 2000. Upper layer cooling and freshening in the Norwegian Sea in relation to atmospheric forcing. *Deep-Sea Research I* **47**: 655–680.
- Boldreel LO, Andersen MS, Kuijpers A. 1998. Neogene seismic facies and deep-water gateways in the Faeroe Bank area, NE Atlantic. *Marine Geology* **152**: 129–140.
- Bond G, Lotti R. 1995. Iceberg discharges into the north Atlantic on millennial time scales during the last glaciation. *Science* **267**: 1005–1010.
- Boulay S. 2000. Variabilité climatique rapide en Atlantique Nord - Un potentiel de réponses: la carotte MD 99-2281 (sud des îles Faeroes). Masters thesis, Université Paris-Sud.
- Boulton G, Hagdorn M. 2006. Glaciology of the British Isles Ice Sheet during the last glacial cycle: form, flow, streams and lobes. *Quaternary Science Reviews* **25**: 3359–3390.
- Byrkjedal Ø, Kvamstø NG, Meland M, *et al.* 2006. Sensitivity of last glacial maximum climate to sea-ice conditions in the Nordic Seas. *Climate Dynamics* **26**: 473–487.
- Chiverrell RC, Thomas GSP. 2010. Extent and timing of the Last Glacial Maximum (LGM) in Britain and Ireland: a review. *Journal of Quaternary Science* **25**: 535–549.
- Clark PU, McCabe AM, Mix AC, *et al.* 2004. Rapid rise of sea level 19,000 years ago and its global implications. *Science* **304**: 1141–1144.
- Clark CD, Hughes ALC, Greenwood SL, *et al.* 2010. Pattern and timing of retreat of the last British-Irish Ice Sheet. *Quaternary Science Reviews* **44**: 112–146.
- CLIMAP Project Members. 1981. *Seasonal reconstructions of the Earth's surface at the last glacial maximum*. Geological Society of America: Boulder, CO.
- de Vernal A, Henry M, Bilodeau G. 1996. Techniques de préparation et d'analyse en micropaléontologie. *Les cahiers du GEOTOP* **3**: 1–29.
- de Vernal A, Hillaire-Marcel C, Turon J-L, *et al.* 2000. Reconstruction of sea-surface temperature, salinity, and sea-ice cover in the northern North Atlantic during the last glacial maximum based on dinocyst assemblages. *Canadian Journal of Earth Sciences* **37**: 725–750.
- de Vernal A, Henry M, Matthiessen J, *et al.* 2001. Dinoflagellate cyst assemblages in surface sediments of the Laptev Sea region (Arctic Ocean) and their relationship to hydrographic conditions. *Journal of Quaternary Science* **16**: 637–649.
- de Vernal A, Eynaud F, Henry M, *et al.* 2005. Reconstruction of sea-surface conditions at middle to high latitudes of the Northern Hemisphere during the Last Glacial Maximum (LGM) based on dinoflagellate cyst assemblages. *Quaternary Science Reviews* **24**: 897–924.
- de Vernal A, Rosell-Melé A, Kucera M, *et al.* 2006. Comparing proxies for the reconstruction of LGM sea-surface conditions in the northern North Atlantic. *Quaternary Science Reviews* **25**: 2820–2834.
- Dokken TM, Jansen E. 1999. Rapid changes in the mechanism of ocean convection during the last glacial period. *Nature* **401**: 458–461.
- Domack E, Duran D, Leventer A, *et al.* 2005. Stability of the Larsen B ice shelf on the Antarctic Peninsula during the Holocene epoch. *Nature* **436**: 681–685.
- Dyke AS, Andrews JT, Clark PU, *et al.* 2002. The Laurentide and Innuitian ice sheets during the last glacial maximum. *Quaternary Science Reviews* **21**: 9–31.
- Ehlers J, Gibbard P. 2004. *Quaternary Glaciations - Extent and Chronology Part I: Europe*. Publisher Elsevier: Amsterdam; 488 pp.
- Ellet DJ, Edwards A, Bowers R. 1986. The hydrography of the Rockall Channel - an overview. *Proceedings of the Royal Society of Edinburgh* **88B**: 61–81.
- Elliot M, Labeyrie L, Dokken T, *et al.* 2001. Coherent patterns of ice-rafted debris deposits in the Nordic regions during the last glacial (10–60 ka). *Earth and Planetary Science Letters* **194**: 151–163.
- Ericson DB. 1959. Coiling direction of *Globigerina pachyderma* as a climatic index. *Science* **130**: 219–220.
- Eynaud F, Turon J-L, Matthiessen J, *et al.* 2002. Norwegian sea-surface palaeoenvironments of marine oxygen-isotope state 3: The paradoxical response of dinoflagellate cysts. *Journal of Quaternary Science* **17**: 349–359.
- Eynaud F, Zaragosi S, Scourse JD, *et al.* 2007. Deglacial laminated facies on the NW European continental margin: the hydrographic significance of British-Irish Ice Sheet deglaciation and Fleuve Manche paleoriver discharges. *Geochemistry, Geophysics, Geosystems* **8**.
- Eynaud F, de Abreu L, Voelker A, *et al.* 2009. Position of the Polar Front along the western Iberian margin during key cold episodes of the last 45 ka. *Geochemistry, Geophysics, Geosystems* **10**.
- Fensome RA, MacRae RA, Williams GL. 1998. DINOFLAJ. *Geological Survey of Canada Open File* 3653.
- Fensome RA, Williams GL. 2004. The Lentin and Williams index of fossil dinoflagellates. *AASP Foundation Contributions Series* 42.
- Fogelqvist E, Blindheim J, Tanhua T, *et al.* 2003. Greenland–Scotland overflow studied by hydro-chemical multivariate analysis. *Deep Sea Research Part I* **50**: 73–102.

- Grousset F, Pujol C, Labeyrie L, *et al.* 2000. Were the North Atlantic Heinrich events triggered by the behavior of the European ice sheet? *Geology* **28**: 123–126.
- Grosswald MG, Hughes TJ. 2002. The Russian component of an arctic ice sheet during the last glacial maximum. *Quaternary Science Reviews* **21**: 121–146.
- Guiot J, de Vernal A. 2007. Transfer functions: methods for quantitative paleoceanography based on microfossils. In Hillaire-Marcel C, de Vernal A (eds.). *Proxies in Late Cenozoic Paleoceanography*. Amsterdam; Elsevier; 523–563.
- Guiot J, de Vernal A. 2011a. Is spatial autocorrelation introducing biases in the apparent accuracy of paleoclimatic reconstructions? *Quaternary Science Reviews* **30**: 1965–1972.
- Guiot J, de Vernal A. 2011b. QSR Correspondence 'Is spatial autocorrelation introducing biases in the apparent accuracy of paleoclimatic reconstructions?' Reply to Telford and Birks. *Quaternary Science Reviews* **30**: 3214–3216.
- Hansen B, Østerhus S. 2000. North Atlantic-Nordic Sea exchanges. *Progress in Oceanography* **45**: 109–208.
- Head MJ, Harland R, Matthiessen J. 2001. Cold marine indicators of the late Quaternary: the new dinoflagellate cyst genus *Islandinium* and related morphotypes. *Journal of Quaternary Science* **16**: 621–636.
- Heinrich H. 1988. Origin and Consequences of Cyclic Ice Rafting in the Northeast Atlantic Ocean during the Past 130,000 Years. *Quaternary Research* **29**: 142–152.
- Hemming SR. 2004. Heinrich events: massive late Pleistocene detritus layers of the North Atlantic and their global climate imprint. *Reviews of Geophysics* **42**: RG1005 1–43.
- Jansen JHF, Van der Gaast SJ, Koster B, *et al.* 1998. CORTEX, a shipboard XRF scanner for element analyses in split sediment cores. *Quaternary Research* **151**: 143–153.
- Johnsen SJ, Dansgaard W, White JW. 1989. The origin of Arctic precipitation under present and glacial conditions. *Tellus* **41**: 452–469.
- Kageyama M, Laine A, Abe-Ouchi A, *et al.* 2006. Last Glacial Maximum temperatures over the North Atlantic, Europe and western Siberia: a comparison between PMIP models, MARGO sea-surface temperatures and pollen-based reconstructions. *Quaternary Science Reviews* **25**: 2082–2102.
- Kageyama M, Paul A, Roche DM, *et al.* 2010. Modelling glacial climatic millennial-scale variability related to changes in the Atlantic meridional overturning circulation: a review. *Quaternary Science Reviews* **29**: 2931–2956.
- Kucera M, Rosell-Melé A, Schneider R, *et al.* 2005a. Multiproxy approach for the reconstruction of the glacial ocean surface (MARGO). *Quaternary Science Reviews* **24**: 813–819.
- Kucera M, Weinelt M, Kiefer T, *et al.* 2005b. Reconstruction of sea-surface temperatures from assemblages of planktonic foraminifera: multi-technique approach based on geographically constrained calibration data sets and its application to glacial Atlantic and Pacific Oceans. *Quaternary Science Reviews* **24**: 951–998.
- Kunz-Pirrung M, Matthiessen J, De Vernal A. 2001. Relationships between dinoflagellate cyst assemblages in surface sediment and hydrographic conditions in the Bering and Chukchi seas. *Journal of Quaternary Science* **16**: 667–680.
- Kutzbach JE, Wright HE Jr. 1986. Simulation of the Climate of 18,000 years B.P.: results for the North American-North Atlantic/European sector and comparison with the geological record of North America. *Quaternary Science Reviews* **4**: 147–187.
- Labeyrie L, Cortijo E, Jansen E. 1999. Rapport scientifique de la mission INTERPOLE MD99-114/812 IMAGES V. In *Les Rapports de Campagne à la Mer à bord du Marion Dufresne*, (IPEV, Ed.), Brest.
- Larsen KMH, Hansen B, Svendsen H. 2008. Faroe Shelf Water. *Continental Shelf Research* **28**: 1754–1768.
- Lekens WAH, Sejrup HP, Haflidason H, *et al.* 2005. Laminated sediments preceding Heinrich event 1 in the Northern North Sea and Southern Norwegian Sea: Origin, processes and regional linkage. *Marine Geology* **216**: 27–50.
- Lézine A-M, Duplessy J-C, Cazet J-P. 2005. West African monsoon variability during the last deglaciation and the Holocene: evidence from fresh water algae, pollen and isotope data from core KW31, Gulf of Guinea. *Palaeogeography, Palaeoclimatology, Palaeoecology* **219**: 225–237.
- Li C, Battisti DS, Schrag DP, *et al.* 2005. Abrupt climate shifts in Greenland due to displacements of the sea ice edge. *Geophys. Res. Lett.* **32**: L19702. DOI: 10.1029/2005GL023492.
- Li C, Battisti DS, Bitz CM. 2010. Can North Atlantic Sea Ice Anomalies Account for Dansgaard-Oeschger Climate Signals? *Journal of Climate* **23**: 5457–5475.
- MARGO Project Members. 2009. Constraints on the magnitude and patterns of ocean cooling at the Last Glacial Maximum. *Nature Geoscience* **2**: 127–132.
- Marret F. 1993. Les effets de l'acétolyse sur les assemblages de kystes de dinoflagellés. *Palynosciences* **2**: 267–272.
- Marret F, Eiriksson J, Knudsen KL, *et al.* 2004. Distribution of dinoflagellate cyst assemblages in surface sediments from the northern and western shelf of Iceland. *Review of Palaeobotany and Palynology* **128**: 35–53.
- Masson DG, Howe JA, Stoker MS. 2002. Bottom-current sediment waves, sediment drifts and contours in the northern Rockall Trough. *Marine Geology* **192**: 215–237.
- McManus JF, Kelgwin L, Francois R, *et al.* 2004. Collapse and rapid resumption of Atlantic meridional circulation linked to deglacial climate changes. *Nature* **428**: 834–837.
- Meland MY, Jansen E, Elderfield H. 2005. Constraints on SST estimated for the northern North Atlantic/Nordic seas during the LGM. *Quaternary Science Reviews* **24**: 835–852.
- Mertens KN, Verhoeven K, Verleye T, *et al.* 2009. Determining the absolute abundance of dinoflagellate cysts in recent marine sediments: the Lycopodium marker-grain method put to the test. *Review of Palaeobotany and Palynology* **157**: 238–252.
- Mix AE, Bard E, Schneider R. 2001. Environmental processes of the ice age: Land, Ocean, Glacier (EPILOG). *Quaternary Science Reviews* **20**: 627–657.
- Moros M, Kuijpers A, Snowball I, *et al.* 2002. Were glacial iceberg surges in the North Atlantic triggered by climatic warming? *Marine Geology* **192**: 393–417.
- Naughton F, Sánchez Goñi M-F, Kageyama M, *et al.* 2009. Wet to dry climatic trend in north-western Iberia within Heinrich events. *Earth and Planetary Science Letters* **284**: 329–342.
- Orvik KA, Niiler P. 2002. Major pathways of Atlantic water in the northern North Atlantic and Nordic Seas toward Arctic. *Geophysical Research Letters* **29**: 1896–1899.
- Peltier WR, Fairbanks RG. 2006. Global glacial ice volume and Last Glacial Maximum duration from an extended Barbados sea-level record. *Quaternary Science Reviews* **25**: 3322–3337.
- Penaud A, Eynaud F, Turon J-L, *et al.* 2009. What forced the collapse of European ice sheets during the last two glacial periods (150 ka B.P. and 18 ka cal B.P.)? Palynological evidence. *Palaeogeography, Palaeoclimatology, Palaeoecology* **281**: 66–78.
- Radi T, de Vernal A, Bonnet S. 2009. Report - DINO8 meeting. Eighth International Conference on Modern and Fossil dinoflagellates. *R. d. Micropaleontologie* **52**: 265–266.
- Rahmstorf S. 2002. Ocean circulation and climate during the past 120,000 years. *Nature* **419**: 207–214.
- Rasmussen TL, Thomsen E, Vanweering TCE, *et al.* 1996a. Rapid changes in surface and deep water conditions at the Faeroe margin during the last 58,000 years. *Paleoceanography* **11**: 757–771.
- Rasmussen TL, Vanweering TCE, Labeyrie L. 1996b. High resolution stratigraphy of the Faeroe-Shetland Channel and its relation to north Atlantic paleoceanography: the last 87 kyr. *Marine Geology* **131**: 75–88.
- Rasmussen TL, Thomsen E. 2008. Warm Atlantic water inflow to the Nordic seas 34–10 ka calibrated ka BP. *Paleoceanography* **23**: 1–13.
- Richter TO, Van Der Gaast S, Koster B, *et al.* 2006. The Avaatech XRF Core Scanner: technical description and applications to NE Atlantic sediments. In *New Techniques in Sediment Core Analysis*, Rothwell RG (ed.). Geological Society Special Publications: London; 39–50.
- Rignot E, Casassa P, Gogineni P, *et al.* 2004. Accelerated ice discharge from the Antarctic Peninsula following the collapse of Larsen B ice shelf. *Geophysical Research Letters* **31**. [doi: 10.1029/2004GL020697]
- Roche DM, Wiersma AP, Renssen H. 2010. A systematic study of the impact of freshwater pulses with respect to different geographical locations. *Climate Dynamics* **34**: 997–1013.

- Rochon A, de Vernal A, Turon J-L, *et al.* 1999. Distribution of dinoflagellate cysts in surface sediments from the North Atlantic Ocean and adjacent basins and quantitative reconstruction of sea-surface parameters. *AASP Special Publication*. American Association of stratigraphic palynologists, Dallas, USA.
- Rosell-Melé A, Bard E, Emeis KC, *et al.* 2004. Sea-surface temperature anomalies in the oceans at the LGM estimated from the alkenone $U^{k^{37}}$ index: comparison with GCMs. *Geophysical Research Letters* **31**. [doi: 10.1029/2003GL018151]
- Ruddiman WF. 1977. Late Quaternary deposition of ice-rafted sand in the subpolar North Atlantic (lat 40° to 65°N). *GSA Bulletin* **88**: 1813–1827.
- Sánchez Goñi M-F, Harrison SP. 2010. Global patterns of vegetation response to millennial-scale variability and rapid climate change during the last glacial period. *Quaternary Science Reviews* **29**: 2957–2980.
- Sarnthein M, Gersonde R, Niebler S, *et al.* 2003. Overview of Glacial Atlantic Mapping (GLAMAP 2000). *Paleoceanography* **18**. [doi: 10.1029/2002PA000769]
- Schmittner A. 2005. Decline of the marine ecosystem caused by a reduction in the Atlantic overturning circulation. *Nature* **434**: 628–633.
- Scourse JD, Haapaniemi AL, Colmenero-Hidalgo E, *et al.* 2009. Growth, dynamics and deglaciation of the last British-Irish ice sheet: the deep-sea ice rafted detritus record. *Quaternary Science Reviews* **28**: 3066–3084.
- Scourse JD, Hall IR, McCave IN, *et al.* 2000. The origin of Heinrich layers: evidence from H2 for European precursor events. *Earth and Planetary Science Letters* **182**: 187–195.
- Stanford JD, Rohling EJ, Hunter SE, *et al.* 2006. Timing of mwp-1a and climate responses to meltwater injections. *Paleoceanography* **21**: PA4103. DOI: 10.1029/2006PA001340.
- Stanford JD, Rohling EJ, Bacon S, *et al.* 2011. A new concept for the paleoceanographic evolution of Heinrich event 1 in the North Atlantic. *Quaternary Science Reviews* **30**: 1047–1066.
- Stockmarr J. 1971. Tablets with spores used in absolute pollen analysis. *Pollen et Spores* **13**: 615–621.
- Stoker MS, Akhurst MC, Howe JA, *et al.* 1998. Sediment drifts and contourites on the continental margin off northwest Britain. *Sedimentary Geology* **115**: 33–51.
- Svensson A, Andersen KK, Bigler M, *et al.* 2008. A 60 000 year Greenland stratigraphic ice core chronology. *Climate of the Past* **4**: 47–57.
- Toucanne S, Zaragosi S, Bourillet J-F, *et al.* 2009. Timing of massive 'Fleuve Manche' discharges over the last 350 kyr: insights into the European ice-sheet oscillations and the European drainage network from MIS 10 to 2. *Quaternary Science Reviews* **28**: 1238–1256.
- Turrell WR, Slesser G, Adams RD, *et al.* 1999. Decadal variability in the composition of Faroe Shetland Channel bottom water. *Deep-Sea Research Part I: Oceanographic Research Papers* **46**: 1–25.
- van Krevelend S, Sarnthein M, Erlenkeuser H, *et al.* 2000. Potential links between surging ice sheets, circulation changes, and the Dansgaard-Oeschger cycles in the Irminger Sea, 60-18 kyr. *Paleoceanography* **15**: 425–442.
- Vidal L, Labeyrie L, Cortijo E, *et al.* 1997. Evidence for changes in the North Atlantic Deep Water linked to meltwater surges during the Heinrich events. *Earth and Planetary Science Letters* **146**: 13–27.
- Waelbroeck C, Labeyrie L, Michel E, *et al.* 2002. Sea-level and deep water temperature changes derived from benthic foraminifera isotopic records. *Quaternary Science Reviews* **21**: 295–305.
- WOA. 1998. *World Ocean Atlas*, Silver Spring, MD. [http://www.nodc.noaa.gov/oc5/woa98.html]
- Weinelt MS, Sarnthein M, Vogelsang E, *et al.* 1991. Early decay of the Barents Shelf Ice Sheet: spread of stable isotope signals across the eastern Norwegian Sea. *Norsk Geologisk Tidsskrift* **71**: 137–140.
- Weinelt M, Sarnthein M, Pflaumann U, *et al.* 1996. Ice-free Nordic seas during the Last Glacial Maximum? Potential sites of deepwater formation. *Paleoclimates* **1**: 283–309.
- Winograd IJ. 2001. The magnitude and proximate cause of ice-sheet growth since 35,000 yr B.P. *Quaternary Research* **56**: 299–307.
- Zaragosi S, Eynaud F, Pujol C, *et al.* 2001. Initiation of the European deglaciation as recorded in the northwestern Bay of Biscay slope environments (Meriadzek Terrace and Trevelyan Escarpment): a multi-proxy approach. *Earth and Planetary Science Letters* **188**: 493–507.
- Zumaque J, Eynaud F, Zaragosi S, *et al.* 2012. An Ocean – ice coupled response during the last glacial: zooming on the marine isotopic stage 3 south of the Faeroe Shetland Gateway. *Climate of the Past*. **8**: 3043–3091. DOI: 10.5194/cpd-8-3043-2012.

La dernière période glaciaire a été ponctuée d'évènements climatiques abrupts connus sous le nom d'évènements d'Heinrich et évènements de Dansgaard-Oeschger. Cette variabilité millénaire a fait l'objet de nombreuses études, mais plusieurs incertitudes demeurent. Ce travail de doctorat vise à étendre et compléter les connaissances existantes sur cette variabilité climatique rapide en ciblant l'étude des variations hydrographiques telles qu'enregistrées au sein de deux archives sédimentaires prélevées au niveau des îles Féroé. Nos principaux résultats, basés sur une approche intégrée multiproxies, mettent en évidence un schéma atypique en Mer de Norvège, où les épisodes froids (stadias, évènements d'Heinrich inclus) sont marqués par des températures océaniques de surface relativement élevées (notamment en été) et un couvert de glace de mer réduit à quelques mois par an, et inversement pour les périodes chaudes (interstadias) qui enregistrent des conditions océaniques de surface froides et une expansion du couvert de glace de mer. Le caractère atypique des stadias paraît lié à une advection accrue d'eaux chaudes atlantiques dans les Mers Nordiques, couplée à un réchauffement de subsurface généralisé au bassin subpolaire Nord-Atlantique et ses mers bordières. Ces deux processus semblent jouer un rôle majeur dans la déstabilisation des *ice-shelves* et glaciers boréaux, et *in fine* dans leur effondrement final et les débâcles d'icebergs qui en résultent. Nos travaux nous permettent également de dégager les principaux mécanismes à l'origine des changements de circulation océanique en Atlantique Nord et des variations de température atmosphérique associées. Sur la base de l'ensemble de nos résultats et de ceux émanant de précédentes études, nous proposons ainsi un nouveau scénario de fonctionnement couplé océan-glace-atmosphère permettant d'expliquer les évènements climatiques abrupts de la dernière période glaciaire.

Mots-clés : évènements d'Heinrich, évènements de Dansgaard-Oeschger, processus hydrographiques, interactions océan-cryosphère-atmosphère, Mers nordiques

The last glacial period was punctuated by abrupt climatic events known as Dansgaard-Oeschger and Heinrich events. Many studies have focused on this millennial climatic variability, but several uncertainties remain. The present work aims at improving our knowledge on this topic through the study of the hydrographical changes recorded in two marine archives retrieved off Faeroes. Our main results, based on a multiproxy approach, reveal a paradoxical scheme in the Norwegian Sea where cold episodes (stadials, including Heinrich events) are characterized by relatively warm sea-surface temperatures (especially during summer) and a reduced sea-ice cover, and warm periods (interstadials) are marked by a reverse pattern with cold sea surface conditions and extended sea ice cover. The atypical stadial features seem to be related to enhanced advection of warm Atlantic waters in the Nordic Seas, combined to a subpolar North-Atlantic and adjacent seas basin-wide subsurface warming. These two processes seem to play a key role in the destabilization of boreal ice-shelves and ice-sheets, and *in fine* to their final collapse and subsequent iceberg discharges. Our work also allows us to identify the main mechanisms responsible for Atlantic Meridional Overturning Circulation changes and associated atmospheric temperature variations. On the basis of our results and of those coming from previous studies, we thus propose a new hydrographical scenario which could explain the abrupt climate events of the last glacial period

Keywords: Heinrich events, Dansgaard-Oeschger events, hydrographical processes, ocean-atmosphere-cryosphere interactions, Nordic seas.